THE UNIVERSITY *of* EDINBURGH

This thesis has been submitted in fulfilment of the requirements for a postgraduate degree (e. g. PhD, MPhil, DClinPsychol) at the University of Edinburgh. Please note the following terms and conditions of use:

- This work is protected by copyright and other intellectual property rights, which are retained by the thesis author, unless otherwise stated.
- A copy can be downloaded for personal non-commercial research or study, without prior permission or charge.
- This thesis cannot be reproduced or quoted extensively from without first obtaining permission in writing from the author.
- The content must not be changed in any way or sold commercially in any format or medium without the formal permission of the author.
- When referring to this work, full bibliographic details including the author, title, awarding institution and date of the thesis must be given.

Physical and morphological studies of polymer blends: a multiscale investigation.

Hannah Jones

A thesis submitted for the Degree of Doctor of Philosophy to the University of Edinburgh.

August 2022

Declaration

I declare that this thesis has been composed solely by myself and that it has not been submitted, in whole or in part, in any previous application for a degree. Except where states otherwise by reference or acknowledgment, the work presented is entirely my own.

Hannah Jones

August 2022

Abstract

Polyolefins, polypropylene (PP) and polyethylene (PE), are two commonly used plastics and account for nearly half of all plastic wastes. As the quantity of plastic wastes surpasses millions of tonnes per year, a focus has been placed on combatting polyolefin plastic wastes to achieve a circular plastic economy. Plastic waste management options include landfill, energy recovery and recycling, with the latter being the most attractive environmental option. Currently, the recycling industry is faced with challenges of poor quality and performance polyolefin recyclate. The poor physical and mechanical performance of recyclate is attributed to the difficulty of PP and PE separation during recycling resulting in the formation of immiscible blends; the presence of thermo-mechanical and thermo-oxidative degradation mechanisms; and contaminants. The quality in recyclate will vary from site to site, and for different waste streams. Studies have been carried out to improve the performance of polyolefin recyclate, for example, through the addition of compatibilisers and fillers. However, understanding performance variability of recycled blends for a range of compositions before addition of other components is just as important in order to achieve a circular plastic economy.

The primary aim of this thesis was to provide a comparative study of the thermal properties, mechanical properties and phase morphology of virgin and recycled PP: high density polyethylene (HDPE) blends prepared by extrusion mixing and injection moulding. There is a lack of comparative studies over a broad range of compositions for virgin and recycled PP:HDPE blends in the literature. Therefore, a range of blend compositions were investigated from PP:HDPE 10: 90 weight percentage (wt%) up to PP:HDPE 90:10 wt%, along with pure PP and HDPE. To understand the thermal properties of the virgin and recycled blends differential scanning calorimetry (DSC) was carried out. Tensile testing and dynamic mechanical analysis (DMA) were used to determine the mechanical properties and finally, scanning electron microscopy (SEM) and atomic force microscopy (AFM) were used to determine the morphology. For the AFM study, a new mode called the Quantitative Imaging (QI) mode was implemented to determine the phase morphology of both the virgin and recycled blends.

The thermal studies concluded that both the virgin and recycled blends were incompatible shown by the presence of two peaks in the melting thermograms. Recycled blends had a lower crystallinity, melting and crystallisation temperatures compared to the virgin blends. These observations were attributed to the polymer degradation during recycling. Mechanical studies began with DMA to understand the effect of recycling and blend composition on the storage modulus, along with the relaxation processes present. There was little variation in the storage modulus of recycled and virgin blends, but the alpha and beta relaxation temperatures were lower in recycled blends due to structural deterioration during the recycling process. The tensile properties of recycled blends were not substantially affected by the recycling process in comparison to the virgin blends. Interestingly, the virgin HDPE (vHDPE) up to PP:HDPE 25:75 wt% exhibited a higher yield strength, lower elongation at yield and at break than expected, due to the high chain orientation caused by the injection moulding process. The deterioration in the thermal and mechanical properties of recycled blends are caused by the presence of degradation mechanisms and contaminants, causing shorter polymeric chains and the formation of imperfect crystallites during reprocessing. AFM was used to complement initial SEM images and found nano-phase morphology that was dependent on composition in both the virgin and recycled blends. The Young's moduli obtained through the QI mode for the virgin and recycled blends were similar in value to the Young's moduli obtained from tensile testing. The morphology was found to be related to changes in the thermal and mechanical properties illustrating the importance of understand the processing-structure-properties relationship.

Lay Summary

Plastic are used on a daily basis and are present in nearly every product we buy, from food packaging to our mobile phones. As a society, we have become dependent on plastics as they possess a diverse range of properties. Consequently, we are required to dispose of millions of tonnes of plastic wastes yearly. Currently, plastic waste management options available include landfill, energy recovery and recycling. Recycling is considered the most attractive environmental option. So how are we going to solve this problem of plastic waste? Can we recycle and re-use every plastic out there to achieve a circular plastic economy? Can we avoid sending recycled plastics to landfill? These are the questions being asked by the plastics industry today.

UK households are encouraged to put their used plastic products in their recycling boxes ready for collection. Within each recycling box, there will be a range of different plastics present, with the most abundant plastics being polypropylene and polyethylene. The plastic wastes are collected and transported to a recycling facility. At the recycling facility, the plastic wastes are separated into the individual types, followed by a reprocessing procedure to produce recycled plastic called recyclate. However, the recycling industry must overcome the challenge of low quality and performance recyclate. This means recyclate is typically used in low demanding applications such as floor decking, and will ultimately end up in landfill. There are three causes for low quality recyclate; firstly, the difficulty of separating the plastics polypropylene and polyethylene during the sorting stage of the recycling process. This means the recyclate will be a blend of the two plastics. The ratio of polypropylene to polyethylene will vary depending on the recycling facility procedures and ultimately, the quantities of the plastics placed in consumers recycling boxes. Secondly, the harsh recycling conditions and thirdly, the presence of contaminants.

It is important to understand the variation in recyclate performance in order to optimise at low cost and increase the presence of recyclate in high demanding applications. Therefore, this thesis is focused on understanding the performance variation in virgin (plastics that have not undergone the recycling process) and recycled polypropylene - high density polyethylene blends at different weight ratios. The mechanical properties

(how the material behaves on the application of a force), thermal properties (how the material behaves on the application of heat) and morphology (the structure of the material) using a range of experimental techniques were investigated. These experiments showed that the recycling process caused structural deterioration causing a reduction in the thermal and mechanical properties in the recycled blends compared to the virgin blends. However, the tensile properties of the recycled blends were not substantially affected by the recycling process. The morphology was found to be dependent upon the blend ratio and were related to the changes in the thermal and mechanical properties.

Acknowledgments

My PhD has been a rollercoaster of highs and lows from start to finish. Therefore, I want to take the time to express my gratitude to the people who helped me along the way. Firstly, I would like to thank my principal supervisor, Professor Vasileios Koutsos for his patience, support and guidance throughout. His advice and insights in our weekly meetings were invaluable. Secondly, I would like to thank my second supervisor Dr Dipa Roy for her time, support, and the opportunity to be lead author on our review paper. Thirdly, to Dr Jake McClements for helping with my AFM experiments and to Dr Laura Charlton for taking time to provide feedback on my AFM results.

I would also like to express my thanks to Professor Colin Hindle for allowing me to use the University of Napier facilities, along with his time and the useful discussions on plastic manufacturing and characterisation. Also to Lynn Chalmers for opening the lab, taking the time to teach me how to use the equipment and helping with the cleaning. Additionally, I would like to thank my industrial supervisor Michail Kalloudis from Impact Solution for his time, resources and input into the project.

My PhD would not have been possible without the funding provided by SOFT-CDT. I began my studies with my cohort who have made my journey unforgettable. I would also like to thank Professor Lian Hutchings for his support during the difficulties I experienced at the start of my PhD.

Thank you to all the people I have met and the friends I have made along the way. To Andy and Eck for filling up the liquid nitrogen bottle before each DMA experiment. To Angus for giving me the opportunity to carry out the internship with Edinburgh Innovations, I learnt so much about the world of patents. To my friends in the lab, Helena, Muhammad, Catherine, James and a big thank you to Danijela for her friendship, laughter and the walks! Finally, to Dr Jeff Steynor for taking me to the hospital after dropping the load cell on my finger and for sending photos of Jack the dog to put a smile on my face.

A big thank you to my amazing friend Aurelie for the laughter, encouragement to keep going and the long Skype chats. To Aunty Kathryn for sending my favourite jelly sweets when things were not going to plan and to my grandparents for their support and kindness and who I miss deeply.

Finally, I would like to thank my family who have been there every step of the way. I am incredibly thankful to my amazing mum and dad for all the hours spent listening to me on facetime, the support and the belief that I can do it. I could not have done this without you! To my cracking brother Matthew and his girlfriend Ellie, for always being there and putting a smile on my face. To Ben, my dog, for knowing when I need a cuddle and for learning paws up when I would phone home. You all mean so much to me!

Table of Contents

List of Figures

Chapter 2.0 Literature Review

Chapter 3.0 Materials and Methods

Chapter 4.0 Thermal and Morphological Properties of Virgin and Recycled PP:HDPE Blends

Chapter 5.0 Mechanical Properties of Virgin and Recycled PP: HDPE Blends

Chapter 6.0 AFM QI Mode Investigation of Virgin and Recycled PP:HDPE Blends

Chapter 7.0 Comparative Study of the Thermal and Tensile Properties of Virgin and Recycled PP:HDPE Blends Using Two Different Manufacturing Methodologies

List of Tables

Chapter 2.0 Literature Review

Chapter 4.0 Thermal and Morphological Properties of Virgin and Recycled PP:HDPE Blends

Chapter 6.0 AFM QI Mode Investigation of Virgin and Recycled PP:HDPE Blends

Chapter 7.0 Comparative Study of the Thermal and Tensile Properties of Virgin and Recycled PP:HDPE Blends Using Two Different Manufacturing Methodologies

List of Acronyms

AFM	Atomic Force Microscopy
CLTE	Coefficient of Linear Thermal Expansion
CM	Brabender Mixing and Compression Moulding
DMA	Dynamic Mechanical Analysis
DMT	Derjaguin-Müller-Toporov
DSC	Differential Scanning Calorimetry
EPDM	Ethylene Propylene Diene Monomer
EPRM	Ethylene Propylene Rubber Monomer
EPS	Expanded Polystyrene
ESCR	Environmental Stress Cracking Resistance
EVA	Ethylene-Vinyl Acetate
EVOH	Ethylene Vinyl Alcohol
HDPE	High Density Polyethylene
IM	Twin Screw Extrusion and Injection Moulding
iPP	Isotactic PP
LCST	Lower Critical Solution Temperature
LCV	Lower Calorific Value
LDPE	Low Density Polyethylene
LLDPE	Linear Low Density Polyethylene
MAPP	Maleated Polypropylene
MFI	Melt Flow Index
MSW	Municipal Solid Waste
PA	Polyamide
PC	Polycarbonate
PE	Polyethylene
PET	Polyethylene Terephthalate
PMMA	Poly(methyl acrylate)
POs	Polyolefins

PP	Polypropylene
PP:HDPE Blends	Polypropylene: High Density Polyethylene Blends
PS	Polystyrene
PSW	Plastic Solid Waste
PVC	Polyvinyl Chloride
QI	Quantitative Imaging
rHDPE	Recycled High Density Polyethylene
rPOs	Recycled Polyolefins
rPP	Recycled Polypropylene
rPP:rHDPE Blends	Recycled Polypropylene: Recycled High Density Polyethylene Blends
SEM	Scanning Electron Microscopy
SPM	Scanning Probe Microscopy
STM	Scanning Tunnelling Microscopy
UCST	Upper Critical Solution Temperature
UHMWPE	Ultra High Molecular Weight Polyethylene
UTS	Ultimate Tensile Strength
vHDPE	Virgin High Density Polyethylene
VLDPE	Very Low Density Polyethylene
vPP	Virgin Polypropylene
vPP:vHDPE Blends	Virgin Polypropylene: Virgin High Density Polyethylene
WPC	Wood–Plastic Composites

List of Symbols

α	Alpha Relaxation
β	Beta Relaxation
E	Young's Modulus
E'	Storage Modulus
E''	Loss Modulus
G	Gibbs Free Energy
tanδ	Tan Delta
T_c	Crystallisation Temperature
T_g	Glass Transition Temperature
T_m	Melting Temperature
wt%	Weight Percentage
γ	Gamma Relaxation
δ	Phase Shift
ΔG_{mix}	Gibbs Free Energy of Mixing
ΔH_c	Enthalpy of Crystallisation
ΔH_{mix}	Enthalpy of Mixing
ΔH_f	Enthalpy of Fusion
ΔS_{mix}	Entropy of Mixing
ΔV_m	Volume of Mixing

1.0 Thesis Overview

1.1. Overview

Plastics are a commodity material that are used on a daily basis within a multitude of products. Plastics are cheap to manufacture, versatile and possess a diverse range of properties, which has resulted in their mass production since the 1950's.[1,2] It is predicted by 2050 there will be 12,000 million tonnes of plastic wastes in landfills and/or the natural environment globally, due to plastics' slow degradability in the ambient environment.[3] During degradation, plastics release toxic, harmful chemicals such as bisphenol A and heavy metals, which can leach into the natural environment, causing ecological harm along with potential detrimental effects to human health.[4-8] Therefore, the management of plastic wastes is extremely important. Management options available include: landfill, recycling and energy recovery; with each option possessing advantages and disadvantages.[9,10] Recycling is an environmentally friendly method of processing plastic wastes and contributes towards the aim of a plastic circular economy.[11,12]

Polyolefin (PO) thermoplastics, polypropylene (PP) and polyethylene (PE), are two commonly used commodity plastics and account for nearly half all of the plastic wastes.[13] At their end of life, these plastics typically undergo the low cost, reliable, secondary mechanical recycling process.[14,15] Secondary mechanical recycling involves sorting and separation of plastics, followed by washing, grinding and shredding to form plastic flakes ready for re-processing.[16-19] The plastics industry is faced with the heterogeneous nature of plastic waste that consequently leads to poor performance recyclate material in comparison to the virgin material.[18,20] Consequently, PO recyclate is typically used in applications of low value, such as in manufacturing plastic lumber.[21]

During secondary mechanical recycling a reduction in mechanical and physical properties are caused by:

1. Thermo-mechanical and thermo-oxidative degradation of the polymer chains.[22-24]
2. Formation of immiscible polymer blends. The complete separation of PP and PE during recycling is challenging and expensive, due to their similar physical properties and densities so typically remain as a polymer blend.[15,25]

3. Presence of low molecular weight contaminants such as ketones and esters.[19]

POs have the lowest recycling rates so there is extensive literature on the addition of a wide variety of compatibilisers, stabilisers, virgin polymers, fillers and fibres, during reprocessing to improve recyclate quality and performance.[13,15,26-36] However, this approach is costly and time consuming, and the quantities required will vary with each recycled waste stream.[37,38] Maintaining a constant recyclate quality is a key challenge for the industry, as the sorting and processing will vary greatly from location to location due to different plastic waste collection processes, waste stream composition, recycling infrastructures, available equipment, and capacity, but also by the recycled plastic type market demand.[11] If recyclate quality and consistency could be improved without a large cost increase, there is the potential for recyclate consisting of PP and PE to be used in a wide range of applications. For example, Andoh et al.[36] proposed a 75 weight percentage (wt%) recycled high density polyethylene (HDPE): 25 wt% bamboo fibre composite which could potentially be used in wind blade manufacturing. This would enable a plastic circular economy to be a reality instead of an unachievable goal.

1.2 PhD Aims

The primary aim of the PhD was to understand and contribute knowledge on the processing-properties-morphology relationship for virgin and recycled PP:HDPE blends to aid efforts to overcome poor performance polyolefin recyclate . The following investigations were carried out.

- The effect of composition on the thermo-mechanical properties and morphology of both the virgin and recycled blends. Recyclate performance varies from site to site due to differing sortation techniques, quantity of contaminants and varying waste sources, resulting in differing ratios of PP to HDPE in each batch. Comparative studies over a wide range of compositions are important in order to optimise the properties of the recycled PP:HDPE (rPP:rHDPE) blends during reprocessing.
- The effect of the recycling process by comparing the thermo-mechanical properties and morphology of the virgin and recycled blends. If the recycled blends are not significantly affected by the reprocessing it may suggest the

possibility that PP and PE separation is not required during reprocessing. This would save the industry time, energy and costs.

- To deduce whether the novel atomic force microscopy (AFM) quantitative imaging (QI) mode can be used to provide information on topography, morphology and quantitative data, in this case, Young's moduli for virgin and recycled blends.

Blends were prepared by injection moulding. The thermo- mechanical properties were investigate by differential scanning calorimetry (DSC), dynamical mechanical analysis (DMA), tensile testing. Morphological studies were carried out using SEM and more extensively with AFM.

1.3 Thesis Structure

This thesis consists of eight chapters. A brief outline of the content in chapters 2 to 8 are discussed below.

Chapter 2 is a literature review providing an overview of the commodity plastics PP and PE, current challenges faced with plastic wastes recycling, thermodynamics polymer blends, in particular PP:HDPE blends and finally briefly discusses methods used to improve recyclate performance. Large amounts of this chapter have been presented in the review paper:

Jones , H.; Saffar, F.;Koutsos, V.; Ray, D. Polyolefins and Polyethylene Terephthalate Package Wastes: Recycling and Use in Composites. *Energies* **2021,** 14, 7306. https://doi.org/10.3390/en14217306

Chapter 3 describes the raw materials and manufacturing methods used to produce the virgin and recycled PP:HDPE blends. Furthermore, this chapter describes the working principles of the characterisation techniques implemented: DSC, AFM, tensile testing and DMA.

Chapter 4 presents the thermal and morphological properties of the virgin and recycled PP:HDPE blends. This chapter implements DSC to study the thermal properties of the virgin and recycled blends. The melting and crystallisation behaviour

of the virgin and recycled blends were compared and discussed. To investigate the effect of varying the PP:HDPE blend composition on the morphology, scanning electron microscopy was used, and complemented by AFM. The AFM data presented in this chapter was obtained in an experiment carried out by Dr Jake McClements.

Chapter 5 presents the mechanical properties for virgin and recycled PP:HDPE blends. The chapter focuses on tensile testing and DMA. The tensile test provided information on the Young's modulus, yield point, ultimate tensile strength, and elongation at yield and at break. From DMA, relaxation processes were identified and the elastic and loss moduli were deduced in the virgin and recycled blends.

Chapter 6 presents a detailed morphological and nanomechanical investigation by AFM. A new AFM mode called the quantitative imaging (QI) mode was implemented. This new mode enables a detailed study of the elastic properties of the blends at nanoscale and was applied to both virgin and recycled PP:HDPE blends over a wide range of compositions to determine the morphology and mechanical properties of the blends.

Chapter 7 presents a short comparative study between the commonly industrially used Brabender mixing and compression moulding process to the twin-screw extrusion mixing and injection moulding process, on the thermal and mechanical properties of virgin and recycled PP:HDPE blends. This study was carried out to understand the unexpected tensile behaviour of vHDPE, which is presented and discussed in chapter 5.

Chapter 8 presents the conclusions from the mechanical, thermal and morphological studies of virgin and recycled PP:HDPE blends. Furthermore, this chapter discusses future work and areas of interest.

Appendix presents the additional AFM images obtained.

References

1. A. Shrivastava, in *Introduction to Plastics Engineering: Plastics Design Library*, S. Ebnesajjad, Williams Andrew Applied Science Publishers, 2018, Ch. 3.
2. R. Geyer, in *Plastic Waste and Recycling*, T. M. Letcher, Elsevier 2020.
3. R. Geyer, J. R. Jambeck, K. L. Law, *Sci. Adv.* **2017**, *3.*
4. C. R. Cook, R. U. Halden, in *Plastic Waste and Recycling*, T. M. Letcher,L. House, Elsevier 2020.
5. R. U. Halden, *Annu. Rev. Public Health* **2010**, *31*, 179.
6. R. Verma, K. S. Vinoda, M. Papireddy, A. N. S. Gowda, *Procedia Environ. Sci.* **2016**, *35*, 701.
7. S. Kubowicz, *Environ. Sci. Technol.* **2017**, *51*, 12058.
8. T. Yamamoto, A. Yasuhara, H. Shiraishi, O. Nakasugi, *Chemosphere* **2001**, *42*, 415.
9. K. Ragaerta, L. Delva, K. V. Geem, *Waste Manage.* **2017**, *69*, 24.
10. S. M. Al-Salem, P. Lettieri, J. Baeyens, *Waste Manage.* **2009**, *29*, 2625.
11. J. N. Hahladakis, E. Iacovidou, *Sci. Total Environ.* **2018**, *630*, 1394.
12. S. Satapathy, *Benchmarking An Int. J.* **2017**, *24*, 415.
13. P. A. Kots, B. C. Vance, D. G. Vlachos, *React. Chem. Eng.* **2022**, *7*, 41.
14. K. Hamad, M. Kaseem, F. Deri, *Polym. Degrad. Stab.* **2013**, *98*, 2801.
15. N. K. Madi, *Mater. Des.* **2013**, *46*, 435.
16. M. E. Grigore, *Recycling* **2017**, *2*, 1.
17. G. Faraca, T. Astrup, *Waste Manage.* **2019**, *95*, 388.
18. E. Kosior, J. Mitchell, in *Plastic Waste and Recycling*, T. M. Letcher,L. House, Elsevier, 2020.
19. B. Luijsterburg, H. Goossens, *Resour., Conserv. Recycl.* **2014**, *85*, 88.
20. J. N. Hahladakis, E. Iacovidou, *Journal of Hazardous Material* **2019**, *380*, 120887.
21. T. Nosker, J. Lynch, in *Handbook of Industrail Polyethylene Technology*, John Wiley and Sons, 2016.
22. M. S. Abbas-Abadi, *J. Therm. Anal. Calorim.* **2021**, *143*, 2867.
23. M. K. Loultcheva, M. Proietto, N. Jilov, F. P. L. Mantia, *Polym. Degrad. Stab.* **1997**, *57*, 77.
24. L. A. Pinheiro, M. A. Chinelatto, S. V. Canevarolo, *Polym. Degrad. Stab.* **2004**, *86*, 445.

25. R. Strapasson, S. C. Amico, M. F. R. Pereira, T. H. D. Sydenstricker, *Polymer Testing* **2005**, *24*, 468.
26. C. Meran, O. Ozturk, M. Yuksel, *Materials & Design* **2008**, *29*, 701.
27. G. W. Curtzwiler, M. Schweitzer, Y. Li, S. Jiang, K. L. Vorst, *J. Clean. Prod.* **2019**, *239.*
28. A.A.S Mariam Atiqah, H.Salmah, Z. Firuz, D. N. U. Lan, *Key Engineering Materials* **2014**, *494*, 837.
29. E. G. Hanna, *J. Eng. Sci. Technol. Rev* **2019**, *12*, 87.
30. P. Brachet, L. T. Høydal, E. L. Hinrichsen, F. Melum, *Waste Manag.* **2008**, *28*, 2456.
31. O. Ammar, Y. Bouaziz, N. Haddar, N. Mnif, *Polym. Sci.* **2017**, *3*, 1.
32. S. Sengupta, D. Ray, A. Mukhopadhyay, *ACS Sustain. Chem. Eng.* **2013**, *1*, 574.
33. N. Phuong, V. Gilbert, B. Chuong, *J. Reinf. Plast. Compos.* **2008**, *27*, 1983.
34. A. M. M. Abdelhaleem, M. Megahed, D. Saber, *J. Compos. Mater.* **2018**, *52*, 1633.
35. S. Svensson, D. Åkesson, M. Bohlén, *J. Polym. Environ.* **2020**, *28*, 1967.
36. P. Y. Andoh, C. K. K. Sekyere, G. K. K. Ayetor, M. N. Sackey, *J. Appl. Eng. Technol. Sci* **2021**, *2*, 125.
37. I. A. Ignatyev, W. Thielemans, B. V. Beke, *ChemSusChem* **2014**, *7*, 1579.
38. J. Hopewell, R. Dvorak, E. Kosior, *Philosophical Transactions of The Royal Society B* **2009**, *364*, 2115.

2.0 Literature Review

2.1 Plastic Packaging

Plastics are used in a variety of different industries such as packaging, building and automotive, due to their advantageous range of properties.[1] The advantages include: their low cost, high toughness, durability, property of being lightweight, easy processability, low thermal conductivity, and high environmental and corrosion resistance.[2] Plastic packaging is the largest end use market and accounts for nearly 70% of all plastic wastes[1,3] Several industries utilise plastic packaging to preserve and protect products of the industrial packing, pharmaceuticals, personal and household care, and electronics industries, but the food and beverage industry possess the largest share in the plastic packaging market.[4,5] The short lifetime, single use, and improper waste management of plastic packaging has led to detrimental environmental effects which are well documented in the literature.[6-8] The prominent plastics found in plastic packaging are HDPE, low density polyethylene (LDPE), PP, and polyethylene terephthalate (PET).[9-12] Plastics present in smaller quantities include polystyrene (PS), expanded polystyrene (EPS), polyvinyl chloride (PVC), and other polymers such as polyamide (PA), ethylene-vinyl acetate (EVA), and ethylene vinyl alcohol (EVOH).[11] This thesis is focused upon the POs, HDPE and PP, found in plastic packaging.

At the end of its life cycle, a plastic product can either undergo recycling, energy recovery, or be placed in landfill.[13-16] In 2019, 17.8 million tonnes of plastic post-consumer packaging wastes were collected from household, industrial, and commercial sources, of which 42% was recycled, 18.5% was landfilled, and 39.5% underwent energy recovery in Europe.[1] A reduction in plastic wastes in landfill is being driven by the reduction in space available for landfill sites along with an imposed landfill tax. However, large amounts of plastic wastes are still ending up in landfill and ultimately causing ecological harm.[17] Interestingly, energy recovery is a commonly used waste management option even with the negative environmental impact. Energy recovery is the process of recovering the energy content within plastic wastes through incineration.[18,19] Energy recovery is a popular choice for plastic waste management due to plastics generating a significant amount of energy due to their high lower calorific value (LCV) and can provide a high electricity-to-heat ratio.[20,21] However, major concern surrounding the incineration of plastic wastes is the production and

release of persistent organic pollutants, particulates, and hazardous toxic compounds such as dioxins and furans into the environment.[22-24]

Achieving a circular plastic economy where all plastic wastes are re-used, recycled, and recovered is the desired solution to prevent further environmental plastic waste contamination.[25] There are several local, UK and worldwide initiatives to achieve a circular economy such as the European Commissions' plastic circular economy strategy set out in 2018.[26,27] For a circular economy to be achieved, it is important to understand and analyse the life cycle of plastics from manufacturing through to reprocessing, but also to design plastic products with end-of-life management in mind.[1,9,28]

2.2 Introduction to Polyolefins

POs, such as PP and PE, are attractive due to their low cost, high abundancy, good mechanical properties and chemical resistance, low density, and ease of processability.[29] For these reasons, 9.8 million tons of PP and 15.1 million tons of PE were manufactured in 2019, which accounted for 49.2% of the total converted plastic European demand (50.7 million tonnes).[1] POs are fully saturated hydrocarbons synthesised by the polymerisation of an olefinic monomer in the presence of a catalyst.[30] The olefinic monomers, ethylene and propylene, depicted in Figure 2.1, are obtained from the cracking of petroleum feeds or the dehydrogenation of alkanes.[29] Different grades of PP and PE exist, such as blow moulding or injection moulding grades, which differ in melt viscosity and can be obtained through the use of co-monomers such as hexane or butane during olefinic polymerisation.[30]

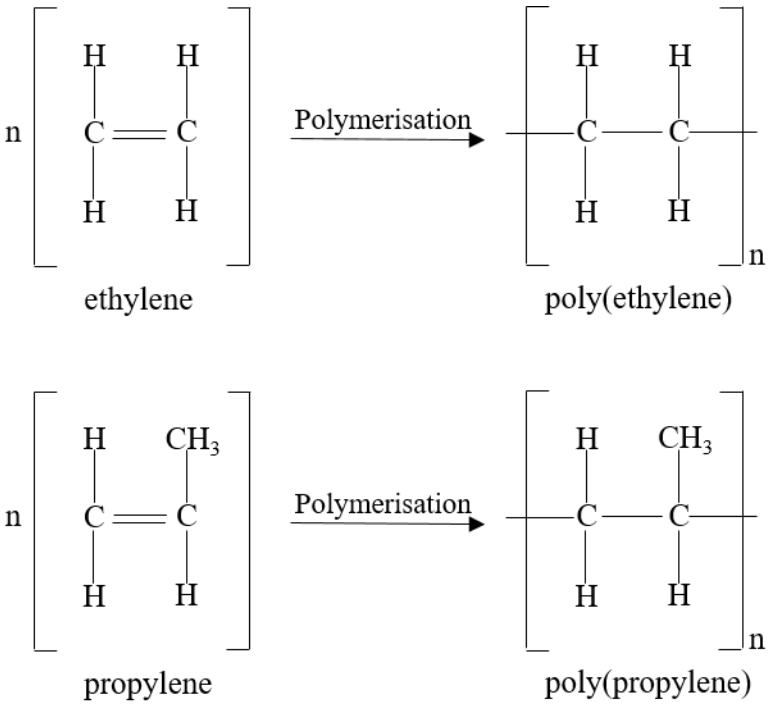

Figure 2.1 Ethylene and propylene monomers for the formation of PE and PP, respectively.

2.2.1 Overview to PP

PP is a semi-crystalline polymer which is widely used in packaging films and household and electrical appliances.[31-33] For example, biaxially orientated PP is commonly used in the manufacturing of flexible and light packaging.[34] PP possesses good mechanical properties and processability; however, its applications are limited by UV degradation, flammability, and poor impact strength at low temperatures.[33,34] There are three different types of PP: atactic PP, syndiotactic PP, and isotactic PP (iPP) (Figure 2.2).[31,32,35] In iPP, the methyl groups are all located on one side of the main chain and it is typically used in research papers due to its stability, homogeneity, and high crystallinity.[31,35]

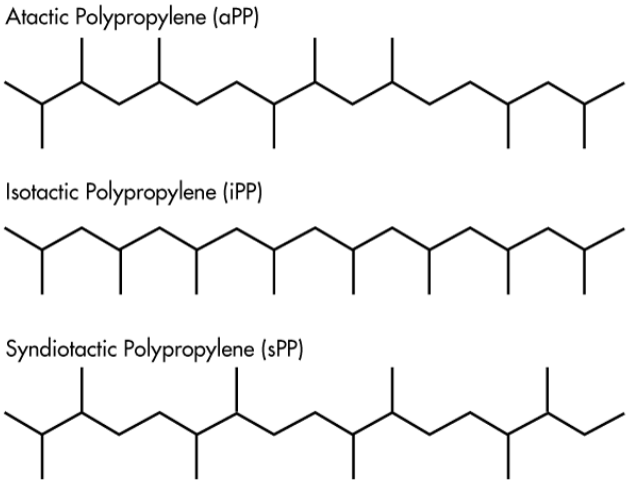

Figure 2.2 Summary of the PP structures. Used with permission.[36]

2.2.2 Overview to PE

PE is a semi-crystalline polymer used in a wide range of applications from packaging to medical devices due to its diverse properties.[31,32,37] Depending on the polymerisation mode, three different PEs can form: HDPE, LDPE, and linear low density PE (LLDPE).[31] The branching degree and the molecular weight influence their physical properties in the melt and solid state.[38-40] There are many other types of PEs which exist on the PO market: for example, ultrahigh molecular weight PE (UHMWPE) and very low-density PE (VLDPE), which are used in very specific applications.[38] UHMWPE is typically incorporated in biomedical applications such as artificial joints,[41] whereas VLDPE is typically used to manufacture films for food packaging.[42] Generally, PEs are limited by poor environmental stress cracking resistance (ESCR).[43] ESCR is affected by molecular weight, molecular weight distribution, density, number of tie molecules between crystalline and amorphous domains, and the testing conditions.[44] Typically, the higher the level of crystallinity, the lower the ESCR.[45] Table 2.1 summarises the structure, properties, and applications of HDPE, LDPE, and LLDPE.

Table 2.1 Structure, properties, and applications of HDPE, LDPE, and LLDPE (non-exhaustive list).[37,38,42,46-50]

Type of PE	Degree of Branching	Crystallinity	Properties	Applications
HDPE 	Minimal branching	High	High tensile strength High heat resistance Rigidity Chemical resistance to acids, alkalis, and solvents	Milk bottles Packaging Toys Electrical insulation Chemical containers
LDPE 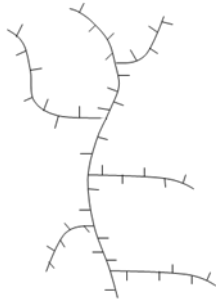	High level of short and long branches	Low	Flexibility Sufficient moisture barrier Chemical resistance to most alcohols, acids, and alkalis	Film packaging Electrical insulation Pipes
LLDPE 	High level of short branches	Low	Transparency Flexibility High toughness	Film packaging

2.3 Recycling

2.3.1 Overview of Recycling Practices

Recycling involves the conversion of waste materials into materials of commercial value for re-use and has been reviewed by several authors.[16,51-55] Recycling plastics has several environmental benefits: a net reduction in greenhouse gases and other potent molecules, net energy savings, and a reduction in the consumption of natural resources in comparison to other waste management methods.[9,56] Recycling is an attractive option to achieve a circular plastic economy as it is a viable method of dealing with plastic waste on an industrial scale with environmental benefits. However, the recycling industry faces several challenges related to high costs and the availability of recycling infrastructure to accommodate for the variation in the recyclate quality.[54] Moreover, the low cost of virgin plastics can hinder the use of recycled plastics by industries.[57] The major problems associated with recycled plastics are the different contaminants present in the plastic wastes, the reduction in their molecular weights on undergoing various recycling steps, and their degradation by oxygen, light, temperature, or water during their service life.[58] There are two forms of recycling: mechanical and chemical. Figure 2.3 summarises their advantages and current limitations.

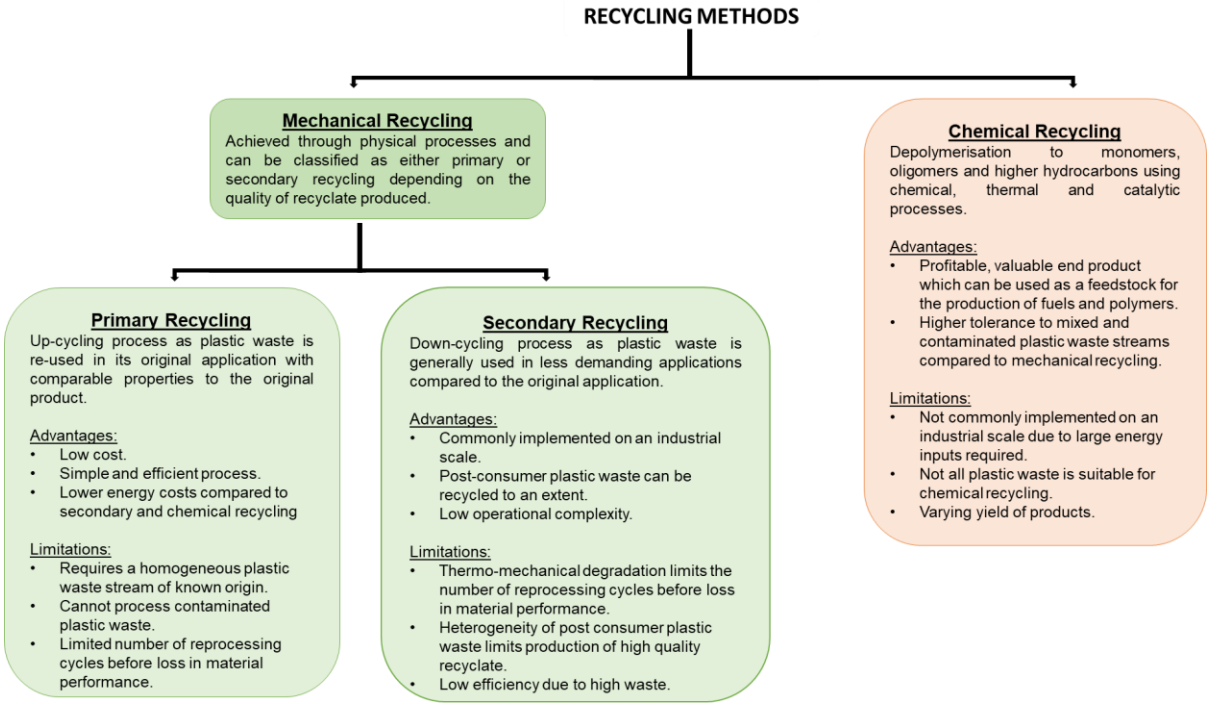

Figure 2.3 A summary of the advantages and limitations of mechanical and chemical recycling.[15,16,18,52,54,59-63]

2.3.1.1 Chemical Recycling

Chemical recycling involves the chemical conversion of polymers to monomers or oligomers which can be achieved through depolymerisation reactions.[15,19,51,64] Chemical recycling can be categorised as either a homogenous or heterogeneous process.[62] Homogenous processes include methanolysis, glycolysis, and alcoholysis.[62] Typical heterogeneous processes for plastic wastes include pyrolysis[65-67] and gasification[65,68] but other novel processes exist such as catalytic cracking[59,69] or microwave-assisted pyrolysis.[59,70,71] These processes result in monomers and other low molecular weight oligomers usually in the form of a liquid oil and syngas, which is a mixture consisting of carbon monoxide, carbon dioxide, and hydrogen.[60,65,72] These molecules can be used as feedstock for the production of new polymers and composites,[73] valuable chemicals, or fuel,[53] and hence contribute towards a circular plastic economy. Chemical recycling of plastic waste has numerous advantages compared to mechanical recycling: higher tolerance to waste contamination, avoidance of recyclate performance losses, and formation of products with economic value, and sortation is not always required; for example, in gasification, all MSW can be treated together without prior sortation.[59,65,74] Currently, chemical recycling is not practiced on an industrial scale due to the large energy costs and limited technology.[18,65,75,76]

2.3.1.2 Mechanical Recycling

Mechanical recycling is the process of recovering plastics through physical processes such as melting, grinding, shredding, and extrusion. There are two categories of mechanical recycling: primary and secondary. Both use mechanical processes to recover plastics, but they differ in the quality of the end product.[46,77] Primary recycling is a closed-loop process where pre-consumer polymers are put back into the reprocessing cycle and extruded. This process produces recyclates of similar performance to the virgin material and can be used to manufacture the same product as the virgin material or for new products for demanding applications.[51,63,78,79] Primary recycling requires knowledge of the waste source origin, previous product application, and history, which ensures low levels of molecular contamination and high polymeric purity.[61,80] PET bottles are an example which typically undergo primary recycling.[81] Primary recycling is desirable due to the production of high quality recyclates, reduction in energy costs, and conservation of natural resources. Secondary recycling

involves the recovery of plastics from municipal solid waste (MSW) and is described as down-cycling due to the recyclate demonstrating a reduction in properties, and consequently it is used in less demanding environments compared to the virgin material.[52,79] For example, recycled polyolefins (rPOs) can be used to manufacture floor tiles.[78] Post-consumer plastic packaging commonly undergoes secondary recycling as it is contaminated by residue, additives, and the presence of composite materials and laminate structures.[77,82]

Secondary mechanical recycling is a commonly used method for recycling POs due to its low cost and reliability.[55] Secondary mechanical recycling is commonly carried out in the United Kingdom. This recycling process begins with kerbside collection of household wastes (MSW).[83,84] After collection, the MSW is taken to a material recovery facility. At this facility, the plastic solid waste (PSW) is sorted from the MSW, e.g., paper and cardboard, by either manual or automated means.[85] The PSW is then transported to a plastic recycling facility where further sortation occurs into single polymer type waste streams, as PSW is a mixture of different plastics, e.g., PP, PE, PVC, PS, and PET.[86] Plastics are sorted and undergo a size reduction by cutting and shredding mechanisms; a washing process involving a hot wash in alkaline and detergent solutions; and drying and reprocessing steps: compounding and pelletizing.[52,83,87] The sorting process is extremely important to limit contamination entering the recycled plastics stream to reduce the waste of target and non-target plastics which will ultimately end up in landfill sites.[9,83,87] Luijsterburg et al.[87] found that the final quality of the recyclate was dependent on the sorting process but also the reprocessing steps. The sorting and processing will vary greatly from location to location due to different plastic waste collection processes, waste stream composition, recycling infrastructures, available equipment, and capacity, but also by the recycled plastic type market demand.[9]

2.3.2 Challenges of Mechanical Secondary Recycling of Polyolefins

Due to the heterogeneity of PSW and difficulty in 100% separation of different plastic types, maintaining a constant recyclate quality and performance is challenging. The complete separation of PP and PE during recycling is challenging and expensive due to their similar physical properties and densities.[47,48] PP:PE blends are commonly found in recycled wastes and are of great commercial interest. The blends display poor

mechanical performance due to immiscibility, thermo-mechanical degradation during reprocessing, and the presence of contaminants.[49] During reprocessing, rPO blends undergo the addition of stabilizers, compatibilizers, and fillers to improve performance, but this can cause issues in processability and cost.

A major challenge of mechanical recycling is the occurrence of thermo-mechanical and thermo-oxidative degradation caused by high temperatures and shear in the presence of oxygen and impurities during reprocessing.[50,88] Degradation mechanisms cause irreversible changes within the polymer structure, causing the deterioration of the thermal, mechanical, and physical performance of the recycled materials.[89,90] During mechanical recycling, two competing degradation mechanisms occur: random chain scission and chain crosslinking (Figure 2.4).[91,92] Random chain scission is the process of breaking bonds in the polymer backbone chain, leading to the formation of reactive free radicals. Chain crosslinking occurs when free radicals react, forming a crosslink between polymer chains to form a network structure.

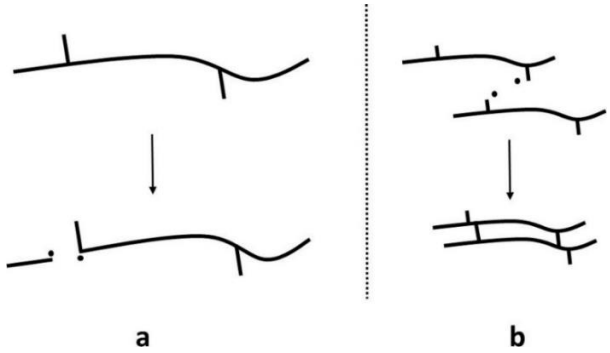

Figure 2.4 Degradation mechanisms: a) random chain scission and b) crosslinking. Used with permission.[16]

Chain scission is considered to be the dominant mechanism and results in a decrease in the polymer molecular weight and an increase in polydispersity showing the presence of different chain lengths.[93] The presence of chain crosslinking, however, increases the molecular weight due to the formation of longer chains and crosslinking.[92] The extent of degradation is dependent upon several factors: the number of re-processing cycles, polymer chemical structure, thermal-oxidative stability of the polymer, and the re-processing conditions.[31,92,94,95] HDPE, LDPE, and PP have been found to have different degradation behaviours during mechanical

reprocessing.[95] HDPE and LDPE have high thermal stability, can be subjected to a high number of extrusion cycles before degradation, and typically undergo chain scission and chain branching/crosslinking. Chain scission has been shown to be the dominant degradation mechanism in HDPE by Abad et al.[96] further supported by Pinherio et al.[92] who both studied HDPE subjected to five extrusion cycles. In comparison to HDPE and LDPE, PP has been found to only undergo chain scission.[97]

2.4 Thermodynamics of Polymer Blends

During the recycling process the complete separation of polyolefins of PP and PE is challenging and a costly process due to their similar physical properties and densities.[47,48] The resulting recyclate will contain a low fraction of other plastics and can therefore, be considered a polymer blend.[93] A polymer blend is a mixture of two or more polymers or copolymers which forms a new material with different physical properties.[98] There is a commercial interest in polymer blends as they offer the opportunity to develop new materials with a combination of advantageous properties from the components.[99] Polymer blends can exhibit either immiscibility, partial immiscibility or miscible behaviour which can be explained by considering thermodynamics.[99-101] Typically, polymer blends are immiscible.[102]

2.4.1 Gibbs Free Energy

On mixing of two polymers together, the immiscibility, partial immiscibility and miscibility can be determined by the Gibbs free energy of mixing, ΔG_{mix},[103]

$$\Delta G_{mix} = \Delta H_{mix} - T\Delta S_{mix} \quad (2.1)$$

where ΔH_{mix} is the enthalpy of mixing, T is the temperature, and ΔS_{mix} is the entropy of mixing.

For a miscible polymer blend, the following two conditions need to be satisfied.[103]

$$\Delta G_{mix} < 0 \tag{2.2}$$

$$\left(\frac{\partial^2 \Delta G_{mix}}{\partial \phi_i^2}\right)_{T,P} > 0 \tag{2.3}$$

where ΔG_{mix} is the Gibbs free energy of mixing, ϕ_i is the volume fraction of *i* component in the binary blend, *T* is temperature and *P* is pressure.

2.4.2 Miscible Blends

Miscible polymer blends are a stable, single-phase material that exhibit homogeneity at the molecular level. Miscible polymer blends are usually associated with a negative ΔH_{mix} due to favourable specific interactions between blend components.[99] Favourable interactions include hydrogen bonding, dipole-dipole or ionic interactions between the blend components.[103] The value of ΔH_{mix} is the dominant factor in promoting polymer-polymer miscibility and ΔS_{mix} needs to exceed ΔH_{mix} in order for miscibility to occur.[103] Typically, for high molecular weight polymers and macromolecules, ΔS_{mix} is negligible whereas for lower molecular weight molecules, ΔS_{mix} has a greater significance and needs to be taken into account. For low molecular weight molecules increasing the temperature can increase the likelihood of miscibility occurring.[101]

2.4.3 Immiscible Blends

It is well documented in the literature that PP:HDPE blends are immiscible. Immiscibility occurs when the mixing of the blend components does not occur at a molecular level causing phase separation.[99,103] In the case of PP:HDPE blends, ΔS_{mix} is either negligible or very small due to the high molecular weight polymer chains which limits the number of possible polymer arrangements. As PP and HDPE possess similar physical properties and densities, ΔH_{mix} is positive due to the limited favourable specific interactions between segments, or portions of segments of PP and HDPE. Hence, ΔG_{mix} is positive and the PP:HDPE blend exhibits high interfacial tension, weak phase adhesion and phase separated morphology, leading to a lower quality of final product properties.[101] This is a major barrier to the use of recycled plastic products.

2.4.4 Phase Diagrams

The phase diagram shown in Figure 2.5, illustrates three distinct regions with different degrees of miscibility.[102,103]

- A single miscible phase between two binodals.
- Four (fragmented) metastable regions between binodals and spinodals.
- Two phase separated regions of immiscibility, bordered by spinodals.

Binodals separate the single phase (miscible) and metastable regions. The spinodals separate the meta-stable and phase separated (immiscible) regions.

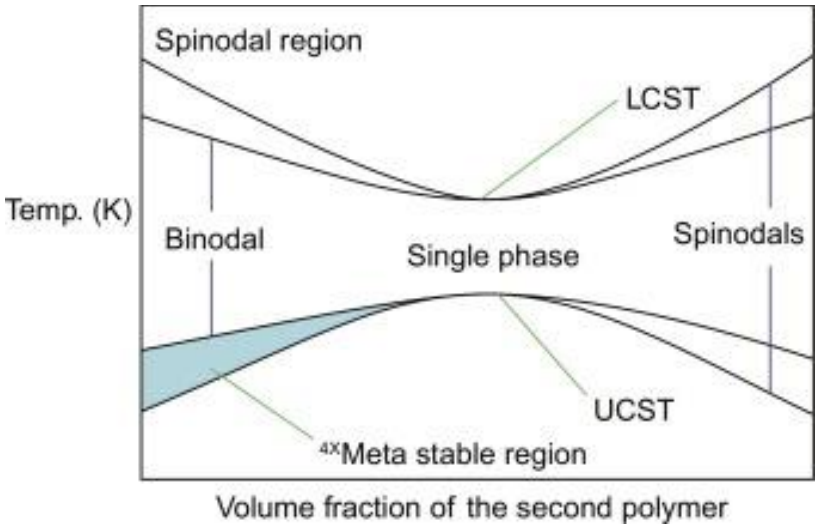

Figure 2.5 Phase diagram. Used with permission.[103]

The phase diagram also illustrates the LCST (lower critical solution temperature) and the UCST (upper critical solution temperature). Above the UCST and below the LCST, the polymer blend components are miscible. Typically, the phase diagrams for polymer blends shows just the LCST, in comparison to mixtures of low molecular weight components where both UCST and LCST are present.[101-103]

The polymer blend undergoes phase separation when it enters either the metastable or the spinodal region. The movement from single phase to multiphase can occur by a change in blend composition, temperature or pressure.[99,102] The mechanism by which phase separation occurs is dependent upon whether the polymer blend enters the metastable or spinodal region. If the polymer blend enters the metastable region,

phase separation will occur via the slow mechanism of nucleation and growth.[102] Whereas, if the polymer blends enters the spinodal region, phase separation proceeds by spinodal decomposition which is a rapid, spontaneous mechanism.[102] It is also possible for phase separation to occur by a combination of nucleation and growth, and spinodal decomposition.[103] The phase separation thermodynamic conditions are given by[103]

$$\text{Spinodal:} \qquad \left(\frac{\partial^2 \Delta G_m}{\partial \phi^2}\right)_{p,T} = 0 \tag{2.4}$$

$$\text{Critical Point:} \qquad \left(\frac{\partial^2 \Delta G_m}{\partial \phi^2}\right)_{p,T} = \left(\frac{\partial^3 \Delta G_m}{\partial \phi^3}\right)_{p,T} = 0 \tag{2.5}$$

where ΔG_{mix} is the Gibbs free energy of mixing, ϕ_i is the volume fraction of *i* component in the binary blend, *T* is temperature, and *p* is pressure.

2.4.5 Flory-Huggins Theory

The Flory[104]-Huggins[105] theory is a lattice model used to predict and model polymers in solutions and polymer blends.[101-103] It is a mean-field model, only average interactions are taken into consideration, and assumes that mixing is entirely random and there is no volume change during mixing (ΔV_m). The Flory-Huggins theory states that the ΔG_{mix} for a binary system is given by[101-103]

$$\Delta G_{mix} = \Delta H_{mix} - T\Delta S_{mix} = RT(x_s ln\phi_s + x_p ln\phi_p + x_s \phi_p X) \tag{2.6}$$

where ΔG_{mix}, ΔH_{mix} and ΔS_{mix} are the Gibbs free energy of mixing, enthalpy of mixing and entropy of mixing respectively, *R* is the universal gas constant, *T* is temperature, x are mole fractions, ϕ are volume fractions, X is the Flory-Huggins binary interaction parameter and the “s” and “p” stand for the solvent and polymer, respectively.

The Flory-Huggins theory introduced a new parameter, X, the binary interaction parameter which is important in assessing the mutual miscibility of blend components.[106] X measures the interaction of the polymer-polymer interaction in

polymer blends and for miscibility to occur X is typically negative indicating attractive interactions.[106,107]

2.5 Improving Recyclate Performance

In the literature, there is focus on the improvement of the performance quality of recyclate through the:

- addition of a compatibiliser and/or
- addition of virgin polymers, or the
- production of composites from rPOs and inorganic/organic fillers, or the
- production of composites from rPOs and fibres

As the focus of the thesis is on binary PP:HDPE blends, the above options for improving recyclate performance are only briefly discussed in sections 2.5.1 to 2.5.4 and do not include all the available literature.

2.5.1 Addition of a Compatibiliser

Compatibilisation improves interfacial properties between the different constituents by stabilizing a desired morphology, reducing interfacial tension, and enhancing phase adhesion, thus leading to the improvement of mechanical properties.[93] Compatibilisers can be graft/block copolymers, nanoparticles, or ionomers and are located at the interface between the phases.[47] Commonly used compatibilisers for rPP/rPE blends are ethylene–propylene rubber monomer (EPRM) and ethylene propylene diene monomer (EPDM), as they are cheap, readily available, and easily processed. Compatibilisers have been successfully used in rPP:rHDPE blends to improve material performance. For example, Atiqah et al.[108] used a maleated PP (MAPP) to improve the tensile properties of rPP:rHDPE blends. They observed an increase in tensile strength, Young's modulus, and elongation at break with the presence of MAPP. This was attributed to the improvement in interfacial adhesion between the rPP and rHDPE phases. The effectiveness of compatibilisation on the performance of PO blends is influenced by the chemical structure of the compatibiliser, the amount of compatibiliser added and the method of blending. It is still hard to predict the type and amount of compatibiliser required for recycled blends due to the inhomogeneity of plastic wastes.

2.5.2 Addition of Virgin Polymers

The addition of virgin polymers to recycled polymer wastes has been shown to be an effective method of improving the performance of recycled materials.[47,109,110] Typically, the same type of polymer is added to the recycled waste, which can minimise the change in melt viscosity. Meran et al.[109] added virgin PP (vPP) to recycled PP (rPP), virgin LDPE (vLDPE) to recycled LDPE (rLDPE), and vHDPE to recycled HDPE (rHDPE). They found that the recycled polymer tensile strength and elongation at break improved upon the addition of virgin polymer. Madi[47] investigated the thermal and mechanical behaviour of rHDPE and vPP blends which contained up to 30 wt% of vPP. They found that the dispersion of vPP through the rHDPE was poor and the presence of vPP affected crystallite formation, resulting in a decrease in crystallinity and enthalpy of fusion (ΔH_f). The tensile strength was observed to improve as the vPP content was increased, but elongation at break decreased, which was caused by HDPE potentially decreasing the plasticity of PP. However, for industry, the quantity of virgin polymer required is of key interest to strike a balance between cost and material performance.

2.5.3 Production of Composites from Recycled Polyolefins and Inorganic/Organic Fillers

To further enhance the performance of recycled materials at low cost, particular fillers can be added along with or instead of compatibilizers to form composite materials. Nano-fillers can stabilise immiscible blend morphology, leading to a finer morphology and improved material performance.[53] A wide range of inorganic and organic fillers have been used in rPP:rPE blends such as calcium carbonate,[111,112] talc,[113,114] fly ash,[115,116] and organoclays.[117] Typically, a coupling agent is added or the surface of the filler is altered to improve the adhesion between the polymer matrix and filler. This is due to the hydrophobic nature of POs compared to the hydrophilic fillers.[118] As an example, Sengupta et al.[115] used stearic acid as a coupling agent in a fly ash, a waste by-product from thermal power plants, and rPP matrix composite to enhance the mechanical properties. Recyclates contain additives such as heat stabilisers which are added during reprocessing. Therefore, the presence of additives in recyclates needs to be taken into account when adding nano-fillers and/or compatibilisers. It is essential that a balance between the quantity of filler and compatibiliser is struck as nano-fillers can affect compatibiliser efficiency if located at the interface.[49]

2.5.4 Production of Composites from Recycled Polyolefins and Fibres

Composites consisting of rPOs and glass fibres[119,120] or carbon nanotubes[121] have been reported in the literature. However, the addition of natural plant-based fibres to recycled plastics to form wood–plastic composites (WPC) is gaining popularity as they are considered to be a sustainable and green material. For example, Inácio et al.[122] suggested that bamboo fibre reinforced rPP/talc/EPDM composites with a PP-g-MA compatibiliser have the potential to be used in the automotive industry. They found that the addition of the bamboo fibres and PP-g-MA resulted in an increase in the tensile strength and modulus, flexural strength, and fatigue life of the composites. There are limitations associated with WPCs, such as poor adhesion between the natural fibre and recycled matrix leading to debonding, along with degradation of the fibres due to the effects of the environmental conditions.

2.6 Literature Limitations

In order to aid the plastic industry with overcoming poor performing polyolefin recyclate, the following areas have been identified as requiring further investigation:

1. Recyclate mechanical and thermal performance over a wide range of composition. Most literature focuses on the wt% extremities, for example, PP:PE blends containing 0-15 wt% PP or PE. After plastic sortation, the PP or PE stream will typically contain up to potentially 20 wt% of PE or PP respectively. However, as previously discussed in section 2.3, the composition of each recyclate batch will vary; therefore, it is important to understand performance of a wide range of compositions. Understanding the performance – composition relationship could reduce time and resources required for optimisation during third component addition.

2. A comparison of the mechanical and thermal performance of virgin to recycled PP:PE blends without the addition of a third component. Even though it is known recycled blends demonstrate a reduced performance, is the performance severely reduced at all blend compositions? Do any blends show a similar performance to the corresponding recycled blend? If the recycle blends are not substantially affected over a range of compositions this leads to discussion of whether PP and PE separation during reprocessing is necessary. This would be a significant change for the industry as it would save time, energy and costs.

3. Investigation of the effect of blend preparation using injection moulding. It is known that blend preparation has an effect on final performance. Large quantities of literature focuses upon blend preparation via compression moulding.

4. Morphological studies of the binary PP:PE blends are usually investigated by scanning electron microscopy (SEM) and are extremely limited in composition range. The images obtained typically lack surface topography sensitivity and usually have to undergo surface etching to provide clarity. Understanding the morphology at different compositions is extremely important, as the final morphology is a contributing factor towards blend performance.

The recycling industry is looking to improve the plastic circular economy by obtaining recycled commingled waste blends with desirable end-use properties acceptable for commercial applications but at low cost; and the starting point should be understanding the variability in recyclate performance before third component addition. The highlighted limited areas above may aid the industry optimise recyclate. Therefore, this thesis investigated the effect of composition and reprocessing on the mechanical and thermal properties and morphology of injection moulded PP:HDPE blends in chapters 4 and 5. To expand the current morphological studies, a full range of composition study using AFM was carried out in chapter 6. The results and conclusions drawn will contribute towards mapping not only the challenges but also the potentially unique opportunities of rPP:rHDPE blends.

2.7 Conclusion

POs, PP and PE, are two commonly used plastics in consumer goods, and are found in high quantities in plastic wastes. Typically, PP and PE undergo secondary mechanical recycling. Currently, the plastics industry is faced with poor quality recyclate that varies with location, available sortation equipment and quality of waste stream. Plastic wastes are heterogeneous in nature, contain contaminants, and the complete separation of PP and PE is time consuming and costly. Consequently, introducing variability in recyclate performance. Maintaining a constant recyclate performance is a current barrier for the use of recyclate in high demanding applications.

There is extensive literature on improving recyclate quality through the addition of other components, such as compatibilisers. Recently, more focus is on introducing green components into the recyclate to meet the demand for sustainability and biodegradability. However, the literature lacks a performance comparison between virgin and recycled PP:HDPE blends over a wide range of compositions. This is crucial to understand the processing-structure-property relationship, which is important for achieving a circular plastic economy.

References

1. Plastic Europe. Plastics - The Facts. 2020. Available at https://www.plasticseurope.org/en/resources/market-data (accessed on 4th January 2021).
2. A. Shrivastava, in *Introduction to Plastics Engineering: Plastics Design Library*, S. Ebnesajjad, Williams Andrew Applied Science Publishers, 2018, Ch. 3.
3. WRAP. The UK Plastics Pact. 2021. Available at https://wrap.org.uk/taking-action/plastic-packaging/the-uk-plastics-pact (accessed on 6 May 2021).
4. G. V. Research. Plastic Packaging Market Trends and Growth 2021-2028. 2021. Available online: https://www.grandviewresearch.com/industry-analysis/plastic-packaging-market#:~:text=The global plas-tic packaging market size was valued,%26 household care are driving the product demand (accessed on 21 April 2021).
5. H. Dahlbo, V. Poliakova, V. Mylläri, O. Sahimaa, R. Anderson, *Waste Manag.* **2018**, *71*, 52.
6. C. R. Cook, R. U. Halden, in *Plastic Waste and Recycling*, T. M. Letcher,L. House, Elsevier 2020.
7. M. Cordier, T. Uehara, *Sci.Total Environ.* **2019**, *670*, 789.
8. O. Kehinde, O. J. Ramonu, K. O. Babaremu, L. D. Justin, *Heliyon* **2020**, *6*, 5131.
9. J. N. Hahladakis, E. Iacovidou, *Sci. Total Environ.* **2018**, *630*, 1394.
10. Plastic Europe. Plastics - The Facts. 2019. Available at https://www.plasticseurope.org/en/resources/market-data (accessed on 2 May 2020).
11. A. Emblem, in *Packaging Technology*, A. Emblem,H. Emblem, Woodhead Publishing, 2012.
12. PlasticEurope. Plastics in Packaging. 2020. Available at Available online: https://www.plasticseurope.org/en/about-plastics/packaging (accessed on 19 November 2020).
13. M. Ilyas, W. Ahmad, H. Khan, S. Yousaf, K. Khan, S. Nazir, *Reviews on Environmental Health* **2018**, *33*, 383.
14. M. Potrykus, V. Redko, K. Glowacka, A. Piotrowicz-Cieslak, P. Szarlej, H. Janik, L. Wolska, *Science of The Total Environment* **2021**, *758*, 143649.
15. A. Rahimi, J. García, *Nat Rev Chem* **2017**, *1*, 46.
16. K. Ragaert, L. Delva, K. V. Geem, *Waste Manage.* **2017**, *69*, 24.

17. N. A. Welden, in *Plastic Waste and Recycling*, T. M. Letcher,L. House, Elsevier, 2020.
18. D. J. d. Silva, H. Wiebeck, *Prog. Rubber, Plast. Recycl. Technol.* **2020**, *36*, 284.
19. S. M. Al-Salem, P. Lettieri, J. Baeyens, *Progress in Energy and Combustion Science* **2010**, *36*, 103.
20. O. Eriksson, G. Finnveden, *Energy Environ. Sci.* **2009**, *2*, 907.
21. J. W. Bujak, *Energy* **2015**, *90*, 1468.
22. R. Verma, K. S. Vinoda, M. Papireddy, A. N. S. Gowda, *Procedia Environ. Sci.* **2016**, *35*, 701.
23. B. Jiang, J. Yu, Y. Liu, *Journal of Environmental & Earth Sciences* **2020**, 2340.
24. L. Makarichi, W. Jutidamrongphan, K. Techato, *Renewable and Sustainable Energy Reviews* **2018**, *91*, 812.
25. k. Winans, A. Kendall, H. Deng, *Renewable and Sustainable Energy Reviews* , *68*, 825.
26. Eurostat. Recording Recycling Rates and Use of Recycled Materials in the EU. 2021. Available at https://ec.europa.eu/eurostat/documents/2995521/9629294/8-04032019-BP-EN.pdf/295c2302-4ed1-45b9-af86-96d1bbb7acb1 (accessed on 2 February 2021).
27. European Commission. A European Strategy for Plastics in a Circular Economy. 2017. Available at https://ec.europa.eu/info/research-and-innovation/research-area/environment/plastics-circular-economy_en#:~:text=The Commission's plan for plastics. In 2018%2C the,waste legislation which were agreed in December 2017. (accessed on 4 May 2021).
28. Ellen MacArthur Foundation; McKinsey & Co. The New Plastics Economy: Rethinking The Future Of Plastics. 2021. Available at https://www.ellenmacarthurfoundation.org/assets/downloads/EllenMacArthurFoundation_TheNewPlasticsEconomy_Pages.pdf (accessed on 11 November 2021).
29. D. J. Lohse, in *Applied Polymer Science: 21st Century*, C. Craver,C. Carraher, Elsevier, 2000.
30. W. Posch, in *Applied Plastics Engineering Handbook*, S. Ebnesajjad, William Andrew Publishing, 2011.

31. O. Agboola, R. Sadiku, T. Mokrani, L. Amer, O. Imoru, *Polyolefins and the environment*, Elsevier, **2017**.
32. B. Manjula, A. B. Reddy, E. R. Sadiku, V. Sivanjineyulu, G. F. Molelekwa, J. Jayaramudu, K. R. Kumar, in *Polyolefin Fibres*, S. C. O. Ugbolue, Woodhead Publishing, 2017, Ch. 18.
33. W. K. Kupolati, E. R. Sadiku, I. D. Ibrahim, A. O. Adeboje, C. Kambole, O. O. S. Ojo, A. A. Eze, P. Paige-Green, J. M. Ndambuki, in *Polyolefin Fibres*, S. C. O. Ugbolue, Woodhead Publishing, 2017, Ch. 16.
34. M. E. G. Rodrigues, S. P. Quevedo, J. d. Souza, J. B. S. d. Farias, *IOSR Journal of Engineering* **2020**, *10*, 11.
35. A. Graziano, S. Jaffer, M. Sain, *J. Elastomers Plast.* **2018**, *51*, 291.
36. All3DP. What is Polypropylene? - All You Need to Know. 2022. Available at https://all3dp.com/1/polypropylene-pp-all-you-need-to-know/ (accessed on 16 Februrary 2021).
37. Y. K. Kim, in *Polyolefin Fibres: Structure, Properties and Industrial Applications*, S. C. O. Ugbolue, Elsevier, 2017.
38. L. W. McKeen, in *The Effect of UV Light and Weather on Plastics and Elastomers*, L. W. McKeen, William Andrew Publishing, 2019, Ch. 8.
39. F. He, L. Zhang, *Polymer Testing* **2014**, *35*, 80.
40. G. Grause, M. Chien, C. Inoue, *Polymer Degradation and Stability* **2020**, *181*, 109364.
41. N. A. Patil, J. Njuguna, B. Kandasubramanian, *Eur. Polym. J.* **2020**, *125*, 109529.
42. Polymer Database. Polymer Properties Database: Very Low Density Polyethylene. 2021. Available at http://www.polymerdatabase.com/Polymer Brands/VLDPE.html#:~:text=Films made from VLDPE have excellent sealing and,films%2C as well as fill and seal packaging (accessed on 26 March 2021).
43. J. J. Cheng, M. A. Polak, A. Penlidisa, *Tunnelling and Underground Space Technology* **2011**, *26*, 582.
44. M. J. Shirkavand, H. Azizi, I. Ghasemi, M. Karabi, *Adv. Polym. Technol.* **2018**, *37*, 770.
45. S. Ebnesajjad, in *Chemical Resistance of Commodity Thermoplastics*, E. Baur,K. Ruhrberg,W. Wishnis, Elsevier, 2016.
46. O. Horodytska, F. J. Valdés, A. Fullanaa, *Waste Manag.* **2018**, *77*, 413.

47. N. K. Madi, *Mater. Des.* **2013**, *46*, 435.
48. R. Strapasson, S. C. Amico, M. F. R. Pereira, T. H. D. Sydenstricker, *Polymer Testing* **2005**, *24*, 468.
49. Y. Kazemi, A. R. Kakroodi, D. Rodrigue, *Polym. Eng. Sci.* **2015**, *55*, 2368.
50. A. A. Cuadri, J. E. Martín-Alfonso, *Polymer Degradation and Stability* **2017**, *141*, 11.
51. S. M. Al-Salem, P. Lettieri, J. Baeyens, *Waste Manage.* **2009**, *29*, 2625.
52. M. E. Grigore, *Recycling* **2017**, *2*, 1.
53. J. Maris, S. Bourdon, J. M. Brossard, L. Cauret, L. Fontaine, V. Montembault, *Polym. Degrad. Stab.* **2018**, *147*, 245.
54. I. A. Ignatyev, W. Thielemans, B. V. Beke, *ChemSusChem* **2014**, *7*, 1579.
55. K. Hamad, M. Kaseem, F. Deri, *Polym. Degrad. Stab.* **2013**, *98*, 2801.
56. S. Satapathy, *Benchmarking An Int. J.* **2017**, *24*, 415.
57. S. Perera, A. Arulrajah, Y. C. Wong, S. Horpibulsuk, F. Maghool, *Construction and Building Materials* **2019**, *221*, 200.
58. N. Torres, J. J. Robin, B. Boutevin, *Eur. Polym. J.* **2000**, *36*, 2075.
59. M. Solis, S. Silveira, *Waste Manag.* **2020**, *105*, 128.
60. G. Cagnetta, K. Zhang, Q. Zhang, J. Huang, G. Yu, *Waste Manag.* **2018**, *75*, 181.
61. V. Goodship, *Science Progress* **2007**, *90*, 245.
62. S. Kumara, A. K. Panda, R. K. Singh, *Resour., Conserv. Recycl.* **2011**, *55*, 893.
63. T. Thiounn, R. C. Smith, *Journal of Polymer Science* **2022**, *58*, 1347.
64. J. R. Banu, V. G. Sharmila, U. V. Amudha, G. Kumar, *Science of The Total Environment* **2020**, *718*, 137287.
65. O. Dogu, M. Pelucchi, R. V. d. Vijver, P. H. M. V. Steenberge, D. R. D'hooge, A. Cuoci, M. Mehl, A. Frassoldati, T. Faravelli, K. M. V. Geema, *Progress in Energy and Combustion Science* **2021**, *84*, 100901.
66. D. Czajczyńska, L. Anguilano, H. Ghazal, R. Krzyżyńska, A. J. Reynolds, N. Spencer, H. Jouhara, *Thermal Science and Engineering Progress* **2017**, *3*, 171.
67. S. D. A. Sharuddin, F. Abnisa, W. M. A. W. Daud, M. K. Aroua, *Energy Conversion and Management* **2016**, *115*, 308.
68. G. Lopez, M. Artetxe, M. Amutio, J. Alvarez, J. Bilbao, M. Olazar, *Renewable and Sustainable Energy Reviews* **2018**, *82*, 576.

69. A. A. Ajibola, J. O. Omoleye, V. E. Efeovbokhan, *Applied Peterochemical Research* **2018**, *8*, 211.
70. K. N. Aishwarya, N. Sindhu, *Procedia Technology* **2016**, *35*, 990.
71. L. Rosi, M. Bartoli, M. Frediani, *Waste Manag.* **2018**, *73*, 511.
72. A. Adrados, I. d. Marco, B. M. Caballero, A. Lopez, M. F. Laresgoiti, A. Torres, *Waste Manag.* **2012**, *32*, 826.
73. M. F. Viante, T. M. P. Zanela, A. Stoski, E. C. Muiz, C. A. P. Almeida, *J. Clean. Prod.* **2018**, *198*, 979.
74. M. P. Aznar, M. A. Caballero, J. A. Sancho, E. Francés, *Fuel Processing Technology* **2006**, *87*, 409.
75. J. M. Garcia, M. L. Robertson, *Science* **2017**, *358*, 870.
76. J. C. Worch, A. P. Dove, *ACS Macro Lett.* **2020**, *9*, 1494.
77. J. N. Hahladakis, E. Iacovidou, *Journal of Hazardous Material* **2019**, *380*, 120887.
78. A. Merrington, in *Applied Plastics Engineering Handbook*, M. Kutz, William Andrew Publishing, 2011.
79. N. Singh, D. Hui, R. Singh, I. P. S. Ahuja, L. Feo, F. Fraternali, *Composites Part B: Engineering* **2017**, *115*, 409.
80. M. T. Brouwer, E. U. T. v. Velzen, A. Augustinus, H. Soethoudt, S. D. Meester, K. Ragaert, *Waste Manag.* **2018**, *71*, 62.
81. F. Welle, *Resour., Conserv. Recycl.* **2011**, *55*
82. M. Pohjakallio, T. Vuorinen, A. Oasmaa, in *Plastic Waste and Recycling*, T. M. Letcher,L. House, Elsevier, 2020.
83. E. Kosior, J. Mitchell, in *Plastic Waste and Recycling*, T. M. Letcher,L. House, Elsevier, 2020.
84. C. Cimpan, A. Maul, M. Jansen, T. Pretz, H. Wenzel, *J. Environ. Manag.* **2015**, *156*, 181.
85. D. Jubinville, E. Esmizadeh, S. Saikrishnan, C. Tzoganakis, T. Mekonnen, *Sustain. Mater. Technol.* **2020**, *25*, 188.
86. G. Faraca, T. Astrup, *Waste Manage.* **2019**, *95*, 388.
87. B. Luijsterburg, H. Goossens, *Resour., Conserv. Recycl.* **2014**, *85*, 88.
88. A. S. F. Santos, J. A. M. Agnelli, D. W. Trevisan, S. Manrich, *Polymer Degradation and Stability* **2002**, *77*, 4410447.

89. S. Saikrishnan, D. Jubinville, C. Tzoganakis, T. H. Mekonnen, *Polymer Degradation and Stability* **2020**, *182*, 109390.
90. M. S. Abbas-Abadi, *J. Therm. Anal. Calorim.* **2021**, *143*, 2867.
91. M. K. Loultcheva, M. Proietto, N. Jilov, F. P. L. Mantia, *Polym. Degrad. Stab.* **1997**, *57*, 77.
92. L. A. Pinheiro, M. A. Chinelatto, S. V. Canevarolo, *Polym. Degrad. Stab.* **2004**, *86*, 445.
93. F. Vilaplana, S. Karlsson, *Macromol. Mater. Eng* **2008**, *293*, 274.
94. M. A. AlMa'adeed, I. Krupa, *Polyolefin Compounds and Materials Fundamentals and Industrial Applications*, Springer, **2016**.
95. S. Yin, R. Tuladhar, F. Shi, R. A. Shanks, M. Combe, T. Collister, *Polymer Engineering and Science* **2015**, *55*, 2899.
96. M. J. Abad, A. Ares, L. Barral, J. Cano, F. J. Diez, S. Garcia-Garabal, J. Lopez, C. Ramirez, *J. Appl. Polym. Sci.* **2004**, *92*, 3910.
97. T. A. Oliveira, R. R. Oliveira, R. Barbosa, J. B. Azevedo, T. S. Alves, *Carbohydrate Polymers* **2017**, *168*, 52.
98. L. A. Utracki, *Can. J. Chem. Eng.* **2002**, *80*, 1008.
99. M. N. Subramanian, *Polymer Blends and Composites: Chemistry and Technology*, Wiley, **2017**.
100. A. Ajji, L. A. Utracki, *Polym. Eng. Sci.* **1996**, *36*, 1574.
101. L. M. Robeson, in *Polymer Blends A Comprehensive Review*, Hanser, 2007, Ch. 2.
102. E. Manias, L. A. Utracki, in *Polymer Blends Handbook*, L. Utracki,C. Wilkie, Springer, 2014.
103. J. Mishra, S. K. Tiwari, M. M. Abolhasani, S. Azimi, G. C. Nayak, in *Micro and Nano Fibrillar Composites (MFCs and NFCs) from Polymer Blends*, R. K. Mishra,S. Thomas,N. Kalarikkal, Woodhead Publishing, 2017, Ch. 2.
104. P. J. Flory, *J. Chem. Phys.* **1942**, *10*, 51.
105. M. K. Huggins, *J. Chem. Phys.* **1941**, *9*, 440.
106. E. Langer, K. Bortel, S. Waskiewicz, M. Lenartowicz-Klik, in *Plasticizers Derived from Post-Consumer PET*, E. Langer,K. Bortel,S. Waskiewicz,M. Lenartowicz-Klik, William Andrew Publishing, 2020, Ch. 3.
107. T. Tadros, in *Encyclopedia of Colloid and Interface Science*, T. Tadros, Springer, 2013.

108. A. A. S. M. Atiqah, H. Salmah, Z. Firuz, D. N. U. Lan, *Key Eng. Mater.* **2014**, *594*, 837.
109. C. Meran, O. Ozturk, M. Yuksel, *Materials & Design* **2008**, *29*, 701.
110. G. W. Curtzwiler, M. Schweitzer, Y. Li, S. Jiang, K. L. Vorst, *J. Clean. Prod.* **2019**, *239*
111. P. Brachet, L. T. Høydal, E. L. Hinrichsen, F. Melum, *Waste Manag.* **2008**, *28*, 2456.
112. A. Elloumi, S. Pimbert, A. Bourmaud, C. Bradai, *Polym. Eng. Sci.* **2010**, *50*, 1904.
113. O. Ammar, Y. Bouaziz, N. Haddar, N. Mnif, *Polym. Sci.* **2017**, *3*, 1.
114. M.Sánchez-Soto, A. Rossa, A. J. Sánchez, J.Gámez-Pérez, *Waste Manag.* **2008**, *28*, 2565.
115. S. Sengupta, P. Maity, D. Ray, A. Mukhopadhyay, *Journal of Applied Polymer Science* **2013**, *130*, 1996.
116. S. Sengupta, D. Ray, A. Mukhopadhyay, *ACS Sustain. Chem. Eng.* **2013**, *1*, 574.
117. N. Phuong, V. Gilbert, B. Chuong, *J. Reinf. Plast. Compos.* **2008**, *27*, 1983.
118. N. Saba, P. M. Tahir, M. Jawaid, *Polymers* **2014**, *6*, 2247.
119. A. M. M. Abdelhaleem, M. Megahed, D. Saber, *J. Compos. Mater.* **2018**, *52*, 1633.
120. C. Annandarajah, A. Langhorst, A. Kiziltas, D. Grewell, D. Mielewski, R. Montazami, *Materials* **2019**, *12*, 3189.
121. S. Svensson, D. Åkesson, M. Bohlén, *J. Polym. Environ.* **2020**, *28*, 1967.
122. A. L. N. Inácio, R. C. Nonato, B. C.Bonse, *Polymer Testing* **2018**, *72*, 357.

3.0 Materials and Methods

3.1 Introduction

This chapter provides an overview to the materials, manufacturing and characterisation techniques used to analyse virgin and recycled PP:HDPE blends. Extrusion mixing and injection moulding was the main manufacturing technique for the polymer blends with Brabender mixing and compression moulding used in a miniature comparative mechanical properties study. The working principles of the following characterisation techniques are discussed: DMA, tensile testing, DSC and AFM.

3.2 Materials

3.2.1 Virgin Materials

PP (Moplen EP440G) supplied by Lyondellbasell (London, UK) had a melt flow index (MFI) of 1.3 g 10 min^{-1} and density of 900 kg m^{-3}. HDPE (HDPE, K46-06-185) supplied by Ineos (Grangemouth, UK) had a MFI of 4.2 g 10 min^{-1} and a density of 946 kg m^{-3}. Virgin PP and HDPE were in the form of pellets.

3.2.2 Recycled Materials

Post-consumer PP and PE, were supplied by Impact Solutions Recycled (Grangemouth, United Kingdom) and has undergone mechanical recycling. The recycled PE was mainly composed of HDPE but small quantities (less than 5 wt%) of LDPE were present. rPP and rHDPE had MFIs of 15 g 10 min^{-1} at 230°C, 2.16 kg and 1.5 g 10 min^{-1} at 190°C, 2.16 kg respectively. Recycled PP and PE were in the form of flakes.

3.3 Blend Preparation

3.3.1 Blend Composition and Notation

Virgin and recycled blends of different compositions of PP and HDPE (P10, P20, P25, P40, P50, P60, P75, P80, P90) were prepared where P denotes PP and the number corresponds to the percentage composition by weight of PP in the blend PP:HDPE. The pure 100 wt% PP and HDPE will be denoted as PP and HDPE, respectively. To denote virgin or recycled the symbols of v and r will be used respectively before the blend composition. For example, virgin P10 would be represented as vP10.

3.3.2 Extrusion Mixing and Injection Moulding

3.3.2.1 Extrusion Mixing

The blending of the polymer components is extremely important for the quality of the final polymer blend. Therefore, the processability window of the polymer components is an important consideration.[1] The processability window informs the user of a range of temperatures, residence time within the extruder and pressures to ensure ease of manufacturing and the quality of the final product.[2,3] The melt viscosity is a major challenge in manufacturing, which is overcome by understanding the processability window.[2] It is important is ensure that processing temperatures do not exceed the degradation temperature and long residence times are avoided to prevent oxidation.[2,3] Extrusion is a commonly used process for mixing, compounding or reactive mixing.[4] Extrusion is the process of forcing a polymer melt through an open-ended die (Figure 3.1).[1,4,5] An extruder can consist of either one or two screws.[4] In a twin-screw extruder, the screws can either be co-rotating or counter-rotating, and intermeshing or non-intermeshing.[4]

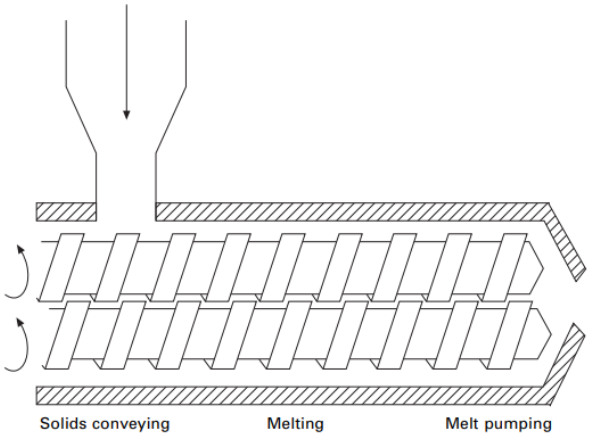

Figure 3.1 A schematic diagram of a twin-screw extruder with the three main zones highlighted. Used with permission.[1]

There are three main zones in an extruder: compaction, melting and pumping:[4-6]

i. Compaction

The solid plastic pellets are feeded into the feed hopper. The pellets are compacted and forced into the screw channel.

ii. Melting

The pellets begin to melt and propelled through the heating barrel by the mechanical screw(s). The pellets are successively compacted and melted to form a homogenous polymer melt. The polymer melt is a viscous fluid and the motion of screws enables the polymer components to blend intensively.

iii. Pumping

The build-up of pressure in the polymer melt enables the melt to be forced through a die orifice. The melt is now termed an extrudate.

3.3.2.2 Injection Moulding

The injection moulding process is a commonly implemented process within the plastic industry.[7] Injection-moulding is a quick and inexpensive method of mass-producing plastic products.[8] The injection-moulding machine consists of a plasticising unit, which similar to an extruder, and a clamping unit (Figure 3.2).[7,9] The plasticising unit differs from a single-screw extruder by the screw moving backwards while rotating. This screw motion is important to push the polymer melt forward and accumulate.[7,9] The clamping unit contains the mould cavity which can vary in size, shape and can be heated. Mould cavities are usually categorised as either single or multi cavity moulds, which enables the production of a variety of plastic products.[9]

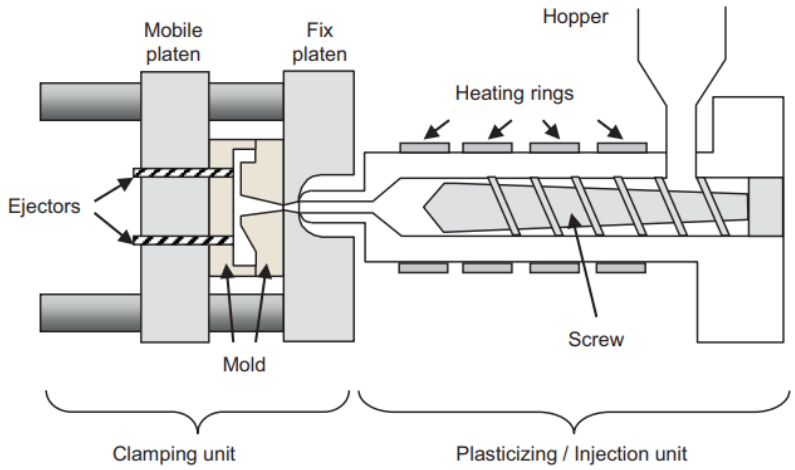

Figure 3.2 A schematic of an injection moulding machine. Used with permission.[9]

The injection moulding cycles consists of plasticising, filling and packing, and ejection. A cycle can vary between 15 seconds up to 1 minute.[7] The melt accumulates in the

screw channel at the front of the plasticising unit, and the screw has proceeded to the rear of the plasticising unit. The screw then acts as a ram to injected the melt into mould cavity.[8] The speed at which the mould cavity fills can vary via sprues and runners.[7] Once the mould cavity is filled, the melt is held underneath pressure while it solidifies. Once cooled, pressure returns to atmospheric pressure, the mould cavity opens and the final product is released.[5,7] The mould closes and the cycle begins again.

3.3.3 Brabender Mixing and Compression Moulding

3.3.3.1 Brabender Mixing

The Brabender is an internal, batch mixer consisting of an opening for polymer pellets, which connects to a mixing chamber. The mixing chamber is heated and has two rotating blades.[10] The blades can either create a tangential or overlapping pathway for the polymer melt.[1] The polymer melt is subjected to compression and folding action.[1] After mixing is complete, the polymer melt is removed from the mixing chamber.

3.3.3.2 Compression Moulding

In compression moulding, the mixed polymer sample is placed between the pre-heated bottom and top half of the mould.[5,11] The bottom and top moulds come together and compressed under pressure for a set amount of time. The polymer sample melts and flows to fill the mould cavities. The polymer melt flows and fills the mould cavities. The mould is cooled at a set rate and the final product is removed from the mould. It is common for thermosets and thermoplastics to be used in compression moulding.[5] Compression moulding is a low cost process that can produce vast quantities.[12]

3.4 Characterisation Techniques

3.4.1 Dynamical Mechanical Analysis

3.4.1.1 Introduction

DMA is an technique used to determine mechanical properties of a material such as storage modulus (E') and damping, as a function of temperature, time and frequency.[13] For polymer samples, DMA is extremely useful to characterise quantitatively and qualitatively their viscoelastic behaviour. DMA is very sensitive to molecular structures and transitions occurring within polymers and has been found to be 100 times more sensitive than DSC in detecting the glass transition temperature (T_g) compared to the

DSC.[14] Limitations of the DMA technique include; destructive technique and the variability in the accuracy of the moduli values obtained. Accuracy of the moduli can vary due to the sensitivity to sample dimensions and loading conditions, such as humidity and the sample clamping force.[13]

3.4.1.2 Viscoelasticity Theory

Polymers are viscoelastic materials which exhibit a combination of elastic and viscous behaviour when undergoing deformation.[15] The viscoelastic behaviour is dependent upon the time and temperature. Elastic behaviour is described by Hooke's law which illustrates that stress and strain are directly proportional,

$$\sigma = E\varepsilon \tag{3.1}$$

where σ is stress, *E* is the Young's modulus and ε is strain.

On removal of the applied force, the polymers will return to their original configuration and act as an elastic solid. This process is called relaxation and typically occur when a force is applied for short time scales.[16] Structural information such as molecular structure can be determined from the elastic response.[17] The viscous behaviour is described by the theory of hydrodynamics,

$$\sigma = \eta \frac{d\varepsilon}{dt} \tag{3.2}$$

where σ is stress, η is the viscosity and $\frac{d\varepsilon}{dt}$ is the strain rate.

Viscous behaviour is described by the polymers resistance to flow by shear forces.[5] The stress is proportional to the strain rate. During the longer time scale of which the force is applied, the polymer chains entangle and flow is irreversible.[16] Therefore, on removal of the applied force the polymers cannot return to their original configuration. The viscous behaviour provides information such as processability and impact resistance.

3.4.1.3 Experimental Set-Up

In a DMA test, a material of known geometry (ISO 557-2296 mould), is subjected to either a stress or strain at a particular frequency and/or temperature. The resulting deformation is monitored as either a strain or stress response. A motor is used to apply the stress or strain to the material via a drive shaft. The resulting stress response is detected by a force transducer, or the strain response is detected by a position sensor.[14,17] There are different experimental set-ups available in DMA.[18] A dynamic oscillatory test such as a multi-frequency set up can determine the materials stiffness and T_g. Whereas, a transient test such as creep, could be used to determine the possible polymer relaxations present. In this thesis, a dynamic oscillatory test was used; single frequency temperature ramp.

DMA offers several modes of deformation; bending, torsion, shear, tension and compression.[18-20] Each mode will have a different clamping arrangement for varying sample geometries and materials and for the modulus under investigation e.g. shear modulus compared to compression modulus. In this thesis, the bending deformation chosen by using the dual cantilever clamping arrangement (Figure 3.3).[19]

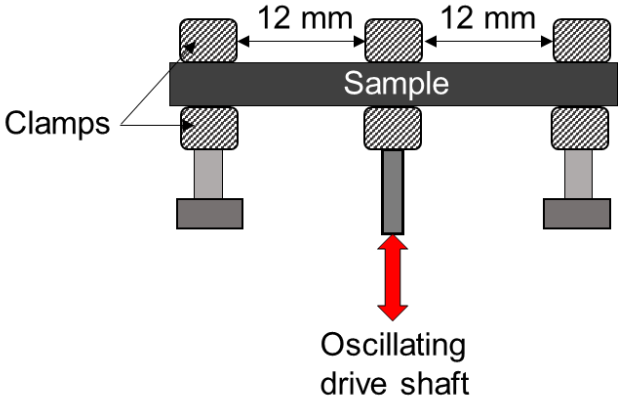

Figure 3.3 Bending deformation using dual cantilever clamping arrangement.[19]

3.4.1.3 Data Obtained

In the dynamic oscillating mode, an oscillating force is applied to the material and causes a sinusoidal stress.[14,21] The applied stress causes material deformation. Deformation is represented by a sinusoidal strain wave (Figure 3.4). The stress and strain are described by the following[14]

$$\sigma = \sigma_0 \sin(\omega t + \delta) \tag{3.3}$$

$$\varepsilon = \varepsilon_0 \sin(\omega t) \tag{3.4}$$

where σ is the stress, σ_0 is the amplitude of the stress wave, ω is the frequency of oscillation, t is the time, δ is the phase shift, and ε_0 is the amplitude of the strain wave.

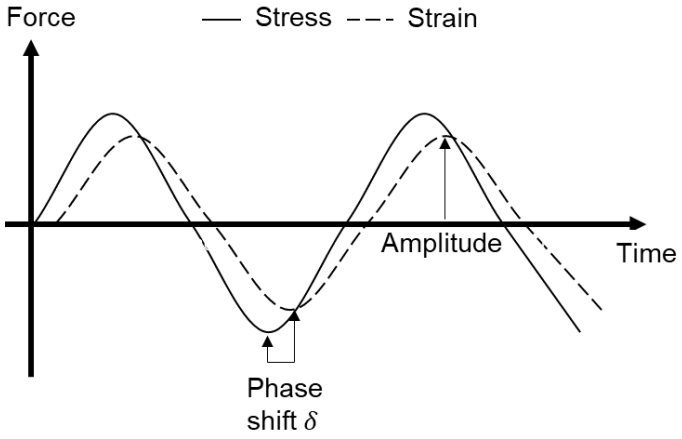

Figure 3.4 A schematic of the applied sinusoidal stress and the strain response.[19-21]

The phase shift (δ), occurs if excess time is required for molecular motions, relaxations and energy dissipation to occur.[20] For purely elastic materials, the phase shift between the stress and strain waves is 0° so the waves are in phase. For purely viscous materials, the phase shift is 90° so the waves are out of phase. Hence, for viscoelastic materials the phase lag is between 0° and 90°.[18] Therefore, the stress equation can be written as an in phase and out of phase component.

$$\sigma = \sigma_0 \sin(\omega t)\, cos\delta + \sigma_0 \cos(\omega t)\, sin\delta \tag{3.5}$$

By dividing through by strain, Equation 3.5 is transformed to

$$\sigma = \varepsilon_0 E' sin(\omega t) + \varepsilon_0 E'' \cos(\omega t) \tag{3.6}$$

where E' is the storage modulus and E'' is the loss modulus.

The complex modulus, E^*, is determined by,

$$E^* = \frac{\sigma}{\varepsilon} \tag{3.7}$$

It is possible to determine E', E'' and the tangent of the phase shift (tanδ) through measurement of the phase shift.[13,22]

$$E' = \frac{\sigma_0}{\varepsilon_0} cos\delta \tag{3.8}$$

$$E'' = \frac{\sigma_0}{\varepsilon_0} sin\delta \tag{3.9}$$

$$\tan\delta = \frac{E''}{E'} \tag{3.10}$$

The E' represents the in phase elastic component and indicates the material's stiffness and ability to store energy.[20] Whereas, E'' is the out of phase viscous component and indicates the ability to dissipate energy.[20,21] The ratio of E'' to E' gives the tangent of the phase difference tanδ and is often termed the damping loss factor. The relationship between the moduli and δ is shown in Figure 3.5.

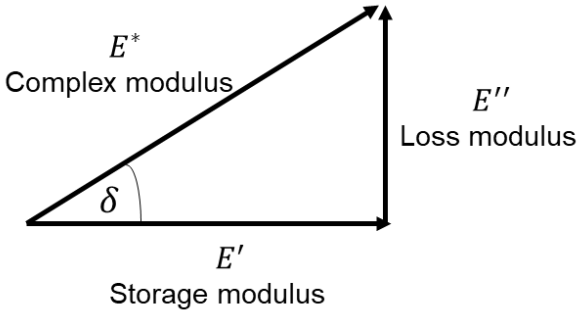

Figure 3.5 Relationship between the storage modulus, loss modulus and phase difference.[22]

By plotting the DMA raw data as a function of temperature, the T_g can be determined from the peak of the E' curve or the tanδ curves.[20] It is also possible to identify relaxation processes from the tanδ curves.

3.4.2 Tensile Testing

3.4.2.1 Introduction

The mechanical properties of a material such as Young's modulus (*E*) can be determined by carrying out a tensile test. A tension tensile test is a simple, relatively

inexpensive, standardised method (ISO 527-2) of obtaining the mechanical properties of a sample.[23] Figure 3.6 illustrates the experimental set-up for a tensile test with the sample shoulders clamped between the grips.[5,24] The crosshead moves upwards away from the lower grip at a specified rate resulting in sample elongation and deformation. A slowly increasing uniaxial loading force is applied across the cross section of the samples gauge section. The test continues until sample fracture.

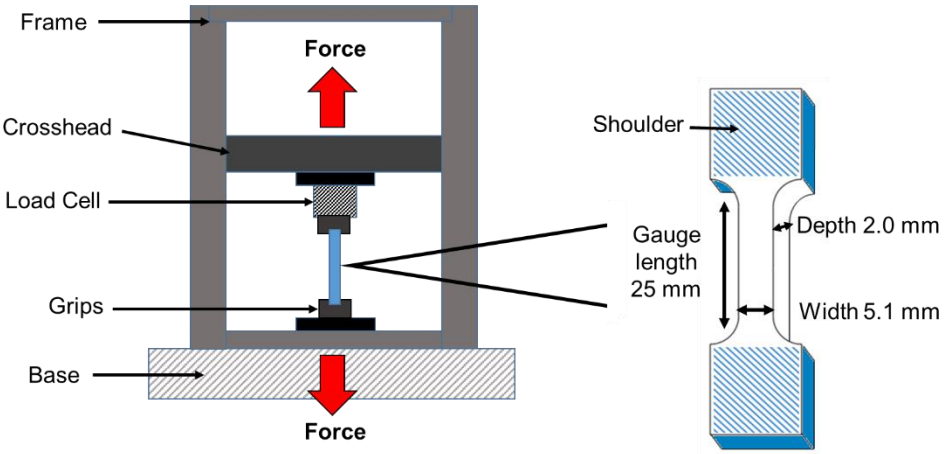

Figure 3.6 A schematic diagram demonstrating the experimental set-up for a tension tensile test including the dimensions of the dog-bone sample (ISO 527-2-1BA).

The positioning and the clamping force of the sample in the grips is extremely important to prevent slippage or pre-mature failure of the sample in the grips which can lead to data errors.[24] For example, the sample shoulders should not be fully within the grip, and the sample should be clamped perfectly vertically. Typically, a pre-tension is applied to the sample to avoid any slippage or movement before starting the experiment. The output of a tensile test is recorded as loading force and elongation, which is converted to a stress-strain curve.[24] Engineering strain, ε, and engineering stress, σ, are determined by Equations 3.11 and 3.12 respectively;

$$\varepsilon = \frac{l_i - l_0}{l_0} = \frac{\Delta l}{l_0} \tag{3.11}$$

$$\sigma = \frac{F}{A_0} \tag{3.12}$$

where l_i is the instantaneous length, l_0 is the gauge length, Δl is the change in length at some instant, F is the force applied and A_0 is the cross sectional area of the sample.

From the stress-strain curves, the E, yield strength, ultimate tensile strength (UTS), elongation at yield and break can be determined.[24,25]

3.4.2.2 Young's Modulus

The E measures the stiffness of the material and is determined from the elastic deformation region in the stress-strain curve. Elastic deformation occurs when deformation is non-permanent. When the force applied to the material is removed the material returns to the original shape. In the elastic deformation region, stress and strain are directly proportional, which is described by Hooke's law:

$$\sigma = E\varepsilon \tag{3.13}$$

where σ is stress, E is Young's modulus and ε is the strain.

Therefore, the E can be determined from the linear gradient in the elastic deformation region. Typically, an extensometer is used to monitor the elongation with high precision as the E is taken within a very small strain region e.g. between 0 – 5% strain.

3.4.2.3 Yield Point and Elongation at Yield

The yield point is the point at which the material transitions from elastic to plastic deformation. Plastic deformation occurs when the material undergoes permanent deformation and no longer obeys Hooke's law. The elongation at yield is determined from the corresponding strain value at the yield point. Typically, the yield point is determined at a strain offset of 0.002.

3.4.2.4 Ultimate Tensile Strength

The UTS is the maximum stress applied to which the material can withstand. The UTS is determined from the maximum stress observed in the stress-strain curve.

3.4.2.5 Elongation at Break

The ductility is determined from the elongation at break, also termed strain at failure. Ductility measures the amount of plastic deformation before the material fractures. Ductility is expressed as percentage of the strain at fracture;

$$Elongation\ at\ break = \frac{l_f - l_0}{l_0} \times 100 \quad (3.14)$$

where l_f is the length at fracture and l_0 is the original length.

3.4.3 Differential Scanning Calorimetry

DSC is a thermal analysis technique that can be used to identify properties such as a materials purity, T_g, melting temperature (T_m) and crystallinity.[26,27] The advantages of DSC include high sensitivity, method simplicity, quick, and requires less than 10 mg of a sample. The DSC technique is a destructive test and challenges arise when analysing heterogeneous samples.[6] The principle of DSC is based on measuring the heat flow difference between the polymer sample and an inert reference sample as a function of time or temperature.[28] The polymer sample and inert reference are subjected to the same heating, cooling or isothermal conditions within a nitrogen gas purged furnace (Figure 3.7). Typically the heating/cooling rate is 10 °C min^{-1} but slower and faster rates are available.[29] Faster heating/cooling rates lower the resolution of transitions and accuracy of the T_g and T_m.[28,30] On the other hand, slow heating/cooling rates increase the time of each DSC scan.

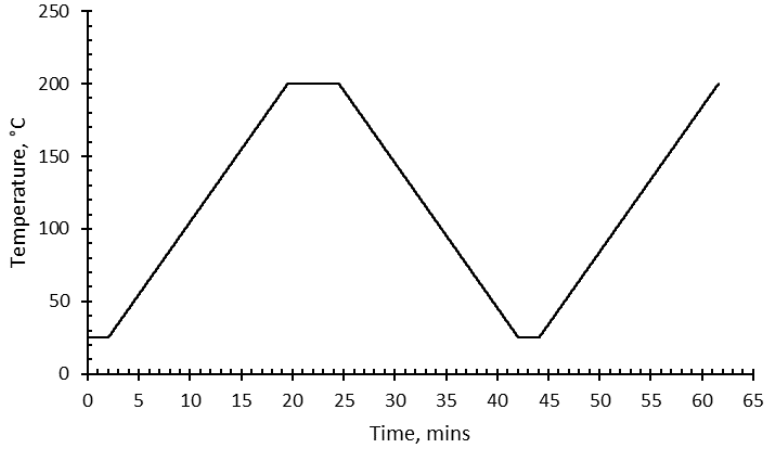

Figure 3.7 An example DSC temperature program with an isotherm, heating, isotherm, cooling, isotherm and second heating segment.

3.4.3.1 DSC Classification

A DSC can either be classed as a heat-flux DSC or a power compensated DSC. In heat-flux DSC, both the sample and the reference are placed within the same furnace.[28] As the temperature is increased or decreased, the DSC monitors the temperature difference between the sample and the reference.[28] In power-compensated DSC, there are two independent micro-furnaces; one for the sample and one for the reference. As the temperature is increased or decreased, the DSC monitors the quantity of thermal power (energy) required to maintain the same temperature of the sample and reference.[26] In this thesis, the polymers and polymer blends were evaluated using a Perkin Elmer DSC 8000, which is categorised as a power compensated DSC.

3.4.3.2 Data Obtained

The DSC data is recorded as a thermogram with heat flow as a function of temperature (Figure 3.8). As the temperature changes, the polymer will undergo thermal phase transitions, such as T_g. Thermal transitions are described by the thermodynamic quantity Gibbs Free Energy (G) (Equation 3.15) and categorised as either; a first order or second order transition.[31,32]

$$G = U - TS + pV = H - TS \tag{3.15}$$

where U is the internal energy, T is temperature, S is entropy, p is pressure, V is volume and H is enthalpy.

First order transitions are characterised by a discontinuity of the first derivative of G.[28,31] Therefore, there is a change in either entropy, enthalpy or volume.[28] First order transitions are usually well defined peaks and include the processes of melting and crystallisation.[31] Melting is an endothermic process and the T_m is the temperature at which the crystalline solid phases shift to an isotropic liquid (a polymer melt).[32] Integration of the area underneath the melting peak gives the ΔH_f. Crystallisation is

an exothermic process and the crystallisation temperature (T_c) is the temperature at which polymer chains in the melt align into ordered crystalline structures.[28] Typically, T_m and T_c are quoted as the peak temperature. Second order transitions are characterised by a discontinuity of the second derivative *G* resulting in a change in heat capacity, isothermal compressibility and the coefficient of thermal expansion.[28,31] The T_g is a second order transition and is the temperature at which the amorphous phase undergoes a phase change from glassy to rubbery.[31] The T_g is an endothermic process and occurs over a wide range of temperatures. The T_g can be quoted from the onset, midpoint, endpoint, or infection point of the step.[28] In this thesis, the T_g is quoted from the midpoint of the T_g step.

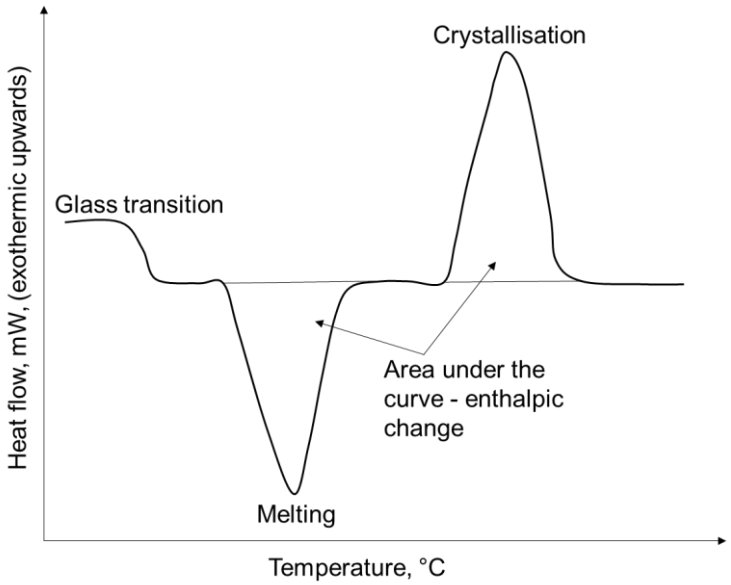

Figure 3.8 A DSC thermogram illustrating the glass transition, melting and crystallisation processes.

3.4.4 Atomic Force Microscopy

3.4.4.1 Introduction

AFM is a surface imaging technique, which is part of the scanning probe microscopy (SPM) family. AFM was first reported in 1986 by Binning, Quate and Gerber who combined their earlier invention, scanning tunnelling microscopy (STM) and stylus profilometer together.[33,34] STM is based on applying a voltage between an atomically sharp metal tip probe in close proximity to the scanning surface.[34] The application of

the bias voltage between the probe and surface causes electron tunnelling. As the probe scans the surface, the tunnelling current intensity is monitored, as the distance between the probe and sample surface varies due to the changes in topography. The SPM ensures the current intensity remains constant by altering the voltage applied. The change in voltage over the sample surface creates the topographical image. STM enabled the imaging of surfaces at nanoscale resolution but imaging was restricted to conducting or semi-conducting surfaces. The AFM technique is the most versatile of the SPM family and overcomes the STM limitations. AFM has a simple operation procedure and can obtain sub-nanometer (10^{-10} m) surface resolutions on a wide range of materials from solid materials such as semi-conductors to biological macromolecules such as bacteria.[35,36] AFM has contributed significantly to understanding the polymer crystallisation process through in-situ real time crystallisation.[37] It is important to note that there are limitations to the AFM. For example, slow scan rates and the susceptibility to surface contamination and instrumentation noise.[35]

3.4.4.2 AFM Experimental Set-Up

In AFM the probe, which consists of a sharp tip mounted onto a cantilever scans over the sample surface to determine the tip-surface force interactions.[35,38,39] The x, y and z position of the probe is controlled by scanners.[39] The scanners are made from piezoelectric materials, such as quartz and lead zirconate titanate ceramics, due to their cost effectiveness and abundant availablity.[38] The scanners are sensitive to changes in voltage, and either contracts or expands proportionally with the voltage applied.[38] The cantilever is flexible and considered as a spring, which can deflect and bend depending on whether the tip-surface interaction is attractive or repulsive. The laser detection system monitors the cantilever deflection. The laser detection system consists of a detection laser beam that hits the cantilever and causes the reflected laser beam to fall onto the detector. The detector is a photodiode that consists of four quadrants. The cantilever deflection will change as the result of the varying tip-surface interaction causing the reflected laser beam to fall onto different positions on the photodiode. The feedback loop maintains the set values such as the cantilever height by adjusting the piezo height. The AFM principle is summarised in Figure 3.9.

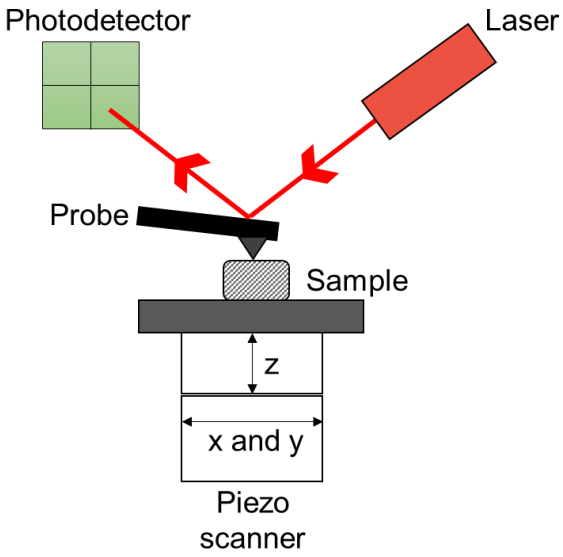

Figure 3.9 A schematic drawing of the AFM.

3.4.4.3 AFM Probe

As previously highlighted, the probe consists of a sharp tip mounted onto a cantilever. The AFM tip is extremely important component as it "touches the surface"[33] and consequently, can determine the resolution of the images acquired.[40] Typically, AFM tips are made from silicon or silicon nitride and pyramidal in shape.[41] Different geometries are available from manufacturers, such as Bruker.[41] Cantilevers can either be rectangular or triangular in nature.[42]

3.4.4.4 AFM Modes

The main modes available are contact, tapping and non-contact. For each mode, it is important to understand tip-sample interaction, which is described by the force-distance plot.[37,43] A force-distance plot shows the change in tip-surface interaction with distance. As the probe approaches the surface from a large distance away, there is an attractive interaction due to van der Waals forces. At very close distances, the tip will "jump" into contact with the surface. When the tip and surface are in contact repulsive interactions take over due to electrostatic forces. Each mode will act within a different region of the force-distance plot.

Contact Mode

The contact mode enables high-resolution, quick scans of surfaces by maintaining the tip in constant contact with the surface.[43] The contact mode acts within the repulsive

region of the force-distance plots. This mode of action works by the feedback loop maintaining a constant cantilever deflection as the tip moves over the surface. The feedback loop adjusts the height of the cantilever through the z piezo to the set point value as the surface height varies.[43] The topography of the surface is therefore directly proportional to the movement of the z piezo.[35] There are limitations to the contact mode due to the combination of the normal force and dragging force as the tip moves across the surface, which can damage the tip and surface.[35] Therefore, contain mode is unsuitable for soft materials such as polymers. The presence of lateral forces may also cause image artefacts which obscure morphological features.[40]

Non-contact Mode

In non-contact mode, there are low tip-surface forces due to the cantilever oscillating near or at its resonant frequency very near to the surface.[43] This mode of action acts within the attractive region of the force-distance plots. The cantilever oscillation will change depending upon the attractive force between the tip and the surface. The feedback loop keeps the amplitude of the oscillation constant by altering the z piezo height. The voltage required to alter the piezo height is converted into an error signal image. Non-contact scan rates are typically slower than in contact and tapping mode but this mode maintains a high sensitivity to the topography.[43]

Tapping Mode

In tapping mode, the cantilever oscillates near or at its resonant frequency and acts in the attractive and repulsive regions. In this mode, the tip touches the surfaces and then retracts away for each oscillation. The tip is intermittently in contact with the surface. The feedback loop maintains the set point amplitude by adjusting the z piezo. Tapping mode enables easy imaging in air and produces image resolution similar to contact mode but with lower forces applied. This mode is most commonly used with soft samples such as polymer samples.[37] In this mode, it is possible to obtain a phase image alongside a topography image. A phase image depicts the interactions between the tip and surface which can give information on the samples composition, viscoelasticity and adhesive properties.[37] Adhesion between the tip and surface or changes in viscoelasticity can cause a damping effect on the cantilever oscillation. This enables different components within the sample to be identified.

Quantitative Imaging Mode

The QI mode is novel, new mode which is based upon the force spectroscopy imaging and provides quantitative data of mechanical interest such as adhesive and Young's modulus. The QI mode is discussed in detail in Chapter 6.1.

References

1. E. K. Silviya, S. Varma, G. Unnikrishnan, S. Thomas, in *Advances in Polymer Processing*, S. Thomas,Y. Weimin, Woodhead Publishing, 2009, Ch. 4.
2. X. Colin, J. Verdu, *Comptes Redus Chimie* **2006**, *9*, 1380.
3. W. Michaeli, M. Koschmieder, in *Comprehensive Composite Materials*, A. Kelly,C. Zweben, Pergamon, 2000, Ch. 2.25.
4. T. A. Osswald, in *Understanding Polymer Processing*, T. A. Osswald, Hanser, 2017, Ch. 4.
5. W. D. Callister, D. G. Rethwisch, *Fundamentals of Materials Science and Engineering. An Integrated Approach*, John Wiley & Sons, **2016**.
6. B. T. Tomoda, P. H. Yassue-Cordeiro, J. V. Ernesto, P. S. Lopes, L. O. Péres, C. F. Silva, M. A. Moraes, in *Biopolymer Membranes and Films*, M. A. Moraes,C. F. Silva,R. S. Vieira, Elsevier, 2020.
7. T. A. Osswald, in *Understanding Polymer Processing*, T. A. Osswald, Hanser, 2017, Ch. 6.
8. S. Fu, B. Lauke, Y. Mai, in *Composite Science and Engineering, Science and Engineering of Short Fibre-Reinforced Polymer Composites*, S. Fun,B. Lauke,Y. Mai, Woodhead Publishing, 2019.
9. J. F. Agassant, P. Avenas, P. J. Carreau, B. Vergnes, M. Vincent, in *Polymer Processing*, J. F. Agassant,P. Avenas,P. J. Carreau,B. Vergnes,M. Vincent, Hanser, 2017, Ch. 7.
10. l. F. R.-D. Valle, in *Handbook of Polymer Synthesis, Characterization, and Processing*, E. Saldívar-Guerra,E. Vivaldo-Lima, Wiley, 2013, Ch. 23.
11. J. L. Hull, in *Handbook of Plastic Processes*, C. A. Harper, Wiley, 2006, Ch. 7.
12. A. A. Elshabini, F. Barlow, P. J. Wang, in *Reference Module in Materials Science and Materials Engineering*, Elsevier, 2017.
13. W. Broughton, in *Adhesive in Marine Engineering*, J. R. Weitzenbock, Woodhead Publishing, 2012.
14. K. P. Menard, N. R. Menard, in *Encyclopedia of Polymer Science and Technology*, 2015.
15. L. Gargallo, D. Radic, in *Physicochemical Behavior and Supramolecular Organization of Polymers*, Springer, 2009.
16. M. P. Stevens, *Polymer Chemistry. An Introduction*, Oxford University Press, **1990**.

17. A. Franck. TA Instruments. 2022. Available at https://www.tainstruments.com/pdf/literature/AAN004_Viscoelasticity_and_DMA.pdf (accessed 21st January 2022).
18. S. Patra, P. M. Ajayan, T. N. Narayanan, *Oxford Open Materials Science* **2021**, *1*, 1.
19. D. M. Price, J. C. Duncan, in *Principles of Thermal Analysis and Calorimetry*, S. Gaisford,P. Haines,V. Kett, Royal Society of Chemistry, 2016, Ch. 9.
20. A. Shrivastava, in *Introduction to Plastics Engineering: Plastics Design Library*, S. Ebnesajjad, Williams Andrew Applied Science Publishers, 2018, Ch. 3.
21. M. A. Bashir, *Solids* **2021**, *2*, 180.
22. K. Dyamenahalli, A. Famili, R. Shandas, in *Shape Memory Polymers for Biomedical Applications*, L. Yahia, Woodhead Publishing, 2015.
23. I. O. f. Standardisation. in Plastics. Determination of tensile properties. Test conditions for moulding and extrusion plastics: 2012.
24. J. R. Davis, *Tensile Testing*, ASM International **2004**.
25. M. Carr, *Phys. Educ.* **2006**, *41*, 57.
26. P. Gill, T. T. Moghadam, B. Ranjbar, *J Biomol Tech.* **2010**, *21*, 167.
27. J. Drzeżdżon, D. Jacewicz, A. Sielicka, L. Chmurzyński, *TrAC Trends in Analytical Chemistry* **2019**, *110*, 51.
28. P. Gabbott, *The Principles and Applications of Thermal Analysis*, Wiley-Blackwell, **2007**.
29. C. Schick, *Analytical and Bioanalytical Chemistry* **2009**, *395.*
30. R. M. Saeed, J. P. Schlegel, C. H. C. Giraldo, R. Sawafta, *IJERT* **2016**, *5.*
31. C. Leyva-Porras, P. Cruz-Alcantar, V. Espinosa-Solís, E. Martínez-Guerra, C. Balderrama, I. C. Martínez, M. Z. Saavedra-Leos, *Polymer* **2019**, *12*, 5.
32. J. D. Menczel, R. B. Prime, *Thermal Analysis of Polymers: Fundamentals and Applications*, Wiley, **2009**.
33. P. Eaton, P. West, in *Atomic Force Microscopy*, Oxford Scholarship Online, 2010, Ch. 1.
34. C. J. Roberts, M. C. Davies, S. J. B. Tendler, P. M. Williams, in *Encyclopedia of Spectroscopy and Spectrometry*, J. C. Lindon, Academic Press, 1999.
35. R. N. Jagtap, A. H. Ambre, *Indian Journal of Engineering & Materials Sciences* **2006**, *13*, 368.
36. J. Chen, K. Xu, *Instrumentation Science & Technology* **2020**, *48*, 667.

37. D. Wang, T. P. Russell, *Macromolecules* **2018**, *51*, 3.
38. P. Eaton, P. West, in *Atomic Force Microscopy*, Oxford Scholarship Online, 2010, Ch. 2.
39. G. Haugstad, *Atomic Force Microscopy. Understanding Basic Modes and Advanced Applications*, John Wiley & Sons, **2012**.
40. R. Nguyen-Tri, P. Ghassemi, P. Carriere, S. Nanda, A. A. Assadi, D. D. Nguygen, *Polymer* **2020**, *12.*
41. Bruker. AFM Probes, Tips and Cantilevers. 2022. Available at https://www.brukerafmprobes.com/ (accessed on 20th January 2022).
42. D. G. Yablon, in *Scanning Probe Microscopy in Industrial Applications Nanomechanical Characterization*, John Wiley & Sons, 2013, Ch. 1.
43. P. Eaton, P. West, in *Atomic Force Microscopy*, Oxford University Press, Oxford Scholarship Online, 2010, Ch. 3.

4.0 Thermal and Morphological Properties of Virgin and Recycled PP:HDPE Blends

4.1 Introduction

This chapter aims to discuss the thermal and morphological properties of virgin and recycled PP:HDPE blends. As PP and HDPE are semi-crystalline polymers, understanding their crystallisation behaviour and the morphology is extremely important due to their influence on the mechanical properties. The crystallization behaviour of the PP:HDPE blends are complex due to both components, PP and HDPE, crystallizing.[1] Thermal studies have shown that both the virgin and recycled PP:HDPE blends are incompatible and the variation in PP and HDPE crystallinity is dependent upon the blend mophology.[2-4] Studies into the crystallinities of rPP, rHDPE and rPP:rHDPE blends, have found that crystallinity is affected by the degradation mechanisms during the recycling process.[5-7] Interestingly, the rPP crystallinity has been found to be higher than that of vPP, by several authors.[5,7,8] Costa et al.[7] suggested a higher value of crystallinity of rPP compared to vPP was caused by a decrease in the molecular weight, which resulted in an increase in chain mobility. Increased chain mobility improved the ability of chains to fold into thicker lamella, and hence an increased crystallisation rate and crystallinity. Therefore, it is important to understand the variation in crystallinity in rPP:rHDPE blends in order to optimise the mechanical performance of recyclate.

During the processing there are several important factors which are important for morphology development in polymer blends, such as composition, viscosity ratio of components, interfacial properties, crystallinity and processing conditions.[2,9-12] Processing conditions, mixing time and intensity, need to be optimised to improve the degree of dispersion but without causing thermal and mechanical degradation.[13] Spardaro and Rizzo[13] found that the mixing time and rate of PP:LDPE blends had significant effects on the tensile properties as during the first two minutes of mixing significant changes in morphology occurred. Many studies have shown that PP:HDPE blends exist in a two phase morphology and the morphology exhibited is dependent upon the blend composition.[2,14,15] Improvement in mechanical properties has been found when blend components have similar physical properties. Lin et al.[3] found that an improved dispersion of HDPE in the continuous PP phase when HDPE and PP have a similar MFI shown by SEM which improved mechanical properties. However, there have been limited studies into the rPP:rHDPE blend morphology over a wide range of compositions by either AFM or SEM.

4.2 Methodology and Characterisation Techniques

4.2.1 Blend Preparation

vPP:vHDPE and rPP:rHDPE blends were prepared using a lab scale Haake MiniCTW twin screw extruder (Karlsruhe, Germany) for 5 minutes with feeder and mixing speeds of 50 rpm and 100 rpm respectively. The conical screws are 4-15 mm in diameter, 109.4 mm in length and co-rotate. The barrel temperature was 180-185 °C. Molten blends were transferred to the Haake MiniJet injection moulder (Karlsruhe, Germany) where the cylinder temperature was 210 °C, mould temperature was 35 °C, injection pressure was 500 bar and time was 10 s.

4.2.2 DSC

The melting and crystallisation behaviour of the vPP:vHDPE and rPP:rHDPE blends were evaluated using a Perkin Elmer DSC 8000 (Waltham, MA, USA). The instrument was calibrated using an Indium sample. Approximately 5-6 mg of the sample was scanned under a nitrogen atmosphere. Samples were exposed to the following thermal cycle: heated from 25 to 200 °C at 10 °C min^{-1}, isothermal at 200 °C for 5 mins, cooled from 200 to 25 °C at 10 °C min^{-1}, isothermal at 25 °C for 2 mins and heated from 25 to 200 °C at 10 °C min^{-1}. The T_m and ΔH_f were obtained from the first heating ramp. The T_c was taken from the cooling ramp.

4.2.2.1 Calculating the Degree of Crystallinity

Two methods were investigated for the calculation of crystallinity in the virgin and recycled PP:HDPE blends, the total peak method and individual peak method.

A. Individual Peak Method

The individual peak method is possible due to the immiscibility of the polymer blends. The immiscibility leads to two separate peaks during the first heating ramp assigned to HDPE and PP (Figure 4.1). The PP and HDPE crystallinities are calculated separately (Equation 4.1).[2]

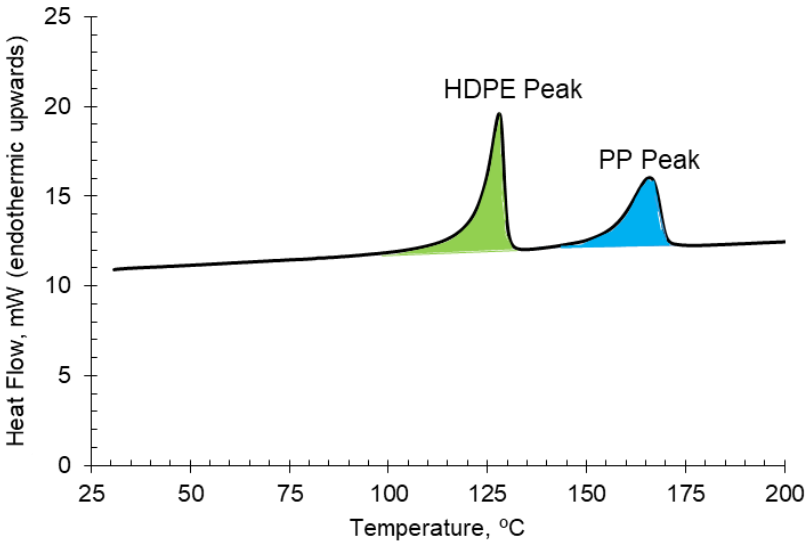

Figure 4.1 DSC thermogram highlighting the individual HDPE and PP peaks for the individual peak method for crystallinity calculation.

The degree of crystallinity was calculated by Equation (4.1),

$$\%\ Crystallinity = \frac{\Delta H_f^{obs}}{\Delta H_f^0} \times\ 100 \qquad (4.1)$$

where ΔH_f^{obs} is the observed enthalpy of fusions for the individual PP and HDPE peaks, and the ΔH_f^0 is the 100% crystalline HDPE or PP which are 287 and 207 J g^{-1}, respectively.[2]

B. Total Peak Method

The total peak method calculates the crystallinity using the total enthalpy of fusion from the combined PP and HDPE peaks (Equation 4.2). This method has been used to determine the crystallinity of composites consisting of a polymer matrix and dispersed fibre.

$$\Delta H_f^{PP} = \Delta H_{total\ obs} \times mol\ fraction\ of\ PP\ in\ the\ blend \qquad (4.2.1)$$

$$\Delta H_f^{HDPE} = \Delta H_{total\ obs} \times mol\ fraction\ of\ HDPE\ in\ the\ blend \qquad (4.2.2)$$

$$Crystallinity = \frac{\Delta H_f^{PP\ or\ HDPE}}{\Delta H_f^0} \times\ 100 \quad (4.2.3)$$

where ΔH_f^{PP} is the PP enthalpy of fusion, ΔH_f^{HDPE} is the HDPE enthalpy of fusion and $\Delta H_{total\ obs}$ is the enthalpy of fusion observed experimental for the combined PP and HDPE peaks.

4.2.3 SEM

Morphology of the virgin blends were studied using a Zeiss Crossbeam 550 FIB-SEM at different magnifications. Cryo-fractured surfaces were exposed to five freeze-thaw cycles. Samples were coated with a thin layer of platinum and examined at an accelerating voltage of 3 kV.

4.2.4 AFM

AFM was carried out on the cryo-fractured vPP:vHDPE blend surfaces using a Bruker Multimode/Nanoscope IIIa (Santa Barbara, CA, USA) in tapping mode at ambient conditions. The RTESPA model probe was used, and purchased from Bruker. A J-scanner with maximum x-y range of ~160 µm was used. The images were collected in the form of height and phase images with the phase images being reported. The freeware Gwyddion (http://gwyddion.net/) was used for image analysis.[16]

4.3 Results and Discussion

4.3.1 Thermal Properties

4.3.1.1 Melting Behaviour of Virgin and Recycled PP:HDPE Blends

PP and HDPE are semi-crystalline polymers, hence their microstructure consists of amorphous and crystalline domains. The crystalline T_m is the temperature at which the ordered crystalline domains become unordered and polymer chains become mobile. Generally, the rPP:rHDPE blends had a lower melting point than the respective vPP:vHDPE blends due to structural deteriorations of the polymeric components during the mechanical recycling process[17] which could imply that less perfect crystallites form.[18] Melting behaviour of both rPP:rHDPE and vPP:vHDPE blends presented two separate peaks assigned to PP and HDPE, suggesting that the blends were immiscible (Figure 4.2 and Table 4.1). The two melting peaks present in the rPP and rPE indicate that contaminants were present due to the challenge of complete

separation of PP and PE during the recycling process.[4,19,20] Little variation in the T_m of virgin and recycled PP, HDPE and their blends suggested that the blending of PP and HDPE did not significantly alter the T_m of PP and HDPE (Table 4.1).[2,4]

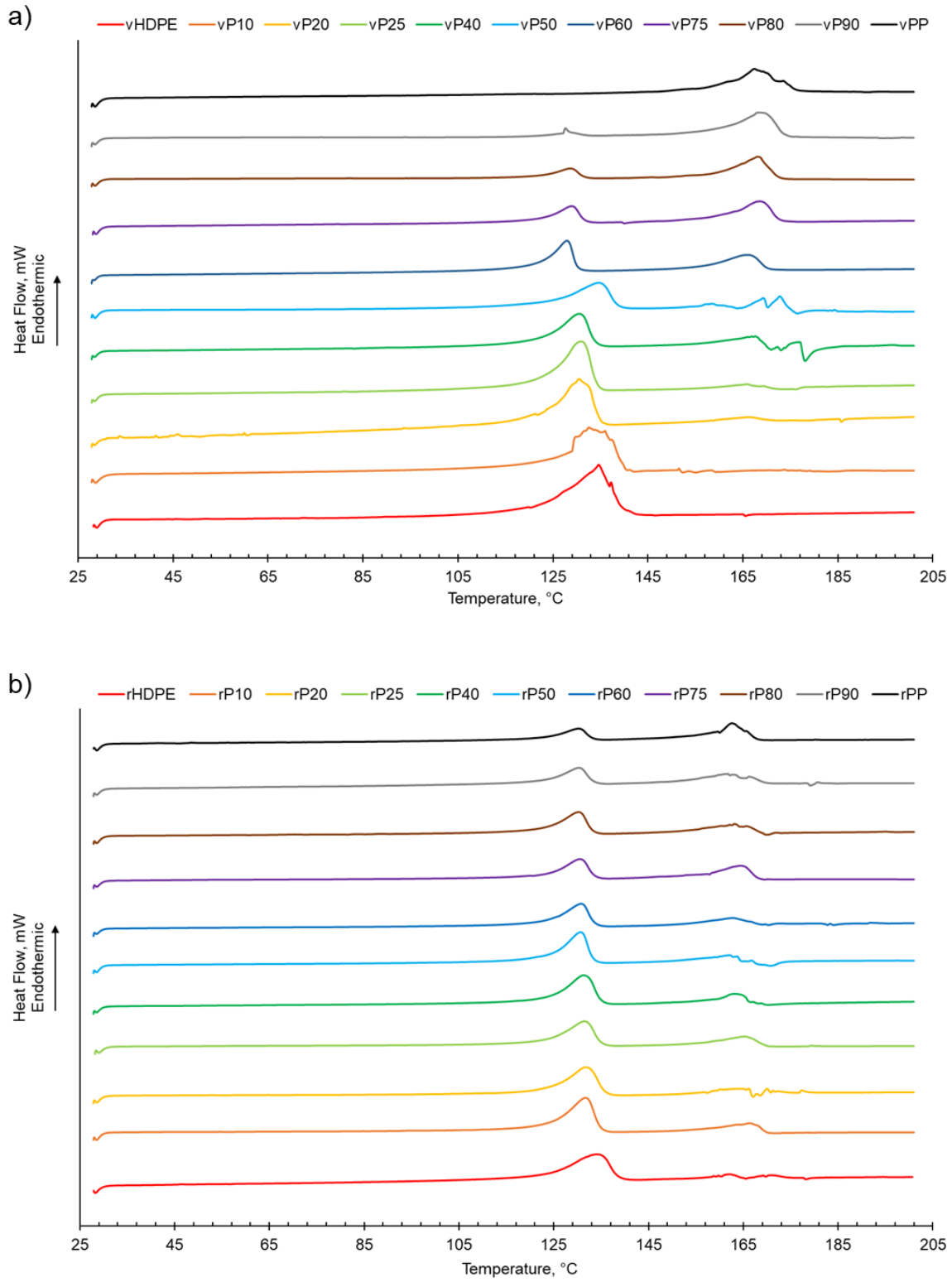

Figure 4.2 The melting behaviour of PP:HDPE blends obtained from DSC a) vPP:vHDPE blends and b) rPP:rHDPE blends.

Table 4.1 Melting and crystallisation behaviour of vPP:vHDPE and rPP:rHDPE blends obtained from the first heating and cooling cycles using DSC. Bold values are vPP:vHDPE and un-bolded numbers are the rPP:rHDPE blends. The individual peak method was used to determine the percentage crystallinity.

PP wt% content in PP:HDPE	Peak Melting Temperature, °C		Enthalpy of Fusion, J g^{-1}		Peak Crystallisation Temperature, °C		Enthalpy of Crystallisation, J g^{-1}	Percentage Crystallinity, %	
	PP	HDPE	PP	HDPE	PP	HDPE	(PP + HDPE)	PP	HDPE
0	**-**	**134.6**	**0.0**	**161.2**	**-**	**118.4**	**161.4**	**0.0**	**56.2**
	159.0	132.9	11.8	115.4	125.0	116.6	147.4	7.3	36.2
10	**173.9**	**132.6**	**3.8**	**161.0**	**-**	**115.6**	**161.6**	**1.8**	**56.1**
	166.4	131.7	27.3	87.8	122.5	118.0	131.4	12.5	30.8
20	**166.1**	**130.5**	**11.4**	**105.8**	**-**	**115.9**	**159.7**	**5.5**	**36.9**
	166.1	131.5	18.9	87.0	123.1	118.4	137.3	14.0	30.4
25	**165.8**	**130.9**	**12.9**	**114.2**	**-**	**116.4**	**148.3**	**6.2**	**36.8**
	165.2	131.5	27.2	72.4	123.4	117.7	116.5	13.9	23.6
40	**167.6**	**130.5**	**31.1**	**78.5**	**124.5**	**117.1**	**131.4**	**15.0**	**27.4**
	163.2	131.3	27.6	79.5	122.0	118.4	129.3	12.0	27.2
50	**172.8**	**134.6**	**41.5**	**79.7**	**126.5**	**117.5**	**110.4**	**20.1**	**27.8**
	162.2	130.7	30.3	68.6	122.4	117.9	125.8	13.6	21.9
60	**165.9**	**127.9**	**38.2**	**55.2**	**124.1**	**117.7**	**117.4**	**18.4**	**19.2**
	162.7	130.8	21.2	60.6	123.1	118.0	116.3	15.7	20.2
75	**168.5**	**128.9**	**50.0**	**36.6**	**123.6**	**116.9**	**108.6**	**24.2**	**12.7**
	164.6	130.5	37.5	50.0	122.0	118.5	110.5	16.9	16.4
80	**168.0**	**128.7**	**55.2**	**24.0**	**124.4**	**116.9**	**94.5**	**26.7**	**8.4**
	163.2	130.2	31.4	53.7	122.2	118.1	105.3	15.6	17.7
90	**168.2**	**128.7**	**66.9**	**5.4**	**121.8**	**116.1**	**88.6**	**32.3**	**1.9**
	161.8	130.3	32.7	41.0	121.8	117.8	107.1	17.0	13.9
100	**167.4**	**-**	**64.4**	**0.0**	**122.3**	**-**	**83.0**	**31.1**	**0.0**
	164.9	129.5	42.8	31.1	122.7	118.2	100.2	19.6	10.6

4.3.1.2 Crystallisation Behaviour of Virgin and Recycled PP:HDPE Blends

Crystallisation takes place during melt processing and consists of nucleation and crystal growth stages.[21,22] Crystallisation is controlled by kinetics, thermodynamics, and hydrodynamic considerations.[23] As the polymer melt cools, the polymer chains fold and orient from the site of nucleation to form lamellar structures.[22] The amorphous regions connect the crystalline lamellae through tie molecules.[24] Typically, aggregates of lamellae form ordered structures called spherulites. Spherulites will continue to grow until spherulite impingement.[21] However, it is possible to form other crystalline morphologies such as drawn fibrillary and shish kebab.[25] The crystallisation behaviour of semi-crystalline polymers is more complex compared to their melting behaviour due to numerous factors which can affect the phase structure; such as polymer composition and distribution, intra and inter molecular interactions and processing conditions.[26,27] The presence of a second semi-crystalline material in the polymer blend also complicates the crystallisation behaviour.[1,27,28] Typically, PP and HDPE crystallise separately and at different rates. HDPE has a quicker nucleation and growth rate compared to PP due to the HDPE's flexible chain and limited intermolecular interactions.[2,19,26] In PP, crystallisation is hindered by the bulky methyl groups on the polymer chain backbone.[26] There have been several studies on the crystallisation kinetics of PP, PE and their blends. Agwuncha et al.[27] suggest that as both PP and HDPE are crystallisable, the final morphology will be strongly dependent upon the processing conditions, temperature and rate of crystallisation.

As shown in Table 4.1, increasing the PP wt% in the virgin or recycled PP:HDPE blends, results in a decrease in the enthalpy of crystallisation. This is in agreement with Jose et al.[2] who suggested that the decrease in enthalpy of crystallisation could be attributed to the differing rates of crystallisation for PP and HDPE and the resulting size of crystallites. PP crystallises at a slower rate compared to HDPE, which enables the formation of large spherulites. The large spherulites in PP liberate less energy during crystallisation compared to smaller crystallites in HDPE.[2]

There was little variation observed in the T_c for the recycled and virgin blends (Table 4.1 and Figure 4.3). Two crystallisation peaks were observed for rPP:rHDPE blends at approximately the individual PP and HDPE crystallisation temperatures. Phase separation is caused by the PP and HDPE crystals growing at different rates.

Crystallisation peaks were observed in the rPP and rPE due to the presence of PE and PP contaminants, respectively. One crystallisation peak was observed for vPP:vHDPE blends up to vP25 suggesting co-crystallisation and/or partial miscibility. However, upon increasing the PP wt% further, two peaks were observed at approximately the individual PP and HDPE crystallisation temperatures, suggesting an onset of independent crystallisation and incompatibility. Literature typically reports a single crystallisation peak for vPP:vHDPE blends over a wide composition range. Lin et al.[3] and Sutar et al.[29] suggested that the addition of HDPE affected the PP crystallisation rate, resulting in one crystallisation peak. Jose et al.[2] who studied a range of PP:HDPE blends reported only one crystallisation temperature which possessed an intermediary T_c value between the T_c's of PP and HDPE. Aumunate et al.[19] found a single crystallisation peak for vPP:vHDPE blends caused by the merging of the vPP and vHDPE peaks due to their close T_c. However, they suggested bimodal behaviour was present at higher vHDPE contents due to the presence of a slight shoulder peak.

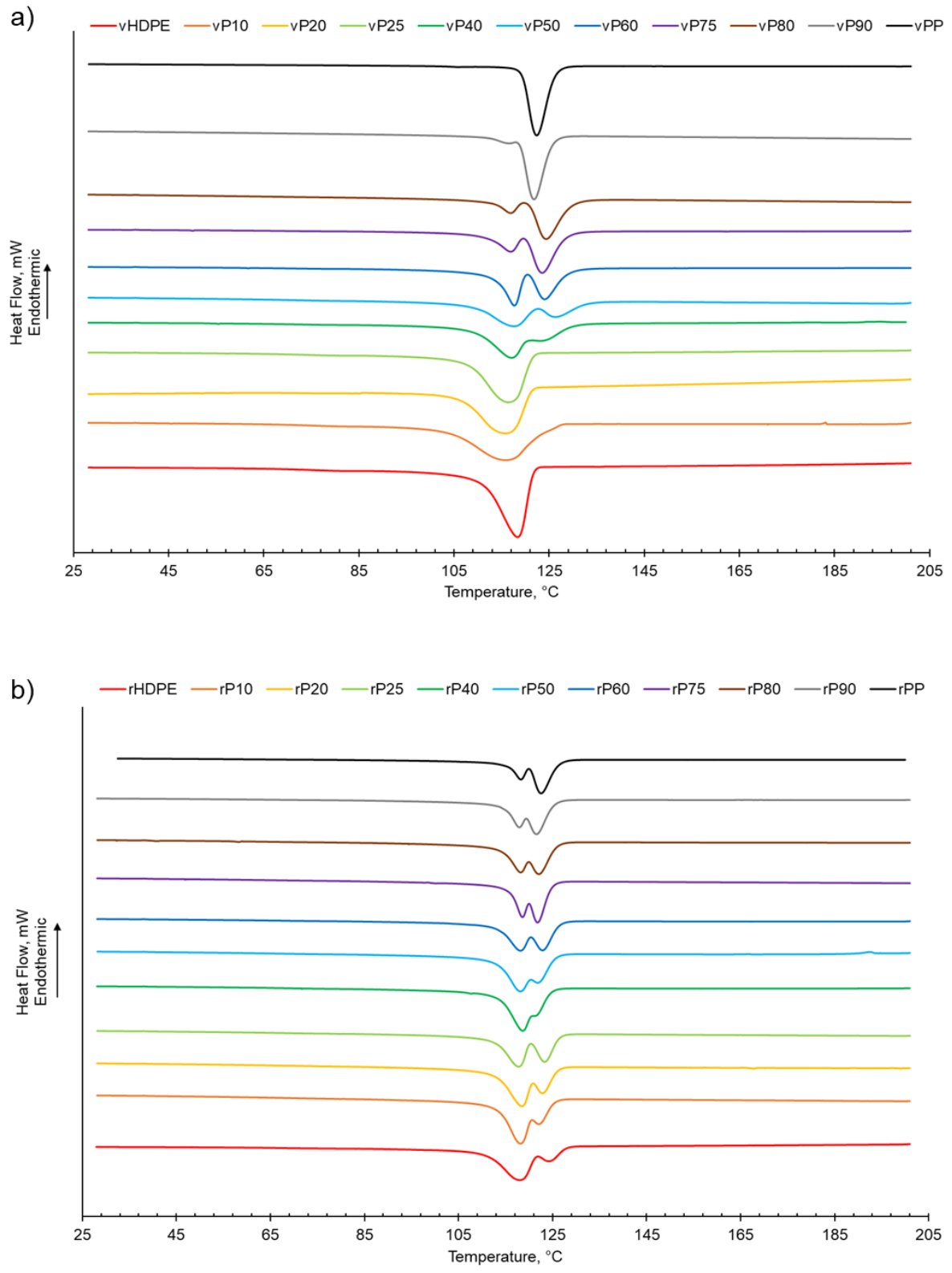

Figure 4.3 The crystallisation behaviour of PP:HDPE blends obtained from DSC a) vPP:vHDPE blends and b) rPP:rHDPE blends.

4.3.1.3 PP and HDPE Crystallinity in Virgin and Recycled PP:HDPE Blends

As discussed in the methodology section (4.2.2.1) the crystallinity of the polymer blends were calculated by two different methods, the individual peak method and the total peak method. Crystallinity did vary depending upon the calculation (Figure 4.4). The total peaks method usually overestimated the crystallinity, possibly due to the placement of the straight line from the start of HDPE peak to the end of the PP peak. This increased the area integrated to find the ΔH_f and hence, affected the crystallinity value. The total peak method is not useful for the rPP and rHDPE due to the presence of contaminants, which increased the ΔH_f observed. Therefore, the individual peaks method was chosen for the crystallinity calculation and discussion.

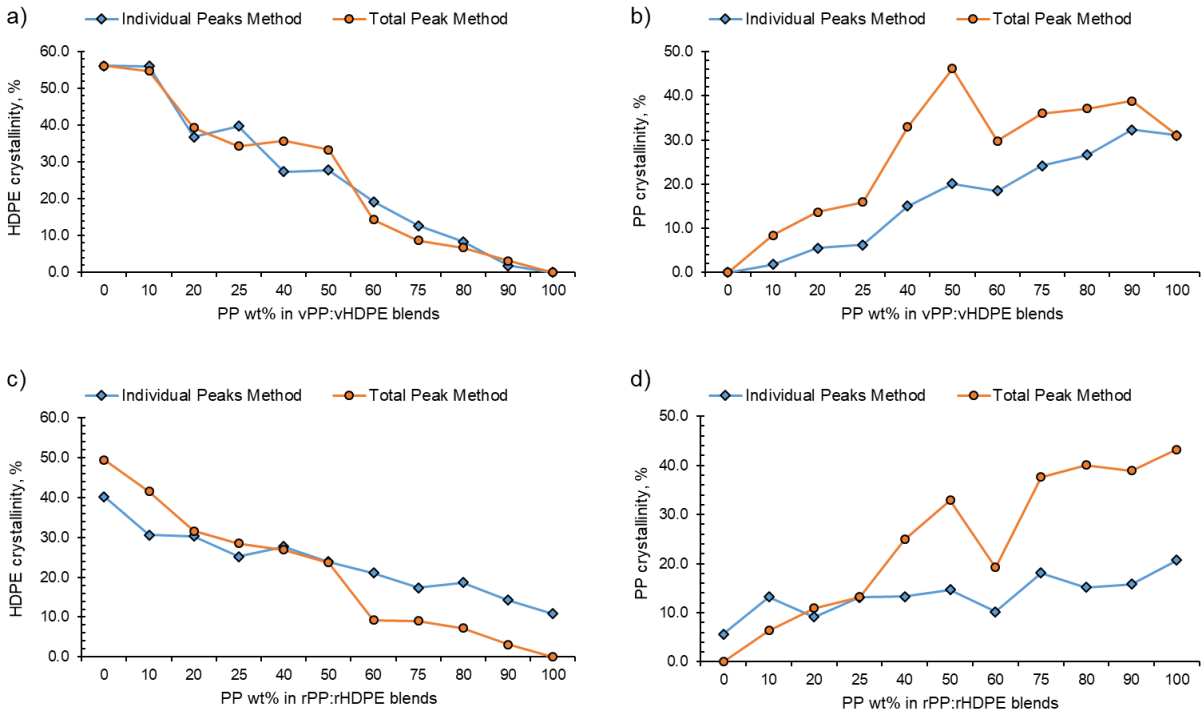

Figure 4.4 Comparison of the percentage PP and HDPE crystallinities in virgin and recycled PP:HDPE blends obtained from the first heating ramp for the individual peak and total peak methods a) HDPE crystallinity in vPP:vHDPE blends, b) PP crystallinity in vPP:vHDPE blends, c) HDPE crystallinity in rPP:rHDPE blends, and d) PP crystallinity in rPP:rHDPE blends.

Using the individual peak method, ΔH_f^{PP} and ΔH_f^{HDPE} were taken from the first heating ramp to calculate the crystallinity. The thermal history of the sample is erased after the first heating ramp.[30] However, very little difference was found when comparing the

crystallinity obtained from the first and second heating ramp for the virgin and recycled blends (Table 4.2 and 4.3). In the literature, the crystallinity obtained from the second heating ramp is larger compared to the first heating. Watt et al.[30] who compared the thermal properties obtained in the first and second heating ramp of vPP and vPP matrix based bio-composites, found that crystallinity increased for vPP (by 21%) and the PP bio-composites on the second heating ramp due to lower amorphous content as thermal history had been erased. It is important to note that crystallinity is affected by the processing method and conditions and the rate of cooling.

Table 4.2: Summary of the crystallinities obtained from the first and second heating ramps for vPP:vHDPE blends.

PP wt% in vPP:vHDPE blends	First Heat Crystallinity, %		Second Heat Crystallinity, %	
	PP	HDPE	PP	HDPE
0	0.0	56.2	0.0	59.2
10	1.8	56.1	1.6	55.2
20	5.5	36.9	5.8	45.4
25	6.2	39.8	6.6	42.3
40	15.0	27.4	13.3	28.2
50	20.1	27.8	12.5	25.0
60	18.4	19.2	20.2	20.3
75	24.2	12.7	27.1	10.5
80	26.7	8.4	28.8	7.0
90	32.3	1.9	32.1	2.6
100	31.1	0.0	42.2	0.0

Table 4.3 Summary of the crystallinities obtained from the first and second heating ramps for rPP:rHDPE blends.

PP wt% in rPP:rHDPE blends	First Heat Crystallinity, %		Second Heat Crystallinity, %	
	PP	HDPE	PP	HDPE
0	5.7	40.2	7.3	36.2
10	13.2	30.6	12.5	30.8
20	9.1	30.3	14.0	30.4
25	13.1	25.2	13.9	23.6
40	13.3	27.7	12.0	27.2
50	14.7	23.9	13.6	21.9
60	10.2	21.1	15.7	20.2
75	18.1	17.4	16.9	16.4
80	15.1	18.7	15.6	17.7
90	15.8	14.3	17.0	13.9
100	20.7	10.8	19.6	10.6

As the PP wt% increased for both the vPP:vHDPE and rPP:rHDPE blends, the PP crystallinity in the blend increased and the HDPE crystallinity decreased (Table 4.1 and Figure 4.5). In Figure 4.5, the rPP crystallinity was higher than vPP crystallinity in HDPE up to the P25 blend. The rHDPE crystallinity was higher than the vHDPE crystallinity from P60 to PP. The increased crystallinities of PP and HDPE in the recycled blends could be attributed to the presence of PP and HDPE contaminants in the recycled materials, which are present in the melting thermograms. The quantity of other plastic contaminants will be dependent on the waste stream composition and the quality of sorting at the material recycling facility.[31,32] Additionally, an increase in crystallinity could be caused by thermo-mechanical degradation which occurs during recycling. Thermo-mechanical degradation results in an increase in polydispersity caused by the presence of shorter polymeric chains.[33] Shorter polymeric chains form crystals more easily compared to long chains due to their low degree of entanglement which may lead to an increase in crystallinity.[34] On the other hand, the crystallinities of rPP and rHDPE were found to be lower than the vPP and vHDPE crystallinities for blends between P40 to PP, and HDPE to P50, respectively. The presence of other plastics, varying chains lengths and branching and, impurities such as oxidative

moieties and additives, can lead to the formation of imperfect crystallites and a heterogeneous crystalline morphology, hence reducing crystallinity.[31,35] Therefore, determining an accurate crystallinity in recycled blends is a challenge.

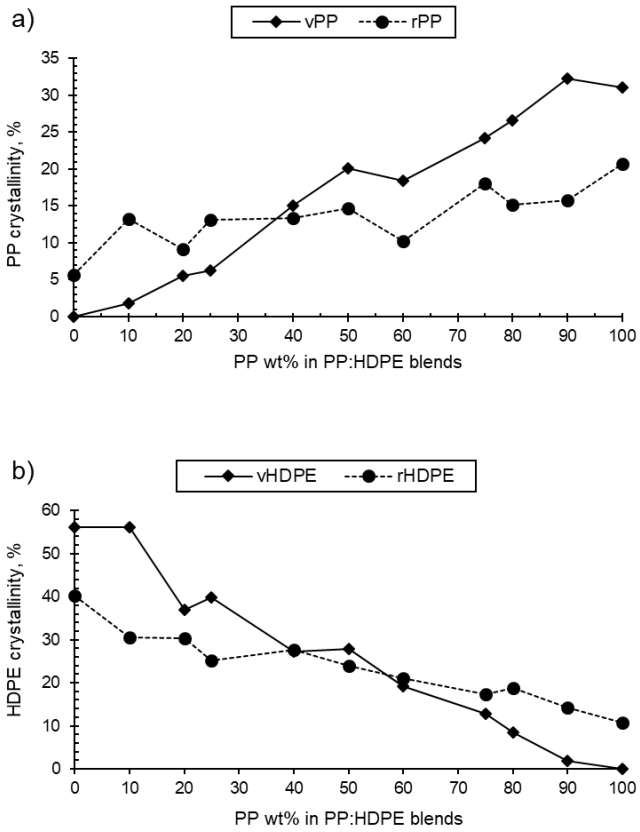

Figure 4.5 Variation of a) virgin and recycled PP percentage crystallinity in PP:HDPE blends and b) virgin and recycled HDPE percentage crystallinity in PP:HDPE blends.

4.3.1.4 Glass Transition Temperature

The T_g of PP and HDPE were not observed in the thermograms as the T_g*'s* are located below the starting temperature of the DSC thermograms.

4.3.2 Morphology of Virgin PP:HDPE Blends

4.3.2.1 SEM

SEM was initially used as a method to determine the morphology of the PP:HDPE blends. SEM is a non-destructive method, which works by firing a high energy electron beam from an electron gun onto the sample surface.[36] The electron beam passes through lenses and apertures to ensure that it is focused onto the sample surface. The electron beam and sample interact, causing the formation of Auger electrons,

backscattered electrons, secondary electrons and X-rays.[37] The electrons and X-rays are detected and their signals are processed to create a morphology image.[36,37]

Initially, the vP50 blend was chosen to determine whether SEM could detect sample morphology. Sample preparation involved subjecting the samples to one freeze thaw cycle before platinum coating. Challenges arose during imaging due to a high level of charging, resulting in low image contrast and lack of PP and HDPE phase clarity. To overcome this issue the samples were subjected up to five freeze thaw cycles. Increasing the number of freeze thaw cycles was thought to improve the contrast between the PP and HDPE phases due to the differing coefficient of linear thermal expansion (CLTE). The CLTE characterises the dimensional changes of the material as the temperature varies. PP has a lower CLTE in comparison to HDPE.[38] Awad et al.[38] suggest that the lower PP CLTE is due to the stronger interatomic forces that slows expansion compared to HDPE. However, this did not improve the phase clarity and there were imaging artefacts present, attributed to moisture on the sample surface caused by the freeze thaw cycles (Figure 4.6). From Figure 4.6, it is unclear as to the morphology of the vP50 blend, which is expected to demonstrate a co-continuous morphology.[2,39] A similar vP50 morphology was obtained by Sutar et al.[29] who investigated a range of PP:HDPE surface morphology by SEM. The researchers carried out SEM on unfractured surfaces but were unable to differentiate the PP and HDPE phases. Interestingly, Jabłońska et al.[40] found that through permanganic surface etching, phase clarity could be achieved for vPP:vHDPE blends. They were able to deduce the overall droplet-matrix morphology and the PP, HDPE domain shapes in a vP20 blend. However, the SEM images lacked surface sensitivity.

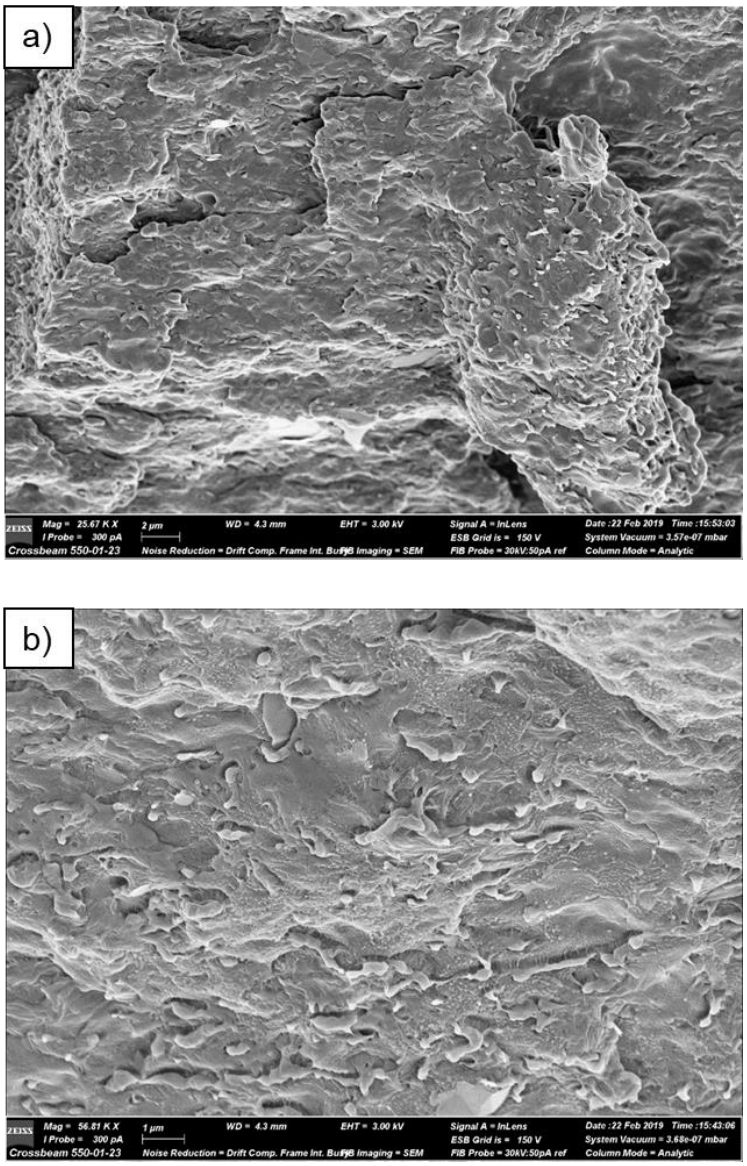

Figure 4.6 SEM images obtained for vP50 blend. a) 25.67 magnification, scale bar 2µm b) 56.81 magnification, 1 µm.

4.3.2.2 AFM

AFM was implemented to deduce the phase separate morphology caused by the immiscibility of PP and HDPE which has been shown by the thermal studies. Tapping mode was implemented on cryo-fractured vPP:vHDPE blends. Tapping mode has been carried out on vHDPE, vPP and with PP:HDPE in binary or ternary polymer blends and composites.[41-44] However, there is limited literature on the use of tapping mode over a range of compositions for PP:HDPE blends. As shown in Figure 4.7, phase separated morphology was observed due to the immiscibility of PP and HDPE. The morphology was found to be dependent upon the blend composition. A

homogenous morphology was observed between vPP to vP80, however vP90 and vP80 could have phase separated morphology on the nanometer scale. A droplet-matrix domain morphology was found at vP75 with the vHDPE dispersed droplet domain and a co-continuous domain morphology at vP50 at the nanoscale. This is in agreement with the literature, as Lin et al.[45] suggested a droplet-matrix structure at vP70 and Jose et al.[2] found a co-continuous domain morphology from vP40 to vP60 determined by SEM. If the reduction in vPP wt% continued below vP50, a phase inverted droplet matrix domain morphology would be expected at vP40 to vP25 with the PP now being the dispersed droplet domain followed by the homogenous phase at vP20.

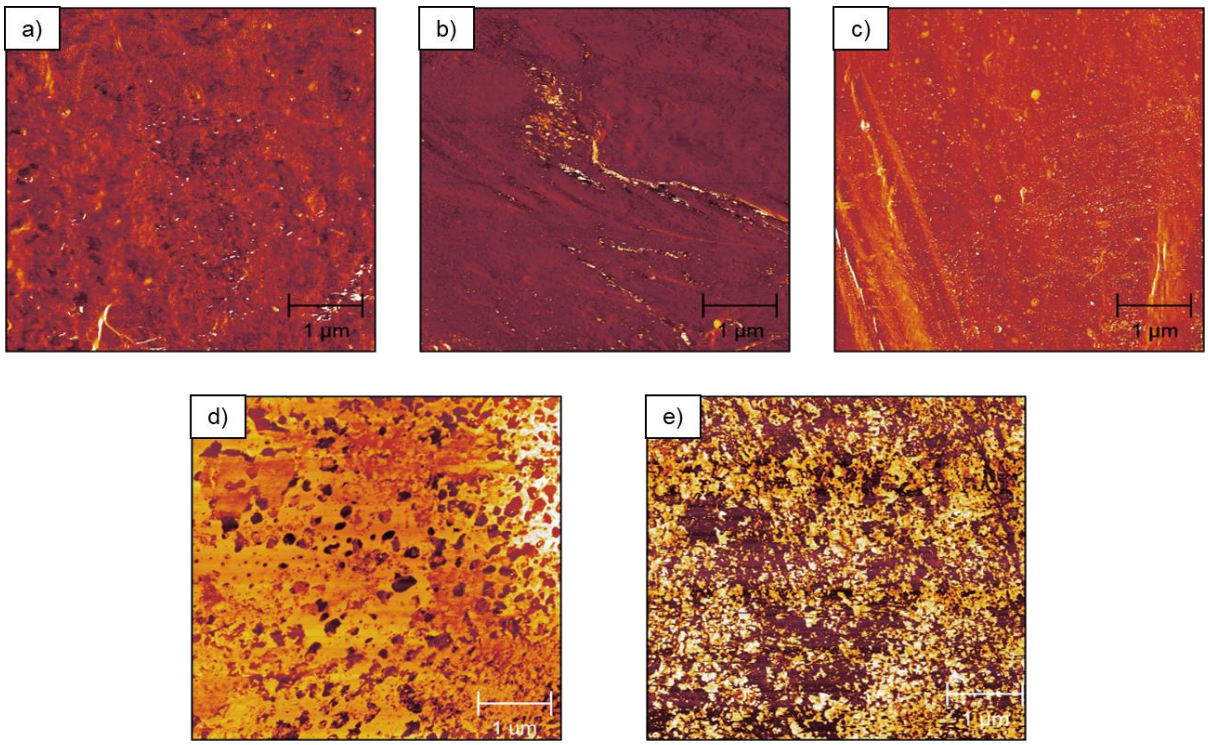

Figure 4.7 AFM phase images of vPP:vHDPE blends at varying wt%. a) vPP showing a homogenous morphology, b) vP90, c) vP80, d) vP75 showing a droplet matrix domain morphology and e) vP50 showing a co-continuous domain morphology.

4.4 Conclusion

This chapter investigated the thermal and morphological properties of virgin and recycled PP:HDPE blends. Thermal studies carried out by DSC confirmed that both the virgin and recycled PP:HDPE blends were immiscible. rPP and rHDPE were found to contain contaminants due to the difficulty of separating PP and HDPE during the recycling process. The recycling process was found to lower the T_m, and crystallinity of the rPP:rHDPE blends due to structural deterioration and the formation of imperfect crystallites. Interestingly, there was little difference in the T_c when comparing the virgin and recycled blends. The PP and HDPE crystallinities were dependent upon the blend composition. As the ratio of PP increased, the crystallinity of PP increased and that of HDPE decreased in the PP:HDPE blends. Initially, SEM was implemented to determine the morphology of the PP:HDPE blends but showed a lack of phase clarity. Therefore, a preliminary AFM study was carried out to complement and provide further insight into PP:HDPE blends morphology. Phase separated morphology, on the nanometer scale, was found in vPP:vHDPE blends to be dependent on the blend composition. As the PP wt% increased, the morphology showed a transition from homogenous to droplet matrix and finally to co-continuous. There is a lack of AFM studies on rPP:rHDPE in the literature. Therefore, as the AFM provided an excellent insight into the morphology of vPP:vHDPE blends, an extensive study was carried out using a new AFM mode, on both the virgin and recycled blends, which is discussed in chapter 6. Overall, this chapter has contributed towards understanding the processing-structure-property relationship of rPP:rHDPE blends in comparison to virgin blends, which is key for improving the circular economy for recycled plastics.

References

1. R. Strapasson, S. C. Amico, M. F. R. Pereira, T. H. D. Sydenstricker, *Polymer Testing* **2005**, *24*, 468.
2. S. Jose, A. S. Aprem, B. Francis, M. C. Chandy, P. Werner, V. Alstaedt, S. Thomas, *Eur. Polym. J.* **2004**, *40*, 2105.
3. J. H. Lin, Y. J. Pan, C. H. Liu, C. L. Huang, C. T. Hsieh, C. K. Chen, Z. I. Lin, C. W. Lou, *Materials* **2015**, *8*, 8850.
4. Y. Kazemi, A. R. Kakroodi, D. Rodrigue, *Polym. Eng. Sci.* **2015**, *55*, 2368.
5. J. Aurrekoetxea, M. A. Sarrioonandia, I. Urrutibeascoa, M. L. Maspoch, *Journal of Materials Science* **2001**, *36*, 2607.
6. S. Yin, R. Tuladhar, F. Shi, R. A. Shanks, M. Combe, T. Collister, *Polymer Engineering and Science* **2015**, *55*, 2899.
7. H. M. d. Costa, V. D. Ramos, M. G. d. Oliveira, *Polymer Testing* **2007**, *26*, 676.
8. K. H. Ha, M. S. Kim, *Materials & Design* **2012**, *34*, 252.
9. C. E. Scott, C. W. Macosko, *Polymer* **1995**, *36*, 461.
10. B. D. Favis, *J. Appl. Polym. Sci.* **1990**, *39*, 285.
11. A. M. Jordan, K. Kim, D. Soetrisno, J. Hannah, F. S. Bates, S. A. Jaffer, O. Lhost, C. W. Macosko, *Macromolecules* **2018**, *51*, 2506.
12. C. Albano, J. González, M. Ichazo, C. Rosales, C. U. d. Navarroc, C. Parrac, *Composites Structure* **2000**, *48*, 49.
13. G. Spadaro, G. Rizzo, *Eur. Polym. J.* **1989**, *25*, 1189.
14. S. Salih, A. Hamood, A. Alsalam, *Mod. Appl. Sci.* **2013**, *7*, 33.
15. J. Li, R. A. Shanks, Y. Long, *J. Appl. Polym. Sci.* **2000**, *76*, 1151.
16. D. Nečas, P. Klapetek, *Cent. Eur. J. Phys.* **2012**, *10*, 181.
17. J. Momanyi, M. Herzog, P. Muchiri, *Recycling* **2019**, *4*, 33.
18. J. Gu, H. Xu, C. Wu, *Adv. Polym. Technol.* **2014**, *33*, 21384.
19. C. Aumnate, N. Rudolph, M. Sarmadi, *Polymers* **2019**, *11*
20. J. Hopewell, R. Dvorak, E. Kosior, *Philosophical Transactions of The Royal Society B* **2009**, *364*, 2115.
21. G. Lamberti, *Chem. Soc. Rev.* **2014**, *43*, 2240.
22. K. M. Seven, *Polymer Engineering and Science* **2016**, *56*, 541.
23. S. Vedantam, V. V. Ranade, *Sadhana* **2013**, *38*, 1287.
24. W. D. Callister, D. G. Rethwisch, *Fundamentals of Materials Science and Engineering. An Integrated Approach*, John Wiley & Sons, **2016**.

25. M. P. Stevens, *Polymer Chemistry. An Introduction*, Oxford University Press, **1990**.
26. D. Mileva, D. Transchida, M. Gahleitner, *Advances in polymer Crystallization, Part 1* **2018**, *1*
27. S. C. Agwuncha, S. J. Owonubi, E. R. Sadiku, K. Varaprasad, S. S. Ray, S. P. Selvam, T. A. Shittu, A. Shanavas, E. Mukwevho, in *Design and Applications of Nanostructured Polymer Blends and Nanocomposite Systems*, Elsevier, 2016, Ch. 14.
28. P. Samanta, R. Srivastava, B. Nandan, H. L. Chen, *Soft Matter* **2017**, *13*, 1569.
29. H. Sutar, P. C. Sahoo, P. S. Sahu, S. Sahoo, R. Murmu, S. Swain, S. C. Mishra, *Materials Science and Applications* **2018**, *9*, 502.
30. E. Watt, M. A. Abdelwahab, M. R. Snowdon, A. K. Mohanty, H. Khalil, M. Misra, *Scientific Reports* **2020**, *10*
31. F. Stangenberg, S. Ågren, S. Karlsson, *Chromatographia* **2004**, *59*, 101.
32. B. Ruj, V. Pandey, P. Jash, V. K. Srivastava, *Journal of Applied Sciences and Engineering Research* **2015**, *4*, 564.
33. L. A. Pinheiro, M. A. Chinelatto, S. V. Canevarolo, *Polym. Degrad. Stab.* **2004**, *86*, 445.
34. M. J. Shirkavand, H. Azizi, I. Ghasemi, M. Karabi, *Adv. Polym. Technol.* **2018**, *37*, 770.
35. F. Vilaplana, S. Karlsson, *Macromol. Mater. Eng* **2008**, *293*, 274.
36. A. Mohammed, A. Abdullah, presented at International Conference on Hydraulics and Pneumatics - HERVEX, Romania**November 7 - 9 2018**.
37. B. Hafner, *Scanning electron microscopy primer*, University of Minnesota-Twin Cities, **2007**.
38. A. H. Awad, R. Elgamsy, A. A. E. Wahab, M. H. Abdellatif, *Engineering Science* **2019**, *4*, 34.
39. C. Zhang, X. S. Yi, D. Asai, M. Sumita, *Journal of Materials Science* **2000**, *35*, 673.
40. M.Jabłońska, S. Reißaus, S. Henning, M. Menzel, A. Hähnel, J. Klehm, U. Hirsch, A. Heilmann, *Micron* **2019**, *124*, 102685.
41. D. G. Yablon, A. Gannepalli, R. Proksch, J. Killgore, D. C. Hurley, J. Grabowski, A. H. Tsou, *Macromolecules* **2012**, *45*, 4363.
42. O. Sahin, N. Erina, *Nanotechnology* **2008**, *19*, 445717.

43. A. Chafidz, I. Ali, M. E. A. Mohsin, R. Elleithy, S. Al-Zahrani, *Journal of Polymer Research* **2012**, *19*, 9860.
44. Y. Wang, H. Zou, Q. Fu, G. Zhang, K. Shen, R. Thomann, *Macromol. Rapid Commun.* **2022**, *23*, 749.
45. Y. Lin, V. Yakovleva, H. Chen, A. Hiltner, E. Baer, *J. Appl. Polym. Sci.* **2009**, *113*, 1945.

5.0 Mechanical Properties of Virgin and Recycled PP: HDPE Blends

5.1 Introduction

The recycling industry is faced with PO recyclate consisting of poor mechanical properties due to the immiscibility between PP and PE, along with the presence of thermo-mechanical and thermo-oxidative degradation during recycling.[1,2] During a recycling cycle, thermal degradation can result in a decrease in the molecular weight, causing the mechanical properties to decrease.[3] For a circular plastic economy to be achieved, recyclate would need to maintain a level of mechanical properties to be used in applications after each recycling cycle. However, the number of recycling cycles has been shown to affect rheological and mechanical properties due to their dependence upon the molecular weight.[4-7] The polymer structure and thermal stability will determine the number of cycles a polymer can endure before a reduction in mechanical performance is observed. As PP and PE are semi-crystalline polymers their degradation in the solid state typically occurs in the amorphous phase.[7] Degradation affects the crystallinity and thus the mechanical properties.[5]

Research has been undertaken in the literature to understand the effect of recycling cycles on the mechanical properties of PP, PE and their blends. For example, Aurrekoetxea et al.[8] subjected PP to 10 successive injection moulding cycles at 200 °C and found that the degree of crystallinity increased with each cycle. This caused an increase in the Young's modulus and yield stress. On the other hand, Oliveira et al.[3] who subjected PP to seven successive cycles at 175–190 °C, suggested a decrease in Young's modulus and yield stress after the third cycle, which was caused by the reduction in tie molecules between the crystalline and amorphous phases. Conflicting observations by Aurrekoetxea et al.[8] and Oliveira et al.[3] for the Young's modulus and yield stress of rPP could be due to differences in the processing methodology. Aurrekoetxea et al.[8] used injection moulding whereas Oliveira et al.[3] opted for a single screw extruder followed by compression moulding. This highlights the importance of the reprocessing methodology but also demonstrates the difficulty of comparing the performance of recycled materials in the literature.

PE can be subjected to a higher number of extrusion cycles before any deterioration in the mechanical properties is observed. Jin et al.[9] found no significant change in crystallinity and hence in mechanical properties of LDPE up to the 40th extrusion cycle. However, a decrease in crystallinity was observed between the 40–50th cycles,

either caused by short side branches in the backbone chain, side groups, or by crosslinking. Oblak et al.[4] subjected HDPE to 100 consecutive extrusion cycles at 220–270 °C. They found that chain branching and chain scission, which occurred up to the 60th cycle resulted, in a decrease in crystallinity and Young's modulus. However, crystallinity and Young's modulus remained stable after the 60th extrusion cycle due to crosslinking. After the 100th cycle, the Young's modulus of rHDPE had only reduced by 20% compared to that of the vHDPE.

Studies have been carried out to understand the mechanical properties of PP:PE blends subjected to recycling cycles.[10-16] Saikrishman et al.[10] found that recycling affected the melt flow behaviour of PP:LDPE blends but found that the tensile properties were not substantially affected (subjected up to 5 recycling cycles). Interestingly, PP underwent chain scission on each recycling cycle but the overall properties of the blend were maintained. However, they only investigated the PP:LDPE up to 10 wt% of LDPE. The literature is typically limited in the blend composition range investigated. However, due to the variability of the waste streams, it is important to understand the mechanical properties for all blend compositions without the addition of a third component initially. This would enable the recycling industry to be reactive to changes in waste stream composition in different locations and batches, and enable more recyclate to re-enter the market. Therefore, this chapter aims to understand the variability in mechanical properties through the use of DMA and tensile testing, for virgin and recycled PP:HDPE blends.

5.2 Experimental

5.2.1 DMA

DMA was used to determine the viscoelastic properties of the virgin and recycled blends. A Triton DMA in dual cantilever mode at a frequency of 1 Hz was used. A temperature sweep from -50 to 150 °C at a heating rate of 5 °C min^{-1} was implemented. Sample dimensions were approximately 45 mm (l) × 10 mm (w) × 2.7 mm (d). A minimum of three samples were tested and the average and standard deviation were calculated for each blend ratio.

The dynamic response was given as the elastic (*E'*), viscous (*E''*) and damping (tanδ) components. The T_g and transition relaxation processes can be seen as changes in

the *E''* or tanδ traces.[17] The tanδ trace was used to quote the T_g and other relaxation peaks present.[18]

5.2.2 Tensile Testing

Tensile properties were determined using an Instron Tensile Machine (Buckinghamshire, UK) with a crosshead speed of 5 mm min^{-1} at ambient temperature in accordance to the ISO 527-2 standard. The Young's modulus was determined using a Zwick Roell Tensile Machine with a video-extensometer. A crosshead speed of 1 mm min-1, gauge length of 25 mm and a 10 kN load cell were used. A minimum of five samples were tested and the average and standard deviation were calculated.

The "rule of mixtures" was used to predict the Young's modulus of the virgin and recycled PP:HDPE blend samples and compared to the experimental data. The rules of mixtures was calculated by Equation (5.1),

$$E_{Blend} = W_{PP}E_{PP} + W_{HDPE}E_{HDPE} \quad (5.1)$$

where E_{Blend} is the Young's modulus of the polymer blend, W_{PP} and E_{PP} is the weight fraction and Young's modulus of PP, respectively, and W_{HDPE} and E_{HDPE} is the weight fraction and Young's modulus of component HDPE, respectively.[19] The experimental Young's modulus of the virgin and recycled homogenous PP and HDPE systems were used for the virgin and recycled E_{PP} and E_{HDPE}.

5.3 Results and Discussion

5.3.1 DMA

5.3.1.1 Storage and Loss Moduli

DMA was used to determine the viscoelastic response of the blends as a function of temperature. The *E'* indicates the relative dynamic stiffness of the material and the *E''* indicates the ability to dissipate energy (Figure 5.1).[20] For virgin and recycled PP, HDPE and their blends, as temperature increased the *E'* decreased and *E''* increased. This is due to material softening and the beginning of relaxation processes.[21] As the PP wt% increased the vPP:vHDPE blends *E''* decreased, whereas the rPP:rHDPE blends did not show an as obvious decrease in *E''* with variation in composition. There was not a large variation in the *E'* as blend composition varied for both the virgin and

recycled blends. The recycled blends, (P20, P40, P60 and P90) have a lower *E'* compared to virgin blends due to structural deteriorations caused by the recycling process which introduced flexibility and mobility to the shorter chains. However, P10, P25, P50, P75 and P80 recycled blends gave a higher *E'* than the corresponding virgin blends. This could be caused by impurities such as fillers in the recycled materials which could impose mechanical restraint.[22] Interestingly, Fang et al.[16] who investigated the storage and loss moduli of rPP:rPE blends, without the addition of a compatibiliser or filler, found an increase in moduli with rPP content. For example, the rP60 blend presented *E'* at 40 °C, which was twice of the rP45 blend. They concluded that an increase in stiffness occurs with an increase in PP wt%. However, the difference in the temperature at which the moduli were taken, manufacturing processes and the unknown MFI of the rPE and rPP, could account for the differences observed.

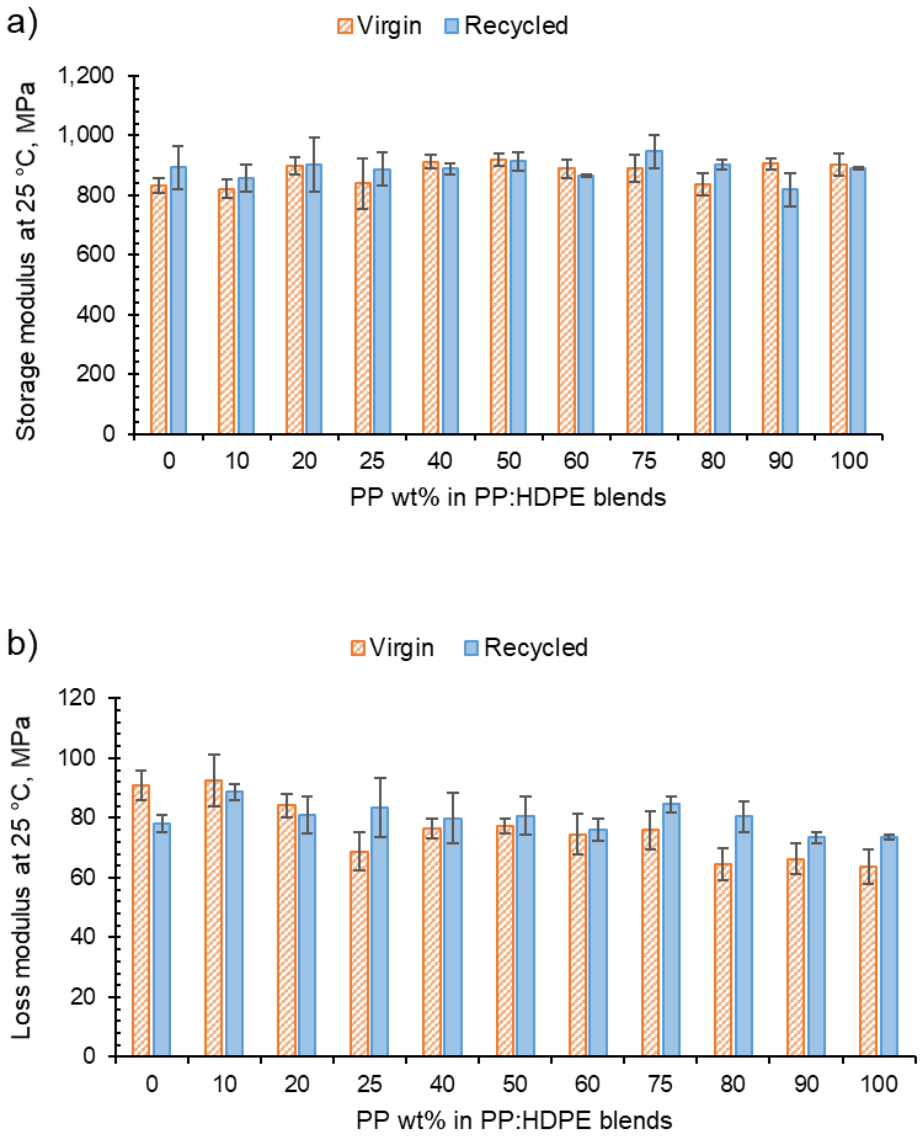

Figure 5.1 a) The variation in storage modulus at 25 °C for vPP:vHDPE and rPP:rHDPE blends and b) the variation in loss modulus at 25 °C for vPP:vHDPE and rPP:rHDPE blends.

5.3.1.2 Relaxation Processes

HDPE and PP both exhibit three relaxation processes: alpha (α), beta (β) and gamma (γ).[18,23] Both the virgin and recycled PP:HDPE blends exhibited the α and β relaxation processes in the tanδ graphs, as shown in Figure 5.2. The γ relaxation was not observed as it typically occurs below -50 °C which was outside the experimental temperature range. The γ relaxation is associated with the motions of the side chain groups attached to the main chain in the amorphous region.[23]

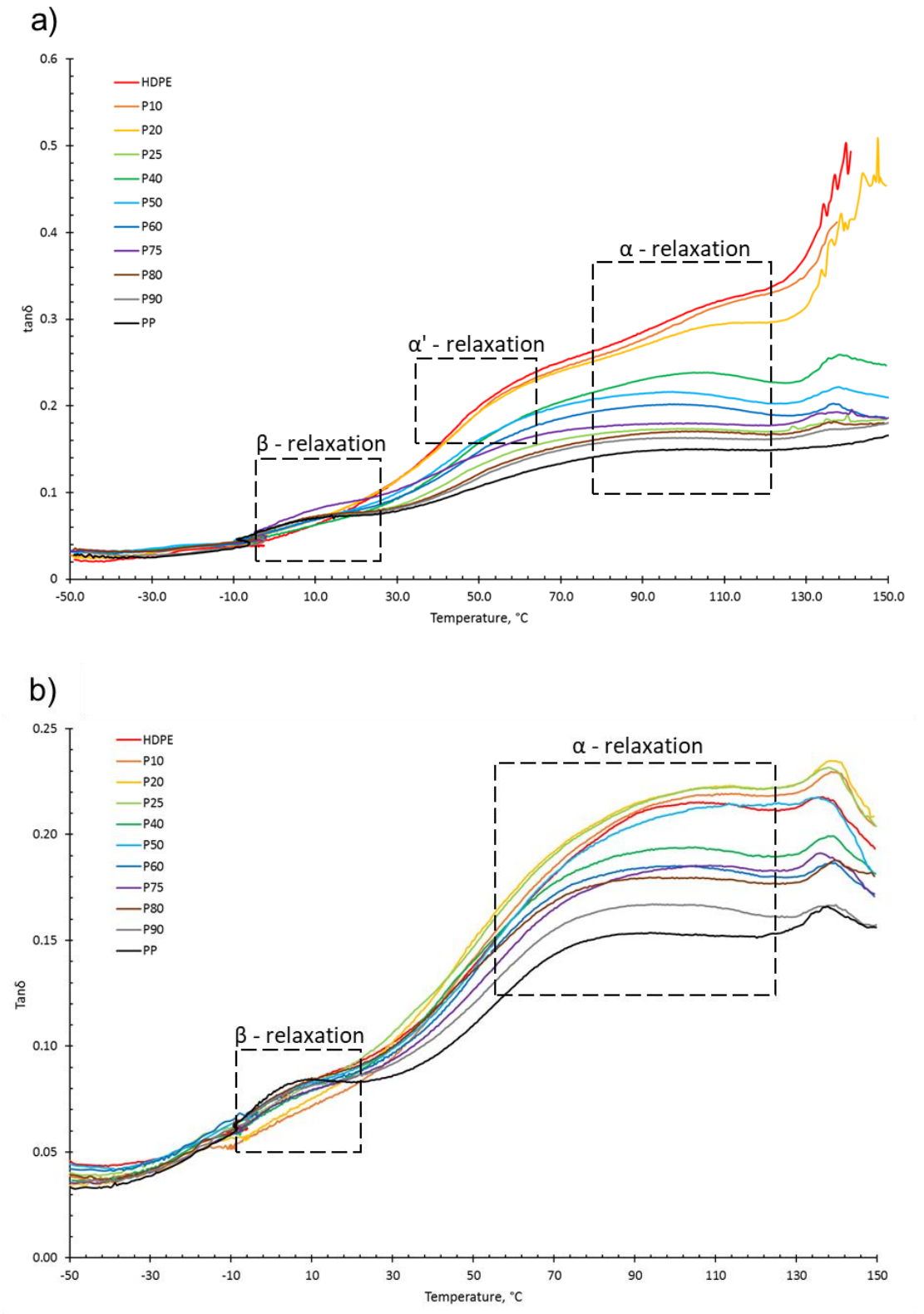

Figure 5.2 tanδ graphs of a) vPP:vHDPE blends and b) rPP:rHDPE blends, with the α and β relaxation regions highlighted.

The α relaxation is associated with the crystalline region where the CH_2 groups within the crystallites have vibrational and re-orientation motion. The chains are flexible and freely rotating.[23-25] The rHDPE and rPP alpha relaxation temperatures (T_α's) were lower compared to the vHDPE and vPP, respectively, possibly caused by imperfect crystallite formation due to recycling (Figure 5.3).[26] The higher T_α of HDPE compared to PP could be due to HDPE's higher crystallinity and amount of crystalline domains compared to PP.[27] The virgin blends T_α's decrease as the PP wt% increases, with a similar trend observed in the recycled blends. The T_α's are intermediary between the T_α of PP and HDPE. As suggested by Karaagac et al.[28] the observed relaxation temperatures of the blends are likely following the rule mixtures and caution must be taken before suggesting partial miscibility at the interface due to the observation of a single peak. As the T_α's of PP and HDPE are close in value, it is possible that there is an overlap in the peaks causing the blend to have a broad T_α peak.

HDPE exhibits an additional relaxation process, α', which is associated with the crystalline region and partially overlaps into the α region.[18] The α' is observed in vHDPE at approximately 40 °C (Figure 5.2). As the vHDPE content in the virgin blends decreases, the α' relaxation decreases in prominence. The α' is not observed in the rHDPE possibly due to the recycling process which causes the formation of imperfect crystallites and the presence of contaminants which decreases the peak prominence.

The β relaxation is associated with the motion of the branches in the amorphous region and is connected to the T_g.[22,24,29] The PP β relaxation temperature (T_β) is the T_g. There are many opposing viewpoints surrounding where the T_g of PE is: a) in the β region just below 0 °C b) in the region of -81 °C and c) in the γ region below -100 °C.[23,30] The magnitude of the T_β is dependent on the amount of amorphous domains as the relaxation occurs in the amorphous domain. The T_β in HDPE may not always be observed due to the low proportion of amorphous domains compared to crystalline domains. Additionally, tie molecules between the crystalline and amorphous domains restrict the complete relaxation of amorphous chains.[22,25] In Figure 5.2 and 5.3, the T_β observed will be that of vPP as the vHDPE T_β is not observed. The vPP T_β is not visible in the vP10 and vP20 blends due to small magnitude of the relaxation. The T_β of PP becomes visible at 12.4 °C for P25. The T_β is present in the rHDPE due to the presence of PP impurities which cannot be completely removed in the recycling process.[31] The

T_β of the recycled blends were lower than the virgin blends and had little variation. The recycling process results in a decrease in molecular weight. Steric hindrance of the low molecular weight chains in the amorphous and crystalline regions causes an increase in free volume and poorer chain packing.[32] Increase in free volume lowers the T_β as less thermal energy is required for chain mobility.

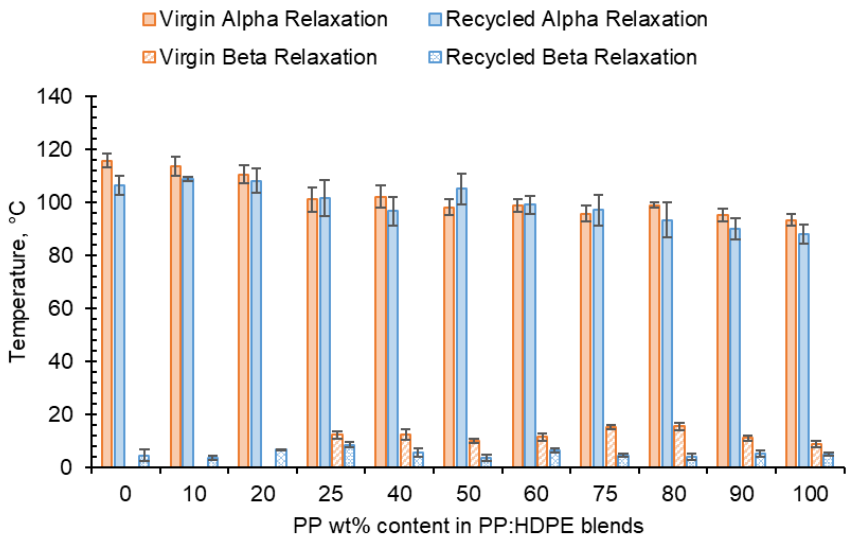

Figure 5.3 Comparison of the T_α and T_β taken from tanδ traces for virgin and recycled PP:HDPE blends.

5.3.2 Tensile Testing

5.3.2.1 Stress-strain behaviour

PP, HDPE and their blends will undergo macroscopic deformation during a tensile test and typically exhibit a strain hardening and a ductile fracture, as shown in Figure 5.4. Initially, the polymers undergo elastic deformation but as the force applied continues to increase, the polymer sample reaches the yield point and enters the region of plastic deformation. At the yield point a small neck forms within the gauge section and the polymer chains align in the direction of elongation.[33] Continuing beyond the yield point, the virgin and recycled PP, HDPE and their blends exhibit the strain-hardening phenomenon. Strain hardening occurs when there is resistance to deformation and the neck region propagates and extends, which is termed necking. The polymer chains continue to orientate and align in the direction of elongation which results in an increase in strength of the plastic. Necking continues until fracture.

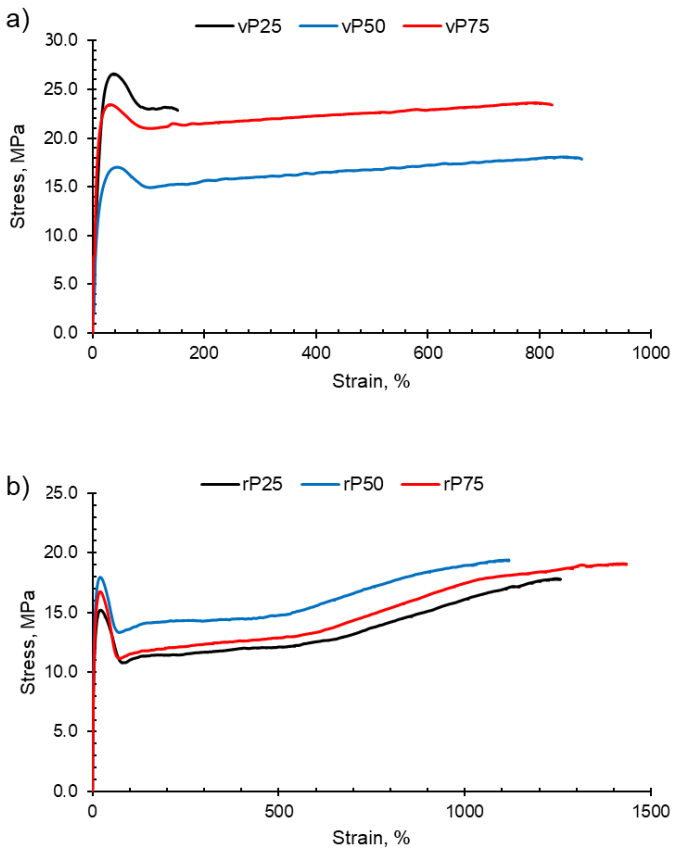

Figure 5.4 Examples of typical stress-strain curves obtained for PP:HDPE blends. The blends P25, P50 and P75 have been shown for a) vPP:vHDPE blends and b) rPP:rHDPE blends.

5.3.2.2 Young's modulus

The recycled blends exhibited deteriorated tensile properties compared to the virgin blends in Young's modulus (Figure 5.5). The Young's modulus of rPP and rHDPE were lower than the virgin polymers due to structural deterioration caused by the recycling process[34,35].

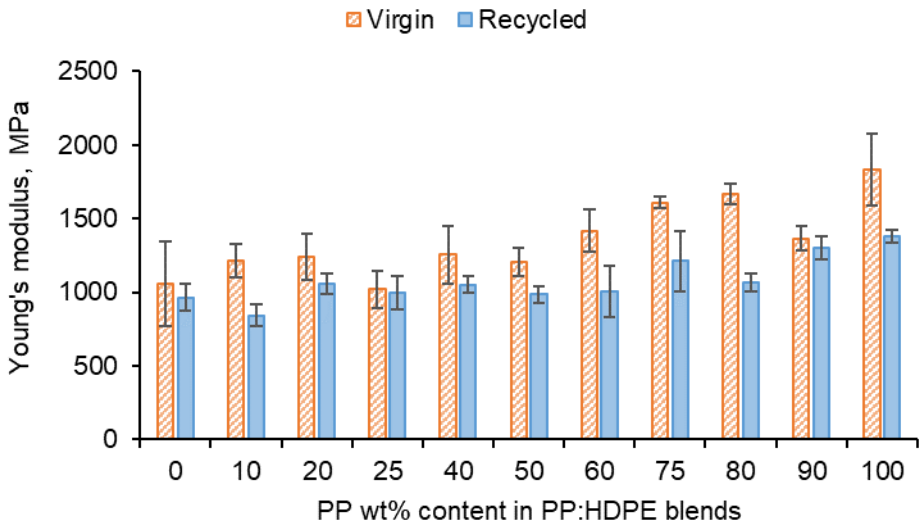

Figure 5.5 Comparison of the Young's moduli for vPP:vHDPE and rPP:rHDPE blends obtained from tensile testing.

The virgin and recycled PP:HDPE blends gave intermediary Young's moduli values between PP and HDPE. Comparing the predicted rules of mixtures to the experimental Young's modulus shows a negative deviation for all recycled blends (Figure 5.6). A negative deviation suggests poor compatibility and weak adhesion between the phases.[36] It is important to note that the rule of mixtures does not take into account interactions between components. The Young's modulus values of the virgin blends showed positive and negative deviations from the rule of mixtures with composition (Figure 5.6). Positive deviation between blends vP10-vP20, minor negative deviation between vP25-vP60, a positive deviation at vP75 and vP80, and a negative deviation at vP90. The vP90 was expected to exhibit a positive deviation however, a negative deviation was observed. Lovinger and Williams[37] suggested that PE can play the role of stiffener to the PP matrix; in sufficient quantities it enhances the intercrystalline links. The alternating regimes of positive and negative deviations suggest a complex interplay of morphological factors and crystallinity as the composition varies. The mechanical properties are dependent upon the morphology, crystallinity and compatibility between the phases. As determined in chapter 4, the PP:HDPE blends are immiscible and crystallinity is dependent upon composition. Additionally, the initial AFM images have shown a variation in the morphology with composition.

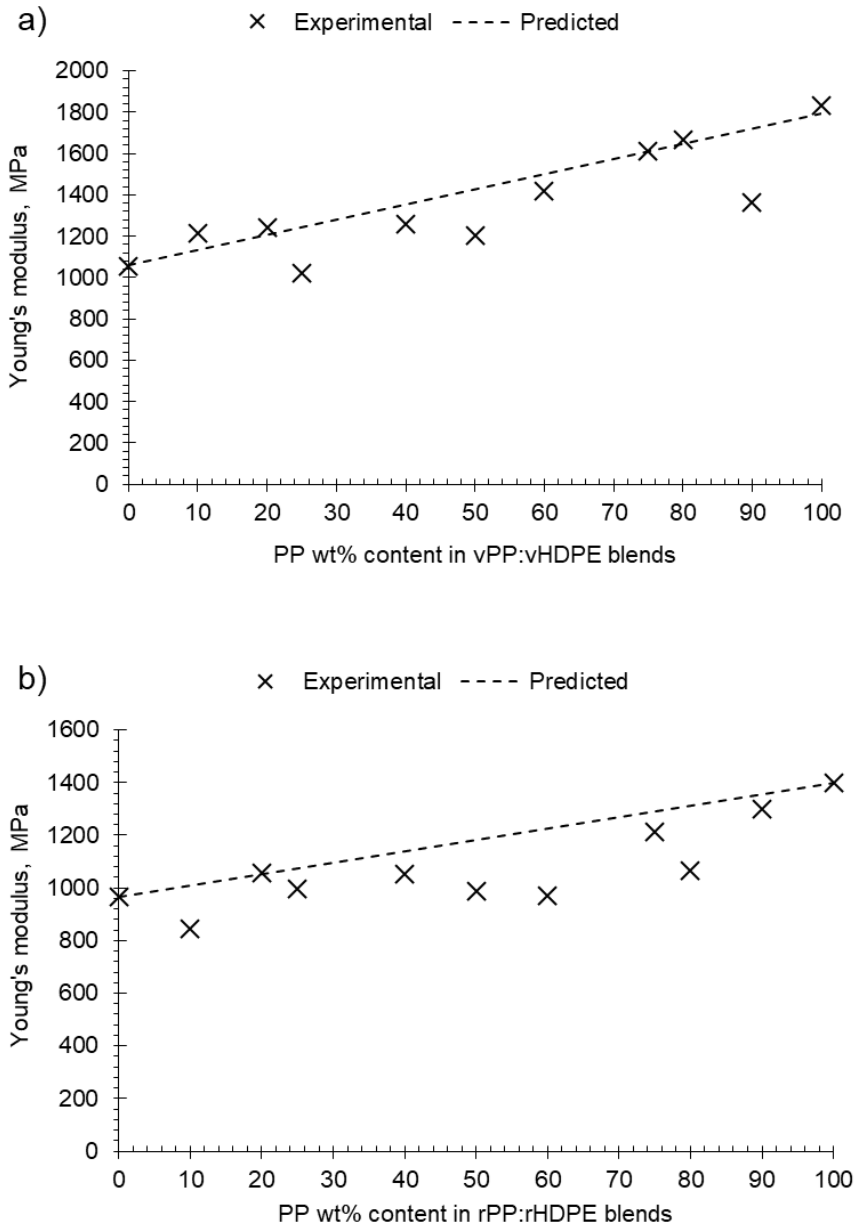

Figure 5.6 Experimental and predicted Young's modulus against PP wt% content in a) vPP:vHDPE blends and b) rPP:rHDPE blends. The predicted Young's modulus was determined by the rules of mixtures.

5.3.2.3 Yield strength and Ultimate Tensile Strength

The rPP:rHDPE blends exhibit deteriorated yield strength and UTS properties compared to the virgin blends (Figure 5.7 and 5.8). However, the rPP:rHDPE blends yield strength and UTS values were similar in value to the virgin blends above rP75. Studies have found that yield strength increases with crystallinity and lamellar thickness, with little or no effect of molecular weight.[38] Additionally, the UTS has been

found to linearly increase with crystallinity.[39] Generally, the crystallinity of the recycled blends is lower compared to the virgin blends and the recycling process results in the formation of imperfect crystals, which was discussed in chapter 4. Hence, causing a reduction in the yield strength and UTS. Generally, there was little variation in the yield strength and UTS for the rPP:rHDPE blends observed.

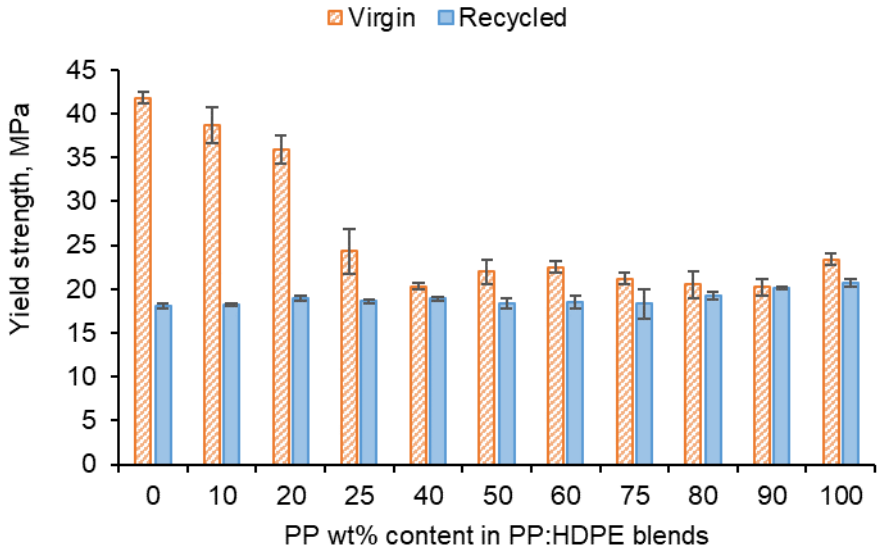

Figure 5.7 Comparison of the yield strength for vPP:vHDPE and rPP:rHDPE blends obtained from tensile testing.

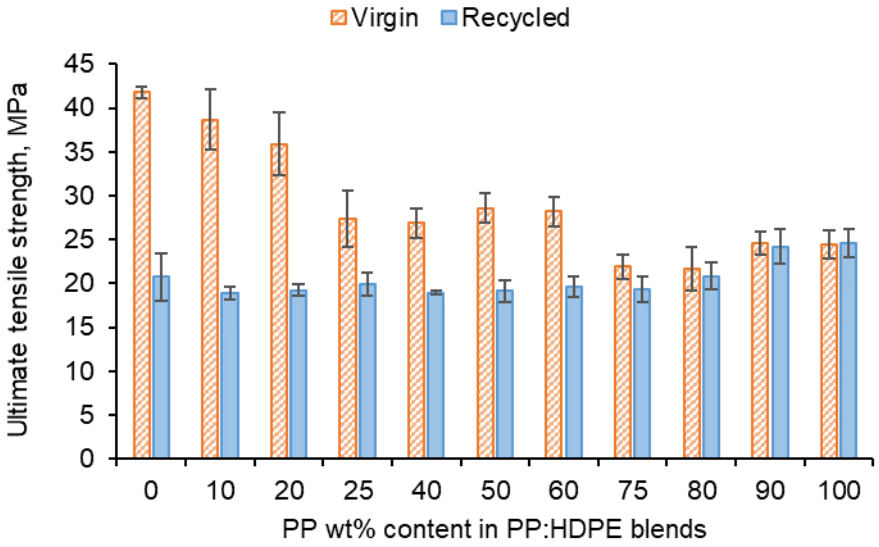

Figure 5.8 Comparison of the ultimate tensile strength for vPP:vHDPE and rPP:rHDPE blends obtained from tensile testing.

When analysing the vPP:vHDPE, the vHDPE demonstrated unexpected behaviour in yield strength, 42 MPa (Figure 5.7) and UTS (Figure 5.8). While conducting the tensile

test, vHDPE did not show typical necking behaviour and a brittle fracture was observed. Initially, it was thought an increase in crystallinity was the cause; however, no change in crystallinity was found when comparing the HDPE crystallinity before and after extrusion and injection moulding by DSC. During the injection moulding process, the polymer melt is exposed to a strong shear and elongational flow in which the chains are stretched and become highly orientated.[40] Flow induced crystallisation increases the HDPE crystallisation rate and forms a highly orientated shish-kebab structure which improves the strength of HDPE.[41] Lei et al.[42] found no necking behaviour when vHDPE was blended with 4% ultra-high molecular weight PE prepared by twin screw extruder and dynamic injection moulding. An increase in the tensile strength in the flow direction was observed from 23 to 76 MPa which was caused by the formation of web-like shish-kebab morphology and chain orientation. Therefore, the high chain orientation of the vHDPE could result in an interlocking of the shish-kebab to form a rigid structure which affected the yield strength and UTS up to vP25 blend.[42-44] The rHDPE did not exhibit the same unexpected behaviour as vHDPE in the yield strength and UTS. This is most likely due to the presence of lower molecular weight chains caused by the recycling processing which have a reduced packing ability and degree of orientation. Additionally, the presence of micro-voids can result in a decrease in compatibility between polymeric components.[45]

5.3.2.4 Elongation at yield

Generally, the rPP:rHDPE blends exhibited a lower elongation at yield in comparison to the virgin blends (Figure 5.9). The recycled blends have shorter range of elastic deformation due to degradation mechanisms during recycling so the yield point is observed at shorter elongations. The unexpected behaviour of vHDPE to vPP:vHDPE 25:75 wt% blend which was observed in the yield strength is observed in the elongation at yield. The possible presence of interlocking rigid crystal structure in vHDPE, as suggested in the yield strength discussion, could explain the low elongation yields obtained.

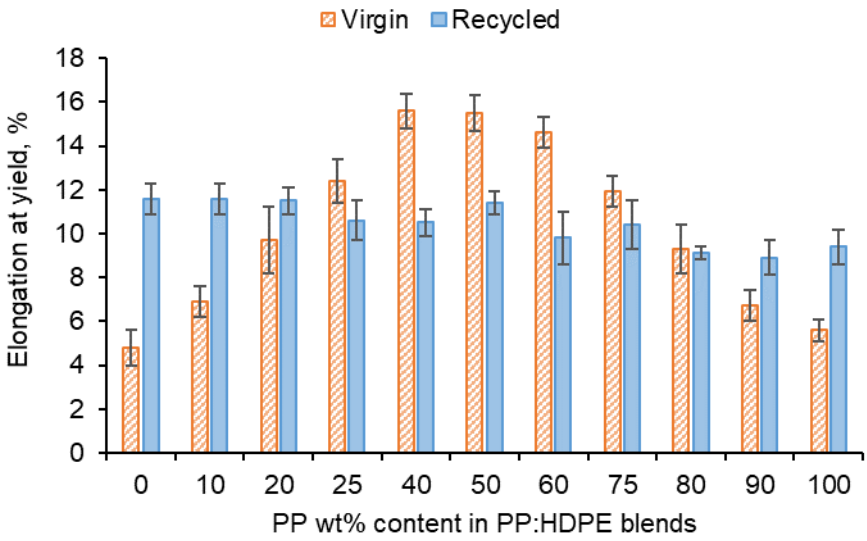

Figure 5.9 Comparison of the elongation at yield for vPP:vHDPE and rPP:rHDPE blends obtained from tensile testing.

5.3.2.5 Elongation at break

The comparison between the elongation at break for the virgin and recycled blends presents interesting results (Figure 5.10). It was expected that recycled blends would have a lower elongation at break compared to the virgin blends due to the structural deterioration during recycling causing a reduction in molecular weight.[46] For example, Fang et al.[16] found that on addition of rPP up to 15 wt% in a PP:PE blend, the elongation at break decreased and over 30 wt% the elongation at break reached a minimum. However, the longer elongation at break observed for recycled blend could be due to the presence of lower molecular weight polymer chains caused by the recycling process.[47] It is possible that the low molecular weight polymer chains locate at the interface between PP and HDPE phases and lower the interfacial tension.[47] Additionally, the lower molecular weight chains increase the capability of molecules sliding over each other resulting in an increase in deformability.[46] The vHDPE up to vP25 presented extremely low elongation at break and samples exhibited brittle fractures. The data sheet provided by Ineos suggests an elongation at break value of 800 % for vHDPE at 2 in min^{-1}. As discussed in the yield strength and UTS, this behaviour could be due to formation of a very rigid crystalline structure, which would explain the brittle fracture observed. Due to this behaviour, a comparison between the virgin and recycled blends is difficult.

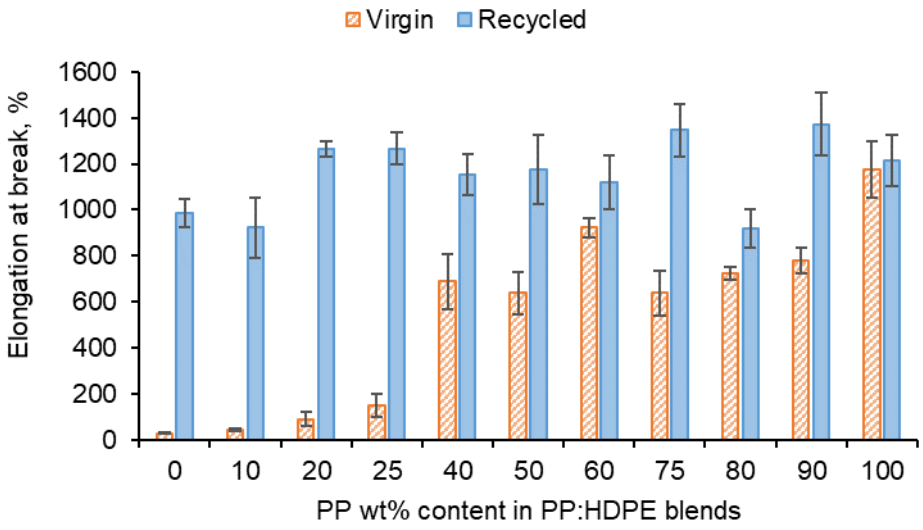

Figure 5.10 Comparison of the elongation at break for vPP:vHDPE and rPP:rHDPE blends obtained from tensile testing.

5.4 Conclusion

This chapter has presented the mechanical properties of virgin and recycled PP:HDPE blends by DMA and tensile testing over a range of compositions. DMA analysis found little variation in the *E'* and *E''* of the virgin and recycled blends with composition. The virgin and recycled blends demonstrated the presence of α and β transitions. The γ transition was not observed as it lies outside the temperature range of the DMA experiment. The T_β observed was associated with PP and not HDPE most likely due to the low proportion of amorphous domains compared to crystalline domains. The recycled blends were found to have lower T_α and T_β due to structural deterioration caused by the recycling process.

From comparing the tensile properties it was found that generally recycled blends had lower Young's modulus, yield strength, elongation at yield and UTS in comparison to virgin blends. However, it was difficult to compare the virgin and recycled blends directly due to the unexpected behaviour of the vHDPE up to vP25. The vHDPE behaviour could be caused by polymer melt being exposed to strong shear and elongation flow during the injection moulding process. Therefore, forming a highly orientated, potentially interlocking crystalline structure, which would significantly increase the strength. Generally, the recycled blends gave a higher elongation at break compared to the virgin blends possibly due to a decrease in interfacial tensile

as the low molecular weight chain align at the PP-HDPE interface. Overall, the tensile behaviour of rPP:rHDPE blends were not substantially affected by the recycling process.

References

1. A. A. Cuadri, J. E. Martín-Alfonso, *Polymer Degradation and Stability* **2017**, *141*, 11.
2. A. S. F. Santos, J. A. M. Agnelli, D. W. Trevisan, S. Manrich, *Polymer Degradation and Stability* **2002**, *77*, 4410447.
3. T. A. Oliveira, R. R. Oliveira, R. Barbosa, J. B. Azevedo, T. S. Alves, *Carbohydrate Polymers* **2017**, *168*, 52.
4. P. Oblak, J. Gonzalez-Gutierrez, B. Zupančič, A. Aulova, I. Emri, *Polymer Degradation and Stability* **2015**, *114*, 133.
5. H. M. d. Costa, V. D. Ramos, M. G. d. Oliveira, *Polymer Testing* **2007**, *26*, 676.
6. K. H. Ha, M. S. Kim, *Materials & Design* **2012**, *34*, 252.
7. J. Dostál, V. Kašpárková, M. Zatloukal, J. Muras, L. Šimek, *Eur. Polym. J.* **2008**, *44*, 2652.
8. J. Aurrekoetxea, M. A. Sarrioonandia, I. Urrutibeascoa, M. L. Maspoch, *Journal of Materials Science* **2001**, *36*, 2607.
9. H. Jin, J. Gonzalez-Gutierrez, P. Oblak, B. Zupančič, I. Emri, *Polymer Degradation and Stability* **2012**, *97*, 2262.
10. S. Saikrishnan, D. Jubinville, C. Tzoganakis, T. H. Mekonnen, *Polymer Degradation and Stability* **2020**, *182*, 109390.
11. C. Aumnate, N. Rudolph, M. Sarmadi, *Polymers* **2019**, *11*
12. V. S. Cecon, P. F. D. Silva, K. L. Vorst, G. W. Curtzwiler, *Polymer Degradation and Stability* **2021**, *10*, 109627.
13. T. I. T. N. Hasanah, D. C. Wijeyesekera, A. J. M. S. Lim, B. Ismail, *Applied Mechanics and Materials* **2013**, *465-466*, 932.
14. A.A.S Mariam Atiqah, H.Salmah, Z. Firuz, D. N. U. Lan, *Key Engineering Materials* **2014**, *494*, 837.
15. N. K. Madi, *Mater. Des.* **2013**, *46*, 435.
16. C. Fang, L. Nie, S. Liu, R. Yu, N. An, S. Li, *Composites Part B: Engineering* **2013**, *55*, 498.
17. A. Shrivastava, in *Introduction to Plastics Engineering: Plastics Design Library*, S. Ebnesajjad, Williams Andrew Applied Science Publishers, 2018, Ch. 3.
18. R. E. Wetton, in *Developments in Polymer Characterisation* Dawkins, Elsevier Applied Science Publications, 1986, Ch. 5.

19. L. E. Nielsen, *Predicting the properties of mixtures : mixture rules in science and engineering*, M. Dekker, **1978**.
20. S. S. Ray, *Environmentally Friendly Polymer Nanocomposites: Types, processing and properties*, Woodhead Publishing Limited, **2013**.
21. M. A. Hidalgo-Salazar, J. P. Correa-Aguirre, S. Garcia-Navarro, L. Roca-Blay, *Polymers* **2020**, *12*, 1507.
22. K. Sewda, S. N. Maiti, *Polym. Bull.* **2013**, *70*, 2657.
23. N.G McCrum, B.E Read, G. Williams, *Anelastic and dielectric effects in polymeric solids*, Dover Publications Inc, **1991**.
24. M. Sethi, N. K. Gupta, A. K. Srivastava, *J. Appl. Polym. Sci.* **2002**, *86*, 2429.
25. E. Suljovrujic, M. Micic, D. Milicevic, *J. Eng. Fibers Fabr.* **2013**, *8*, 131.
26. J. Gu, H. Xu, C. Wu, *Adv. Polym. Technol.* **2014**, *33*, 21384.
27. R. Popli, M. Glotin, L. Mandelkern, R. S. Benson, *J. Polym. Sci., Polym. Phys. Ed.* **1984**, *22*, 407.
28. E. Karaagac, T. Koch, V. M. Archodoulaki, *Waste Manage.* **2021**, *119*, 285.
29. Y. P. Khanna, E. A. Turi, T. J. Taylor, V. V. Vickroy, R. F. Abbott, *Macromolecules* **1985**, *18*, 1302.
30. S. Fakirov, B. Krasteva, *J. Macromol. Sci., Part B: Phys.* **2000**, *39*, 297.
31. J. Hopewell, R. Dvorak, E. Kosior, *Philosophical Transactions of The Royal Society B* **2009**, *364*, 2115.
32. B. A. Morris, in *The Science and Technology of Flexible Packaging: Multilayer Films from Resin and Process to End Use*, B. A. Morris, William Andrew Publishing, 2017, Ch. 4.
33. W. D. Callister, D. G. Rethwisch, *Fundamentals of Materials Science and Engineering. An Integrated Approach*, John Wiley & Sons, **2016**.
34. K. Ragaerta, L. Delva, K. V. Geem, *Waste Manage.* **2017**, *69*, 24.
35. L. A. Pinheiro, M. A. Chinelatto, S. V. Canevarolo, *Polym. Degrad. Stab.* **2004**, *86*, 445.
36. S. Jose, A. S. Aprem, B. Francis, M. C. Chandy, P. Werner, V. Alstaedt, S. Thomas, *Eur. Polym. J.* **2004**, *40*, 2105.
37. A. J. Lovinger, M. L. Williams, *J. Appl. Polym. Sci.* **1980**, *25*, 1703.
38. R. A. Chivers, D. R. Moore, *Polymer (Guildf)* **1994**, *35*, 110.
39. F. Addiego, A. Dahoun, C. G'Sell, J. Hiver, O. Godard, *Polymer Engineering and Science* **2009**, *49*, 1198.

40. H. R. Yang, J. Lei, L. Li, Q. Fu, Z. M. Li, *Macromolecules* **2012**, *45*, 6600.
41. B. Zhao, X. Li, Y. Huang, Y. Cong, Z. Ma, C. Shao, H. An, T. Yan, L. Li, *Macromolecules* **2009**, *42*, 1428.
42. J. Lei, Z. Zhang, C. Jiang, K. Shen, *Polymer International* **2006**, *55*, 1021.
43. C. Deng, J. Lei, X. Gao, Z. Chen, K. Shen, *Polym.-Plast. Technol. Eng* **2010**, *47*, 716.
44. R. K. Bayer, F. J. B. Calleja, E. L. Cabarcos, H. G. Zachiviann, A. Paulsen, F. Brüning, W. Meins, *J. Mater. Sci.* **1989**, *24*, 2643.
45. D. Murugan, S. Varughese, T. Swaminathan, *Polym.-Plast. Technol. Eng* **2006**, *45*, 885.
46. F. P. L. Mantia, L. Botta, M. C. Mistretta, A. D. Fiore, V. Titone, *Polymers* **2020**, *12*, 2297.
47. A. Dorigato, *Advanced Industrial and Engineering Polymer Research* **2021**, *4*, 53.

6.0 AFM QI Mode Investigation of Virgin and Recycled PP:HDPE Blends

6.1 Introduction

This chapter aims to provide further understanding of the morphology present in virgin and recycled PP:HDPE blends using the QI AFM mode. The QI mode is a new mode of action which generates quantitative data of mechanical interest, and is based on force spectroscopy imaging. Force spectroscopy measures cantilever deflection as the cantilever-sample surface distance changes.[1] For every pixel, the QI mode generates a complete force distance plot from which the Young's modulus and adhesion can be calculated[2] (Figure 6.1). The force-distance plots can be divided into three stages[1,2]:

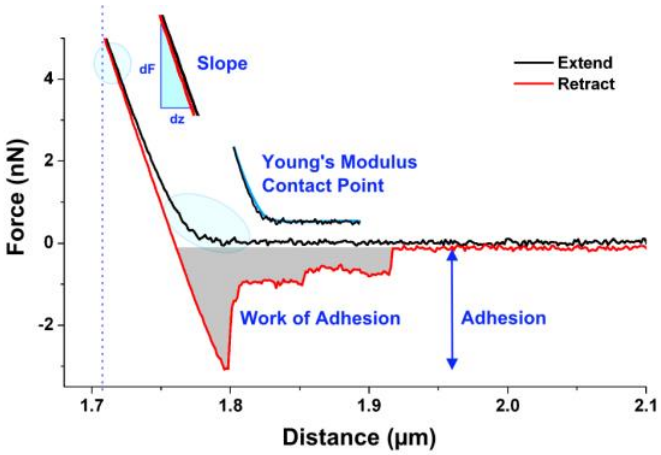

Figure 6.1 Force-distance curve showing the extended and retracted paths along with a summary of the extraction of the mechanical properties; Young's modulus and adhesion.[2]

Stage 1: Approach

As piezo moves towards the sample, the cantilever approaches the surface and the tip begins to experience long distance interactions. Typically, these interactions are at very small forces so the cantilever remains unaffected e.g. no deflection. At nanometers to atomic distances away, the tip experiences strong attractive forces, such as van der Waals, with the surface causing a "snap-in" into contact.

Stage 2: Contact

The tip touches, compresses and in some cases indents the surface with a pre-determined force. During tip-sample contact, the cantilever is deflected and the interaction is repulsive.

Stage 3: Retraction

As the piezo moves away, the cantilever begins to retract from the surface to the set-point height, the tip remains deflected and in contact with the surface. This is caused by adhesion between the tip and the surface. At some point “pull-off” will occur where the force applied is enough for the cantilever to overcome the adhesion. The tip will break contact with the surface.

The change in cantilever deflection during the approach – contact – retraction stages causes the reflective laser beam to change position on the four quadrant photodiode which delivers an electric signal in volts which is then converted into either units of distance or force.[2,3] The cantilever can be considered as a spring and cantilever deflection is directly proportional to the force applied and is calculated using Hooke’s Law (Equation 6.1)[2,4]

$$F = -kx \tag{6.1}$$

where F is force, k is the cantilever’s spring constant and x is the cantilever deflection expressed as a distance.

The QI mode differs from force spectroscopy by offering a higher scan velocity and the option to adjust parameters in the single force curves and the pixel to pixel movement. There is no feedback loop in QI mode allowing for independent pixel imaging and no optimisation required during imaging.[2,5] As there is complete cantilever retraction between pixels the QI mode has the ability to scan sticky, soft and loosely attached samples; can be used at very low imaging forces and on rough samples.[2] The QI mode has mainly been used for the imaging and determination of the mechanical properties for biological cells[6-8], but it has been effectively used on polymer nanocomposites.[9,10] The literature is limited on the use of the AFM to determine the morphology of PP:HDPE blends. In particular, the QI mode has not been seen in the literature to determine the morphology and Young’s moduli for virgin and recycled PP:HDPE blends. Therefore, this chapter aims to contribute to the missing knowledge and provide a deeper understanding of the processing-structure-property relationship for extrusion mixing and injection moulded virgin and recycled PP:HDPE blends.

6.2 Methodology

6.2.1 Sample Preparation

A “V” shaped notch was made in the centre of each virgin and recycled PP:HDPE blend. Each sample was submerged in liquid nitrogen for 10 minutes. On removal the sample was fractured in the centre to enable AFM scanning of the sample’s cross section. Pressurised air was passed over the cryo-fractured surface to removed debris. The cryo-fractured samples were adhered to a glass slide using double sided sticky tape.

6.2.2 QI Mode Procedure

AFM was carried out on the cryo-fracture virgin and recycled PP:HDPE blend surfaces using a Bruker/JPK AFM, Nanowizard 4 XP, in QI mode.[5] The JPK SPM software was used for acquiring the QI data and images. All imaging was carried out in air at ambient temperature.

6.2.2.1 Cantilevers

A NTESPA model cantilever was used throughout and purchased from Bruker (Table 6.1). Cantilevers were rectangular in geometry and made from antimony doped silicon. The nominal spring constant was 40 N m^{-1} which reflects a stiff cantilever. The nominal tip radius was 8 nm.

Table 6.1 Summary of the cantilever specification (NTESPA model) used in the AFM QI Mode obtained from Bruker.

Model	Material	Dimensions	Coating
NTESPA	0.01-0.025 Ωcm antimony (n) doped silicon	Thickness (T): 3.75 µm Length (L): 125 µm Resonant frequency (f_0): 300 kHz Spring constant (k): 40 N m^{-1}	Front Side: None Back Side: Reflective aluminium

6.2.2.2 Calibration

Manufacturers provide an approximate spring constant within a specified range for the cantilever. Calibration is an important process to ensure the precision of the cantilever's sensitivity and spring constant. During an AFM scan, the cantilever deflection is measured through the changing laser position on the four quadrant photodiode.[5] The photodiode signal is measured in volts so the calibration process converts the vertical cantilever deflection from volts to units of length or force.[5] Calibration ensures the accuracy for the tip-sample force and hence, the values of mechanical properties obtained.[3]

Contact free calibration was carried out before each measurement. In contact free calibration, the cantilever does not touch the surface unlike contact based calibration. This method of calibration was preferred over contact based calibration to prevent damaging the cantilever tip as there no requirement to obtain a force curve in advance of calibration. Contact free calibration involves acquiring a thermal noise measurement to determine the quality factor Q and resonance frequency; and the user inputting the physical environmental conditions (Temperature: 25 °C, environment: air) and the cantilever model/ dimensions. The JPK software then calculates the spring constant and sensitivity of the cantilever. The cantilever spring constant calculation (Equation 6.2) is based on the theory presented by Sader et al.[11] who suggested;

$$k = 0.1906\rho_f b^2 L Q_f \Gamma_i(\omega_f)\omega_f^2 \qquad (6.2)$$

where *k* is the spring constant, ρ_f is the density of the fluid, *b* is the cantilever width, *L* is the cantilever length, Q_f is the quality factor in fluid, Γ_i is the imaginary components of the hydrodynamic function Γ and ω_f is the fundamental mode resonant frequency.

Sader et al.[11] suggest that the spring constant is related to the dimensions of the cantilever. It is important to note that Equation 6.2 can only be applied to rectangular shaped cantilevers.

6.2.2.3 QI Mode Settings

After calibration the sample properties are inputted into the JPK SPM software: “”Expected height” of the features were 300 nm and “Adhesion” was medium. From the inputted sample properties the JPK SPM software calculates suggested imaging parameters. The QI Control window enabled modification of the suggested parameters. The “set point” which determine the maximum force applied to the surface ranged between 85 – 100 nN and the “z length” which determines the distance covered by the piezo during the force curve ranged between 0.1 to 0.15 µm. Speed of imaging was 53.6 µm s^{-1}. The parameters were altered if on examination of the force curves break through events were observed or the baseline was tilted upwards. Additionally, the QI Control window enabled the scan size to be set to either 5 x 5 μm^2 or 10 x 10 μm^2 along with the scan resolution, changeable by the number of pixels: 256 x 256 pixels (lowest resolution image), 512 x 512 pixels or 1024 x 1024 pixels (highest resolution image).

6.2.2.4 Capturing QI Images and Data

Scans were taken at sites throughout the sample to understand the morphology. Each scan generated QI data and images. The images of interest were height measured, stiffness and adhesion. The measured height corresponds to the height at 80% of the set point force of the smoothed extended curves. For each sample, images of varying resolution were taken due to high resolution scans taking longer periods of time. For example, high resolution 1024 x 1024 pixel scan took a minimum of 2 hours so was reserved for areas of interest. Each sample had the following: 2 scans x 1024 pixels, 1 scan x 512 pixels, 5 or more scan at 256 pixels. Additional scans not presented in this chapter are shown in Appendices 1 to 8. JPK SPM Data Analysis package (version 7.0.128) was used for QI image and data analysis.[12]

6.2.3 Data Analysis

6.2.3.1 QI Image Analysis

The JPK SPM Data Analysis software enables the QI-image files obtained to be processed. The processing operations undertaken for stiffness, height measured, and adhesion images for the virgin and recycled PP:HDPE blends are summarised in Table 6.2.

Table 6.2 Summary of the typical processing operations undertaken by the JPK SPM Data Analysis Software on the stiffness, height and adhesion images.

Image	**Linear Plane Fit**	**Line Levelling**	**Median Pass Filter**	**Low Pass Filter**
Stiffness	x		x	(x)
Height	x	x	x	(x)
Adhesion	x		x	(x)

The processing operations undertaken and reasoning is listed below (Figure 6.2).[12]

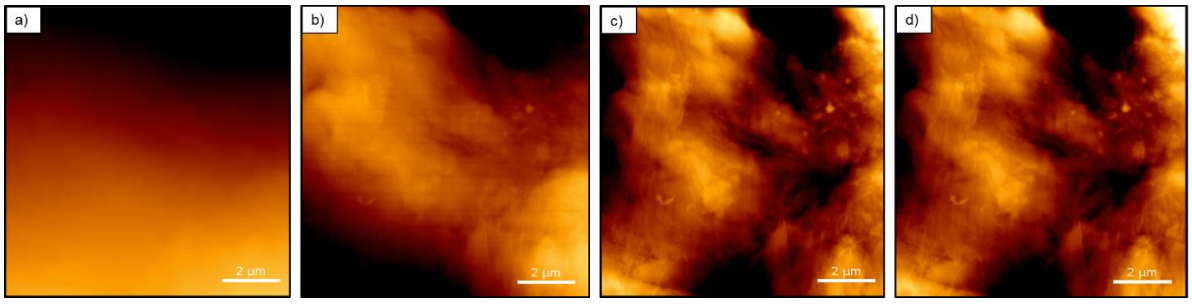

Figure 6.2 Sequential application of the processing operations to an example height image obtained for vP40. a) original height image, b) linear plane fit, c) line levelling, and d) median pass filter.

1. Linear Plane Fit

A linear plane fit of 1 was applied to the whole sample to remove the effect of an overall sample tilt in the height measured. During mounting the samples were not perfectly flat to the glass slide which consequently requires a z-data adjustment. As the linear plane fit was applied to the whole sample the relationship between adjacent scan lines remains unaffected.

2. Line Levelling

Line levelling was applied only to the height image due to the offset between adjacent scans line being noticeable. A line levelling fit of a polynomial of 1 degree was applied.

3. Median Filter

The median filter was applied to replace any outlier pixels with the median value of neighbouring pixels. The neighbouring pixels which are considered are determined by the mask shape and size. There are different masks available: constricted square, square, cross. The constricted square shape was used with a low mask width, either 5 or 7. The tolerance level was set to 3 so fewer points were considered as outliers.

4. Low Pass Filter

The low pass filter was applied to remove noise from the image. The Savitzky-Golay filter was used with a smoothing width of 5 and order 4. Not all images required the application of the low pass filter.

6.2.3.2 QI-Data Analysis

The aim of the QI-data analysis was to extract the Young's modulus. Each scan generated QI data which was saved as jpk-qi-data files. A jpk-qi-data file contained the individual force-distance curves at each pixel. To analysis the individual force-distance curves the jpk-qi-data files were split into qi-imaging series files. These files were then batched processed by applying a sequence of operations (Figure 6.3).

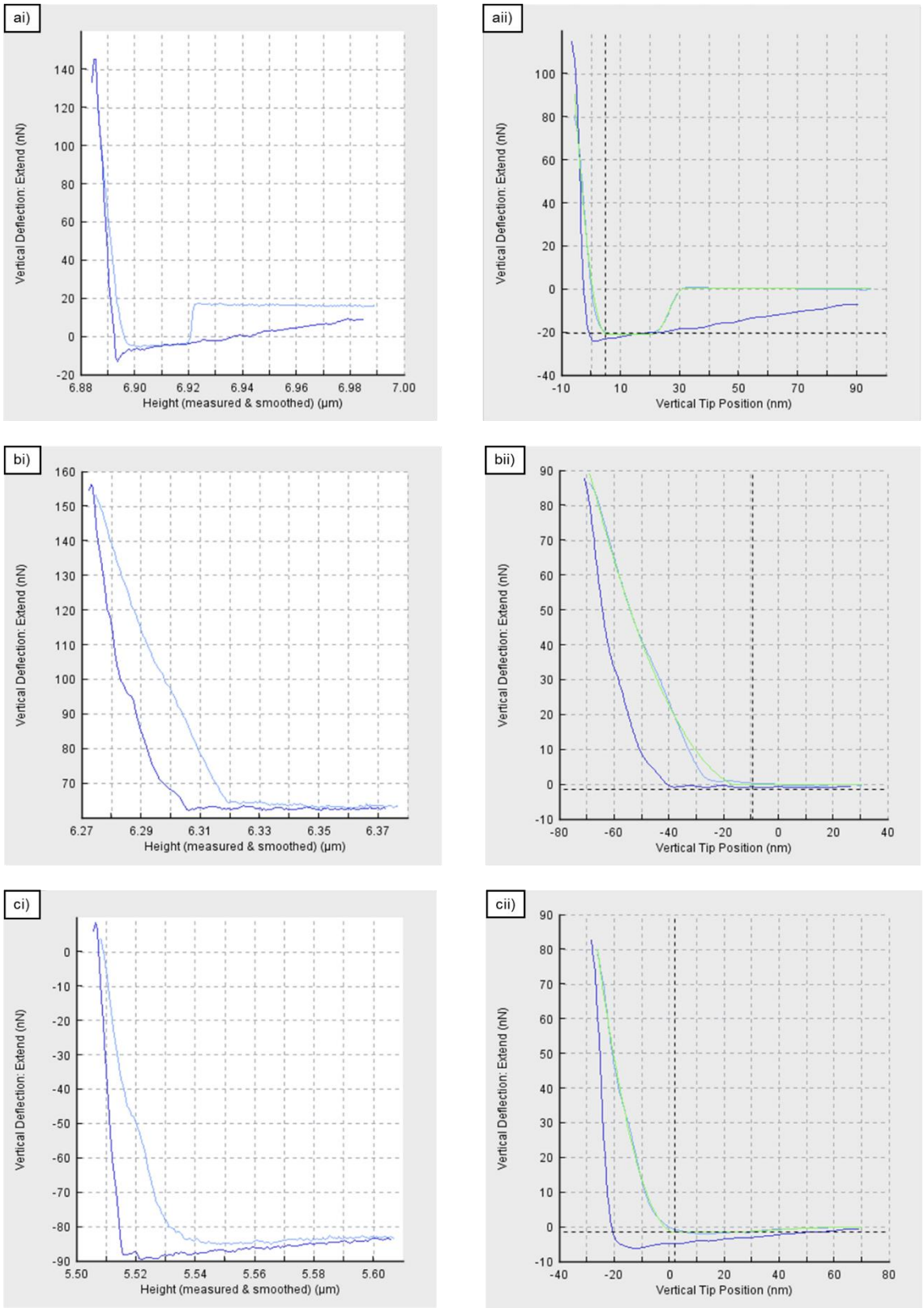

Figure 6.3 An example of the batch processing applied to a force-distance curve where i) is the raw curve and ii) the processed curve for a) vHDPE, b) vP50 and c) rP50 blends. The retract curve is shown in dark blue and the extend curve is shown in light blue. The DMT model fit is shown by the green curve.

1. Calibration

The calibration operation was applied to the vertical deflection by using value of the cantilever spring constant and sensitivity. Cantilever spring constant and sensitivity values were determined experimentally by the contact free calibration, which was carried out before each measurement.

2. Data Smoothing

The data smoothing was applied to the curves to reduce noise before applying the Derjaguin-Müller-Toporov (DMT) model. A Gaussian smoothing method was chosen and improve the fit between the data curves and DMT model.

3. Baseline Subtraction

The baseline subtraction was applied to remove baseline offset in the vertical deflection. The baseline offset is determined from the vertical deflection against position force curves. The baseline offset is an average value calculated in the flat region of the curve. Even though this region should have a zero force as there is no force between the tip and sample surface, there is usually a force present. The force present could be caused by environmental factors altering the deflection. The baseline offset is applied to the whole curve.

4. Contact Point

The contact point operation adjusts height offset (x axis) by calculating the point where the force curve first crosses axis and sets this point to zero.

5. Vertical Tip Position

The vertical tip position operation was applied to allow the elastic fit operation to be fitted. The vertical tip operation corrects the height signal for the cantilever deflection. The height signal is derived from piezo displacement so includes both the distance the cantilever is moved towards the sample and the deflection of the cantilever. However, to enable the calculation of the Young's modulus, the force against vertical tip position is required rather than piezo displacement.

6. Elasticity fit

The elasticity fit operation applies a contact mechanics model to the extended curve to determine the Young's modulus of the scan region.

6.2.3.3 Contact Mechanic Models

The JPK SPK software offers two model options: Hertz Model and DMT.

Hertz model

Hertz model has been used to determine the Young's modulus of a range of polymers such as polycarbonate (PC), poly(methyl acrylate) (PMMA) and PP.[13,14] The Hertz model is based on the elastic deformation of two spherical bodies with radii R_1 and R_2.[15] When a force is applied, the region of contact between the two spheres deforms elastically to form a circular contact area. This model focuses on non-adhesive contact, assumes no surface forces, and can be applied to sphere-on-sphere and on sphere-on flat geometry scenarios.[15]

The Hertz model also makes the following assumptions[15-17]:

- The bodies are homogenous, isotropic and exhibits linear elastic behaviour.
- Each body is considered to be an elastic half space.
- There are no attractive interactions.
- Surfaces are frictionless and continuous.
- The strain is small in comparison to the body's dimensions (no major plastic deformation).

Hertzian contact of two spheres

Under the assumptions stated above, the contact radius, a, and total deformation, δ, can be calculated by:

$$a = \left(\frac{3RF_L}{4E^*}\right)^{1/3} \tag{6.3}$$

$$\delta = \frac{a^2}{R} = \left(\frac{9F_L^2}{16RE^{*2}}\right)^{1/3} \tag{6.4}$$

where R is the composite radius of curvature, F_L is the applied load force and E^* is the effective elastic modulus.

With the composite radius of curvature, R, given by

$$\frac{1}{R} = \frac{1}{R_1} + \frac{1}{R_2} \quad (6.5)$$

where R_1 and R_2 are the radii of the spheres 1 and 2 respectively,

and the effective elastic modulus, E^*, given by

$$\frac{1}{E*} = \frac{1-\nu_1^2}{E_1} + \frac{1-\nu_2^2}{E_2} \quad (6.6)$$

where E_1 and E_2 are the elastic moduli of the spheres 1 and 2 respectively, and ν_1, ν_2 is the poison ratio for sphere 1 and 2 respectively.

Hertzian contact between sphere and a flat surface

In the case of an AFM experiment, the tip touches, compresses and in some cases indents a surface, so a sphere on flat geometry is appropriate. The Hertz model assumes that the tip is a perfect sphere and indents a flat, smooth surface with an indentation depth significantly less than the tip radius. This is achieved by setting the radius R_1 and elastic modulus E_1 to infinite. This gives rise to the following Equation[16]

$$F_L = \frac{4}{3}\frac{E}{1-\nu^2} R^{\frac{1}{2}} \delta^{\frac{3}{2}} \quad (6.7)$$

where F_L is the force applied, E is the Young's modulus of the sample, ν is the poison ratio of the sample, R is the tip radius and δ is the indentation depth.

By applying the Hertz model to the initial repulsive region of the extend curve in the force-distance plot, the Young's modulus can be calculated from the applied force and the measured deformation.[13]

DMT Theory

The DMT[18] theory is an extension of the Hertz model which accounts for adhesion between an elastic spherical body on a flat/rigid surface or between two spherical bodies. In AFM experiments, the DMT theory takes into account the attractive forces between the tip and the sample surface. DMT is applicable to solid surfaces of weak energy of adhesion with small asperities.[15] The DMT theory assumes that the attractive adhesion stress does not affect the deformation of the bodies.[19] Adhesive stresses act outside the contact area.[19] Deformation is caused by the effective force of the tip on the sample surface[15],

$$F_{eff} = F_L + F_{ad} \tag{6.8}$$

where F_{eff}, F_L and F_{ad} are the effective total force, external applied force and the adhesion force respectively.[17,19]

The adhesive force (F_{ad}) is assumed to be constant when the tip is in contact with the surface. The adhesive force is quantified by[20]

$$F_{ad} = 2\pi R\Delta\gamma \tag{6.9}$$

$$\Delta\gamma = \gamma_1 + \gamma_2 - \gamma_{12} \tag{6.10}$$

where R is the equivalent radius of curvature, γ_1 and γ_2 are the surface energies of the bodies and γ_{12} is the interfacial energy.

So the DMT theory can be written as;

$$\frac{4E^* a^3}{3R} = F_{eff} - 2\pi R\Delta\gamma \tag{6.11}$$

where E^* is the effective elastic modulus and a is the radius of contact.

JPK SPM Software Input

To determine the Young's modulus, the DMT model was implemented and applied to each individual extended force curve generated in a scan. After the DMT model was selected the following was inputted into the software:

- Tip Shape: Quadratic Pyramidal. The software applies a modification factor to correct for the tip geometry as the Hertz/DMT model applies to tips of circular geometry (Equation 6.12).

$$F = 0.7453\frac{E}{1-\nu^2}\delta^2\tan\alpha \qquad (6.12)$$

$$a_e = 0.709\delta\tan\alpha$$

where *F* is the force, *E* is the Young's modulus, ν is the Poisson's ratio, δ is the indentation, α is the half-angle to face of a pyramid, and a_e is the equivalent radius of contact circle.

- Half-angle to face: 15.0 degrees.
- Poisson ratio is set to 0.45.

The DMT model was then applied to each force curve using the Levenberg-Marquardt algorithm.[12] If the model was successfully fitted to the data a residual RMS value was generated and each scan generated a histogram of the residual RMS values obtained (Figure 6.4). The smaller the residual RMS value the greater the quality of the fit between the DMT model and the data. If the DMT model function did not converge, no Young's modulus value was generated for that particular force curve.

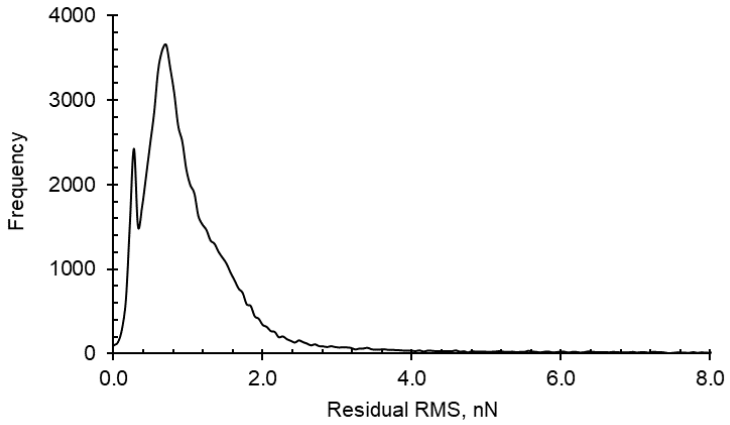

Figure 6.4 Example histogram of the residual RMS values obtained for vP50 blend of scan size 5 x 5 μm^2 and 256 x 256 pixels.

Each scan generated a histogram of distributed Young's moduli along with statistical measurements, mean and standard deviation. For each sample, the DMT model was applied to a minimum of three scan areas.

6.3 Results and Discussion

6.3.1 Influence of Topography

The height images show the surface topography by the height variation of the surface features. Surface roughness did vary for each sample (Figure 6.5). No surface was measured with a height features greater than 3 μm. These rough surfaces could result in the underside of the cantilever touching the surface causing poor surface resolution and unwanted artefacts[21]. If the surface topography is rough it can obscure small features[22], such as phase separation. In all experiments, the height images were compared to the stiffness image to ensure the stiffness image features observed were not attributed to surface topography. For example, if a feature of interest was observed in the stiffness image, a check would be carried out in the corresponding area of the height image. If no similar height feature was found, the feature of interest would attributed to the surface morphology. On the other hand, if a similar height feature was found in the corresponding area, the feature would be attributed to the topography and not morphology.

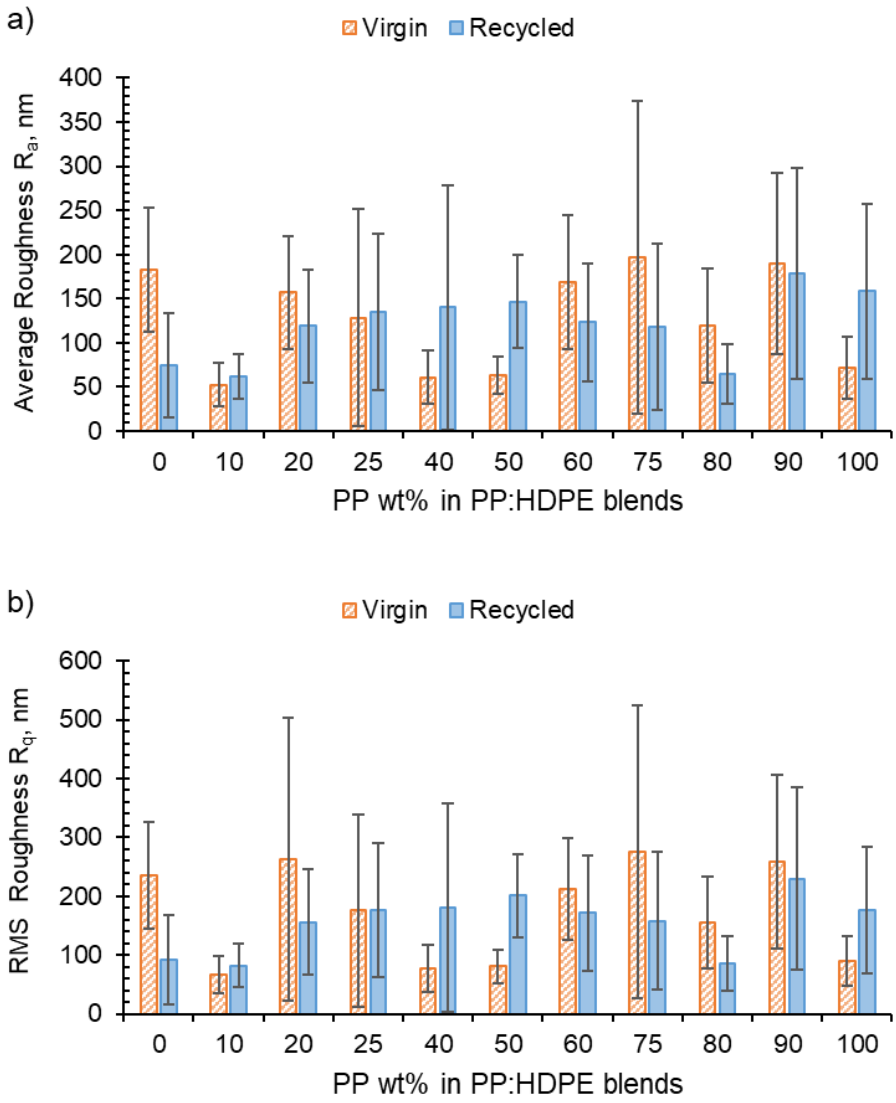

Figure 6.5 Roughness of the virgin and recycled PP:HDPE blends. An average and standard deviation over at least five scan areas were calculated are shown, a) Average roughness R_a and b) RMS roughness R_q.

6.3.2 Stiffness Images of Virgin and Recycled PP:HDPE Blends

6.3.2.1 Virgin PP:HDPE Blends

vHDPE and vPP are semi-crystalline polymers which undergo thermal induced crystallisation and flow induced crystallisation during the injection moulding process.[23] During extrusion mixing and injection moulding HDPE and PP are subjected to shear and extensional flow which alters the crystallisation kinetics and causes molecular orientation along the direction of flow, as discussed in Chapter 4.[23] Consequently, the injection moulding process produces a sample with multi-layer structure, commonly

referred to a skin-core morphology. The skin-core morphology is caused by varying shear stress and temperature gradient throughout the sample melt.[24,25] Typically, the core has low level orientation whereas the skin has high level orientation.[26] The skin layer morphology is dependent on the polymer melt viscosities and processing.[27] During crystallisation spherulites grow from nucleation sites, and contain ordered crystalline structures called lamella, which connect to amorphous polymer regions.[28] The stiffness images could provide information on the phase separated morphology formed in the PP:HDPE blends. This is due to PP and HDPE having different stiffness values. For example, it is highly likely the spherulites are observed in the vHDPE and vPP stiffness images, with the vPP spherulites being less defined (Tables 6.3 and 6.4). It is expected that the core morphology would present isotropic spherulites due to low shear influence.[29] Flow induced crystallisation can lead to a higher orientation shish-kebab structures which are typically found in the skin layer.[29,30] The formation mechanism of shish-kebab structure is still debated[24] and further investigation would be required to deduce their presence in the skin layer.

As shown in Tables 6.3 and 6.4, morphology is dependent upon the blend composition; as the PP wt% is increased from 0 to 100 % the morphology changes. Clear morphology can be observed at vP25, vP40, vP75, vP90 as droplet-matrix, continuous, droplet-matrix (phase inverted) and droplet-matrix (phase inverted) morphology respectively. It is harder to ascertain the morphology at vP10, vP20, vP50 and vP80. This could be due to the presence of skin-core morphology caused by the injection moulding process or the surface roughness which reduces the resolution. If the scan area is within the skin region, the morphology is affected greatly by the flow direction. For example, vP10, the morphology is orientated in the same direction which reduces the resolution. Additionally, the lack of detailed morphology for vP10 main be due to the addition of 10 wt% PP which obscures or affects the HDPE spherulites.

Table 6.3: AFM stiffness images of vPP:vHDPE blends at 1024 x 1024 pixels, size 5 x 5 μm^2.

vHDPE	vP10	vP20
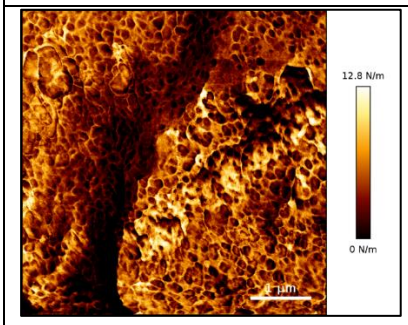	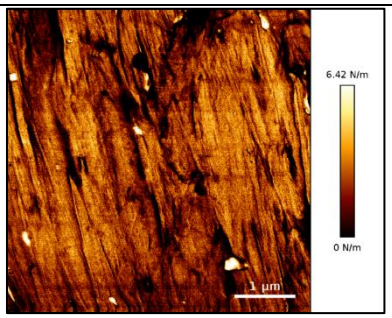	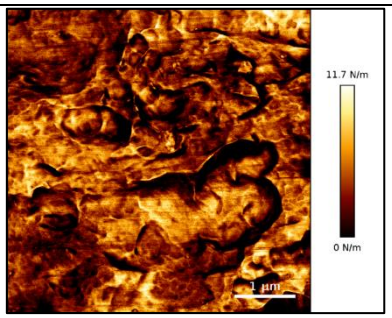
vP25	**vP40**	**vP50**
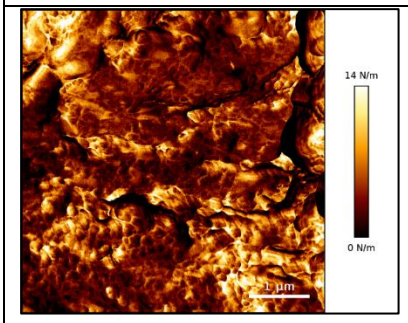	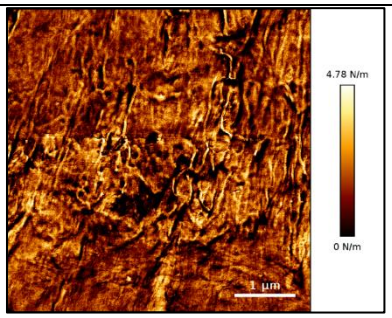	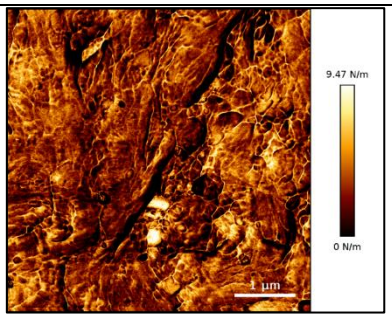
vP60	**vP75**	**vP80**
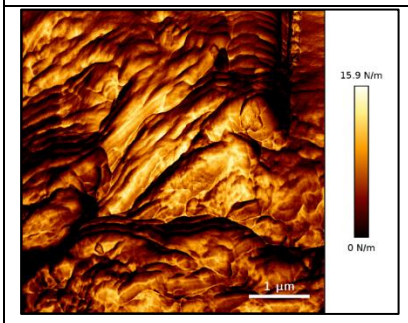	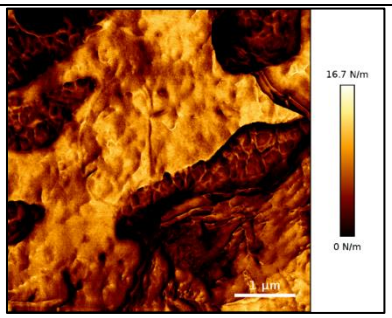	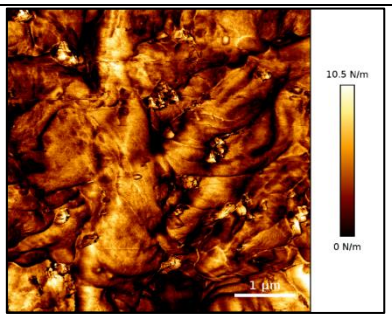
vP90	**vPP**	
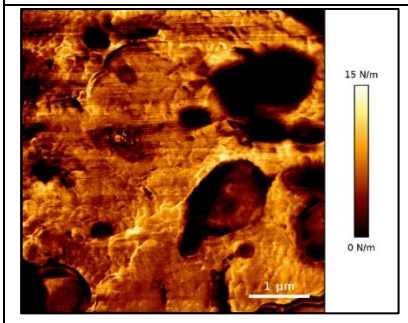	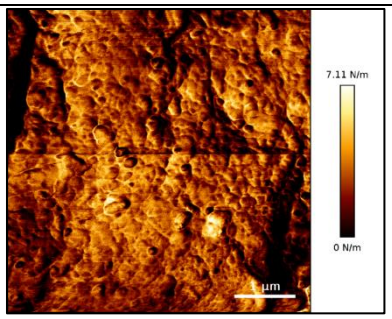	

Table 6.4 AFM stiffness images for vPP:vHDPE blends at 502 x 502 pixels, size 5 x 5 μm^2.

vHDPE	vP10	vP20
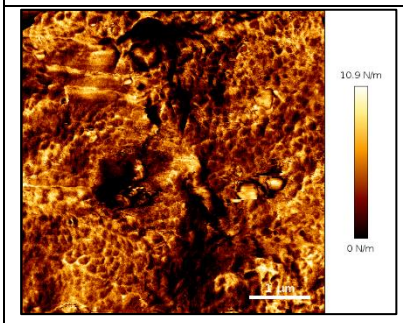	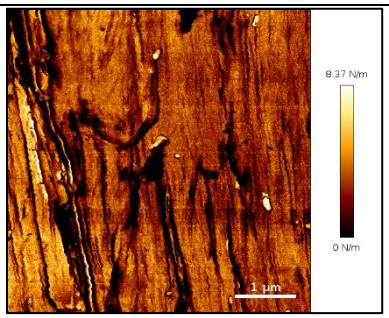	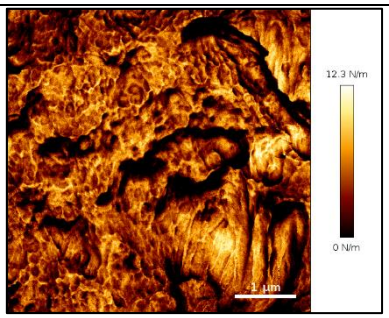
vP25	**vP40**	**vP50**
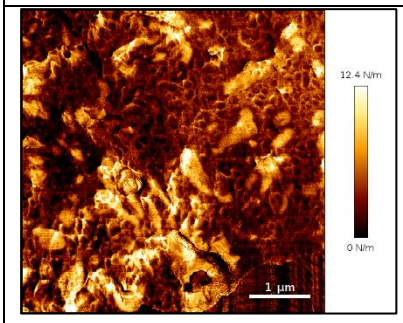	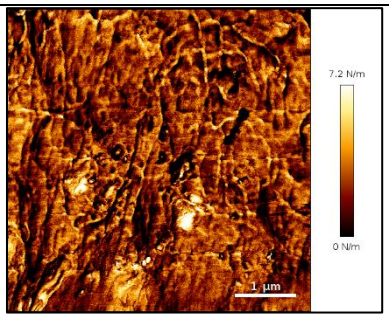	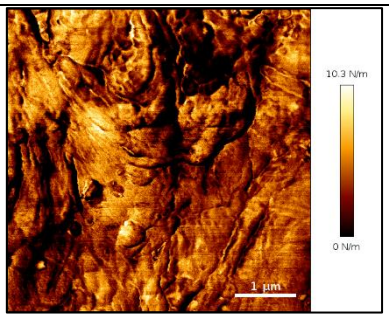
vP60	**vP75**	**vP80**
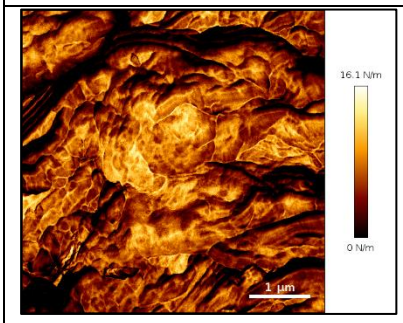	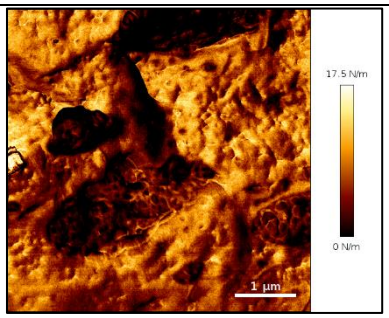	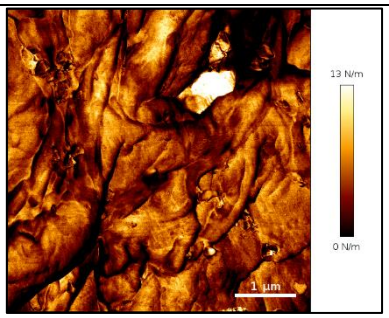
vP90	**vPP**	
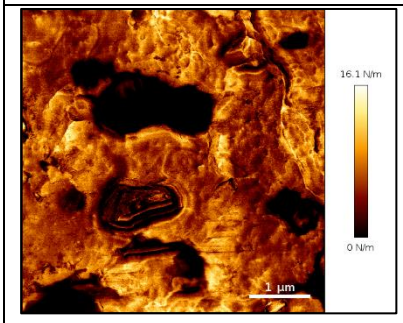	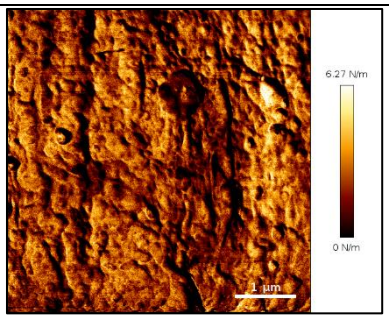	

6.3.2.2 Recycled HDPE:PP Blends

As observed in the vPP:vHDPE blends, the recycled morphology is dependent upon the blend composition (Tables 6.5 and 6.6). As the PP wt% is increased from 0% the morphology transitions from homogenous, droplet-matrix, continuous, droplet-matrix.

Table 6.5 AFM stiffness images of rPP:rHDPE blends at 1024 x 1024 pixels, size 5 x 5 μm^2.

rHDPE	rP10	rP20
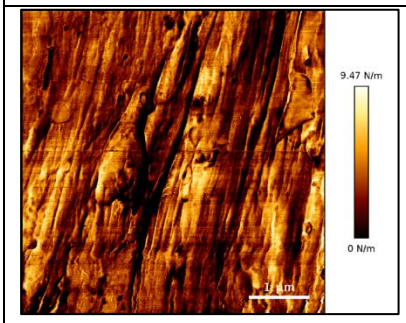	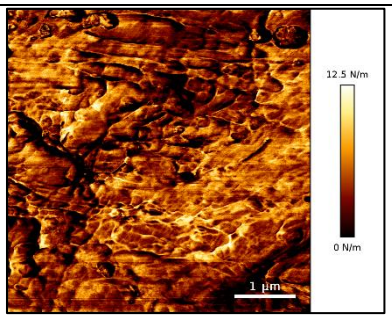	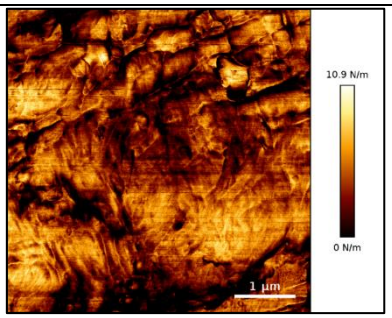
rP25	**rP40**	**rP50**
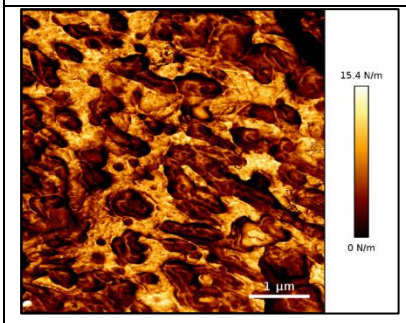	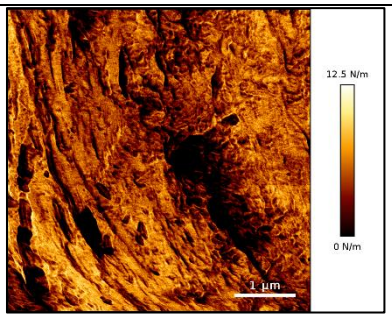	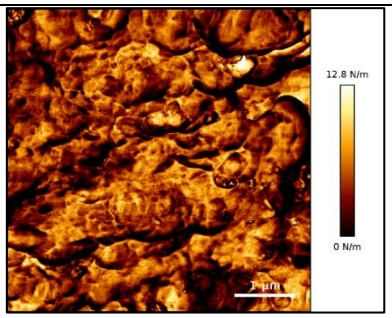
rP60	**rP75**	**rP80**
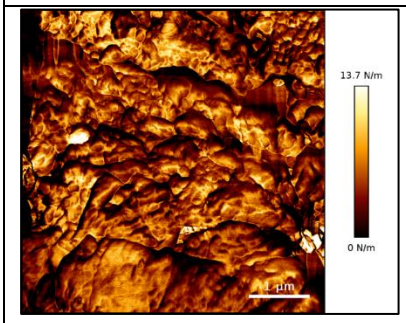	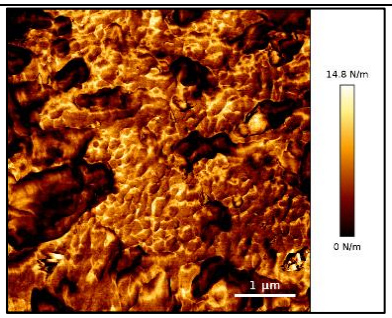	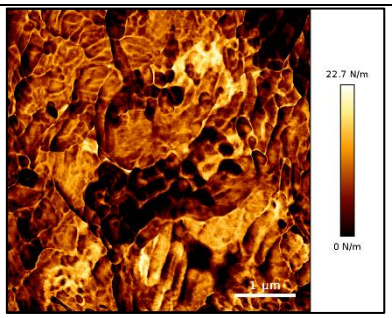
rP90	**rPP**	
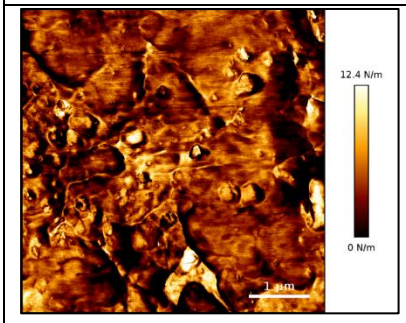	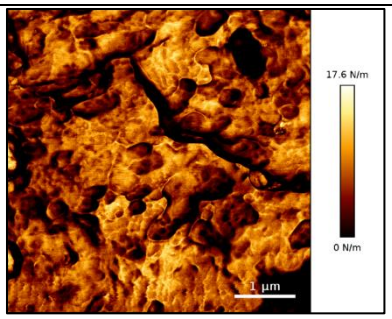	

Table 6.6 AFM stiffness images for rPP:rHDPE blends at 502 x 502 pixels, size 5 x 5 μm^2.

rHDPE	rP10	rP20
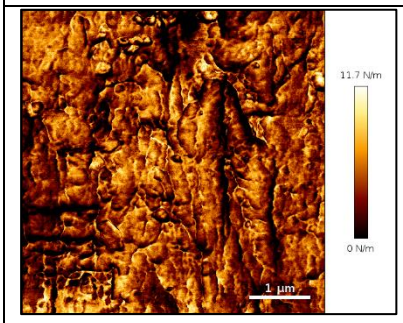	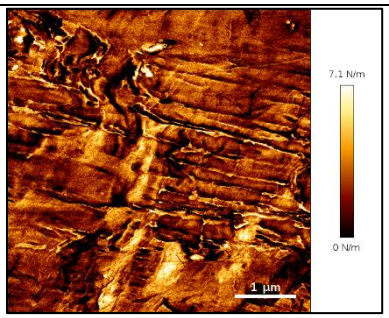	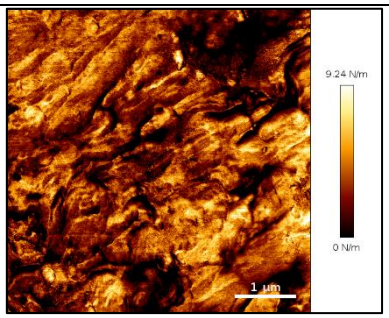
rP25	**rP40**	**rP50**
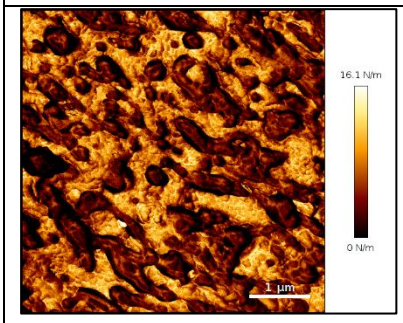	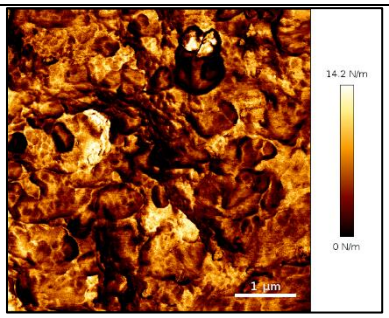	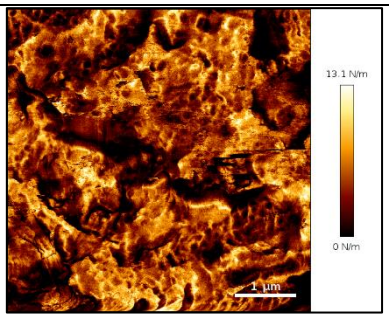
rP60	**rP75**	**rP80**
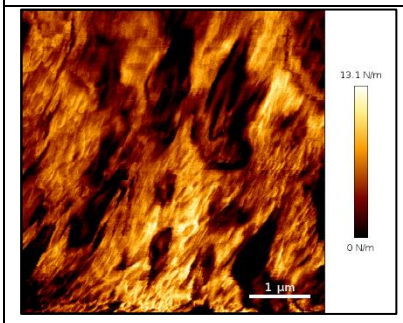	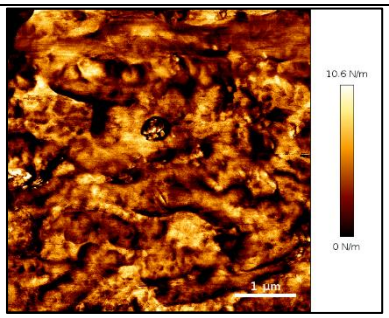	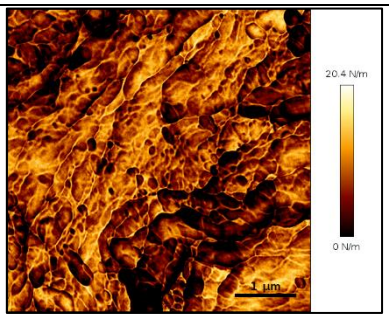
rP90	**rPP**	
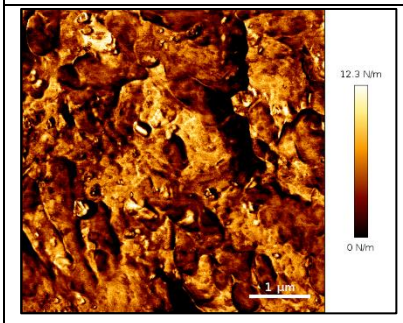	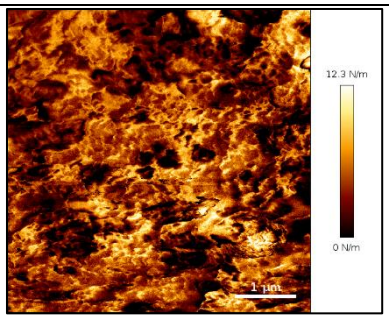	

6.3.2.3 Comparison of Virgin and Recycled PP:HDPE Blends

There is a difference in morphology when comparing the vHDPE and vPP with rHDPE and rPP respectively (Table 6.7). The spherulites are not distinct in rHDPE compared to vHDPE which could be caused by the presence of PP contaminants, discussed in Chapter 4. Therefore, the rHDPE presents similar morphology as a P10 blend. The rPP morphology is affected by the present of HDPE contaminants. The rP50 blend presents a coarser morphology compared to vP50 which could be caused by polymer degradation during the recycling process and the presence of contaminants.

At P25 and P75, both the virgin and recycled blends presents a dispersed droplet-matrix morphology. The size of dispersed phase is influenced by the viscosity ratio between the dispersed phase and matrix.[31] In the virgin blends, the viscosity of vHDPE is greater than vPP, see Chapter 3 for MFI's. In vP25, the high viscosity HDPE is the matrix and the lower viscosity PP is the dispersed phase. Whereas, in the vP75, phase inversion occurs resulting in HDPE being the dispersed phase and PP the matrix. Jose et al.[32] suggests a more viscous matrix compared to the dispersed phase will hinder the diffusion of the dispersed phase. Limited diffusion leads a reduction in the likelihood of coalescence and hence, smaller domains are observed. Smaller dispersed domains are observed in vP25 compared to vP75 due to the viscous HDPE matrix preventing PP diffusion. The viscosity of rHDPE and rPP are similar in value so there is not a large difference in the dispersed phase size of rHDPE in rP75 and rPP in rP25. The viscosity of rHDPE and rPP are less viscous compared to the vHDPE and vPP. This is due to the degradation mechanisms occurring during recycling which reduces the polymer chains molecular weight. It could be expected that recycled blends to form larger domains compared to virgin blends due to the increased likelihood of coalescence. However, the final morphology is not only affected by the viscosity ratio between the matrix and dispersed phase, but by additional factors such as processing conditions, crystallinity, interfacial tension and presence of contaminants. Kazemi et al.[33] suggest that the presence of nano-contaminants in post-consumer PP/PE blends reduce the domain size of recycled blends.

Table 6.7 Comparison of HDPE, P25, P50, P75 and PP stiffness images for the virgin and recycled PP:HDPE blends at 1024 x 1024 pixels, 5 x 5 μm^2.

PP:HDPE blends	Virgin	Recycled
HDPE	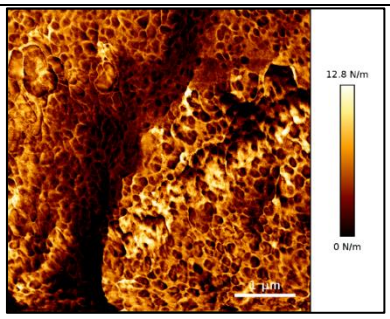	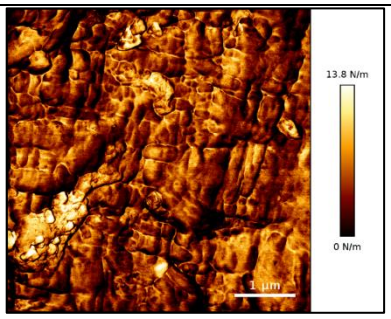
P25	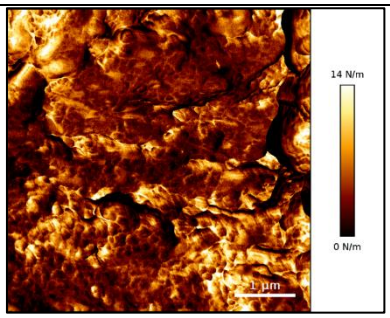	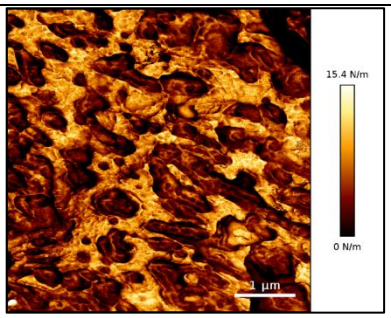
P50	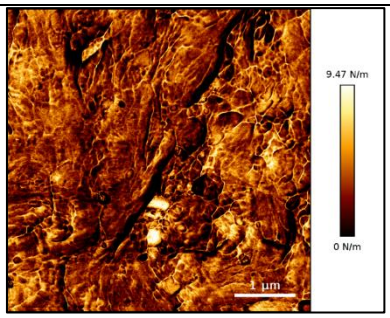	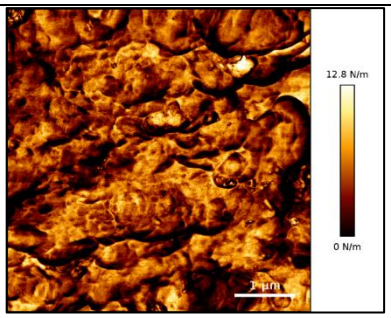
P75	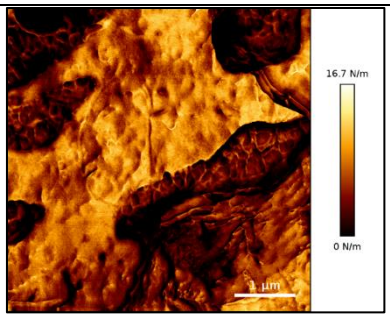	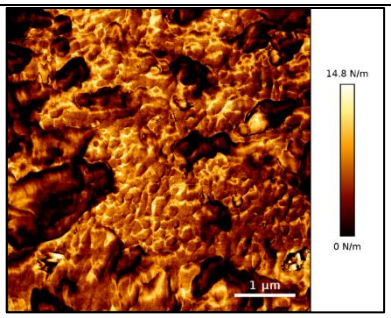
PP	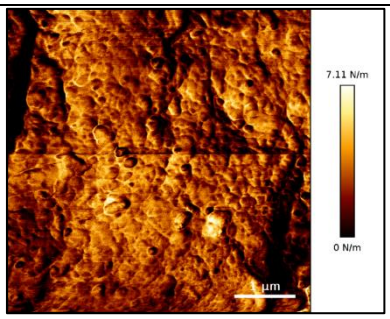	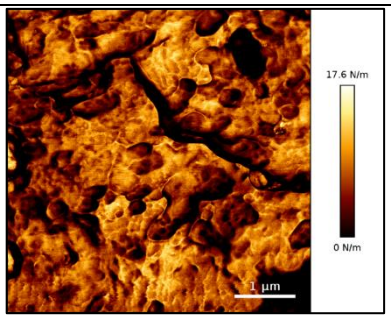

6.3.3 Elasticity Images of Virgin and Recycled PP:HDPE Blends

The JPK software enabled the production of a Young's modulus map. Table 6.8 and 6.9 summarise one Young's modulus map obtained for each of the virgin and recycled blends with their corresponding height and stiffness images. There was good correlation between the stiffness and Young modulus images.

Table 6.8 Summary of the height, stiffness and Young's modulus images obtained for the vPP:vHDPE blends at 512 x 512 pixels, size 5 x 5 μm^2.

PP:HDPE blend	Height, nm	Stiffness, N m^{-1}	Young's modulus, GPa
vHDPE	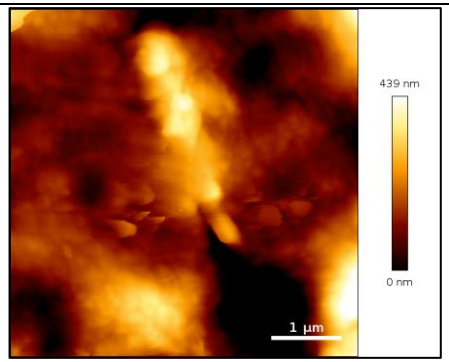	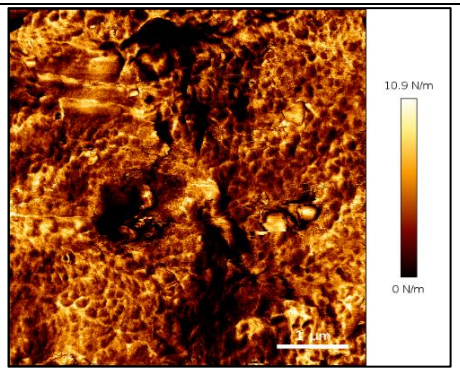	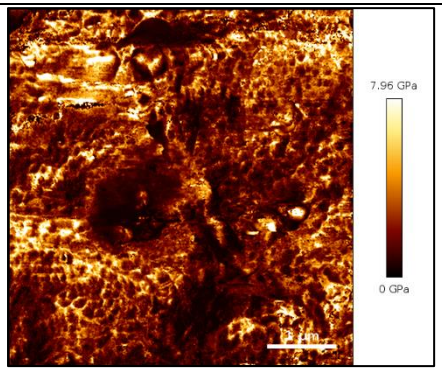
vP10	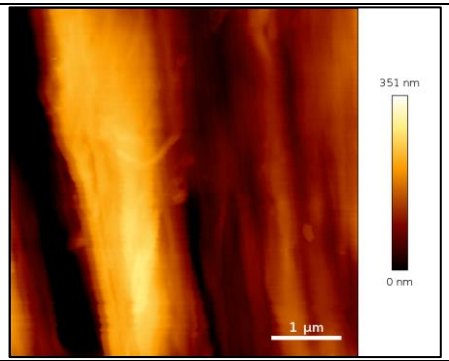	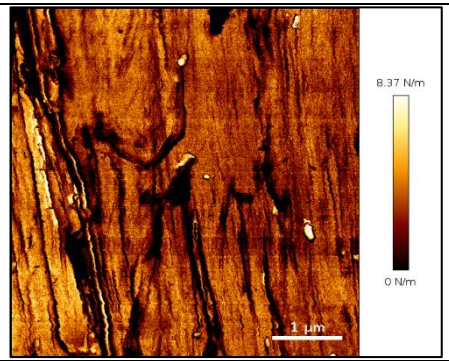	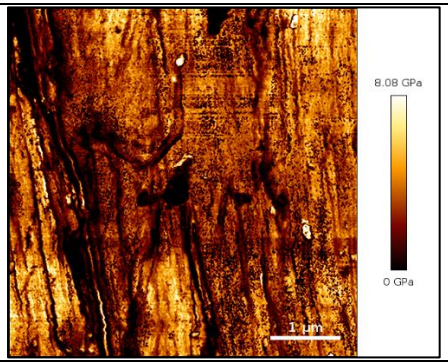

vP20	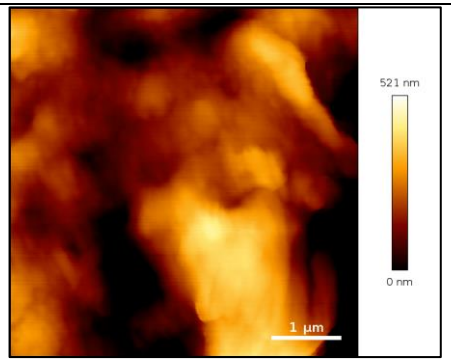	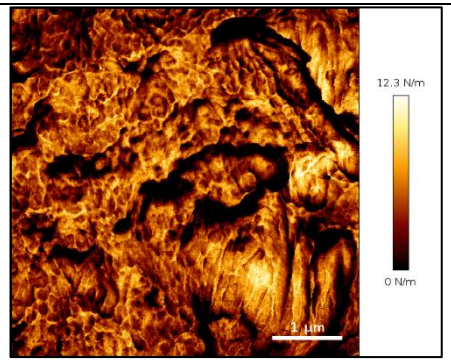	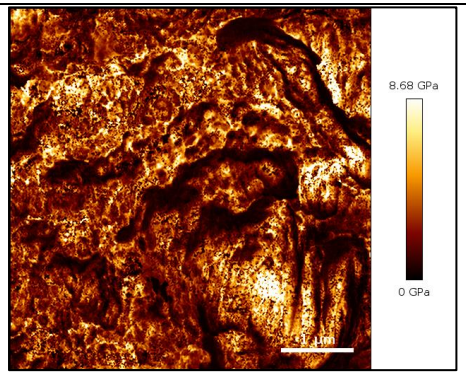
vP25	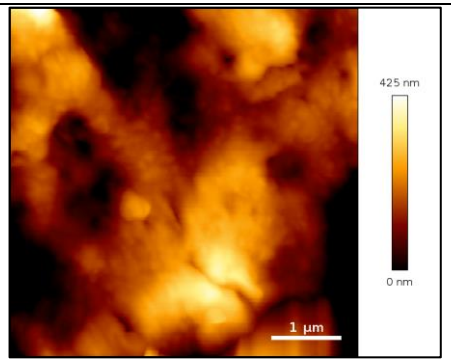	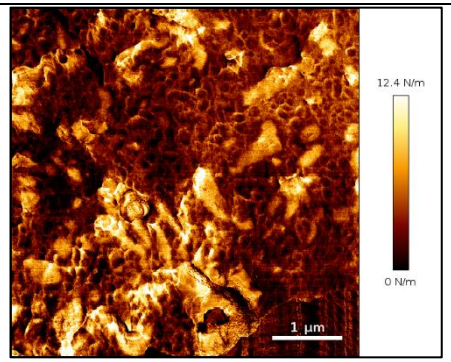	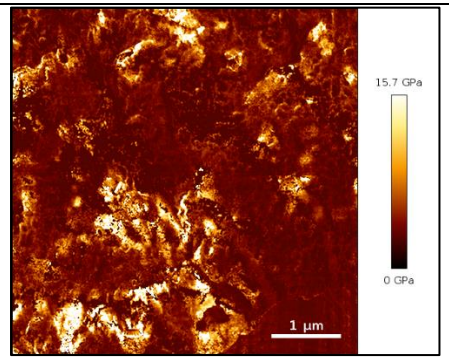
vP40	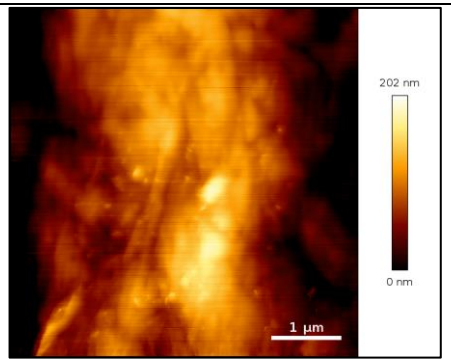	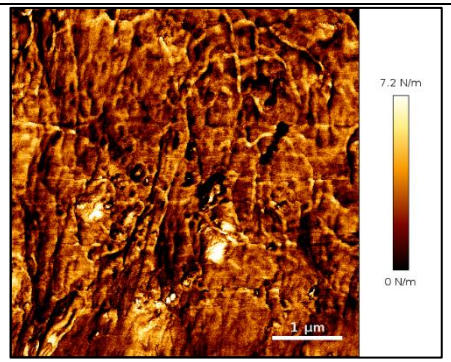	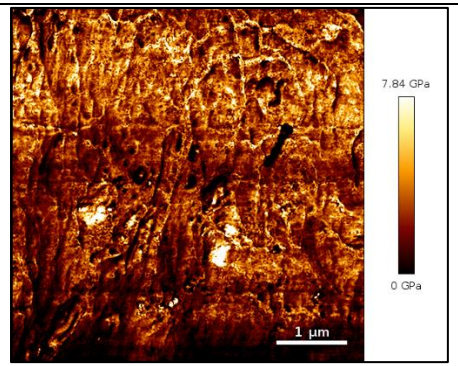

vP50	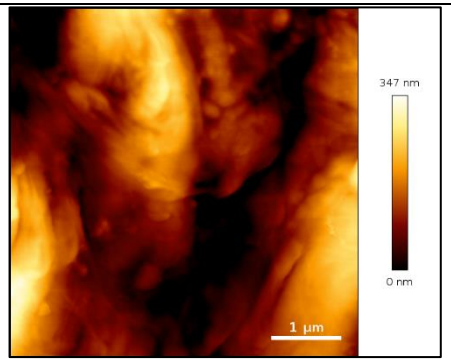	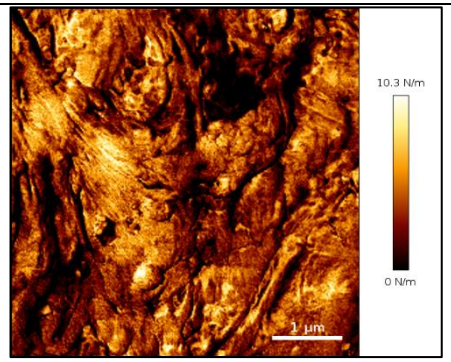	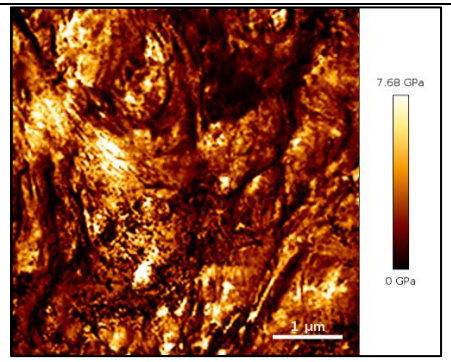
vP60	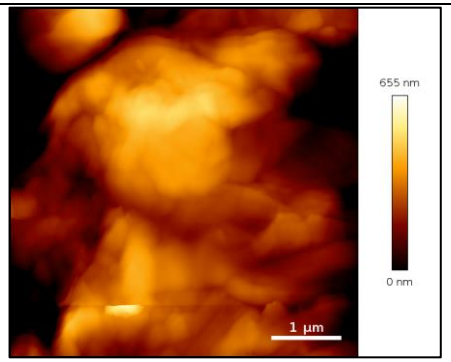	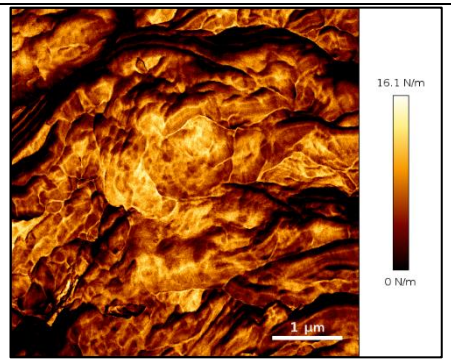	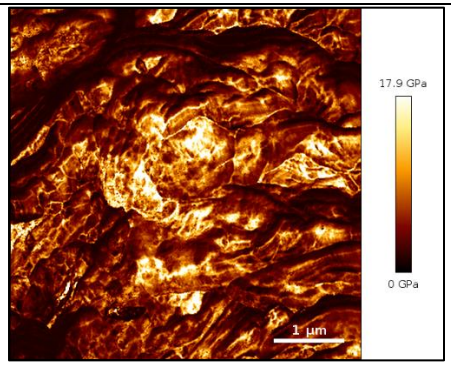
vP75	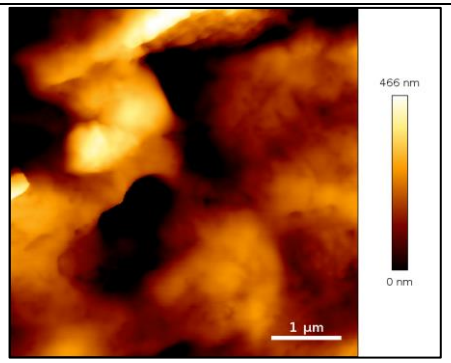	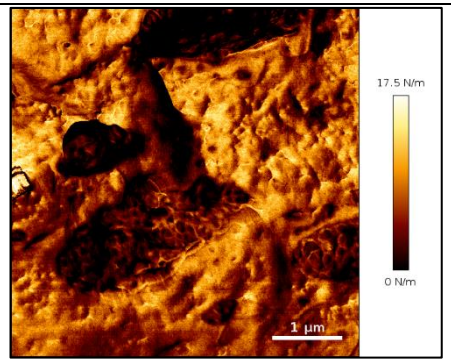	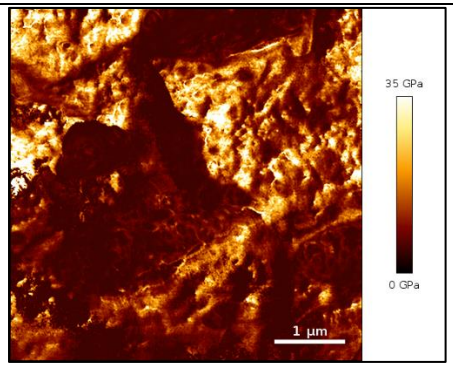

vP80	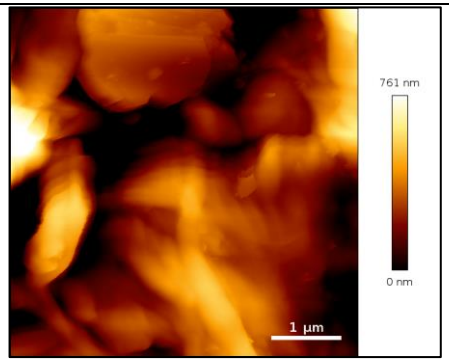	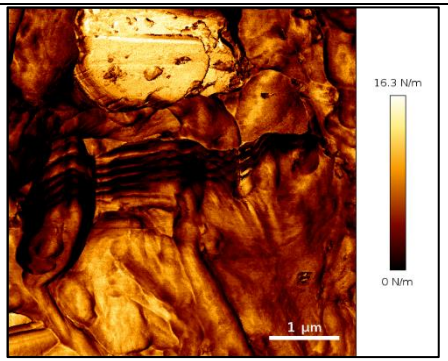	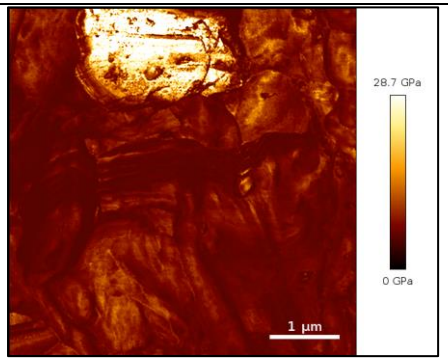
vP90	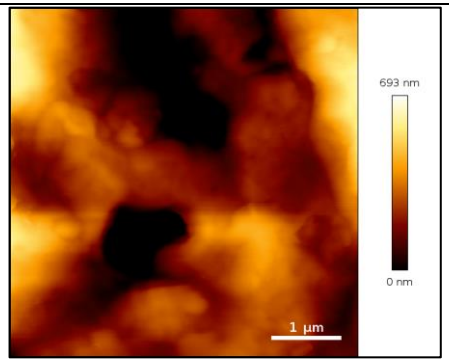	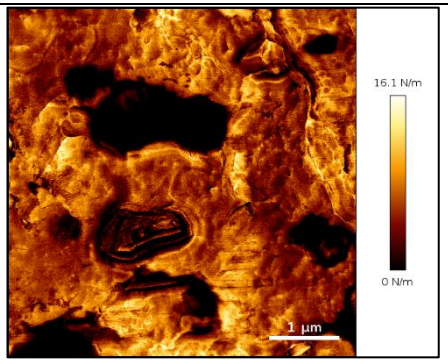	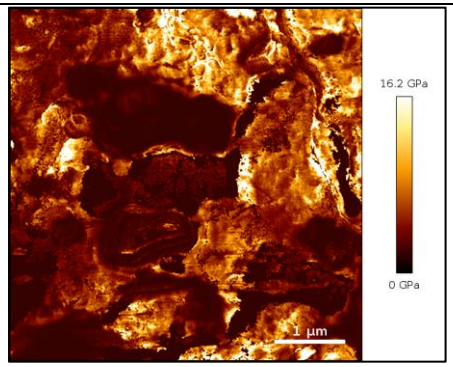
vPP	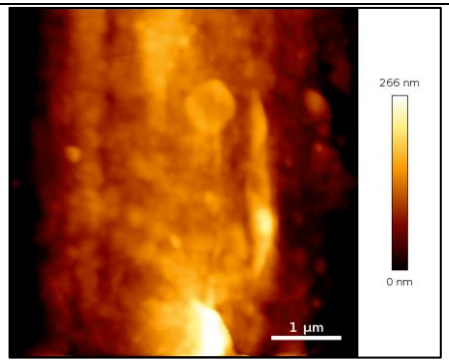	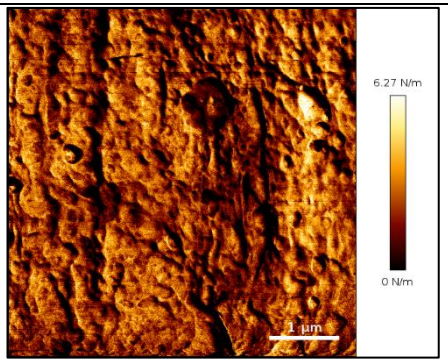	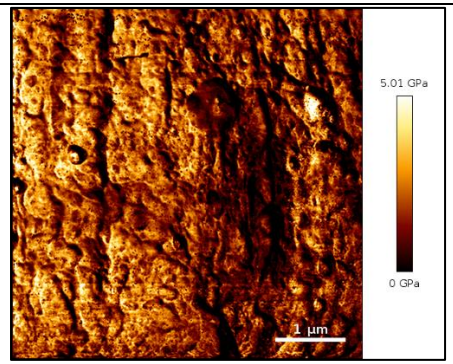

Table 6.9 Summary of the height, stiffness and Young's modulus images obtained for the rPP:rHDPE blends at 512 x 512 pixels, size 5 x 5 μm^2.

PP:HDPE blend	Height, nm	Stiffness, N m^{-1}	Young's modulus, GPa
rHDPE	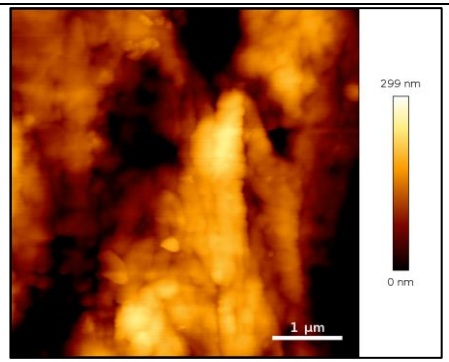	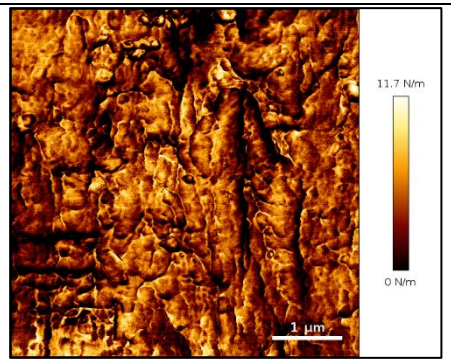	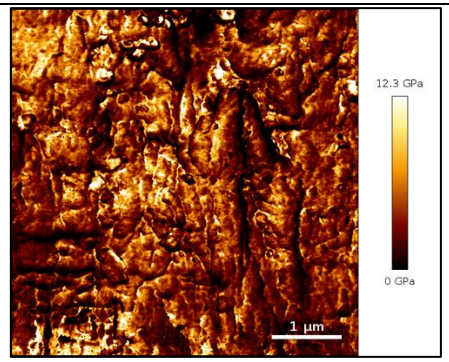
rP10	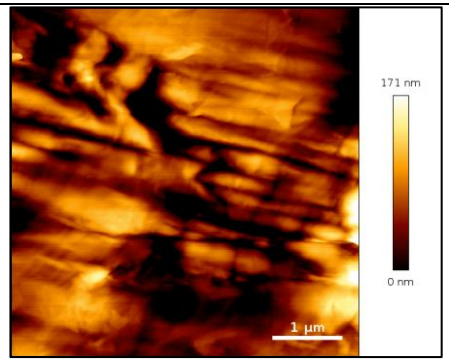	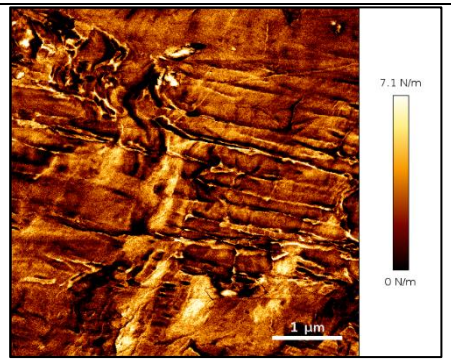	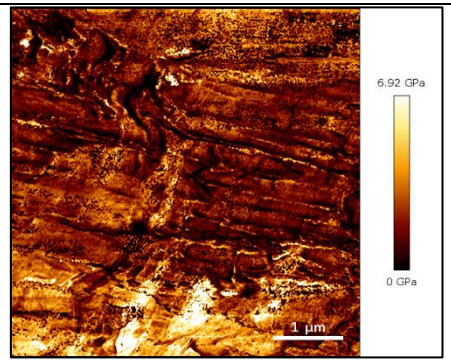

rP20	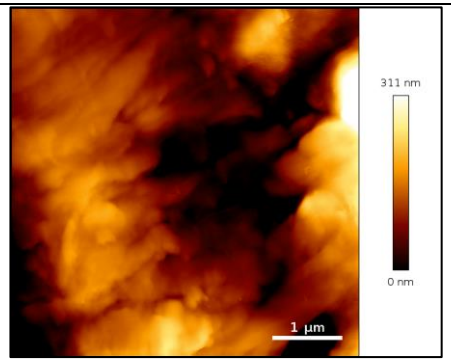	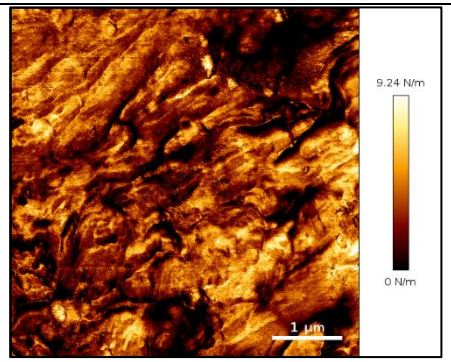	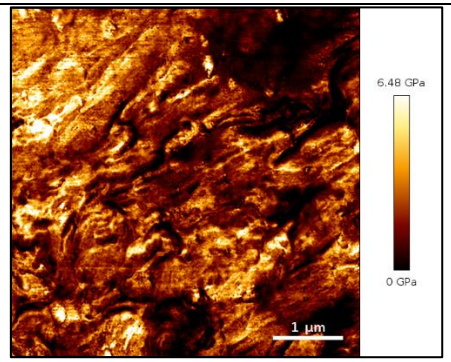
rP25	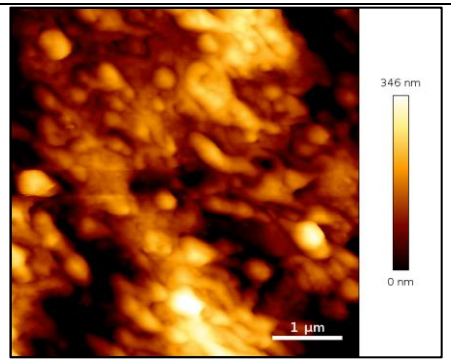	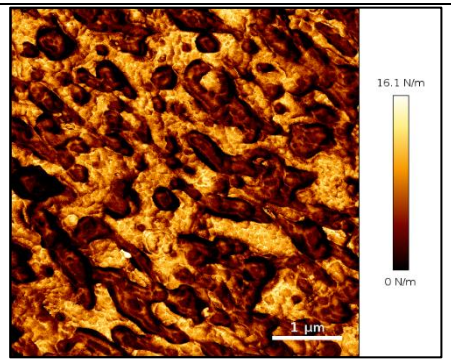	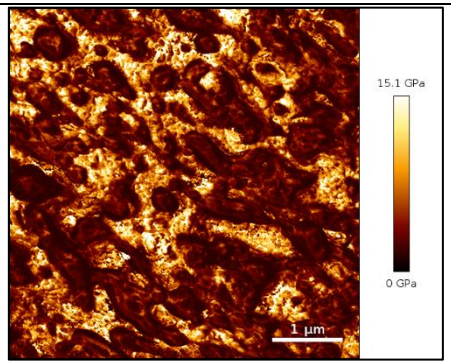
rP40	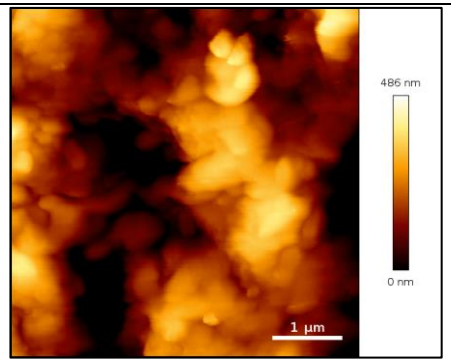	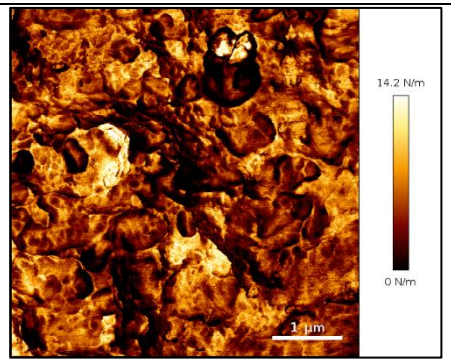	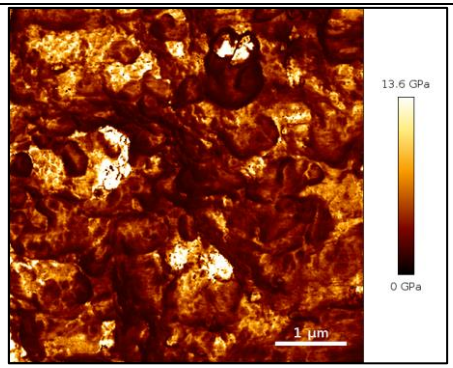

rP50	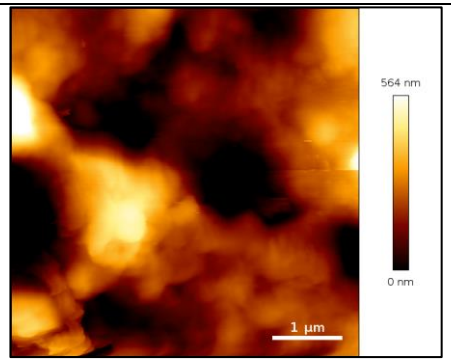	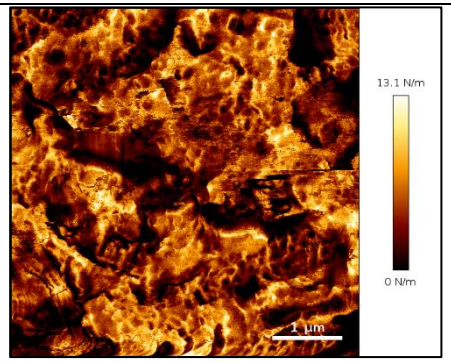	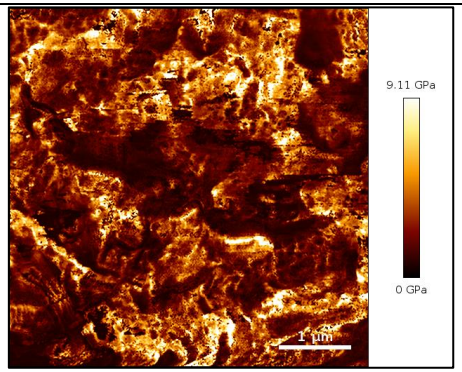
rP60	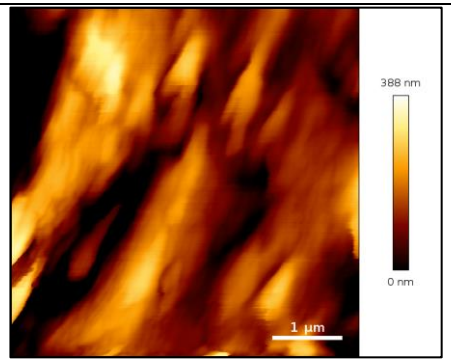	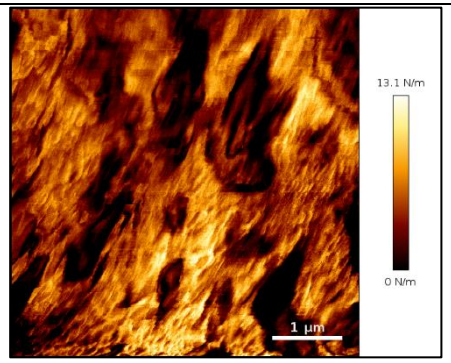	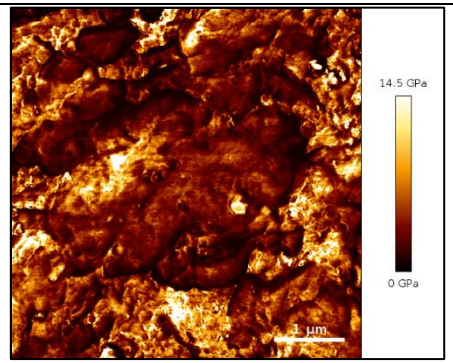
rP75	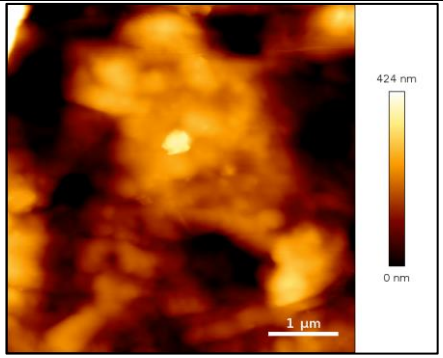	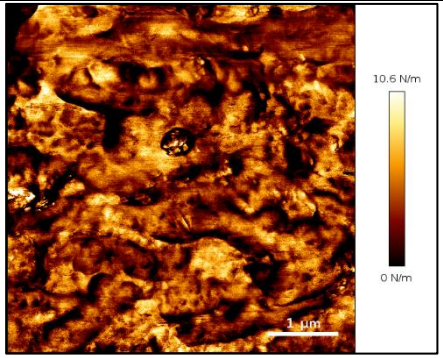	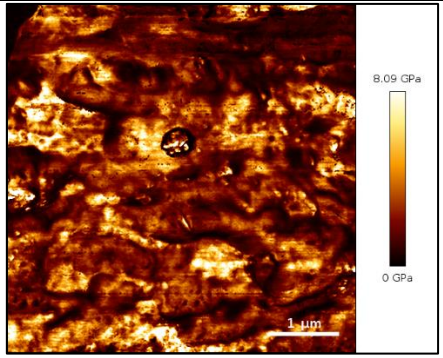

rP80	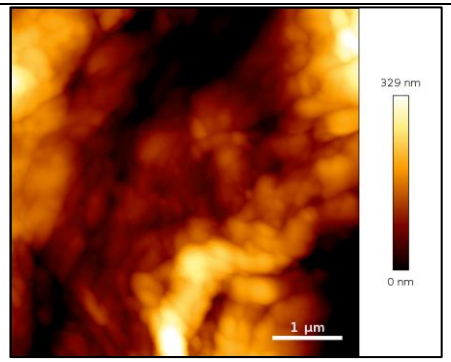	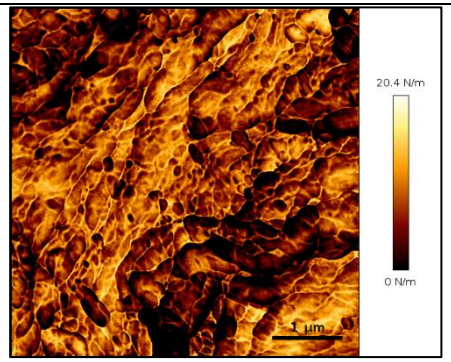	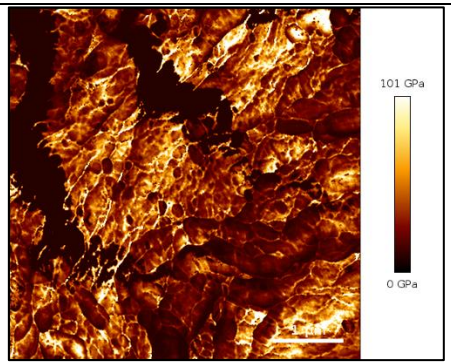
rP90	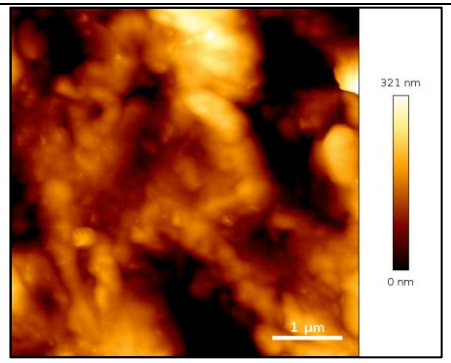	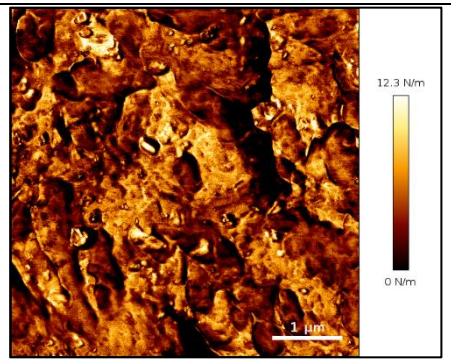	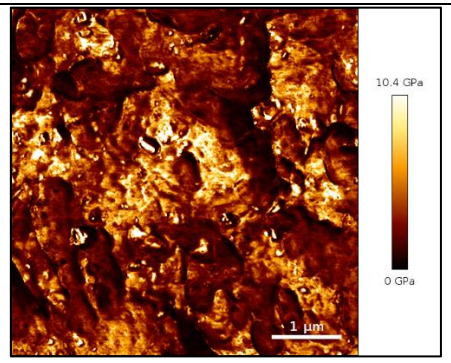
rPP	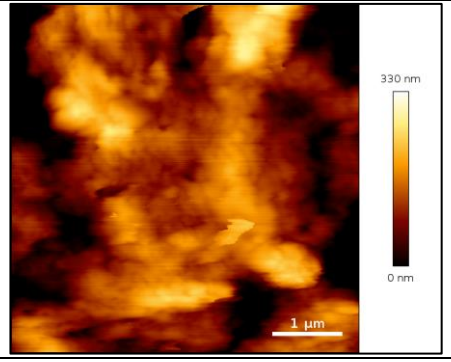	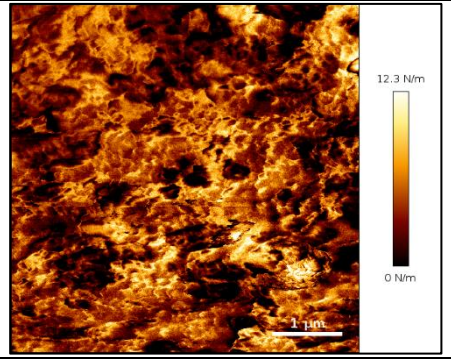	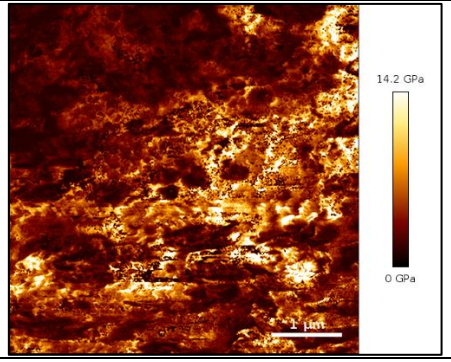

6.3.3.1 Young's Modulus

The Young's modulus (using the DMT model) was determined for each pixel to produce a histogram of moduli distribution. Two methods were used to determine Young's moduli of the PP:HDPE blends; firstly, by quoting the arithmetic mean, and secondly, by quoting the highest frequency Young's modulus value in the histogram distribution (value at the peak of the distribution).

6.3.3.2 Arithmetic Mean Young's Moduli

Generally, the Young's moduli for virgin and recycled blends were similar in value with the exception at rP80 where the recycled blend was higher than the virgin blend (Figure 6.6). Large standard deviations were observed which could be attributed to the sample roughness causing variation in the contact area.[34] Additionally, large residual RMS values could contribute to an overestimate of the Young's modulus value due to the poor fit between the data and the DMT model. Large standard deviations could be attributed to the phase separated PP and HDPE phases. For example, one scan region might be PP rich whereas the following scan might be HDPE rich, thus affecting the standard deviation. This is a limitation of this methodology as it is not possible to attribute a Young's modulus value to PP and HDPE in each blend ratio.

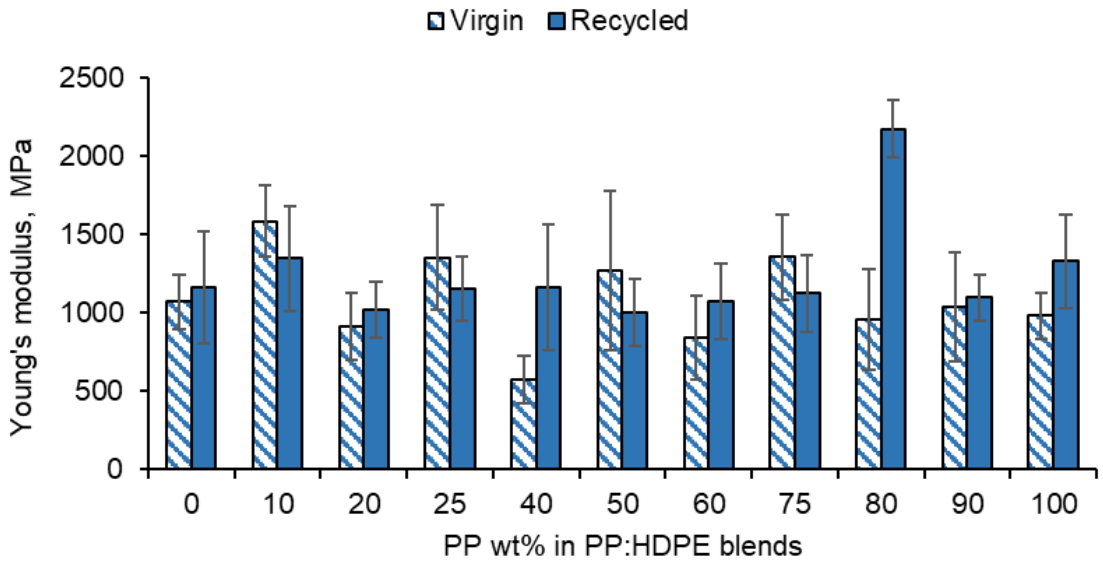

Figure 6.6 Plot of the mean Young's modulus value obtained from JPK Software using the mechanical DMT model for virgin and recycled PP:HDPE blends. An average of three scans and standard deviation is quoted.

6.3.3.3 Young's Moduli of Highest Frequency

Generally, the virgin blends Young's moduli were higher than the recycled blends (Figure 6.7). Interestingly, rPP and rHDPE Young's moduli were slightly larger than vPP and vHDPE respectively. This could be attributed to PP/HDPE contaminants in the rPP and rHDPE, which have been shown to be present by DSC, see Chapter 4. The large variation in the standard deviation could be attributed to the surface roughness and the poor fitting of the DMT model to the data.

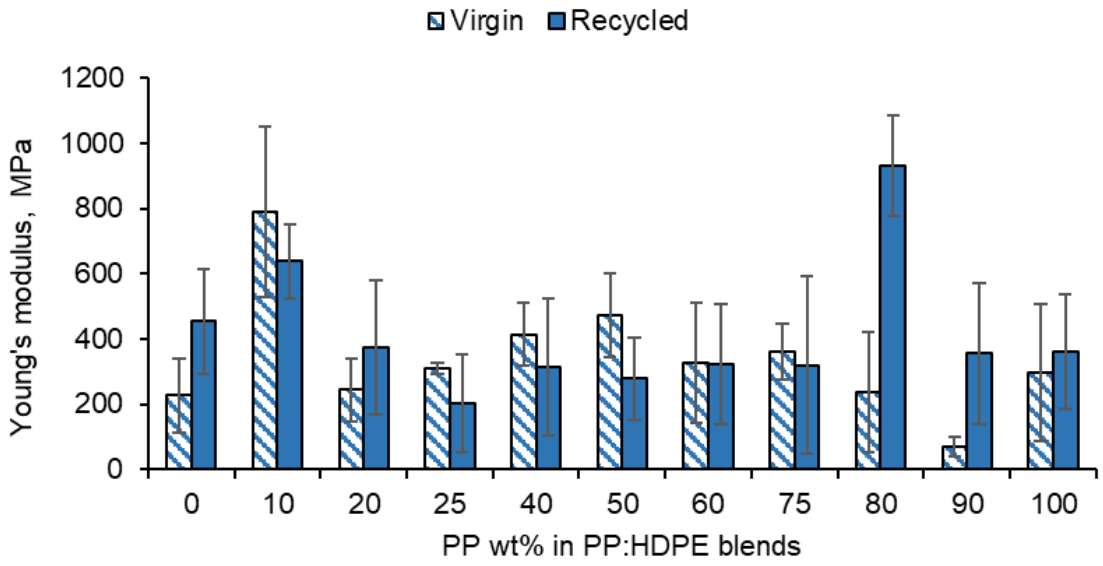

Figure 6.7: Plot of the Young's modulus values for virgin and recycled PP:HDPE blends obtained from the peak of the histogram distribution. The highest frequency Young's modulus value in the histogram for each scan is determined and an average over a minimum of three scans is quoted.

As the PP wt% increased from P10 to P90, it was expected that two distinct peaks would be observed in the Young's modulus histograms (Table 6.10). The expected peaks were to be attributed to pure PP and HDPE Young moduli respectively, due to the phase separated morphology. The absence of two distinct peaks could possibly be attributed to the closeness of the Young's modulus values for PP and HDPE, resulting in peak overlap. Schona et al.[34] investigated the Young's modulus using HarmoniX Tapping Mode AFM and Peak Force Tapping Mode of polyurethane samples. They found a broadening on the Young's modulus values due confinement's effects leading to the soft and hard segments potentially mutually influencing each

other. As a result an averaging moduli occurred in the regime of the contact area of the AFM tip.

Table 6.10 Young's modulus histograms obtained with the corresponding Young's moduli image for the vPP:vHDPE blends.

	Young's moduli Images	**Histogram – Young's modulus distribution**
vHDPE	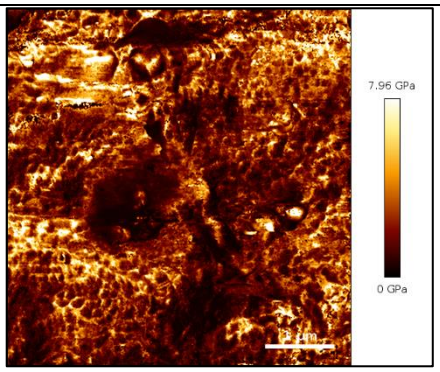	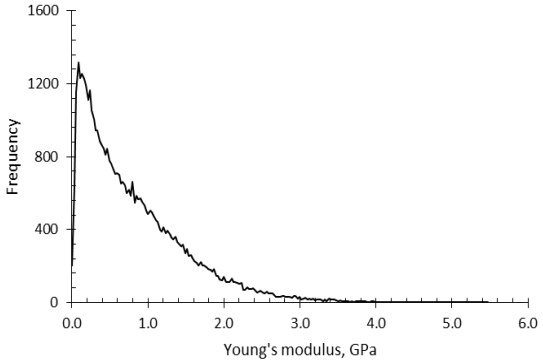
vP25	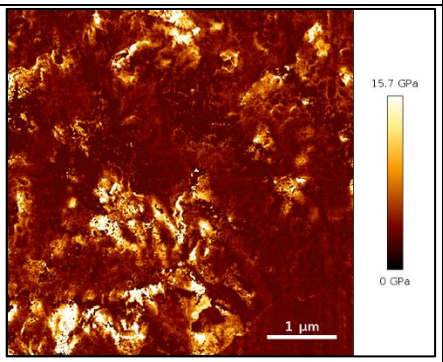	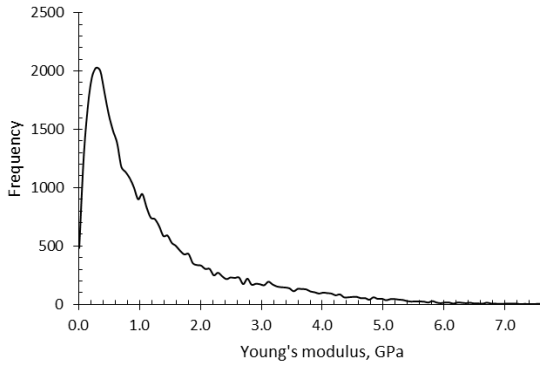
vP50	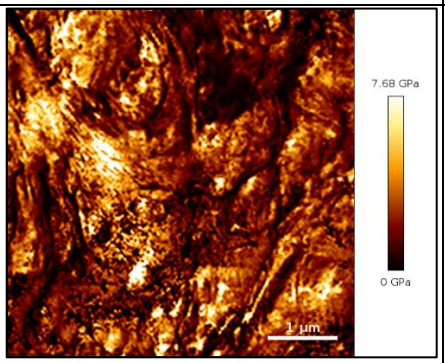	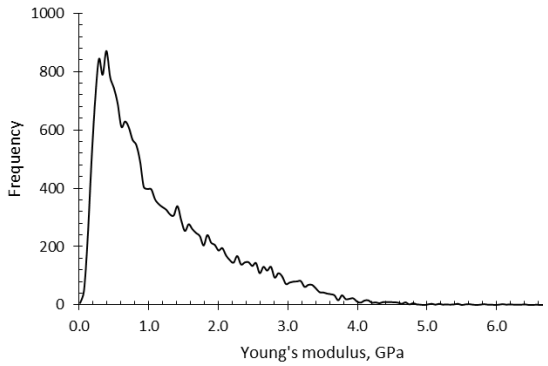

vP75	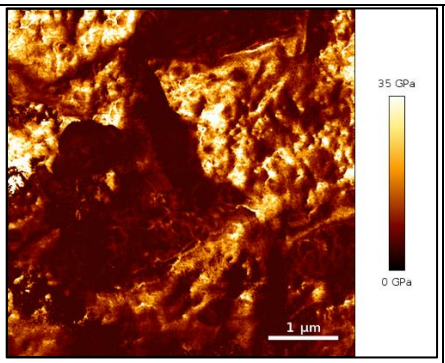	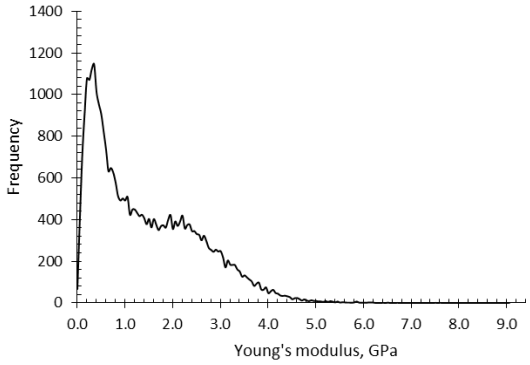
vPP	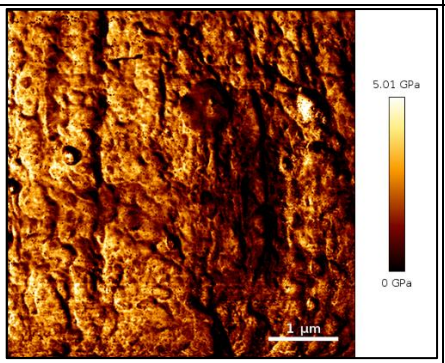	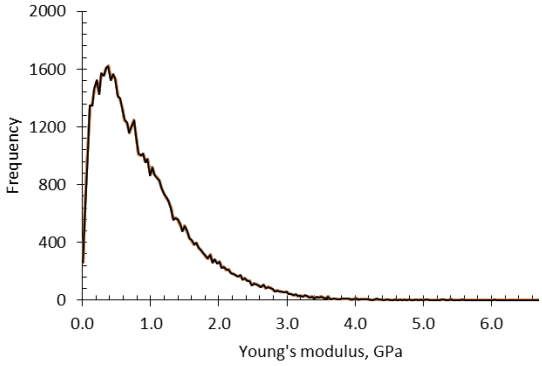

6.3.3.4 Comparing the Young's Modulus Obtained from AFM to Tensile Testing

There is discrepancy between the two methodologies to obtain the Young's moduli from the QI mode (Figure 6.8). The peak distribution Young's moduli obtained from the histograms underestimates the Young's modulus compared to the arithmetic mean methodology for all virgin and recycled PP:HDPE blends. This could be due to the broad distribution of moduli values obtained.

When comparing the Young's moduli obtained from AFM and tensile testing it is important to consider the differences in the procedures. In AFM, the modulus is obtained from each individual pixel to produce a distribution of moduli and an arithmetic mean, whereas tensile testing is a single average bulk modulus is obtained.[34] There is not a substantial difference in the surface properties when comparing nanoscale (AFM –value at peak methodology) properties to the bulk properties (tensile testing). This is supported by the findings by Longo et al.[35] who compared the Young's modulus of membranes by AFM and traditional tensile tests.

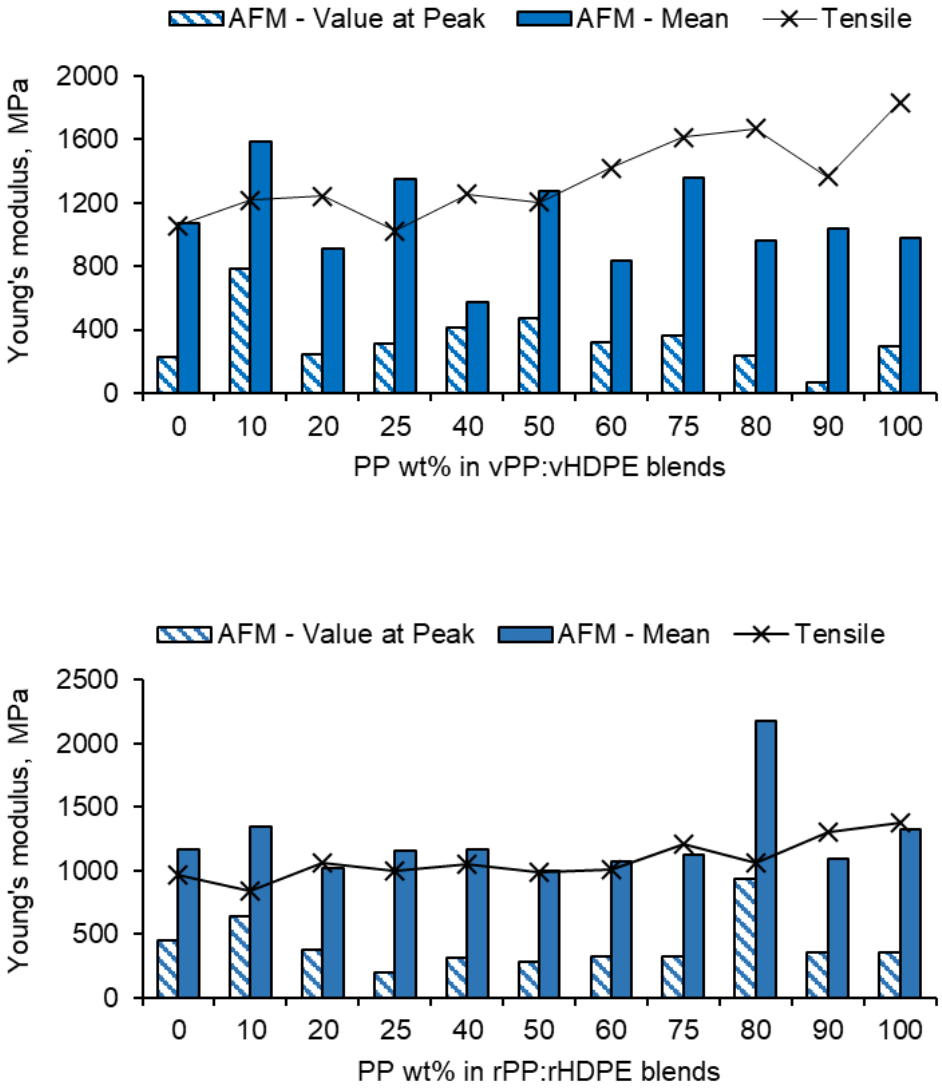

Figure 6.8 Comparison of Young's modulus values of the a) vPP:vHDPE blends and b) rPP:rHDPE blends, obtained from i) AFM Young's modulus value at peak of distribution ii) AFM mean of the distribution and iii) tensile testing.

6.4 Conclusion

This chapter has contributed to knowledge towards the use of the QI mode to determine the morphology and Young's moduli of virgin and recycled PP:HDPE blends. This is an area which is currently limited in the literature. The morphology was found to be dependent on the blend composition in both the virgin and recycled blends. In the virgin and recycled PP:HDPE blends, droplet matrix morphology was observed at P25 and P75 along with co-continuous morphology at P50. The injection moulding process orientates the polymer chains in the direction of flow to produce skin-core

morphology. Phase separation was not clearly observed in some blends due to the imaging of the skin and/or large surface roughness. The QI mode can be used to determine the Young's moduli by applying the DMT model and extracting the arithmetic mean for each scan region. Extracting the Young's moduli from the peak of distribution in the histogram underestimated the Young's moduli. However, the arithmetic mean gave similar Young's moduli values as obtained from tensile testing.

References

1. P. Eaton, P. West, in *Atomic Force Microscopy*, Oxford University Press, Oxford Scholarship Online, 2010, Ch. 3.
2. Bruker Nano GmbH. NanoWizard AFM Handbook Version 6.0. 2018.
3. D. G. Yablon, in *Scanning Probe Microscopy in Industrial Applications Nanomechanical Characterization*, John Wiley & Sons, 2013, Ch. 1.
4. R. Nguyen-Tri, P. Ghassemi, P. Carriere, S. Nanda, A. A. Assadi, D. D. Nguygen, *Polymer* **2020**, *12*
5. Bruker Nano GmbH. NanoWozard Series User Manual. 2019.
6. L. Chopinet, C. Formosa, M. P. Rols, R. E. Duval, E. Dague, *Micron* **2013**, *48*, 26.
7. S. Lyonnais, M. Hénaut, A. Neyret, P. Merida, C. Cazevieille, N. Gros, C. Chable-Bessia, D. Muriaux, *Sci Rep* **2021**, *11*, 11885.
8. K. Casdorff, T. Keplinger, I. Burgert, *Plant Methods* **2017**, *13*
9. H. Gojzewski, M. Sadej, E. Andrzejewska, M. Kokowska, *Eur. Polym. J.* **2017**, 205.
10. L. Marsich, D. Borin, O. Sbaizero, C. Schmid, *Polymer Testing* **2020**, *90*, 106632.
11. J. E. Sader, J. W. M. Chon, P. Mulvaney, *Rev. Sci. Instrum.* **1999**, *70*, 3967.
12. Bruker Nano GmbH. JPK DP Data Processing Software Manual Version 6.0. 2019.
13. M. Griepentrog, G. Krämer, B. Cappella, *Polymer Testing* **2013**, *32*, 455.
14. D. Tranchida, S. Piccarolo, M. Soliman, *Macromolecules* **2006**, *39*, 4547.
15. T. D. B. Jacobs, C. M. Mate, K. T. Turner, R. W. Carpick, in *Scanning Probe Microscopy in Industrial Applications: Nanomechanical Characterization*, D. G. Yablon, John Wiley & Sons, 2014.
16. S. V. Kontomaris, A. Malamou, *Mater. Res. Express* **2020**, *7*, 033001.
17. M. Krieg, G. Fläschner, D. Alsteens, B. M. Gaub, W. H. Roos, G. J. L. Wuite, H. E. Gaub, C. Gerber, Y. F. Dufrêne, D. J. Müller, *Nat. Rev Phys* **2019**, *1*, 41.
18. B. V. Derjaguin, V. M. Muller, Y. P. Toporov, *Journal of Colloid and Interface Science* **1975**, *53*, 314.
19. G. Violano, L. Afferrante, *Tribology International* **2019**, *130*, 36.
20. G. G. Adams, in *Encyclopedia of Tribology*, Q. J. Wang,Y. W. Chung, Springer, 2013.

21. V. J. Morris, A. R. Kirby, A. P. Gunning, *Atomic Force Microscopy for Biologists*, Imperial College Press London, **2009**.
22. G. K. H. Pang, K. Z. Baba-Kishi, A. Patel, *Ultramicroscopy* **2000**, *81*, 35.
23. A. Tabatabaei, L. H. Mark, C. B. Park, *Polymer* **2016**, *101*, 48.
24. T. Liao, X. Zhao, X. Yang, P. Coates, B. Whiteside, Z. Jiang, Y. Men, *Polymer* **2019**, *180*, 121698.
25. L. Wang, M. Yang, Q. Zhang, R. Zhang, J. Wu, J. Feng, *Polymers for Advanced Technologies* **2013**, *24*, 541.
26. M. Leung, M. Gnatowski, G. Sun, A. Stanese, T. Wong, *J. Appl. Polym. Sci.* **2019**, *136*, 47507.
27. B. A. Schrauwen, L. C. A. Breemen, A. B. Spoelstra, L. E. Govaert, G. W. M. Peters, H. E. H. Meijer, *Macromolecules* **2004**, *37*, 8618.
28. C. Leyva-Porras, A. Balderrama-Aguilar, Y. Estrada-Ávila, I. Espelosín-Gómez, M. Mendoza-Duarte, C. Piñón-Balderrama, M. Z. Saavedra-Leos, I. Estrada-Moreno1, *Polymers* **2021**, *13*, 3597.
29. C. Ruan, K. Liang, E. Liu, *Polymers* **2017**, *9*, 699.
30. X. Liu, M. Lian, Y. Pan, X. Wang, G. Zheng, C. Liu, D. W. Schubert, C. Shen, *Macromol. Mater. Eng* **2018**, *303*, 1700465.
31. M. Hemmati, H. Nazokdast, H. S. Panahi, *J. Appl. Polym. Sci.* **2000**, *82*, 1129.
32. S. Jose, A. S. Aprem, B. Francis, M. C. Chandy, P. Werner, V. Alstaedt, S. Thomas, *Eur. Polym. J.* **2004**, *40*, 2105.
33. Y. Kazemi, A. R. Kakroodi, D. Rodrigue, *Polym. Eng. Sci.* **2015**, *55*, 2368.
34. P. Schöna, K. Bagdi, K. Molnár, P.Markus, B. Pukánszky, G. J. Vancso, *Eur. Polym. J.* **2011**, *47*, 692.
35. M. Longo, M. P. D. Santo, E. Esposito, A. Fuoco, M. Monteleone, L. Giorno, J. C. Jansen, *Polymer* **2018**, *156*, 22.

7.0 Comparative Study of the Thermal and Tensile Properties of Virgin and Recycled PP:HDPE Blends Using Two Different Manufacturing Methodologies

7.1 Introduction

Injection moulding and compression moulding are commonly used techniques within the plastics industry. Compression moulding is used due to its simplicity and low cost. Injection moulding is a popular alternative to compression moulding for complex shapes, high repeatability and mass scale production.[1,2] The literature contains studies that investigate the effect of manufacturing methodology on the mechanical properties of polymer blends and composites.[3,4] For example, Nolly et al.[5] and Barlett et al.[6] found that compression moulding PP:HDPE blends resulted in lower strength and ductility compared to injection moulding blends. Xie et al.[7] compared the morphology and mechanical properties of UHMWPE:PP blends prepared by injection and compression moulding. They found that the injection moulded blends developed a skin core structure whereas the compression moulded blends phase morphology was isotropic throughout. The skin core structure of injection moulded blends formed by shear–induced orientation and crystallization has been found to increase the Young's modulus and yield strength.[7,8]

Before undergoing injection or compression moulding, the polymers are subjected to mixing. There are different mixing methods available but extrusion mixing and internal mixers are typically associated with injection and/or compression moulding. The mixing conditions need to be taken into account, as these factors will contribute towards the final polymer blend performance. For example, mixing time and intensity needs to be optimised to improve the degree of dispersion but without causing thermal and mechanical degradation.[9] Spadaro and Rizzo[9] found that the mixing time and rate of PP:LDPE blends had significant effects on the tensile properties as during the first two minutes of mixing significant changes in morphology occurred.

The first aim of this chapter was to gain an understanding of whether the unexpected tensile behaviour of the vHDPE up to v25 blend was caused by the twin screw extruder and injection moulding process. The second aim was to investigate whether an improvement in the thermal and tensile behaviour of rPP:rHDPE blends was observed by varying the manufacturing method. To achieve these aims a comparative study of the thermal and tensile behaviour of 5 virgin and recycled PP:HDPE blends were prepared by two manufacturing methods. Firstly, extrusion mixing and injection moulding, and secondly, Brabender mixing and compression moulding.

7.2 Methodology

7.2.1 Manufacturing

Virgin and recycled HDPE, PP, and the P25, P50 and P75 blends, were investigated in this study.

7.2.1.1 Extrusion Mixing and Injection Moulding

vPP:vHDPE and rPP:rHDPE blends were prepared using a lab scale Haake MiniCTW twin-screw extruder (Karlsruhe, Germany) for 5 minutes with feeder and mixing speeds of 50 rpm and 100 rpm respectively. The conical screws are 4-15 mm in diameter, 109.4 mm in length and co-rotate. The barrel temperature was 180-185 °C. Molten blends were transferred to the Haake MiniJet injection moulder (Karlsruhe, Germany) where the cylinder temperature was 210 °C, mould temperature was 35 °C, injection pressure was 500 bar and time was 10 s. The ISO 527-2-1BA was used for the dog bone shaped samples.

7.2.1.2 Brabender Mixing and Compression Moulding

vPP:vHDPE and rPP:rHDPE blends were prepared in a Brabender Mixer with z blades (Duisburg, Germany). For the melt mixing process, the rotation speed, time and temperature of the mixing chamber were set to 30 rpm for 5 min at 190°C. Blends were compression moulded using a Moore Hydraulic Press Compression Moulder. The blends were placed within a metal frame of dimension 149(l) x 120(w) x 1.2(d) mm^3 and then sandwiched between two steel plates to form a sheet. Preheated at 180°C under atmospheric pressure for 5 mins, compressed at 20 tons of 5 inch Ram for 3 mins, 180°C and promptly quenched in another cold Moore Hydraulic Press at approximately 50 °C min^{-1} to room temperature at 16 tons of 4.5 inch Ram. The ISO 527-2-5A mould was used to cut the dog bone shaped samples from the sheet.

7.2.1.3 Limitations of Proposed Manufacturing Routes

It is important to note that a direct results comparison from the two manufacturing methods is not possible. This was due to equipment limitations. The twin-screw extruder was limited to a maximum of 10g per cycle. The compression moulding technique required a minimum of 40 g to form a single sheet. Therefore, three options were considered:

1. All blending occurs in the Brabender mixer.
2. All blending occurs in the twin-screw extruder.
3. Blending occurs in the twin-screw extruder for the injection moulding process, and occurs in the Brabender mixer for the compression moulding process.

Options 1 and 2 were excluded. Firstly, there was no method to transfer the polymer blend from the Brabender mixer to the injection moulder. Secondly, if all blending occurred in the twin-screw extruder, at least 4 mixing batches (4 x 10 g) would be required to make a single sheet (40 g) by compression moulding. This could lead to a sheet with zones of varying degrees of mixing which would ultimately affect the properties. Therefore, option three was chosen, so general trends and observations could be discussed even though it would not be possible to attribute effects to either mixing, processing or both with certainty. The mechanical and thermal properties results for the virgin and recycled PP:HDPE blends prepared by twin screw extrusions and injection moulding are discussed in chapters 4 and 5. This chapter will focus on the mechanical and thermal properties of virgin and recycled PP:HDPE blends prepared by Brabender mixing and compression moulding, followed by a comparison of the two manufacturing routes.

7.2.1.4 Abbreviations

The figures shown in this chapter use the following abbreviations for the two manufacturing routes of interest:

- CM – Brabender mixing followed by compression moulding
- IM – twin screw extruder mixing followed by injection moulding

7.2.2 Characterisation

7.2.2.1 DSC

The melting and crystallisation behaviour of the vPP:vHDPE and rPP:rHDPE blends were evaluated using a Perkin Elmer DSC 8000 (Waltham, MA, USA). The instrument was calibrated using an Indium sample. Approximately 5-6 mg of the sample was scanned under a nitrogen atmosphere. Samples were exposed to the following thermal cycle: heated from 25 to 200 °C at 10 °C min^{-1}, isothermal at 200 °C for 5 mins,

cooled from 200 to 25 °C at 10 °C min^{-1}, isothermal at 25 °C for 2 mins and heated from 25 to 200 °C at 10 °C min^{-1}. The T_m and ΔH_f were obtained from the first heating ramp. The T_c and ΔH_c were obtained from the cooling ramp.

7.2.2.2 Tensile Testing

Tensile properties were determined using an Instron Tensile Machine (Buckinghamshire, UK) with a crosshead speed of 5 mm min^{-1} at ambient temperature in accordance to the ISO 527-2 standard. The Young's modulus was determined using a Zwick Roell Tensile Machine with a video-extensometer. A crosshead speed of 1 mm min-1, gauge length of 20 mm and a 10 kN load cell were used. A minimum of five samples were tested and the average and standard deviation were calculated.

7.3 Results and Discussion

7.3.1 Thermal Properties

Generally, the rPP:rHDPE blends prepared by Brabender mixing and compression moulding had a lower T_m and T_c compared to the corresponding vPP:vHDPE blends. This was caused by polymer chain degradation during the recycling process, as discussed in chapter 4 (Table 7.1). Two T_m and T_c peaks were observed in the rPP and rHDPE due to the presence of PE and PP contaminants (Table 7.1 and Figure 7.1). Both the virgin and recycled blends presented two peaks in their melting and crystallisation behaviour suggesting phase separation (Figure 7.1 and 7.2). This was also observed in the extrusion mixed and injection moulded blends where the peaks were attributed to the individual PP and HDPE phases in the blend (Figure 7.1 and 7.2). There was little or no variation in the T_m and T_c of the virgin and recycled PP:HDPE blends prepared by the two methods (Figure 7.1 and 7.2). This suggests that both manufacturing methods form immiscible blends and that blending PP and HDPE has no effect on the T_m.

Table 7.1 Melting and crystallisation behaviour of vPP:vHDPE and rPP:rHDPE blends prepared by Brabender mixing and compression moulding obtained from DSC. Bold values are vPP:vHDPE blends and un-bolded numbers are rPP:rHDPE blends.

PP wt% content in PP:HDPE	**Peak Melting Temperature, °C**		**Enthalpy of Fusion, J g^{-1}**		**Peak Crystallisation Temperature, °C**		**Enthalpy of Crystallisation, J g^{-1}**
	PP	HDPE	PP	HDPE	PP	HDPE	(PP + HDPE)
0	-	**134.3**	**-**	**134.3**	**-**	**116.0**	**174.4**
	165.8	132.8	25.0	89.93	123.5	118.2	145.2
25	**166.8**	**133.2**	**15.3**	**116.9**	**-**	**116.4**	**149.7**
	164.3	132.0	28.5	81.7	123.6	118.4	137.2
50	**166.1**	**130.4**	**33.6**	**74.8**	**122.2**	**117.4**	**125.6**
	162.0	131.2	32.6	60.9	123.2	118.6	123.4
75	**168.2**	**130.6**	**47.5**	**37.4**	**121.3**	**116.5**	**105.6**
	161.8	130.8	37.0	41.4	123.3	118.8	110.6
100	**168.7**	**-**	**66.1**	**-**	**123.3**	**-**	**79.6**
	160.8	129.3	42.0	29.3	122.4	118.1	108.1

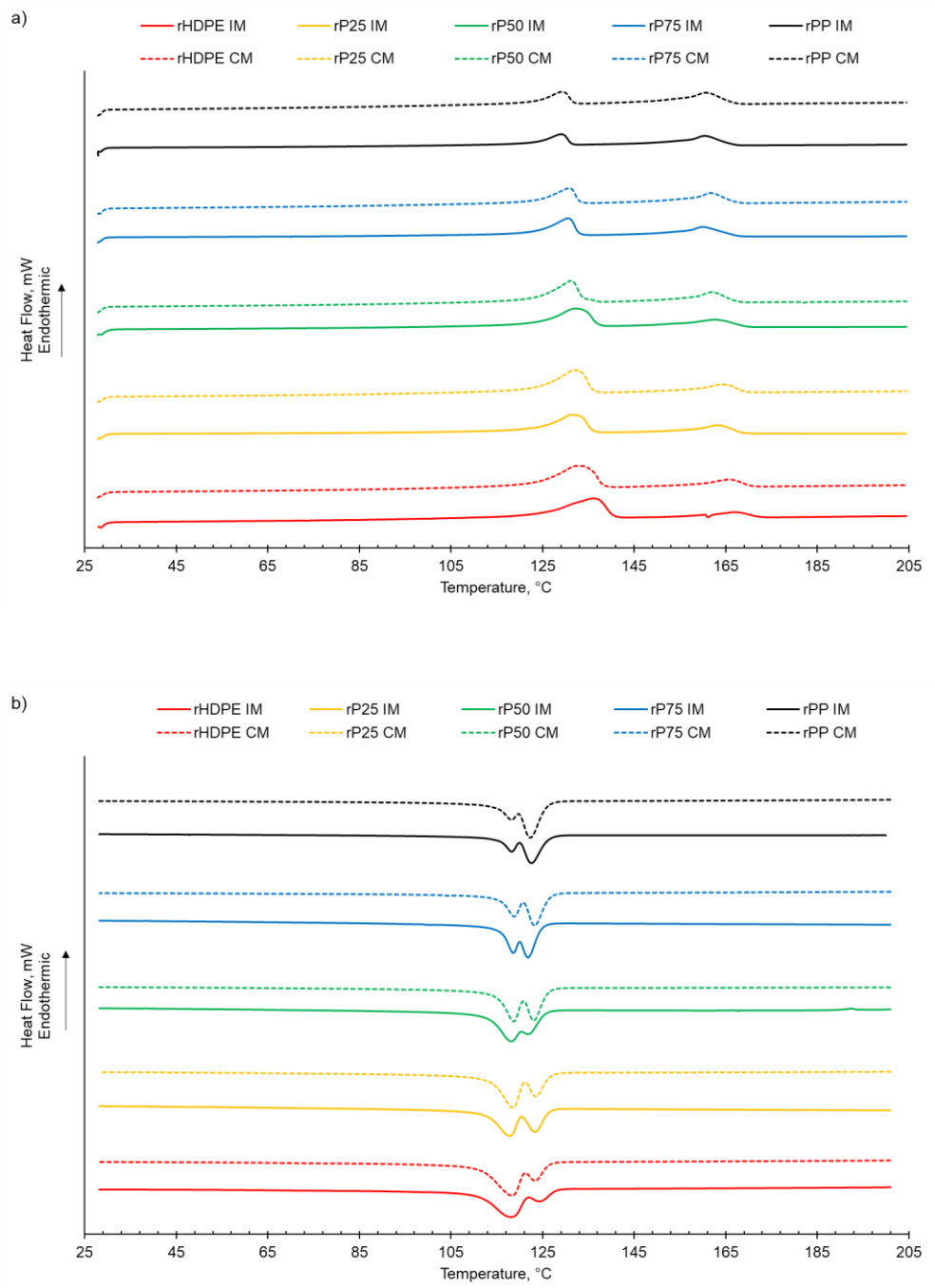

Figure 7.1 Comparison of melting and crystallisation behaviour of rPP:rHDPE blends prepared by CM (Brabender mixing and compression moulding) and IM (twin screw extrusion mixing and injection moulding) where a) melting behaviour b) crystallisation behaviour.

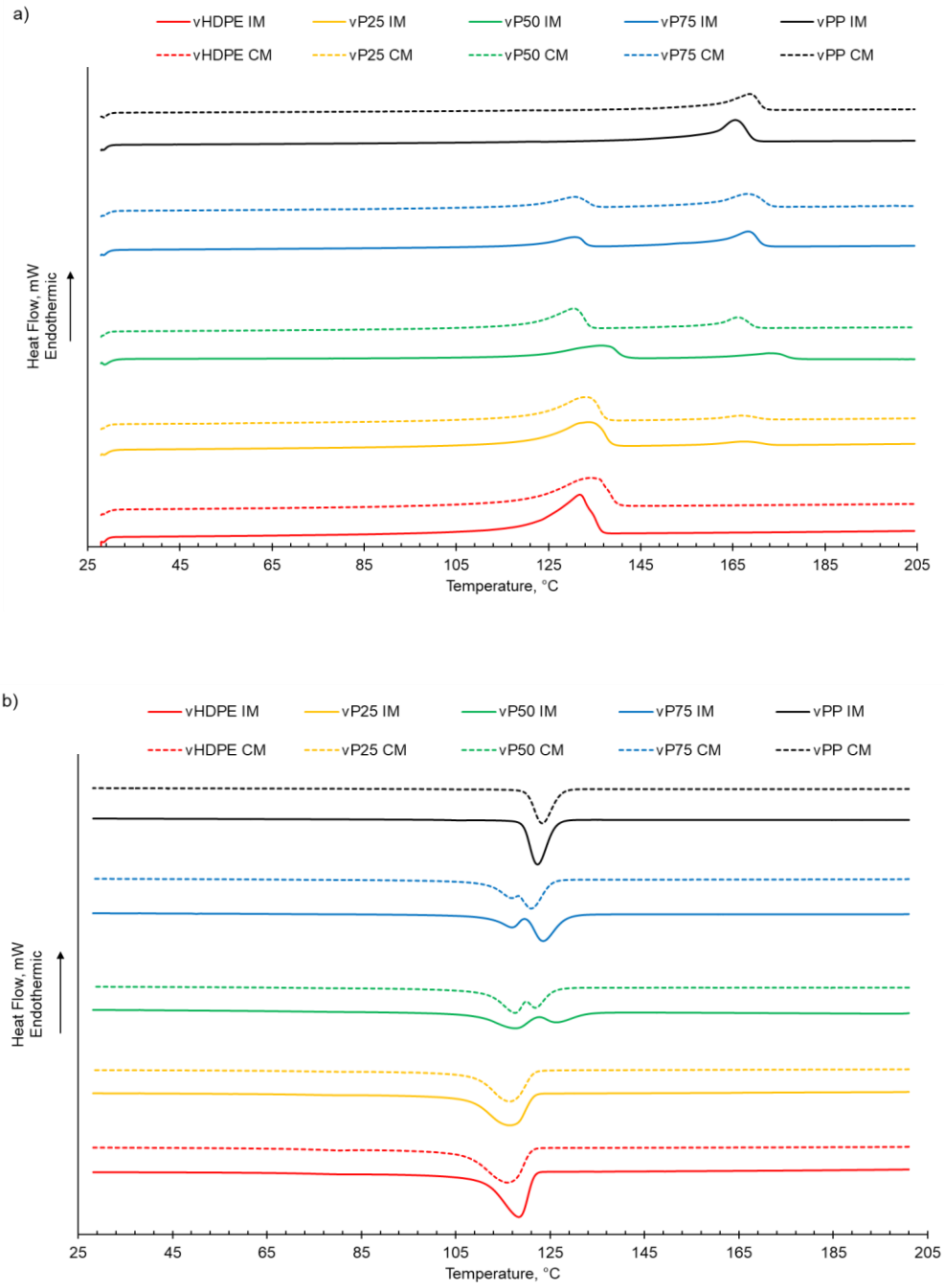

Figure 7.2 Comparison of melting and crystallisation behaviour of vPP:vHDPE blends prepared by CM (Brabender mixing and compression moulding) and IM (twin screw extrusion mixing and injection moulding) where a) melting behaviour b) crystallisation behaviour.

Variation is observed when comparing the crystallinity of rPP:rHDPE blends prepared by the two methods (Figure 7.3). The variation was attributed to the presence of contaminations in the rPP and rHDPE material. Quantities of contaminates will vary

from batch to batch. Very little variation is observed for the vPP and vHDPE crystallinities in the vPP:vHDPE blends prepared by the two methods. The manufacturing method of extrusion mixing and injection moulding, was expected to give a higher crystallinity compared to Brabender mixing and compression moulding due to flow-induced crystallisation and orientation during the injection moulding process. However, several authors have found the opposite.[7,10,11] Mejia et al.[11] found that the crystallinity of vHDPE prepared by compression moulding was higher compared to injection moulding. They suggested that the conditions in the compression moulding technique enabled the vHDPE melt to cool down slowly to room temperature. A slower rate of cooling resulted in larger spherulites size and compact packing. It is important to not only consider the compression moulding experimental conditions, such as cooling rate, but also effects caused by the mixing method. For example, Jaafar et al.[12] discussed the effects of different types of mixers before proceeding with the compression moulding technique for the preparation of a natural fibre composite. They suggested that an internal mixer provided a more efficient mixing and orientation compared to extrusion mixing.

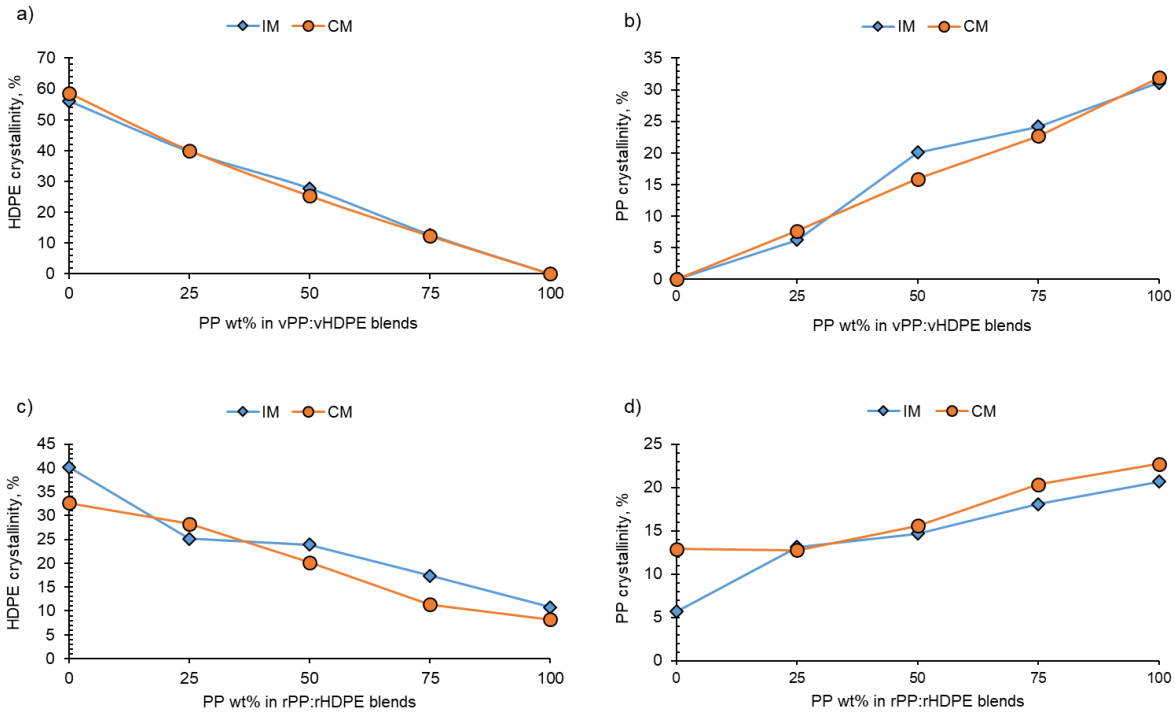

Figure 7.3 Comparison of the PP and HDPE crystallinity in vPP:vHDPE and rPP:rHDPE blends prepared by either IM (twin screw extrusion mixing and injection moulding) or CM (Brabender mixing and compression moulding), a) HDPE crystallinity

in vPP:vHDPE blends b) PP crystallinity in vPP:vHDPE blends c) HDPE crystallinity in rPP:rHDPE blends, and d) PP crystallinity in rPP:rHDPE blends.

7.3.2 Tensile Properties

Generally, the rPP:rHDPE blends had lower tensile properties compared to the vPP:vHDPE blends when prepared by Brabender mixing and compression moulding (Figures 7.4 and 7.5). The extrusion mixing and injection moulded virgin and recycled blends gave a higher *E*, yield strength and UTS compared to the Brabender mixing and compression moulded samples (Figures 7.4 and 7.5). This is in agreement with Nolley et al.[5] and Bartlett et al.[6] who also compared the two processing methods for PP:HDPE blends. The higher *E*, yield strength and UTS can be attributed to the skin-core structure which forms due to shear-induced orientation and crystallization.[7,8]

The extrusion mixing and injection moulded virgin and recycled blends gave a higher elongation compared to the Brabender mixing and compression moulded blends, with the exception of vHDPE and vP25. If mixing was carried out by the same method, comparing injection to compression moulded blends, the injection moulded blends would be expected to have a lower elongation at break due to the molecular orientation in the flow direction. However, the opposite is seen. For the recycled blends, the twin screw extrusion mixing and injection moulded samples gave larger elongation break values compared to ones prepared by Brabender mixing and compression moulding. For example, rP50 gave 1175% and 17% elongation at break for twin screw extrusion mixing and injection moulding, and Brabender mixing and compression moulding respectively. These results indicate that both the crystalline and amorphous domains, are affected dramatically by the extrusion mixing and injection moulding process. At larger strain, tensile behaviour is affected largely by the polymer components compatibility[13]. Song et al.[14] found that interfacial adhesion was dominated by phase compatibility. The twin screw extruder used in the injection moulding process has a greater mixing ability resulting in an improved phase dispersion and finer phase separation compared to the Brabender used in compression moulding[15]. The increase in ductility in recycled injection moulded blends compared to compression moulded blends could be due to the formation of entanglements are the interface as suggested by Salih et al.[16] but also due to improved phase dispersion resulting in better interfacial adhesion[17].

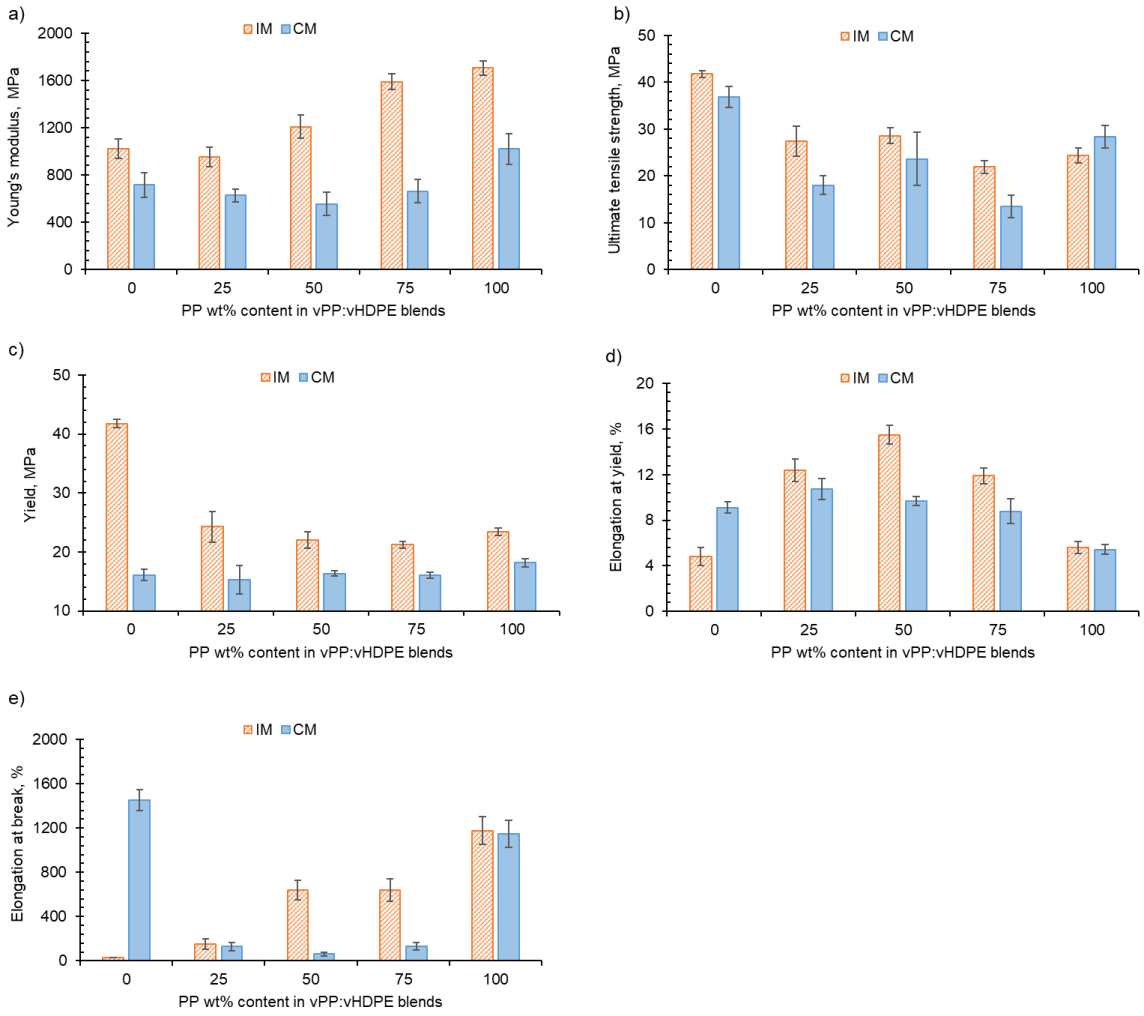

Figure 7.4 Tensile behaviour of vPP:vHDPE blends prepared by either IM (twin screw extrusion mixing and injection moulding) or CM (Brabender mixing and compression moulding) a) Young's modulus, b) ultimate tensile strength, c) yield strength, d) elongation at yield, and, e) elongation at break.

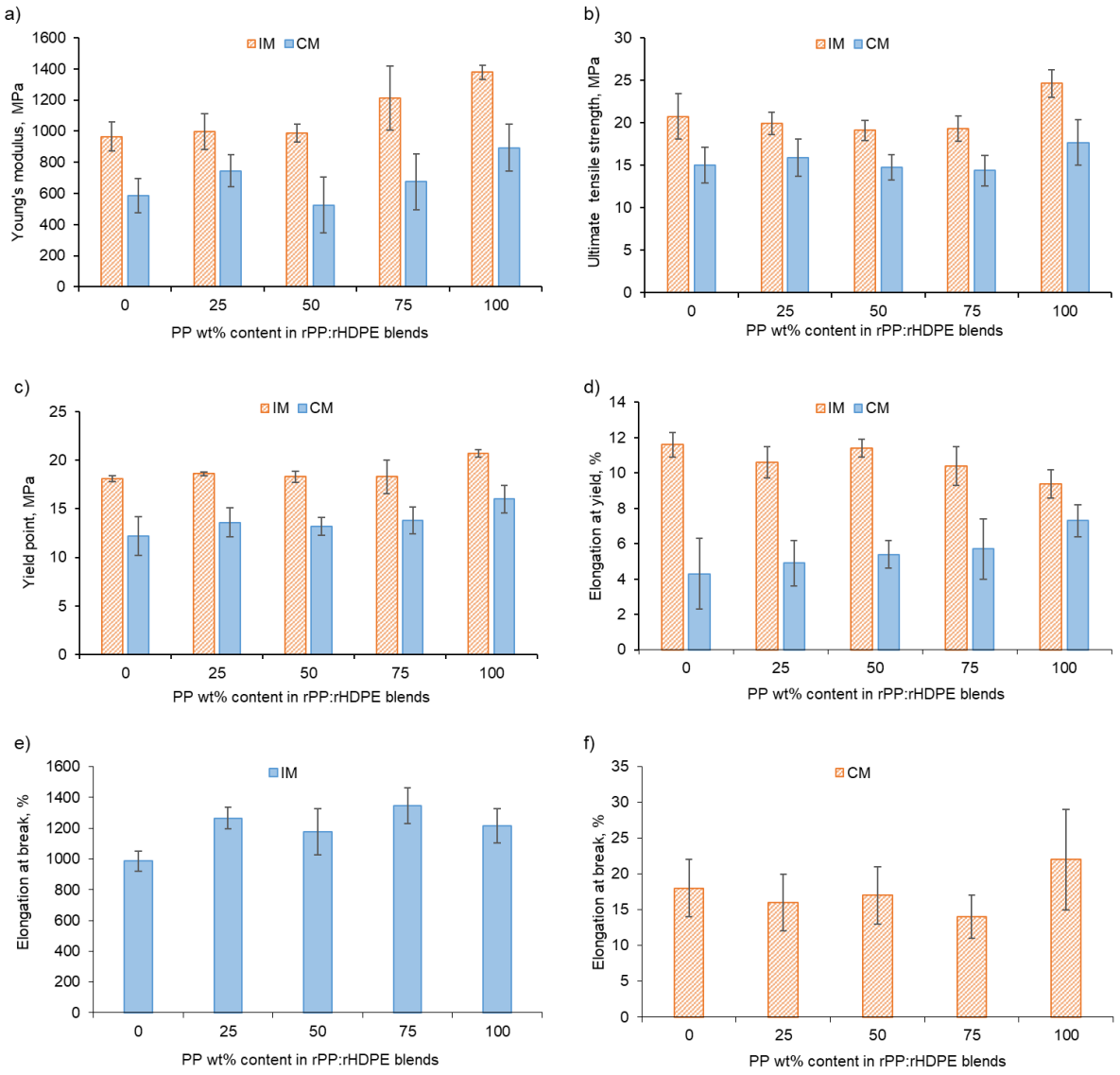

Figure 7.5 Tensile behaviour of rPP:rHDPE blends prepared by either IM (twin screw extrusion mixing and injection moulding or CM (Brabender mixing and compression moulding) a) Young's modulus, b) ultimate tensile strength, c) yield strength, d) elongation at yield, e) elongation at break for IM, and, f) elongation at break for CM.

7.4 Conclusion

This comparative chapter investigated 5 virgin and recycled PP:HDPE blends prepared by two different methodologies, extrusion mixing/injection moulding, and Brabender mixing/compression moulding. The method of blend preparation had little difference on the thermal behaviour of either the virgin or recycled PP:HDPE blends. As there was little difference in the crystallinity in the two manufacturing methods for the PP:HDPE blends suggests that crystallinity does not have a great influence on the mechanical properties. This is supported by Xie et al.[7] who investigated the

mechanical properties of UHMWPE:PP blends by injection moulding and compression moulding. They deduced that even though compression moulding gave a slightly higher crystallinity there was a lower Young's modulus and yield strength compared to injection moulding. It was concluded that crystallinity was less influential to the mechanical properties compared with morphology and blend composition.

The tensile behaviour of the virgin and recycled PP:HDPE blends was found to be affected by the manufacturing method. The unexpected behaviour of vHDPE up to vP25 is attributed to the polymer chain orientation caused by the twin screw extrusion mixing and injection moulding process. Both virgin and recycled PP:HDPE blends by injection moulding gave improved tensile properties compared to compression moulding which has been attributed to the formation of a skin-core structure. Extrusion mixed and injection moulded recycled blends gave significant increase in elongation at break compared to the Brabender mixed and compression moulded recycled blends. This indicated that both the crystalline and amorphous domains, and the phase behaviour are affected dramatically by the manufacturing process.

References

1. S. Hong, J. Hwang, J. Kang, K. Yoon, *Korea Aust Rheol J* **2015**, *27*, 309.
2. G. Zhong, Z. Li, *Polymer Engineering and Science* **2005**, *45.*
3. A. K. Bledzki, O. Faruk, *Polymer Plastics Technology and Engineering* **2004**, *43.*
4. D. Pérez-Rocha, A. B. Morales-Cepeda, F. Navarro-Pardo, T. Lozano-Ramírez, P. G. LaFleur, *International Journal of Polymer Science* **2015**, *2015*, 493206.
5. E. Nolley, J. Barlow, D. R. Paul, *Polym. Eng. Sci.* **1980**, *20*, 364.
6. D. W. Bartlett, J. W. Barlow, D. R. Paul, *J. Appl. Polym. Sci.* **1982**, *27*, 2351.
7. M. Xie, J. Chen, H. Li, *J. Appl. Polym. Sci.* **2009**, *111*, 890.
8. W. Cao, K. Wang, Q. Zhang, R. Du, Q. Fu, *Polymer* **2006**, *47*, 6857.
9. G. Spadaro, G. Rizzo, *Eur. Polym. J.* **1989**, *25*, 1189.
10. J. S. Godinho, A. Cunha, R. J. Crawford, *Proceedings of the Institution of Mechanical Engineers, Part L: Journal of MAterials: Design and Applications* **2002**, *216*, 179.
11. E. B. Mejia, A. I. Mourad, A. S. B. Faqer, D. F. Halwish, H. O. A. Hefeiti, S. M. A. Kashadi, N. Cherupurakal, M. S. Mozumder, presented at Advances in Science and Engineering Technology International Conferences (ASET)**2019**.
12. J. Jaafar, J. P. Siregar, C. Tezara, M. H. M. Hamdan, T. Rihayat, *The International Journal of Advanced Manufacturing Technology* **2019**, *105*, 3437.
13. S. Jose, A. S. Aprem, B. Francis, M. C. Chandy, P. Werner, V. Alstaedt, S. Thomas, *Eur. Polym. J.* **2004**, *40*, 2105.
14. J. Song, A. Bringuier, S. Kobayashi, A. M. Baker, C. W. Macosko, *Polymer Journal* **2012**, *44*, 939.
15. T. Kallel, V. Massardier-Nageotte, M. Jaziri, J. Gérard, B. Elleuch, *J. Appl. Polym. Sci.* **2003**, *90*, 2475.
16. S. Salih, A. Hamood, A. Alsalam, *Mod. Appl. Sci.* **2013**, *7*, 33.
17. Z. K. Marwat, M. K. Baloch, *Int J Thermophys* **2015**, *36*, 2755.

8.0 Conclusions and Future Work

8.1 General Conclusions

Improving the consistency and performance of recyclate to obtain desirable end-use properties at a low cost is a key challenge in order to achieve a circular plastic economy. PO waste contributes nearly half of all plastic wastes so understanding the variability in PO recyclate before optimisation is important. The aim of this thesis was to provide a comparative study of the mechanical properties, thermal properties and phase morphology over a range of compositions for virgin and recycled PP:HDPE blends. The mechanical properties were determined by DMA and tensile testing. The thermal properties by DSC and the phase morphology by SEM and AFM.

The key conclusions for the performance of virgin and recycled PP:HDPE blends are as follows:

1. PP:HDPE blend composition

PP:HDPE blend performance was found to be dependent upon the composition for:

- The crystallinity, thermal properties (T_m, ΔH_c) and phase morphology of both the virgin and recycled blends. For example, the AFM studies found as PP wt% increased, the morphology showed a transition from homogenous to droplet matrix and finally to co-continuous.
- The tensile properties of the virgin and recycled blends. For example, the Young's moduli were compared to the predicted moduli determined by the Rules of Mixtures. Positive and negative deviations were observed as the composition varied and were additionally related to changes in morphology.

2. The effect of the recycling process on PP:HDPE blends

The recycling process was found to effect the properties of virgin and recycled PP:HDPE blends due to the presence of thermo-mechanical and thermo-oxidative degradation mechanisms. The studies concluded:

- Presence of contaminates in rPP and rHDPE. Contaminates were present due to the challenge and high cost of PP and PE separation during the recycling process.
- Recycled blends had lower T_m and crystallinity compared to the virgin blends due to structural deterioration and the formation of imperfect crystals.

- The recycled blends had lower T_α and T_β due to structural deterioration caused by the recycling process.
- The *E'*, *E''* and tensile behaviour of the recycled blends were not substantially affected by the recycling process.

3. Tensile behaviour of vHDPE

The unexpected tensile behaviour of vHDPE up to the vP25 blend was observed in the yield strength, elongation at yield and at break. This tensile behaviour was not observed in the comparative study, which involved blend preparation by Brabender mixing and compression moulding. Therefore, it was concluded that the exposure to twin screw extrusion mixing and strong shear and elongation flow during injection moulding caused a highly orientated, potentially interlocking crystalline structure.

4. Nanomechanical investigations by QI mode (AFM)

The QI mode was successfully implemented to determine information on the topography, morphology and Young's moduli of virgin and recycled PP:HDPE blends. The stiffness and Young's moduli maps provided an insight into the PP and HDPE phase distributions in the blends. There was good correlation between the phase distributions observed in the tapping mode and QI mode. However, it has to be noted that tapping mode is expected to have a better resolution. It was found extracting the Young's moduli via the arithmetic mean gave similar values obtained from tensile testing, whereas the highest frequency peak from the histogram underestimates.

Overall Summary

In conclusion, the mechanical properties of virgin and recycled PP:HDPE blends were not only dependent upon composition but also on the crystallinity and the compatibility between the phases. Overall, this thesis has shown the relationship between the processing-structure-property relationship for virgin and recycled PP:HDPE blends. The limitations of the work include the recyclate being subjected to only one reprocessing cycle, and the recyclate being obtained from only one recycling plant. Therefore, the results obtained were site specific and may not be applicable to recyclate which have undergone further reprocessing cycles. To overcome this, section 8.2 discusses that future work will include investigating the scale of recyclate

variability along with dealing with a variation in MFI causes by several reprocessing cycles. Finally, it was not possible to identify a recyclate blend ratio or ratios, which provided an optimal thermo-mechanical performance due to the complicated processing-crystallinity-thermo-mechanical properties-morphology relationship.

8.2 Future Work

The work set out and discussed in this thesis could be expanded further in the following areas.

8.2.1 Scale of Variability

The rPP and rHDPE used in this study were obtained from one recycling facility only. However, it is known that recyclate performance, for example MFI, varies greatly from location to location. Therefore, future work would include mapping the mechanical properties, thermal properties and phase morphology of recyclate obtained from different recycling facilities from around the UK and rest of the world. This would contribute to understanding the variability from site to site and the factors affecting variability such as plastic waste sorting techniques used.

8.2.2 Mixing Different Recyclate Grades

To improve a recyclate performance a third component such as a compatibiliser, is typically added. Literature studies have added virgin polymers into rPO blends and found an improvement in overall performance. However, this is not aiding the circular economy initiative by introducing virgin polymers into reprocessing. Therefore, it would be an interesting study to understand the effect of adding high MFI PO recyclate as the third component on the overall blend performance. This has the potential of leading to tuning recyclate performance depending upon desired end application.

8.2.3 Manufacturing Methodology

Future work would include expanding the initial comparison of manufacturing techniques, which was discussed in Chapter 7. The study would include investigating the effects of the mixing technique and processing, by the following routes:

a. Brabender mixer and injection moulding
b. Brabender mixer and compression moulding
c. Twin screw extruder and injection moulding
d. Twin screw extruder and compression moulding

8.2.4 Tapping Mode

As discussed in Chapter 4, AFM in tapping mode was used to determine the morphology of virgin PP:HDPE blends. Future work would therefore include expanding the study to recycled blends. A comprehensive profile of the stiffness, Young's modulus, height, and phase images would then be achieved via the QI and tapping AFM modes.

Appendix 1 AFM QI mode height, stiffness and Young's modulus images obtained at 256 x 256 pixels for vPP:vHDPE blends.

PP:HDPE Blend		Height, nm	Stiffness, N m^{-1}	Young's modulus, GPa
vHDPE	Site 1	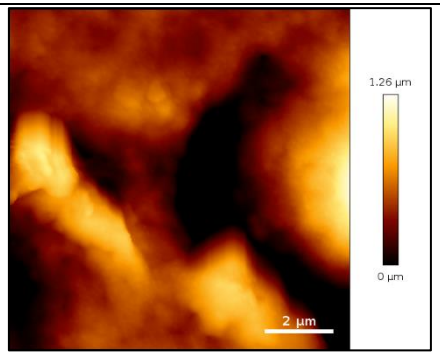	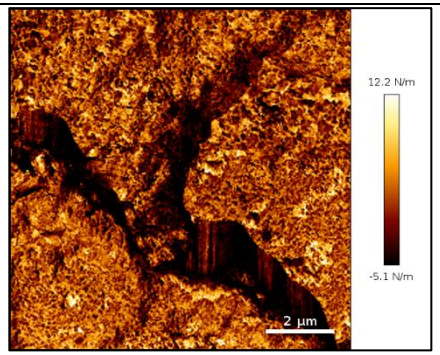	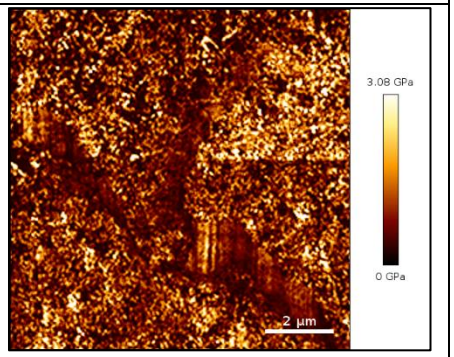
	Site 2	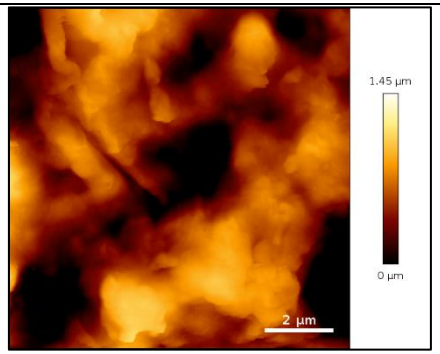	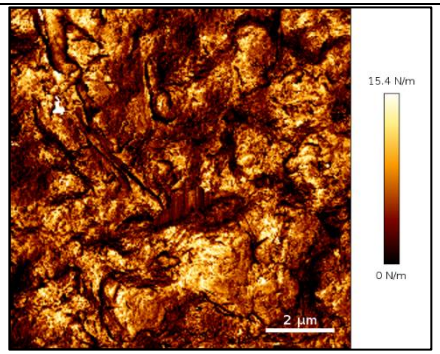	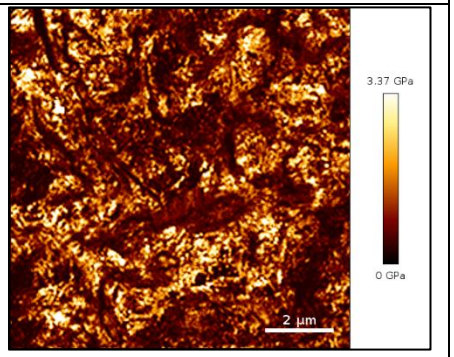
		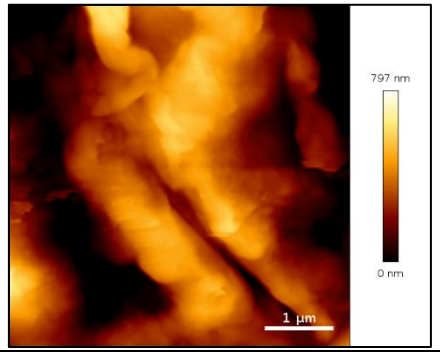	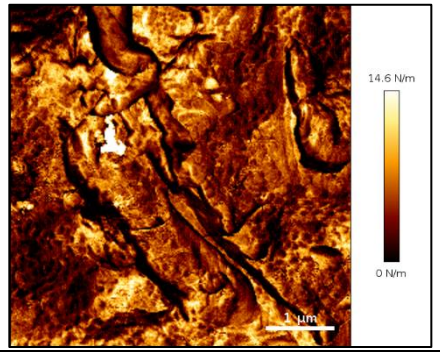	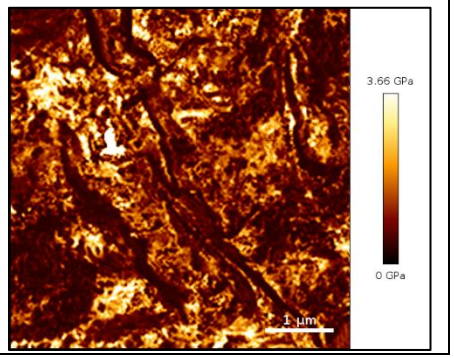

Appendix 1

	Site 3	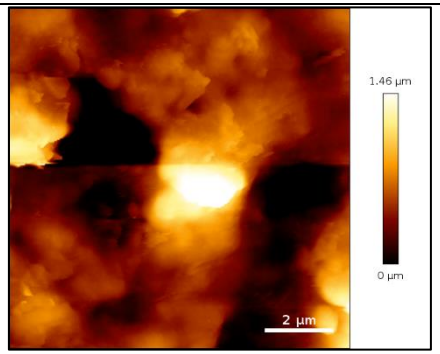	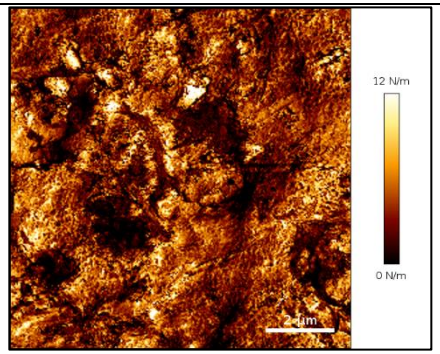	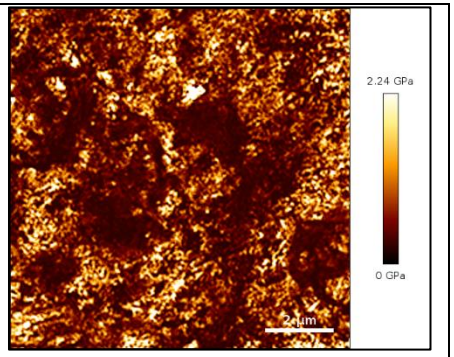
		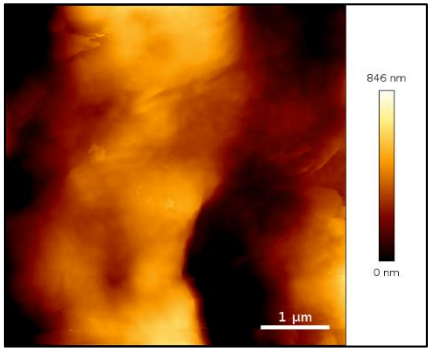	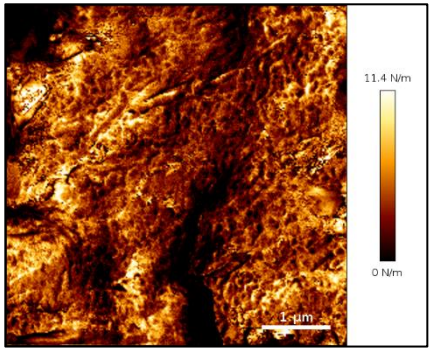	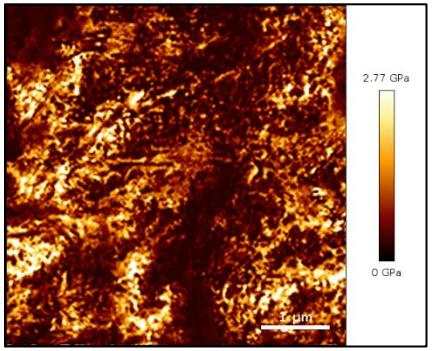
	Site 4	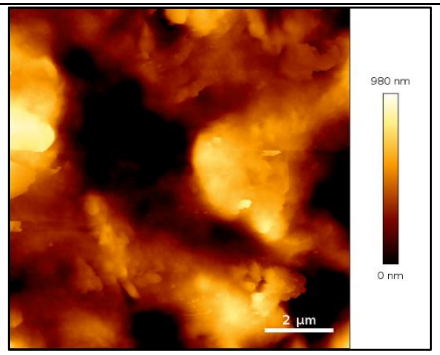	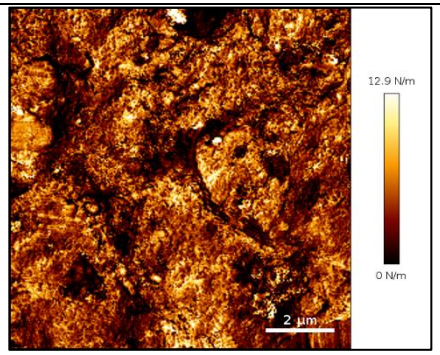	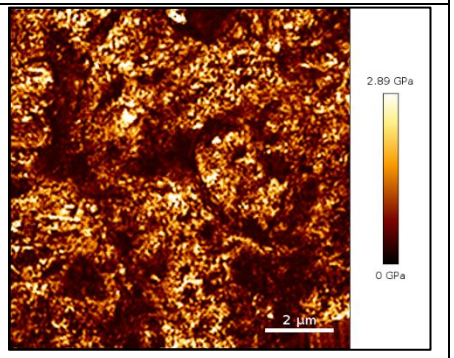

Appendix 1

		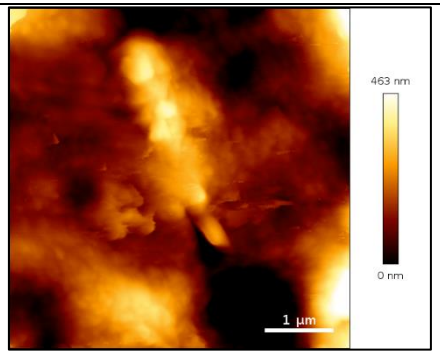	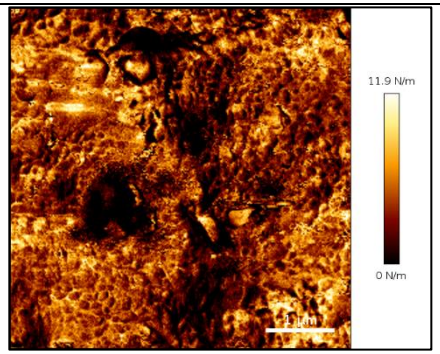	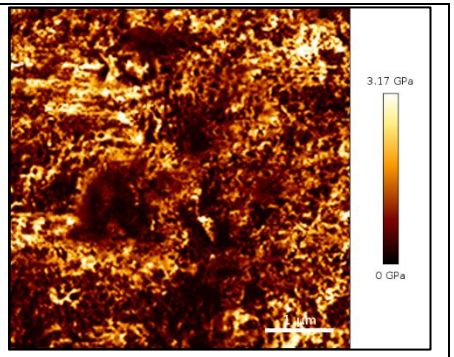
vP10	Site 1	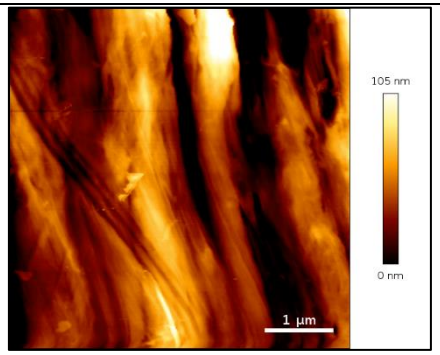	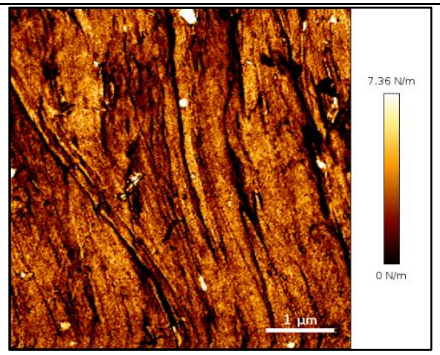	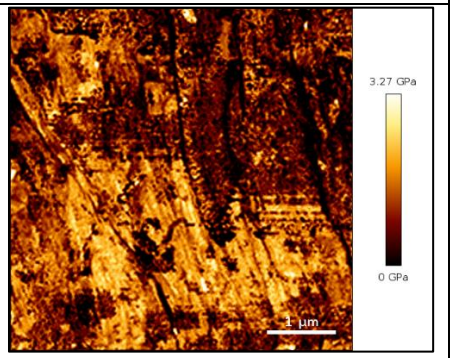
	Site 2	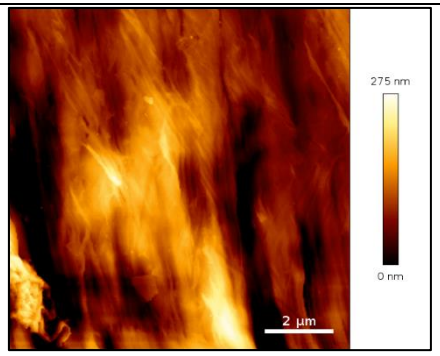	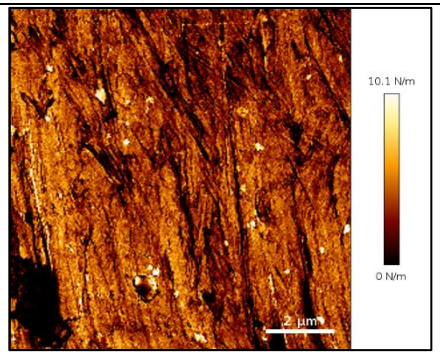	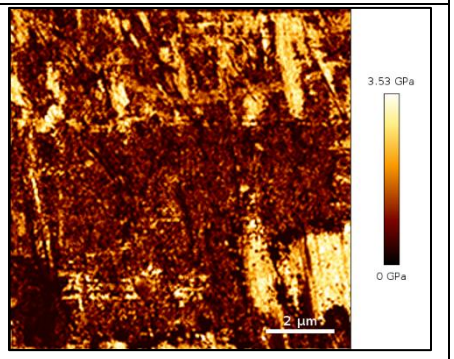

Appendix 1

		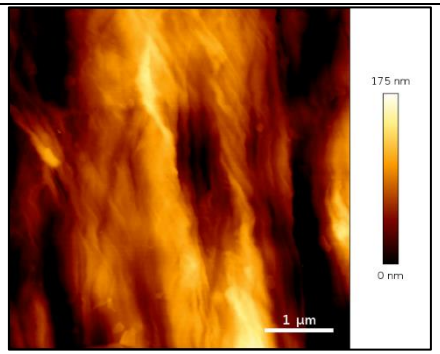	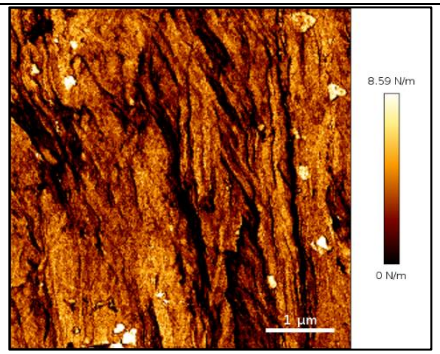	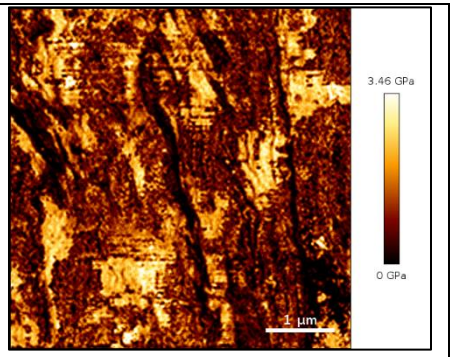
	Site 3	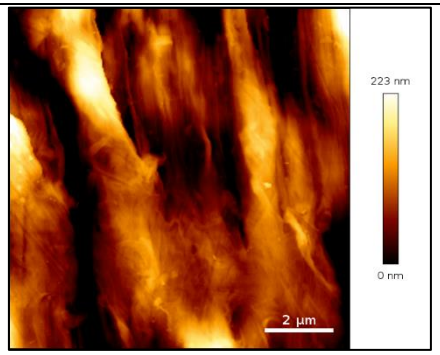	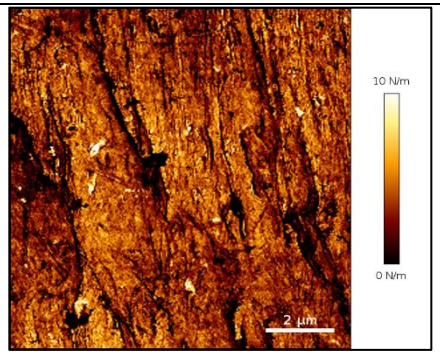	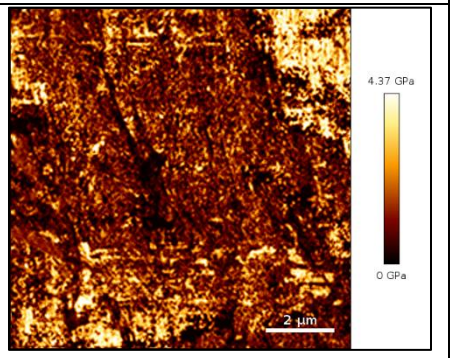
		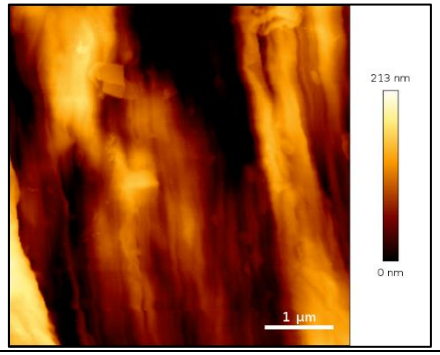	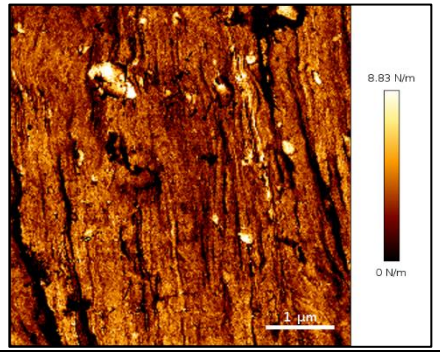	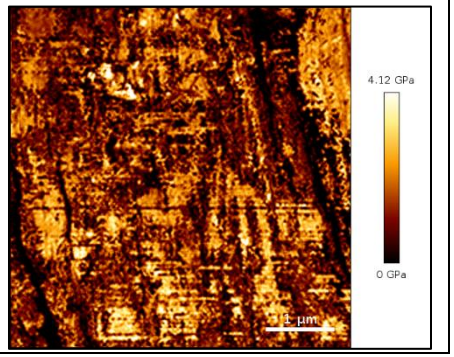

	Site 4	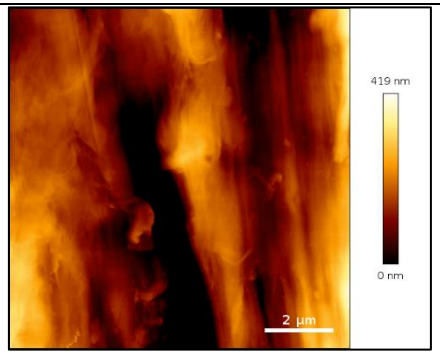 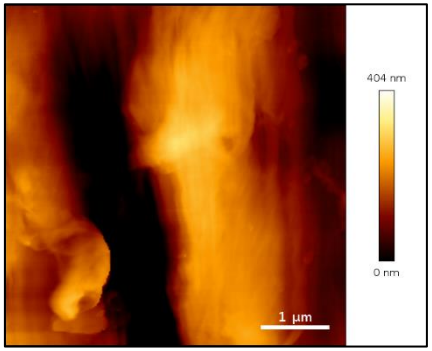	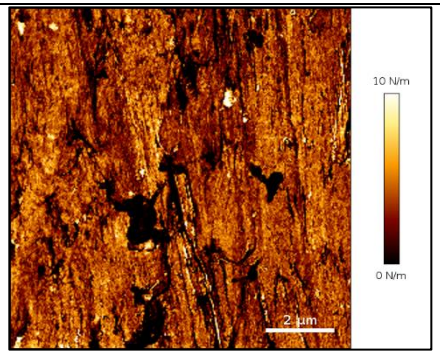 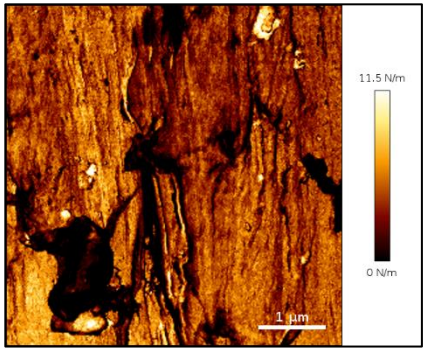	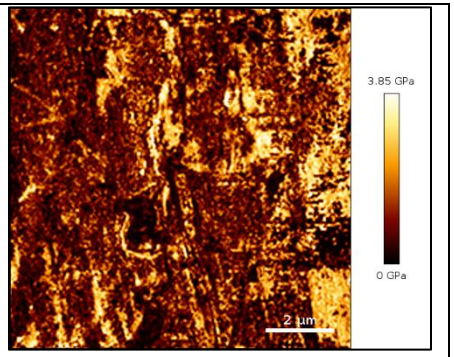 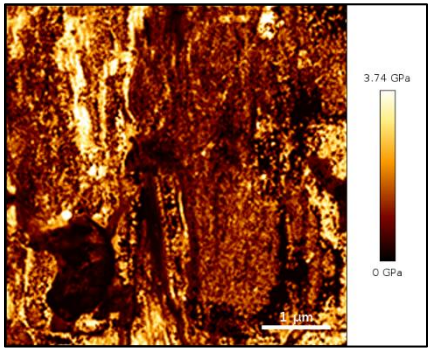
vP20	Site 1	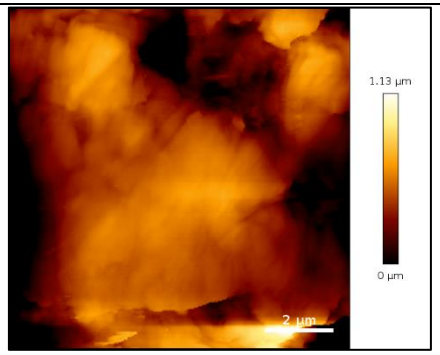	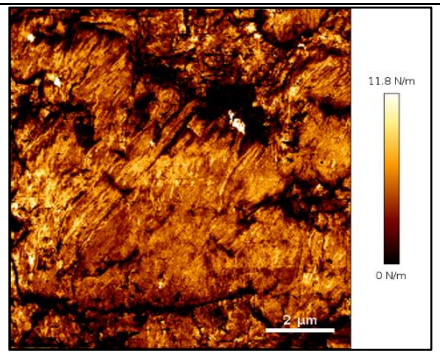	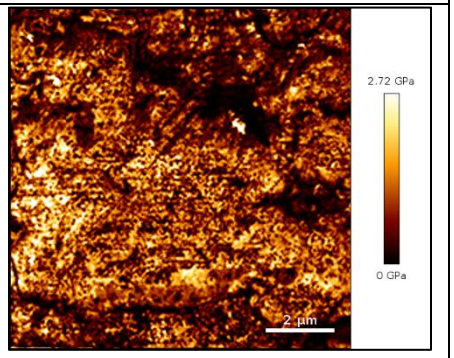

Appendix 1

		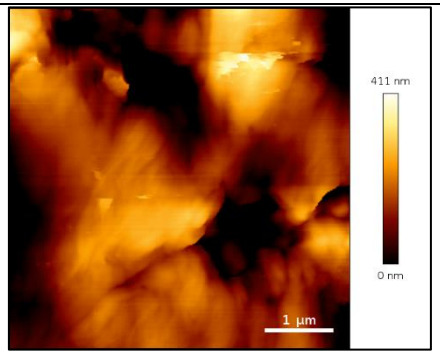	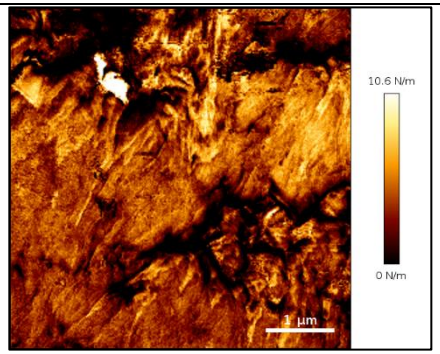	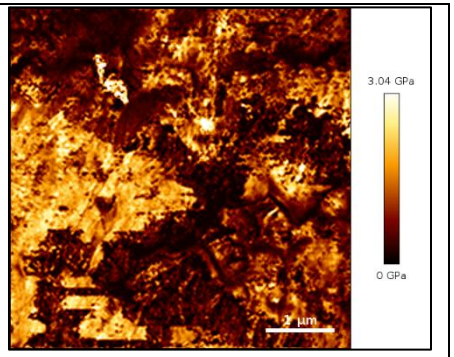
	Site 2	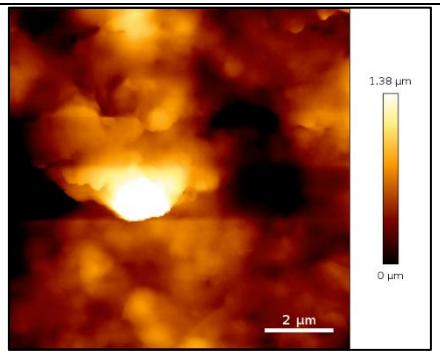	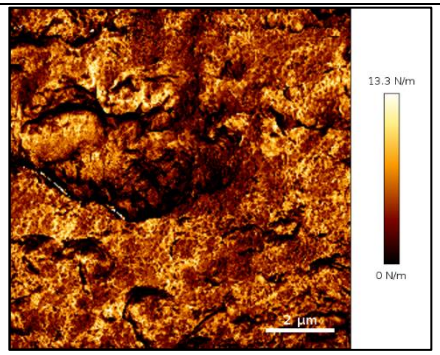	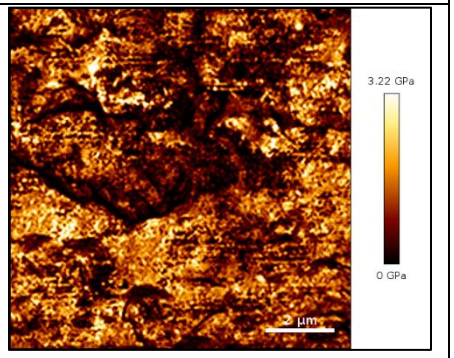
		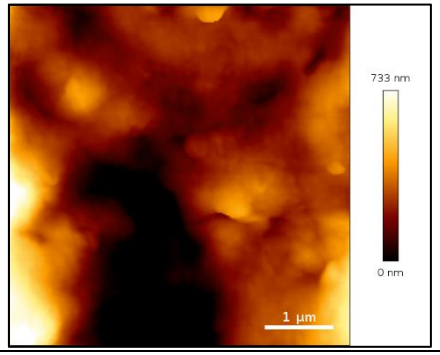	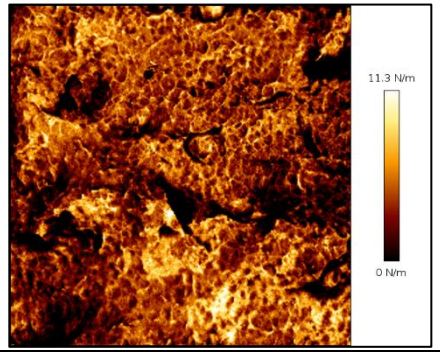	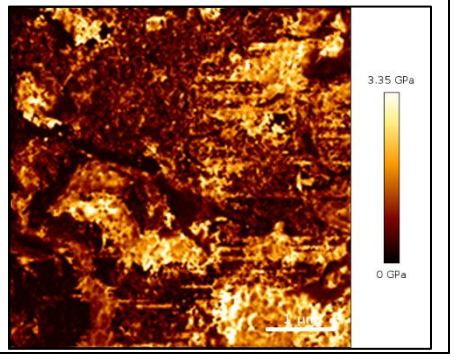

	Site 3	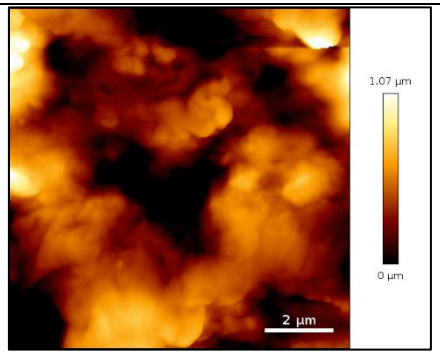 1.07 µm 0 µm 2 µm	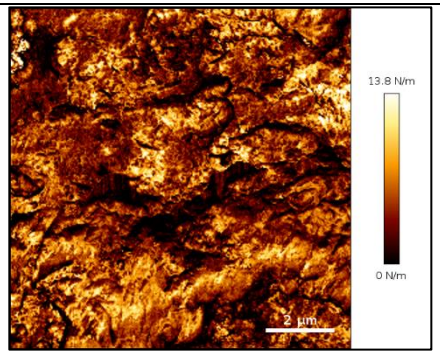 13.8 N/m 0 N/m 2 µm	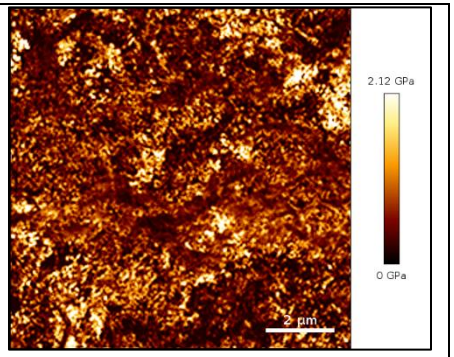 2.12 GPa 0 GPa 2 µm
		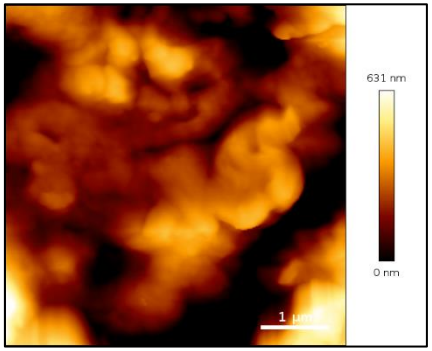 631 nm 0 nm 1 µm	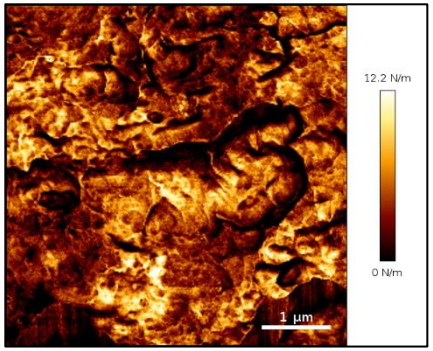 12.2 N/m 0 N/m 1 µm	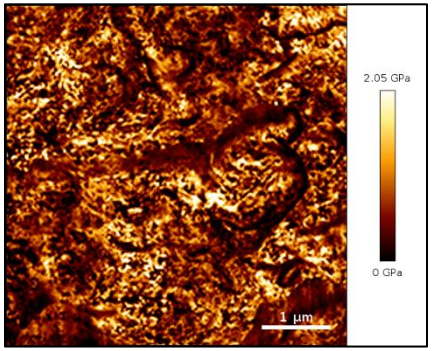 2.05 GPa 0 GPa 1 µm
	Site 4	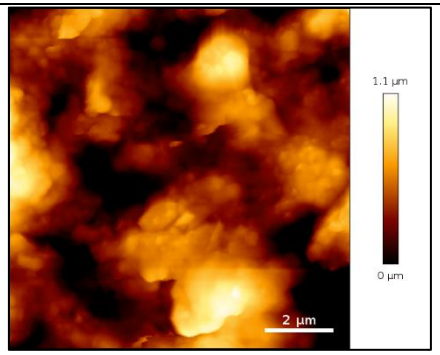 1.1 µm 0 µm 2 µm	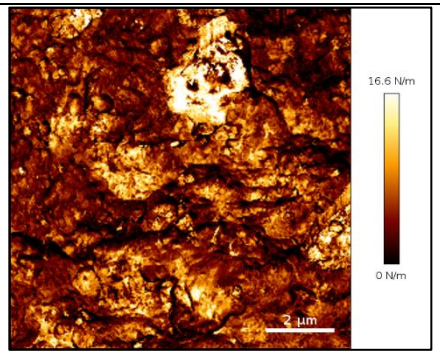 16.6 N/m 0 N/m 2 µm	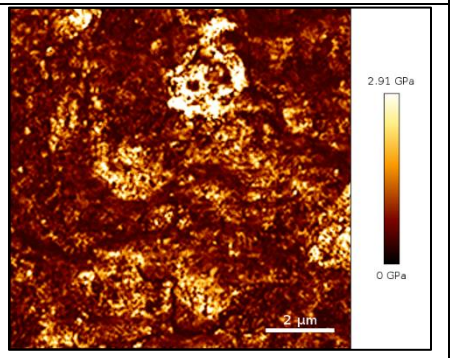 2.91 GPa 0 GPa 2 µm

		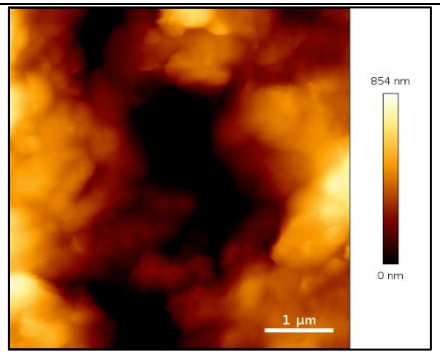	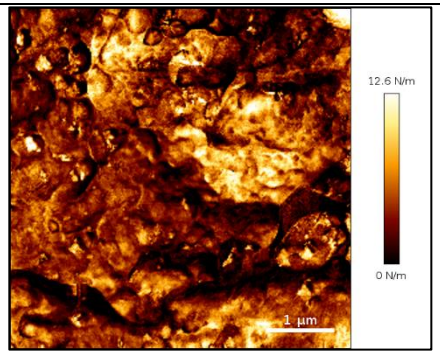	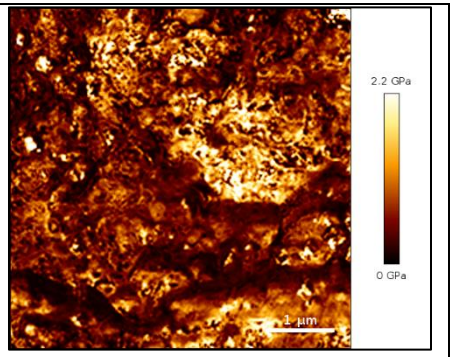
vP25	Site 1	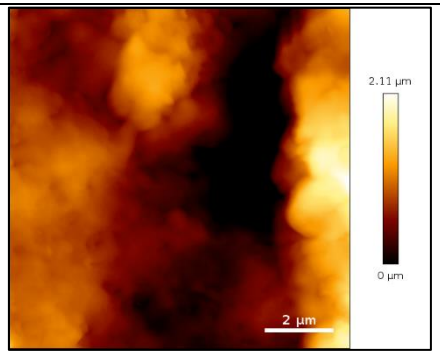 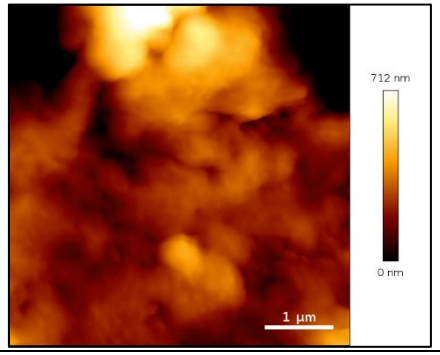	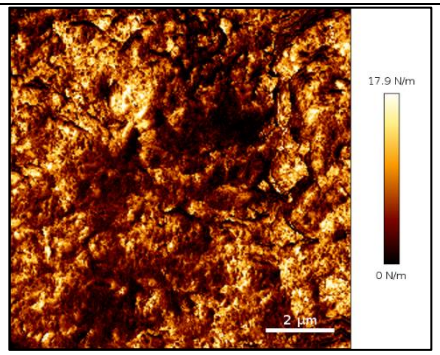 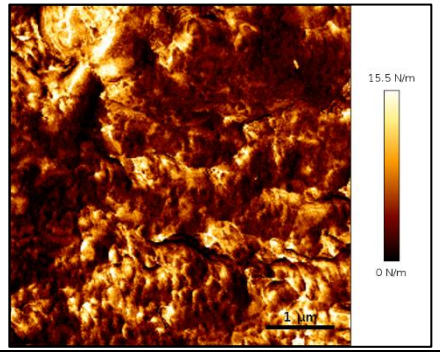	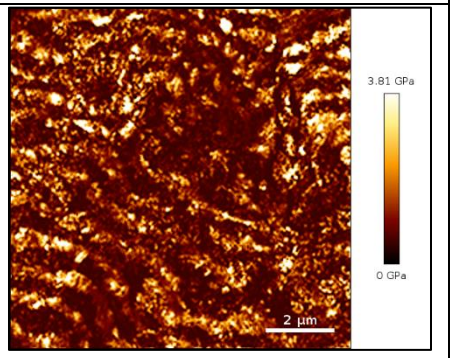 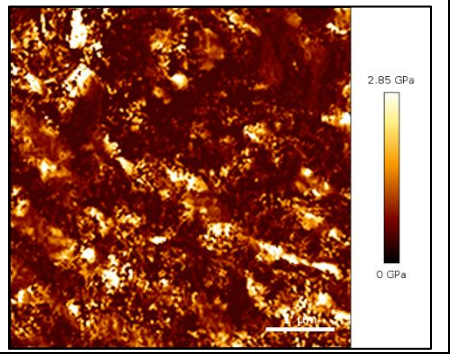

	Site 2	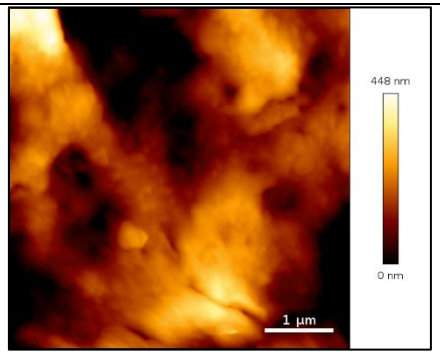	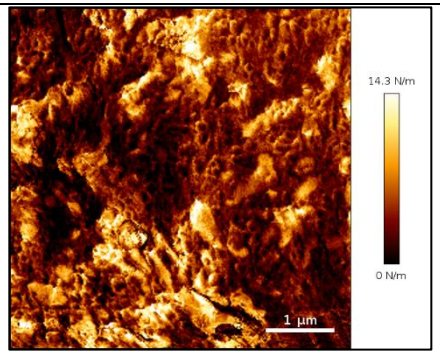	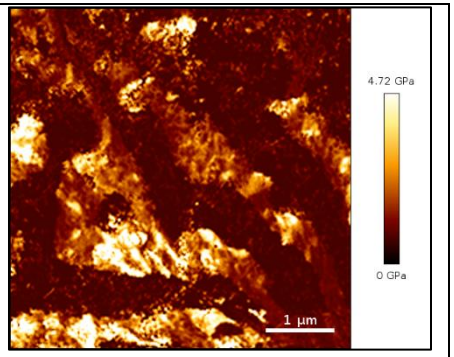
	Site 3	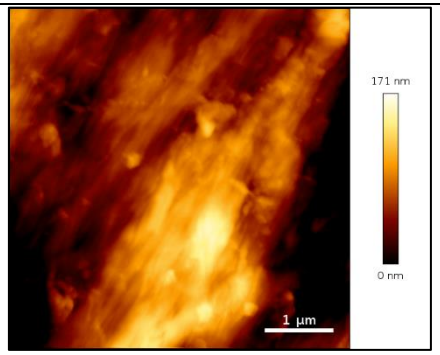	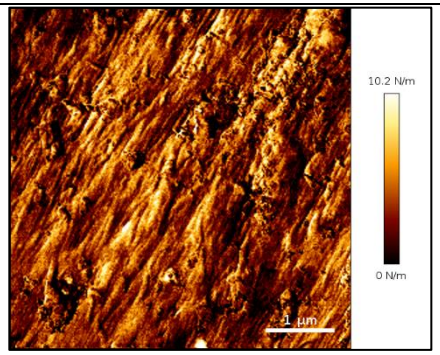	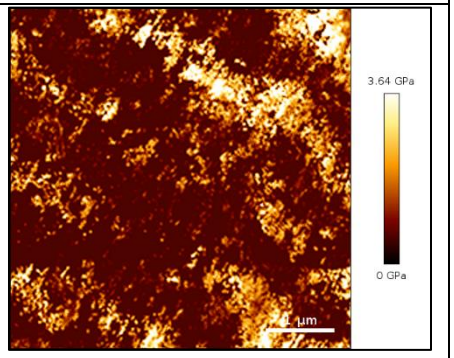
	Site 4	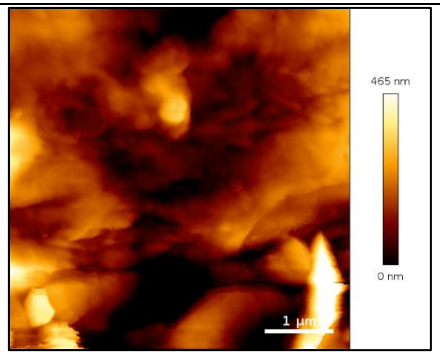	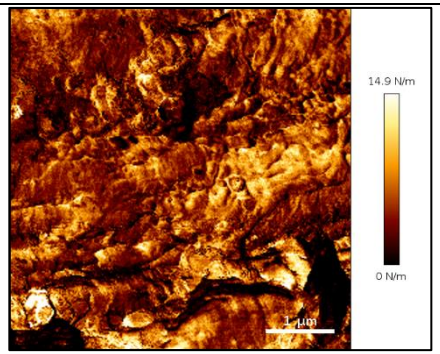	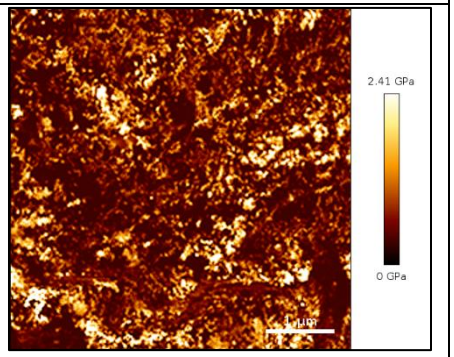

Appendix 1

vP40	Site 1	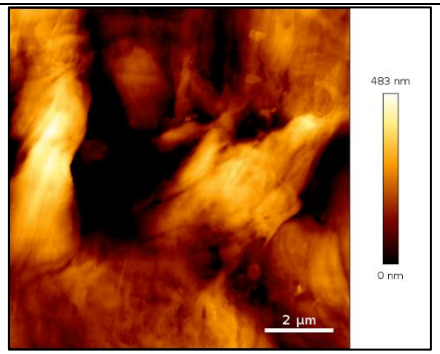	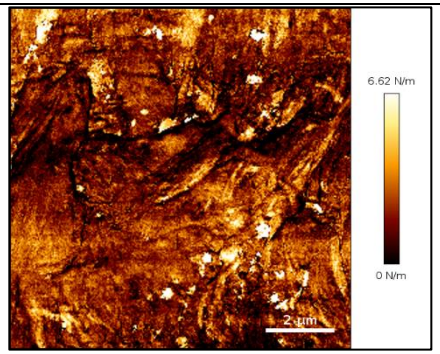	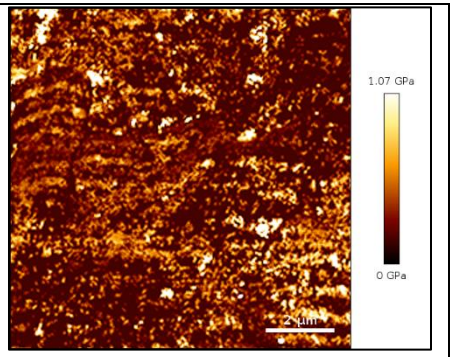
		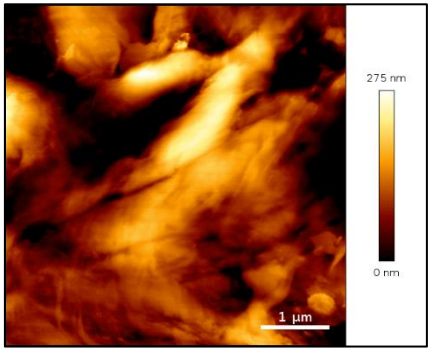	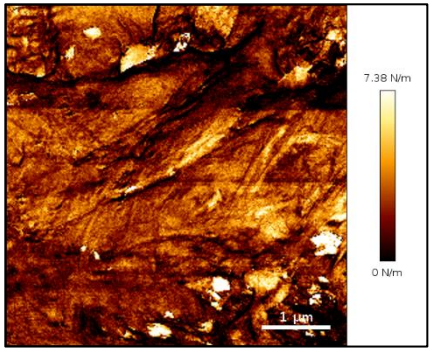	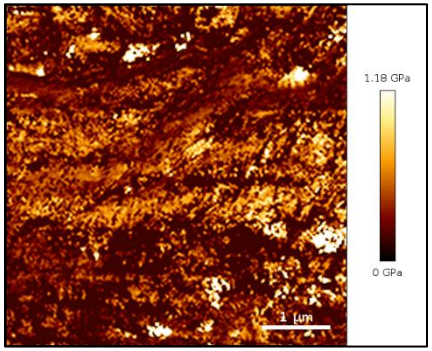
	Site 2	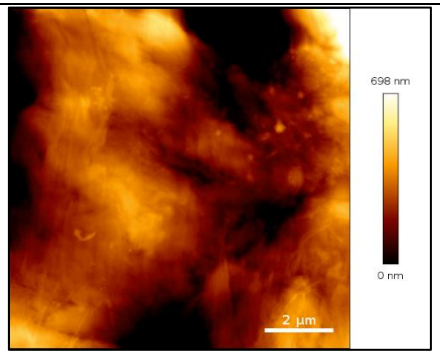	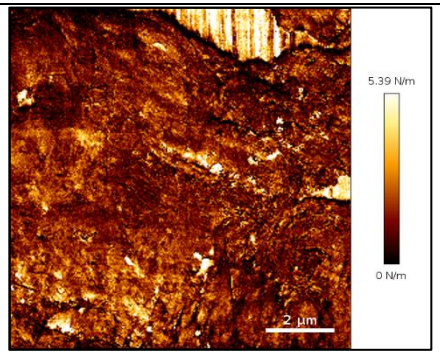	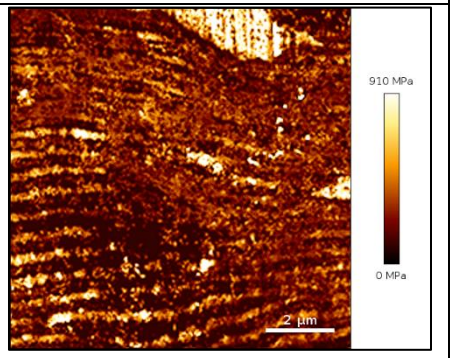

		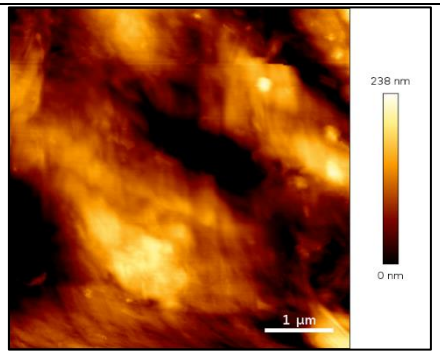	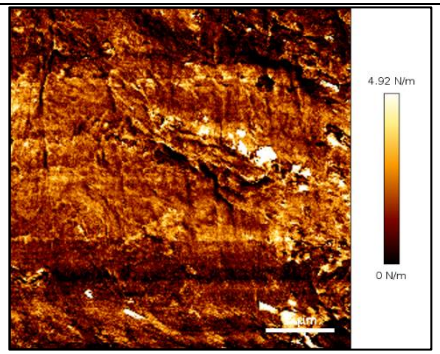	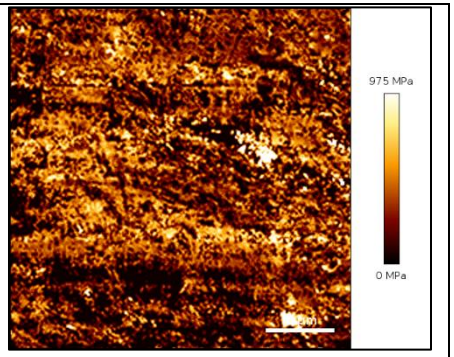
	Site 3	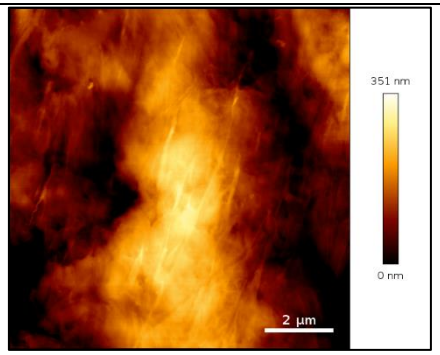 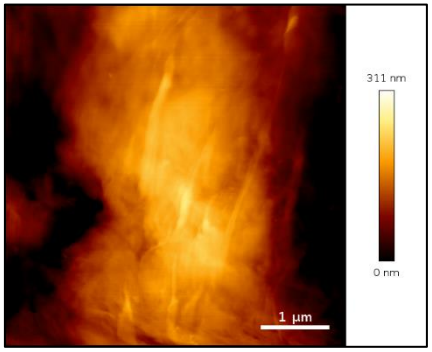	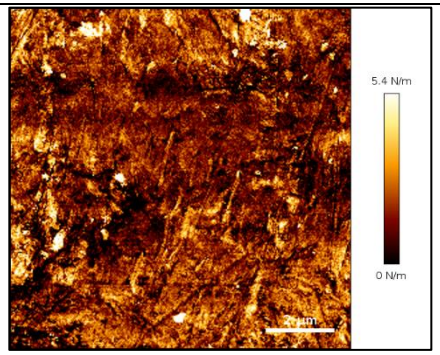 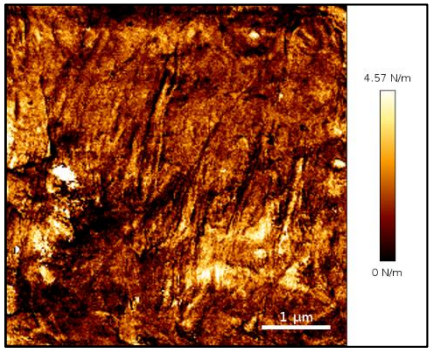	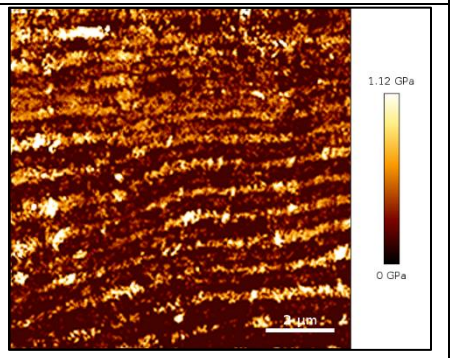 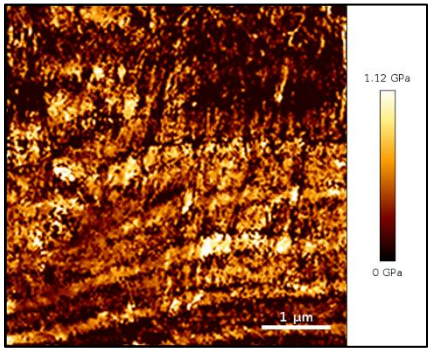

Appendix 1

	Site 4	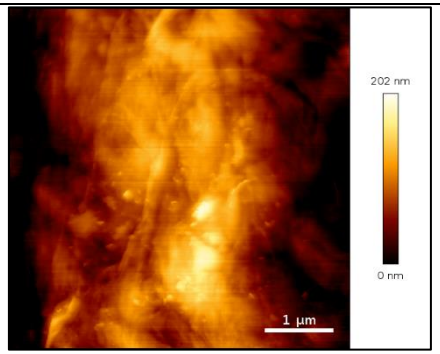	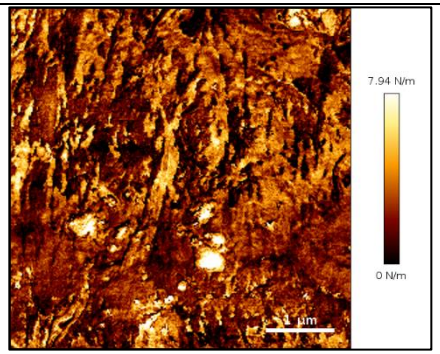	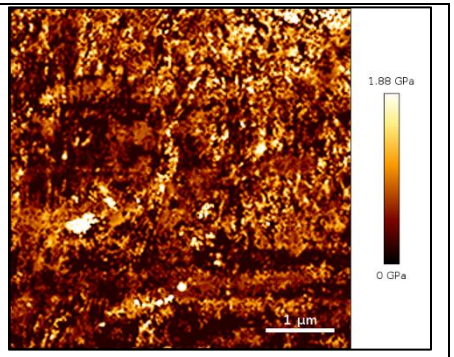
vP50	Site 1	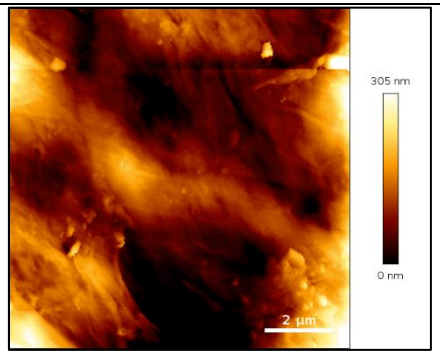 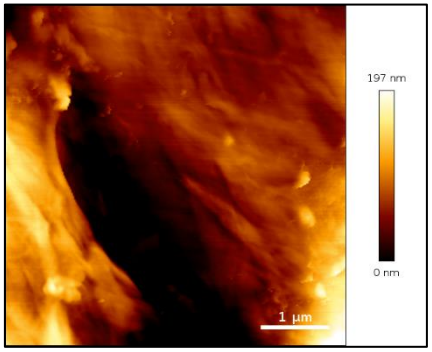	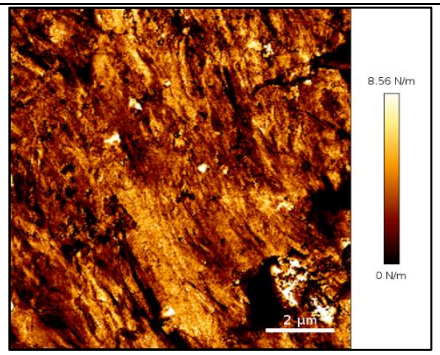 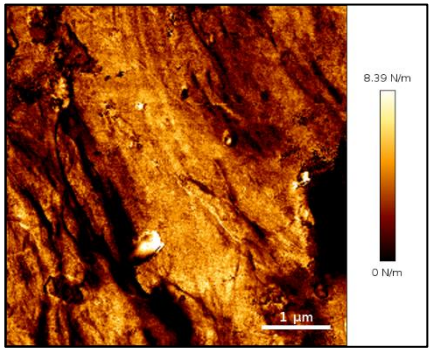	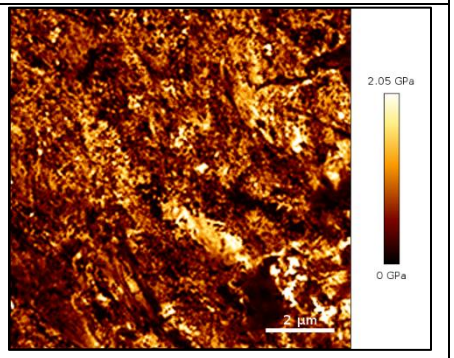 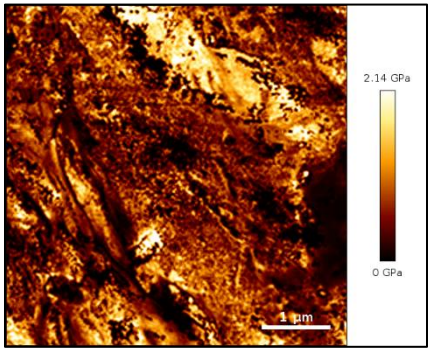

Appendix 1

	Site 2	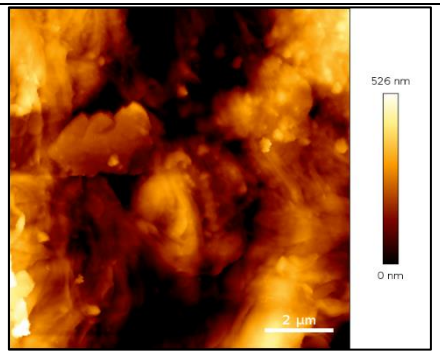	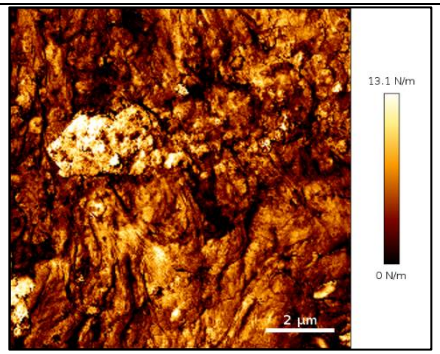	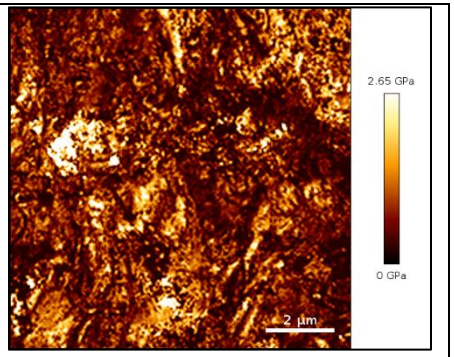
		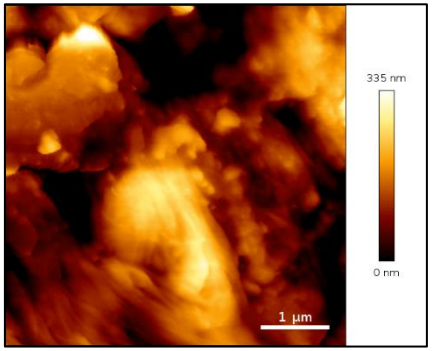	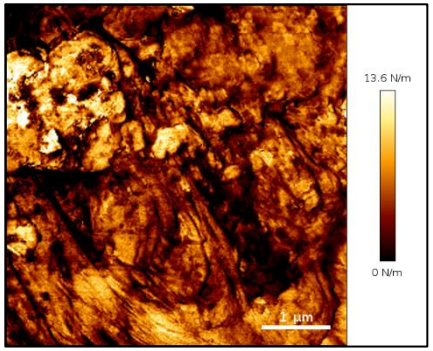	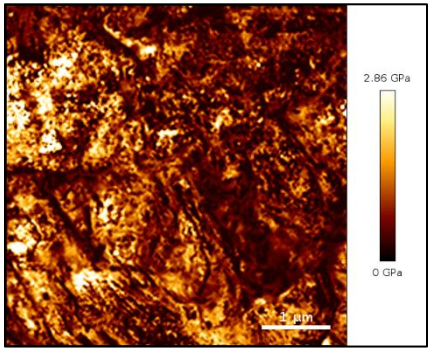
	Site 3	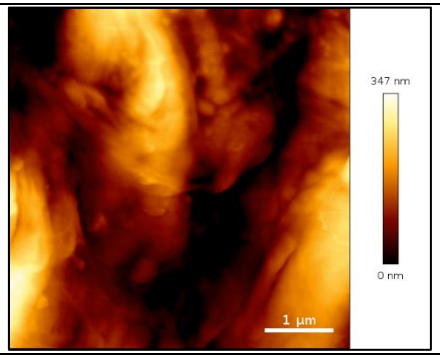	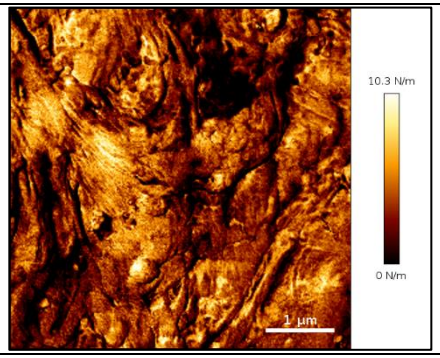	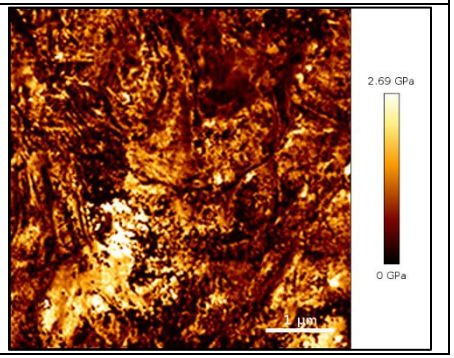

	Site 4	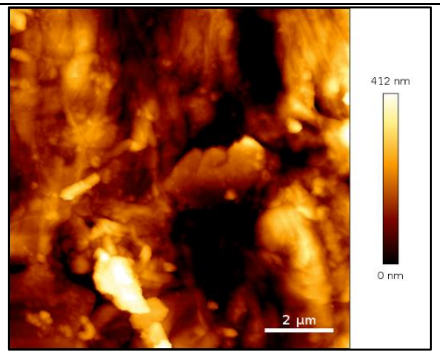	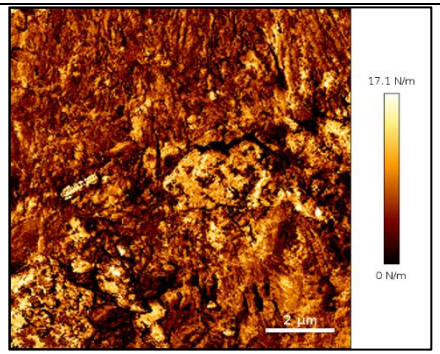	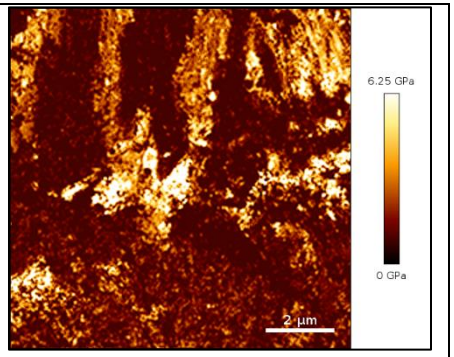
		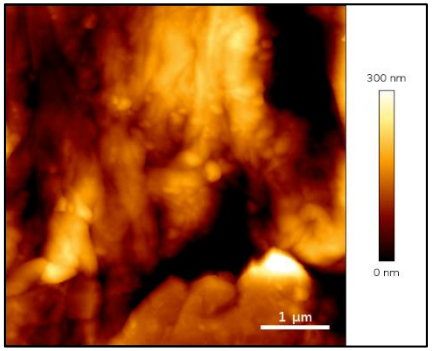	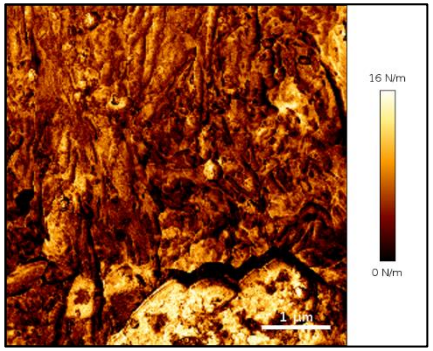	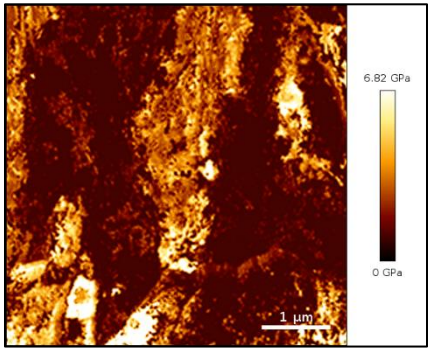
vP60	Site 1	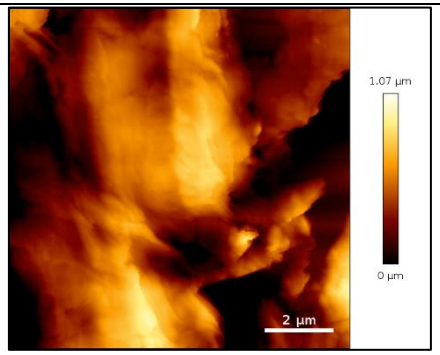	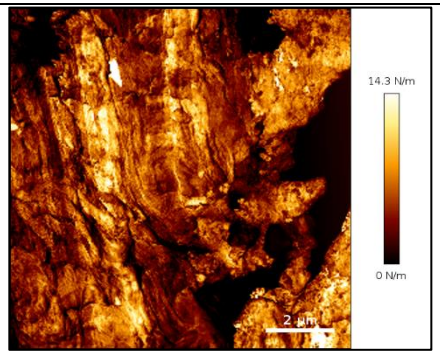	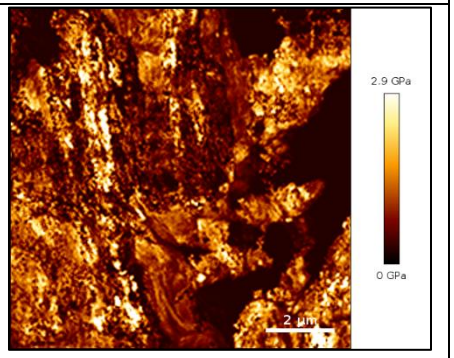

Appendix 1

		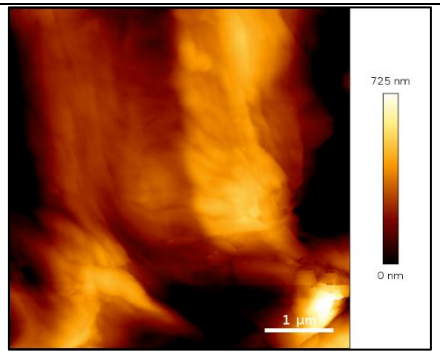	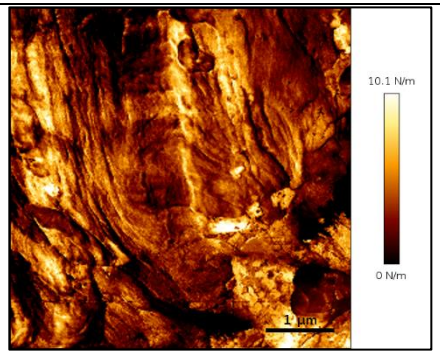	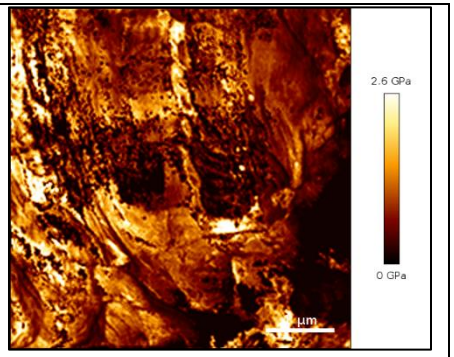
	Site 2	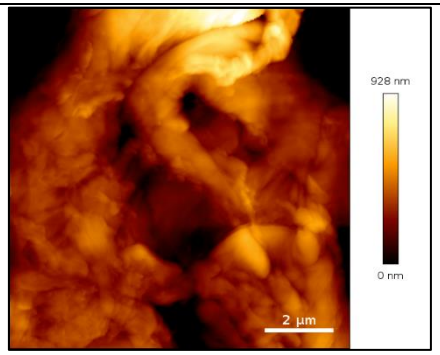	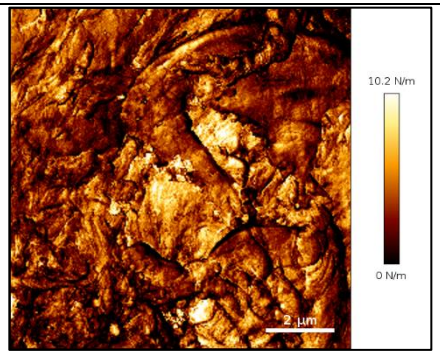	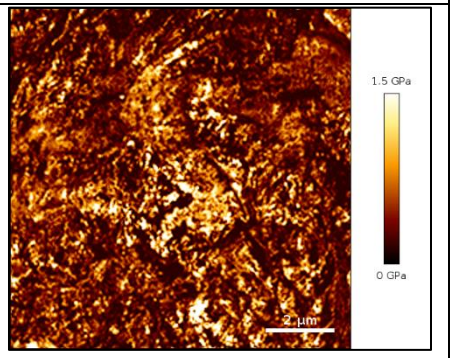
		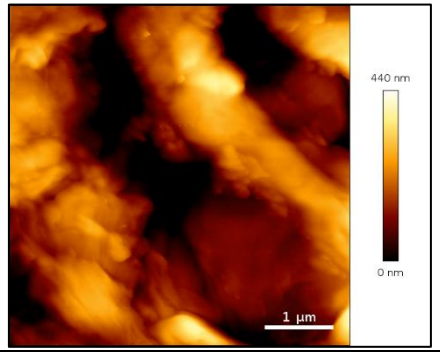	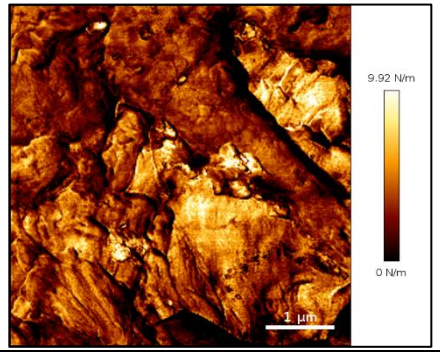	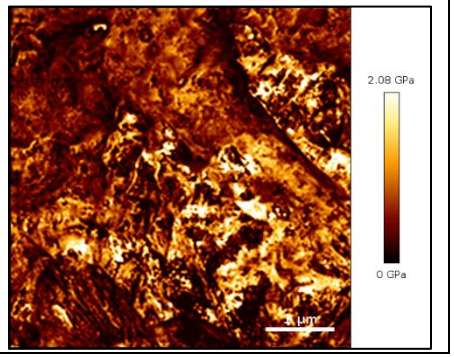

Appendix 1

	Site 3	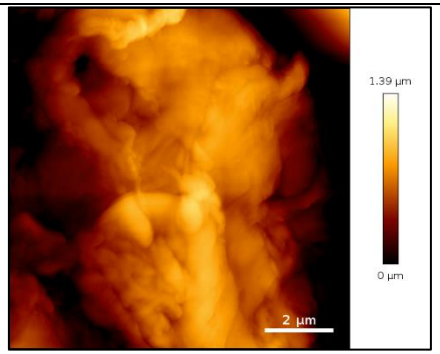	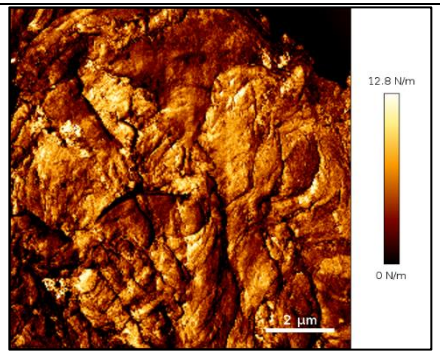	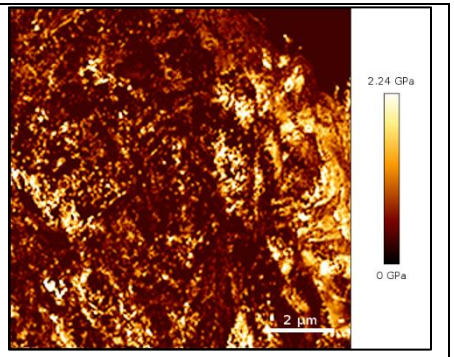
		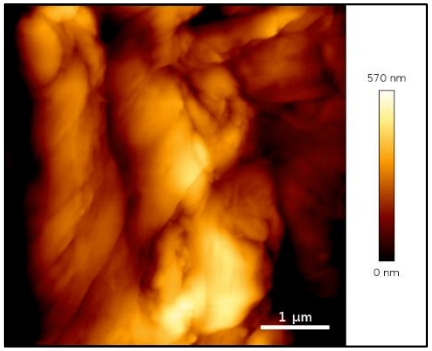	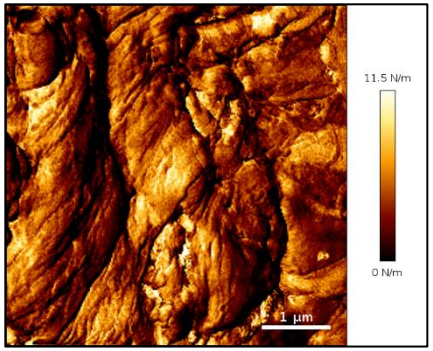	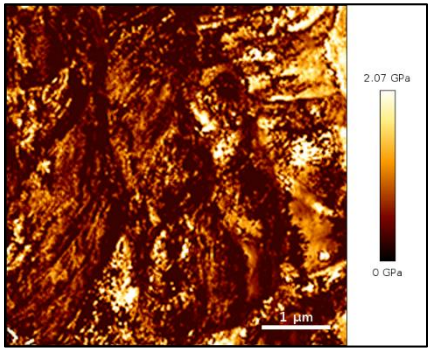
	Site 4	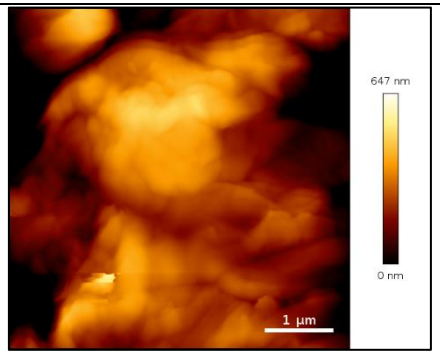	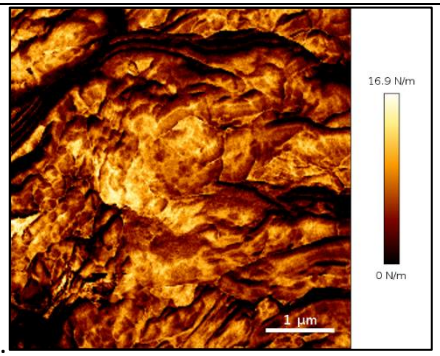	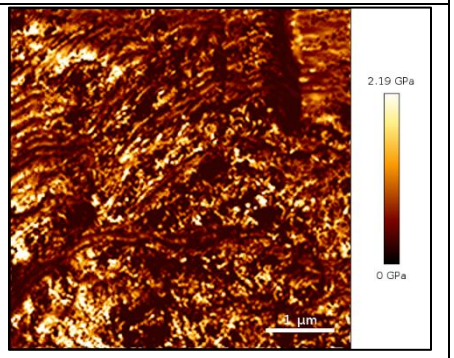

.

Appendix 1

vP75	Site 1	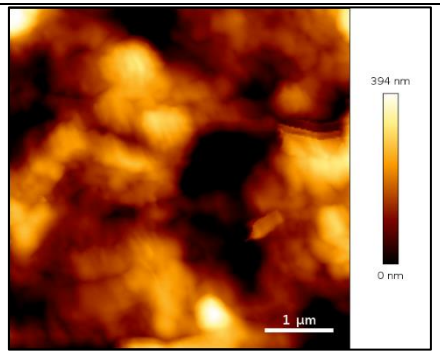	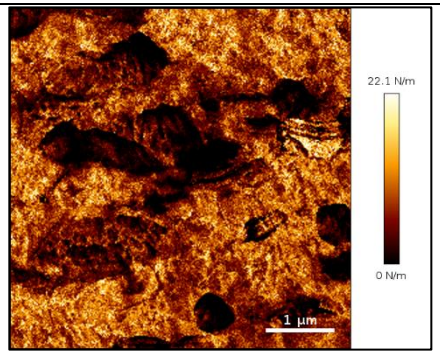	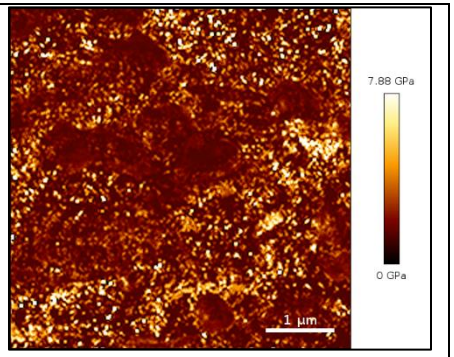
	Site 2	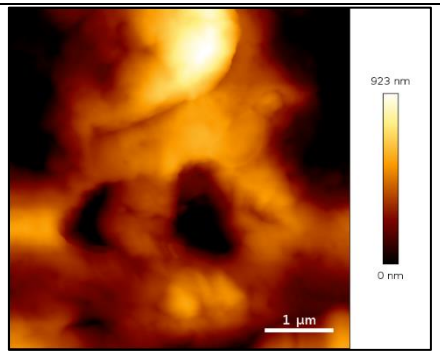	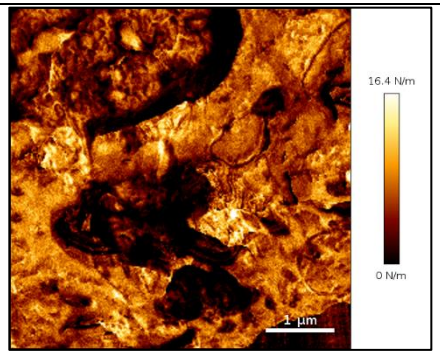	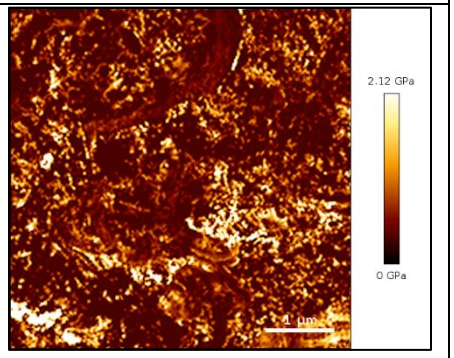
	Site 3	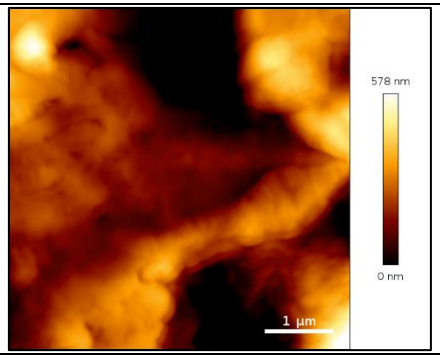	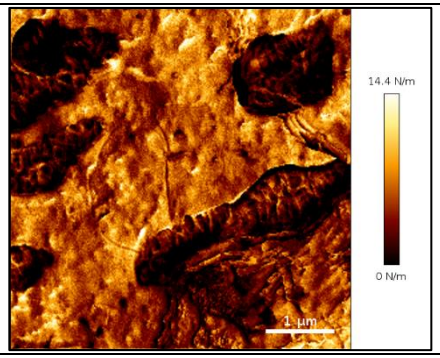	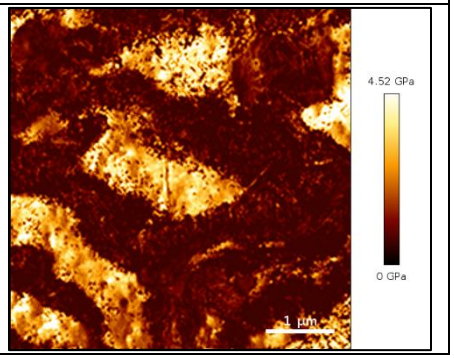

Appendix 1

	Site 4	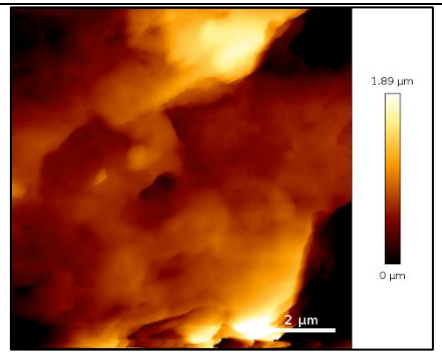	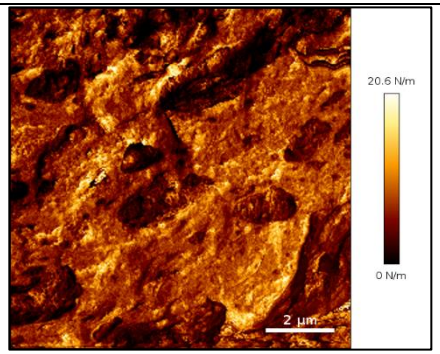	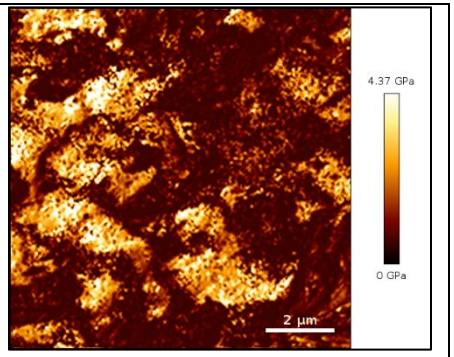
		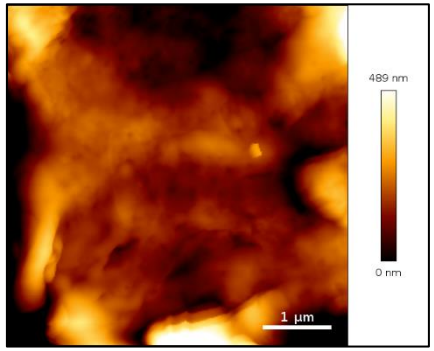	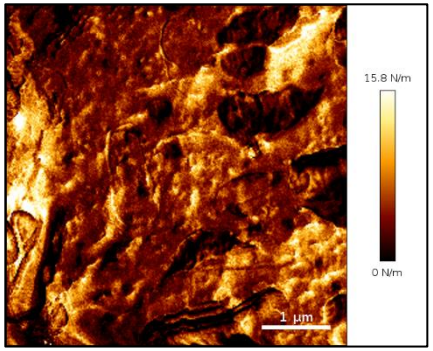	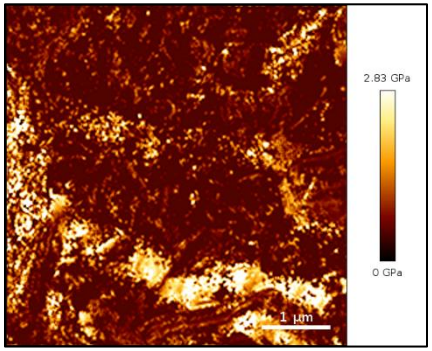
vP80	Site 1	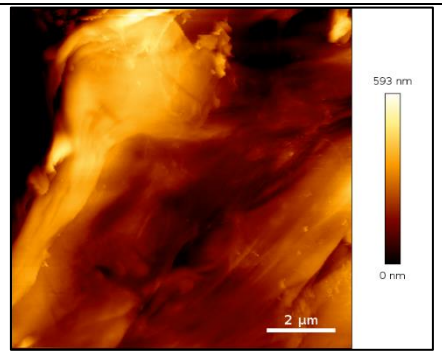	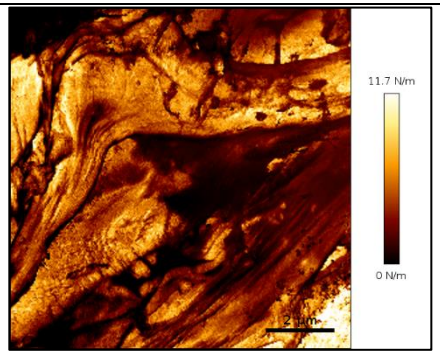	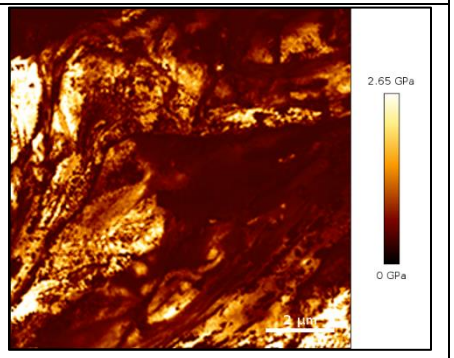

Appendix 1

		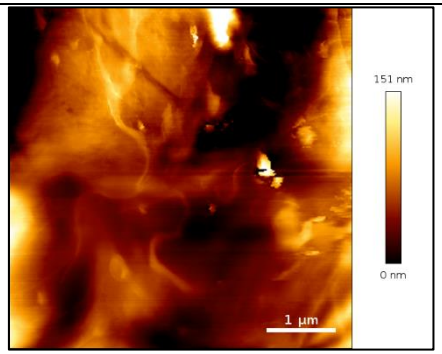	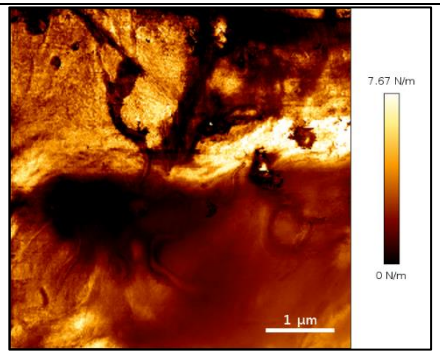	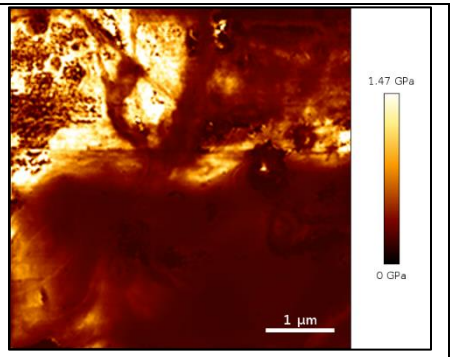
	Site 2	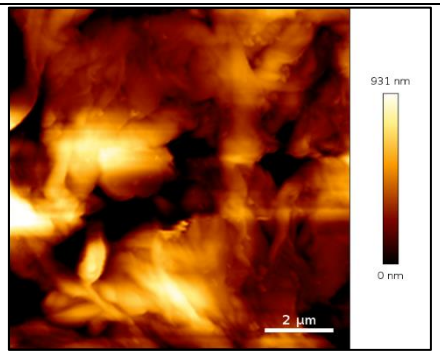 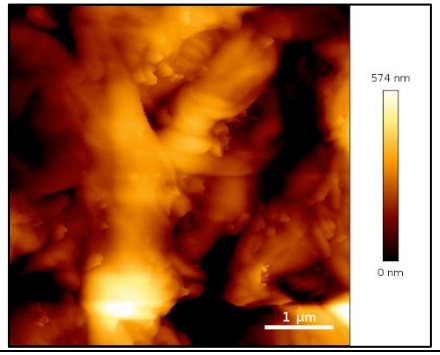	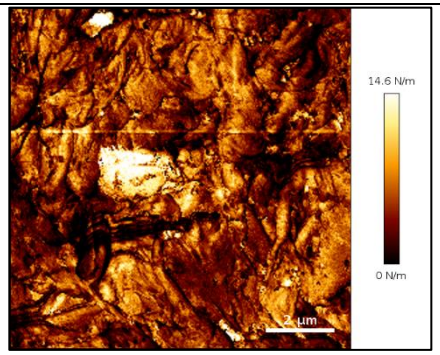 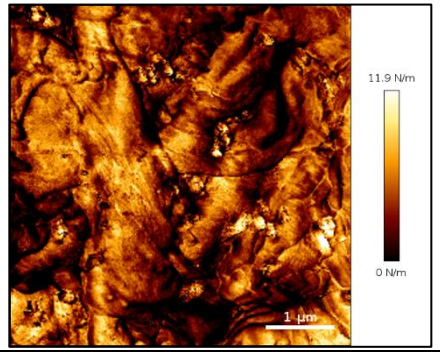	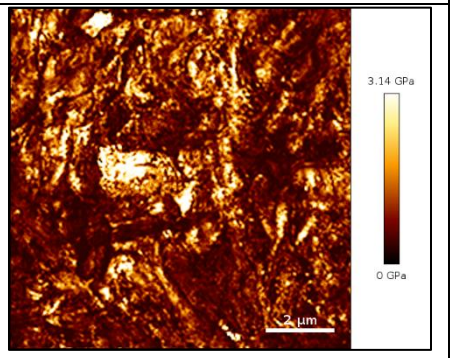 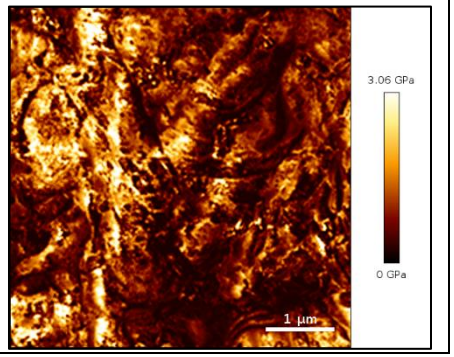

	Site 3	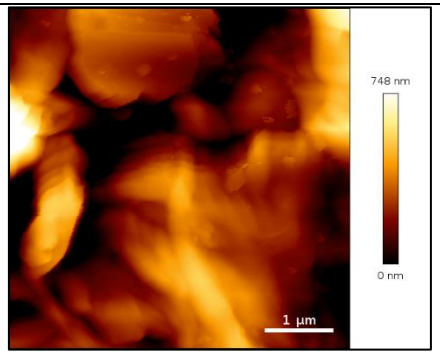	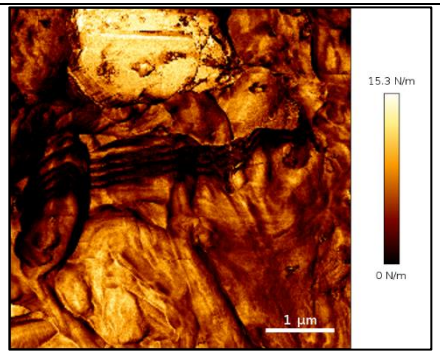	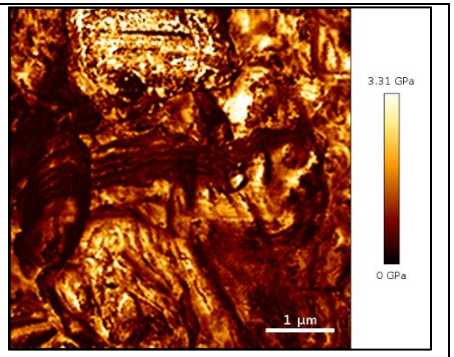
	Site 4	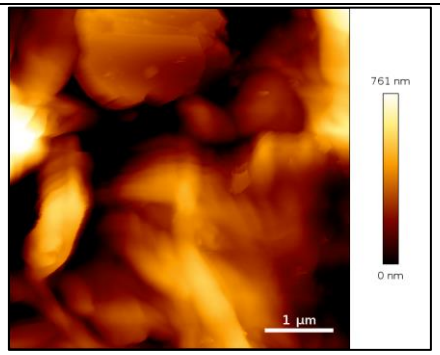	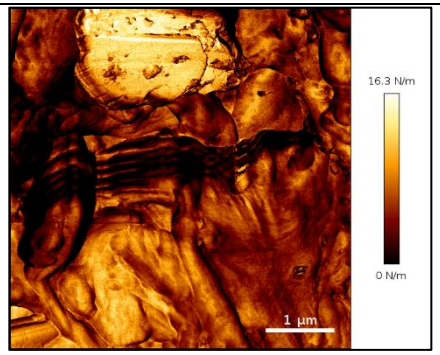	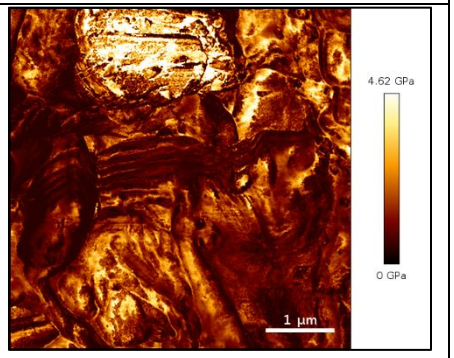
vP90	Site 1	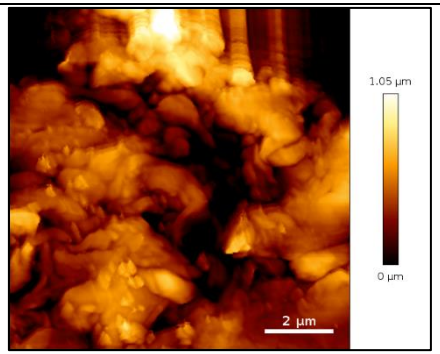	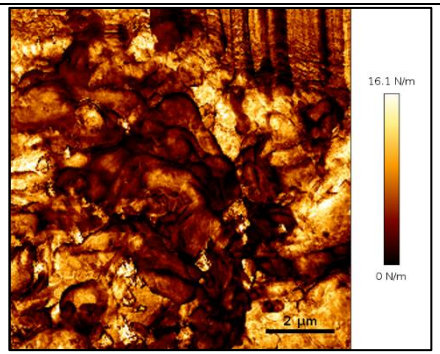	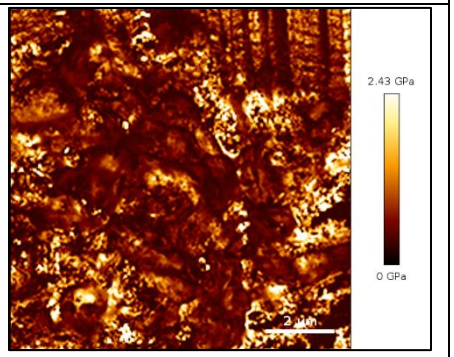

Appendix 1

		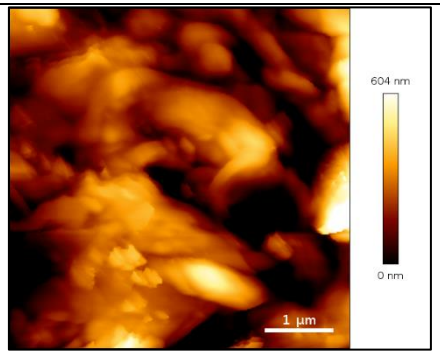	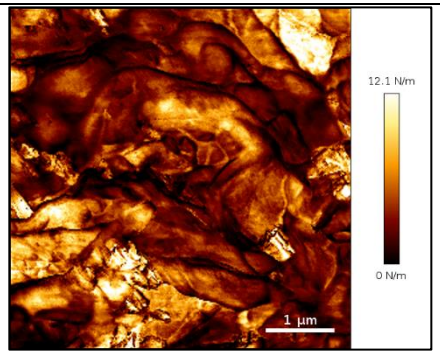	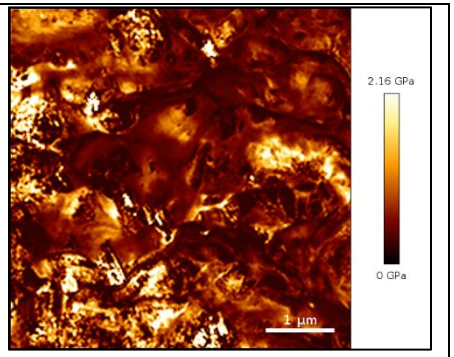
	Site 2	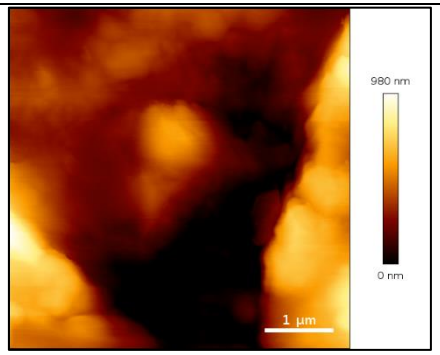	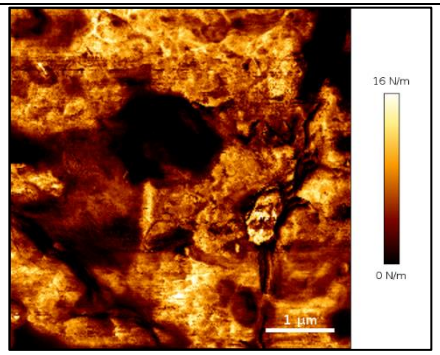	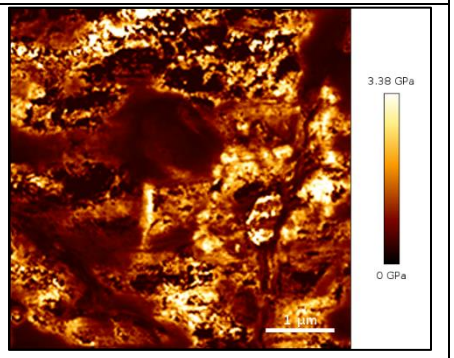
	Site 3	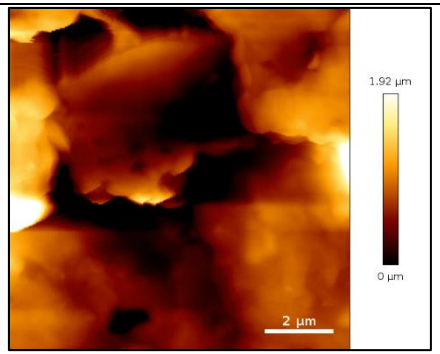	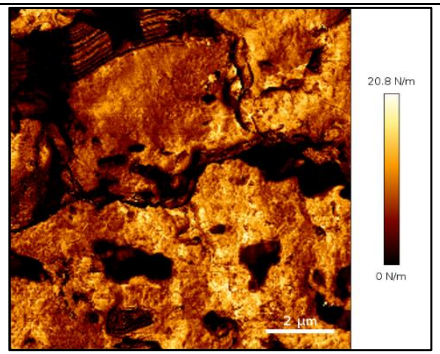	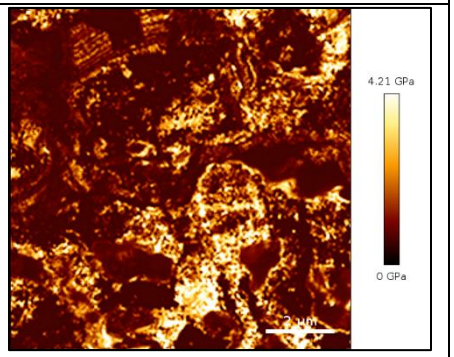

		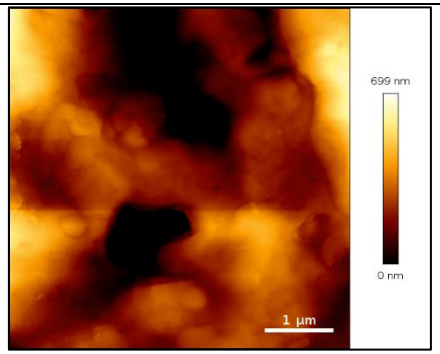	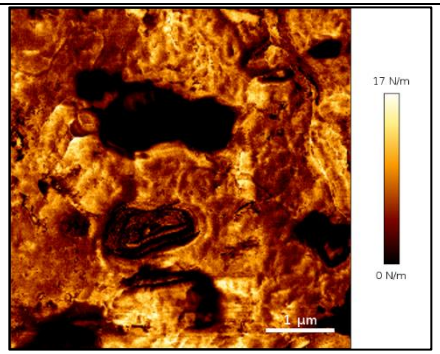	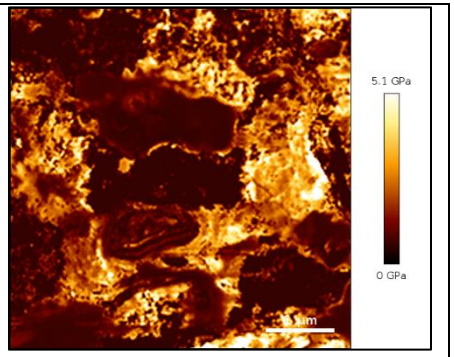
	Site 4	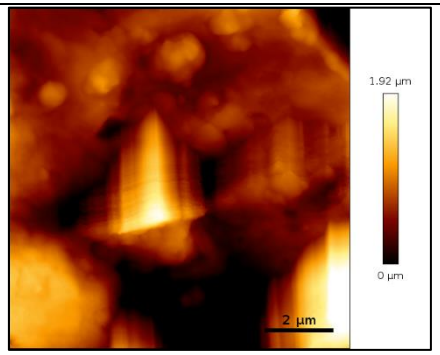 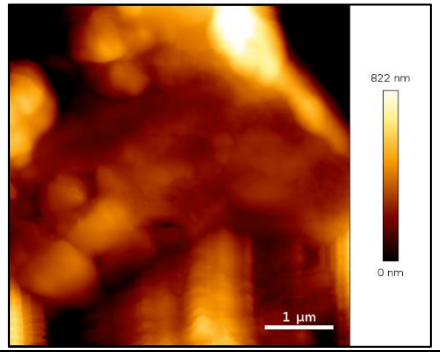	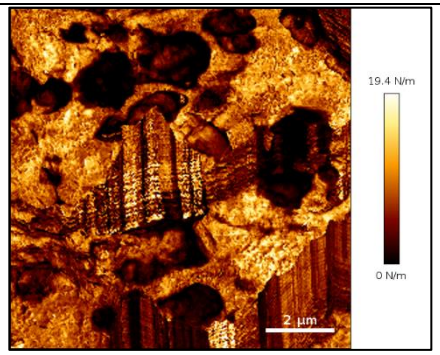 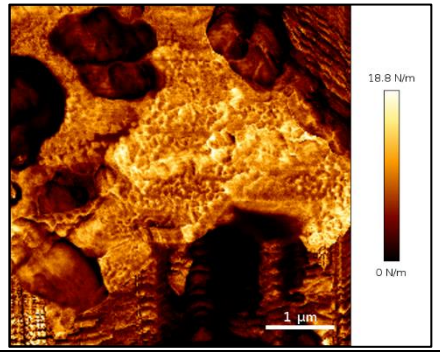	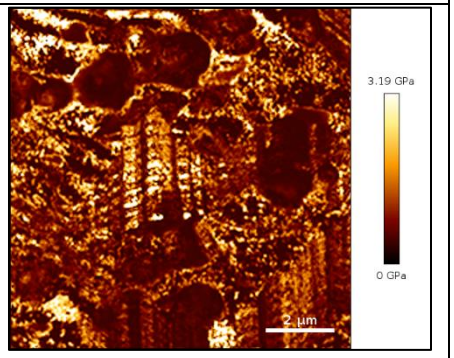 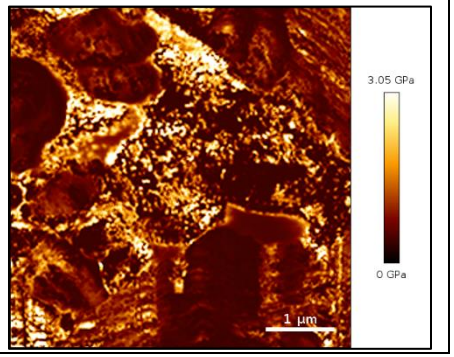

Appendix 1

vPP	Site 1	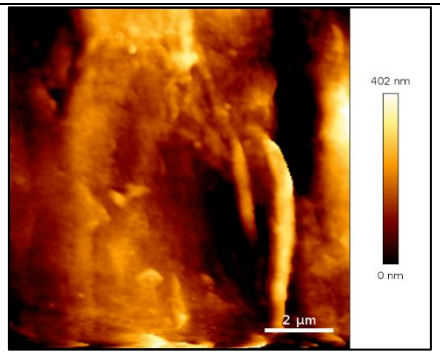	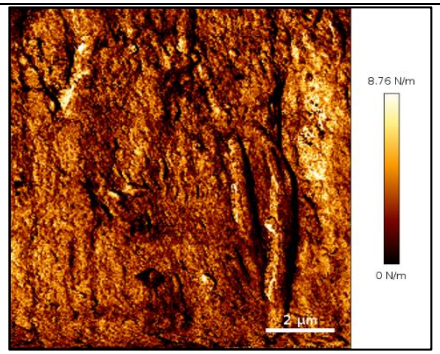	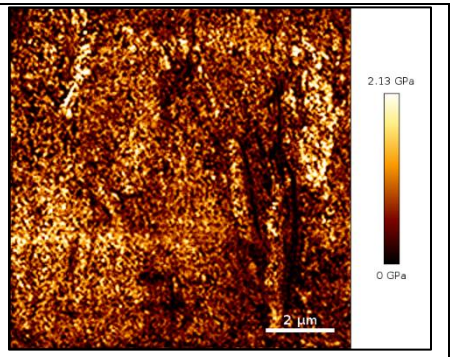
	Site 2	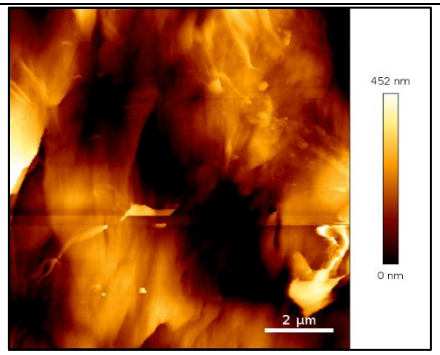 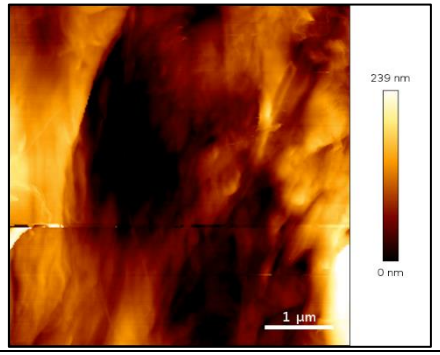	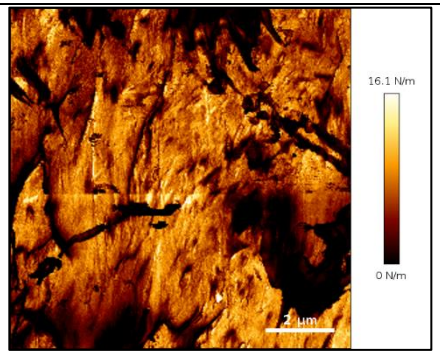 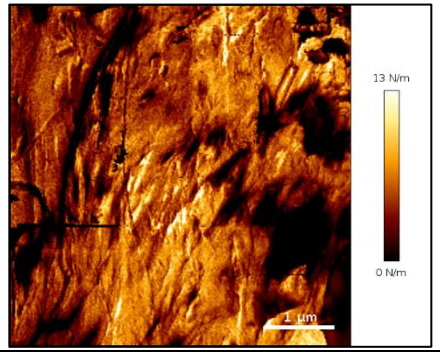	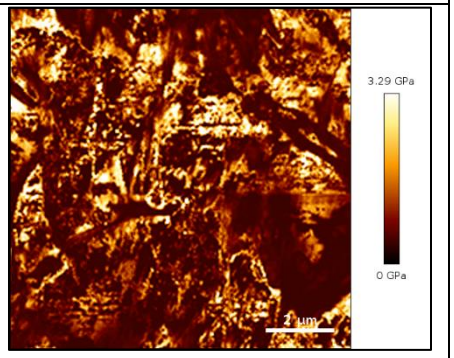 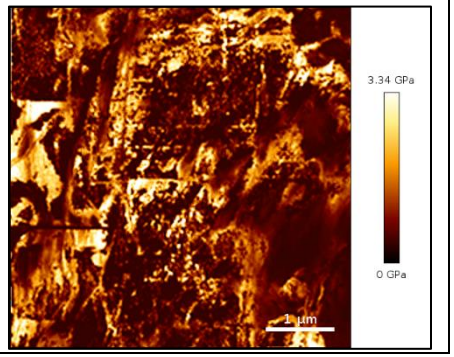

	Site 3	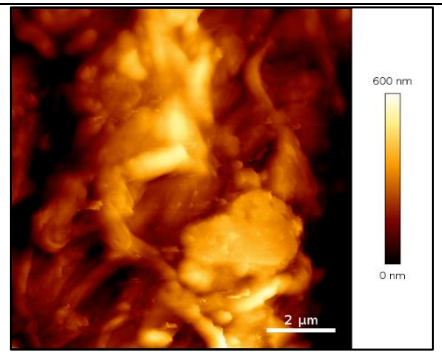 600 nm 0 nm 2 µm	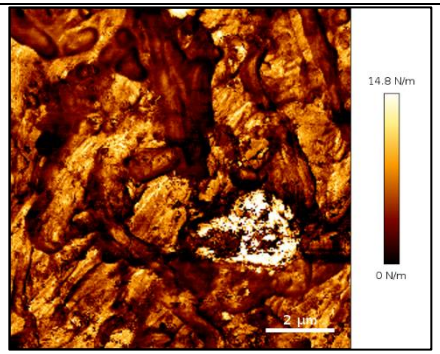 14.8 N/m 0 N/m 2 µm	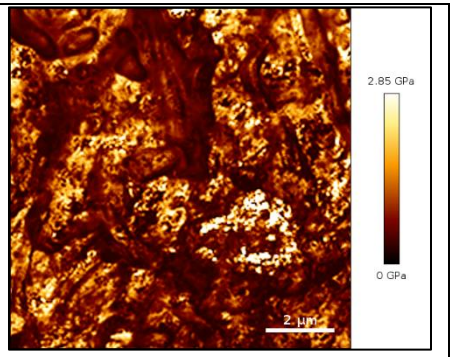 2.85 GPa 0 GPa 2 µm
		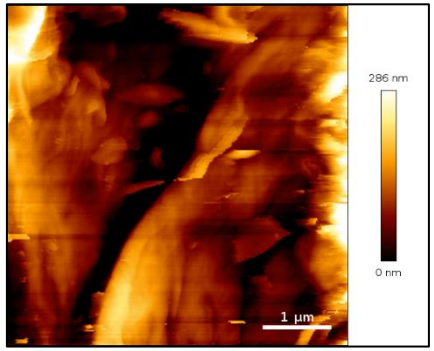 286 nm 0 nm 1 µm	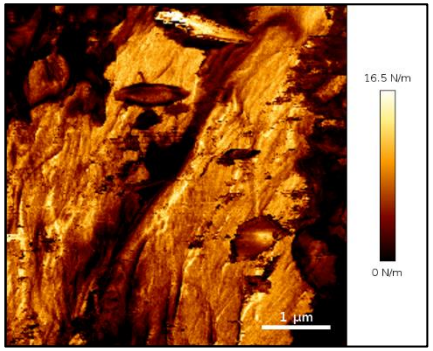 16.5 N/m 0 N/m 1 µm	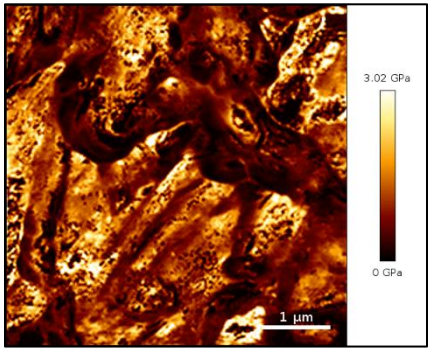 3.02 GPa 0 GPa 1 µm
	Site 4	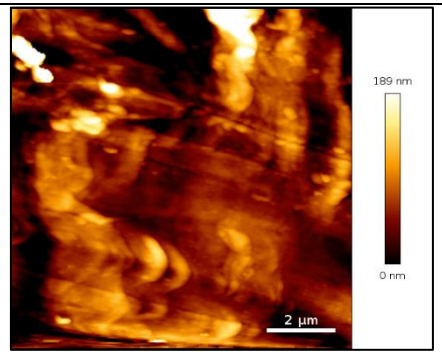 189 nm 0 nm 2 µm	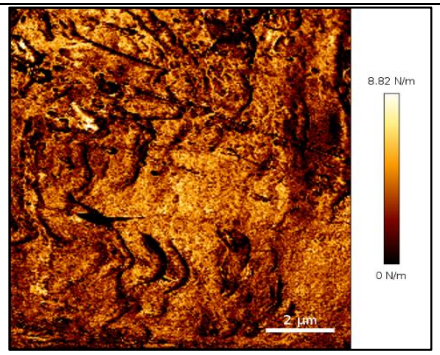 8.82 N/m 0 N/m 2 µm	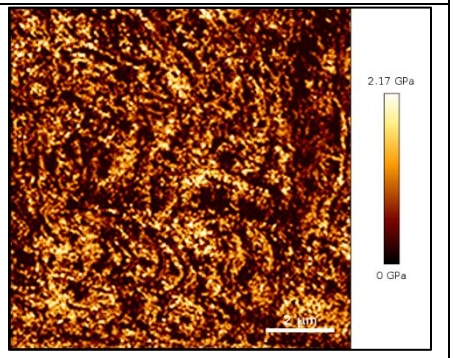 2.17 GPa 0 GPa 2 µm

Appendix 2 AFM QI mode height, stiffness and Young's modulus images obtained at 256 x 256 pixels for rPP:rHDPE blends.

PP:HDPE Blend		Height, nm	Stiffness, N m^{-1}	Young's modulus, GPa
rHDPE	Site 1	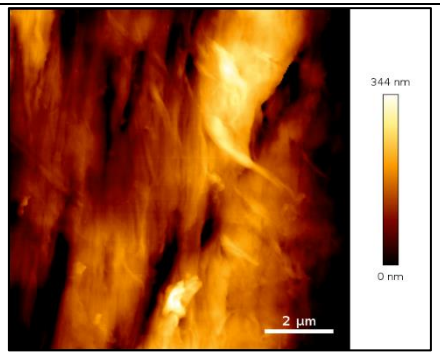	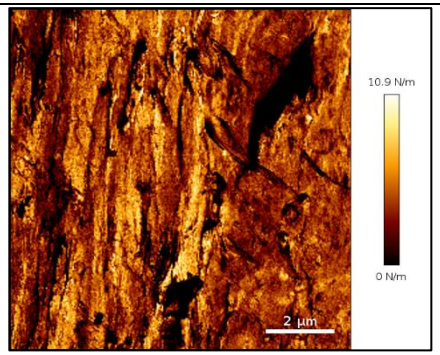	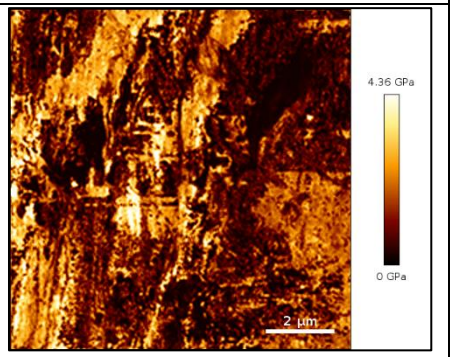
		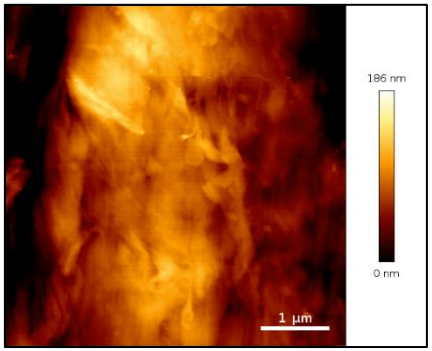	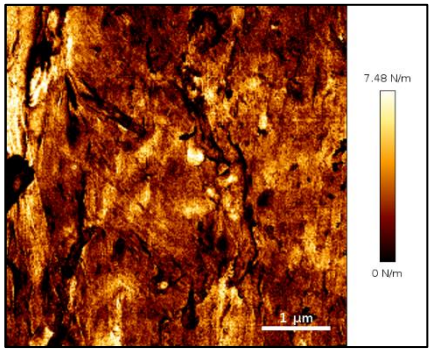	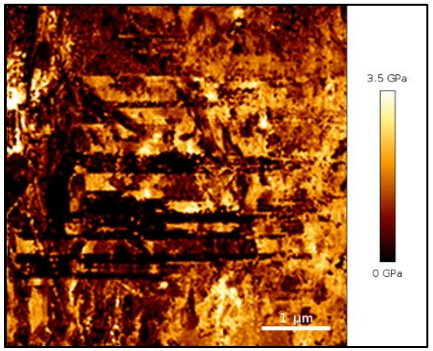
	Site 2	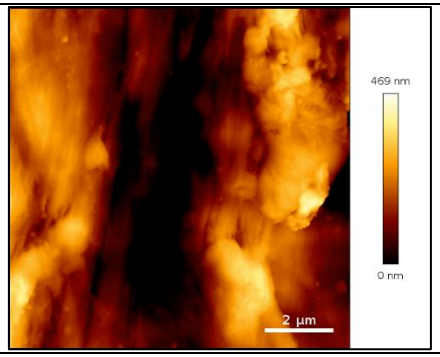	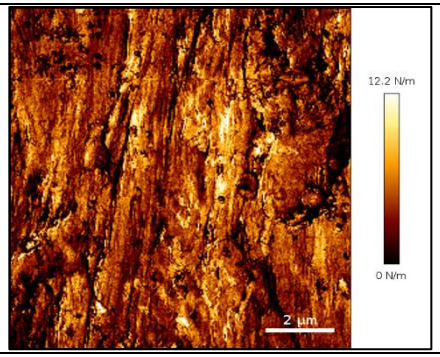	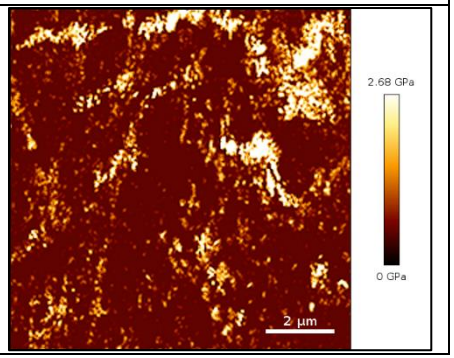

		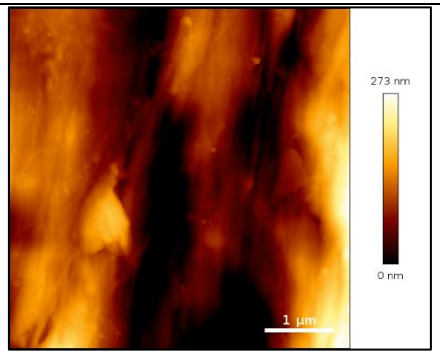	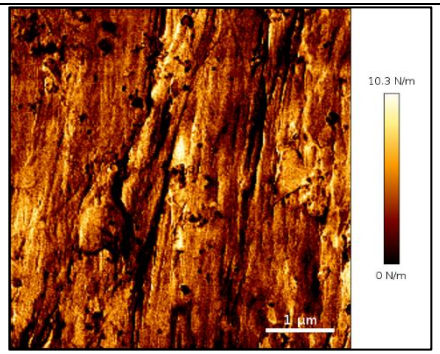	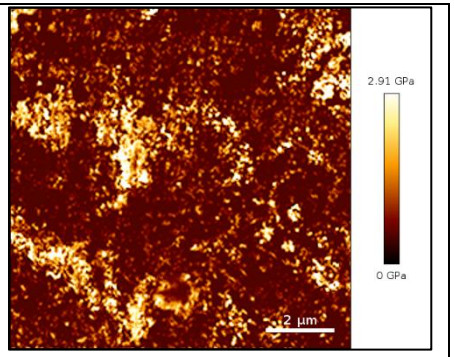
	Site 3	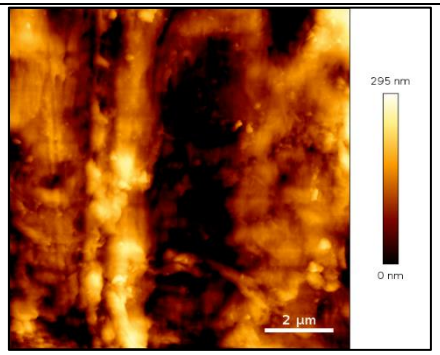 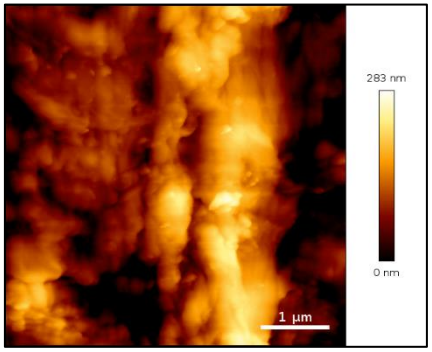	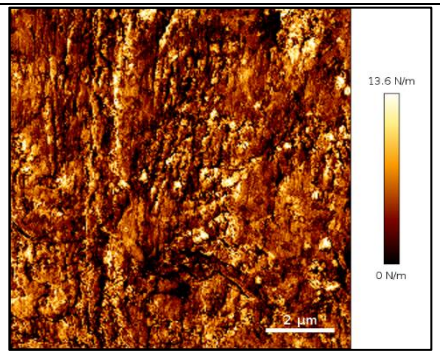 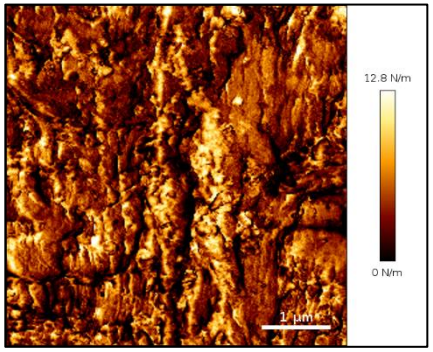	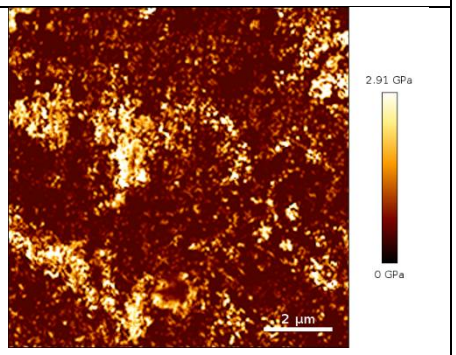 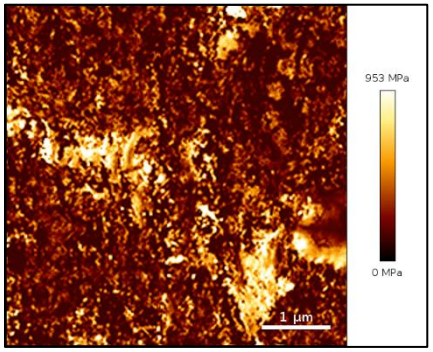

	Site 4	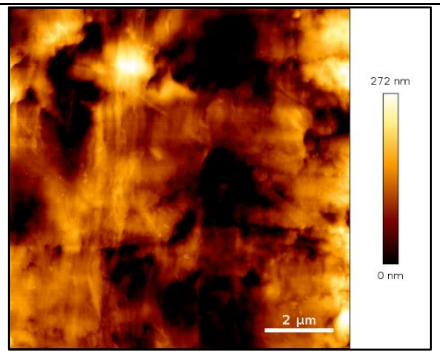	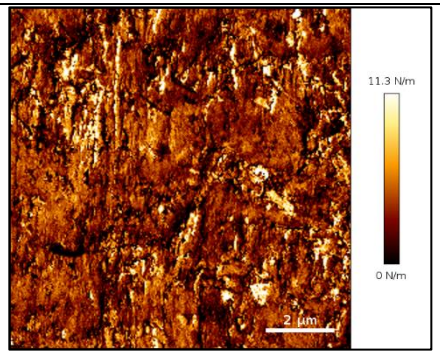	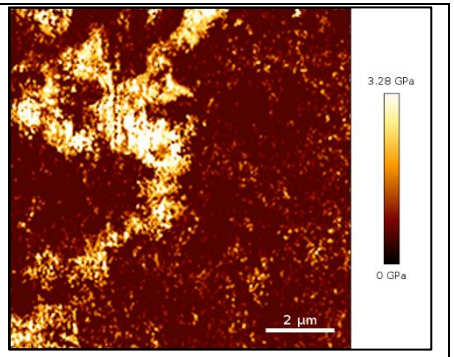
		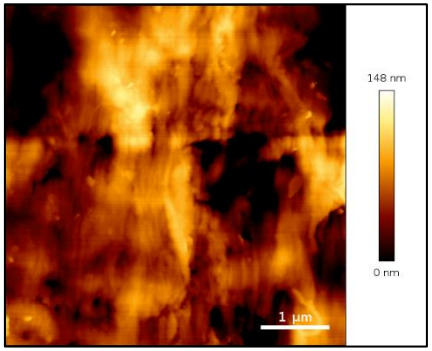	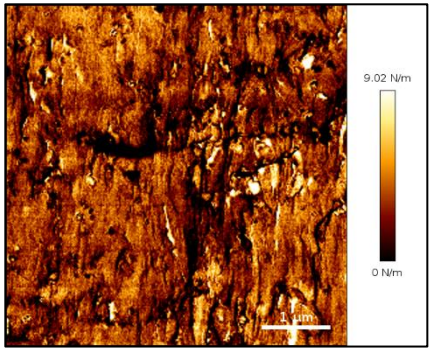	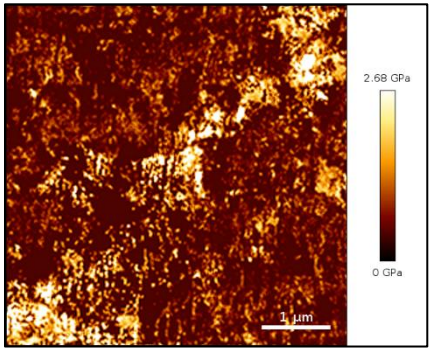
rP10	Site 1	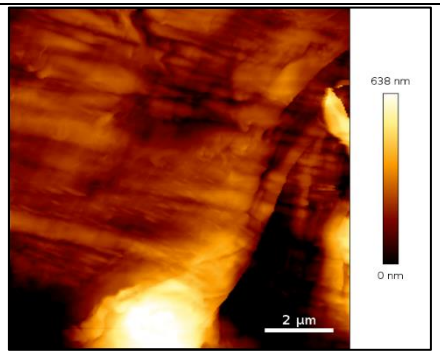	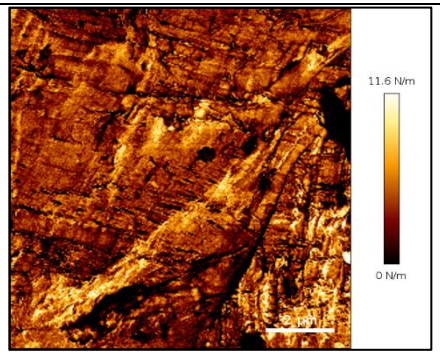	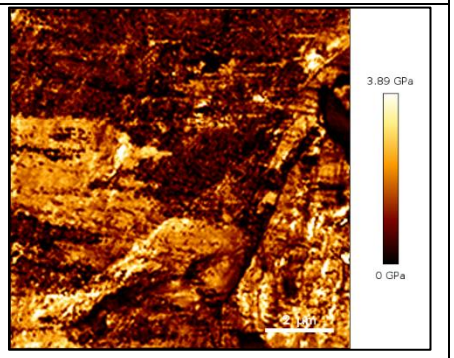

		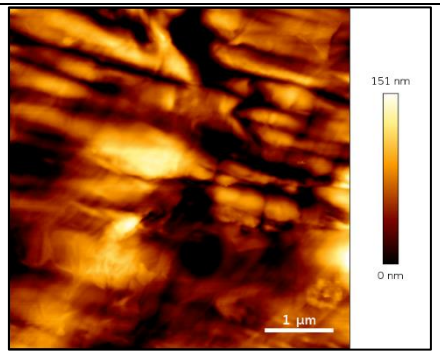 151 nm 0 nm 1 µm	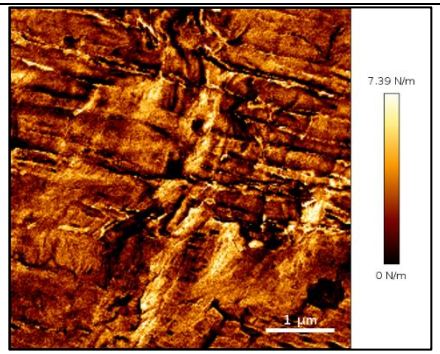 7.39 N/m 0 N/m 1 µm	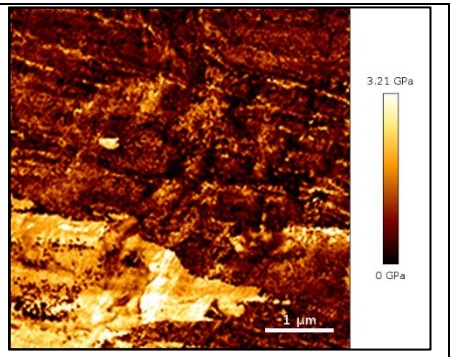 3.21 GPa 0 GPa 1 µm
	Site 2	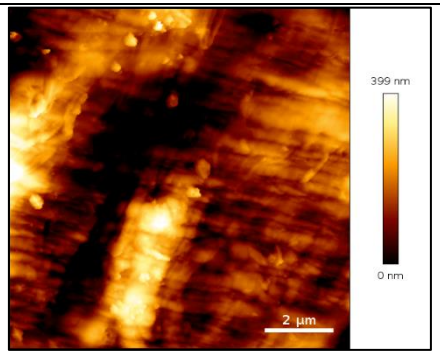 399 nm 0 nm 2 µm	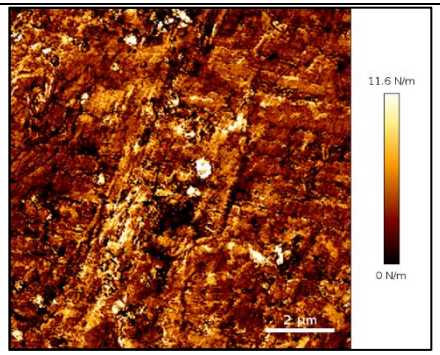 11.6 N/m 0 N/m 2 µm	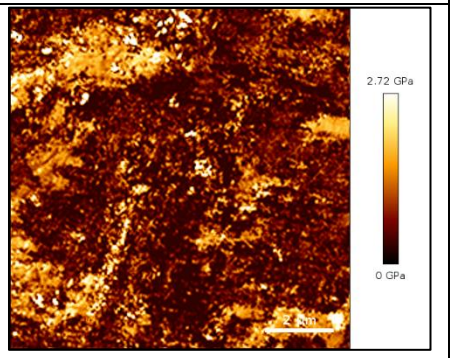 2.72 GPa 0 GPa 2 µm
		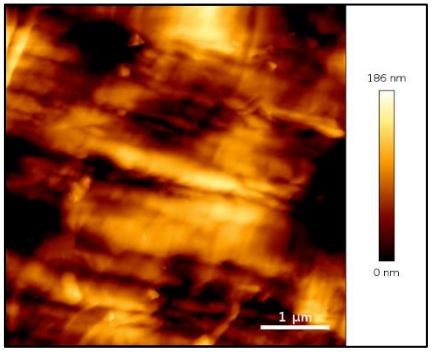 186 nm 0 nm 1 µm	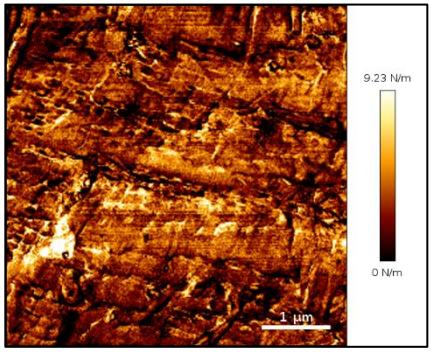 9.23 N/m 0 N/m 1 µm	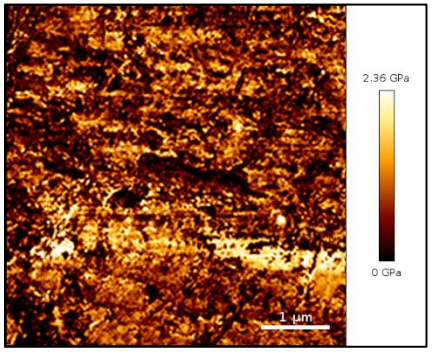 2.36 GPa 0 GPa 1 µm

	Site 3	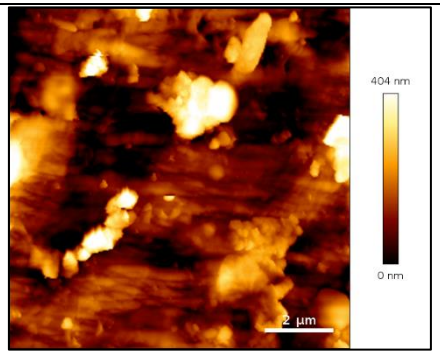	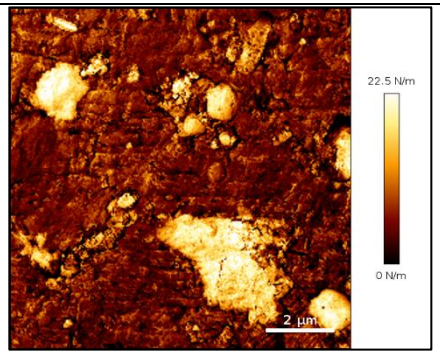	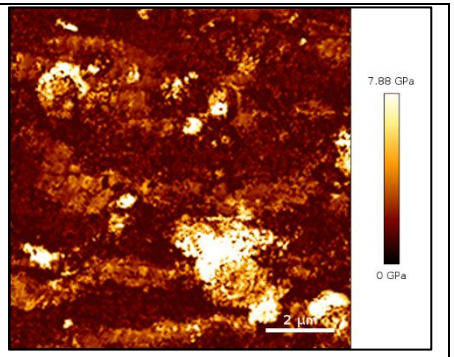
	Site 4	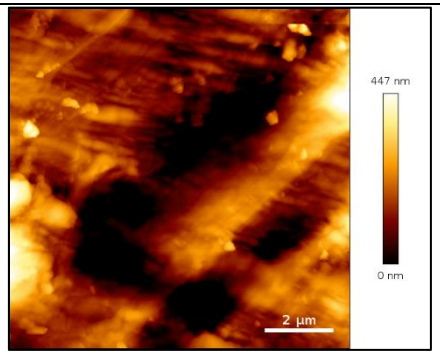 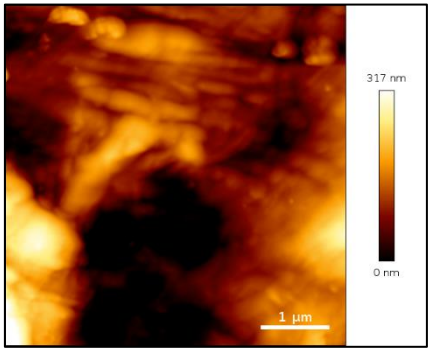	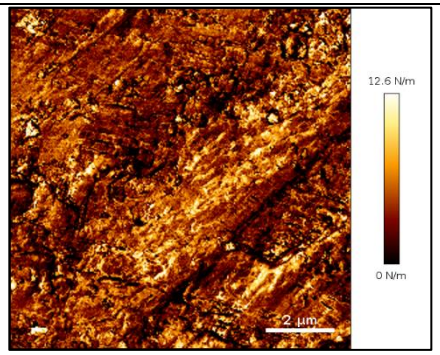 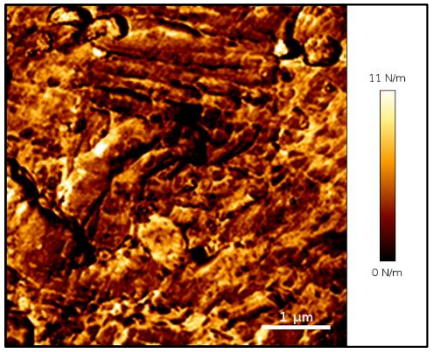	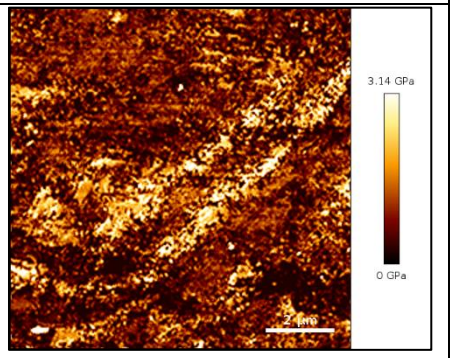 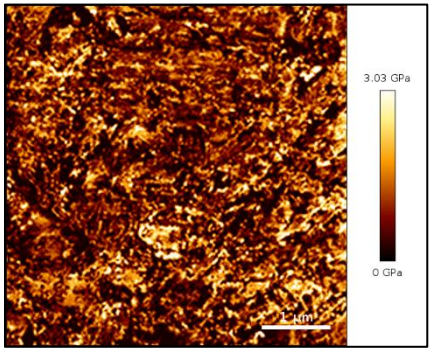

Appendix 2

rP20	Site 1	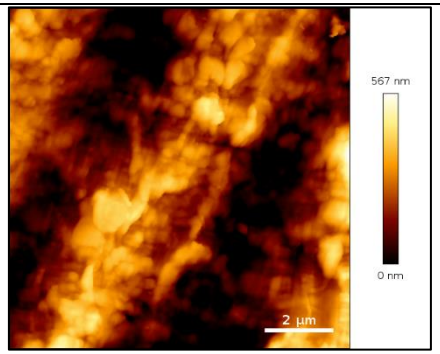	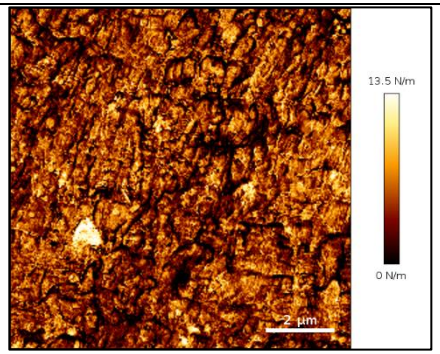	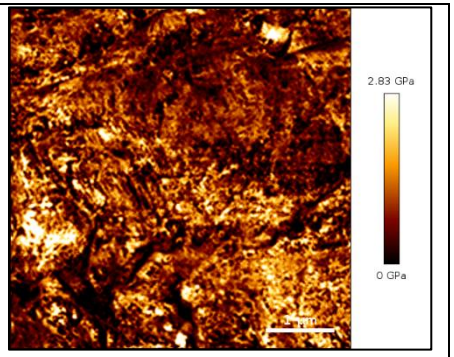
		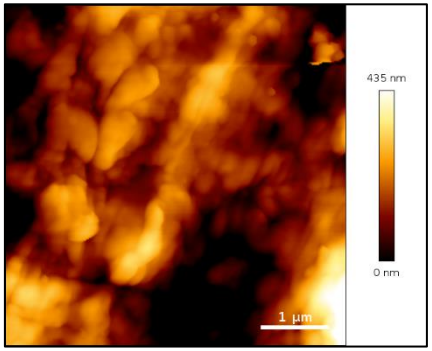	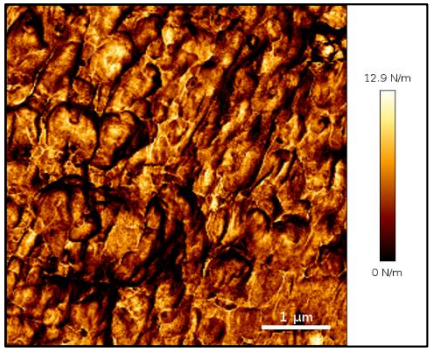	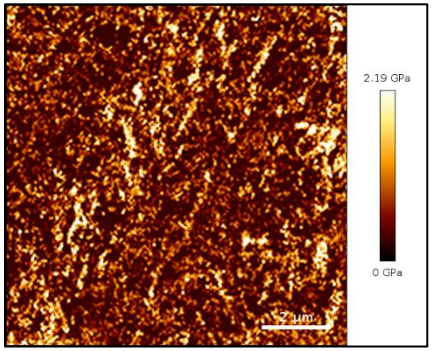
	Site 2	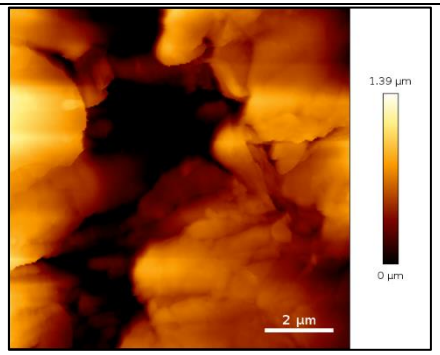	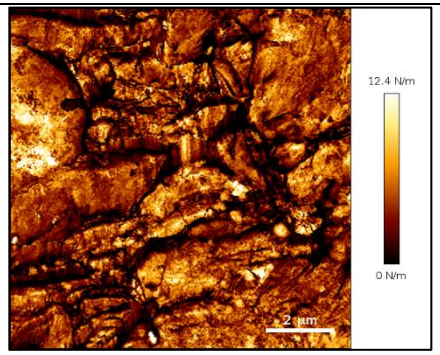	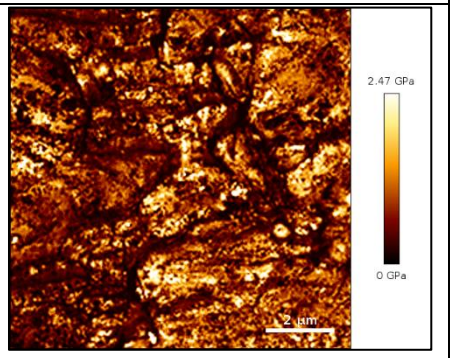

		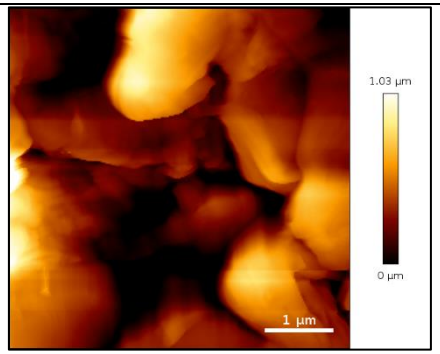 1.03 µm 0 µm 1 µm	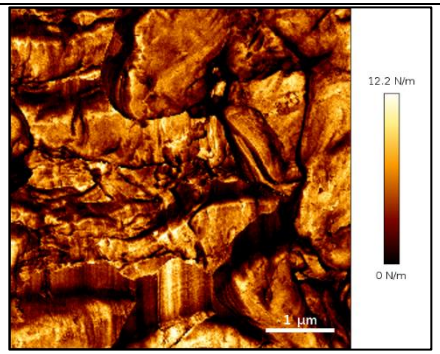 12.2 N/m 0 N/m 1 µm	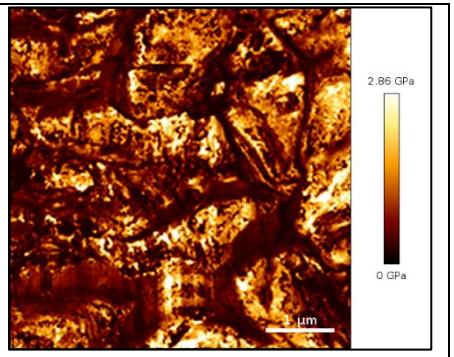 2.86 GPa 0 GPa 1 µm
	Site 3	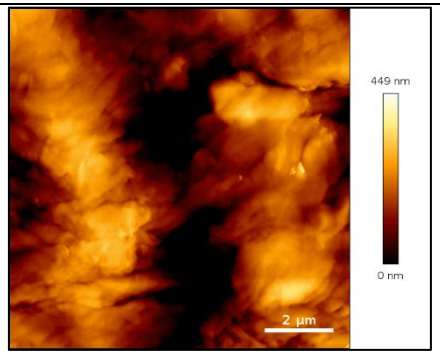 449 nm 0 nm 2 µm	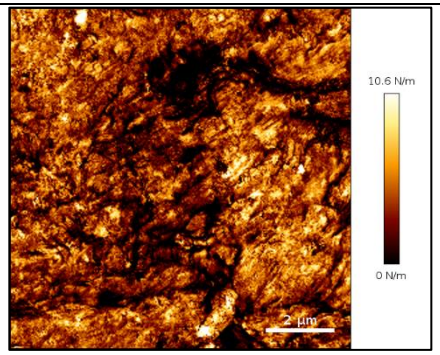 10.6 N/m 0 N/m 2 µm	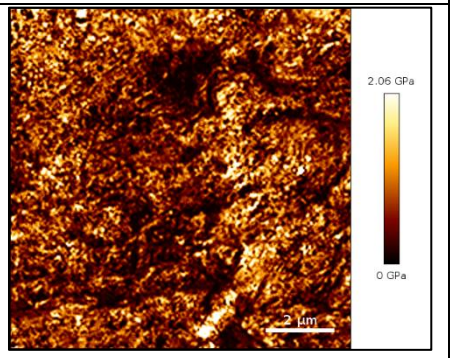 2.06 GPa 0 GPa 2 µm
		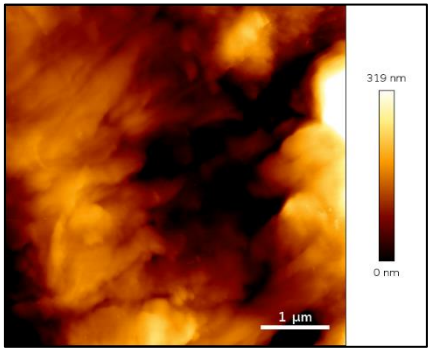 319 nm 0 nm 1 µm	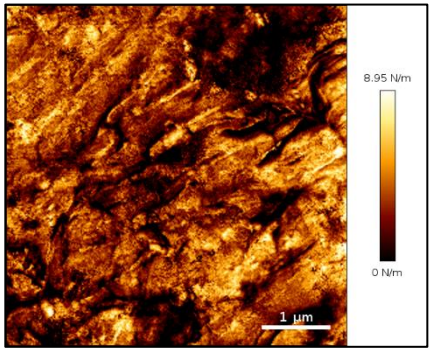 8.95 N/m 0 N/m 1 µm	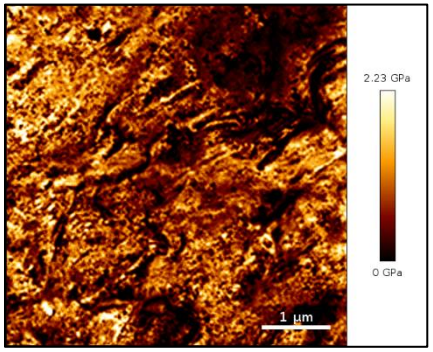 2.23 GPa 0 GPa 1 µm

	Site 4	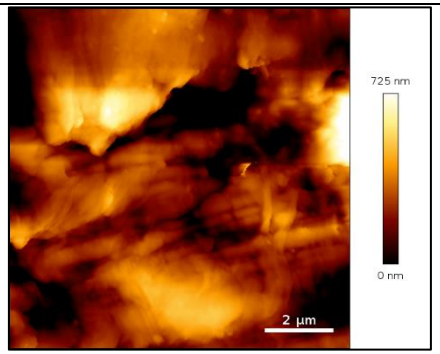	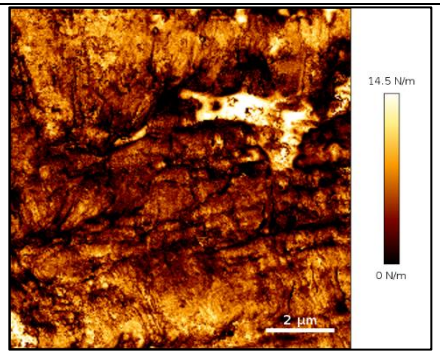	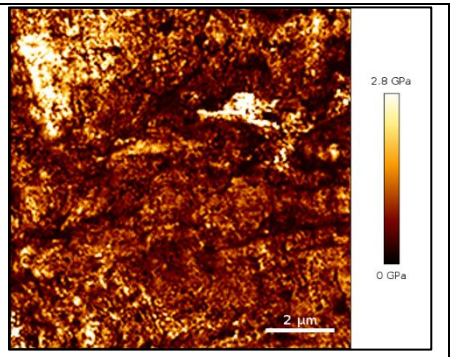
		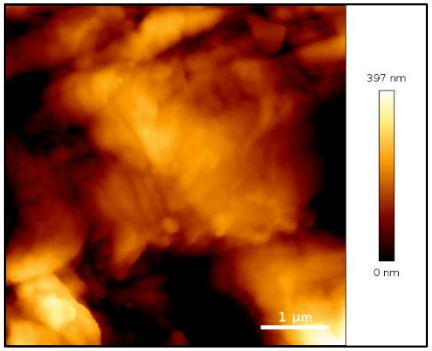	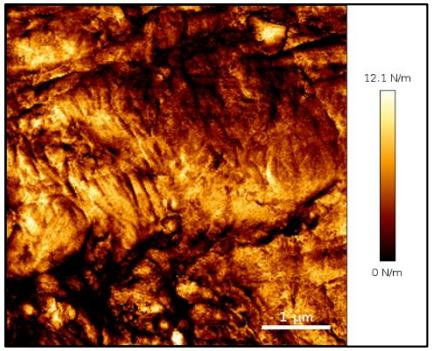	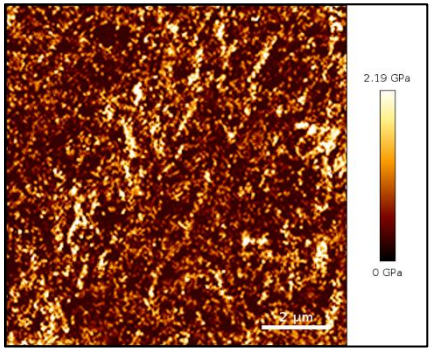
rP25	Site 1	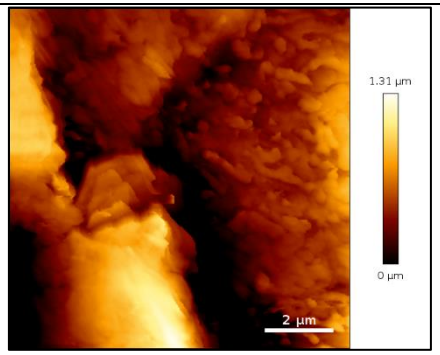	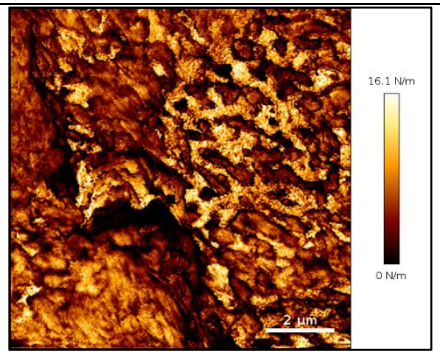	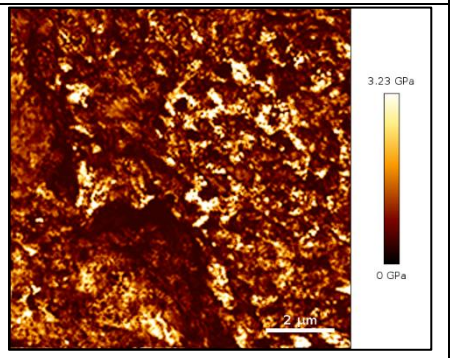

		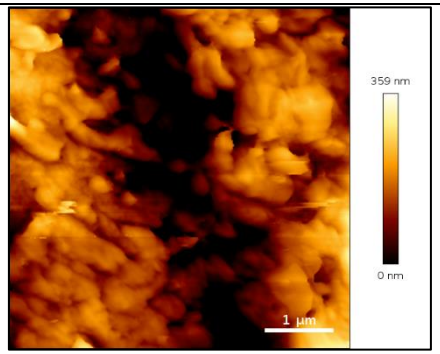	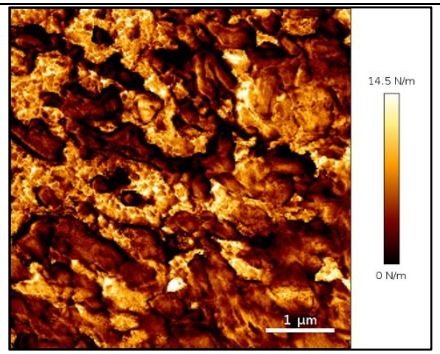	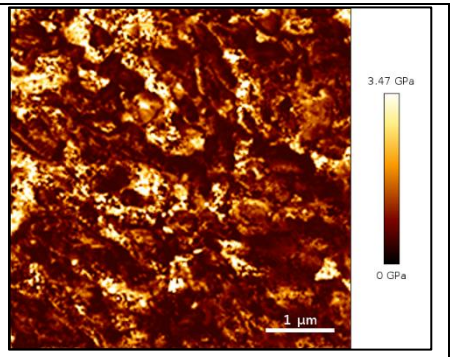
	Site 2	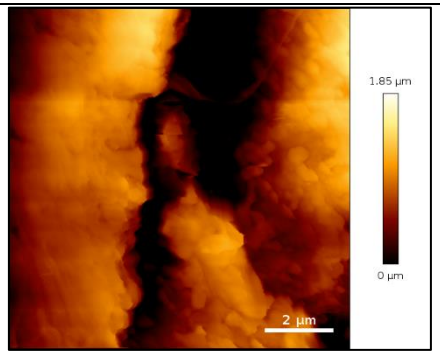 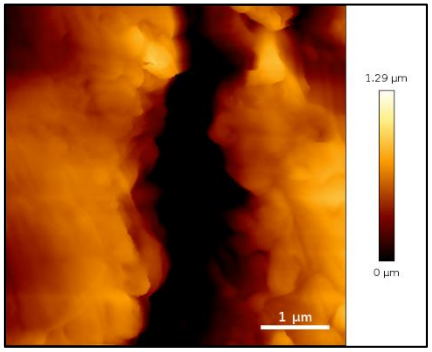	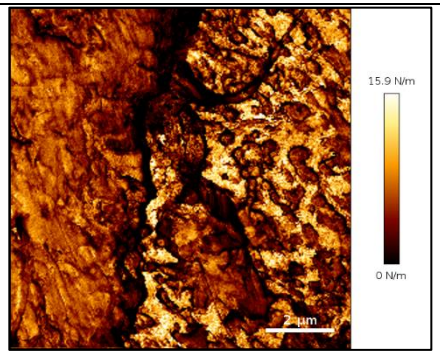 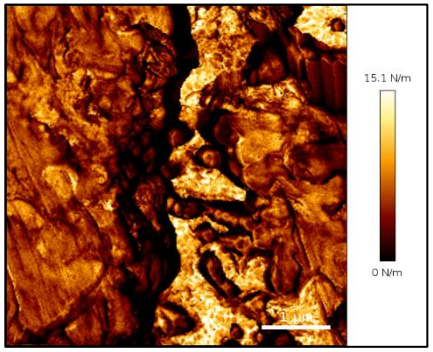	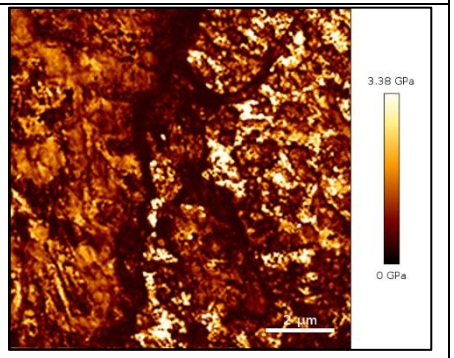 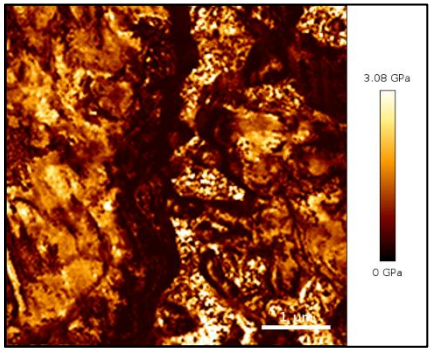

	Site 3	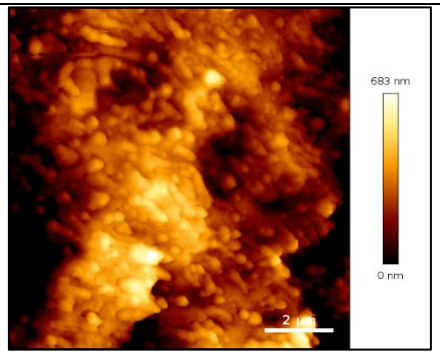 683 nm 0 nm 2 µm	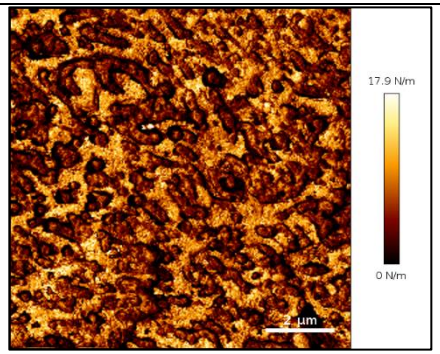 17.9 N/m 0 N/m 2 µm	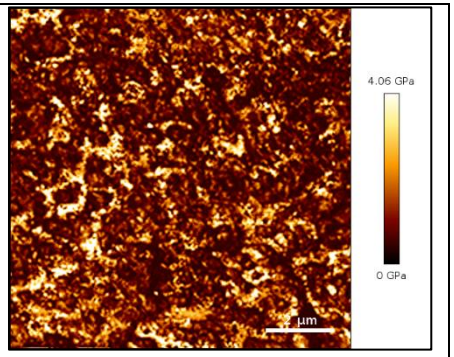 4.06 GPa 0 GPa 2 µm
		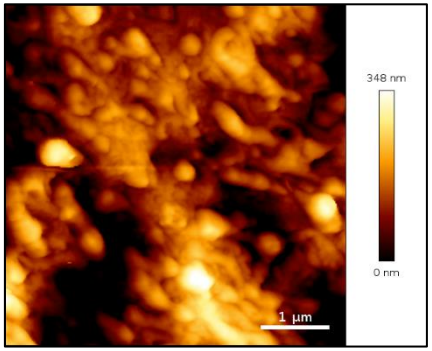 348 nm 0 nm 1 µm	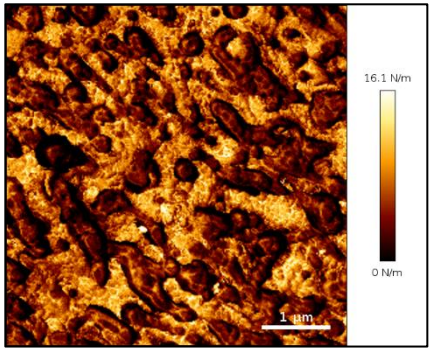 16.1 N/m 0 N/m 1 µm	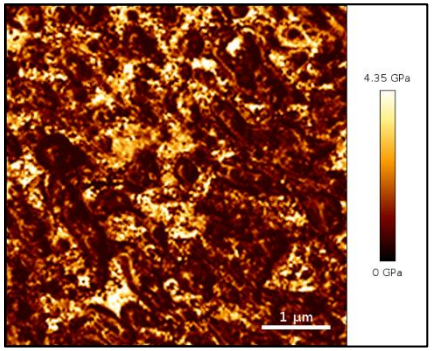 4.35 GPa 0 GPa 1 µm
	Site 4	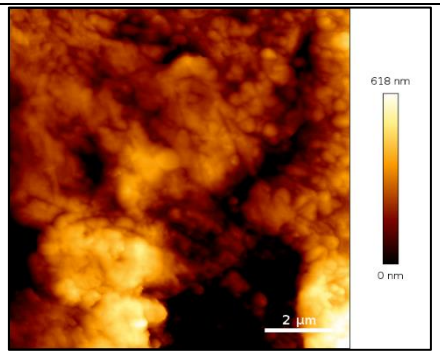 618 nm 0 nm 2 µm	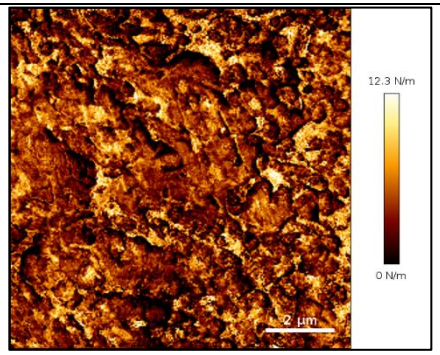 12.3 N/m 0 N/m 2 µm	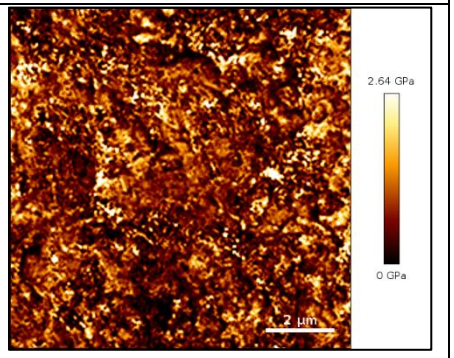 2.64 GPa 0 GPa 2 µm

		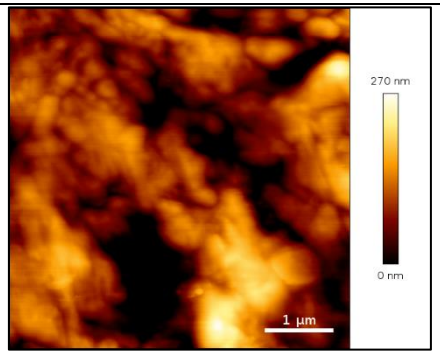	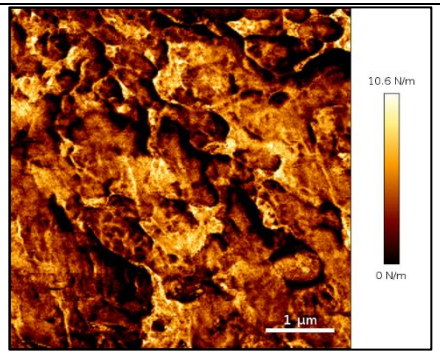	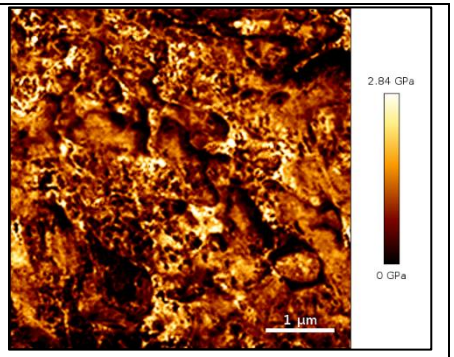
rP40	Site 1	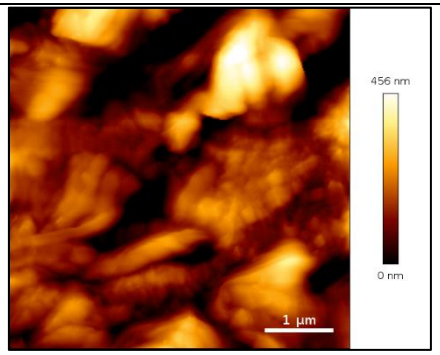	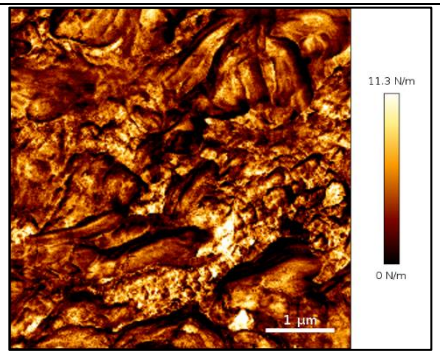	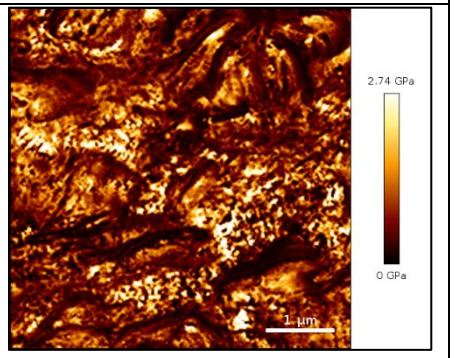
	Site 2	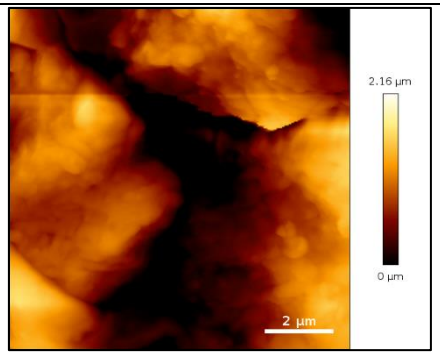	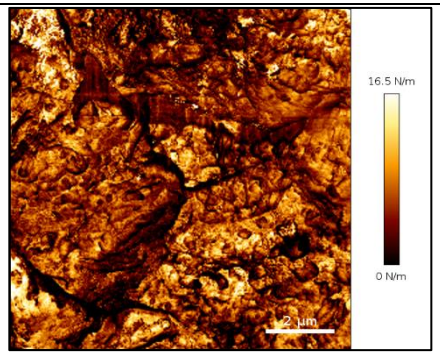	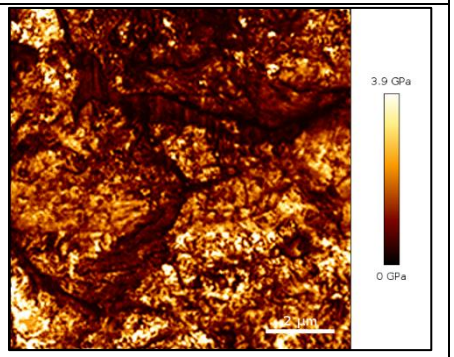

		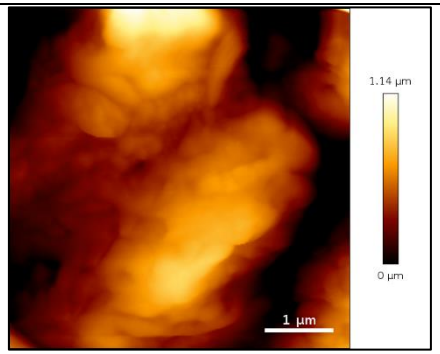	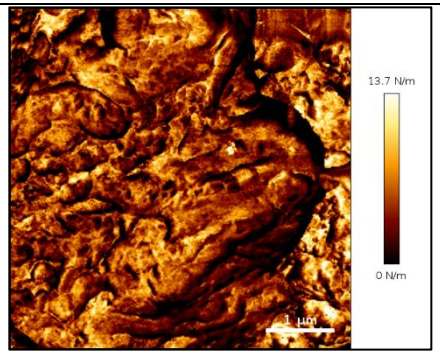	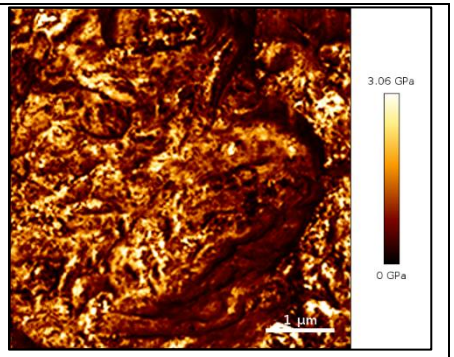
	Site 3	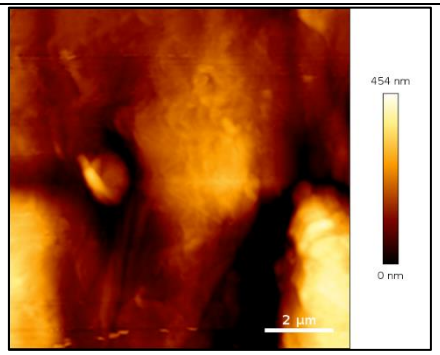 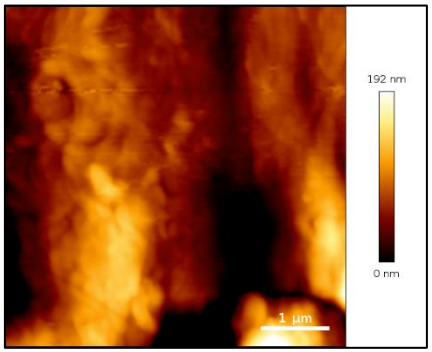	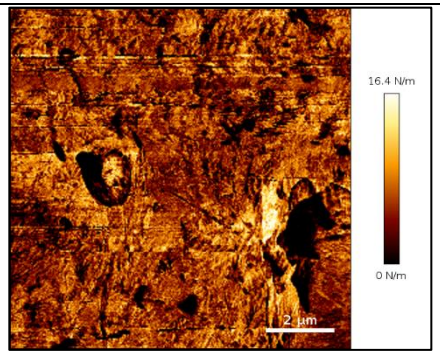 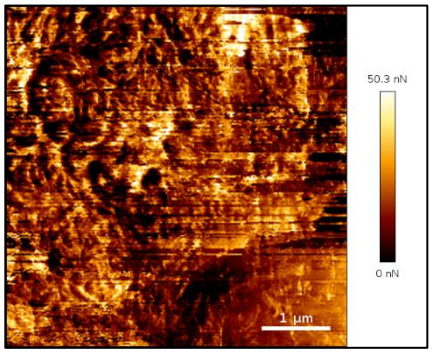	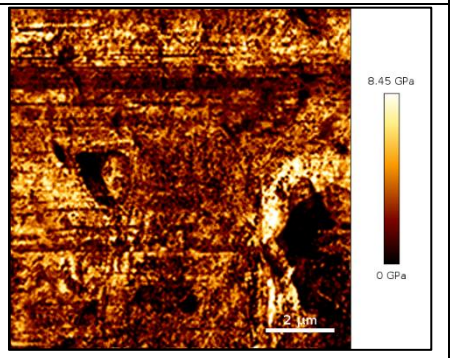 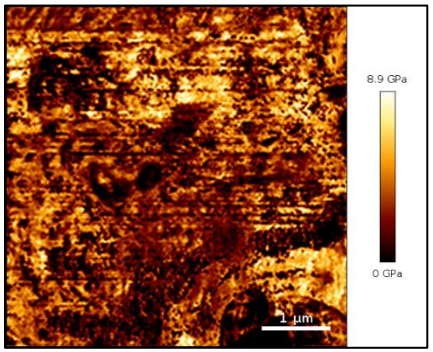

Appendix 2

	Site 4	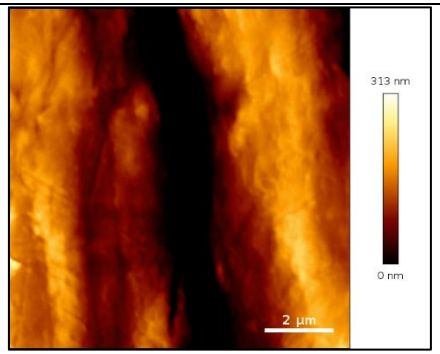	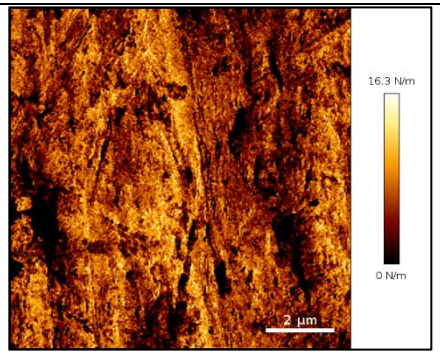	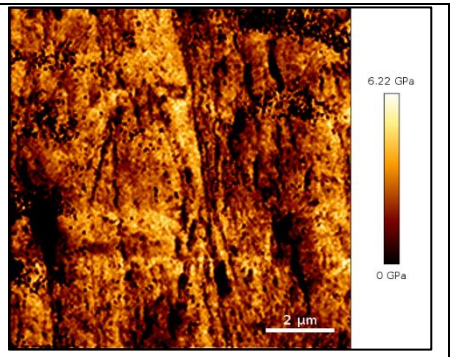
rP50	Site 1	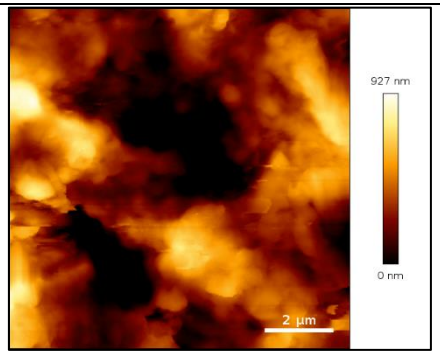 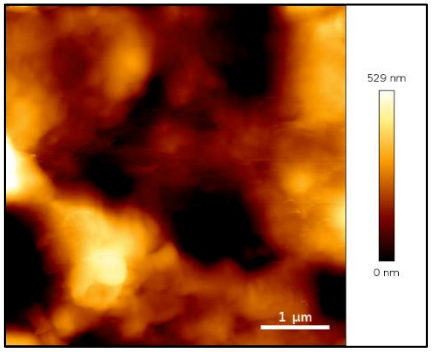	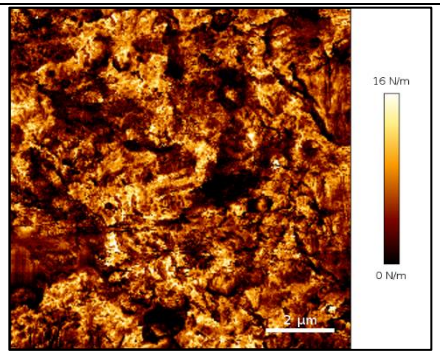 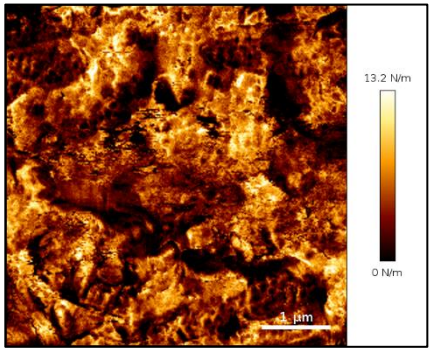	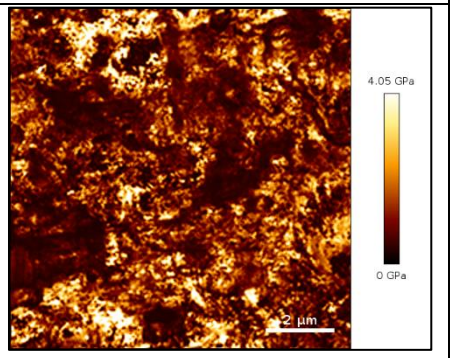 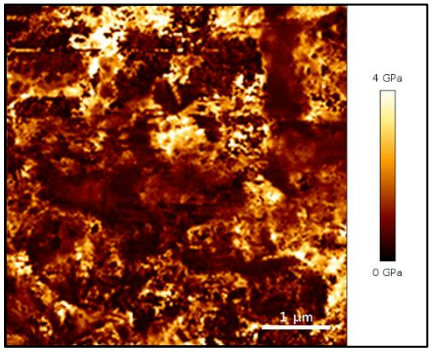

	Site 2	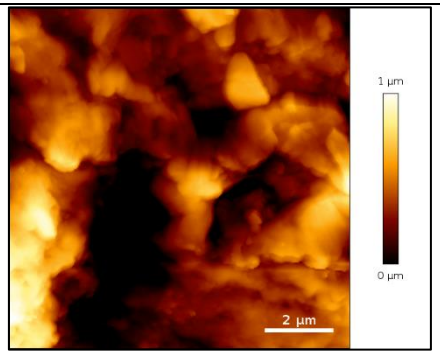 1 µm 0 µm 2 µm	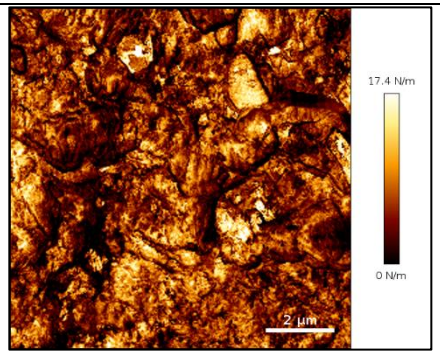 17.4 N/m 0 N/m 2 µm	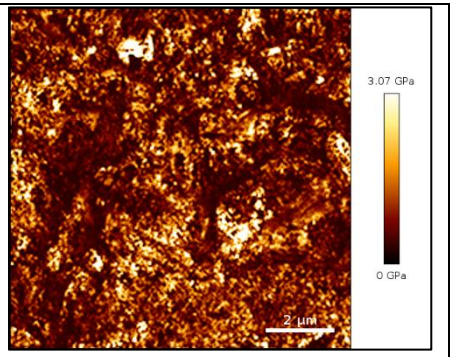 3.07 GPa 0 GPa 2 µm
		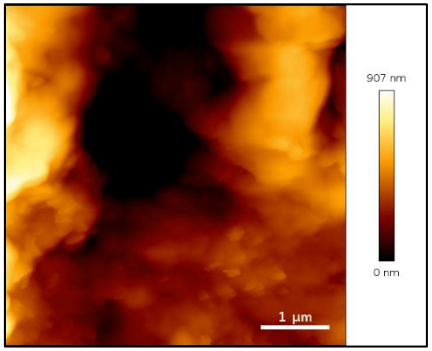 907 nm 0 nm 1 µm	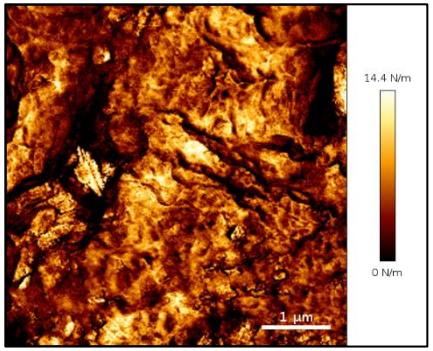 14.4 N/m 0 N/m 1 µm	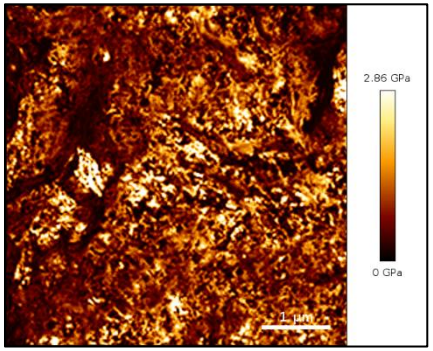 2.86 GPa 0 GPa 1 µm
	Site 3	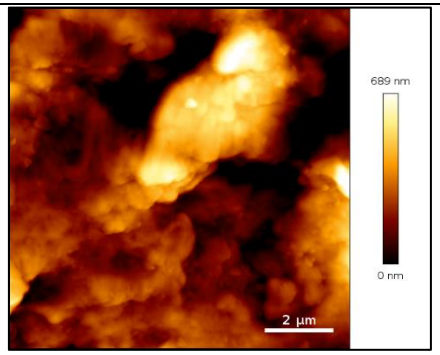 689 nm 0 nm 2 µm	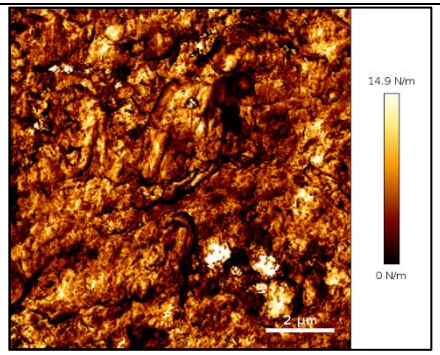 14.9 N/m 0 N/m 2 µm	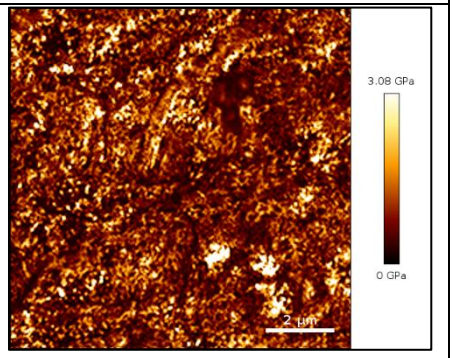 3.08 GPa 0 GPa 2 µm

		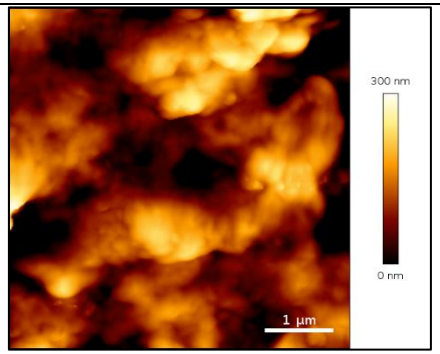	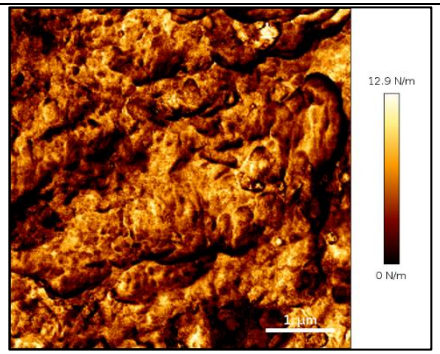	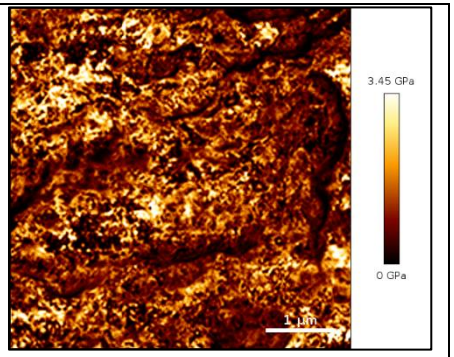
	Site 4	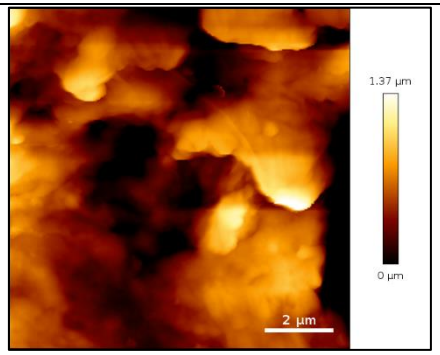 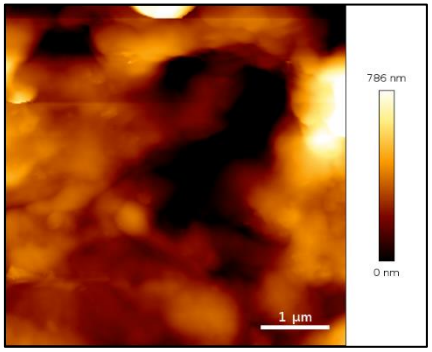	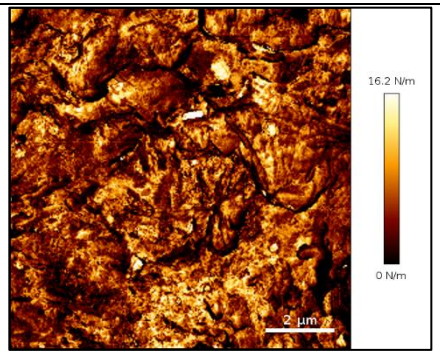 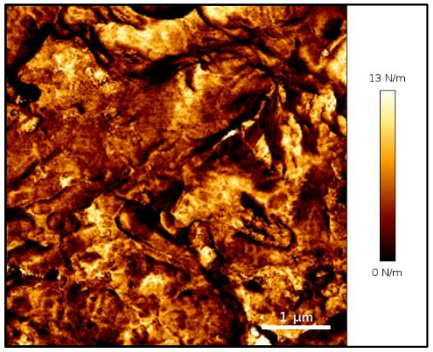	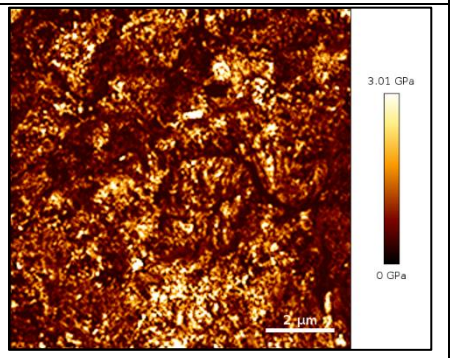 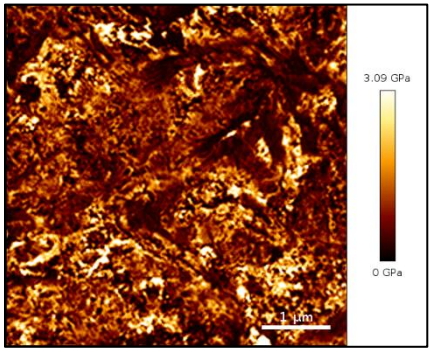

rP60	Site 1	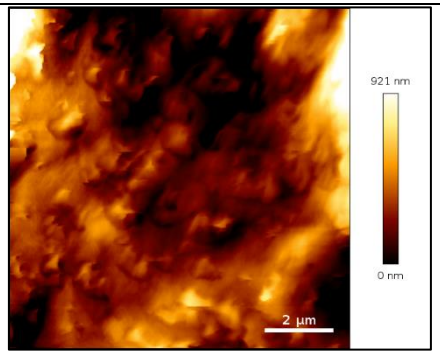	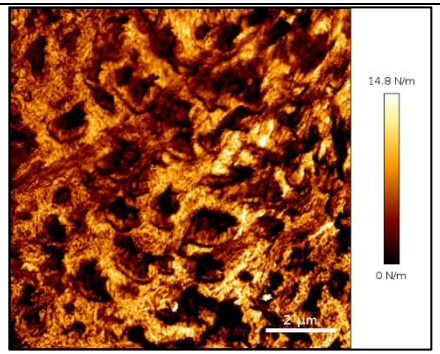	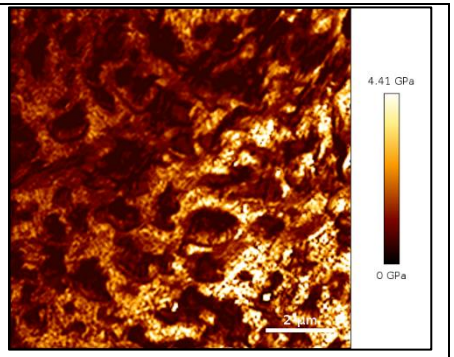
		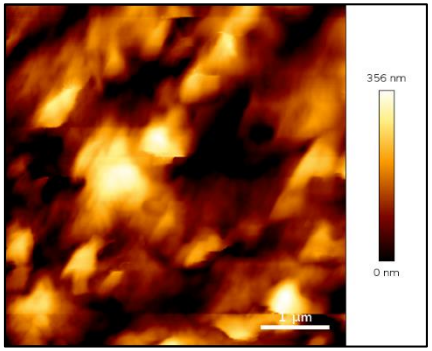	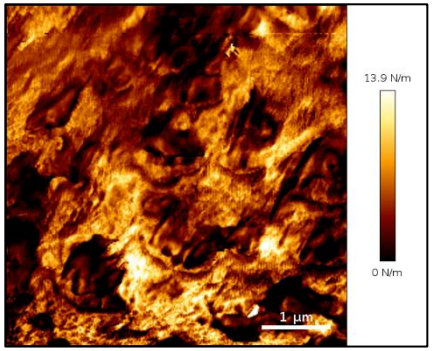	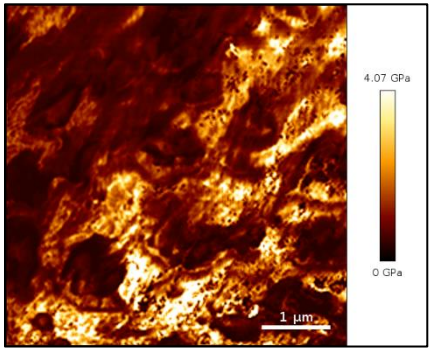
	Site 2	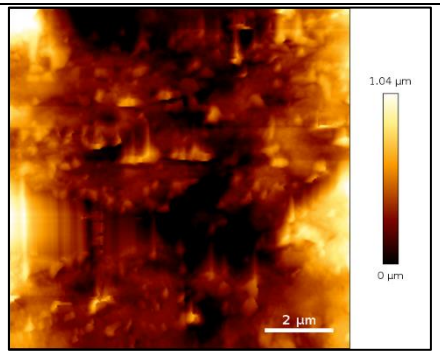	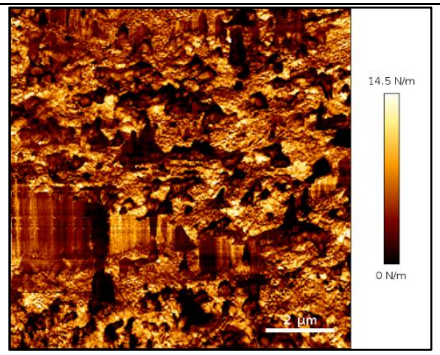	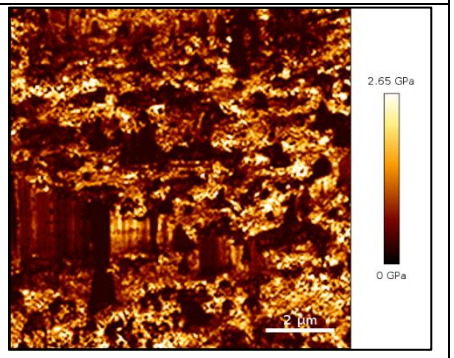

		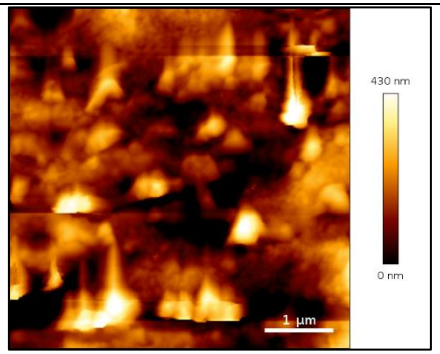	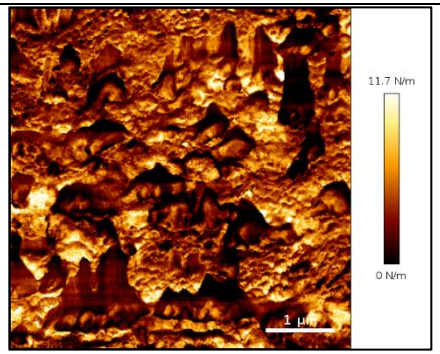	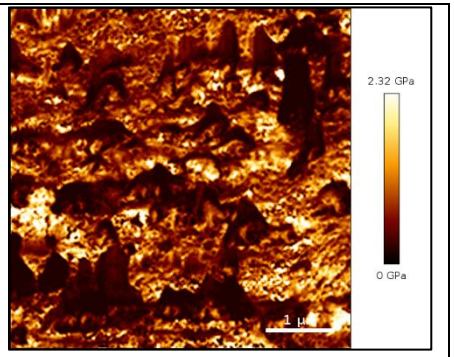
	Site 3	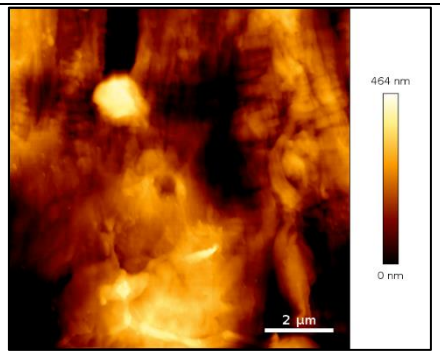 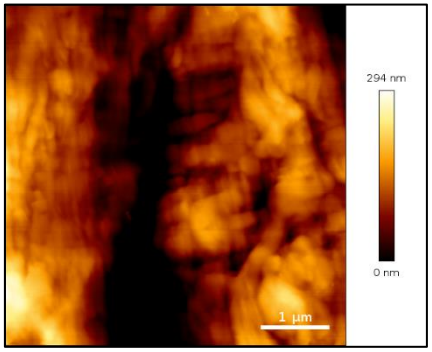	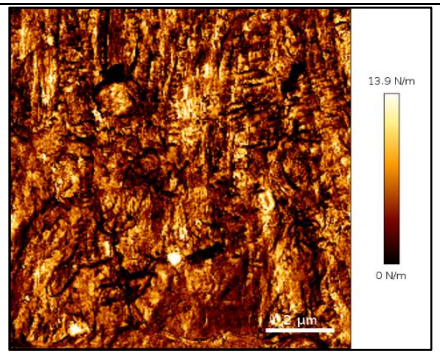 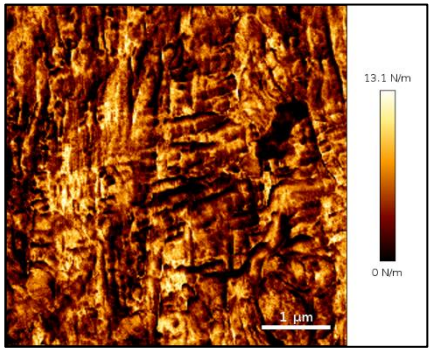	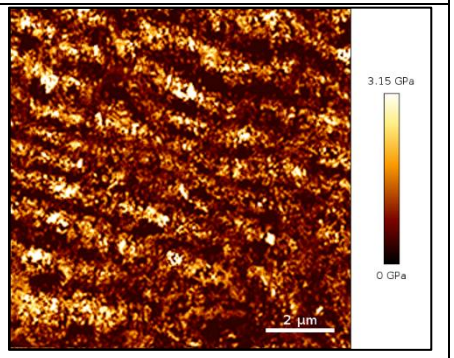 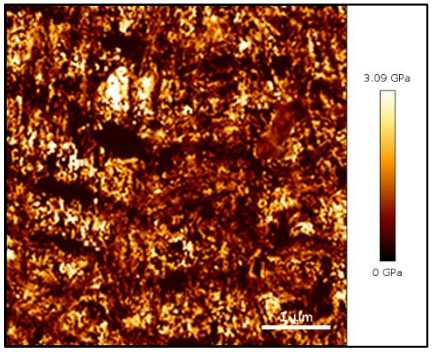

Appendix 2

	Site 4	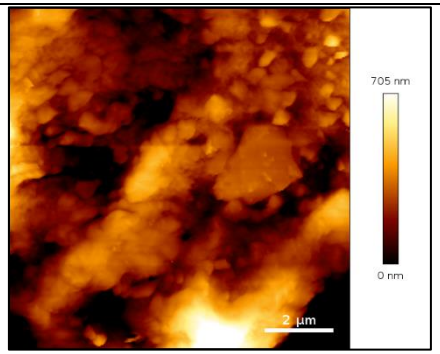	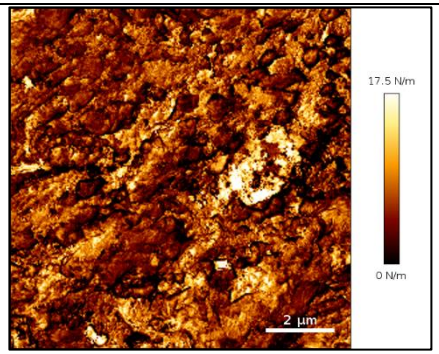	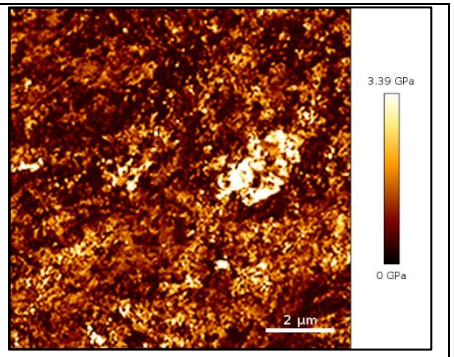
		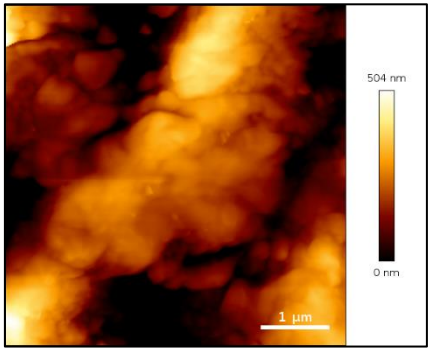	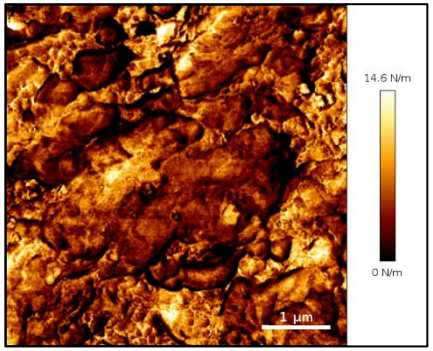	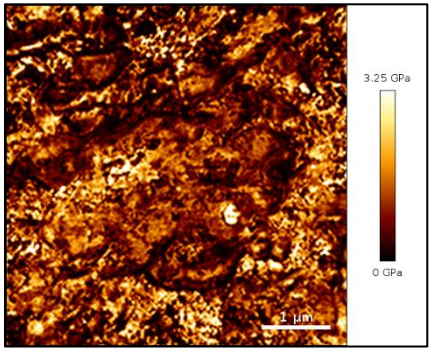
rP75	Site 1	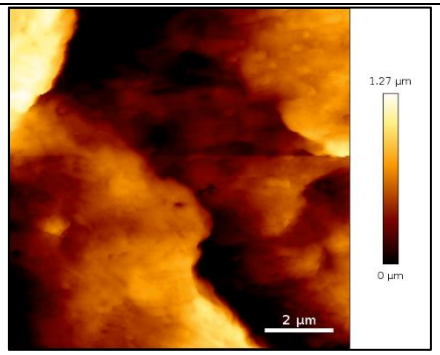	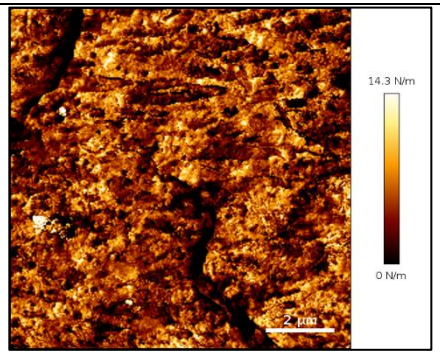	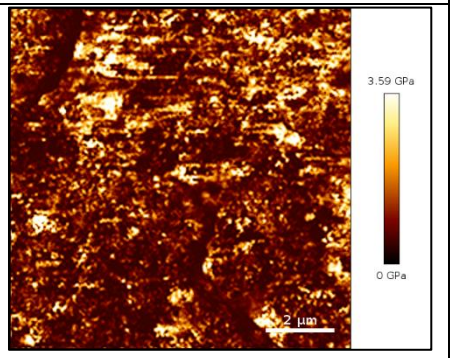

		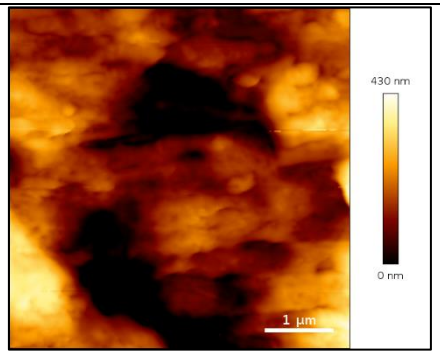 430 nm 0 nm 1 µm	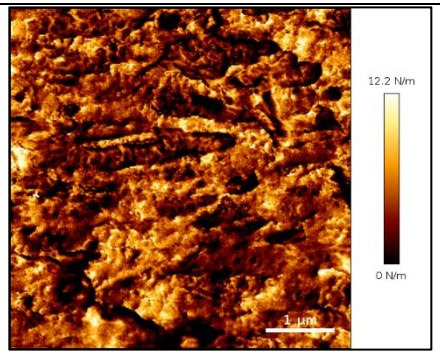 12.2 N/m 0 N/m 1 µm	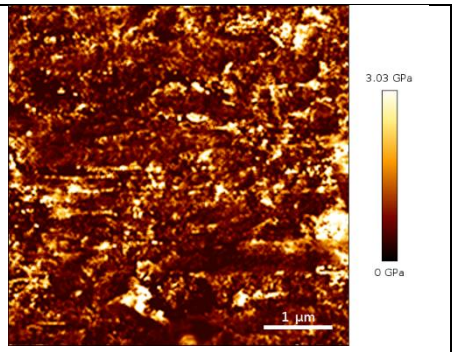 3.03 GPa 0 GPa 1 µm
	Site 2	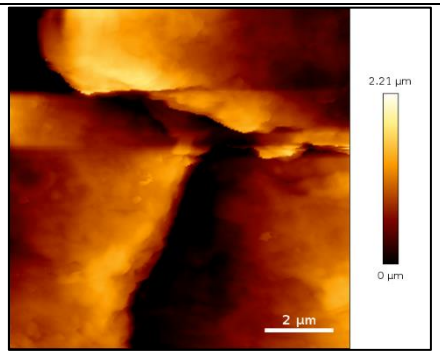 2.21 µm 0 µm 2 µm	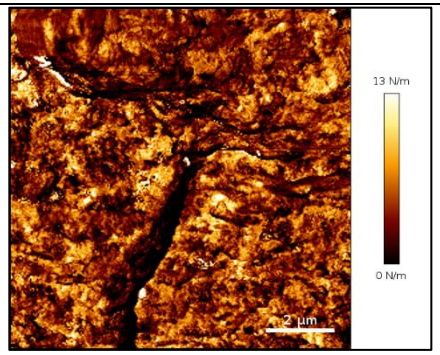 13 N/m 0 N/m 2 µm	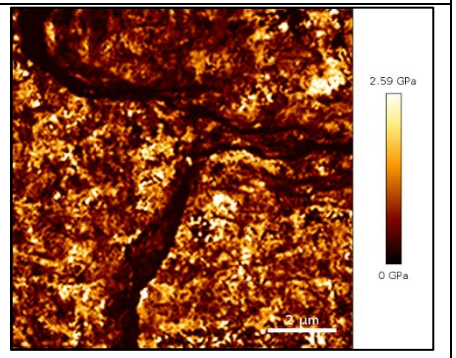 2.59 GPa 0 GPa 2 µm
		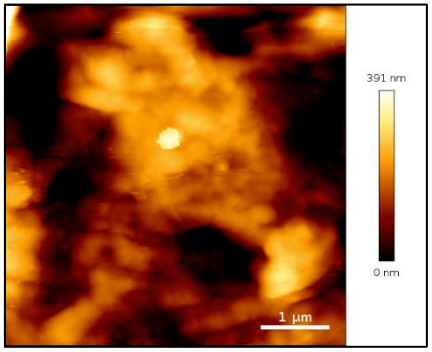 391 nm 0 nm 1 µm	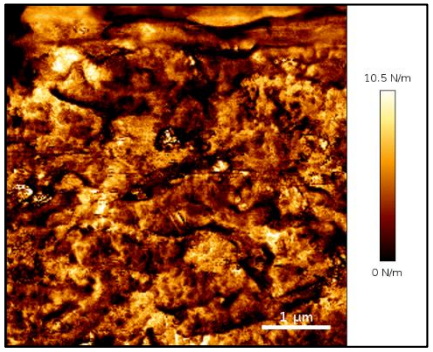 10.5 N/m 0 N/m 1 µm	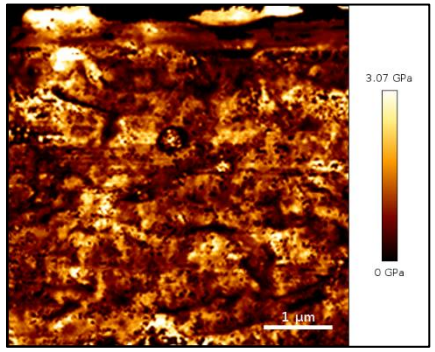 3.07 GPa 0 GPa 1 µm

	Site 3	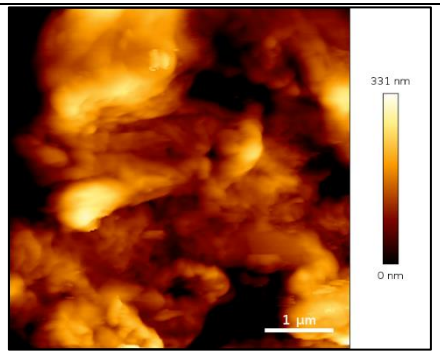	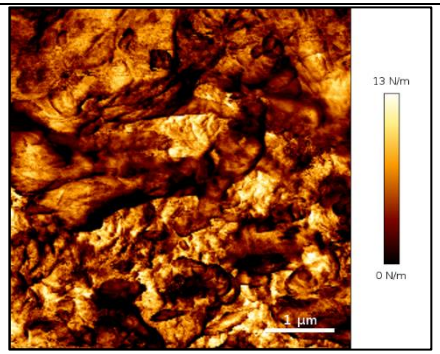	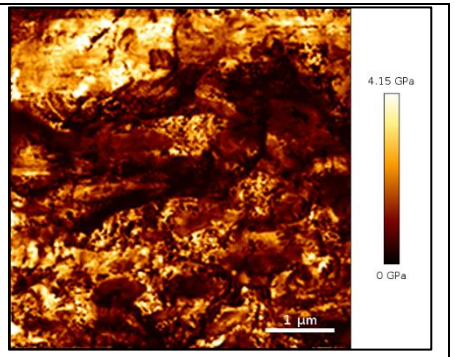
	Site 4	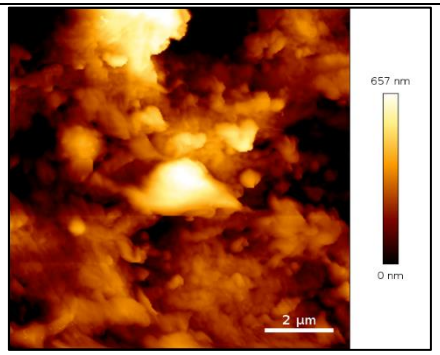 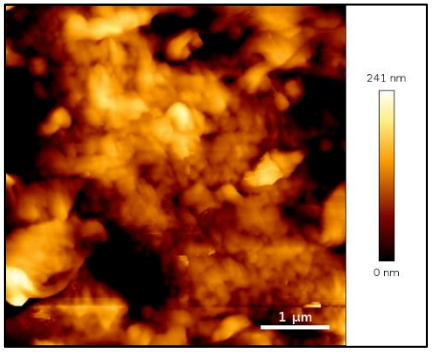	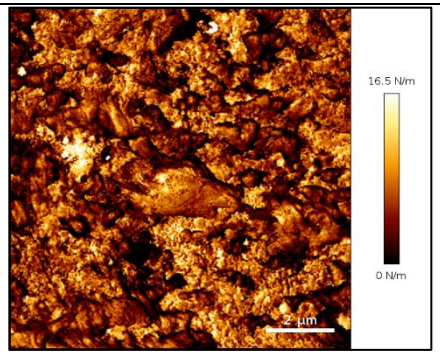 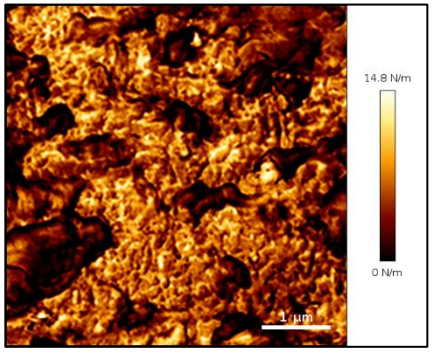	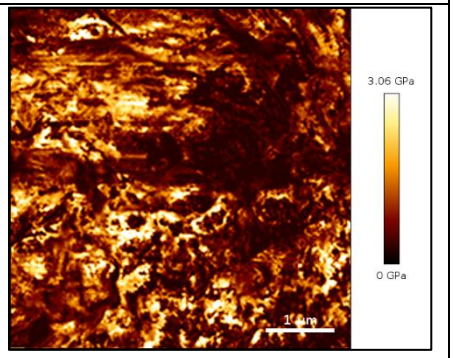 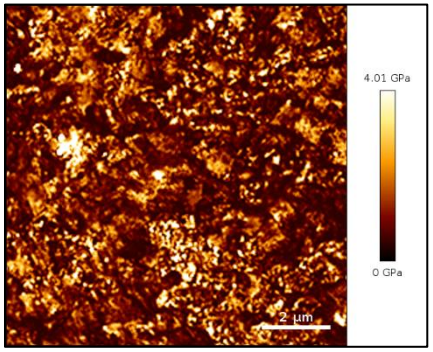

rP80	Site 1	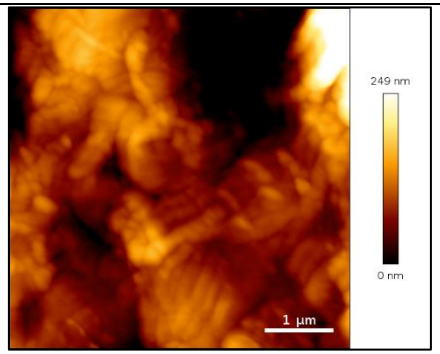	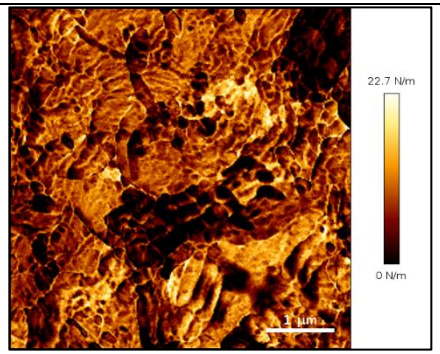	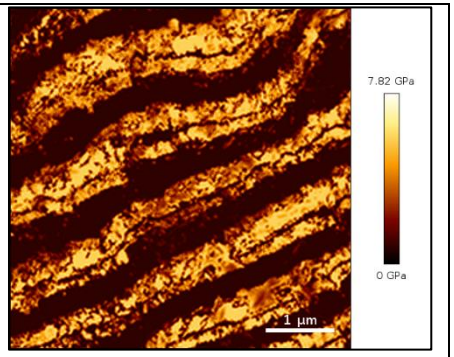
	Site 2	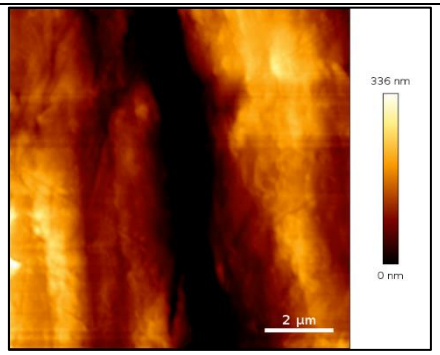 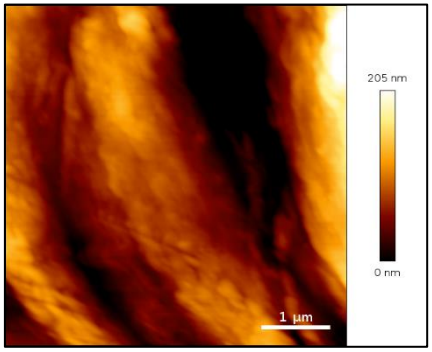	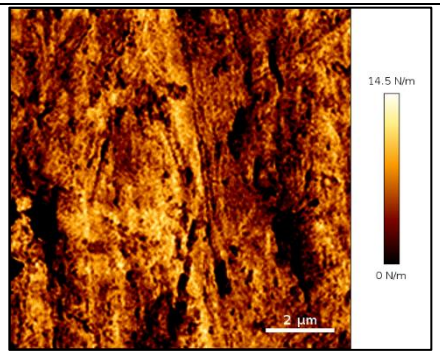 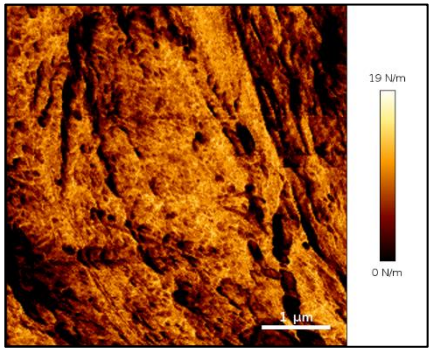	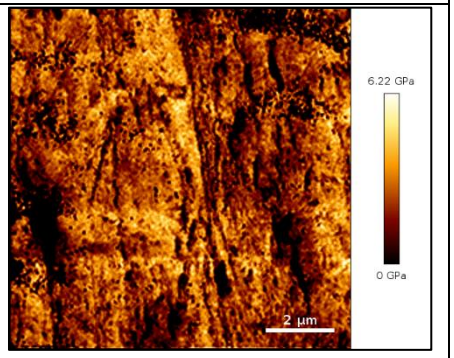 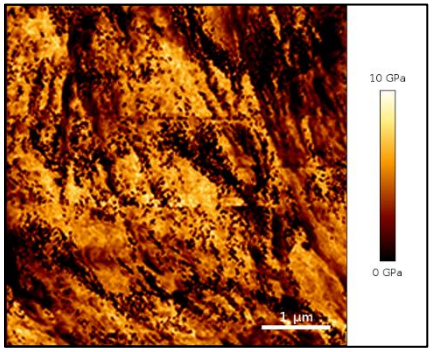

	Site 3	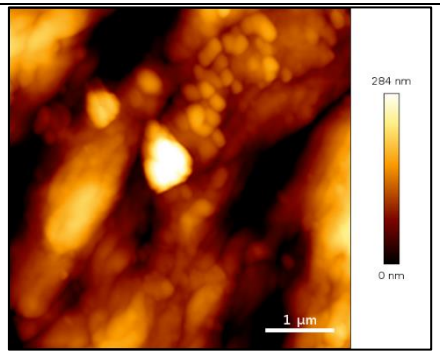	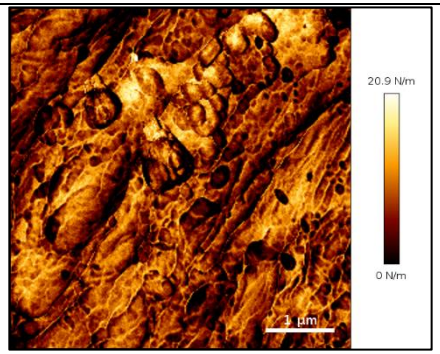	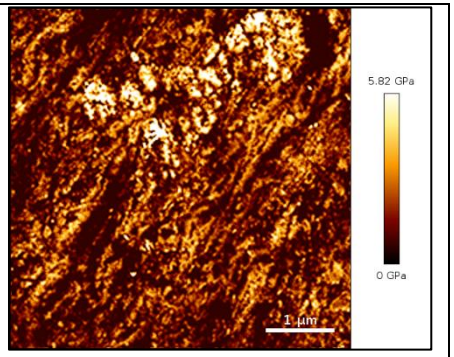
	Site 4	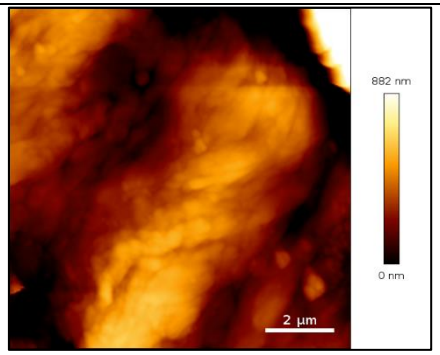 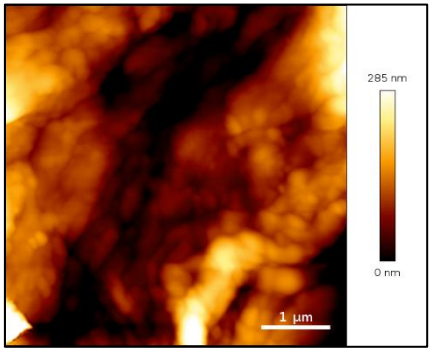	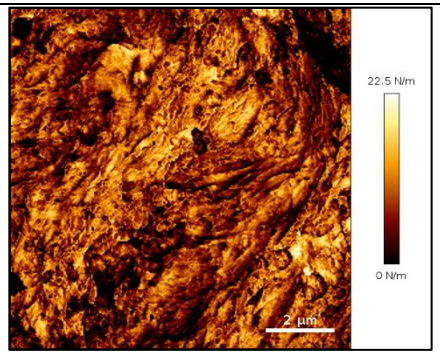 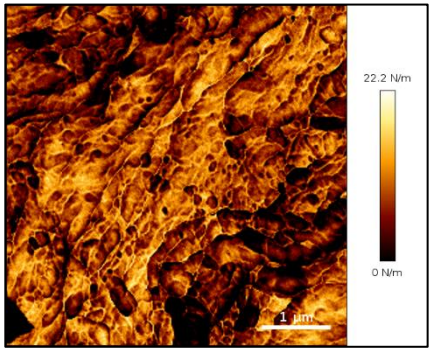	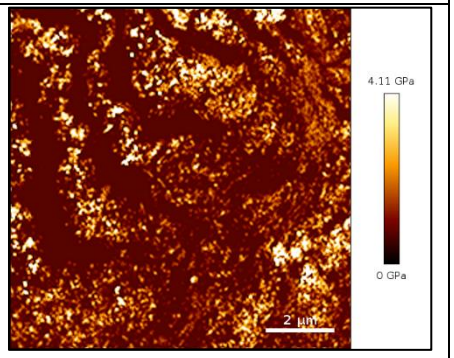 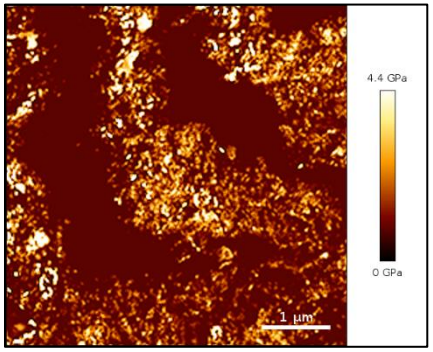

Appendix 2

rP90	Site 1	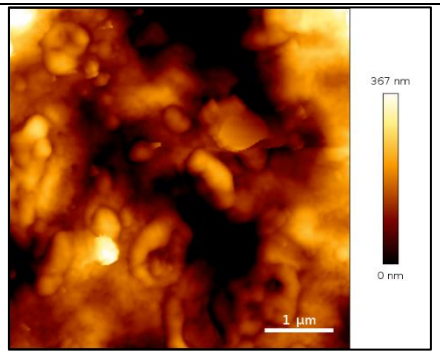	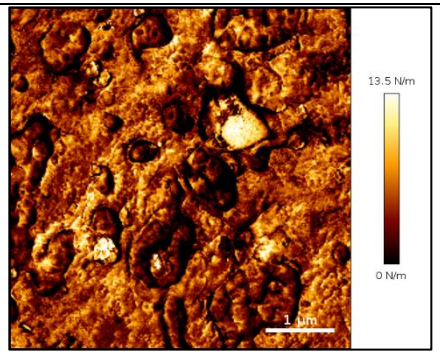	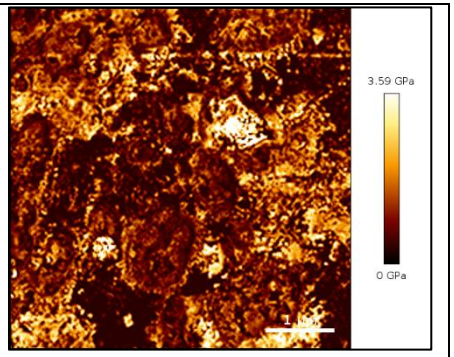
	Site 2	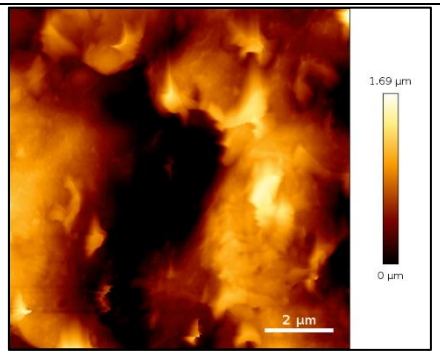 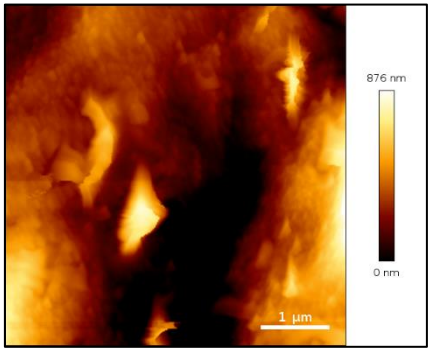	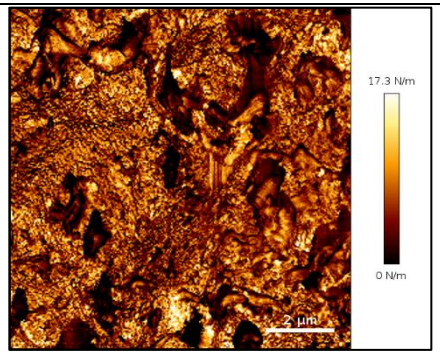 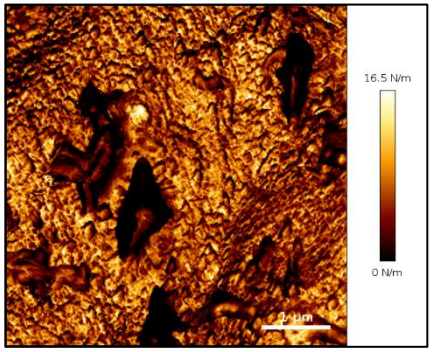	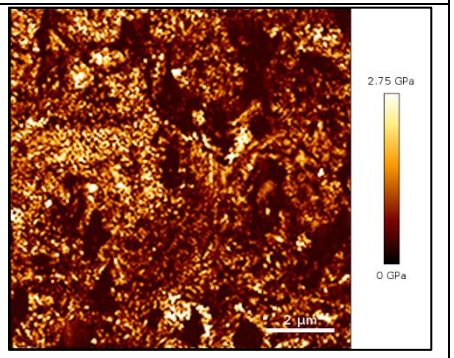 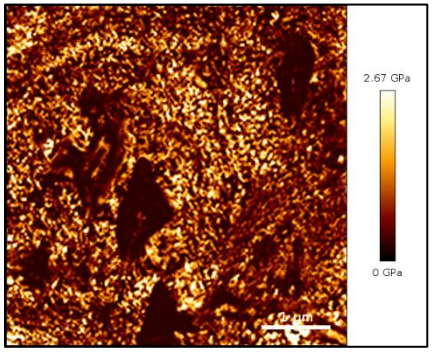

	Site 3	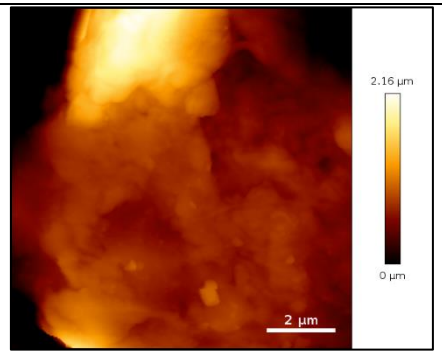 2.16 µm 0 µm 2 µm	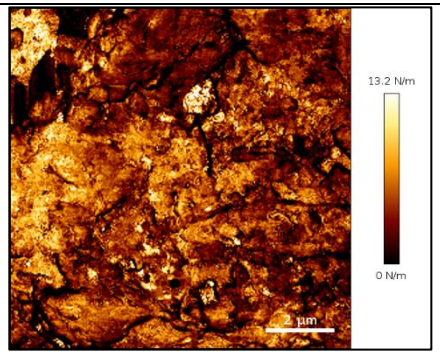 13.2 N/m 0 N/m 2 µm	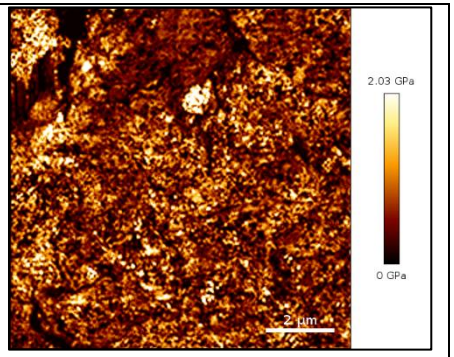 2.03 GPa 0 GPa 2 µm
		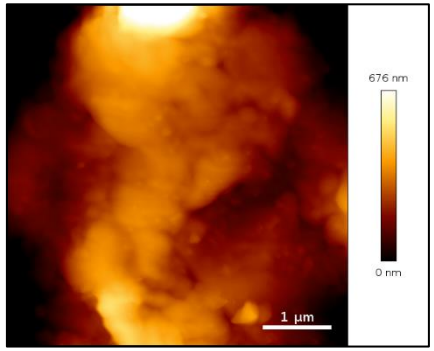 676 nm 0 nm 1 µm	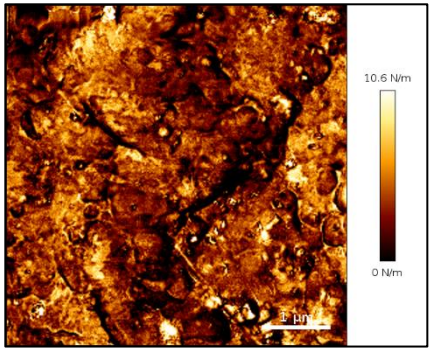 10.6 N/m 0 N/m 1 µm	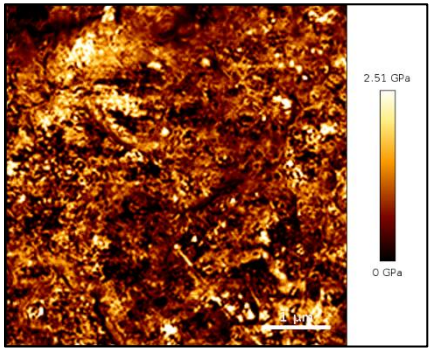 2.51 GPa 0 GPa 1 µm
	Site 4	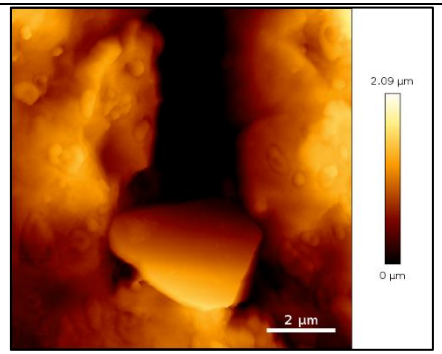 2.09 µm 0 µm 2 µm	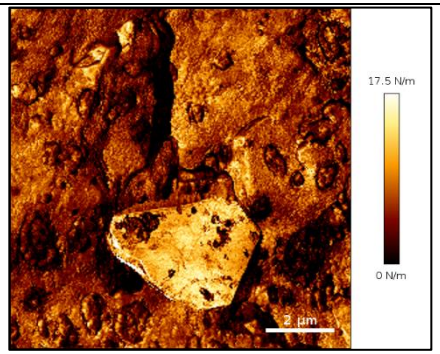 17.5 N/m 0 N/m 2 µm	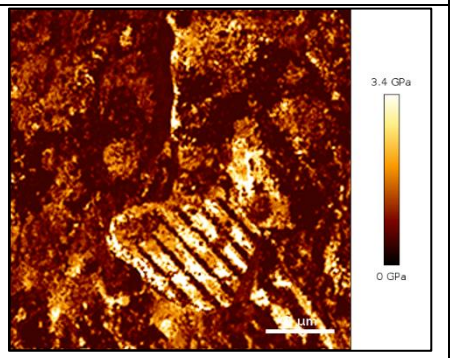 3.4 GPa 0 GPa 1 µm

		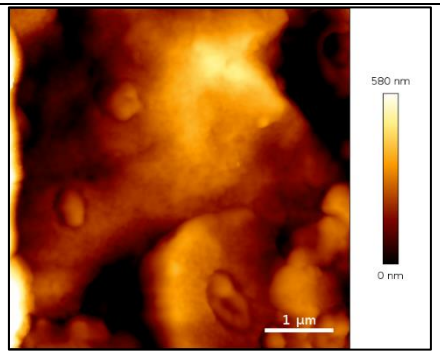	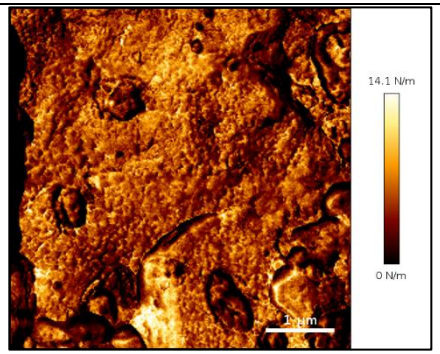	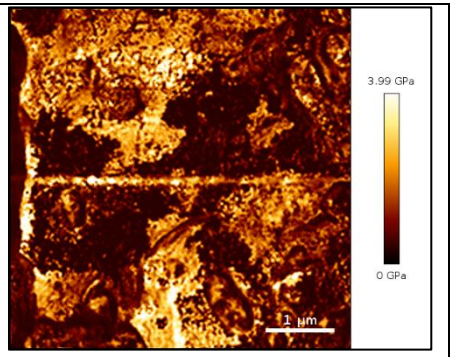
rPP	Site 1	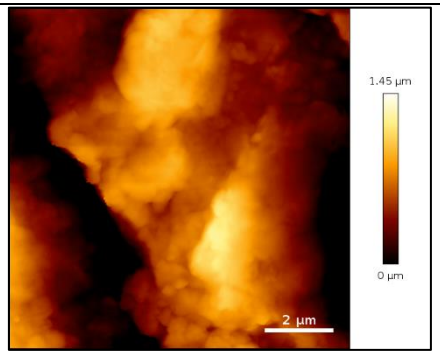 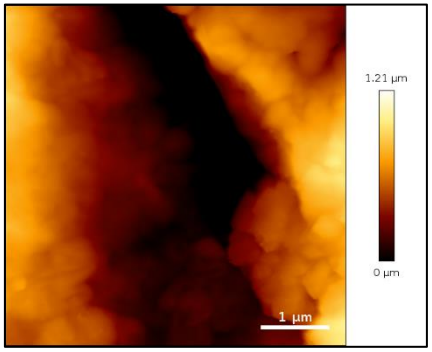	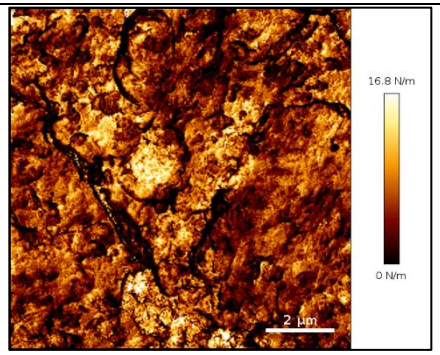 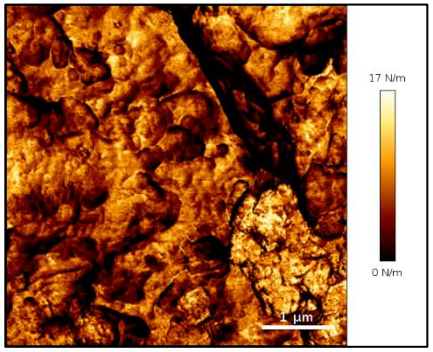	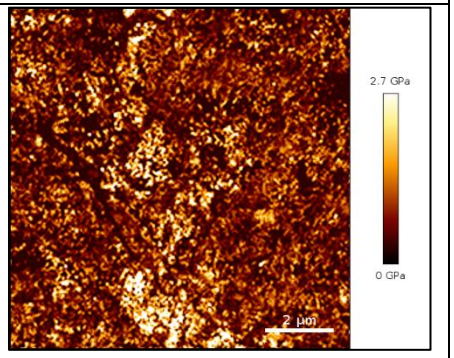 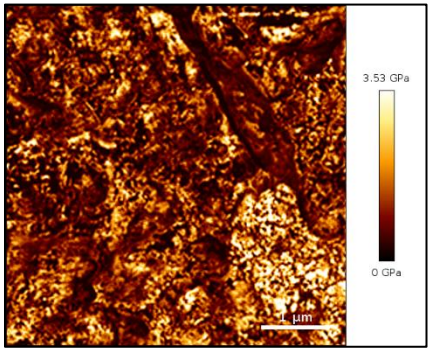

	Site 2	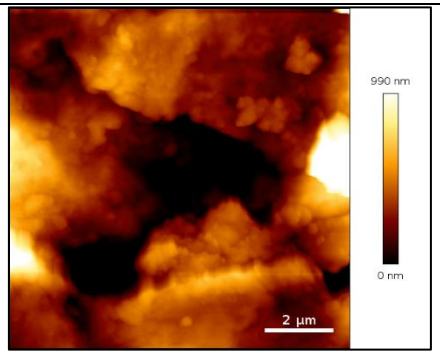 990 nm 0 nm 2 µm	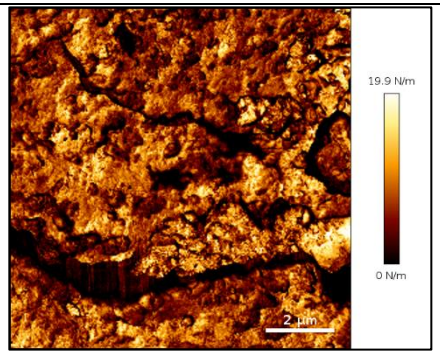 19.9 N/m 0 N/m 2 µm	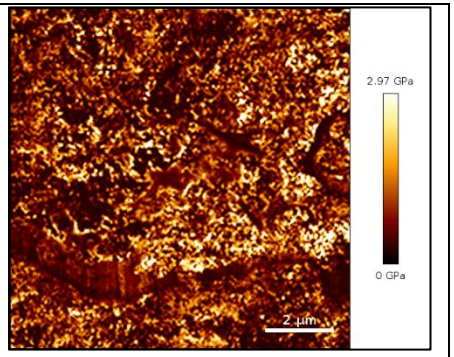 2.97 GPa 0 GPa 2 µm
		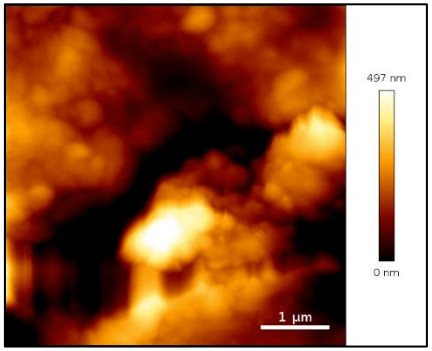 497 nm 0 nm 1 µm	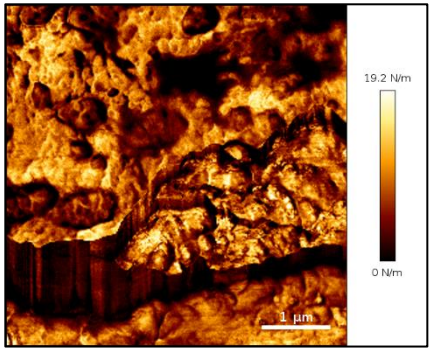 19.2 N/m 0 N/m 1 µm	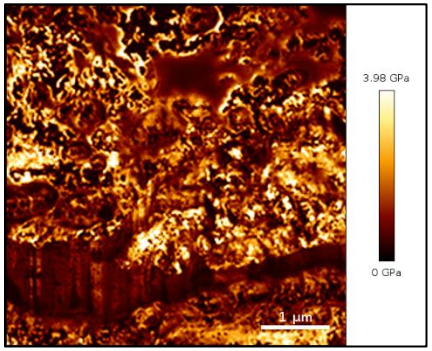 3.98 GPa 0 GPa 1 µm
	Site 3	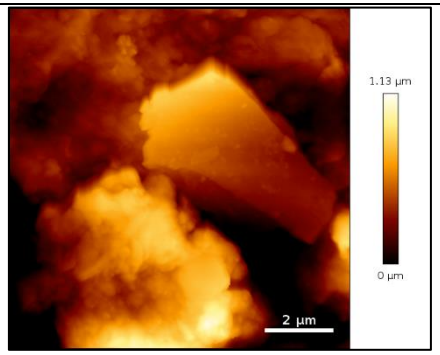 1.13 µm 0 µm 2 µm	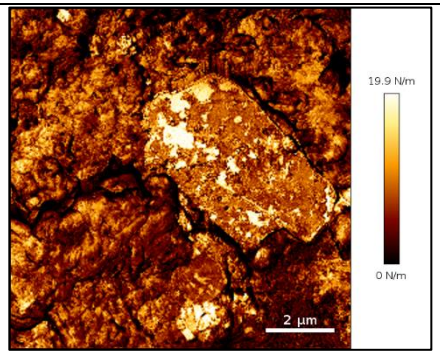 19.9 N/m 0 N/m 2 µm	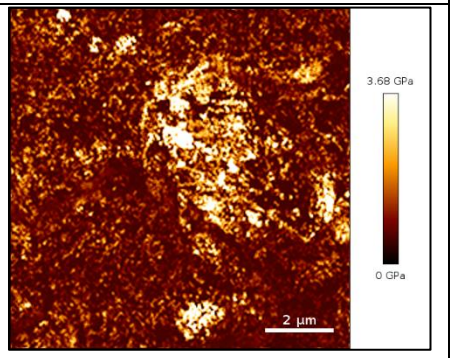 3.68 GPa 0 GPa 2 µm

		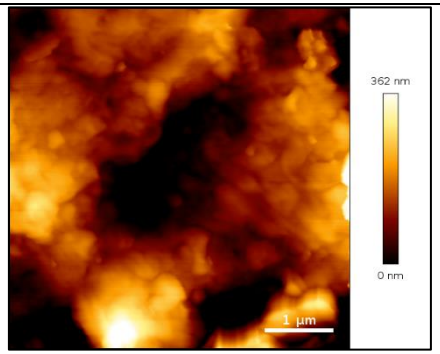	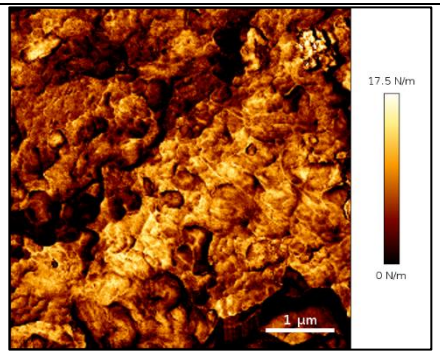	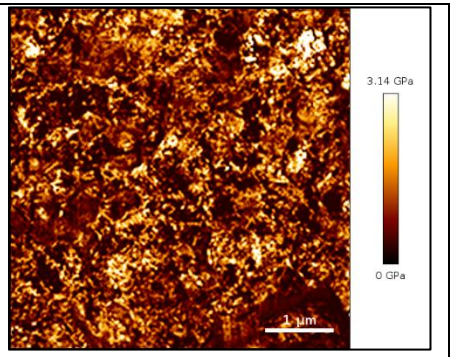
	Site 4	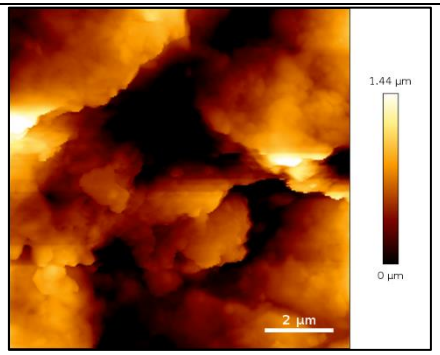 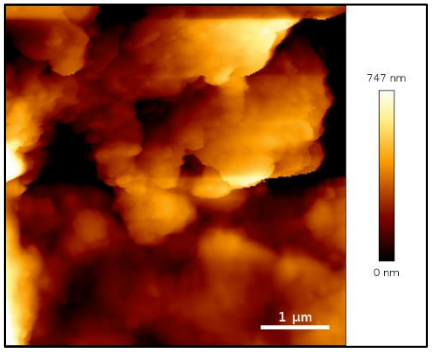	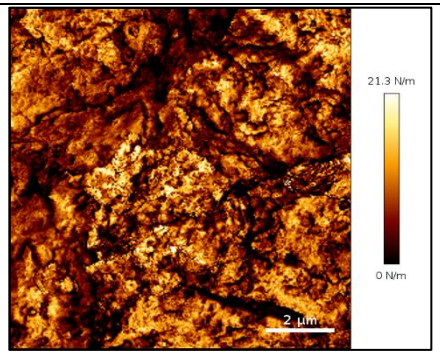 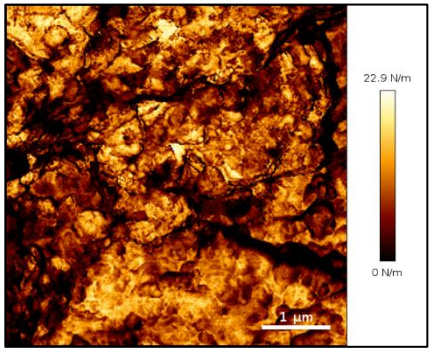	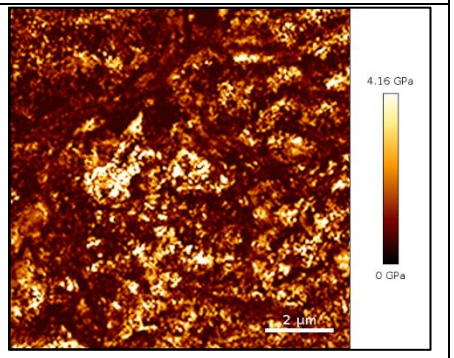 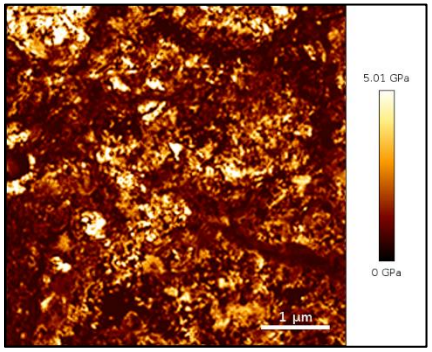

Appendix 3 AFM QI mode height, adhesion and Young's modulus images obtained at 256 x 256 pixels for vPP:vHDPE blends.

PP:HDPE Blend		Height, nm	Adhesion, nN	Young's modulus, GPa
vHDPE	Site 1	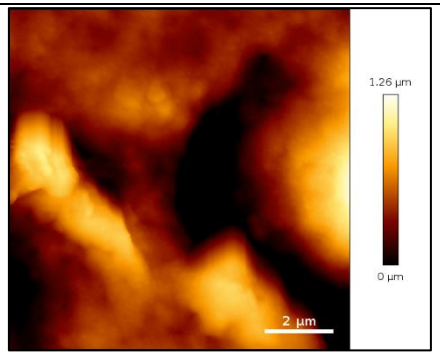	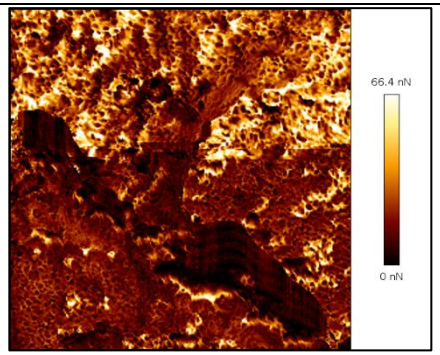	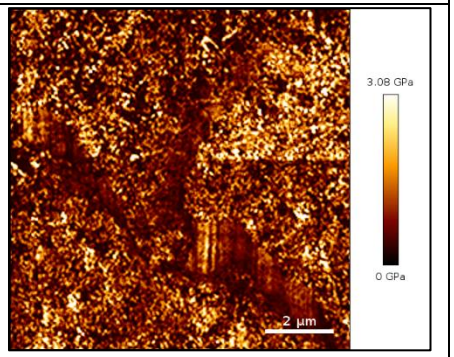
	Site 2	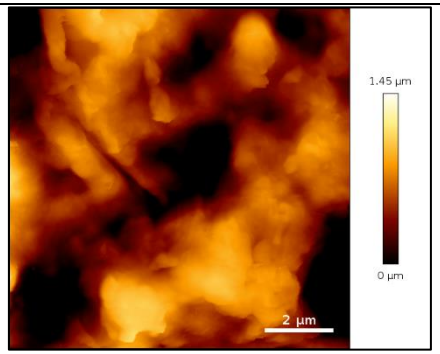	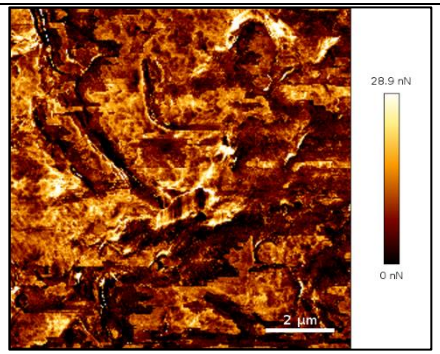	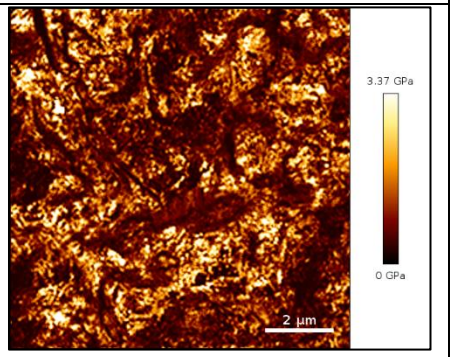
		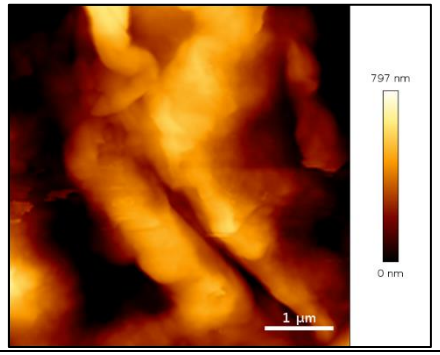	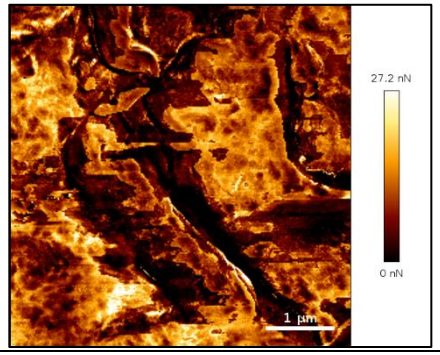	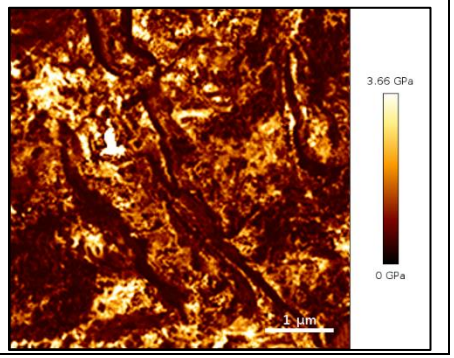

	Site 3	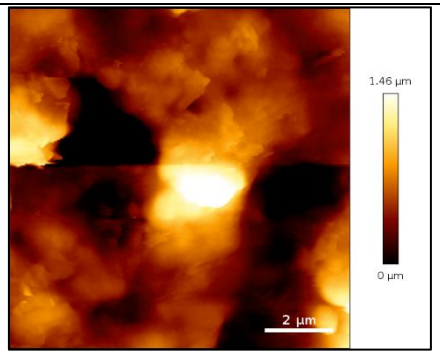 1.46 µm 0 µm 2 µm	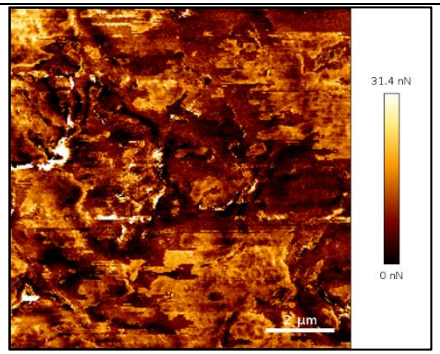 31.4 nN 0 nN 2 µm	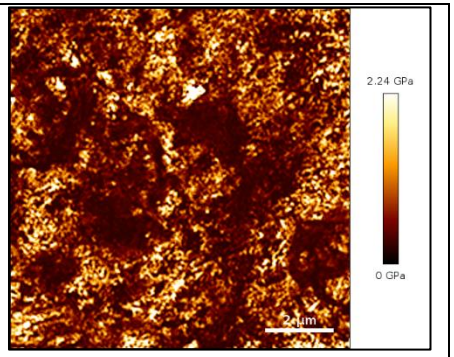 2.24 GPa 0 GPa 2 µm
		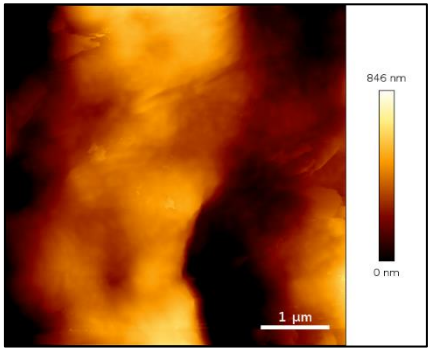 846 nm 0 nm 1 µm	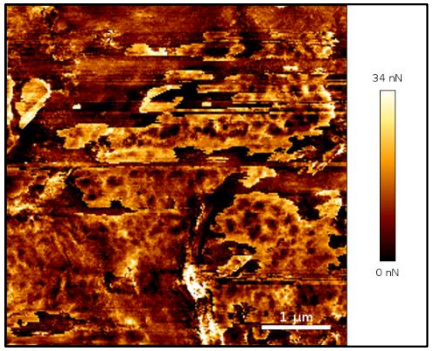 34 nN 0 nN 1 µm	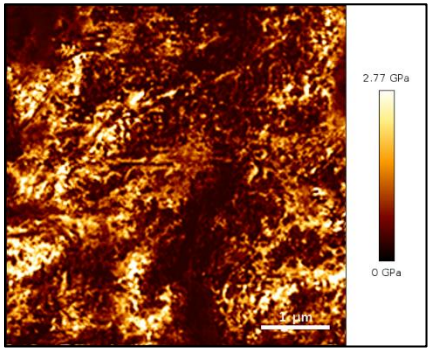 2.77 GPa 0 GPa 1 µm
	Site 4	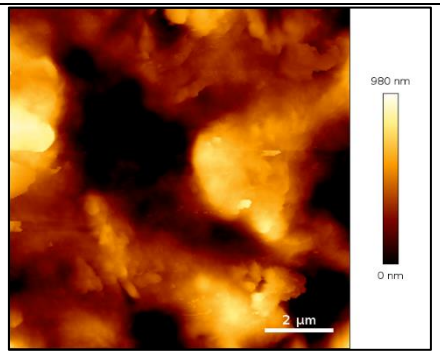 980 nm 0 nm 2 µm	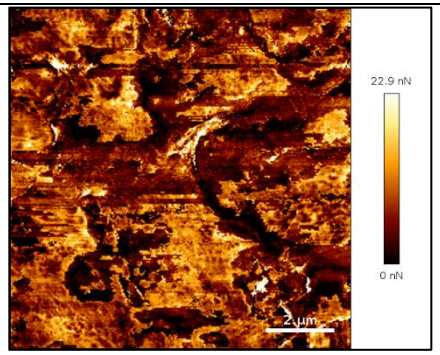 22.9 nN 0 nN 2 µm	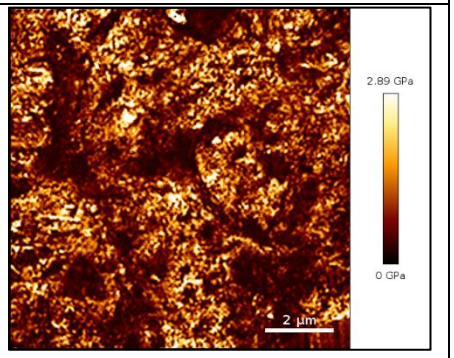 2.89 GPa 0 GPa 2 µm

		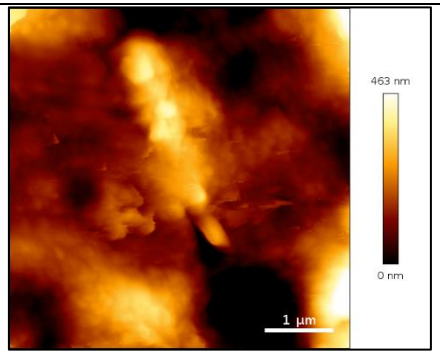	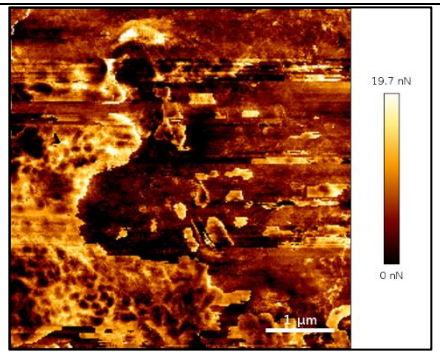	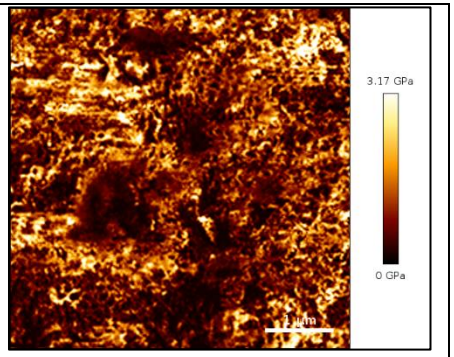
vP10	Site 1	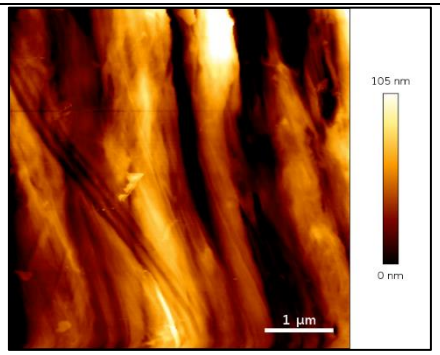	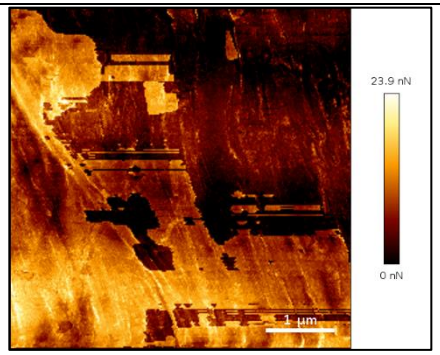	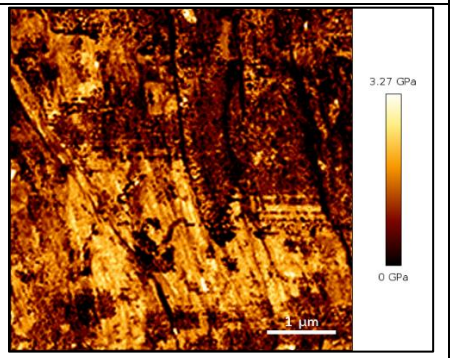
	Site 2	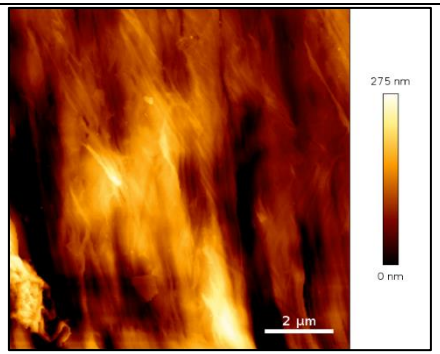	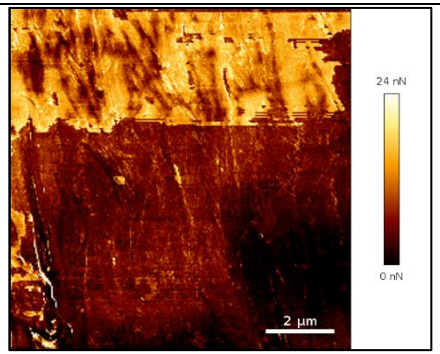	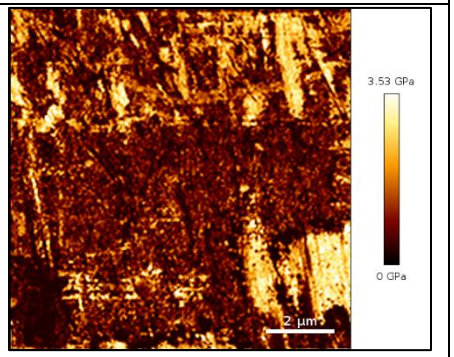

		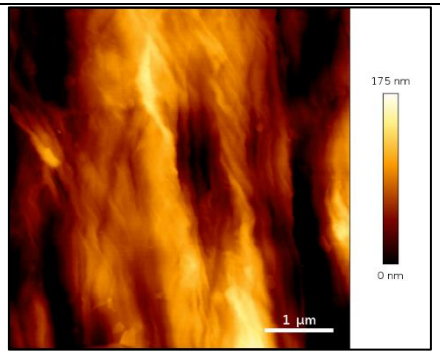 175 nm 0 nm 1 µm	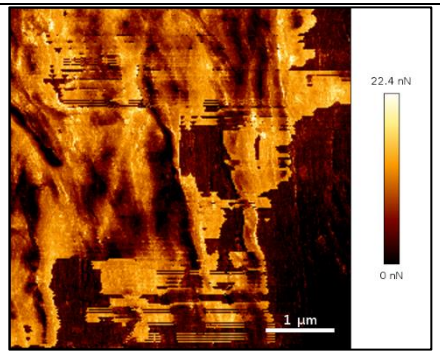 22.4 nN 0 nN 1 µm	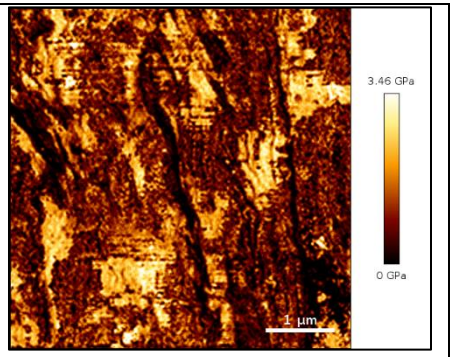 3.46 GPa 0 GPa 1 µm
	Site 3	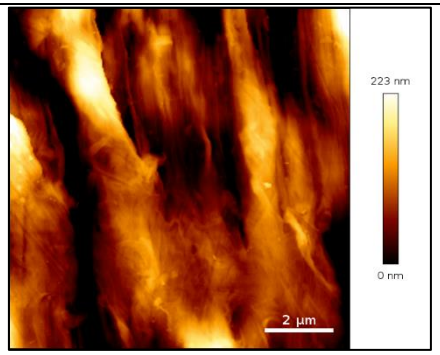 223 nm 0 nm 2 µm	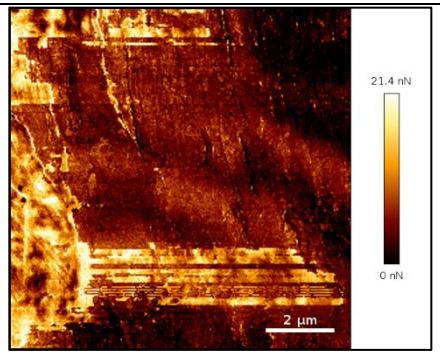 21.4 nN 0 nN 2 µm	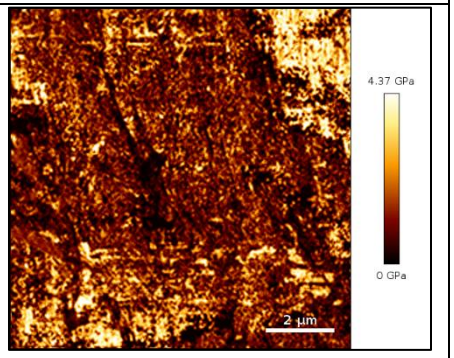 4.37 GPa 0 GPa 2 µm
		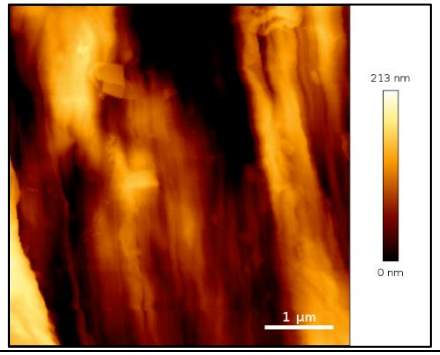 213 nm 0 nm 1 µm	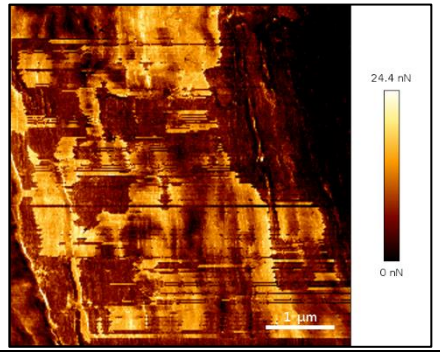 24.4 nN 0 nN 1 µm	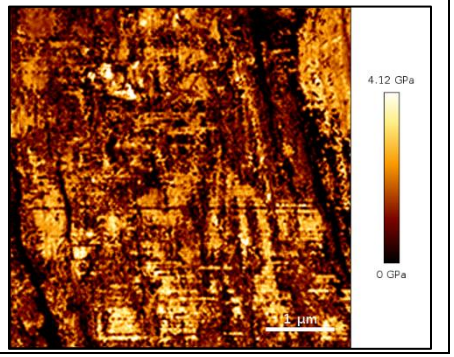 4.12 GPa 0 GPa 1 µm

	Site 4	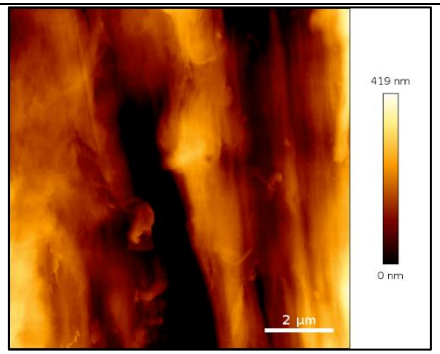	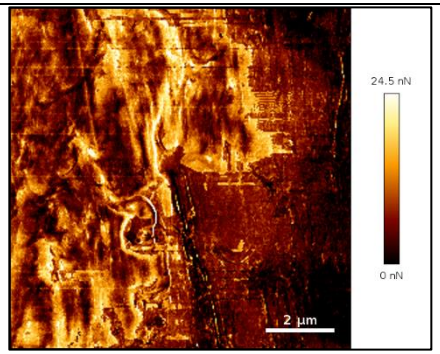	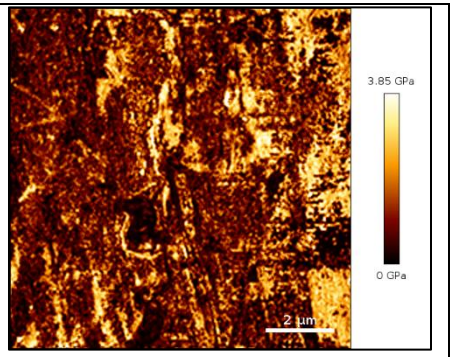
		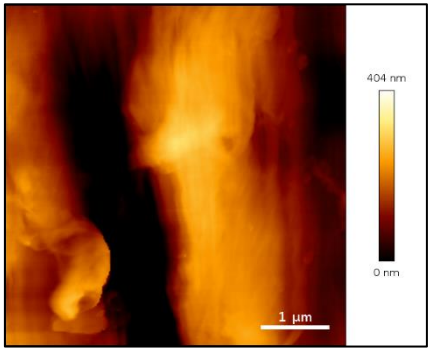	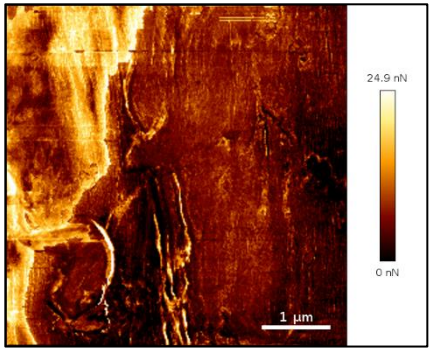	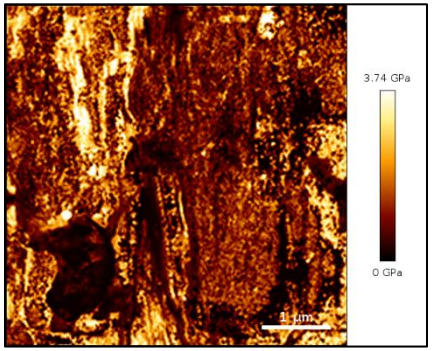
vP20	Site 1	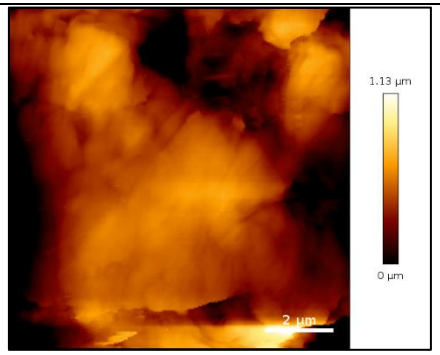	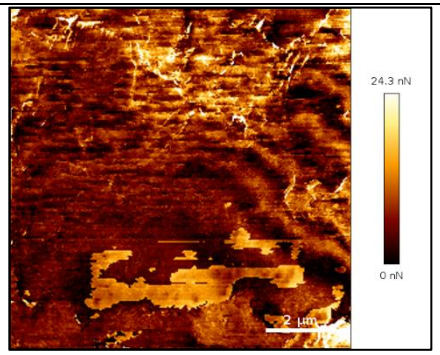	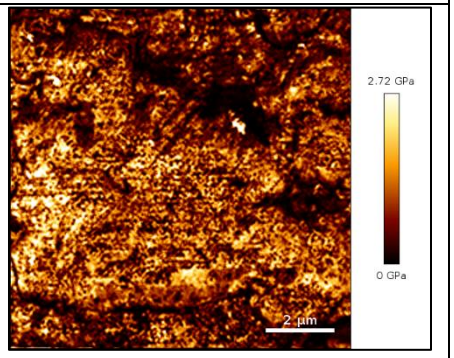

		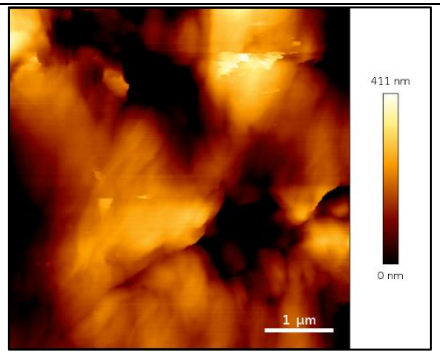 411 nm 0 nm 1 µm	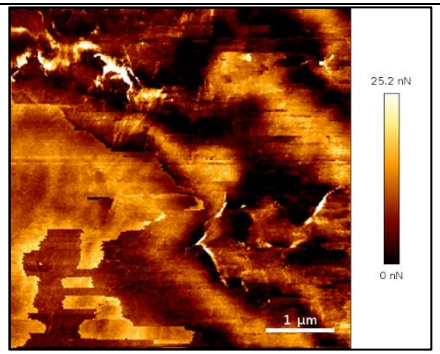 25.2 nN 0 nN 1 µm	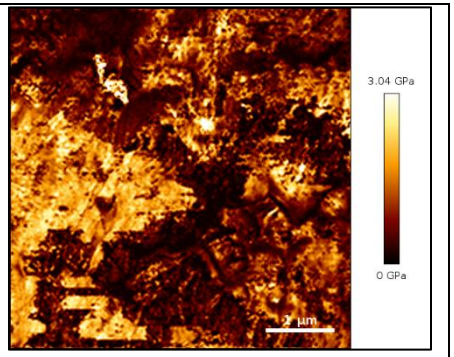 3.04 GPa 0 GPa 2 µm
	Site 2	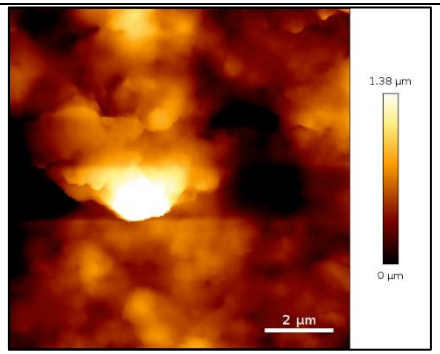 1.38 µm 0 µm 2 µm	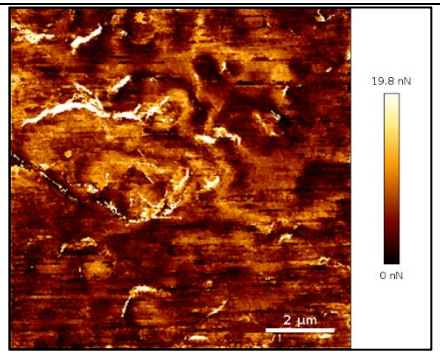 19.8 nN 0 nN 2 µm	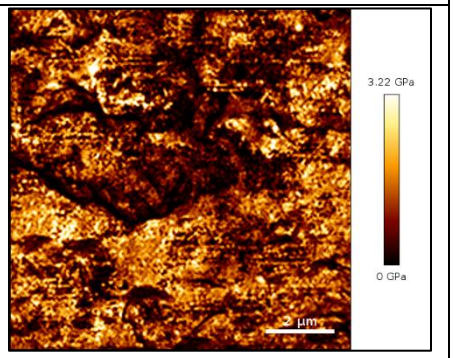 3.22 GPa 0 GPa 2 µm
		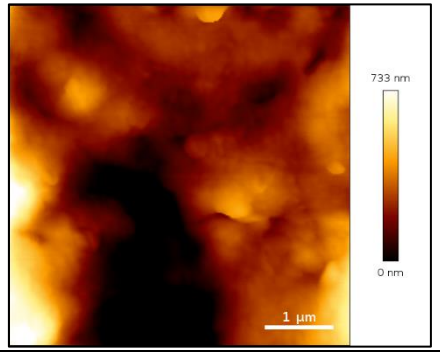 733 nm 0 nm 1 µm	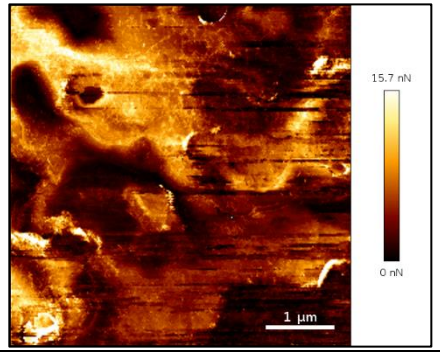 15.7 nN 0 nN 1 µm	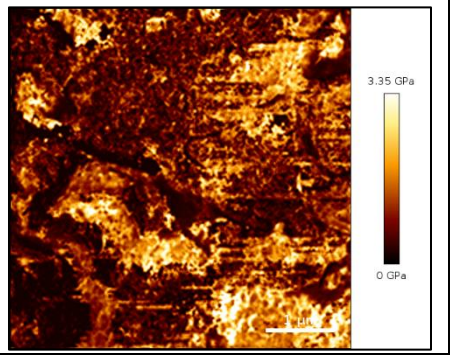 3.35 GPa 0 GPa

	Site 3	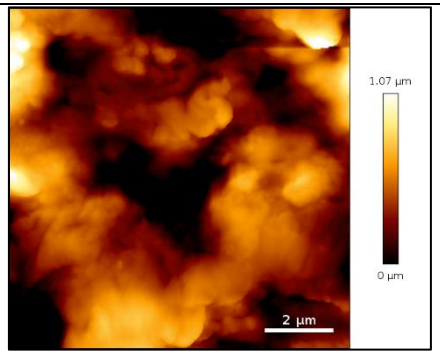 1.07 µm 0 µm 2 µm	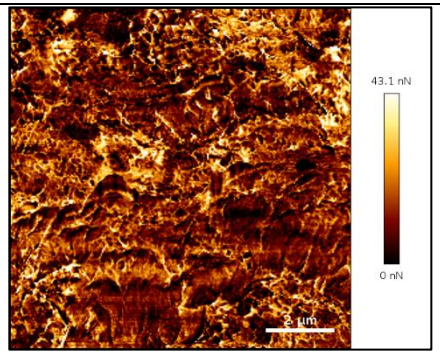 43.1 nN 0 nN 2 µm	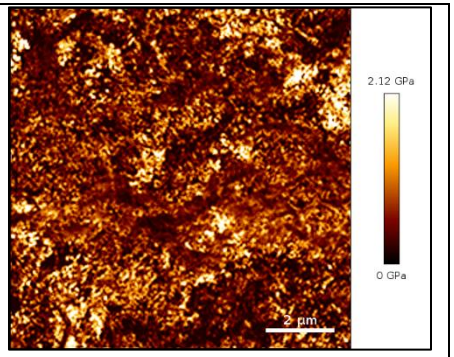 2.12 GPa 0 GPa 2 µm
		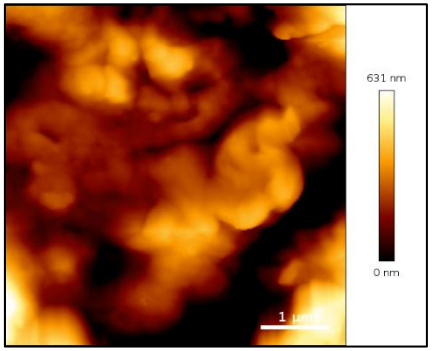 631 nm 0 nm 1 µm	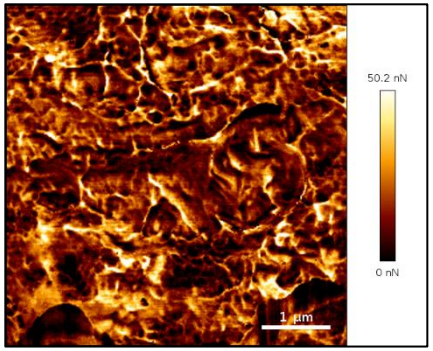 50.2 nN 0 nN 1 µm	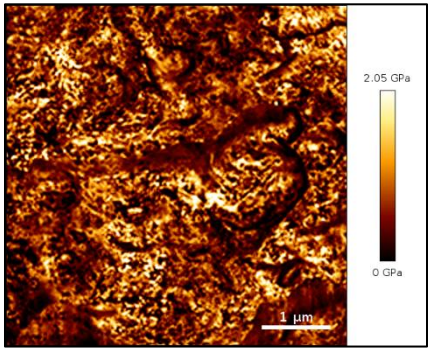 2.05 GPa 0 GPa 1 µm
	Site 4	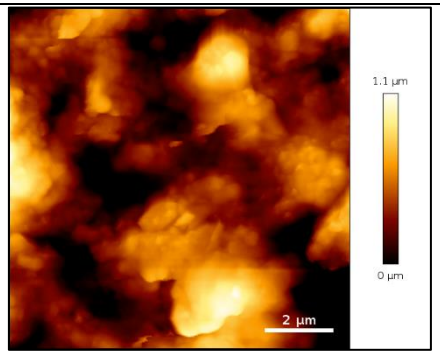 1.1 µm 0 µm 2 µm	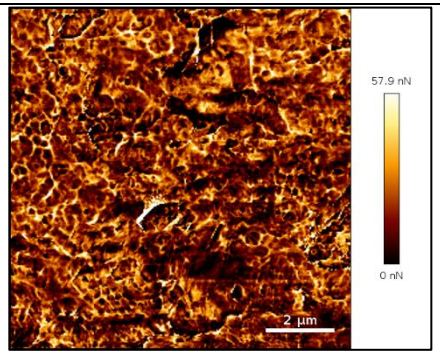 57.9 nN 0 nN 2 µm	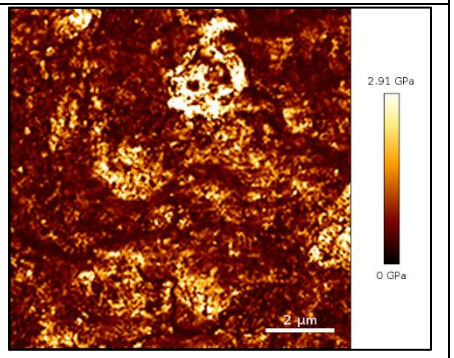 2.91 GPa 0 GPa 2 µm

		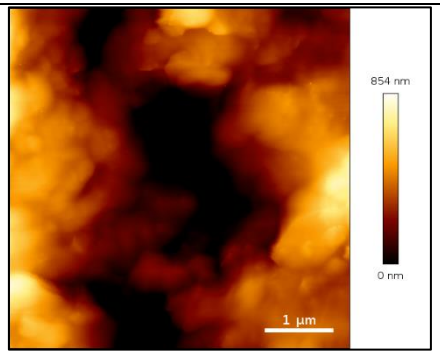	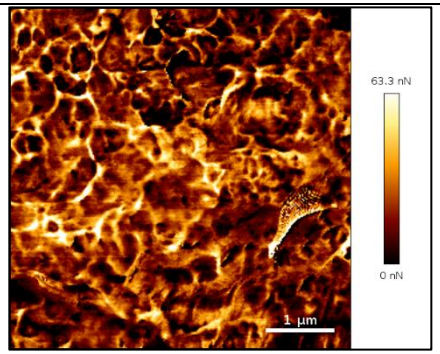	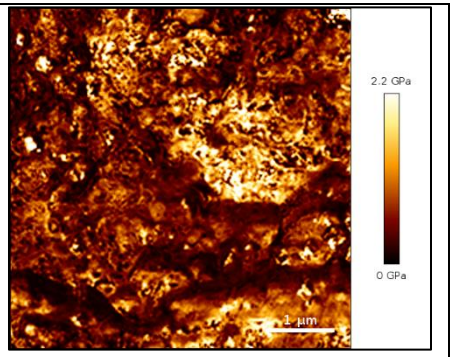
vP25	Site 1	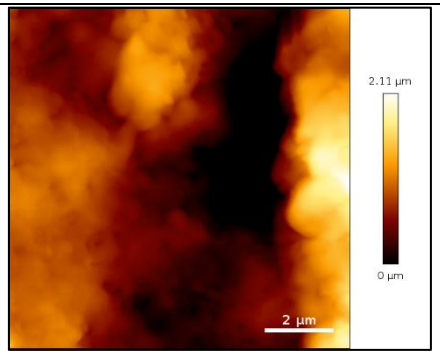 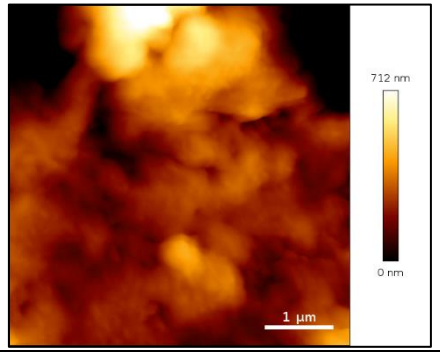	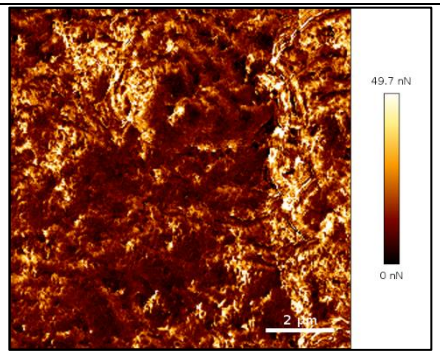 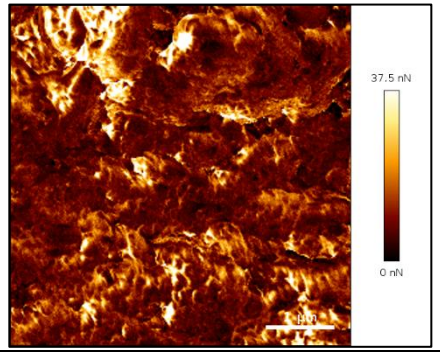	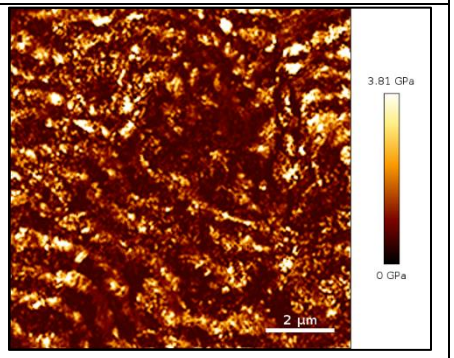 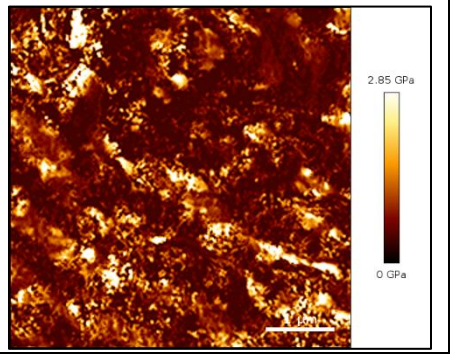

	Site 2	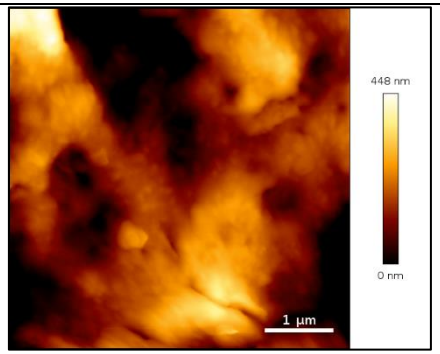	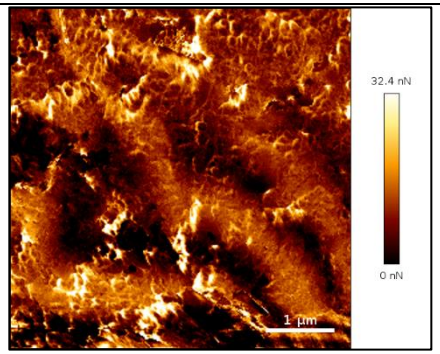	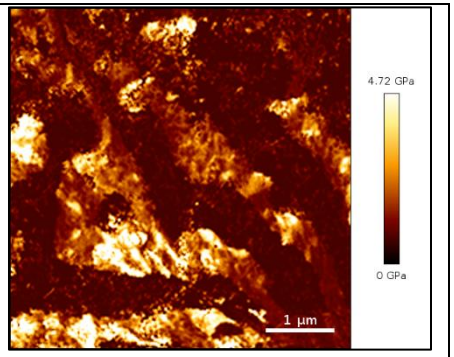
	Site 3	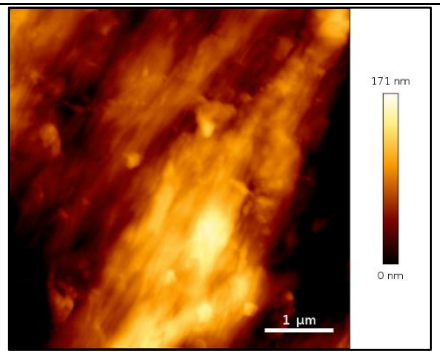	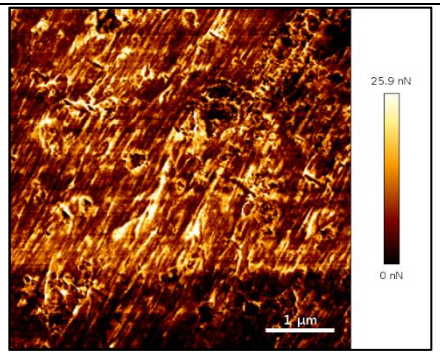	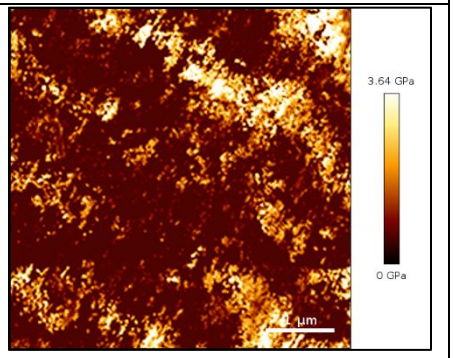
	Site 4	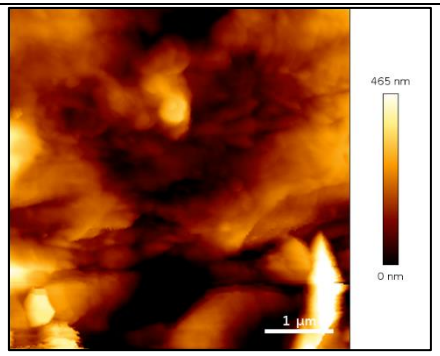	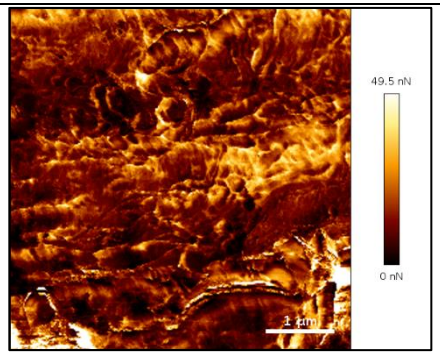	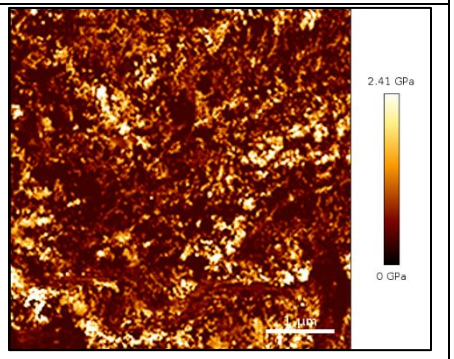

Appendix 3

vP40	Site 1	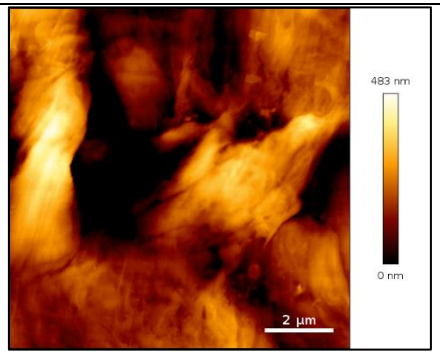	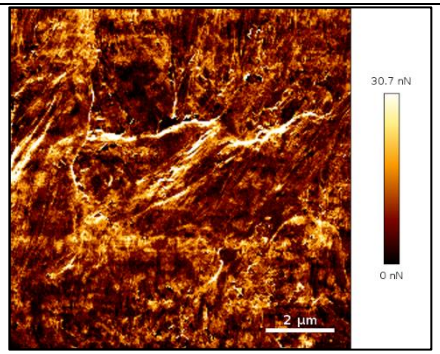	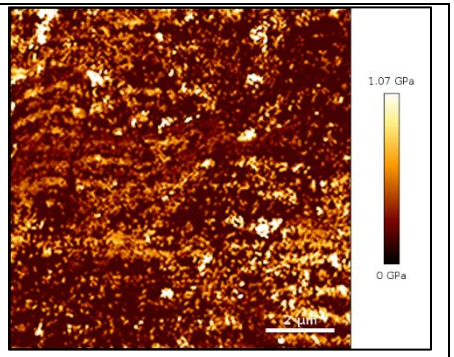
		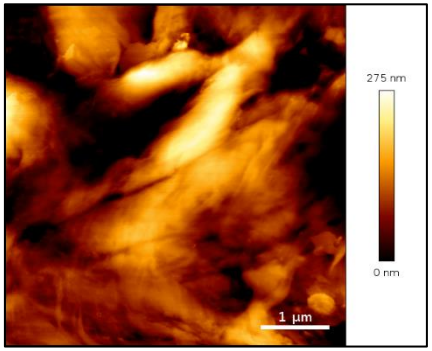	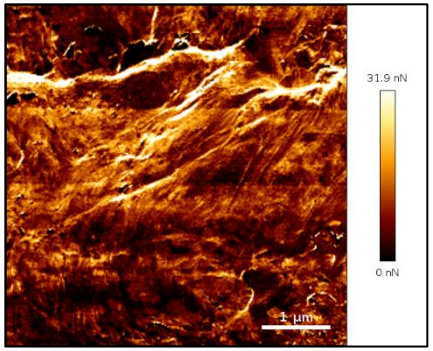	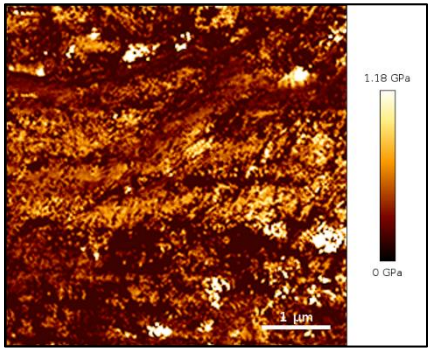
	Site 2	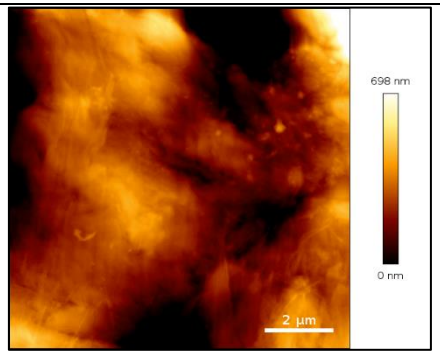	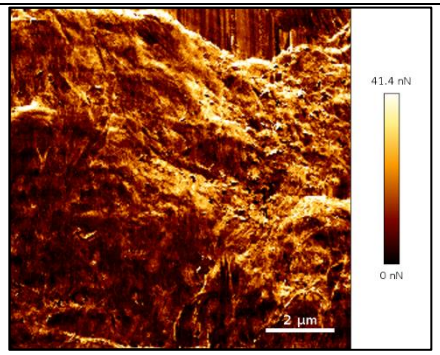	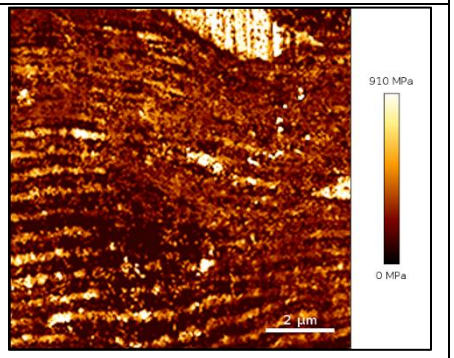

		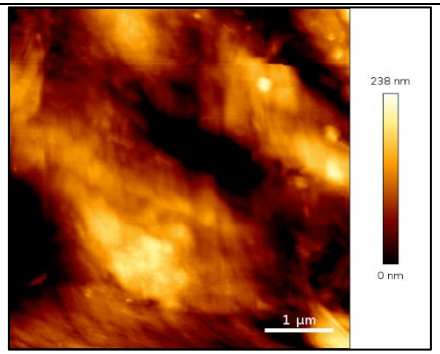	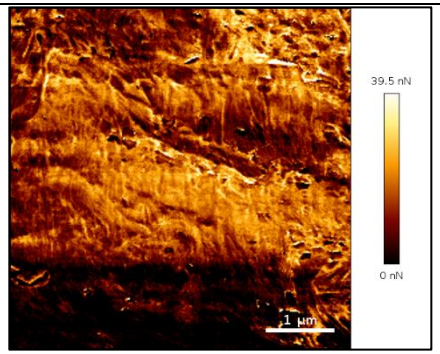	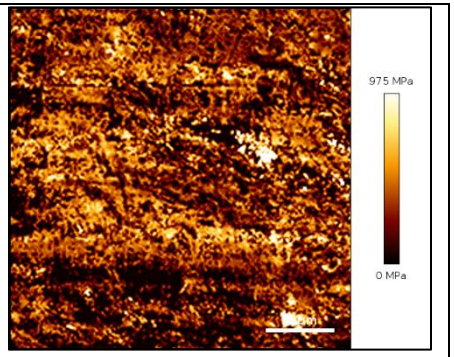
	Site 3	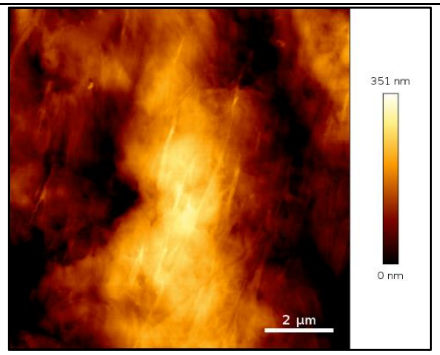 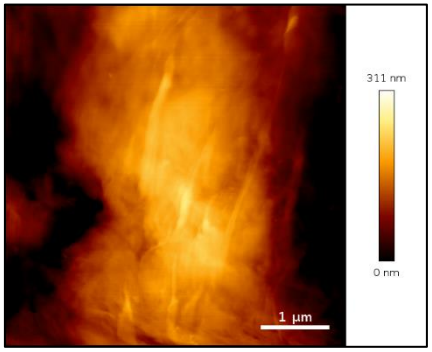	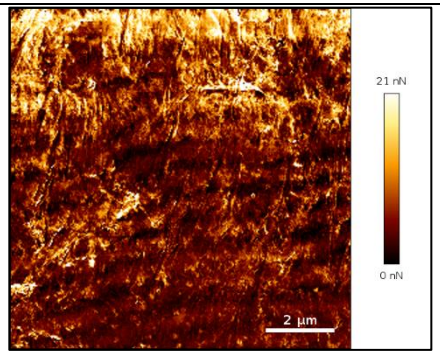 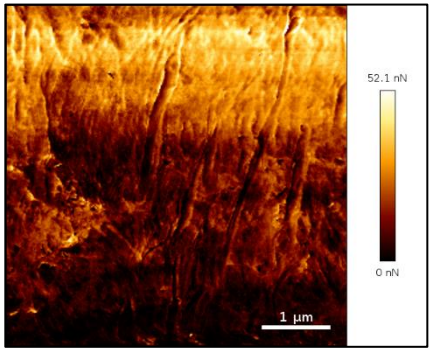	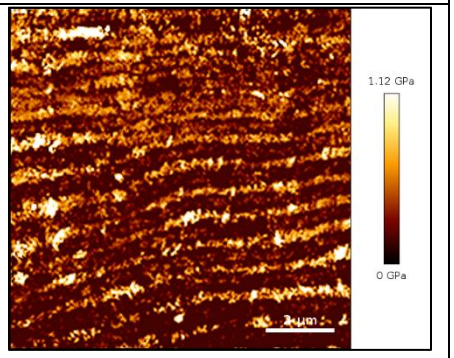 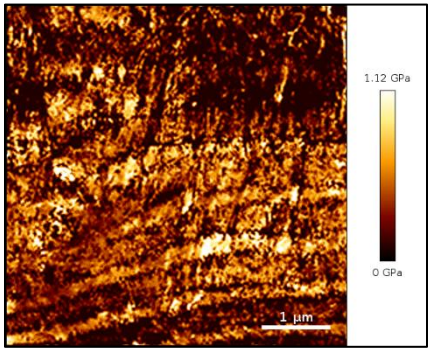

	Site 4	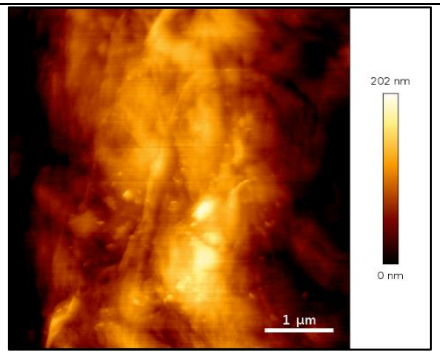	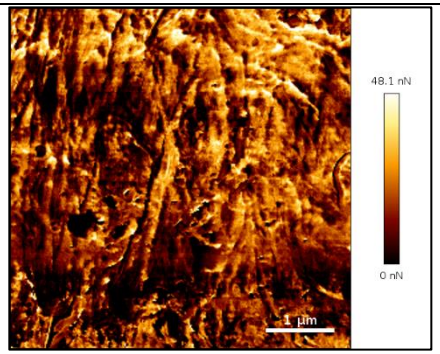	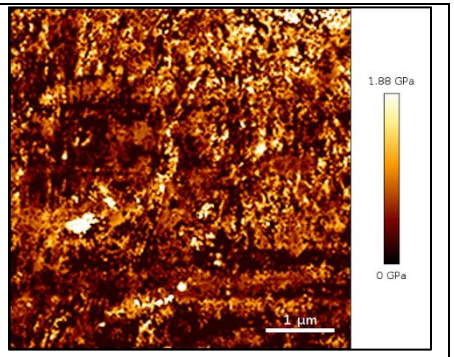
vP50	Site 1	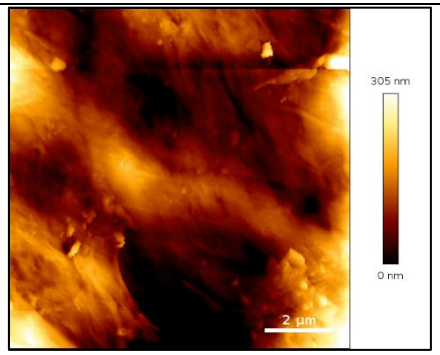 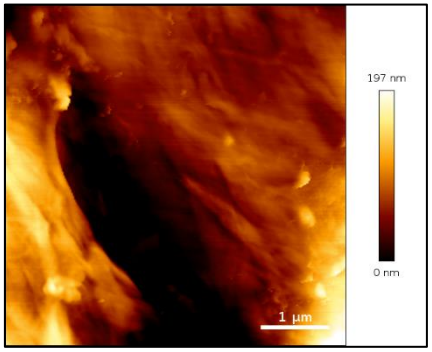	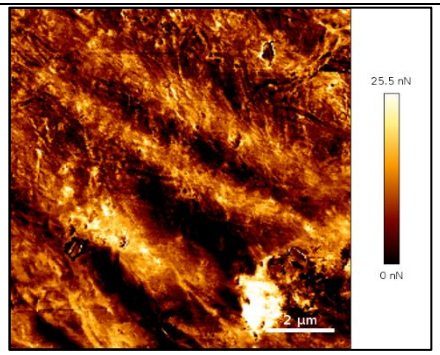 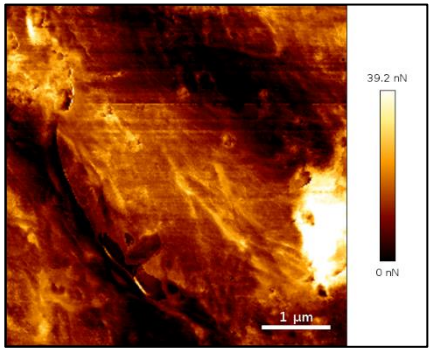	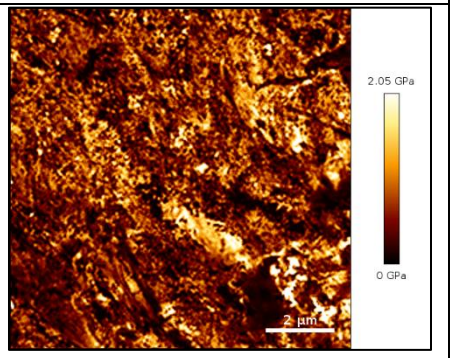 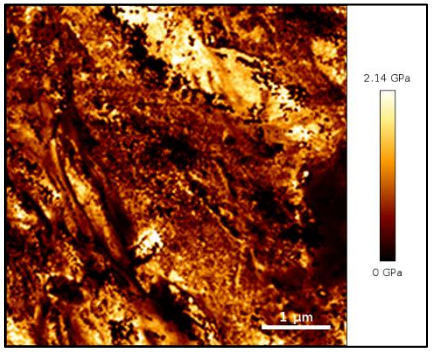

	Site 2	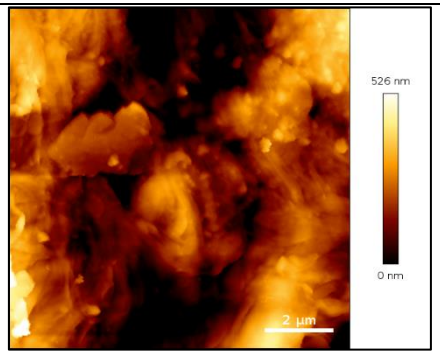 526 nm 0 nm 2 µm	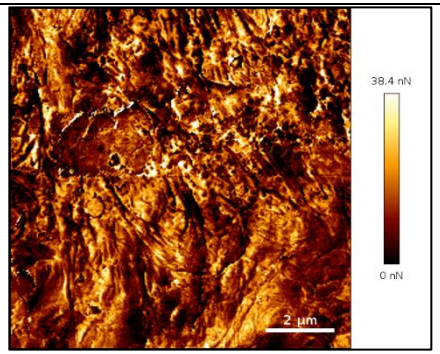 38.4 nN 0 nN 2 µm	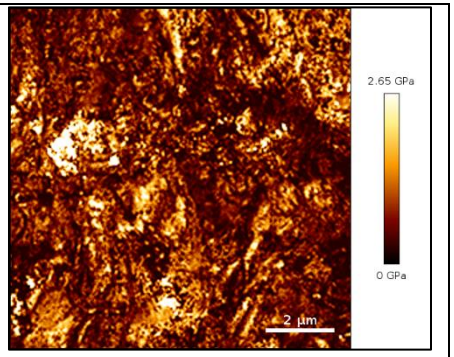 2.65 GPa 0 GPa 2 µm
		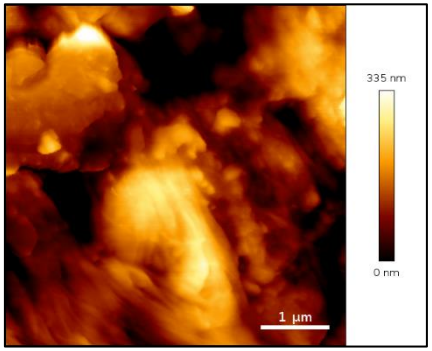 335 nm 0 nm 1 µm	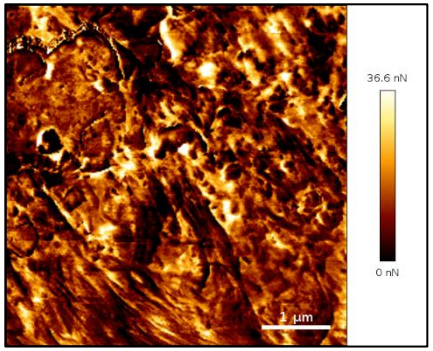 36.6 nN 0 nN 1 µm	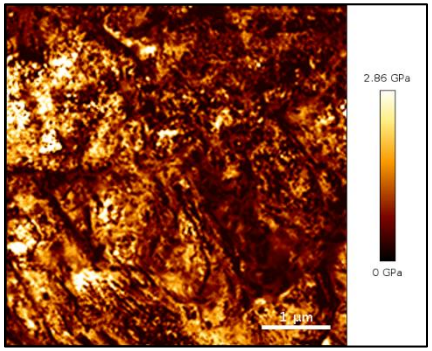 2.86 GPa 0 GPa 1 µm
	Site 3	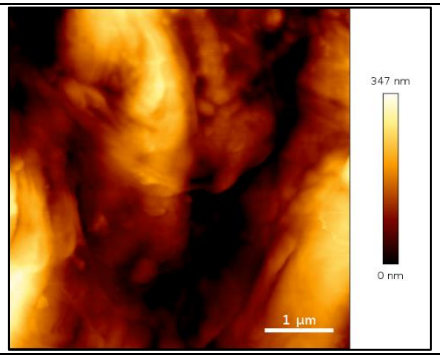 347 nm 0 nm 1 µm	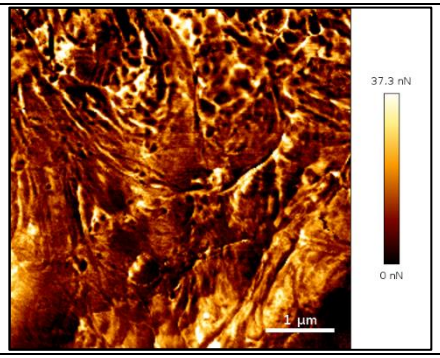 37.3 nN 0 nN 1 µm	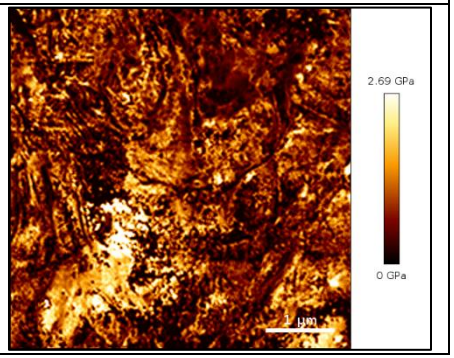 2.69 GPa 0 GPa 1 µm

	Site 4	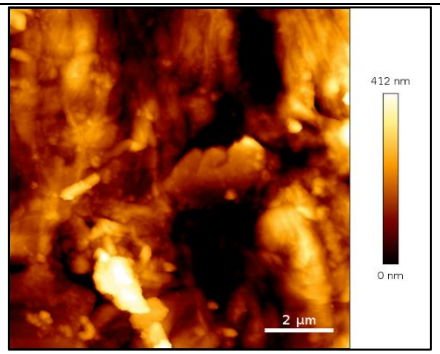	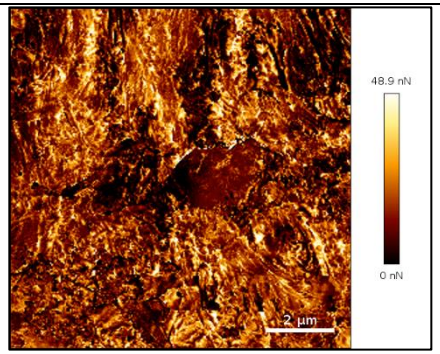	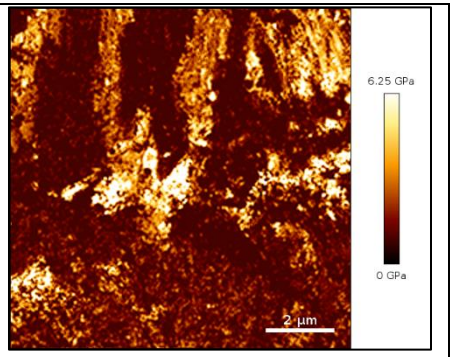
		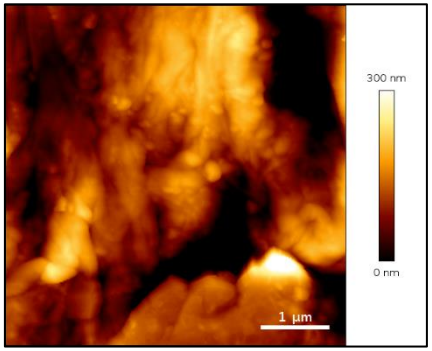	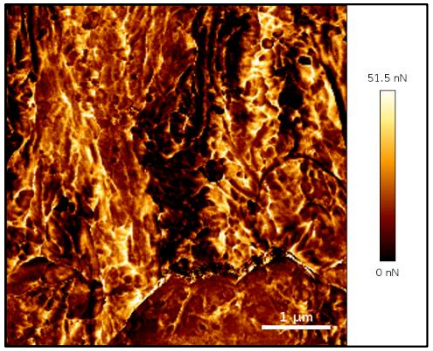	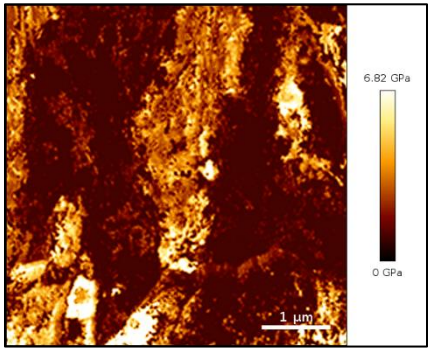
vP60	Site 1	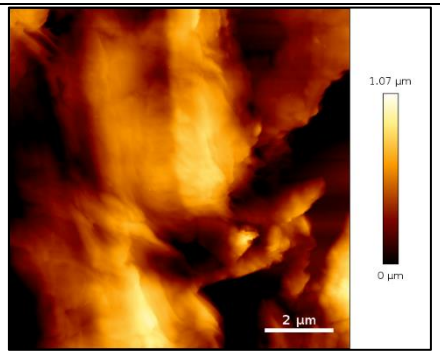	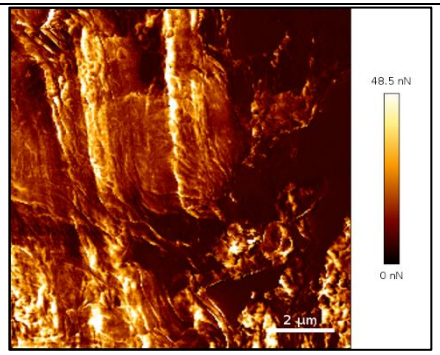	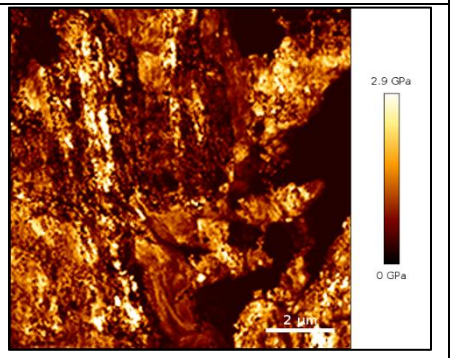

		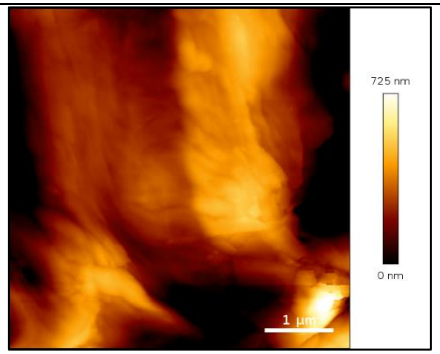 725 nm 0 nm 1 µm	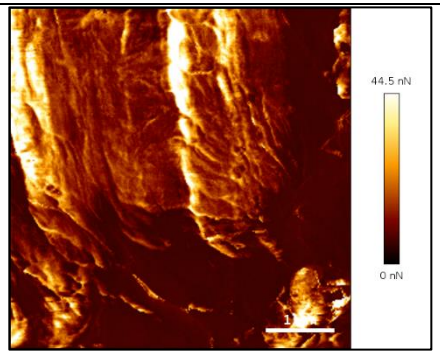 44.5 nN 0 nN	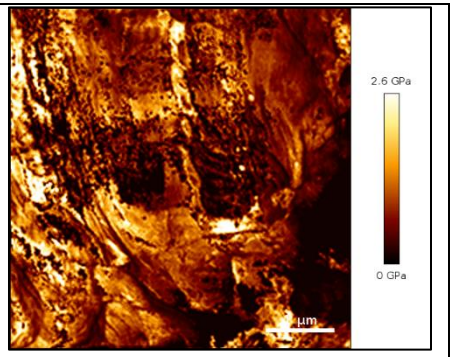 2.6 GPa 0 GPa
	Site 2	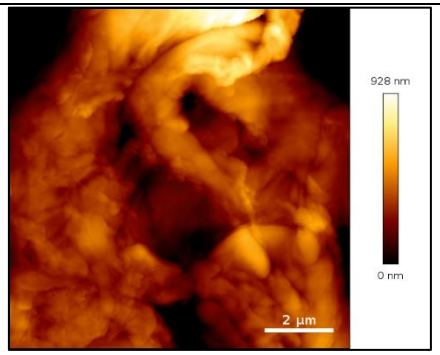 928 nm 0 nm 2 µm	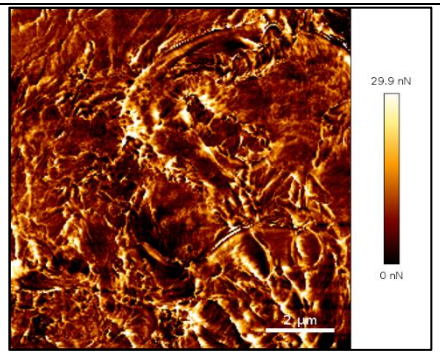 29.9 nN 0 nN 2 µm	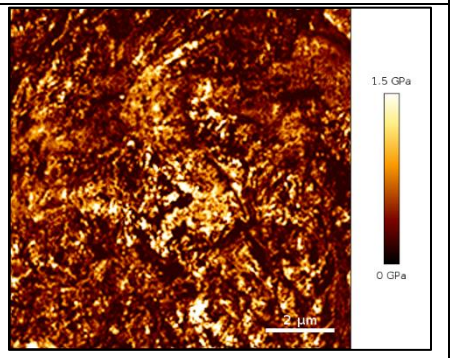 1.5 GPa 0 GPa 2 µm
		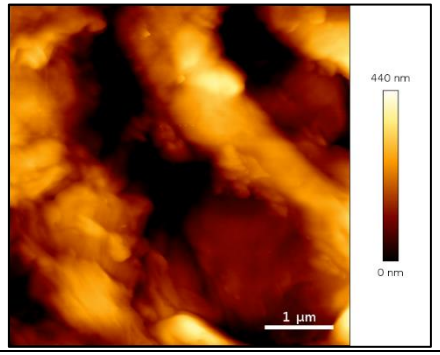 440 nm 0 nm 1 µm	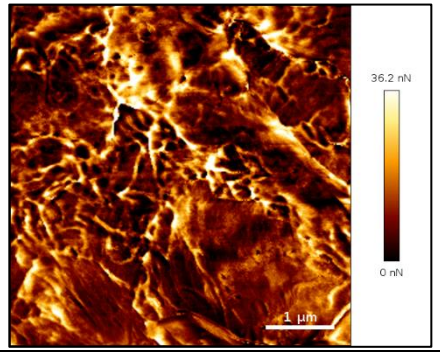 36.2 nN 0 nN 1 µm	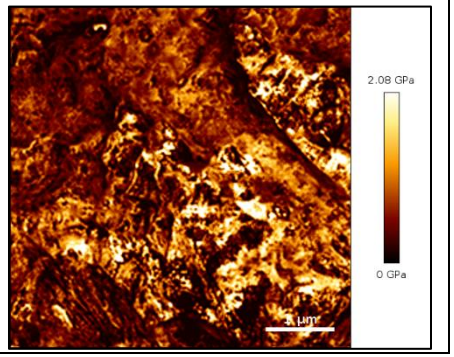 2.08 GPa 0 GPa 1 µm

	Site 3	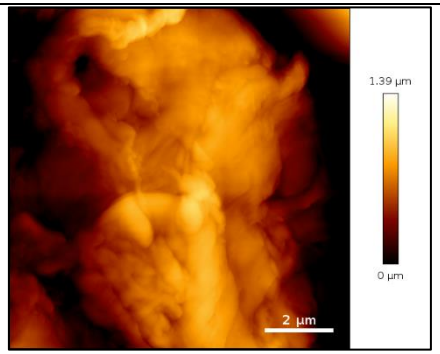 1.39 µm 0 µm 2 µm	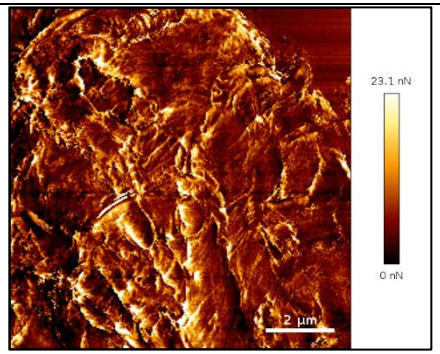 23.1 nN 0 nN 2 µm	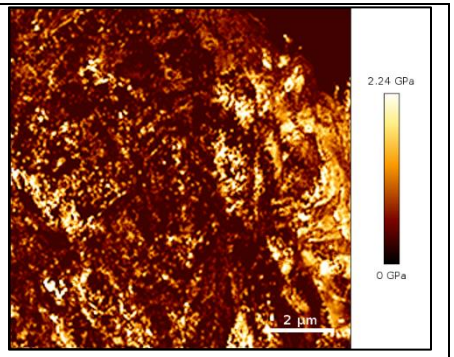 2.24 GPa 0 GPa 2 µm
		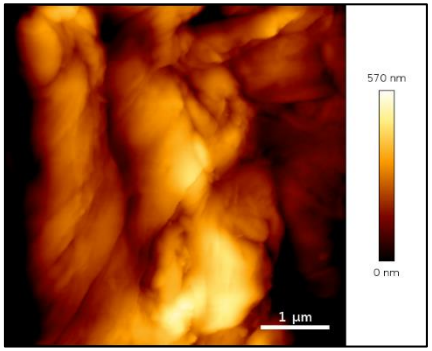 570 nm 0 nm 1 µm	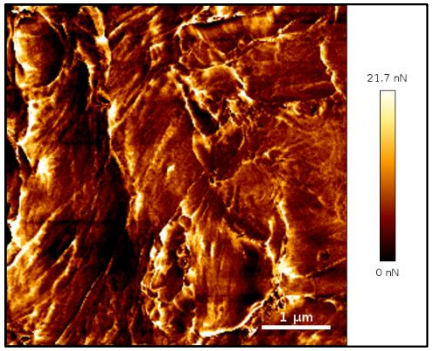 21.7 nN 0 nN 1 µm	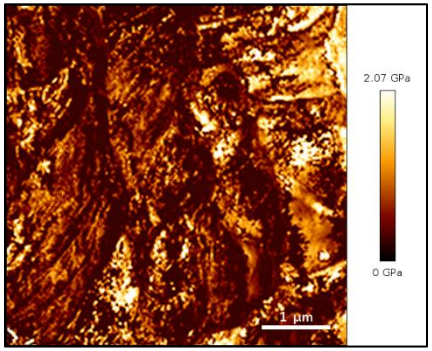 2.07 GPa 0 GPa 1 µm
	Site 4	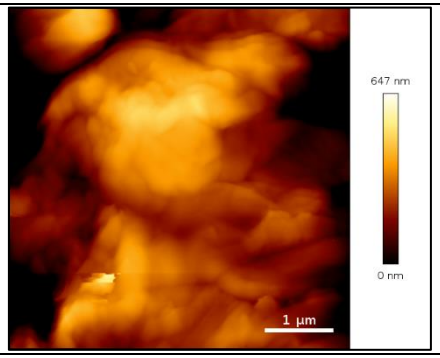 647 nm 0 nm 1 µm	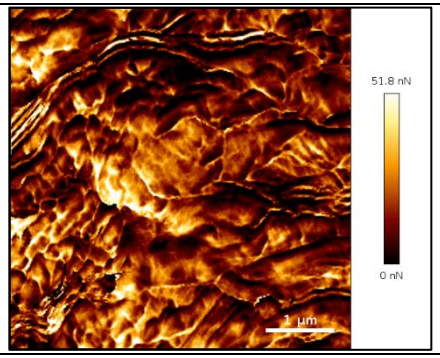 51.8 nN 0 nN 1 µm	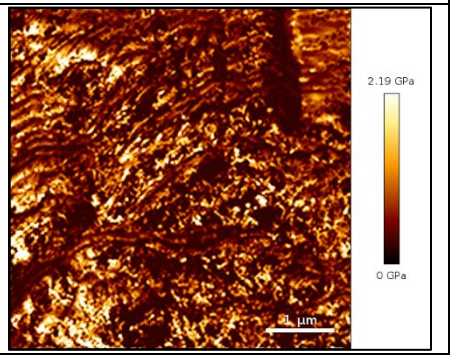 2.19 GPa 0 GPa 1 µm

Appendix 3

vP75	Site 1	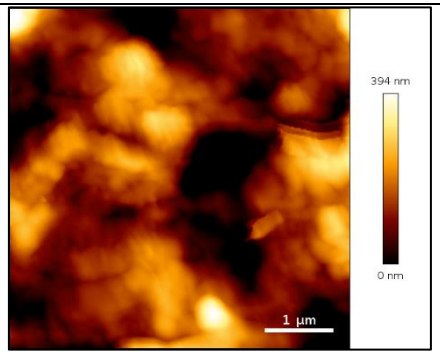	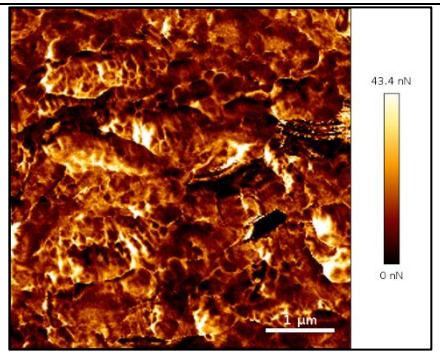	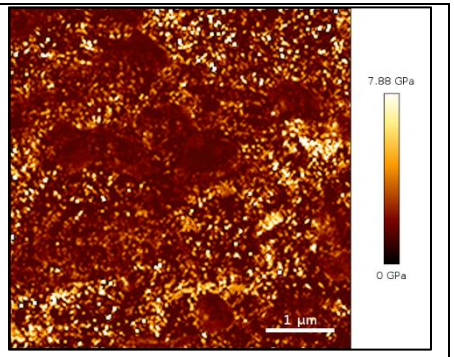
	Site 2	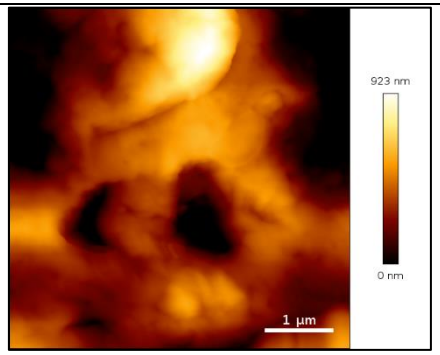	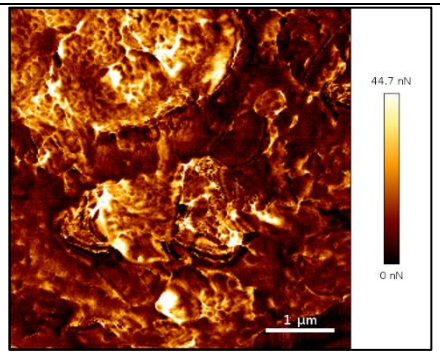	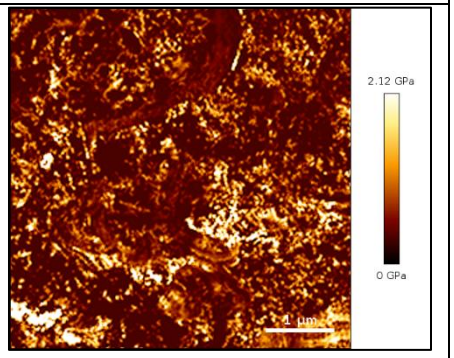
	Site 3	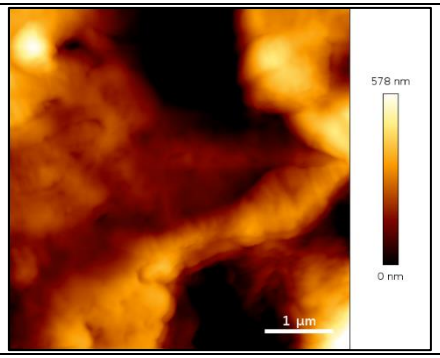	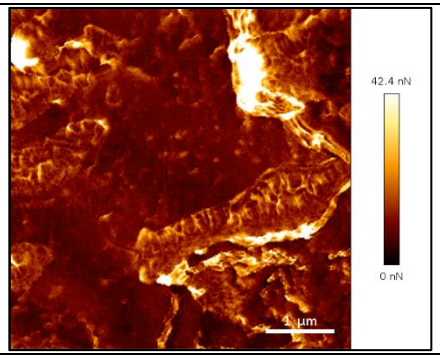	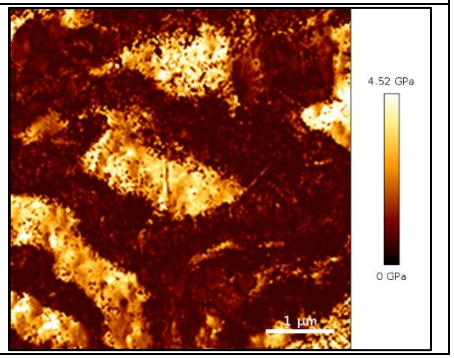

	Site 4	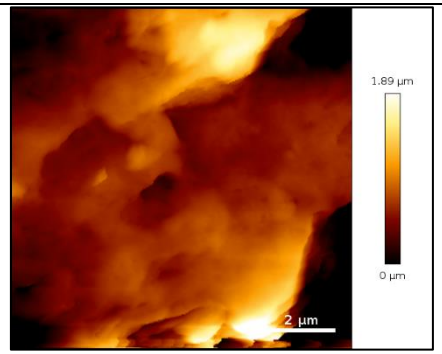	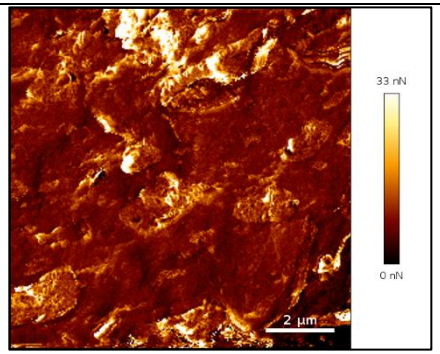	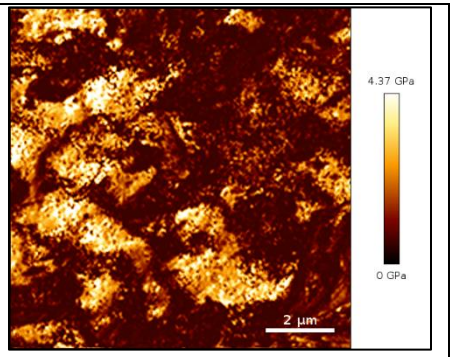
		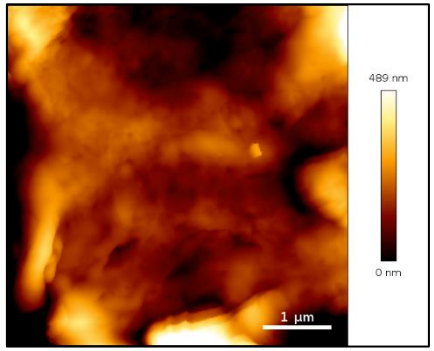	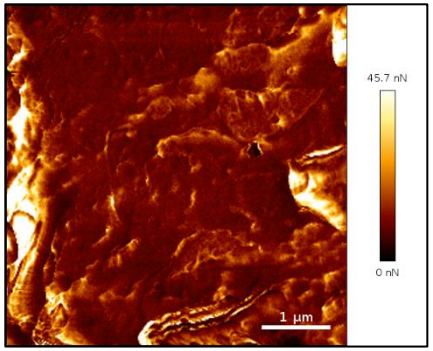	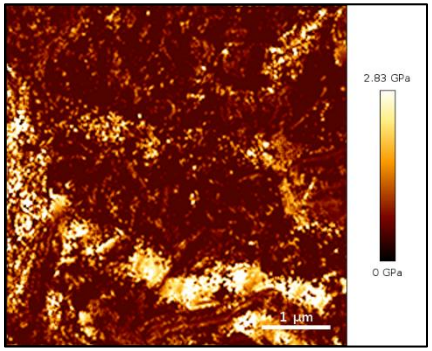
vP80	Site 1	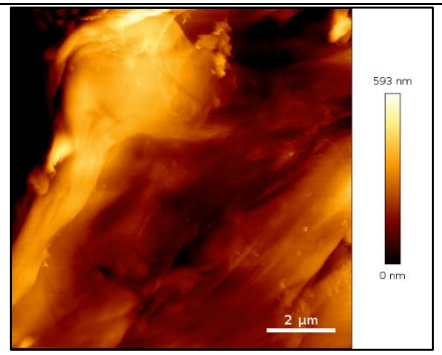	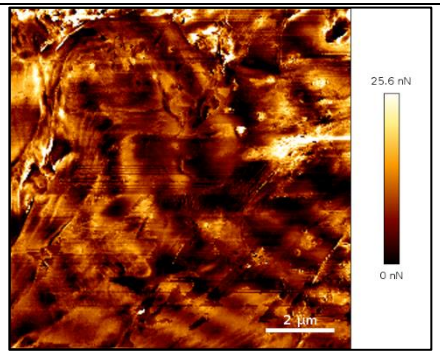	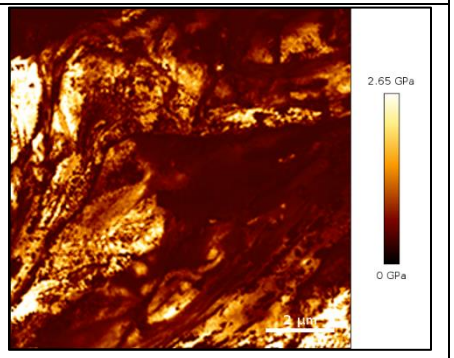

		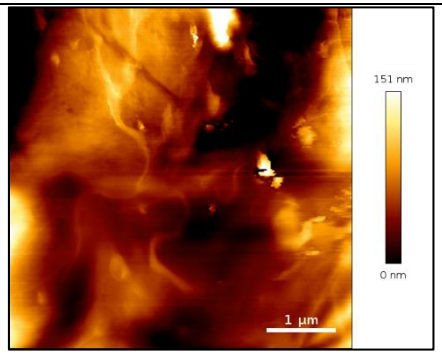 151 nm 0 nm 1 µm	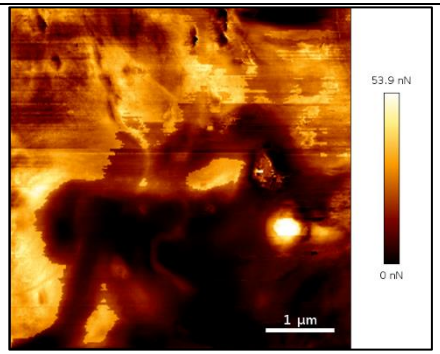 53.9 nN 0 nN 1 µm	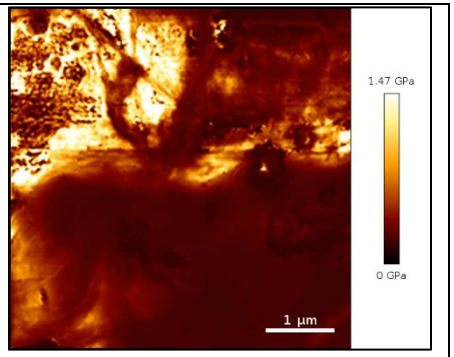 1.47 GPa 0 GPa 1 µm
	Site 2	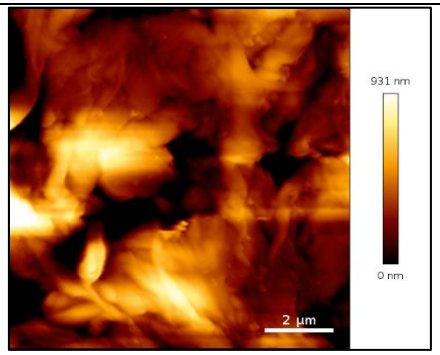 931 nm 0 nm 2 µm	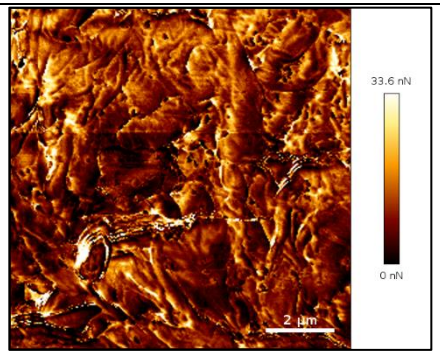 33.6 nN 0 nN 2 µm	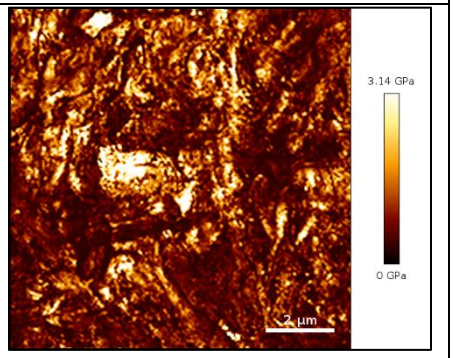 3.14 GPa 0 GPa 2 µm
		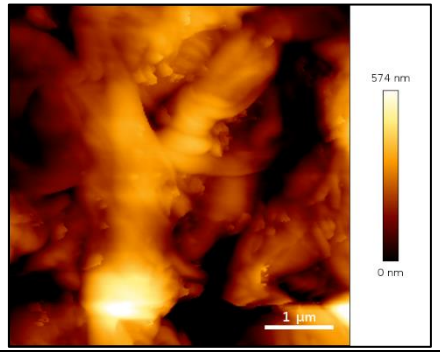 574 nm 0 nm 1 µm	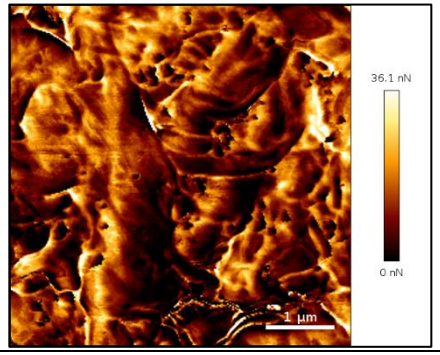 36.1 nN 0 nN 1 µm	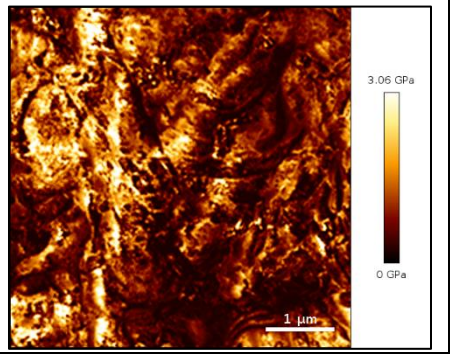 3.06 GPa 0 GPa 1 µm

	Site 3	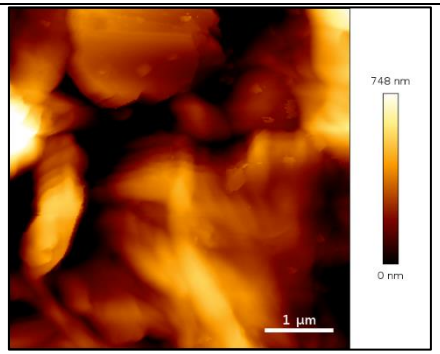	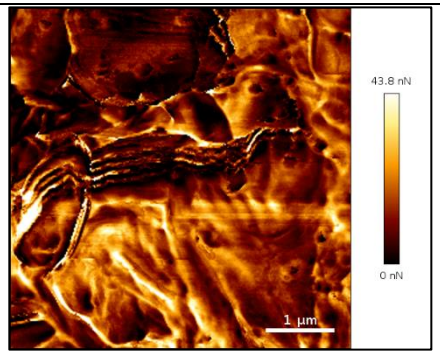	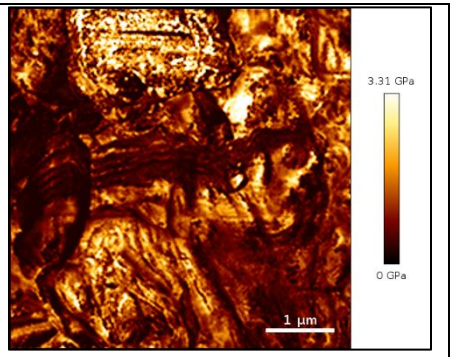
	Site 4	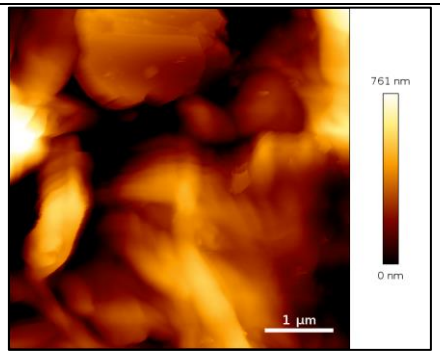	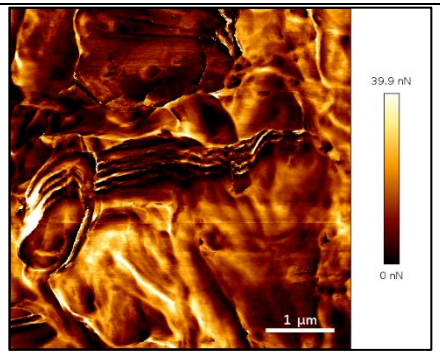	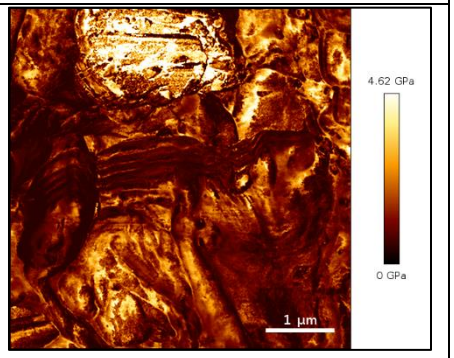
vP90	Site 1	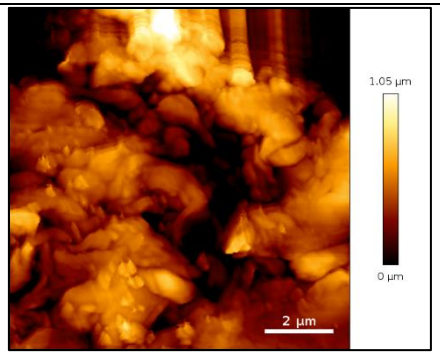	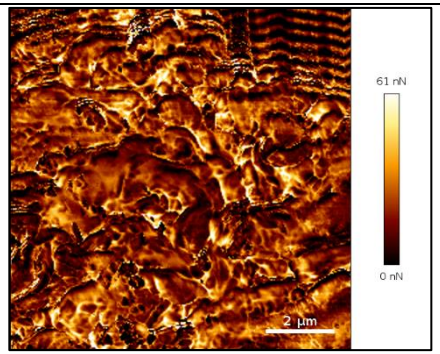	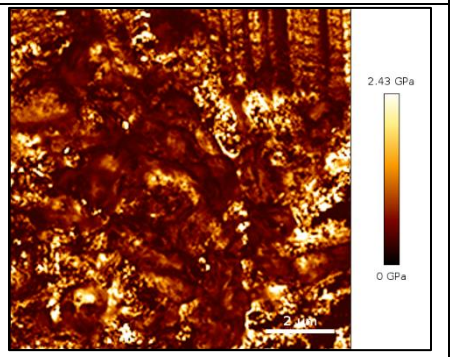

		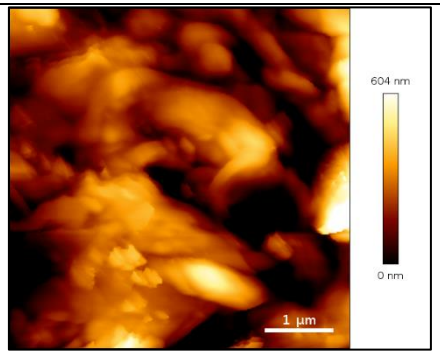 604 nm 0 nm 1 µm	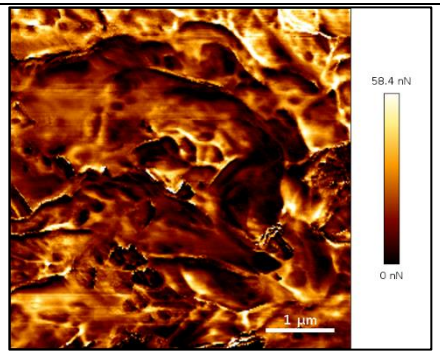 58.4 nN 0 nN 1 µm	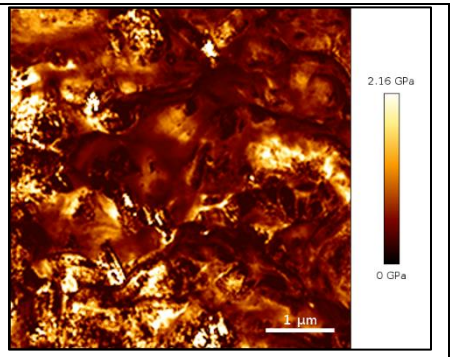 2.16 GPa 0 GPa 1 µm
	Site 2	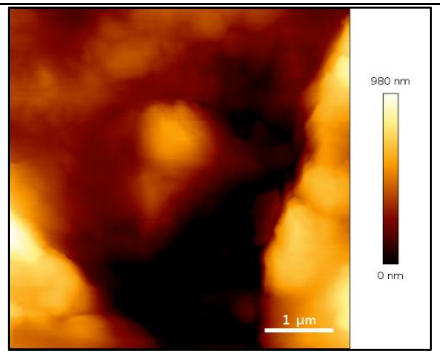 980 nm 0 nm 1 µm	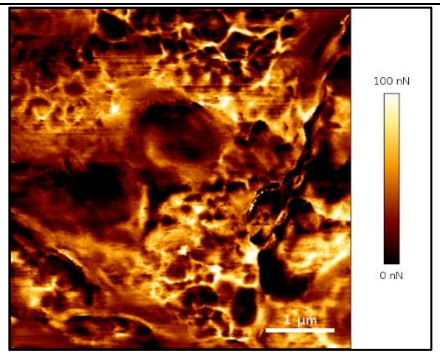 100 nN 0 nN 1 µm	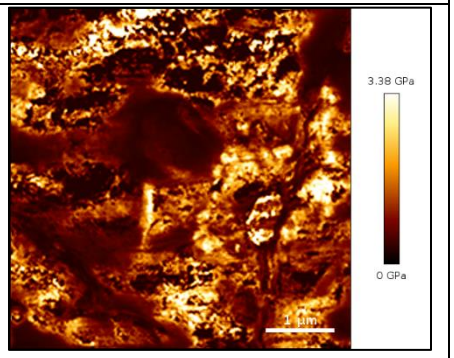 3.38 GPa 0 GPa 1 µm
	Site 3	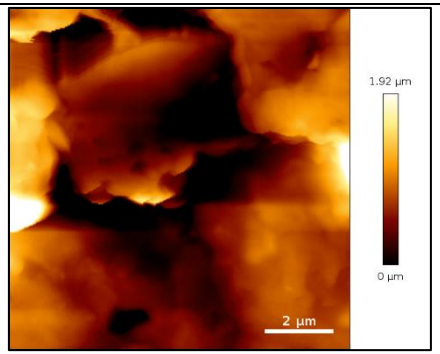 1.92 µm 0 µm 2 µm	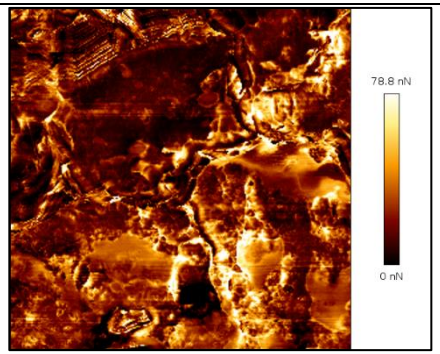 78.8 nN 0 nN	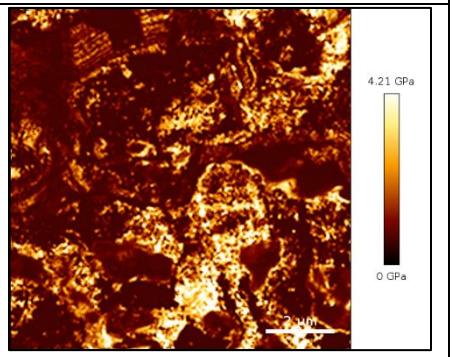 4.21 GPa 0 GPa

		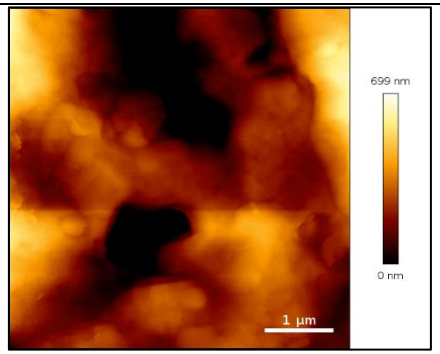 699 nm 0 nm 1 µm	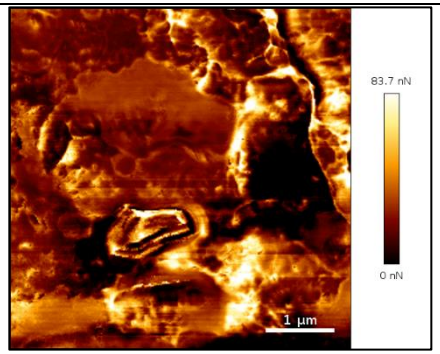 83.7 nN 0 nN 1 µm	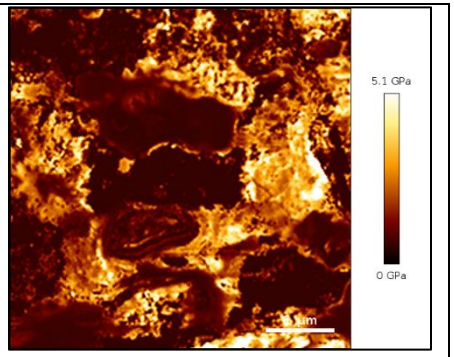 5.1 GPa 0 GPa
	Site 4	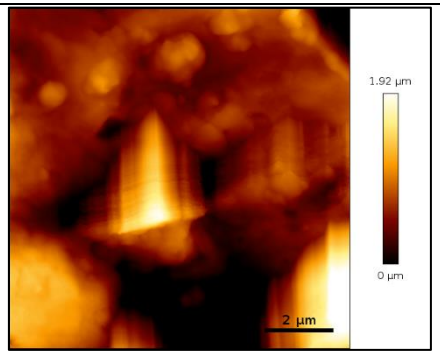 1.92 µm 0 µm 2 µm	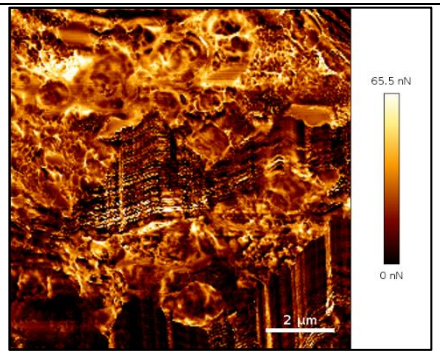 65.5 nN 0 nN 2 µm	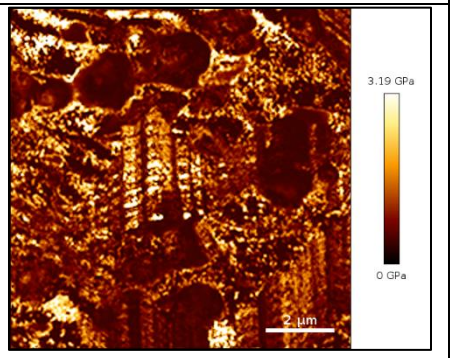 3.19 GPa 0 GPa 2 µm
		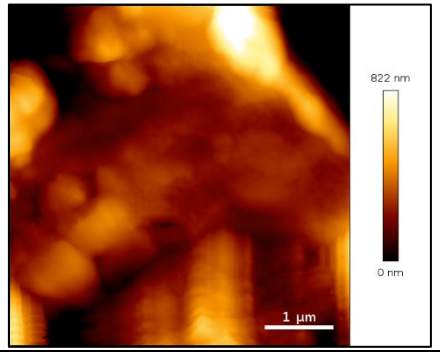 822 nm 0 nm 1 µm	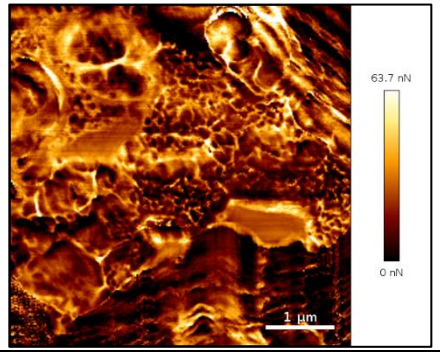 63.7 nN 0 nN 1 µm	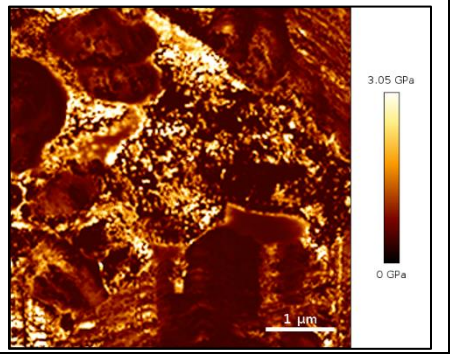 3.05 GPa 0 GPa 1 µm

Appendix 3

vPP	Site 1	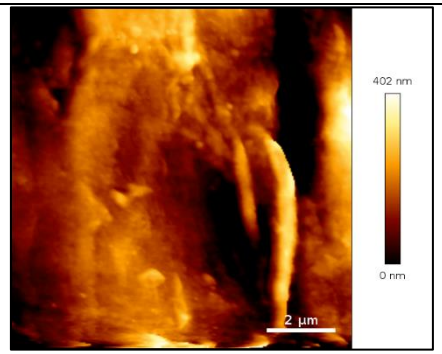	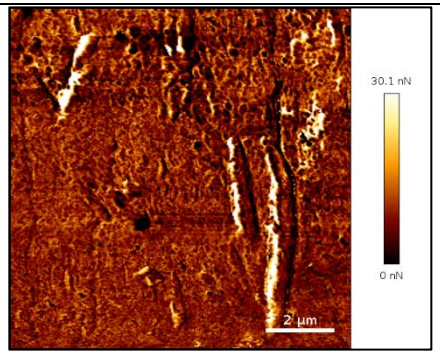	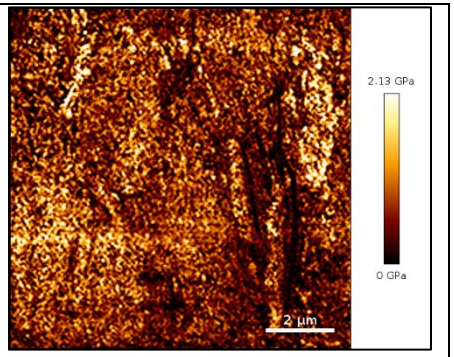
	Site 2	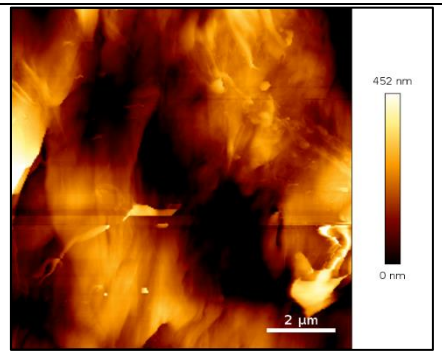 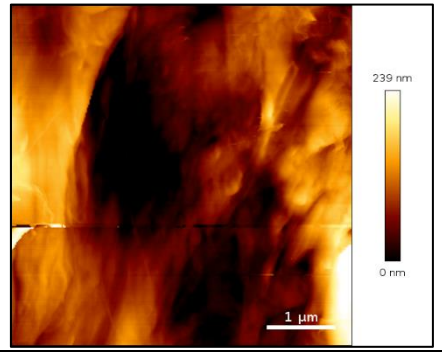	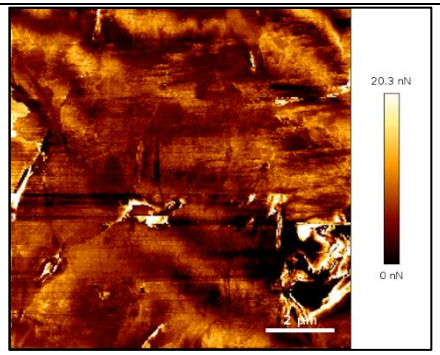 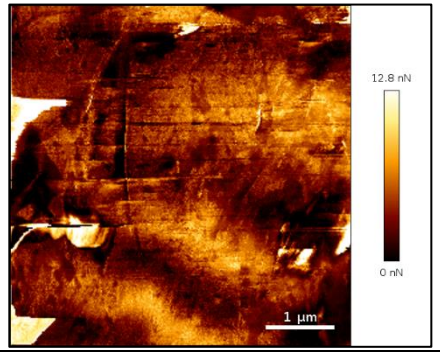	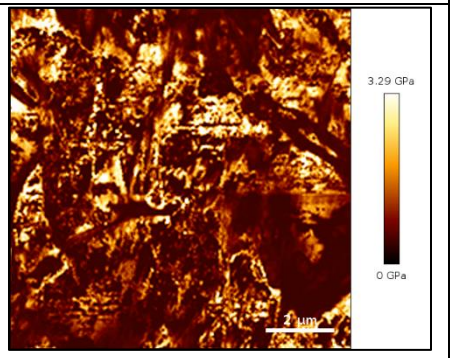 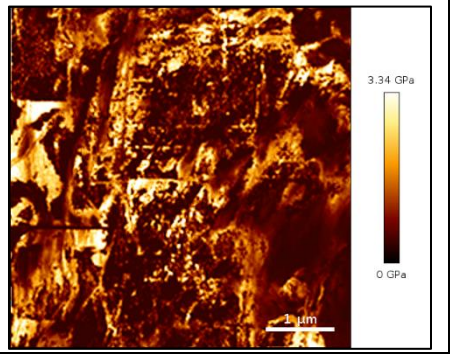

	Site 3	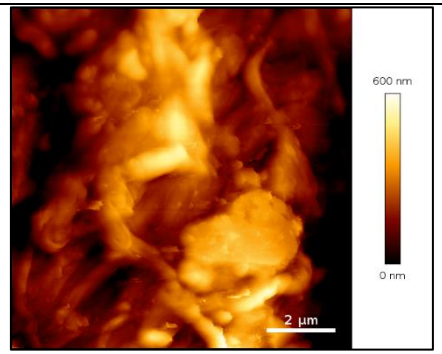 600 nm 0 nm 2 µm	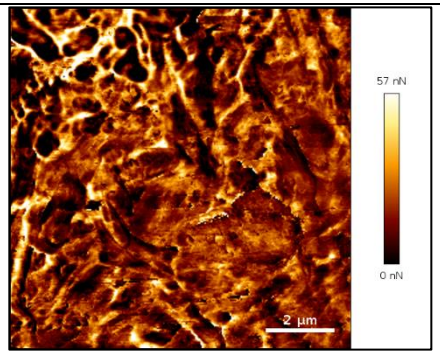 57 nN 0 nN 2 µm	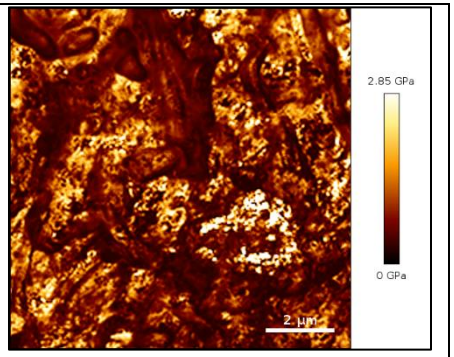 2.85 GPa 0 GPa 2 µm
		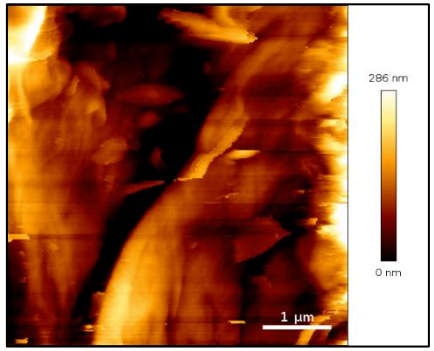 286 nm 0 nm 1 µm	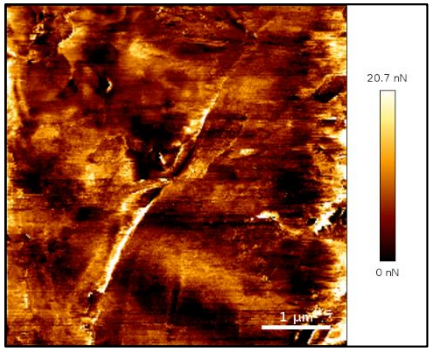 20.7 nN 0 nN 1 µm	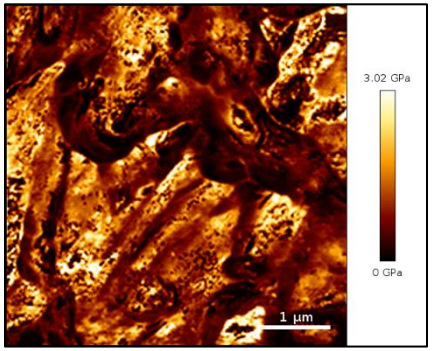 3.02 GPa 0 GPa 1 µm
	Site 4	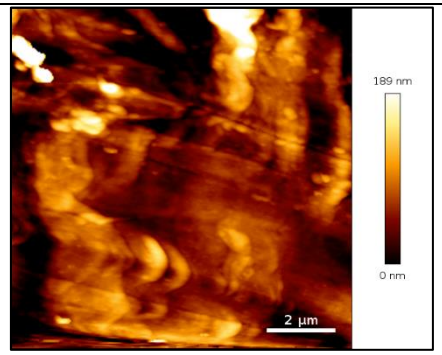 189 nm 0 nm 2 µm	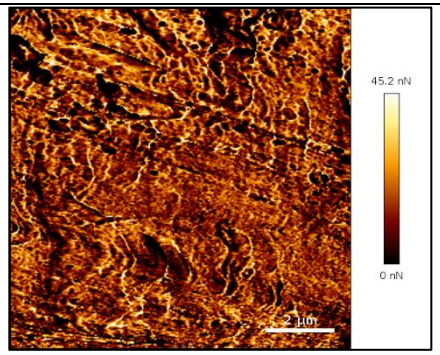 45.2 nN 0 nN 2 µm	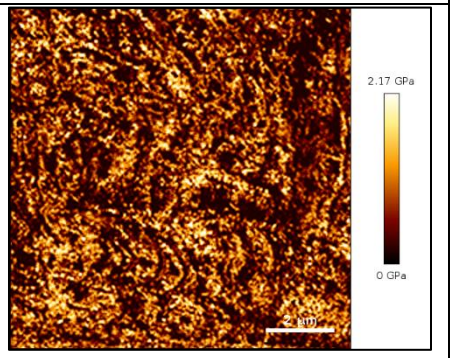 2.17 GPa 0 GPa 2 µm

Appendix 4 AFM QI mode height, adhesion and Young's modulus images obtained at 256 x 256 pixels for rPP:rHDPE blends.

PP:HDPE Blend		Height, nm	Adhesion, nN	Young's modulus, GPa
rHDPE	Site 1	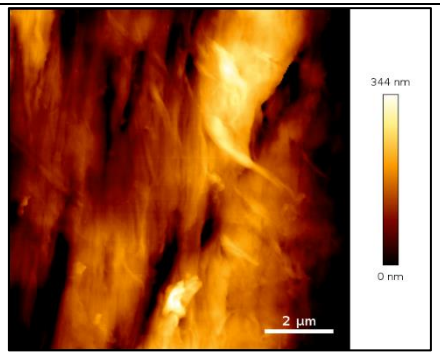	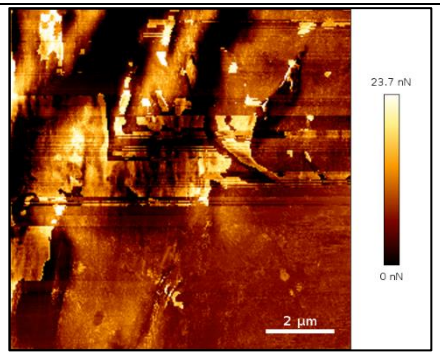	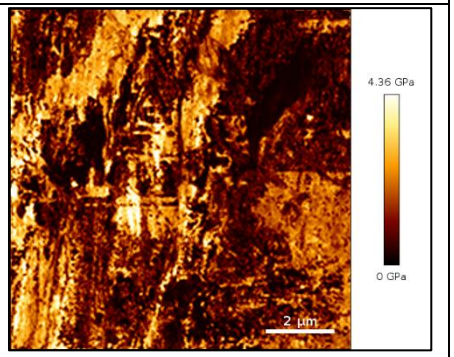
		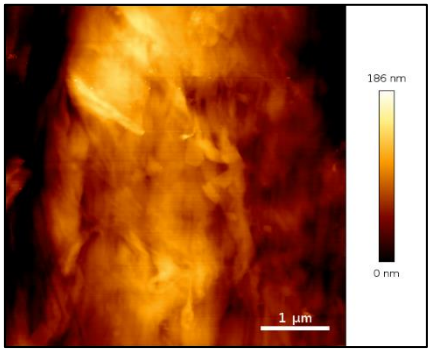	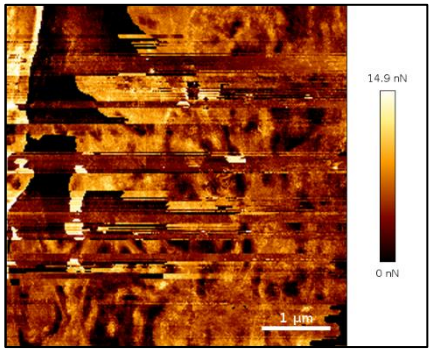	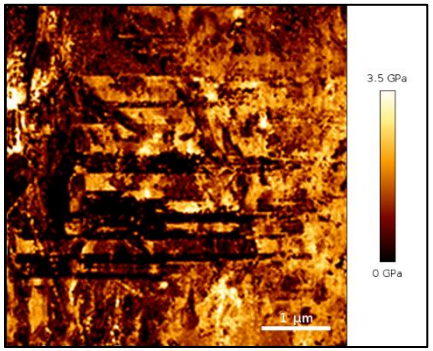
	Site 2	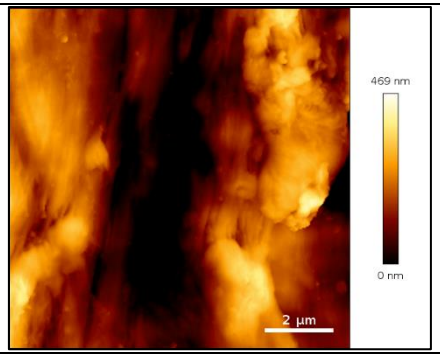	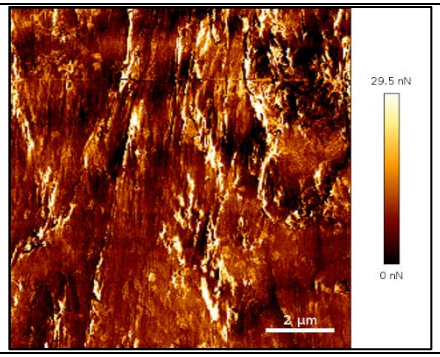	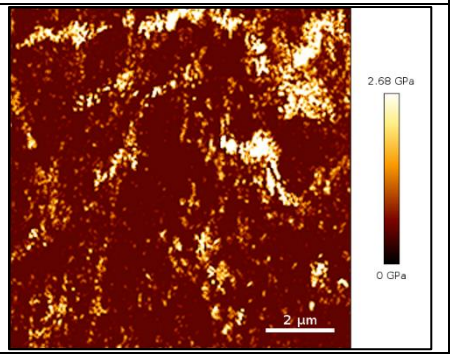

		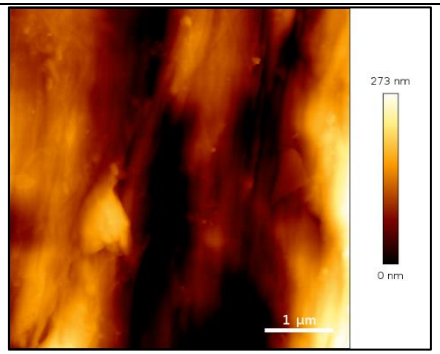	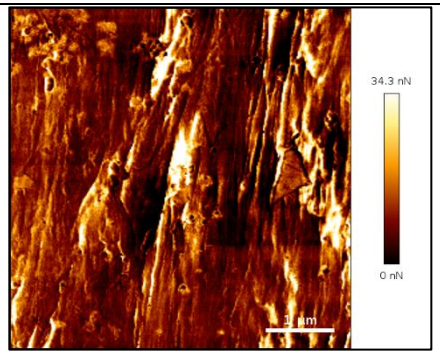	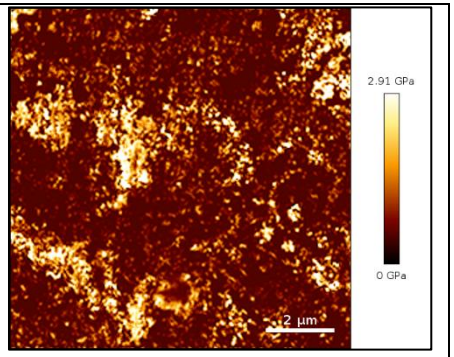
	Site 3	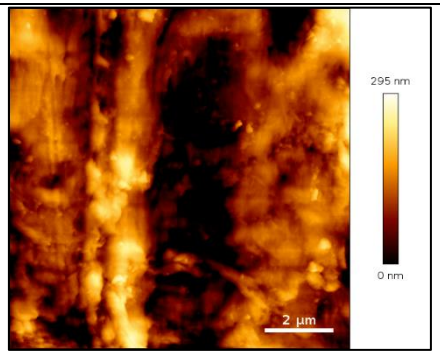 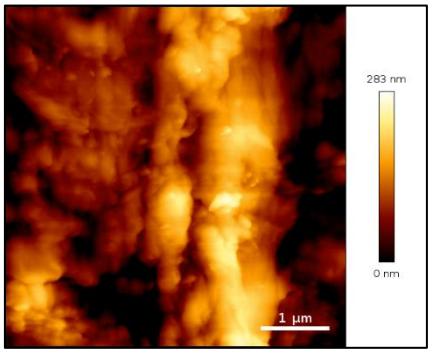	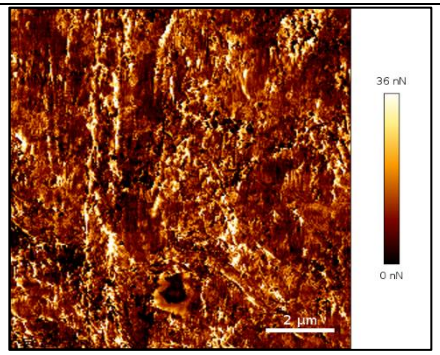 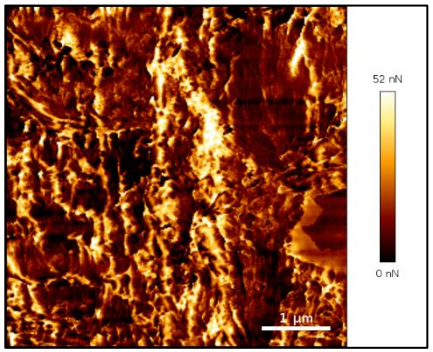	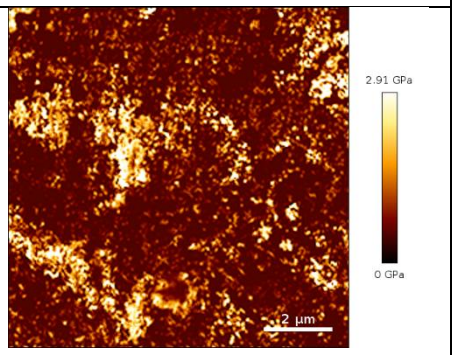 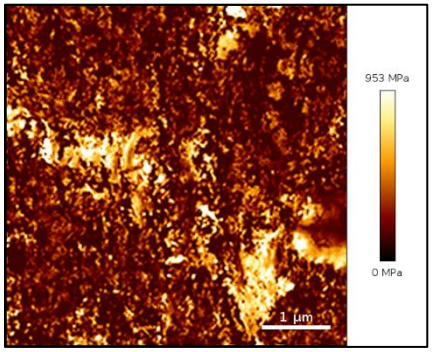

	Site 4	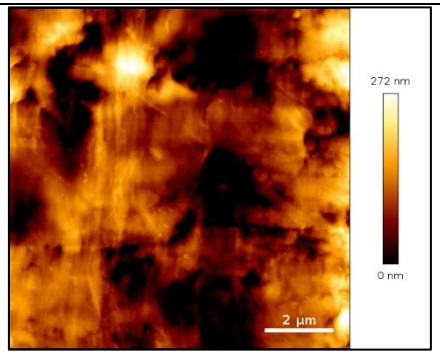	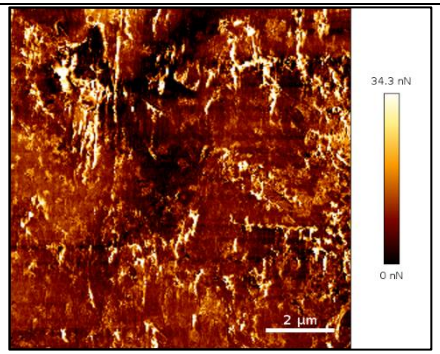	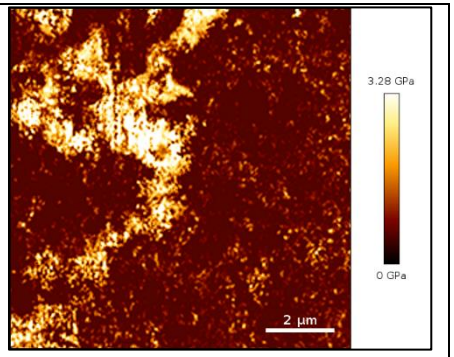
		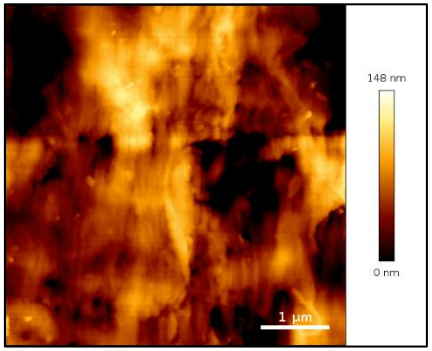	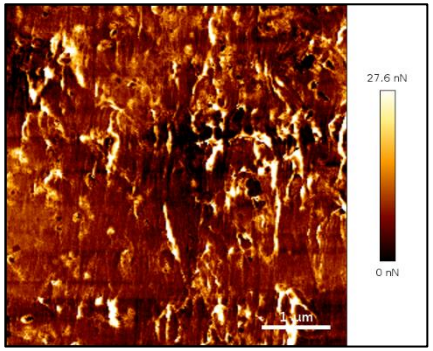	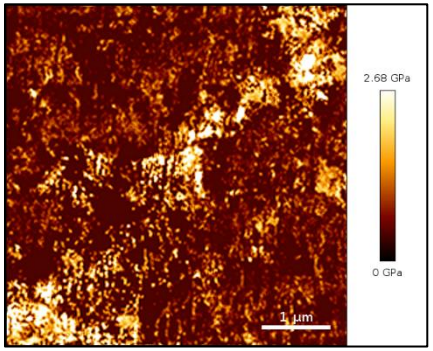
rP10	Site 1	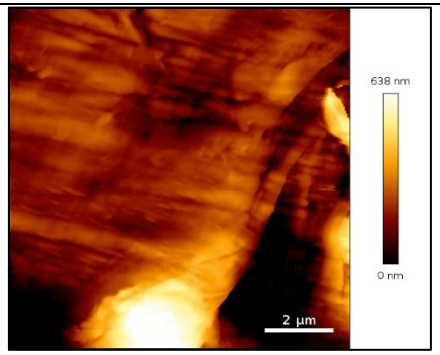	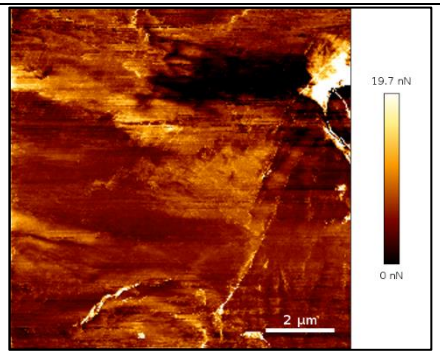	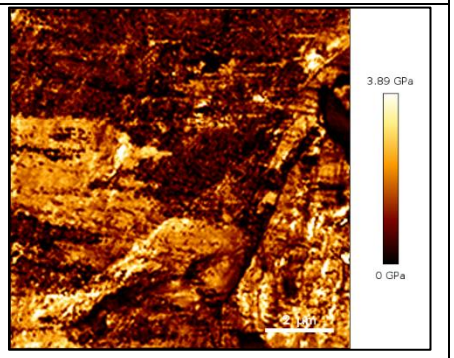

		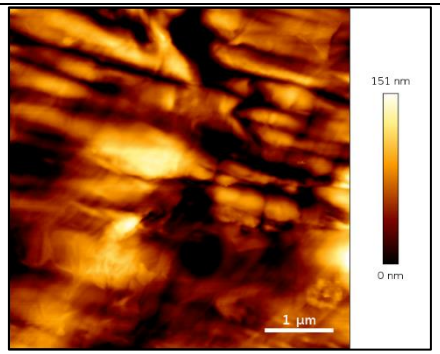 151 nm 0 nm 1 µm	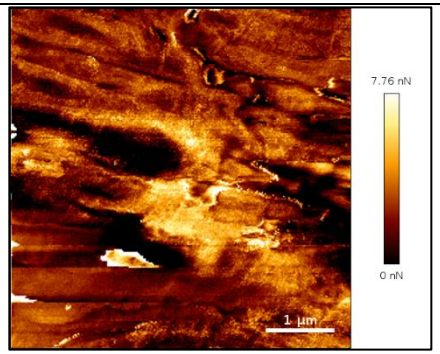 7.76 nN 0 nN 1 µm	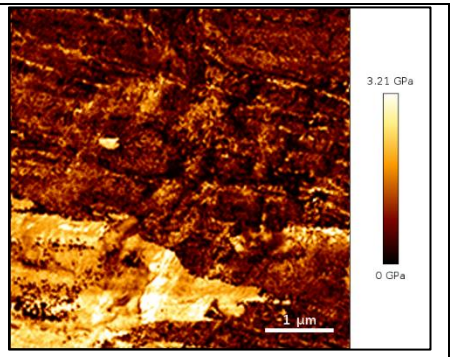 3.21 GPa 0 GPa 1 µm
	Site 2	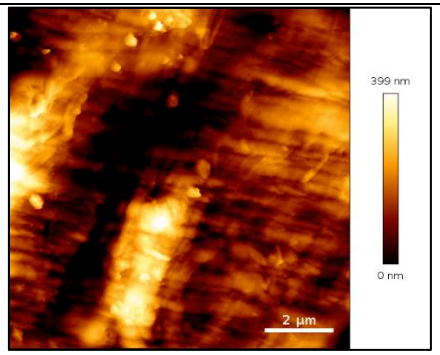 399 nm 0 nm 2 µm	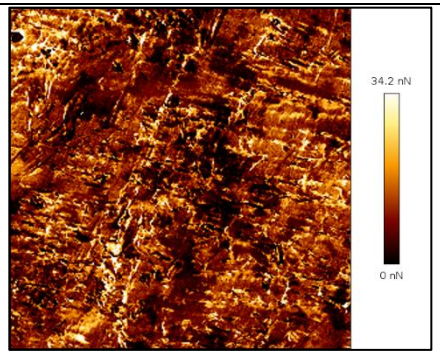 34.2 nN 0 nN	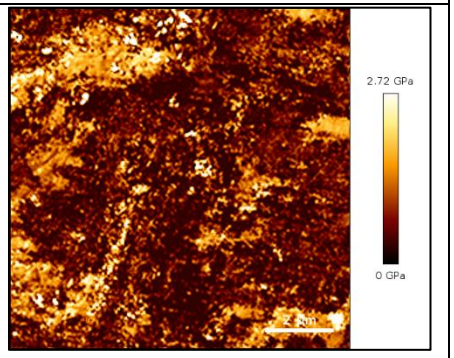 2.72 GPa 0 GPa
		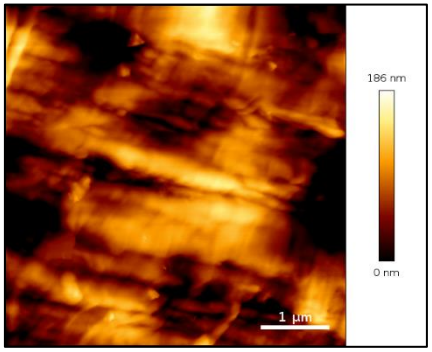 186 nm 0 nm 1 µm	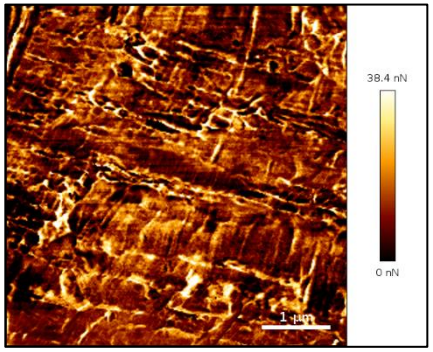 38.4 nN 0 nN 1 µm	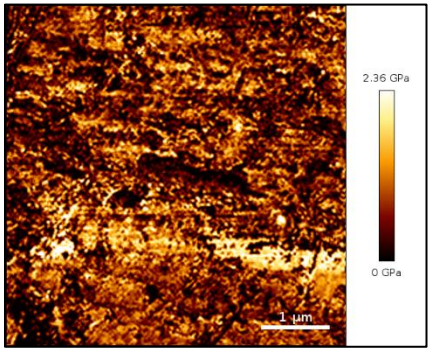 2.36 GPa 0 GPa 1 µm

	Site 3	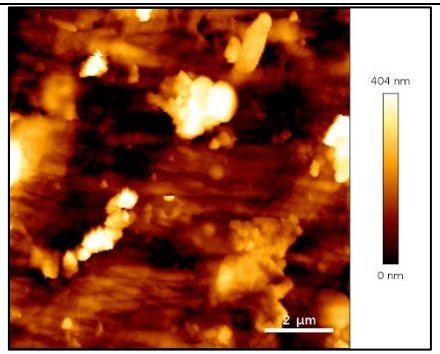	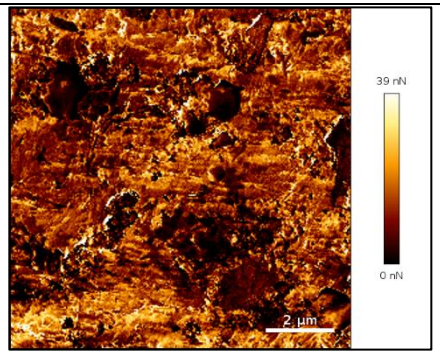	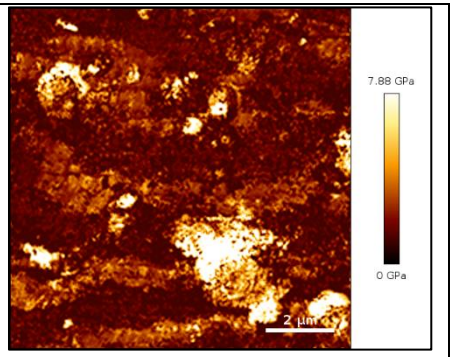
	Site 4	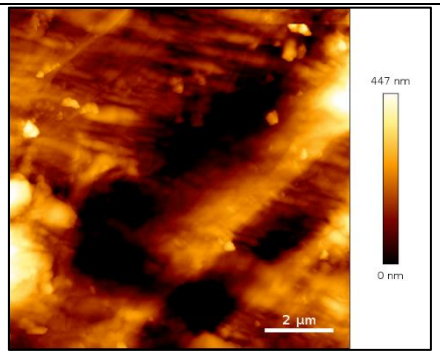 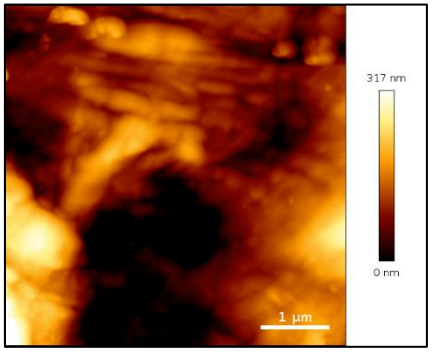	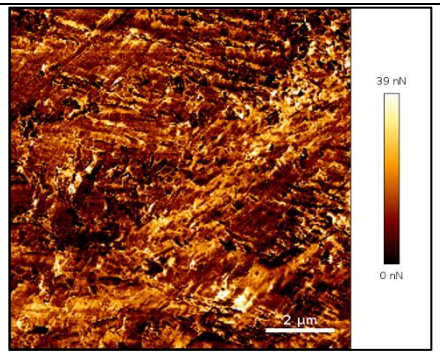 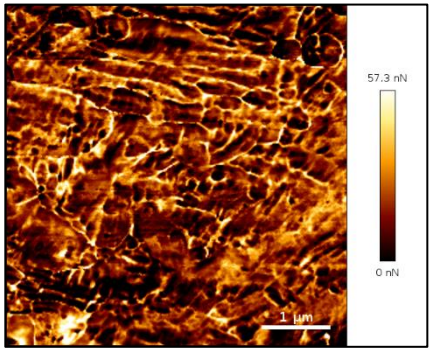	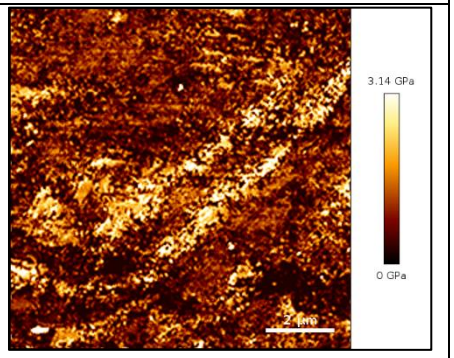 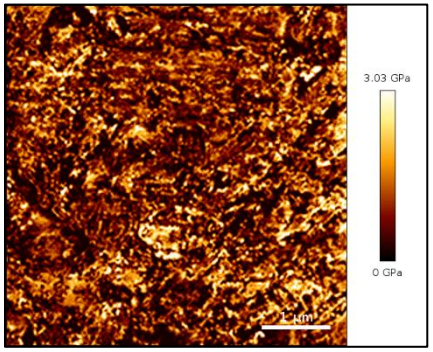

Appendix 4

rP20	Site 1	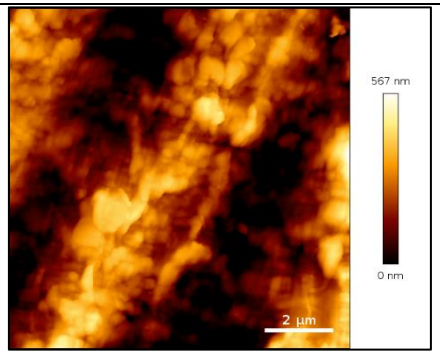	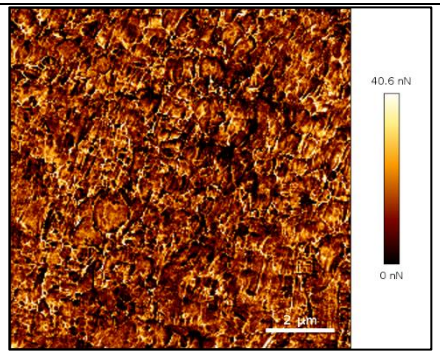	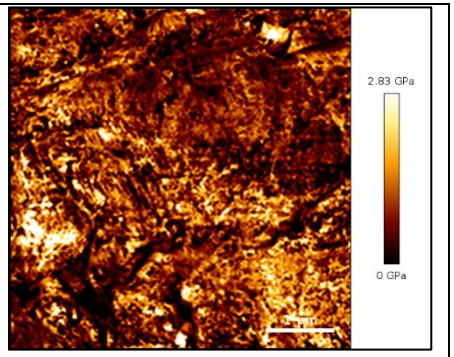
		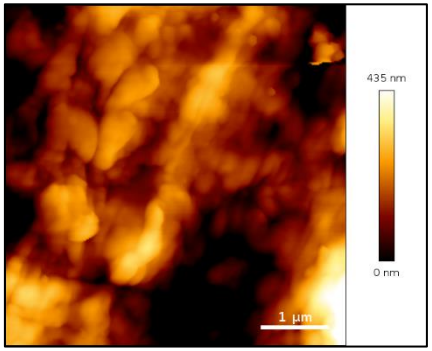	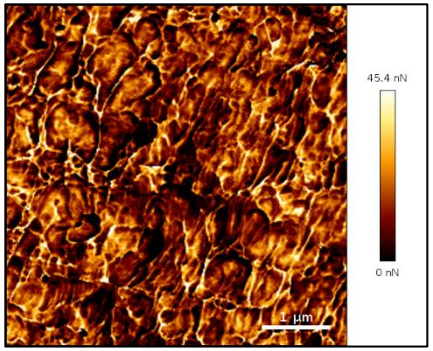	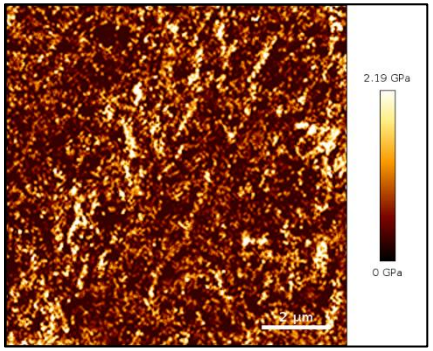
	Site 2	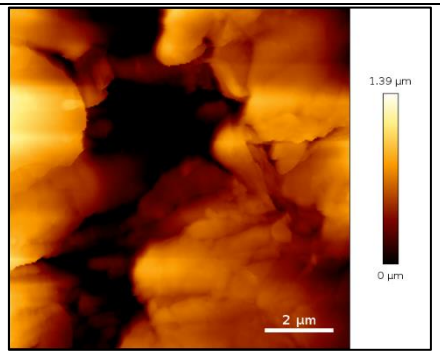	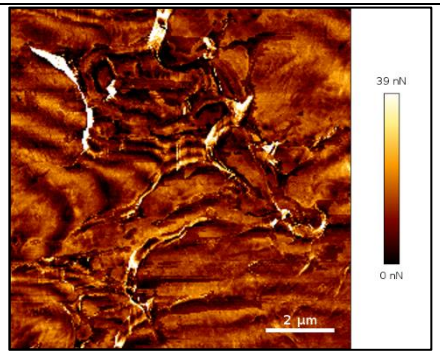	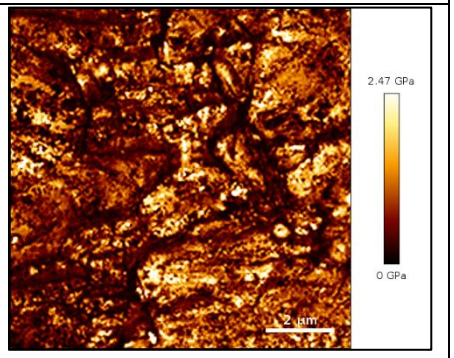

		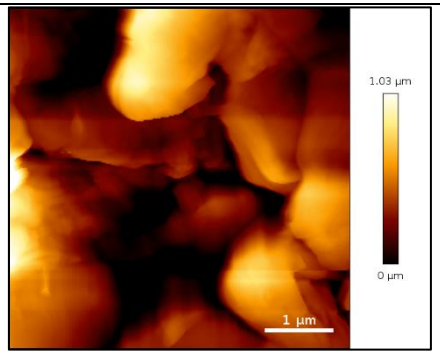	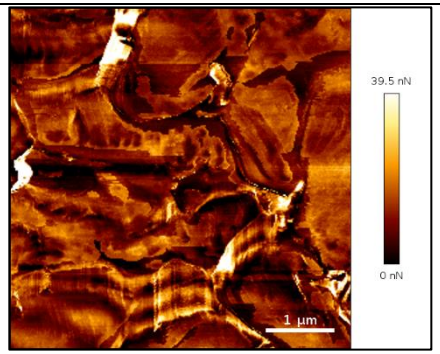	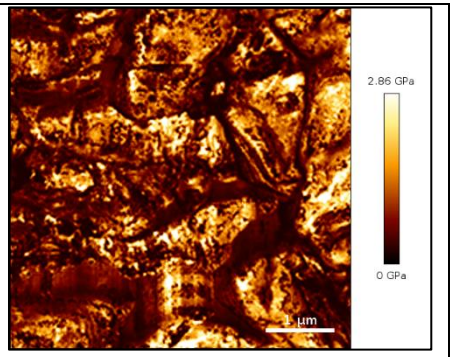
	Site 3	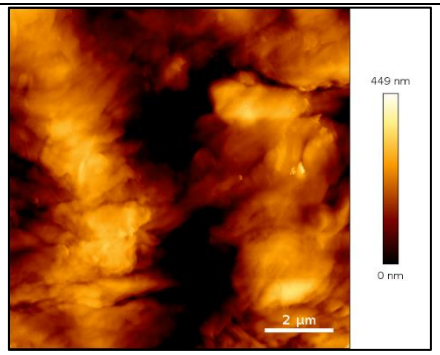 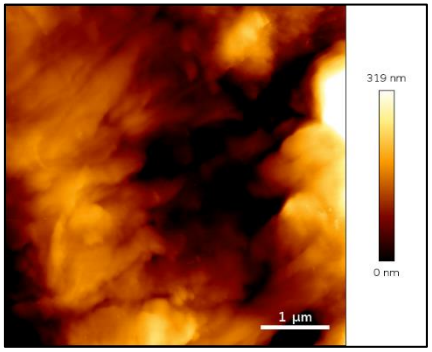	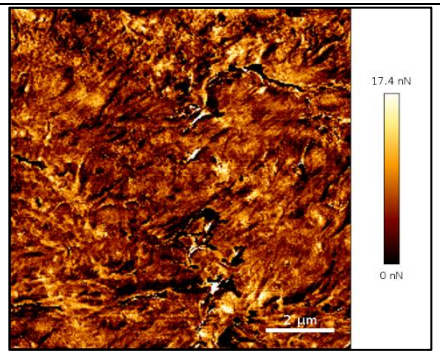 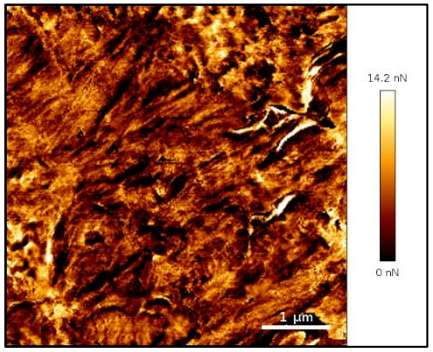	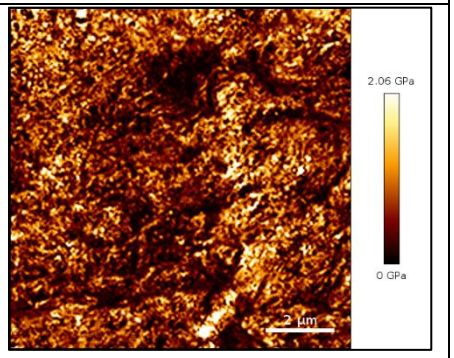 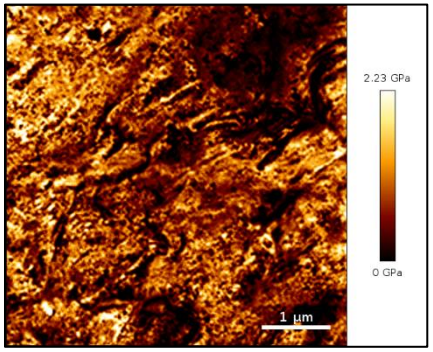

Appendix 4

	Site 4	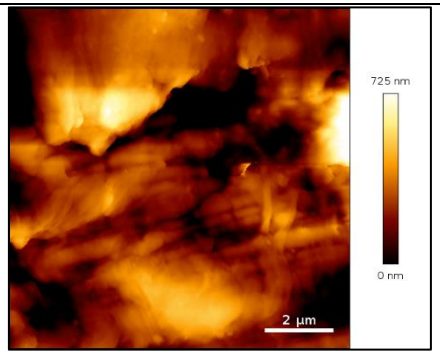 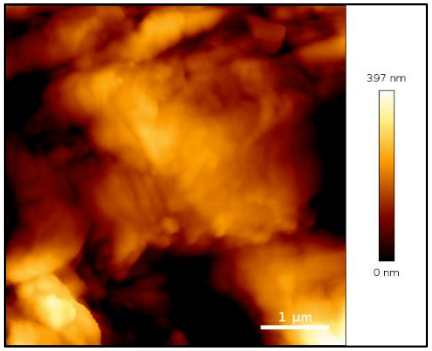	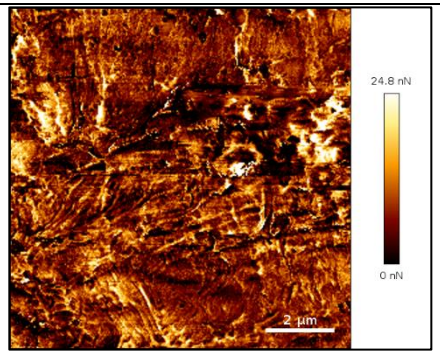 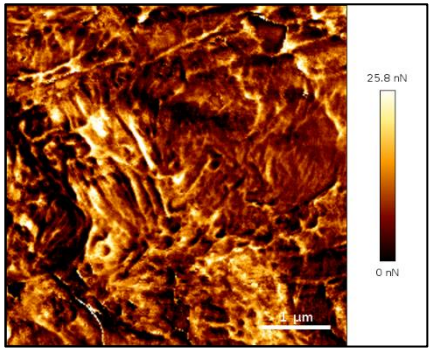	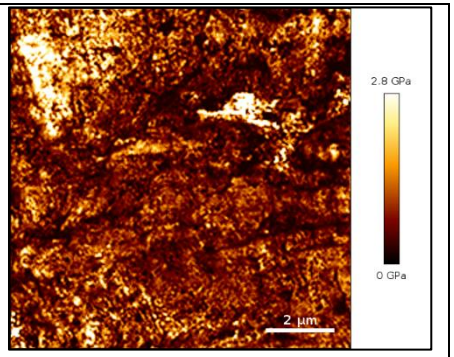 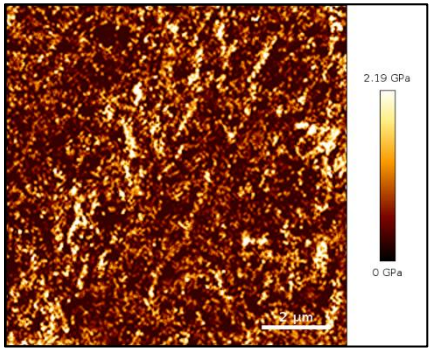
rP25	Site 1	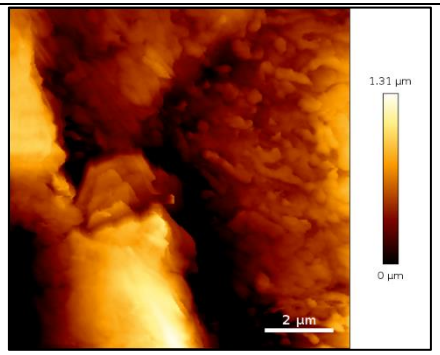	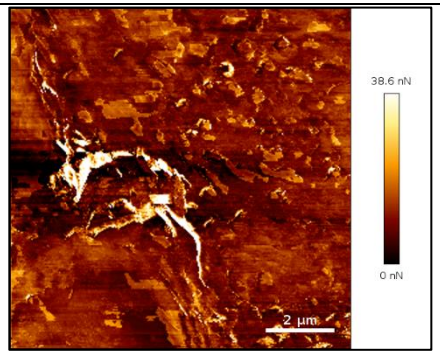	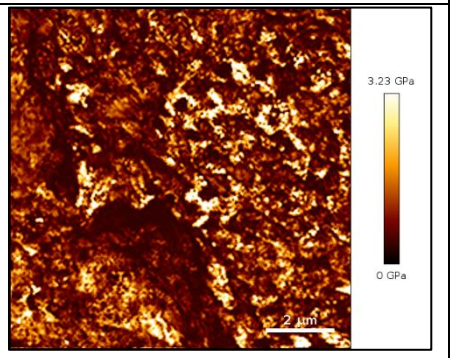

		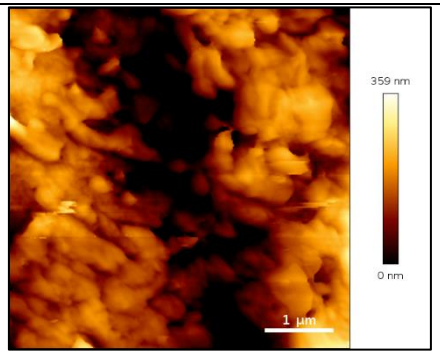 359 nm 0 nm 1 µm	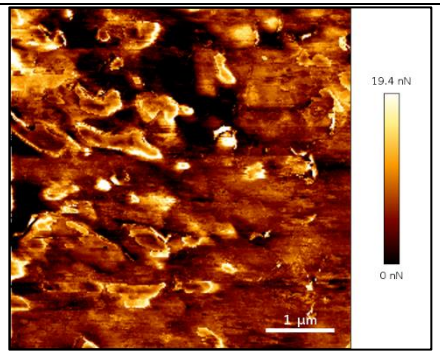 19.4 nN 0 nN 1 µm	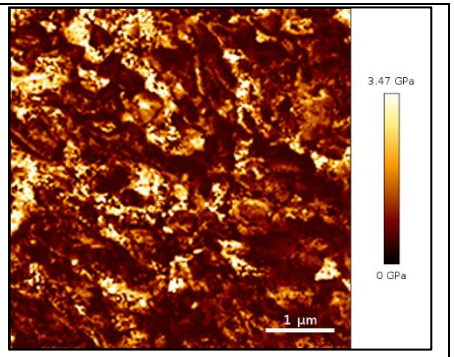 3.47 GPa 0 GPa 1 µm
	Site 2	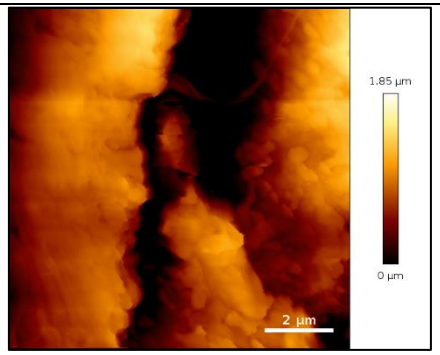 1.85 µm 0 µm 2 µm	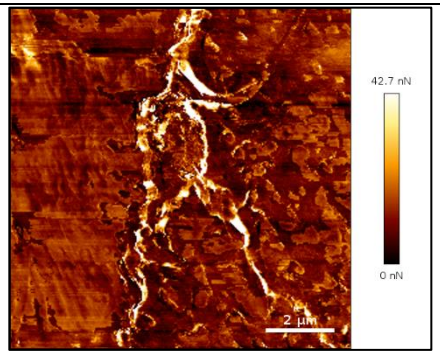 42.7 nN 0 nN 2 µm	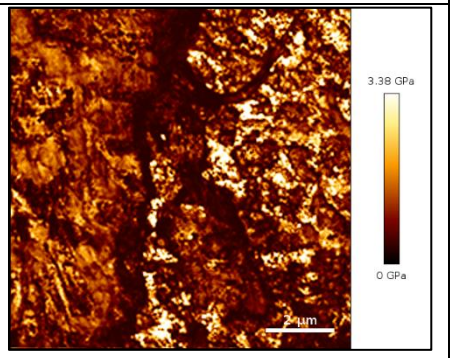 3.38 GPa 0 GPa 2 µm
		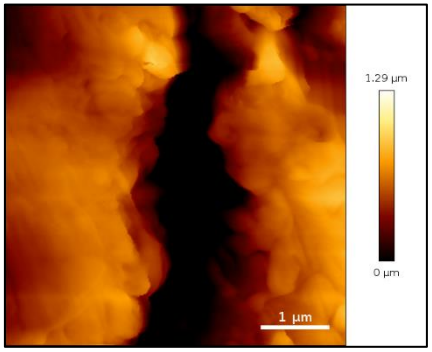 1.29 µm 0 µm 1 µm	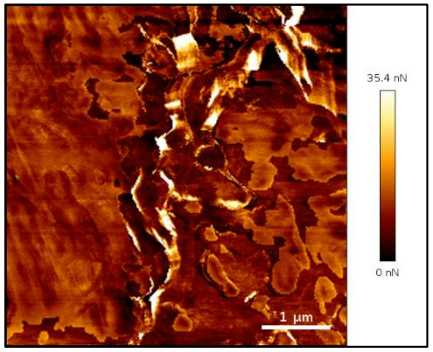 35.4 nN 0 nN 1 µm	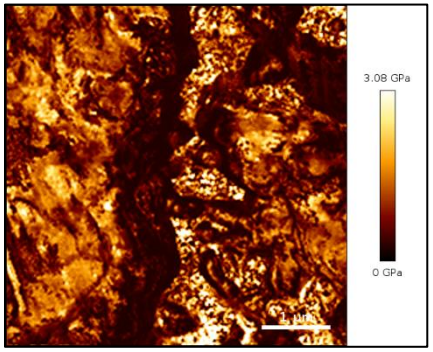 3.08 GPa 0 GPa

	Site 3	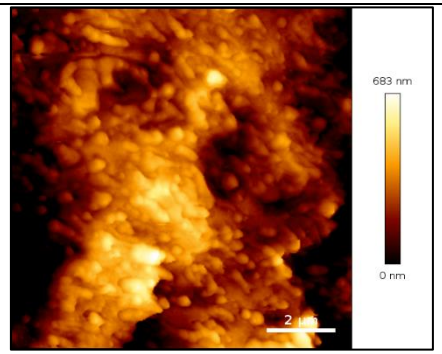 683 nm 0 nm 2 µm	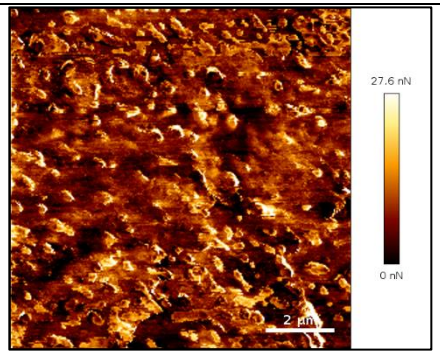 27.6 nN 0 nN 2 µm	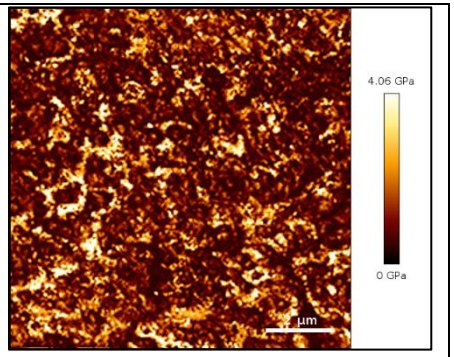 4.06 GPa 0 GPa 2 µm
		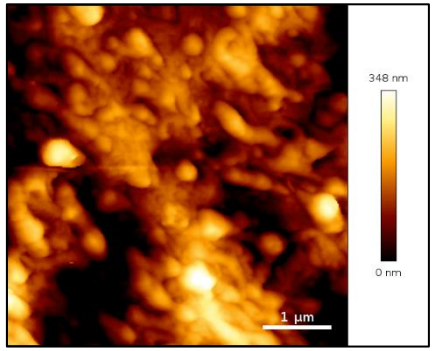 348 nm 0 nm 1 µm	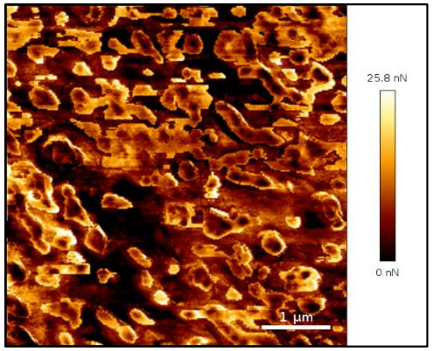 25.8 nN 0 nN 1 µm	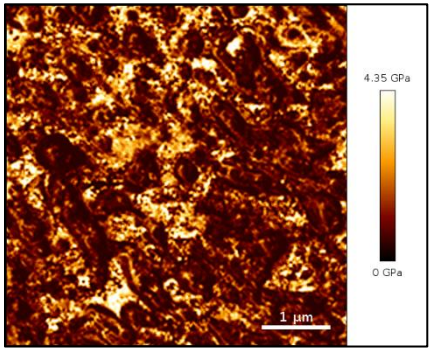 4.35 GPa 0 GPa 1 µm
	Site 4	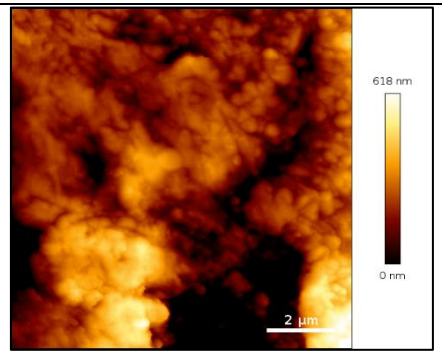 618 nm 0 nm 2 µm	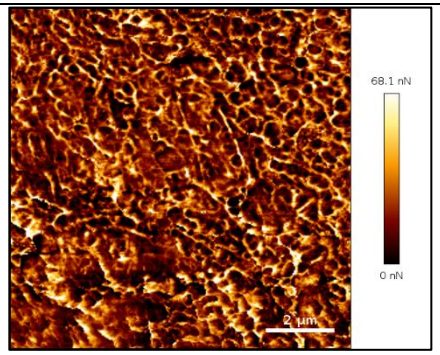 68.1 nN 0 nN 2 µm	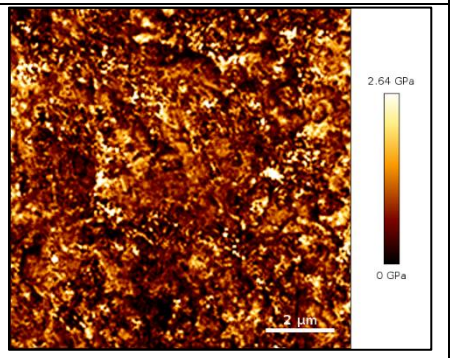 2.64 GPa 0 GPa 2 µm

Appendix 4

		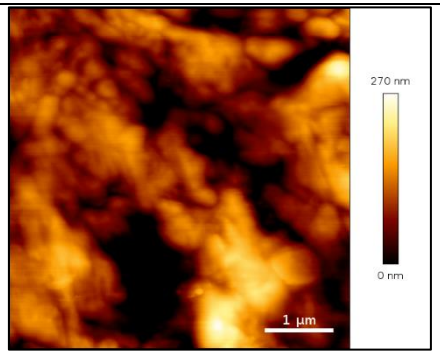	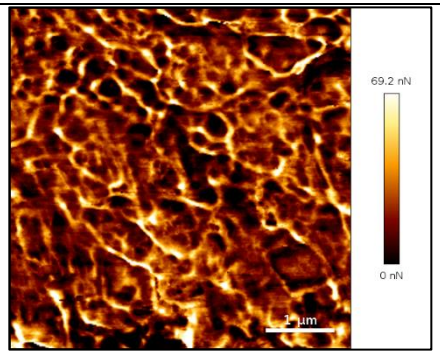	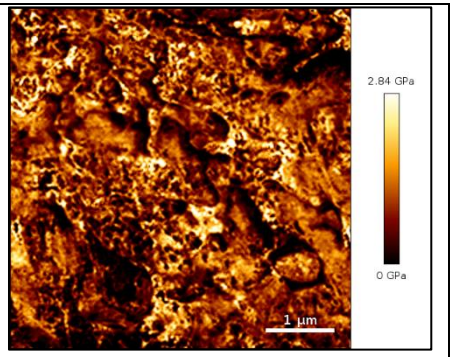
rP40	Site 1	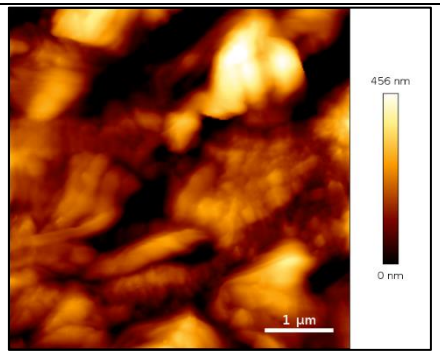	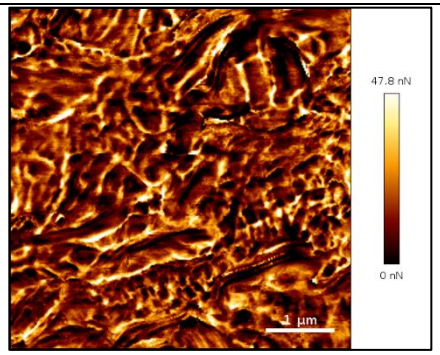	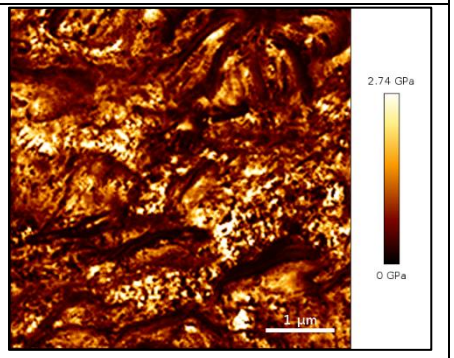
	Site 2	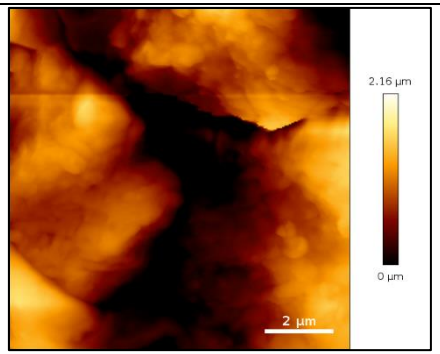	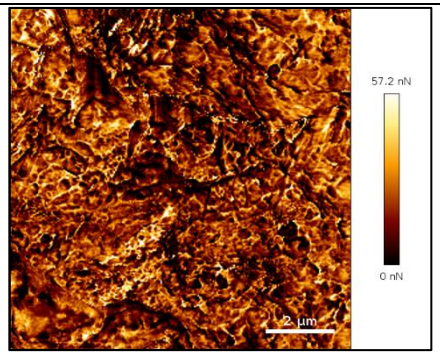	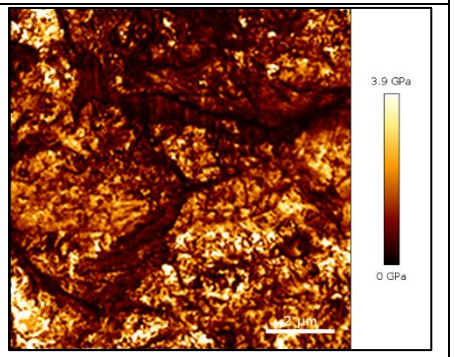

		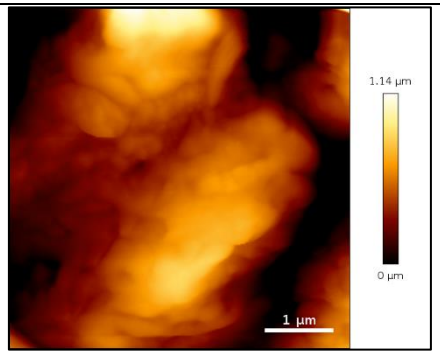	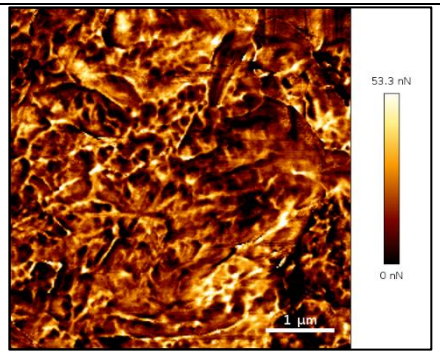	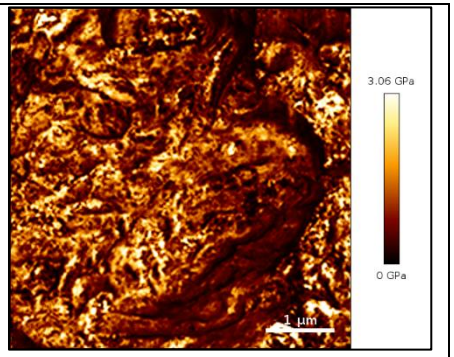
	Site 3	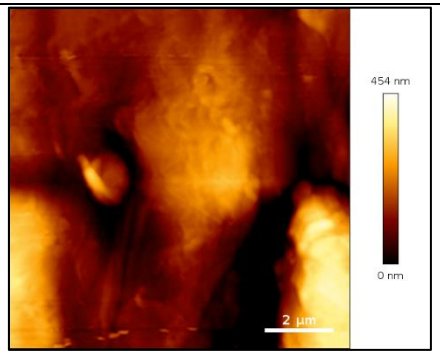 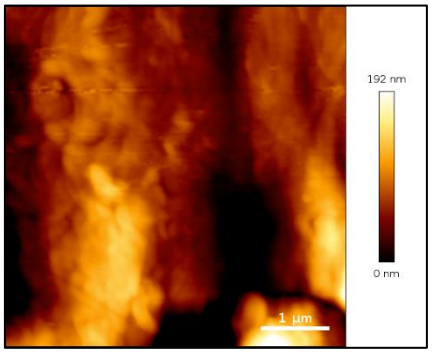	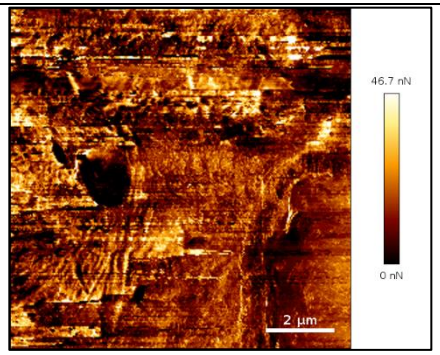 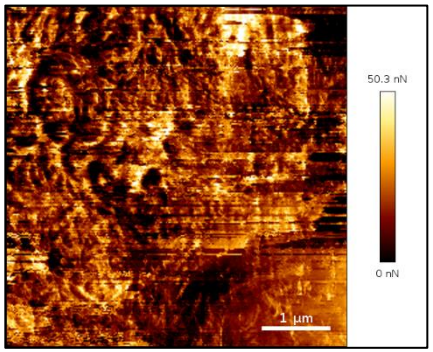	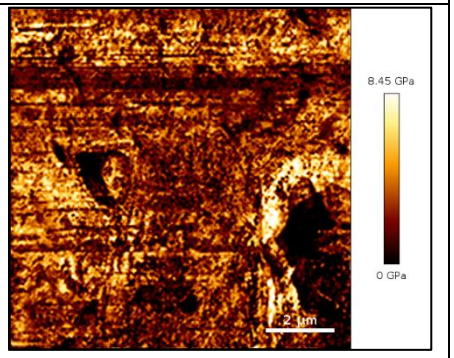 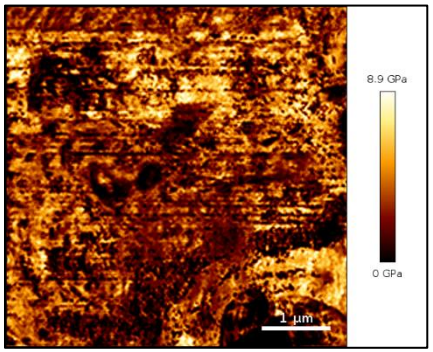

Appendix 4

	Site 4	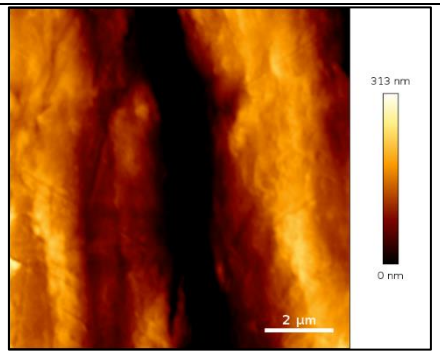	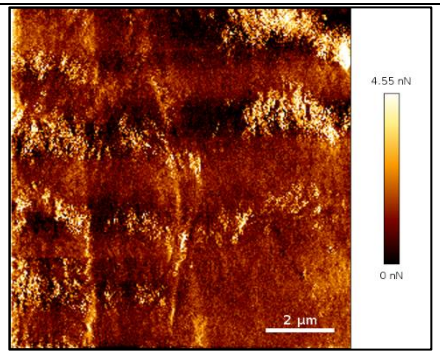	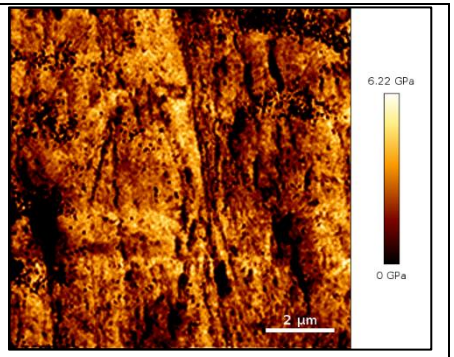
rP50	Site 1	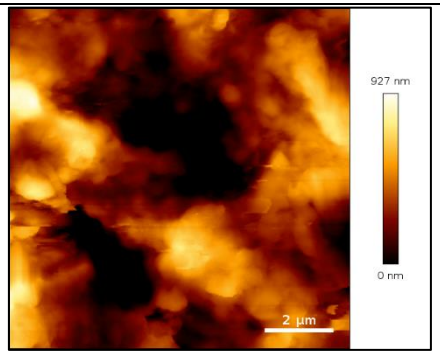 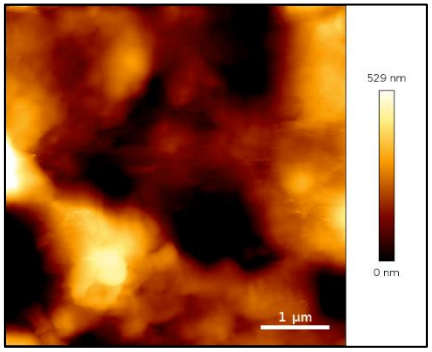	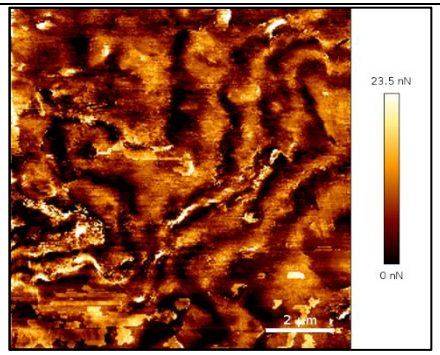 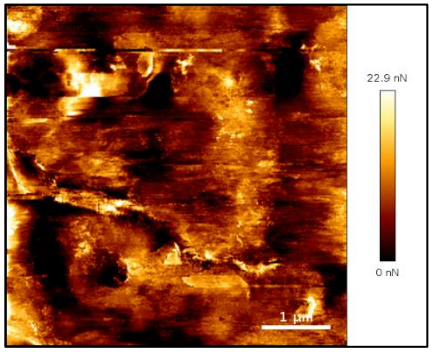	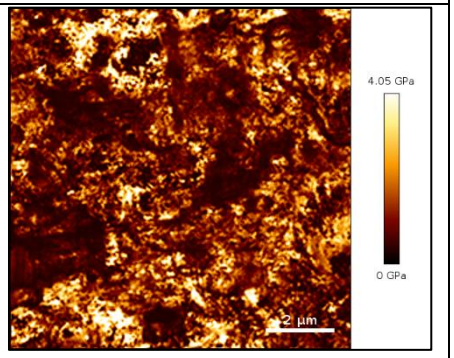 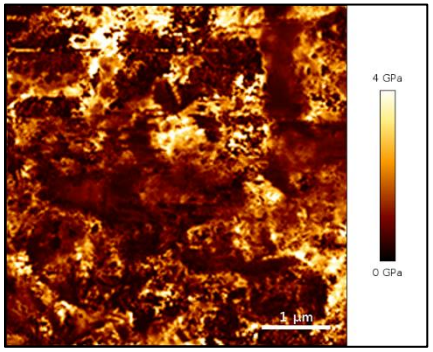

Appendix 4

	Site 2	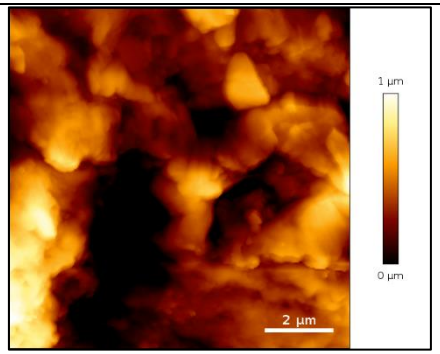	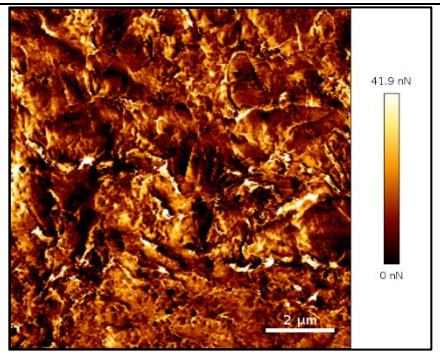	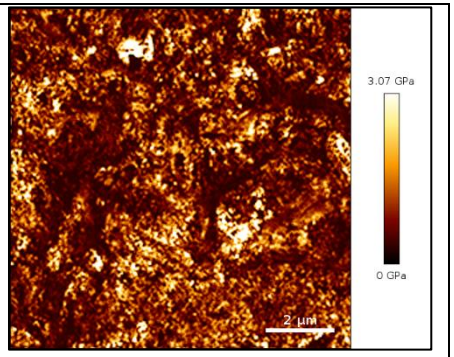
		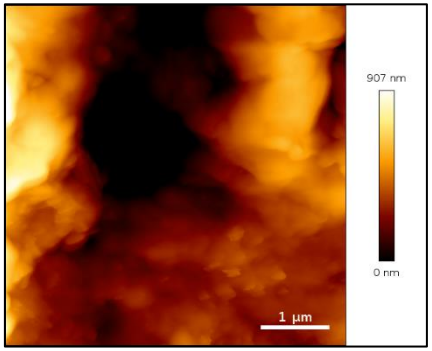	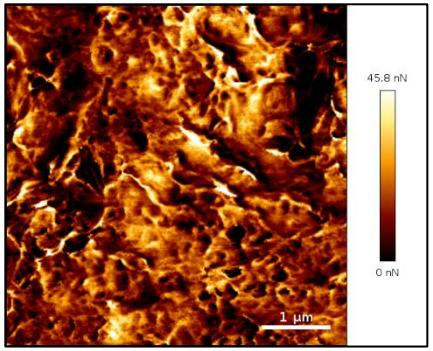	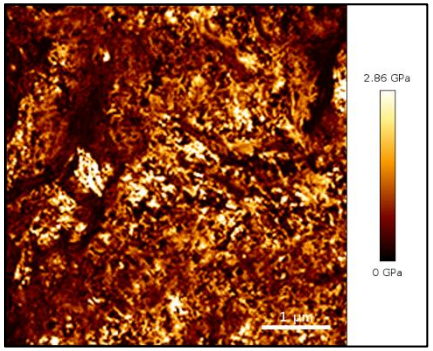
	Site 3	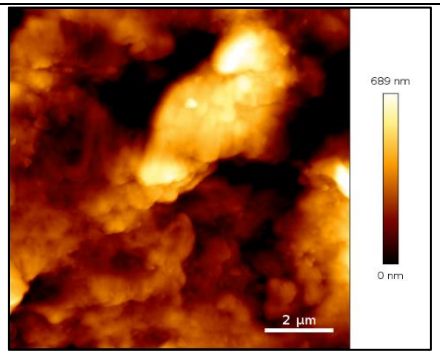	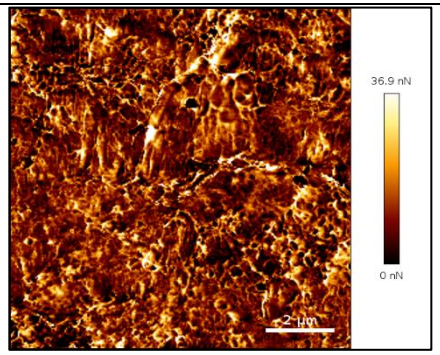	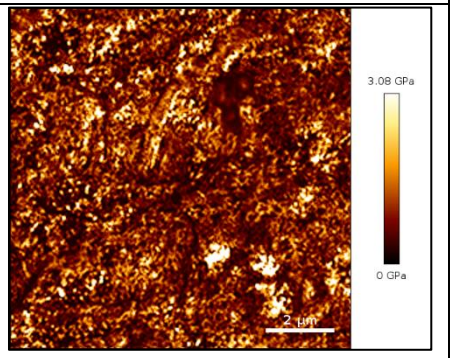

		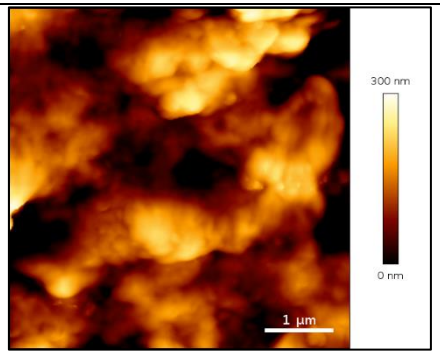	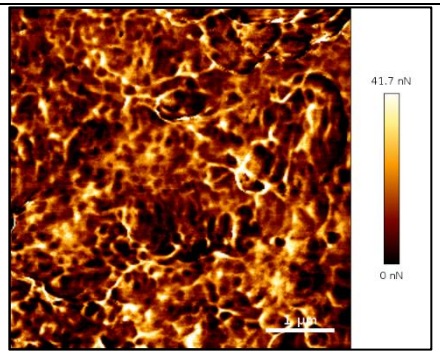	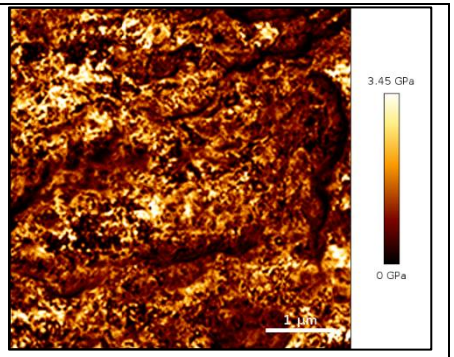
	Site 4	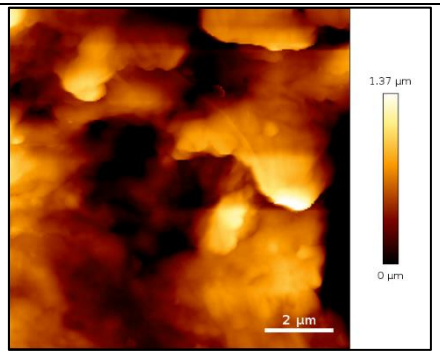 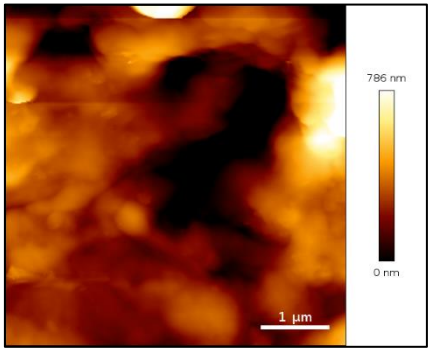	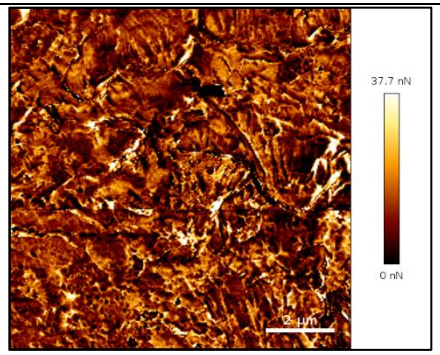 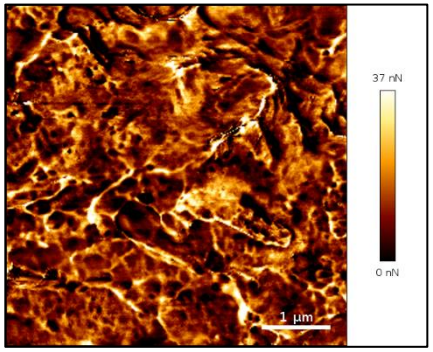	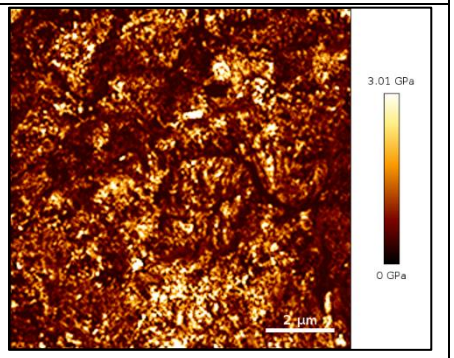 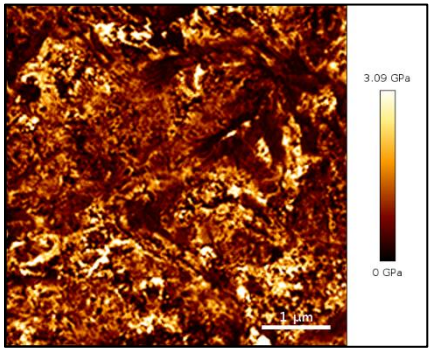

Appendix 4

rP60	Site 1	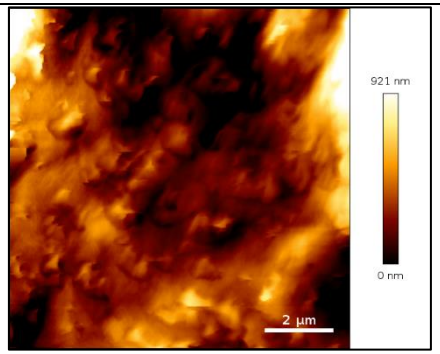	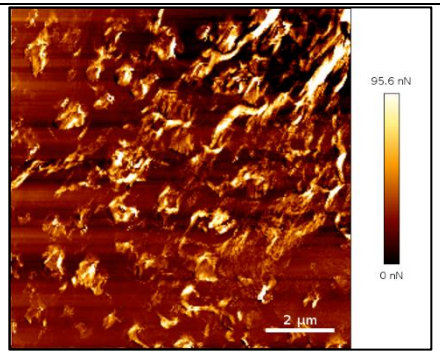	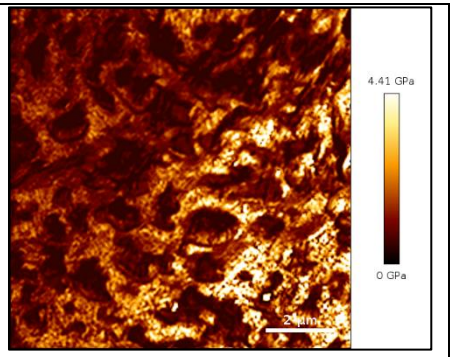
		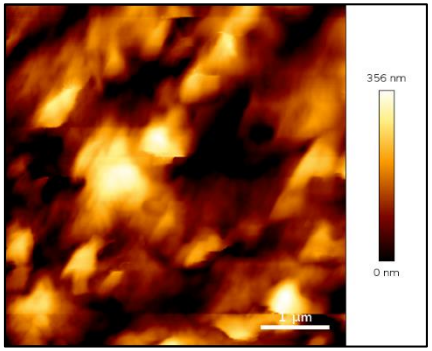	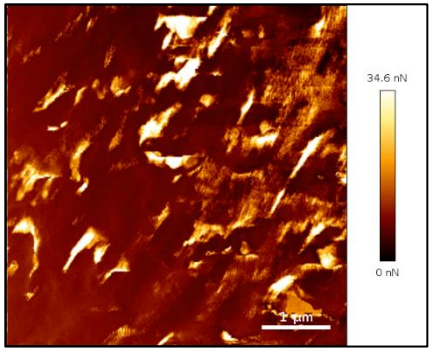	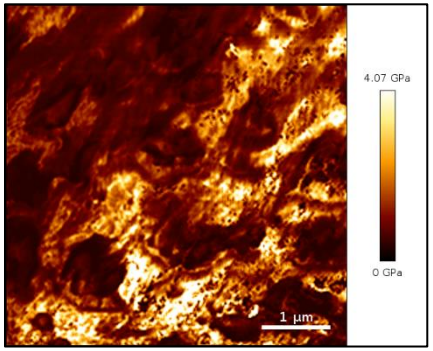
	Site 2	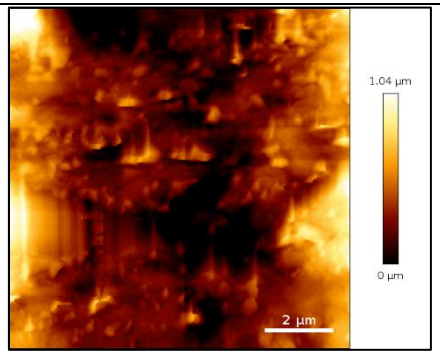	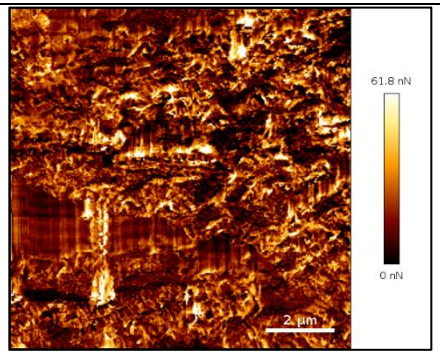	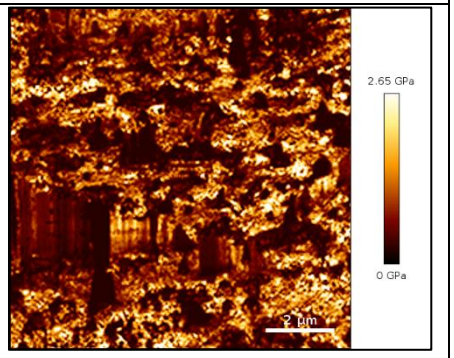

		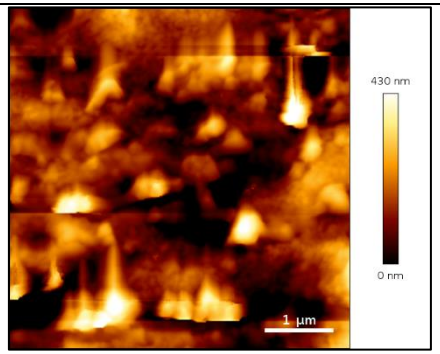	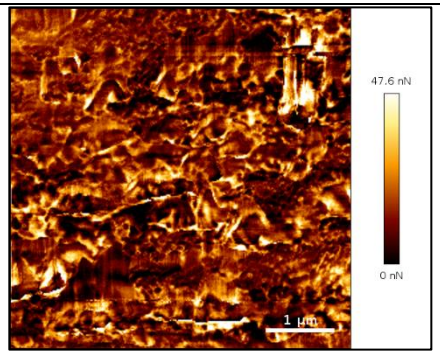	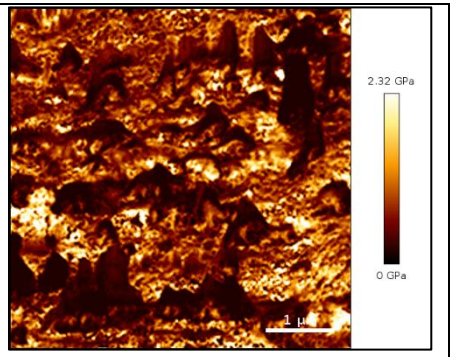
	Site 3	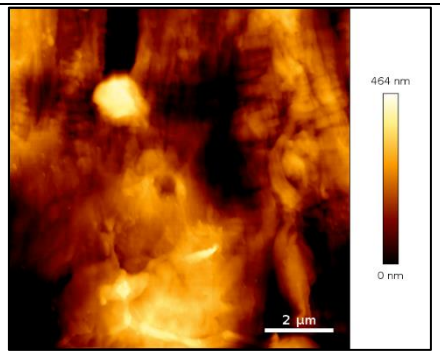 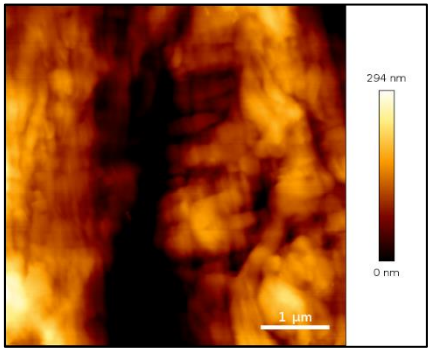	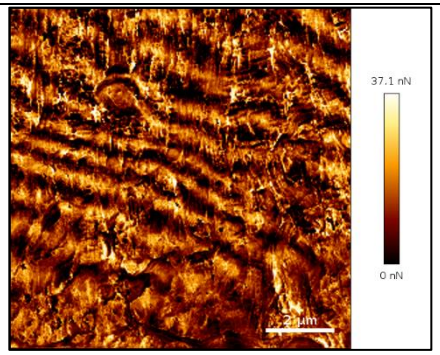 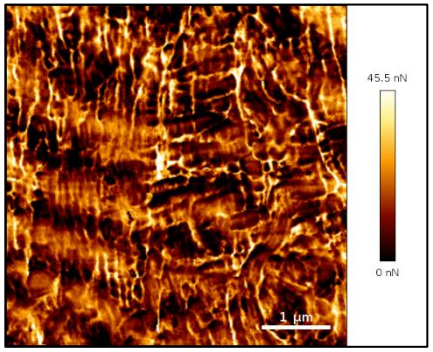	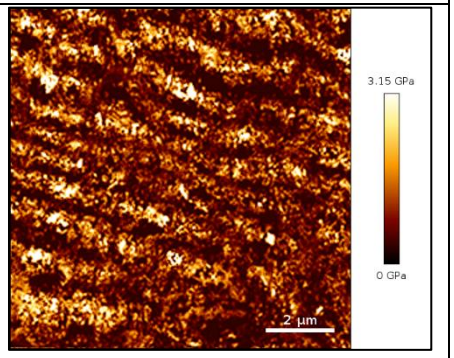 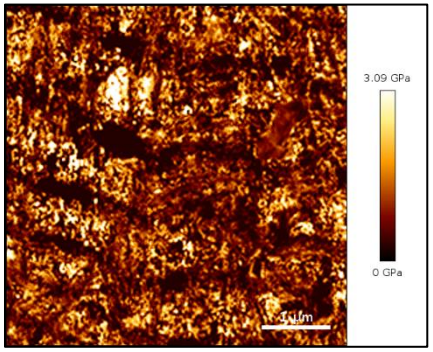

	Site 4	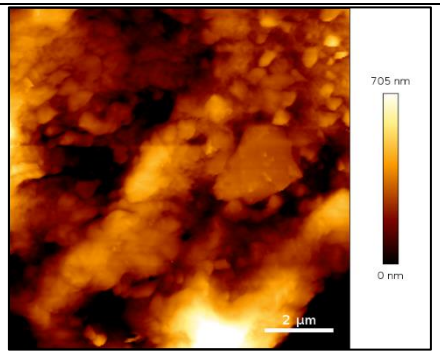	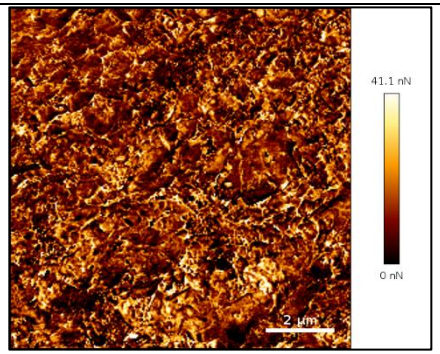	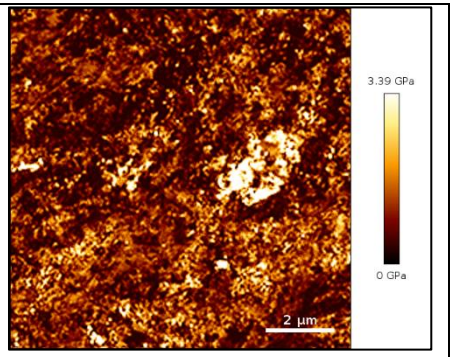
		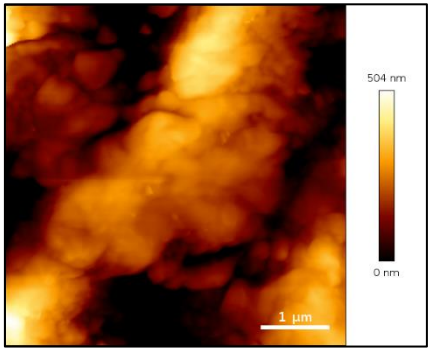	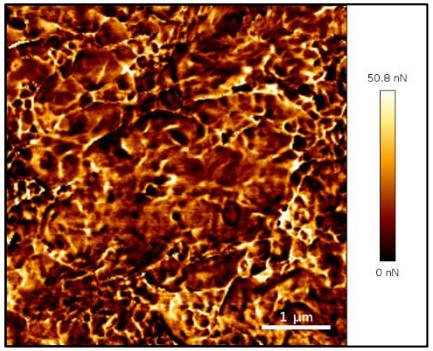	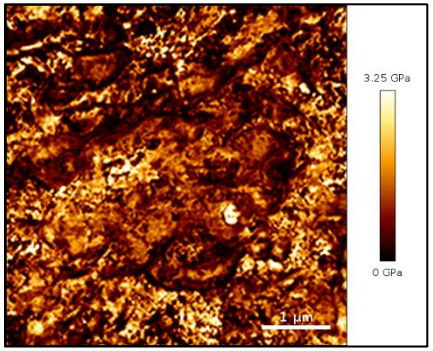
rP75	Site 1	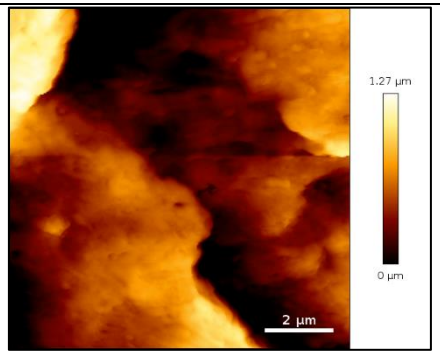	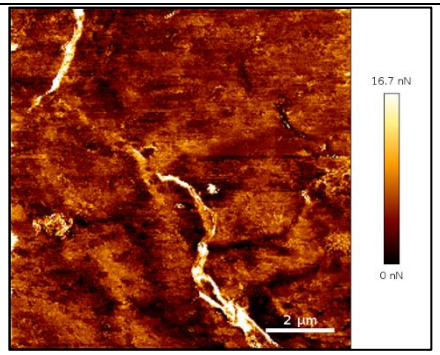	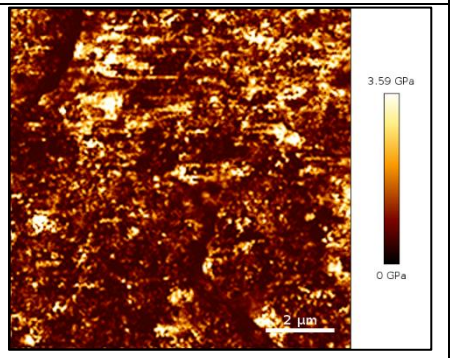

		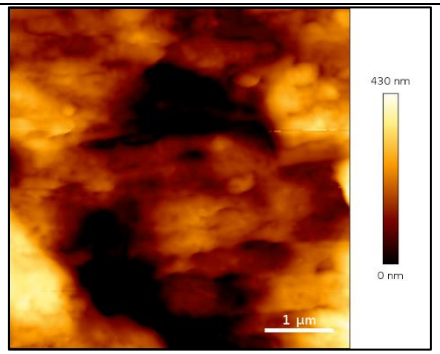 430 nm 0 nm 1 µm	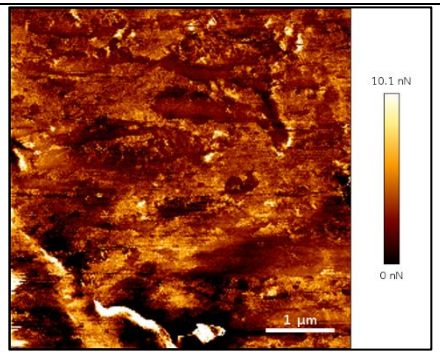 10.1 nN 0 nN 1 µm	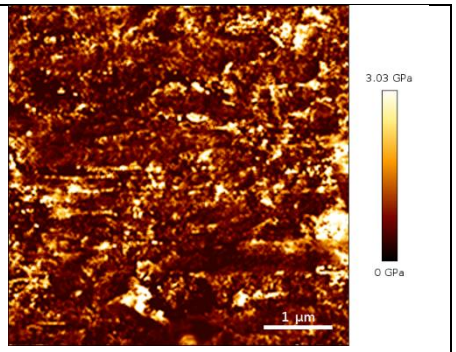 3.03 GPa 0 GPa 1 µm
	Site 2	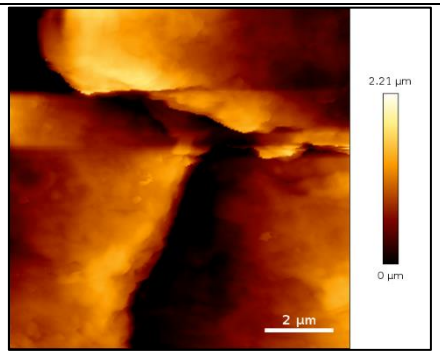 2.21 µm 0 µm 2 µm	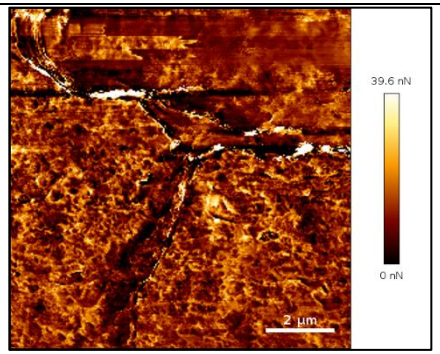 39.6 nN 0 nN 2 µm	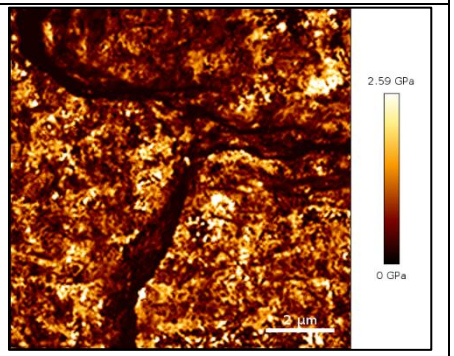 2.59 GPa 0 GPa 2 µm
		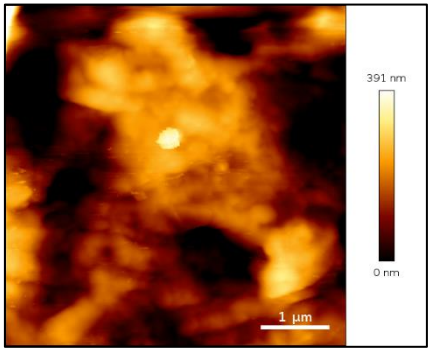 391 nm 0 nm 1 µm	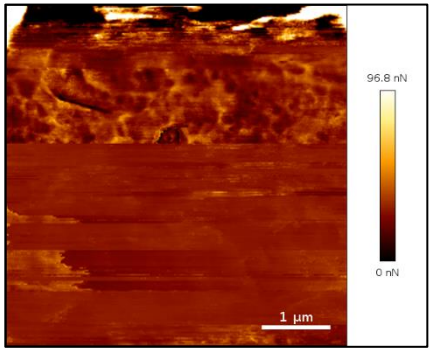 96.8 nN 0 nN 1 µm	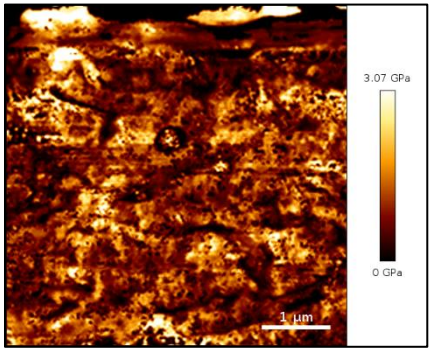 3.07 GPa 0 GPa 1 µm

	Site 3	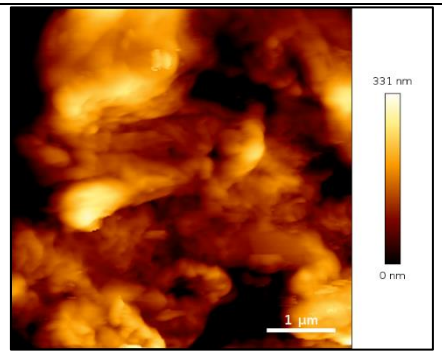	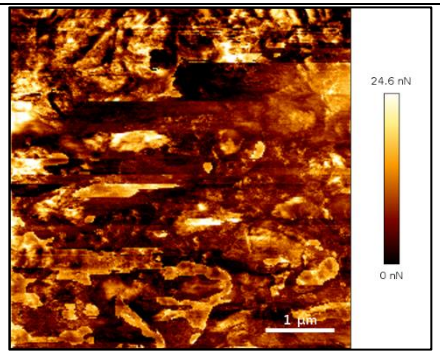	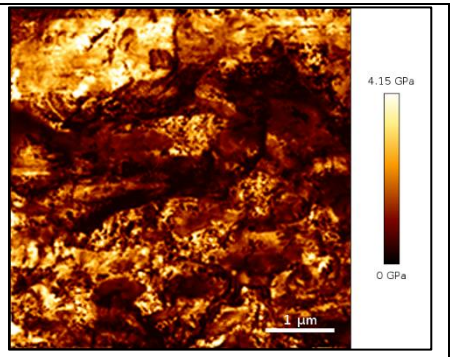
	Site 4	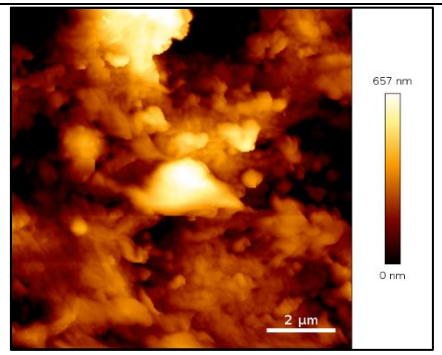 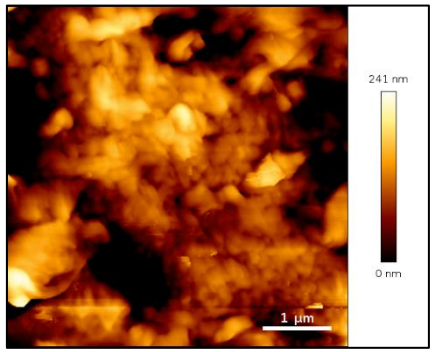	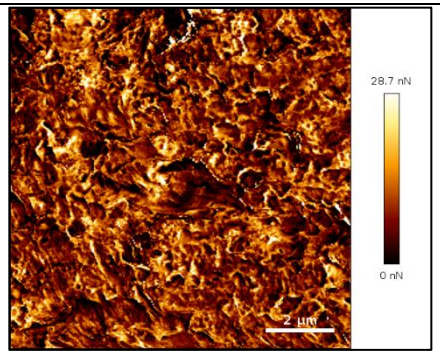 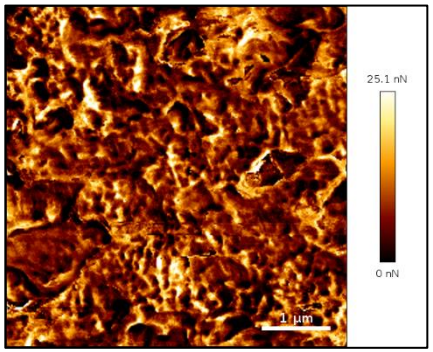	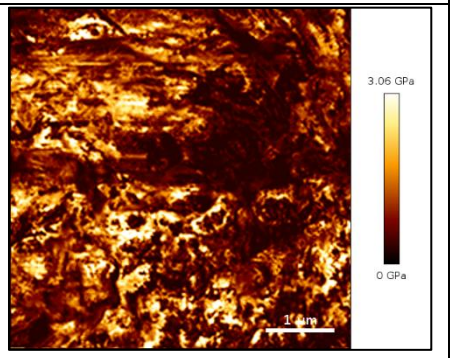 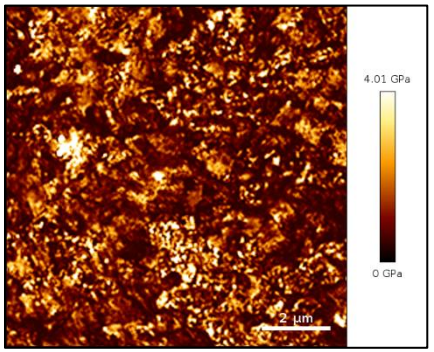

Appendix 4

rP80	Site 1	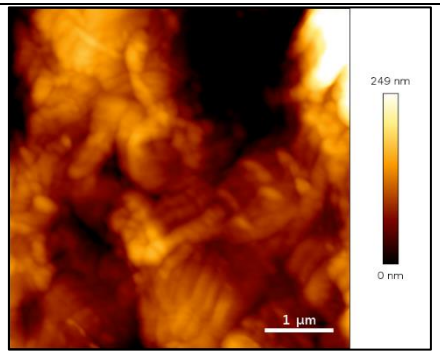	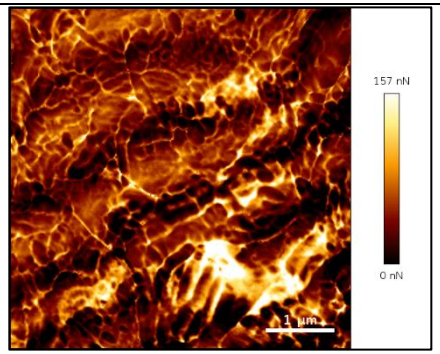	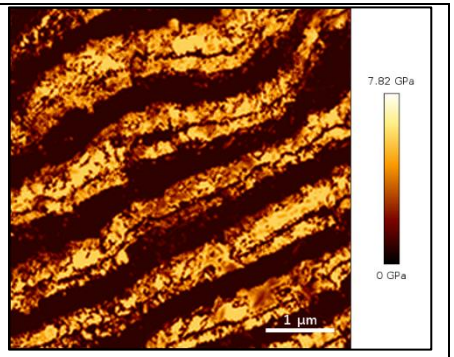
	Site 2	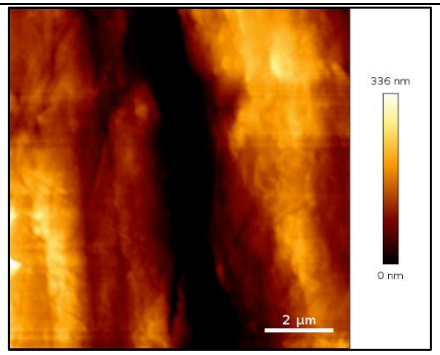 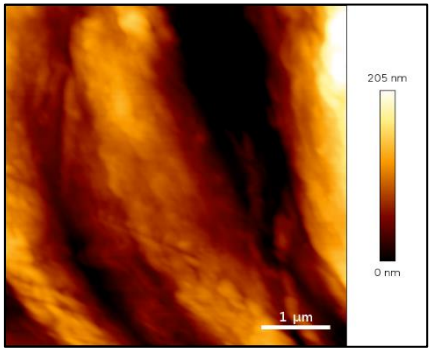	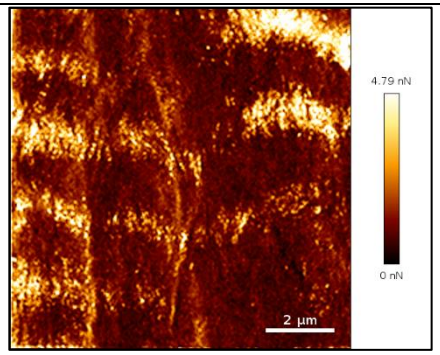 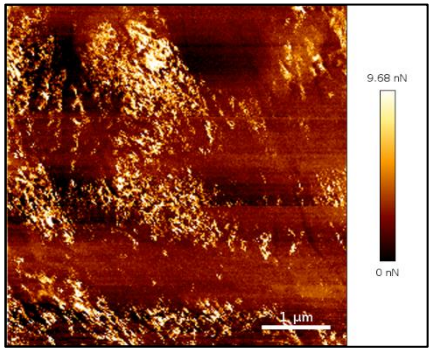	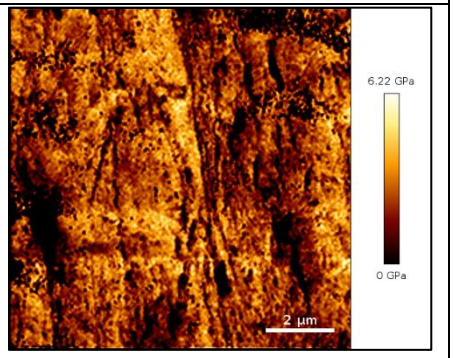 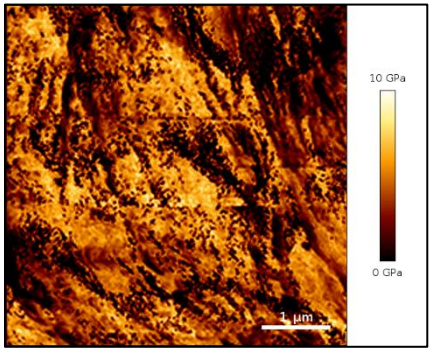

	Site 3	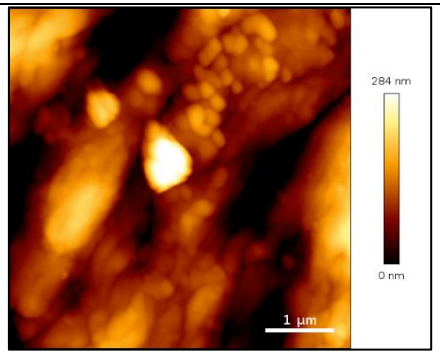	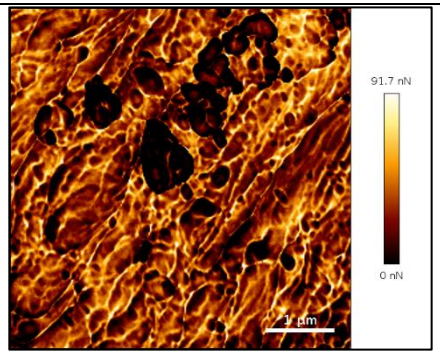	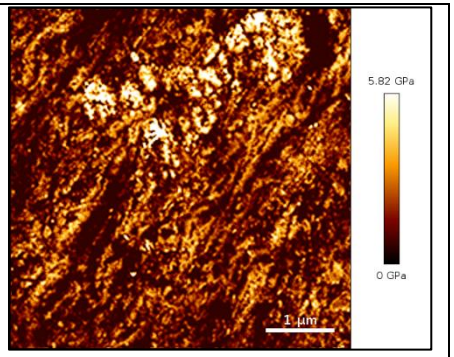
	Site 4	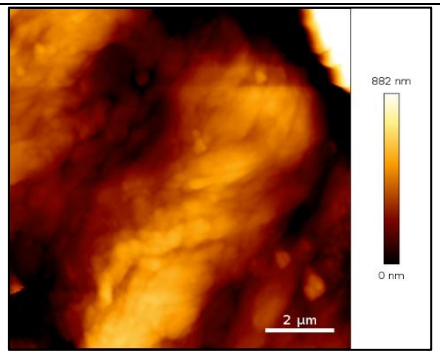 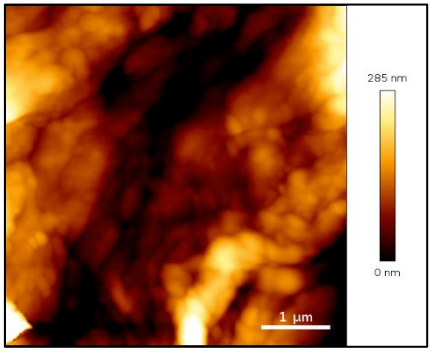	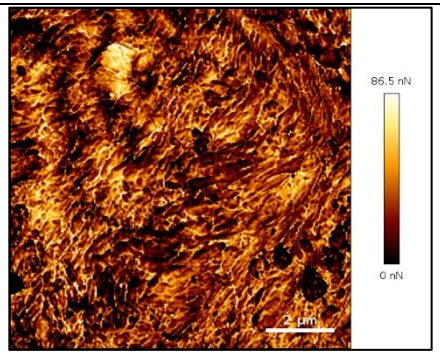 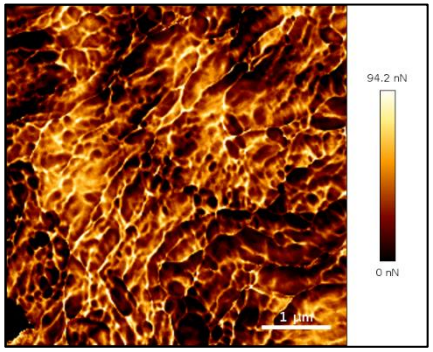	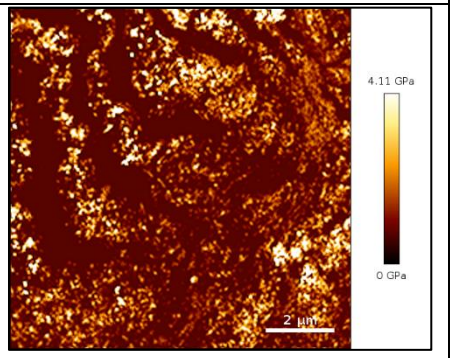 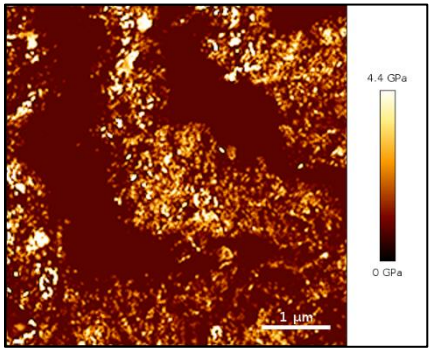

Appendix 4

rP90	Site 1	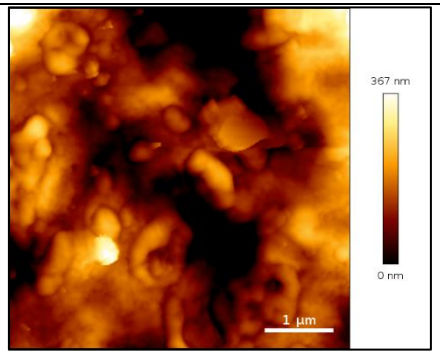	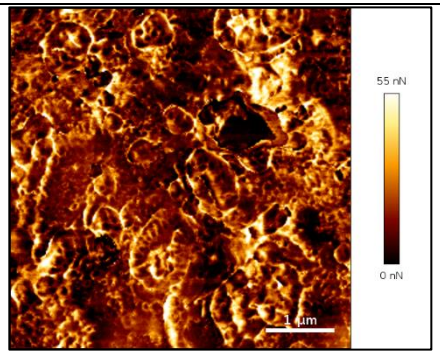	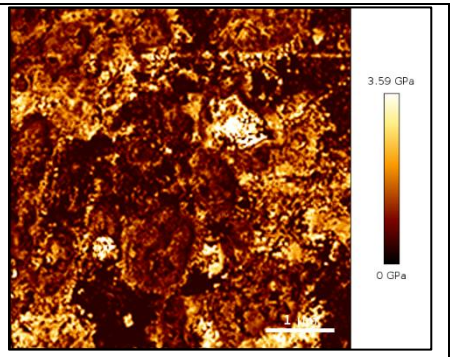
	Site 2	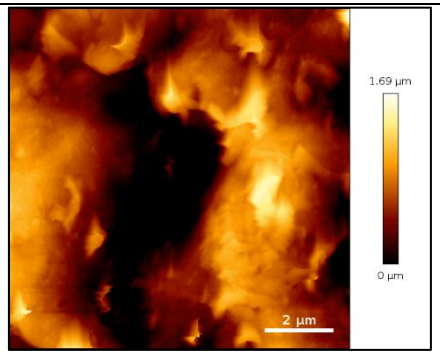 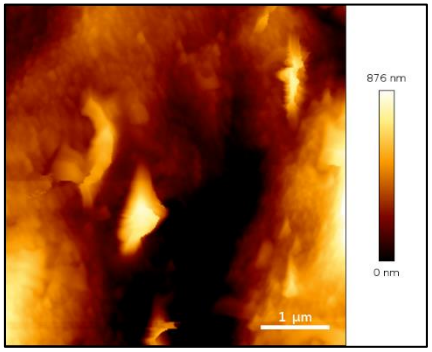	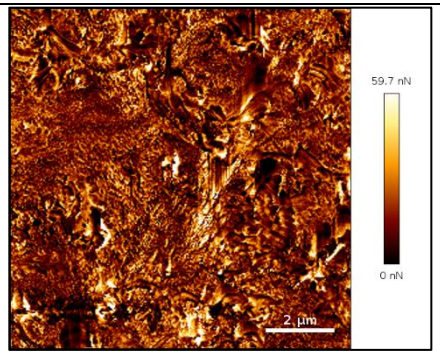 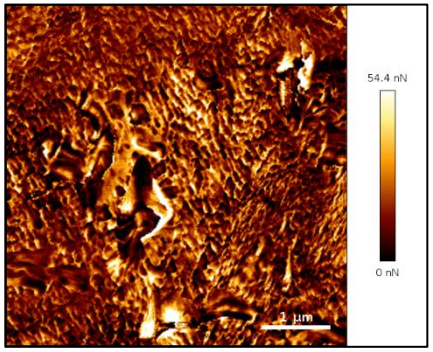	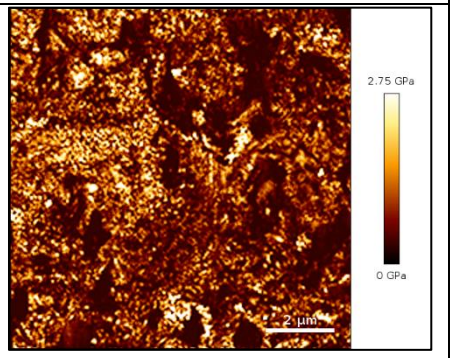 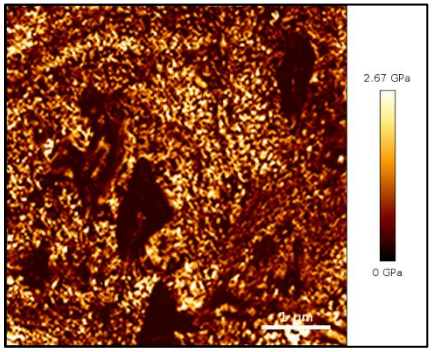

	Site 3	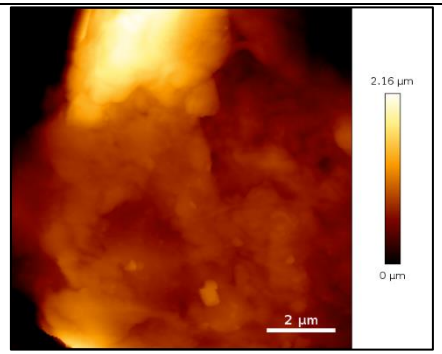 2.16 µm 0 µm 2 µm	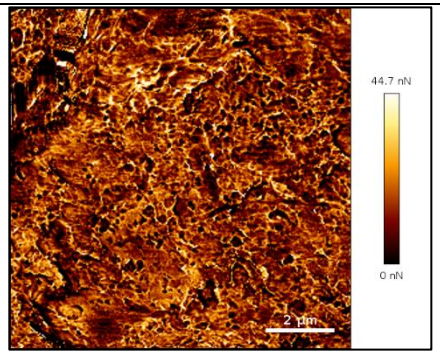 44.7 nN 0 nN 2 µm	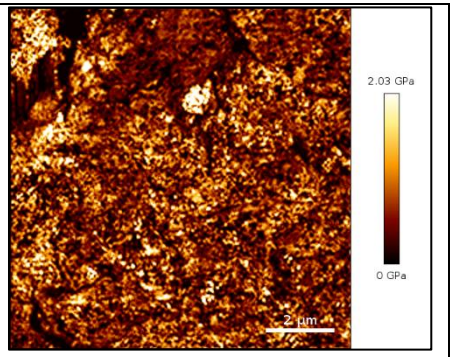 2.03 GPa 0 GPa 2 µm
		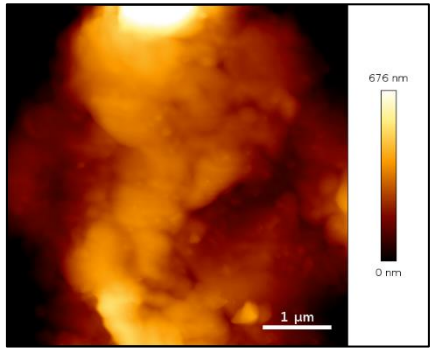 676 nm 0 nm 1 µm	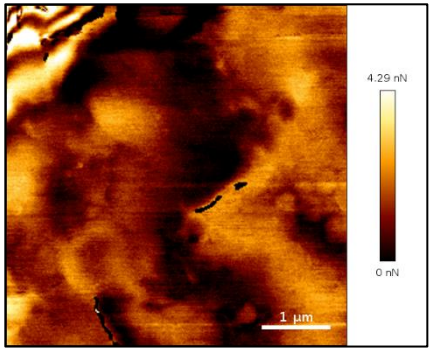 4.29 nN 0 nN 1 µm	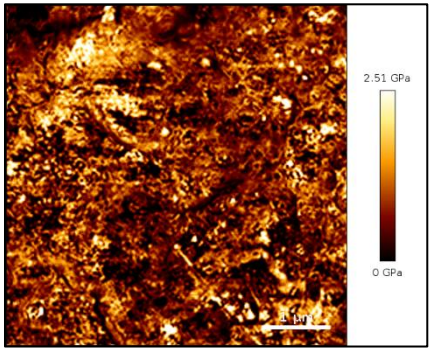 2.51 GPa 0 GPa
	Site 4	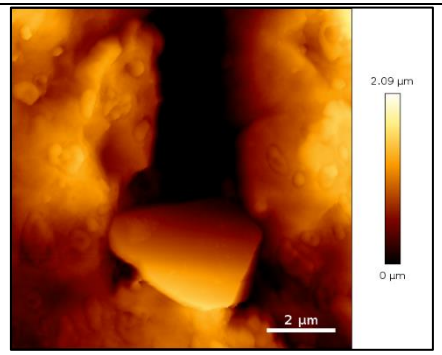 2.09 µm 0 µm 2 µm	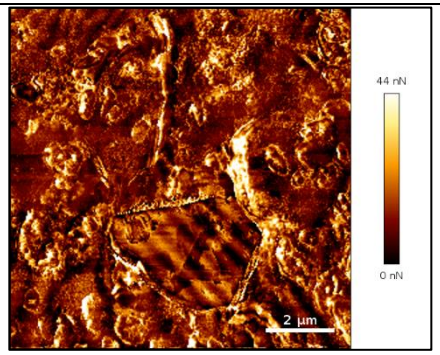 44 nN 0 nN 2 µm	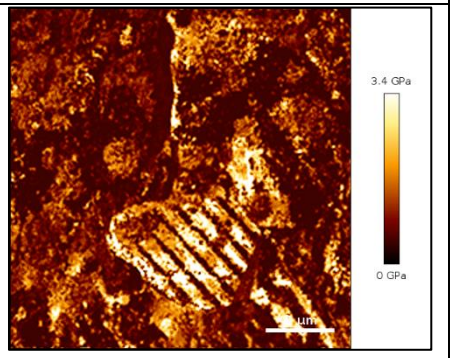 3.4 GPa 0 GPa

Appendix 4

		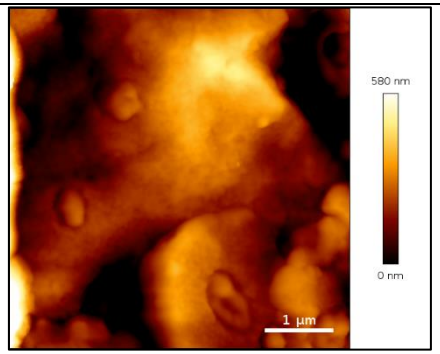	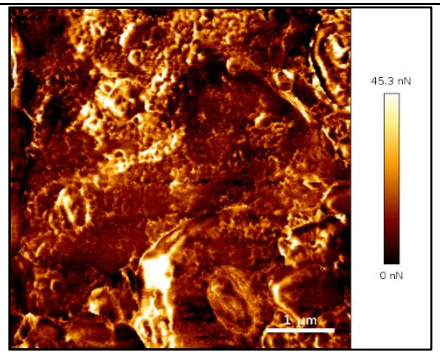	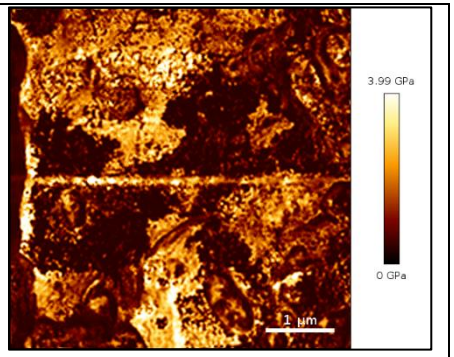
rPP	Site 1	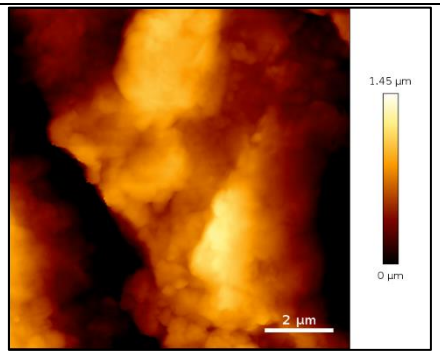 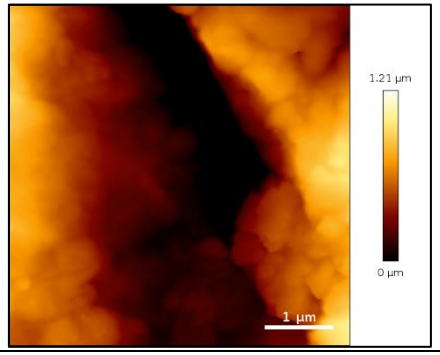	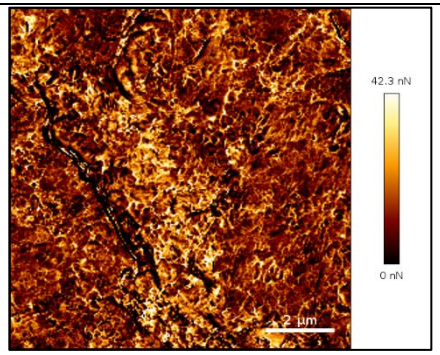 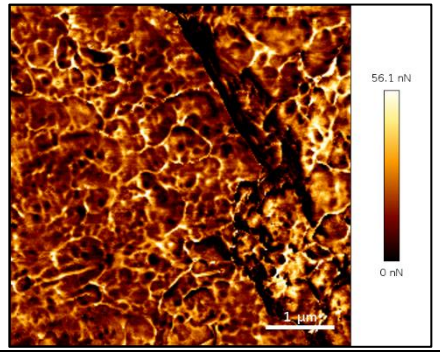	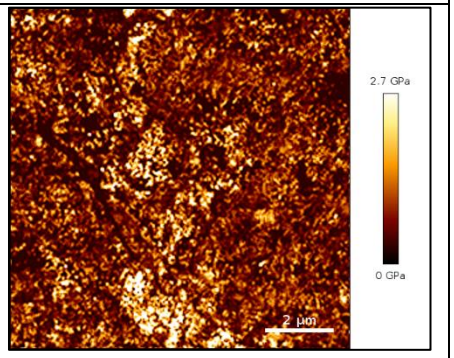 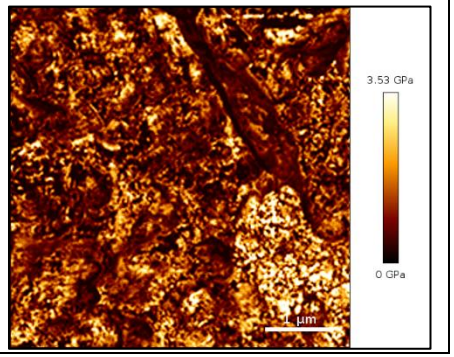

	Site 2	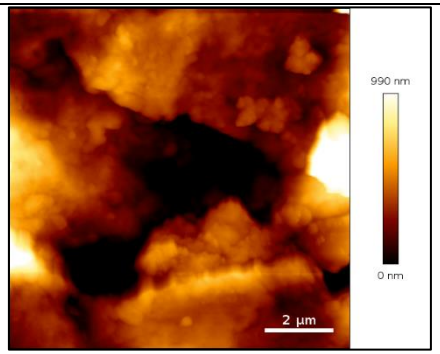 990 nm 0 nm 2 µm	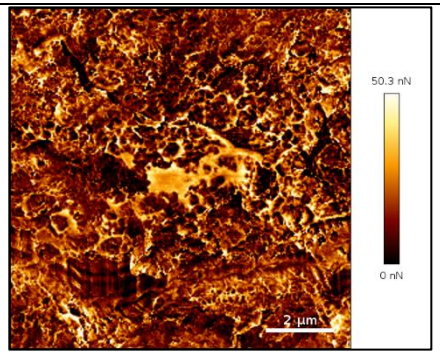 50.3 nN 0 nN 2 µm	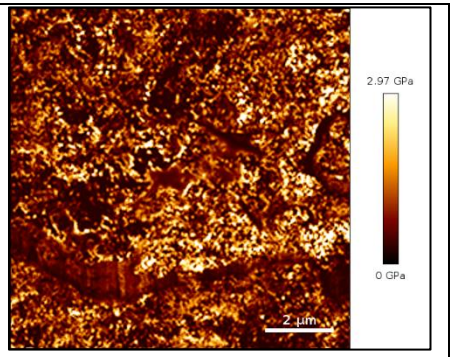 2.97 GPa 0 GPa 2 µm
		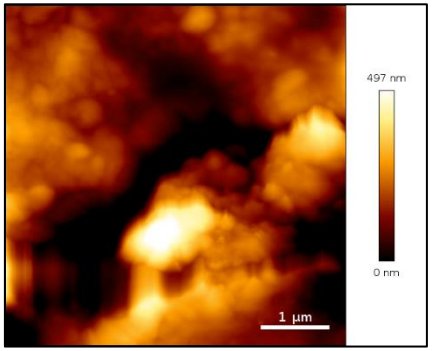 497 nm 0 nm 1 µm	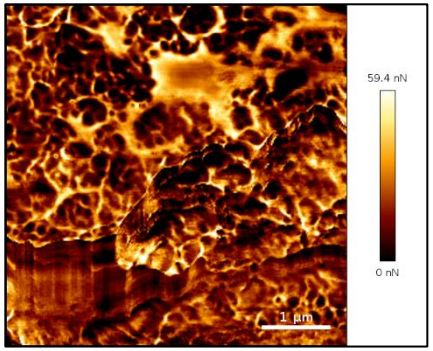 59.4 nN 0 nN 1 µm	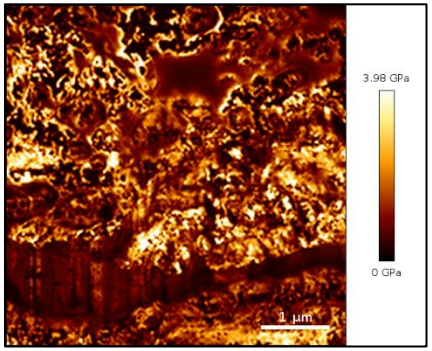 3.98 GPa 0 GPa 1 µm
	Site 3	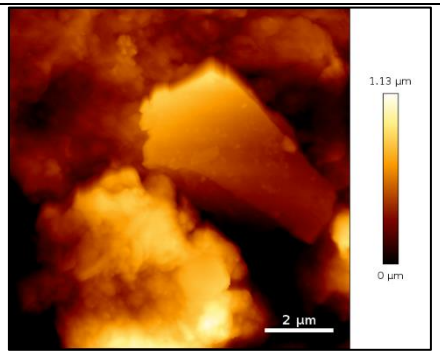 1.13 µm 0 µm 2 µm	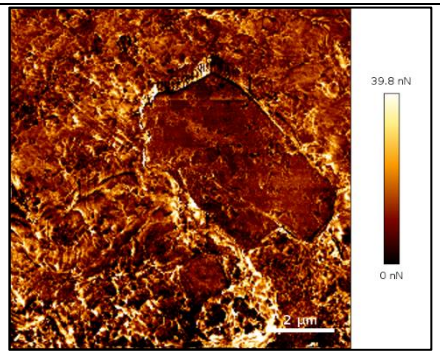 39.8 nN 0 nN 2 µm	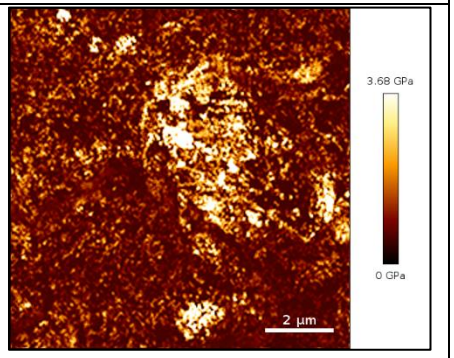 3.68 GPa 0 GPa 2 µm

		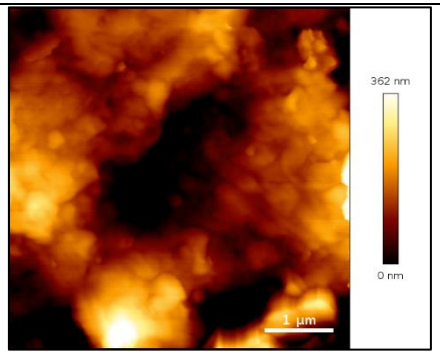	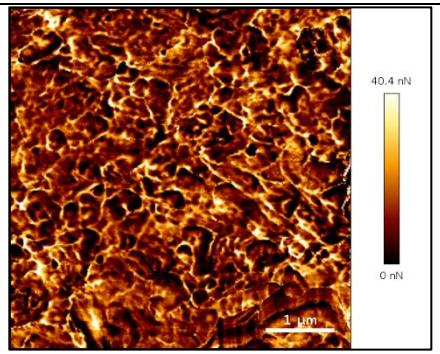	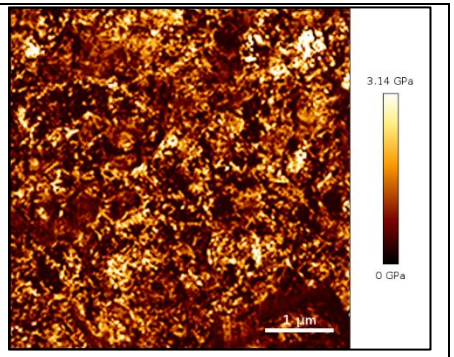
	Site 4	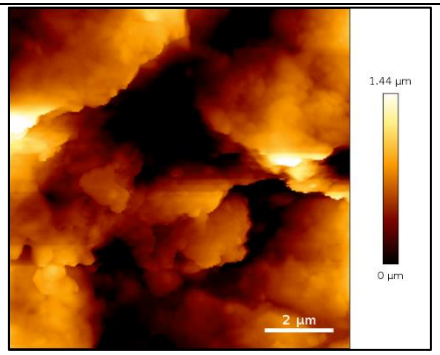 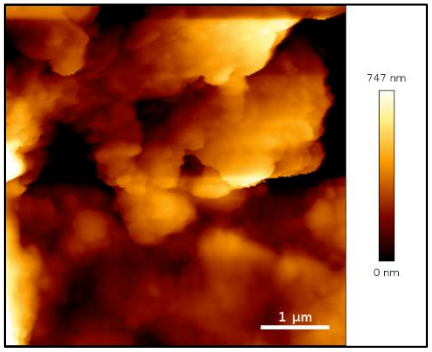	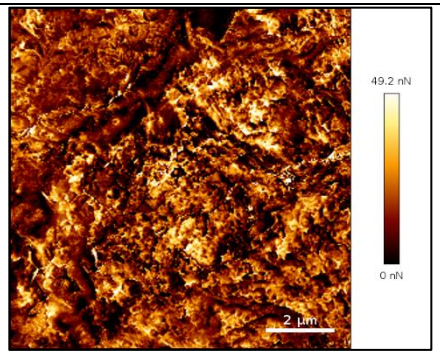 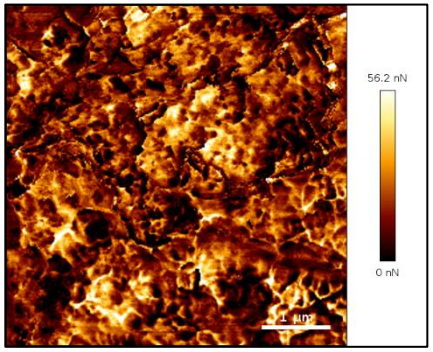	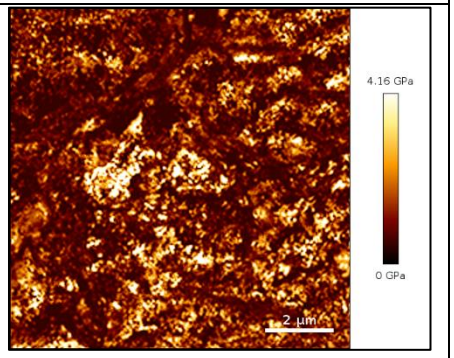 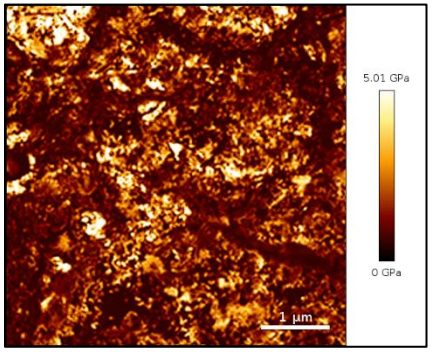

Appendix 5 AFM QI mode height, stiffness and adhesion images obtained at 1024 x 1024 pixels for vPP:vHDPE blends.

PP:HDPE Blend	Height, nm	Stiffness,	Adhesion, nN
vHDPE	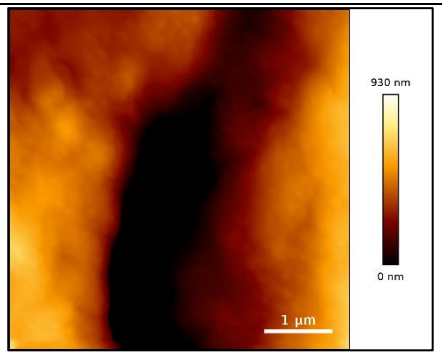	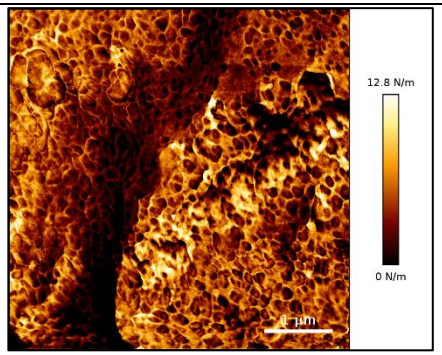	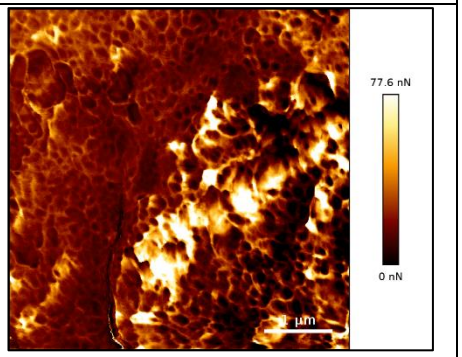
	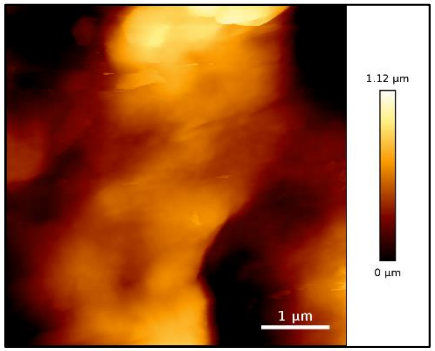	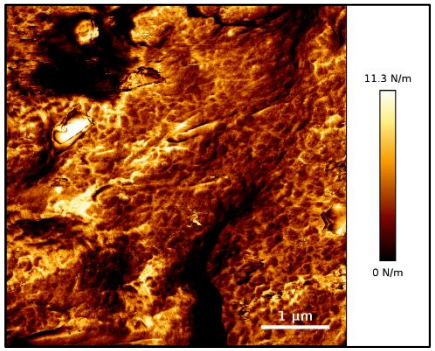	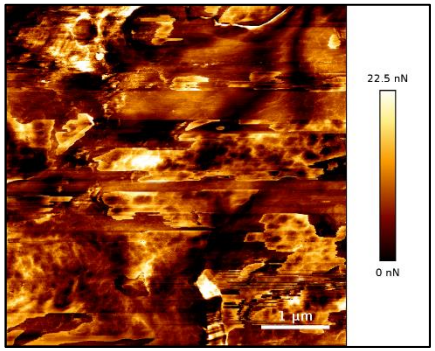
vP10	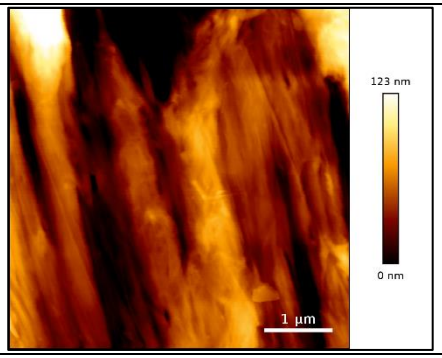	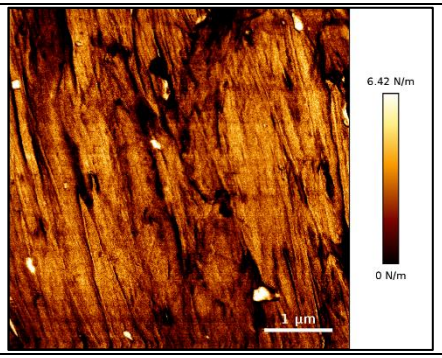	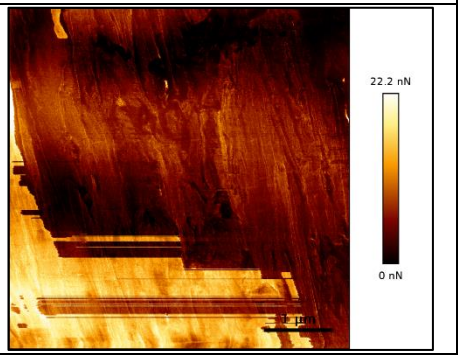

Appendix 5

	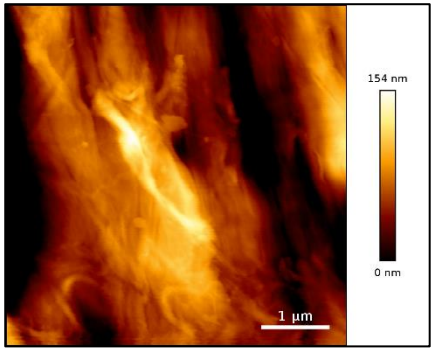	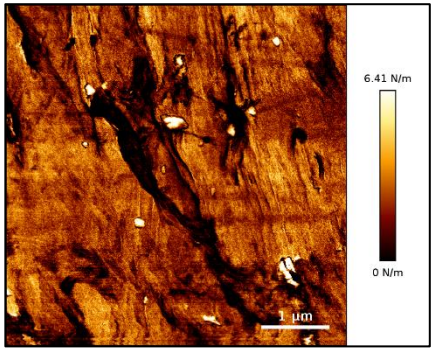	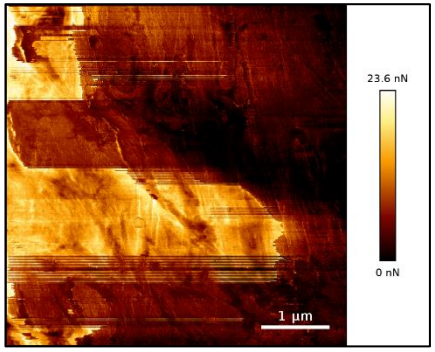
vP20	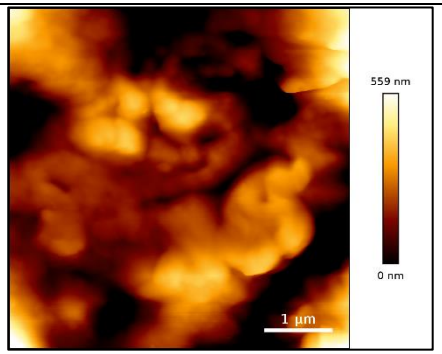 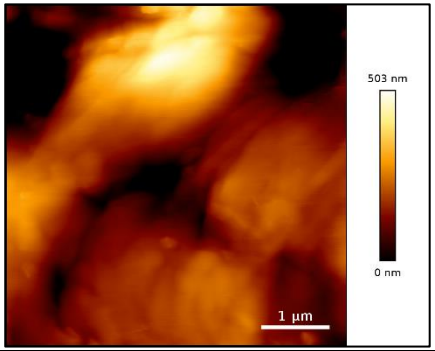	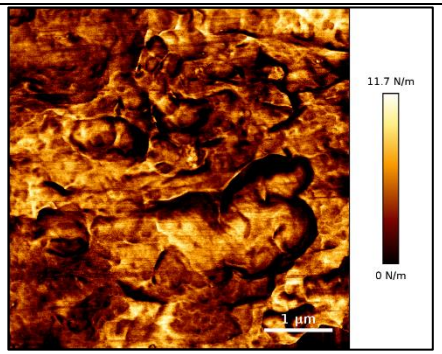 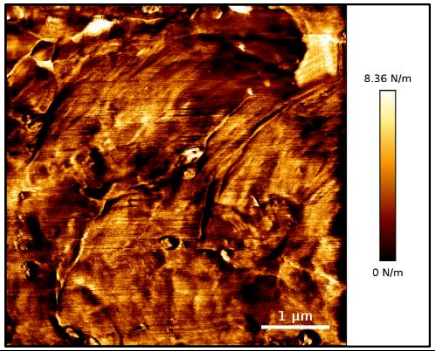	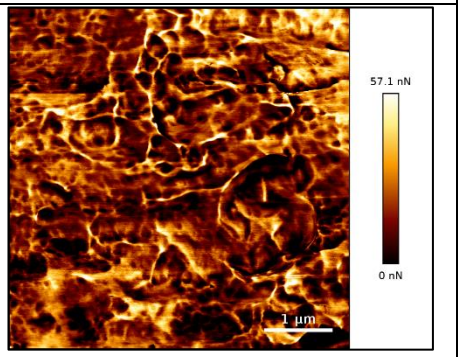 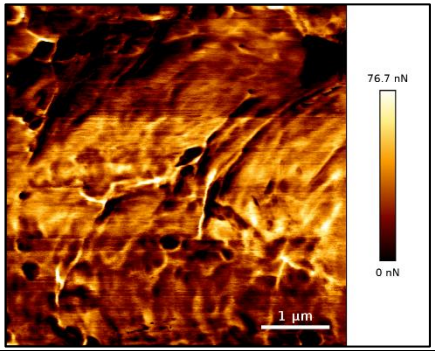

Appendix 5

vP25	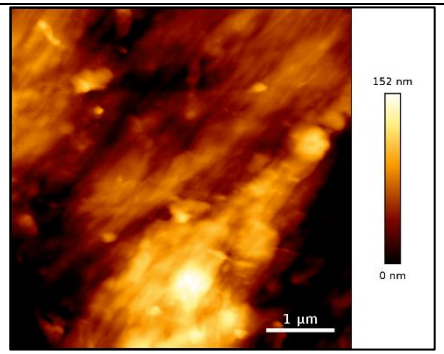	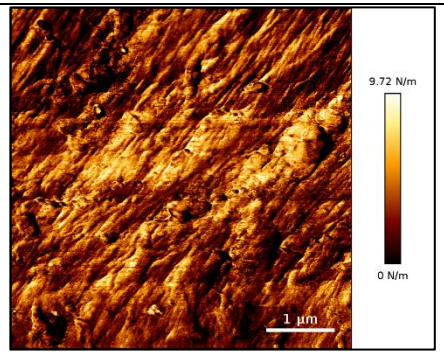	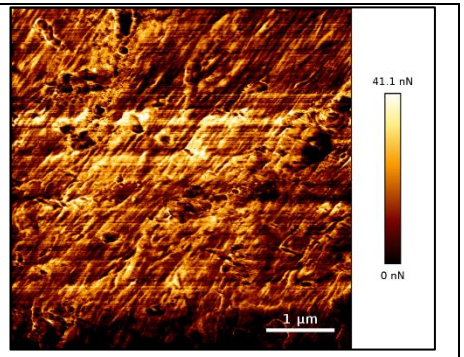
	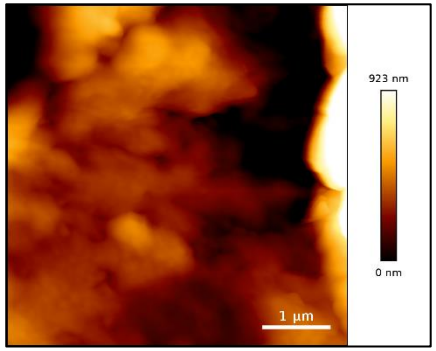	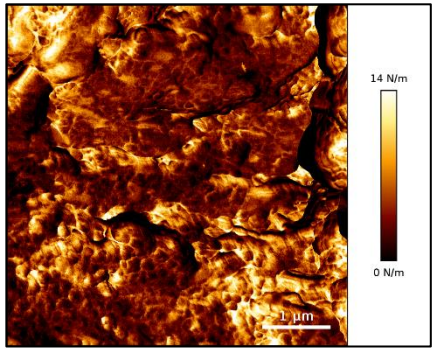	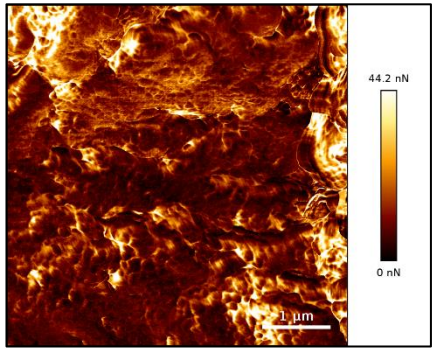
vP40	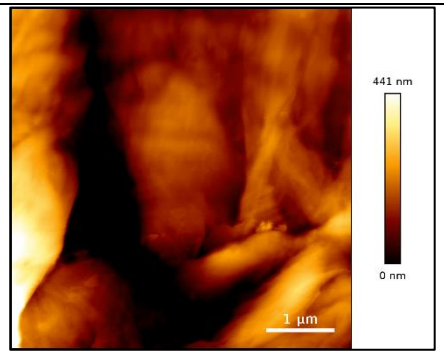	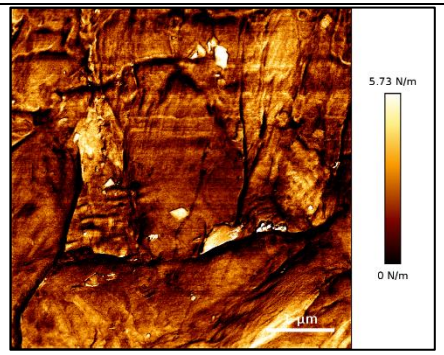	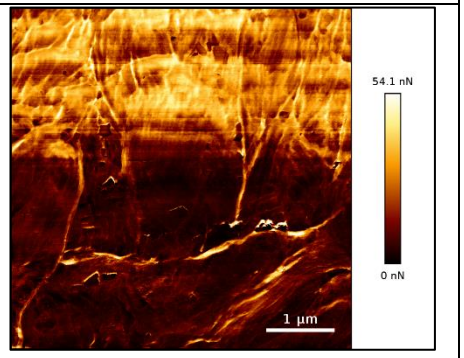

Appendix 5

	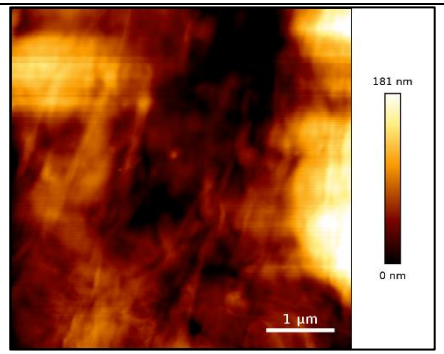	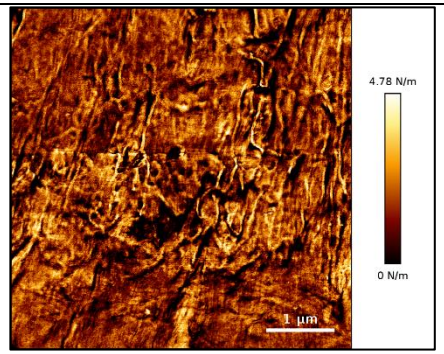	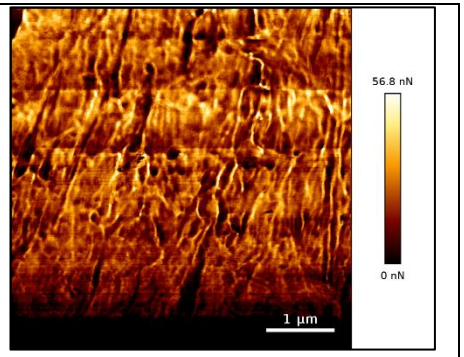
vP50	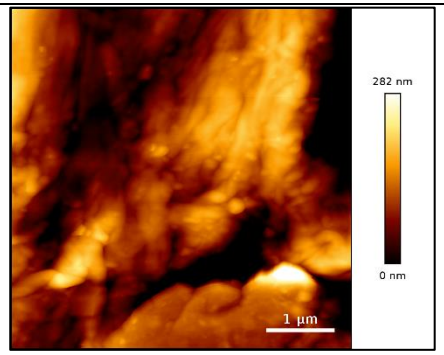 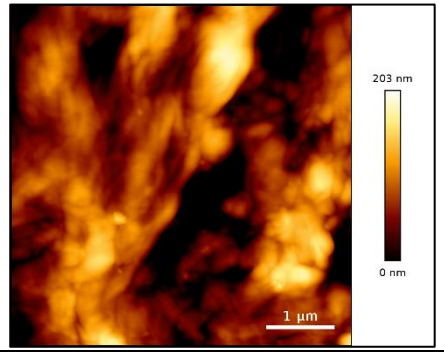	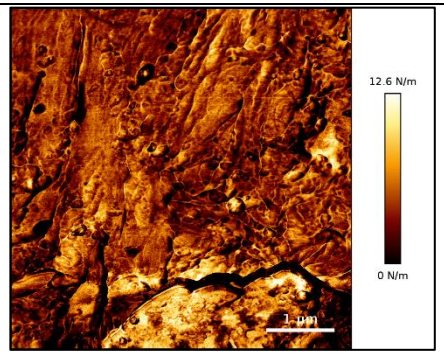 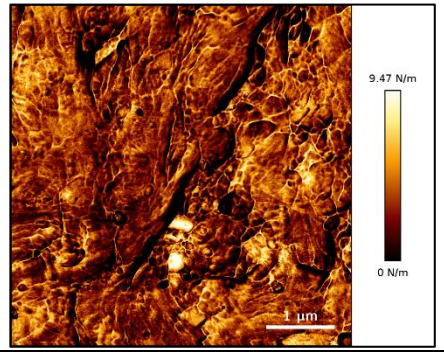	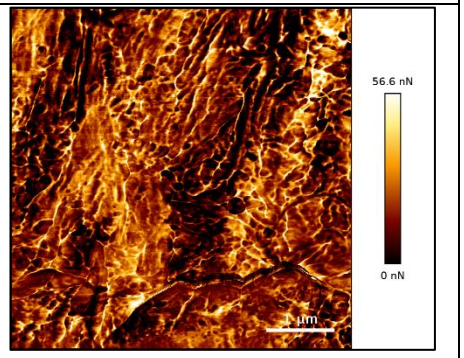 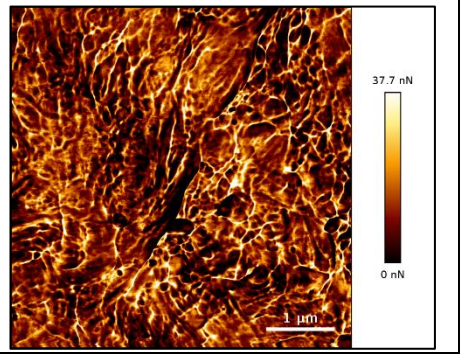

Appendix 5

vP60	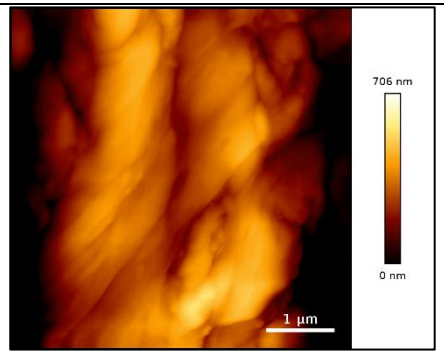	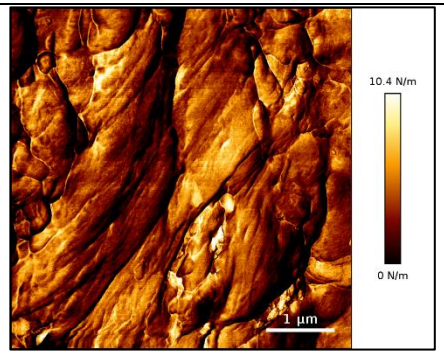	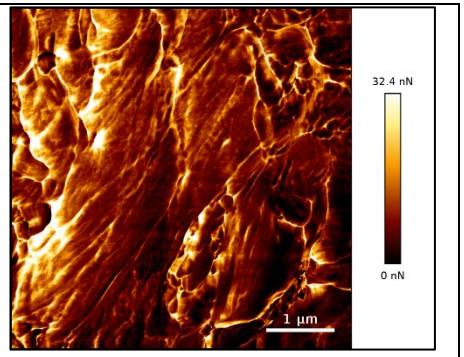
	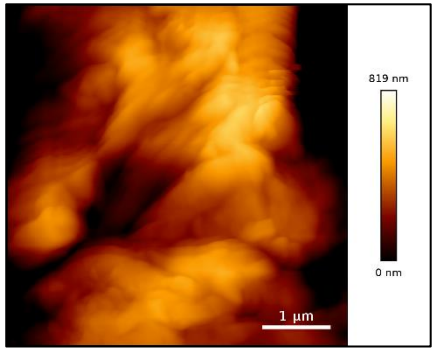	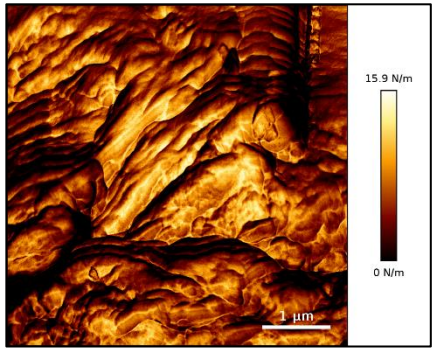	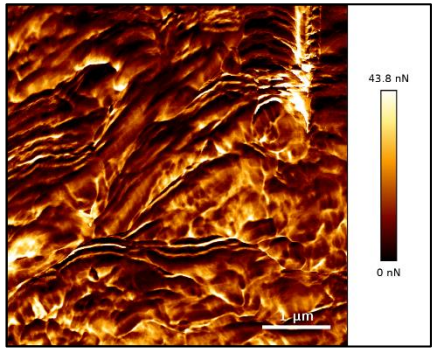
vP75	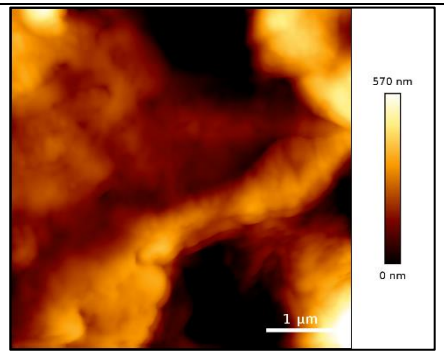	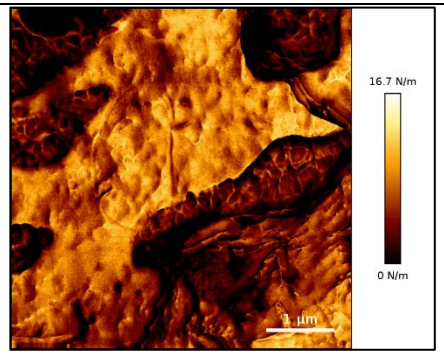	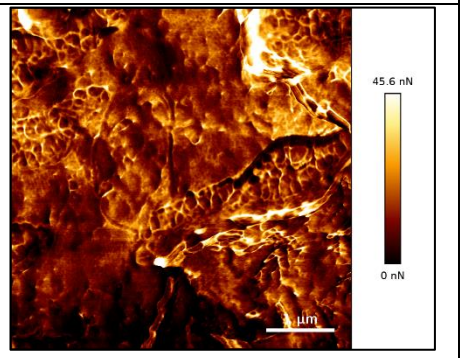

Appendix 5

	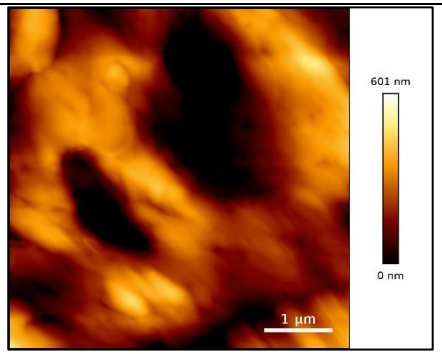	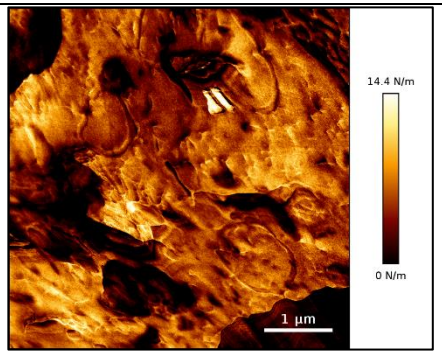	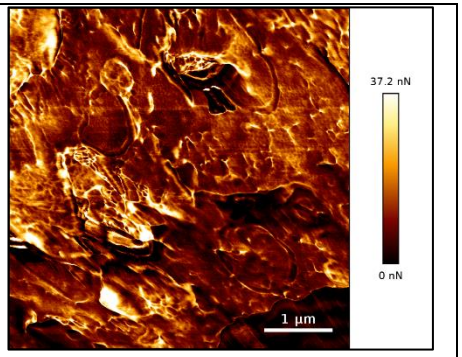
vP80	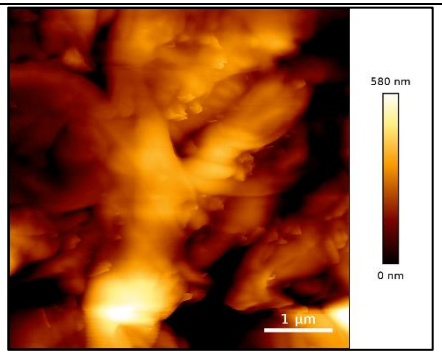 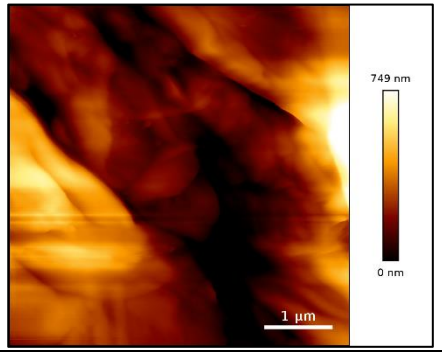	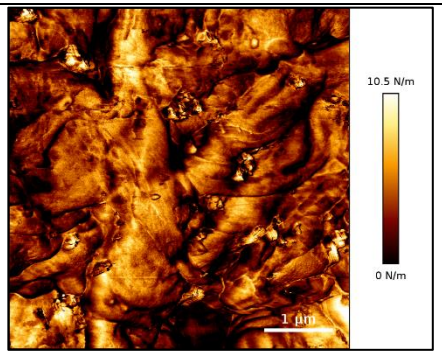 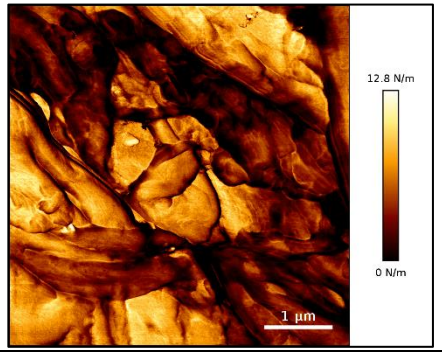	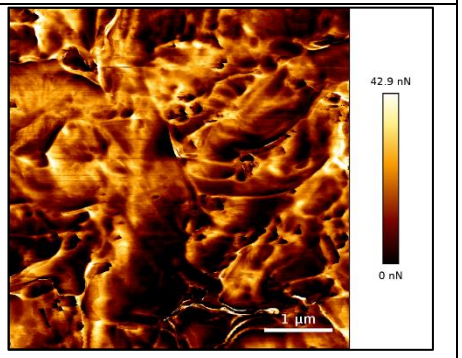 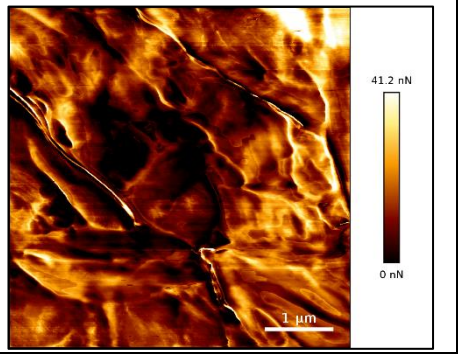

Appendix 5

vP90	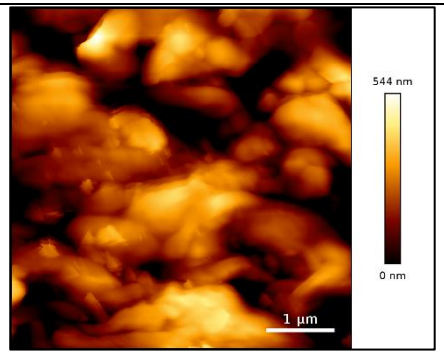	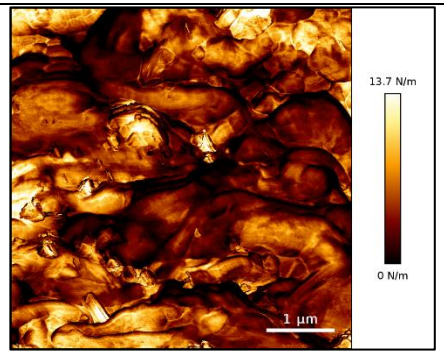	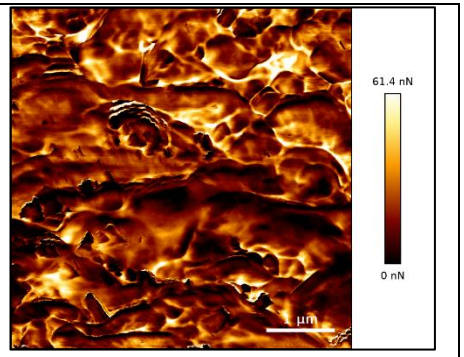
	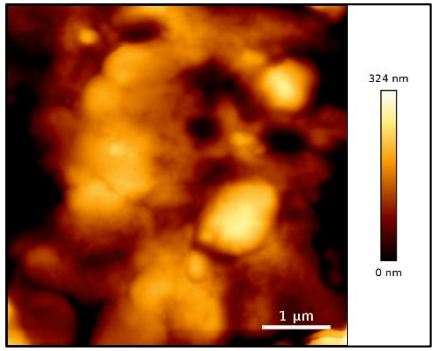	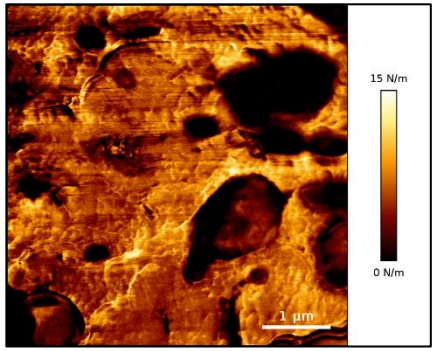	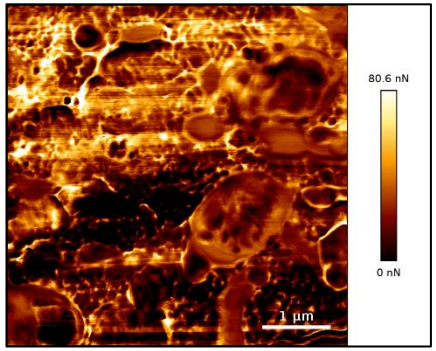
vPP	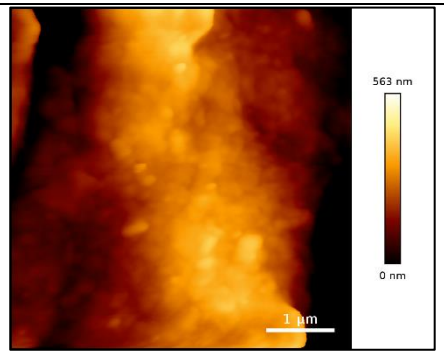	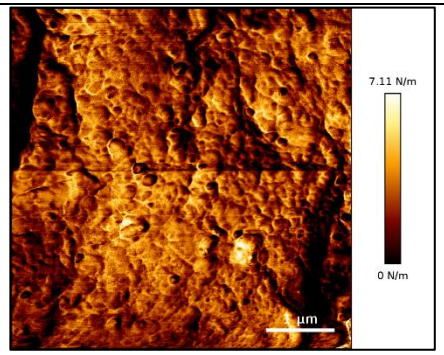	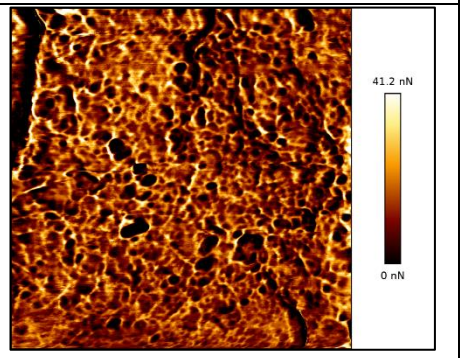

Appendix 5

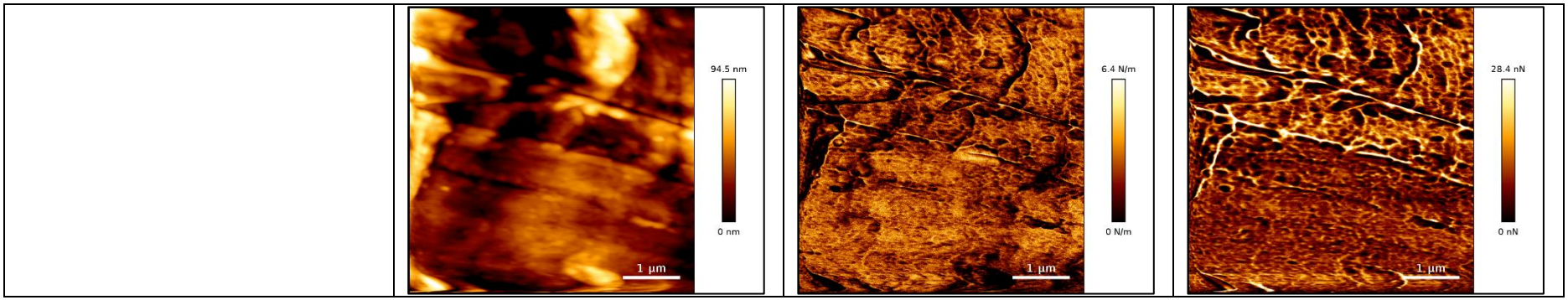

Appendix 6 AFM QI mode height, stiffness and adhesion images obtained at 1024 x 1024 pixels for rPP:rHDPE blends.

PP:HDPE Blend	Height, nm	Stiffness, N m^{-1}	Adhesion, nN
rHDPE	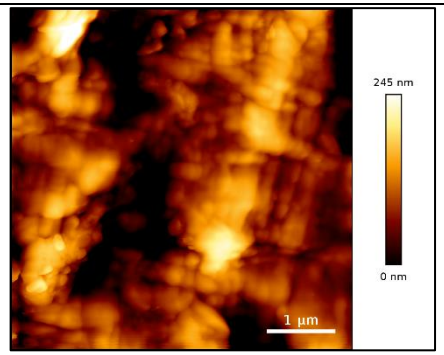	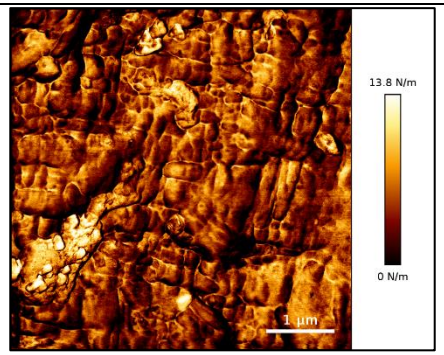	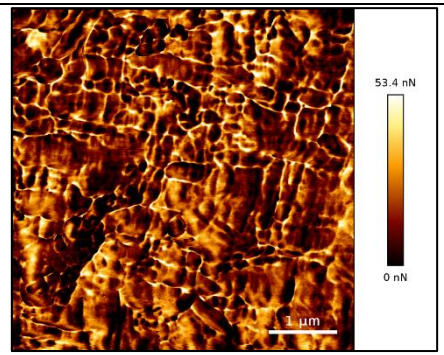
	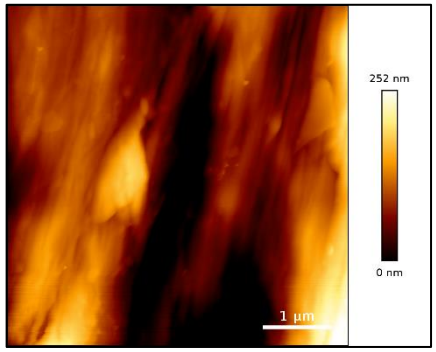	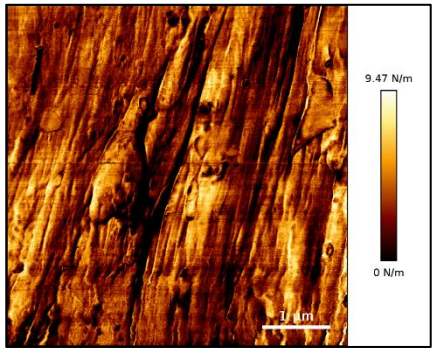	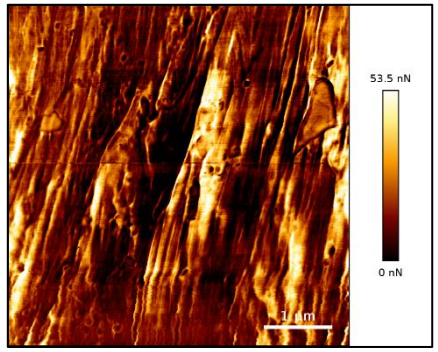
rP10	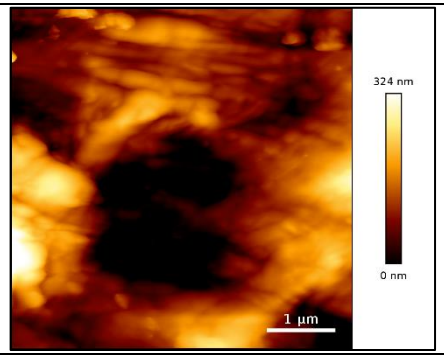	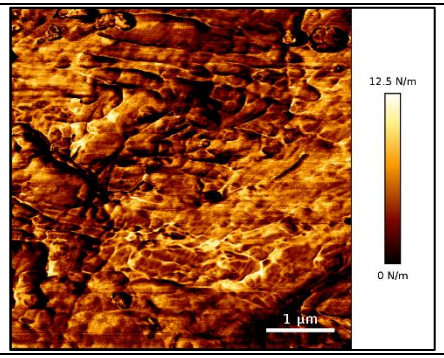	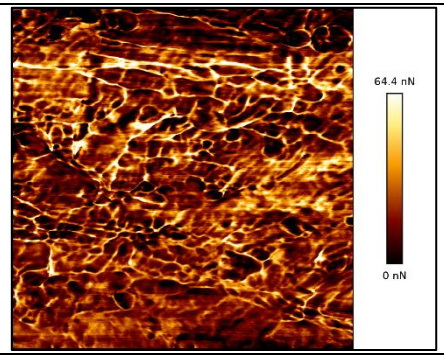

Appendix 6

	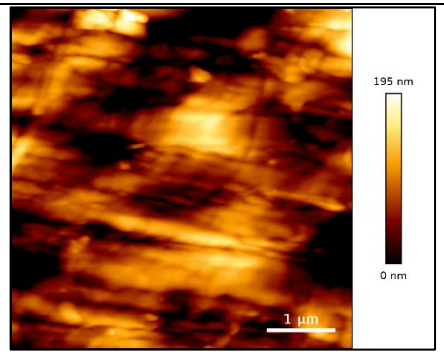	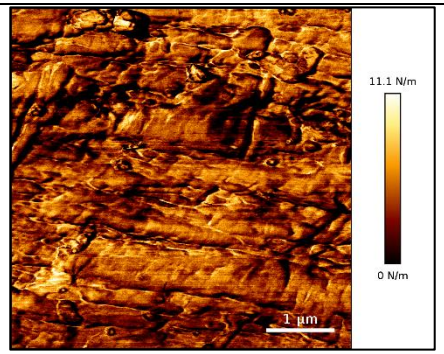	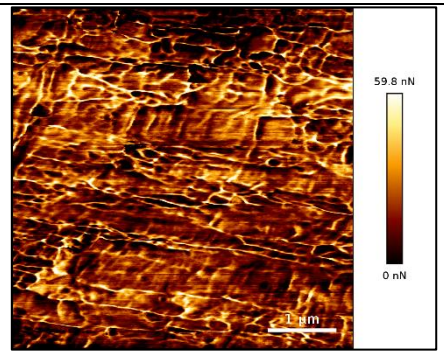
rP20	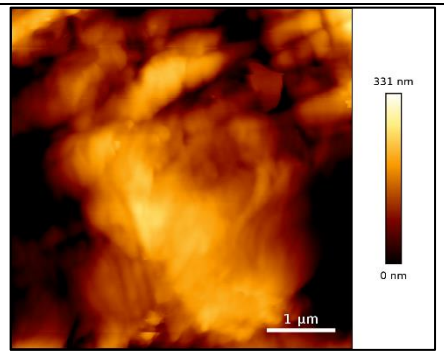 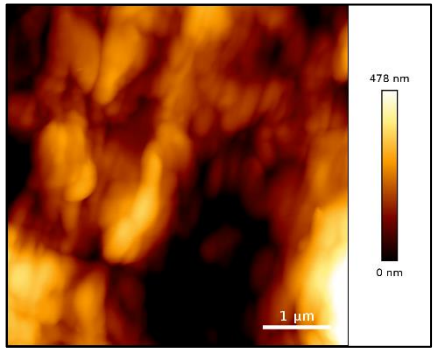	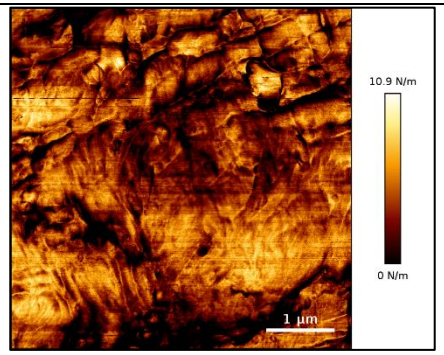 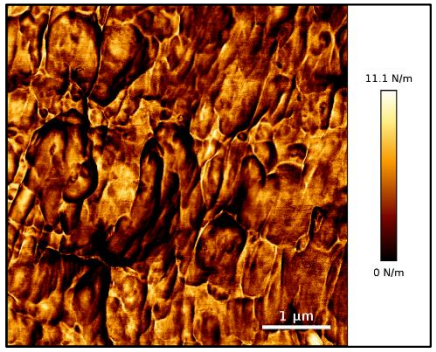	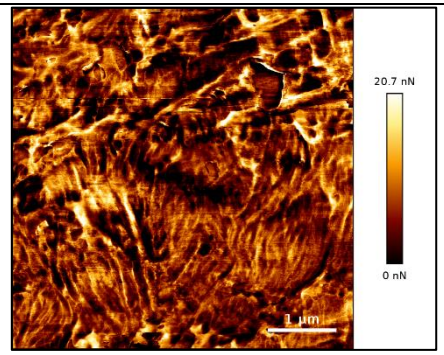 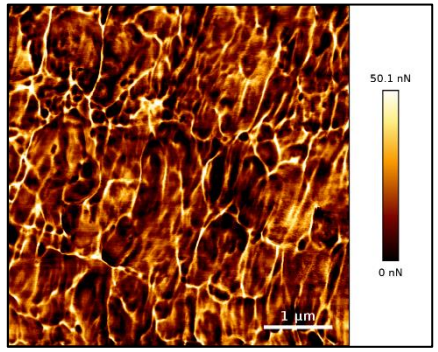

Appendix 6

rP25	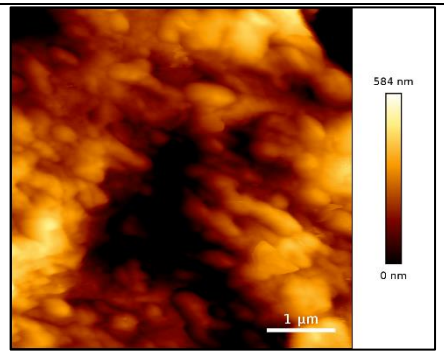	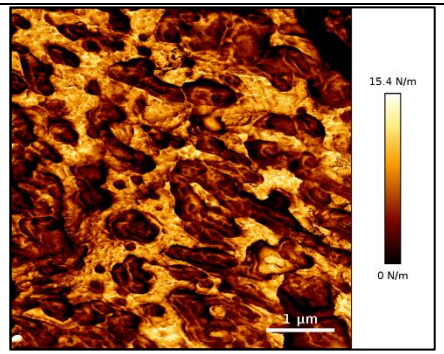	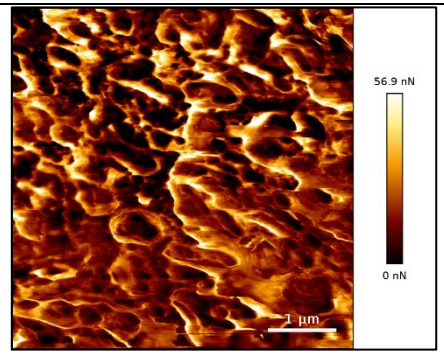
	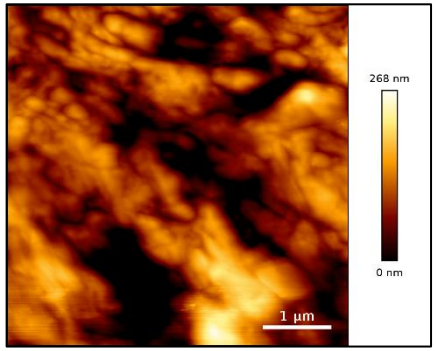	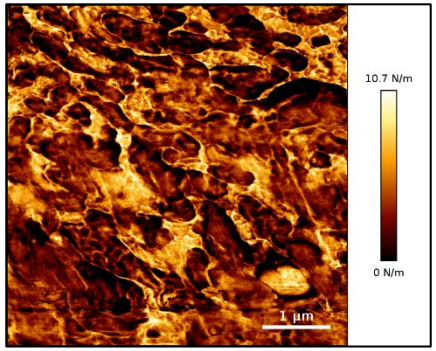	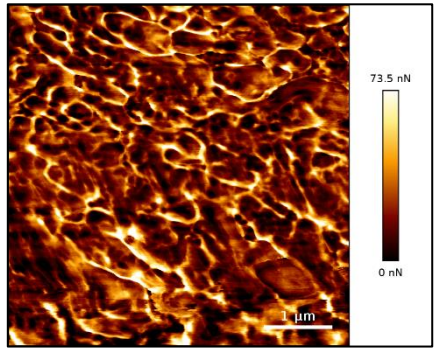
rP40	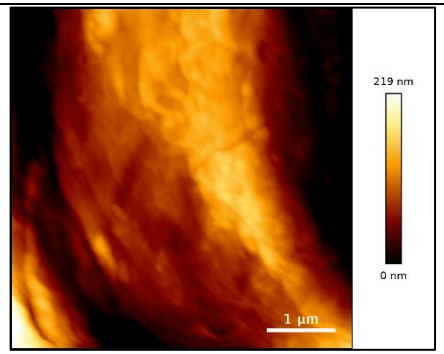	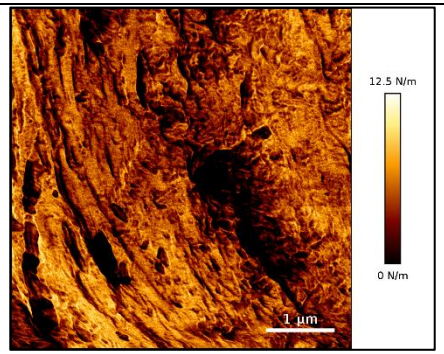	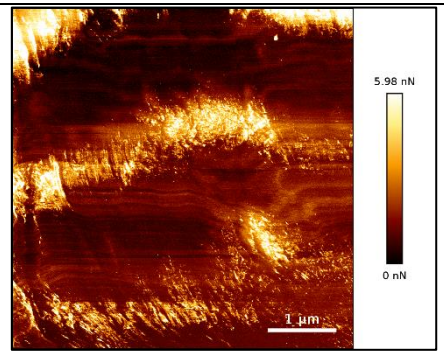

Appendix 6

	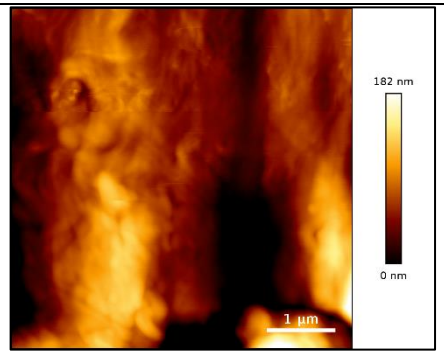	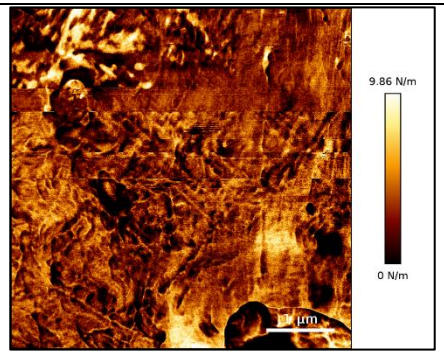	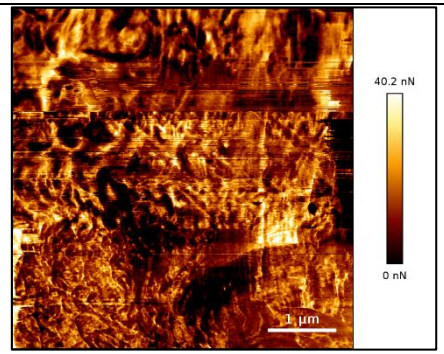
rP50	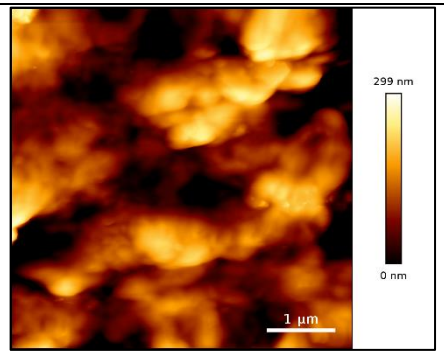 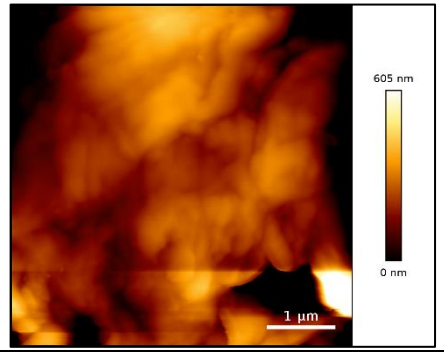	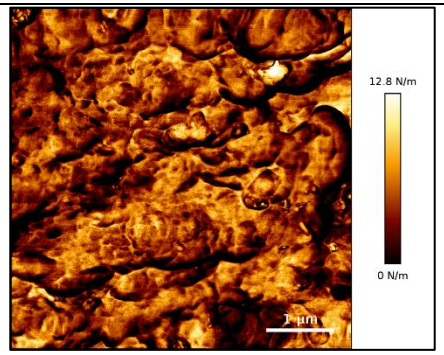 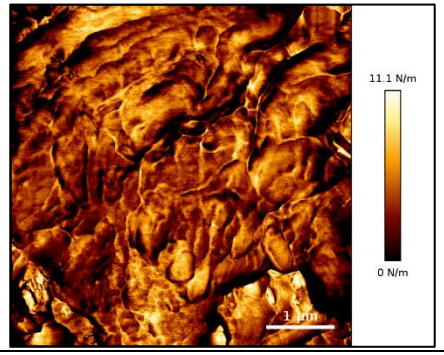	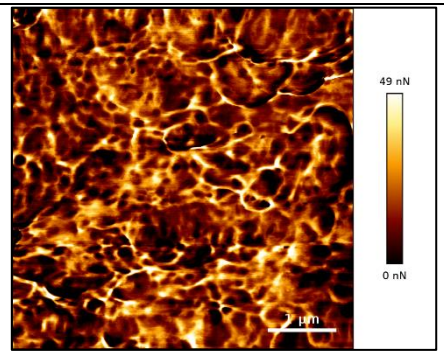 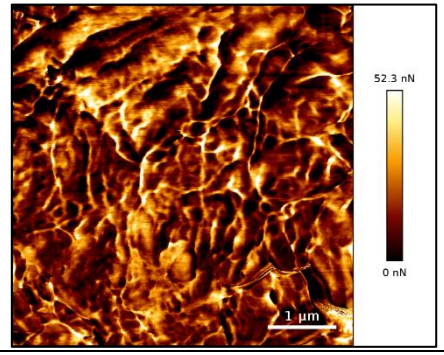

Appendix 6

rP60	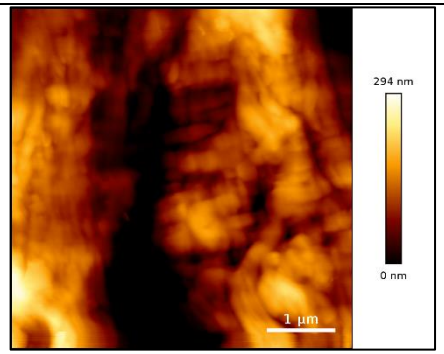	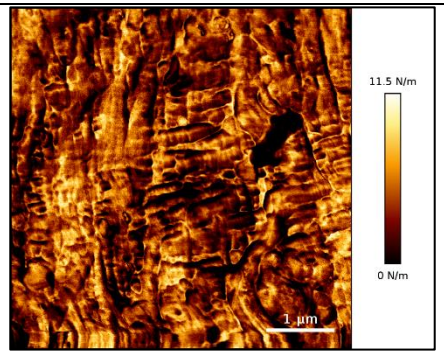	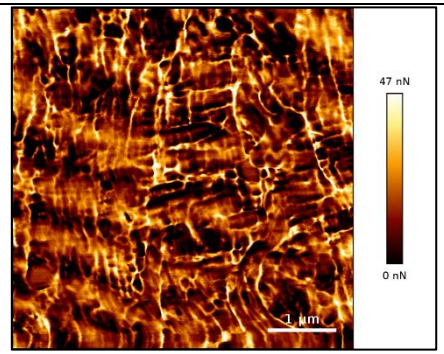
	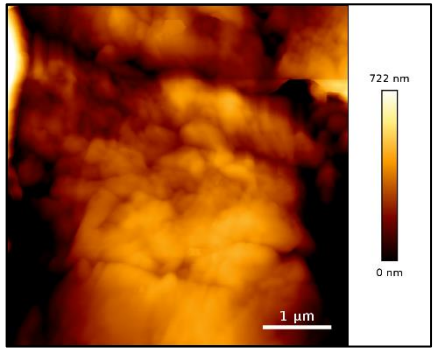	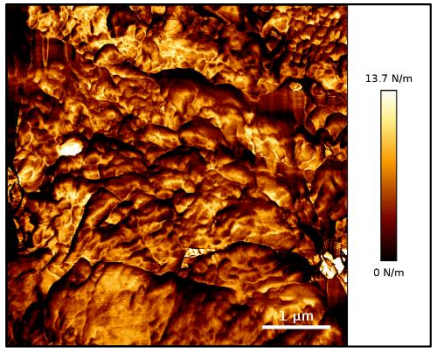	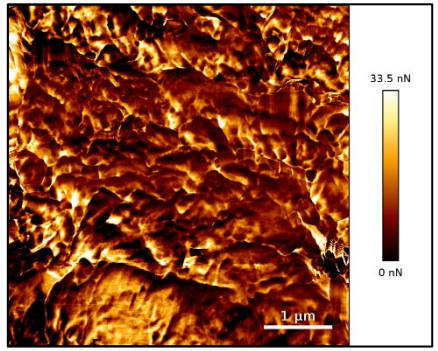
rP75	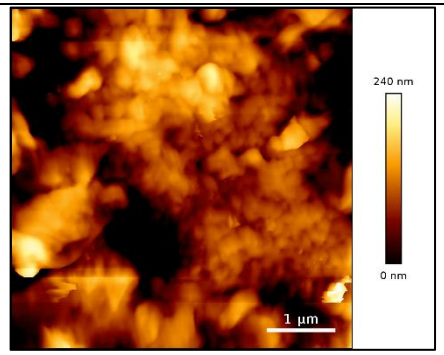	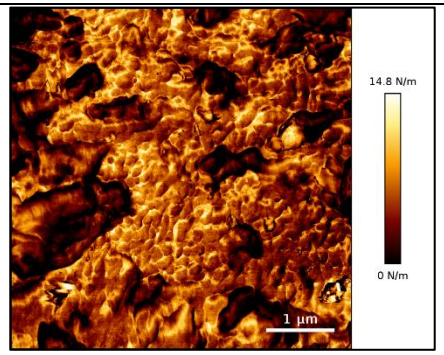	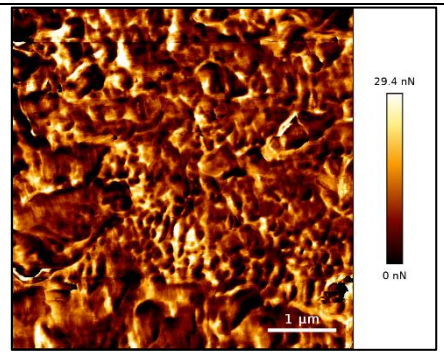

Appendix 6

	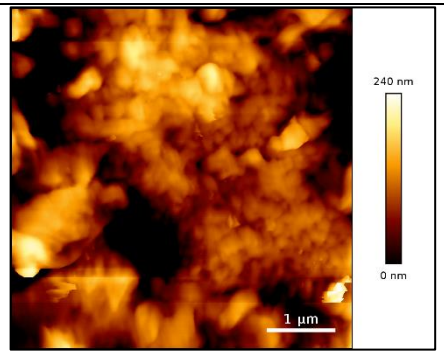	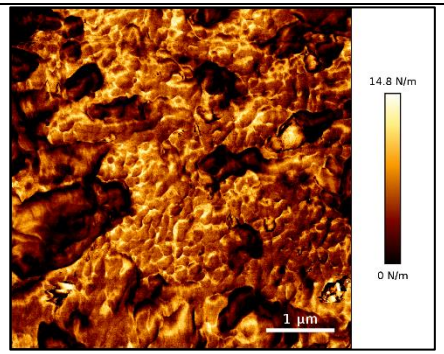	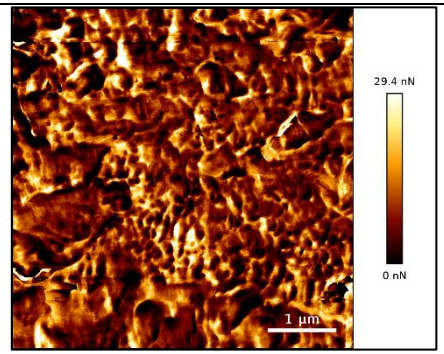
rP80	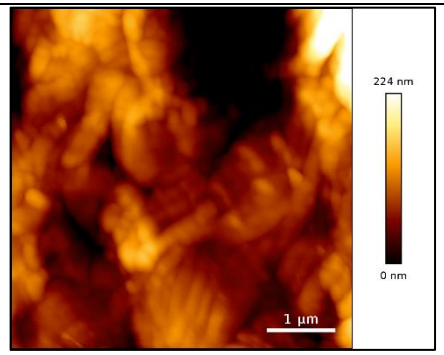 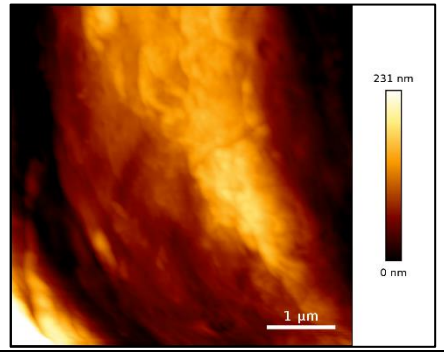	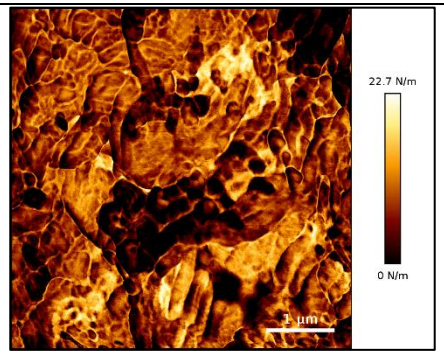 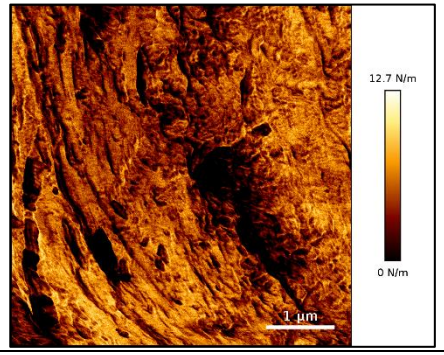	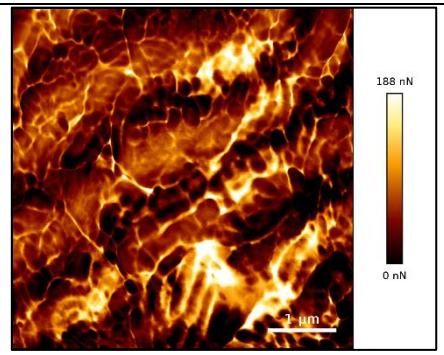 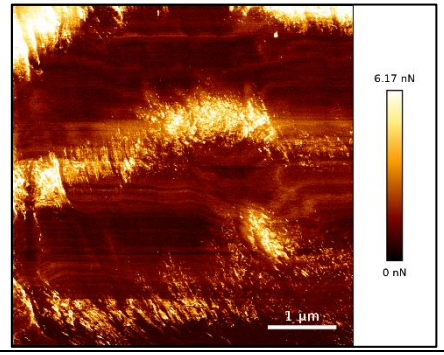

Appendix 6

rP90	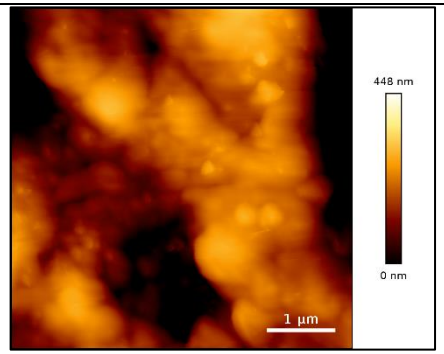	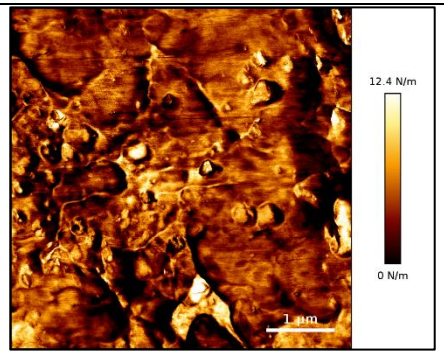	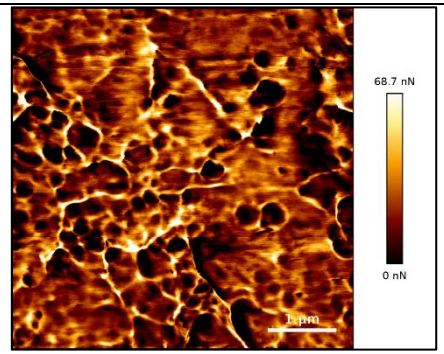
	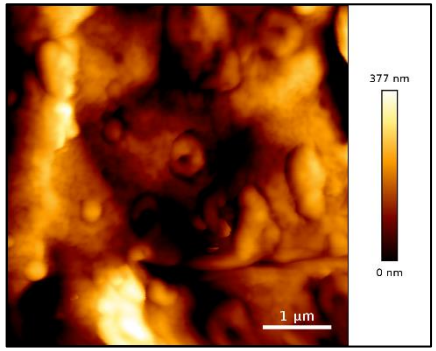	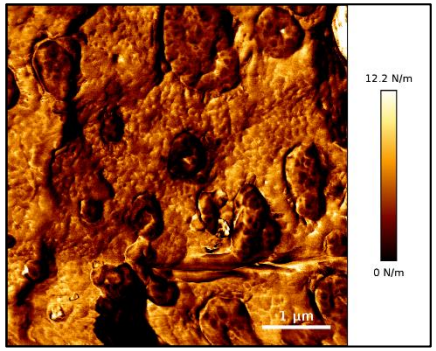	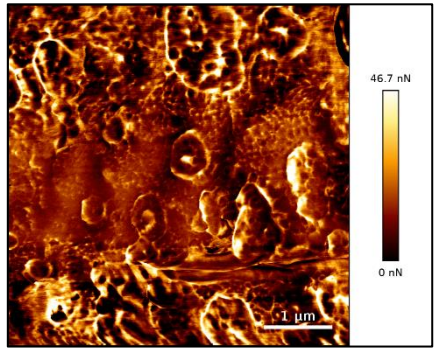
rPP	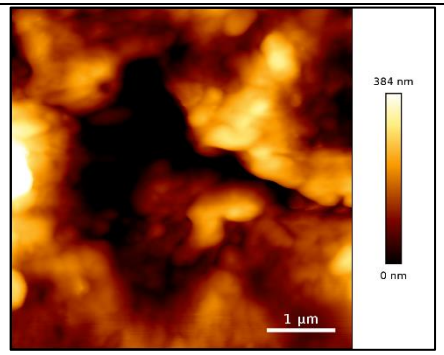	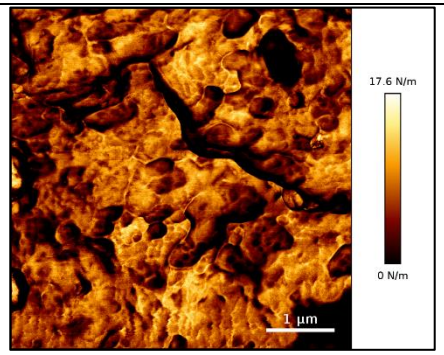	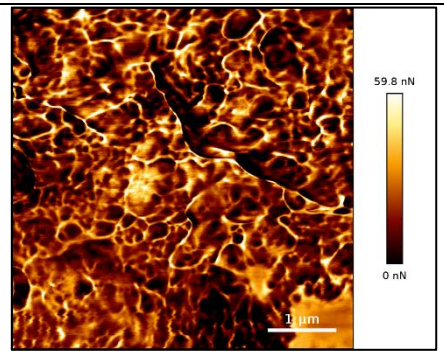

Appendix 6

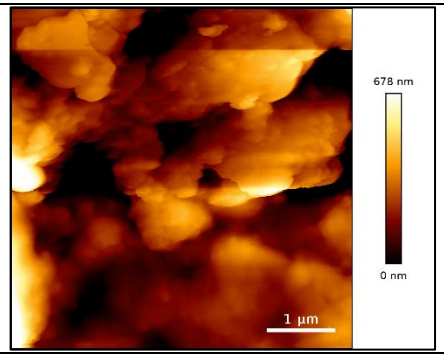

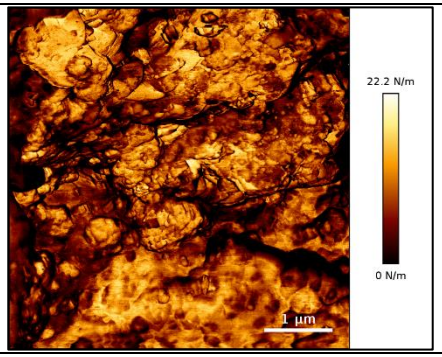

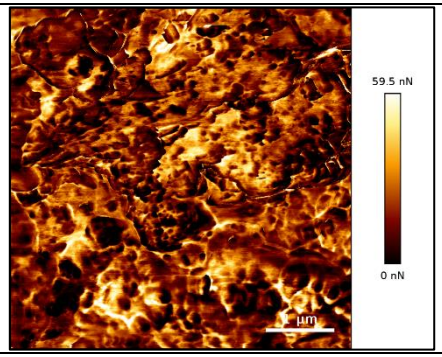

Appendix 7 AFM QI mode height, stiffness and adhesion images obtained at 512 x 512 pixels for vPP:vHDPE blends.

PP:HDPE Blend	Height, nm	Stiffness, N m^{-1}	Adhesion, nN
vHDPE	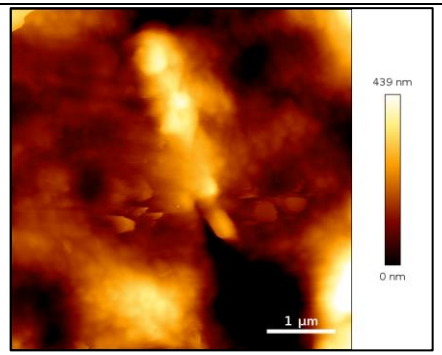	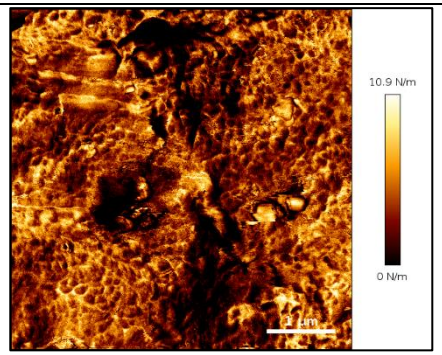	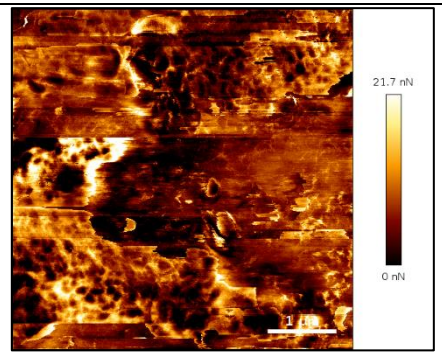
vP10	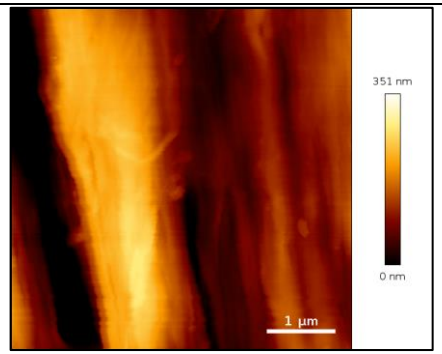	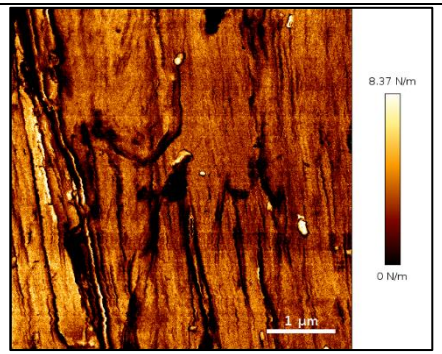	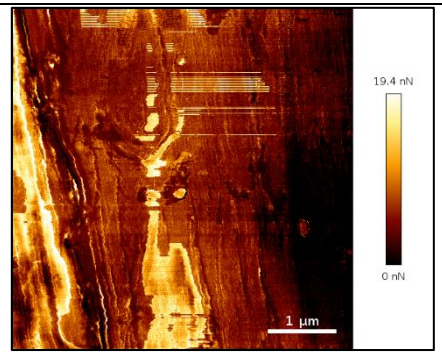

Appendix 7

vP20	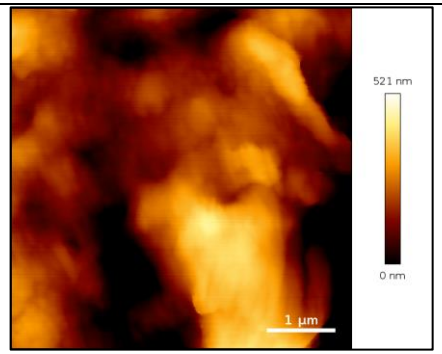	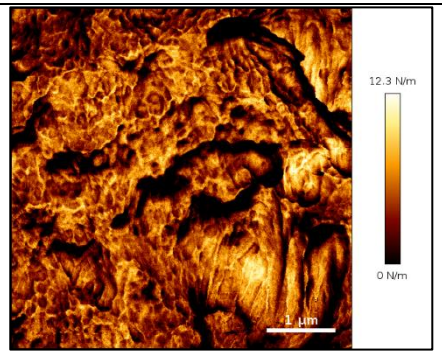	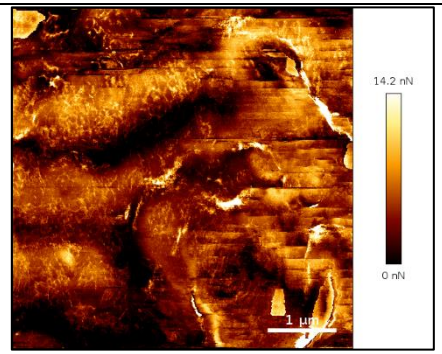
vP25	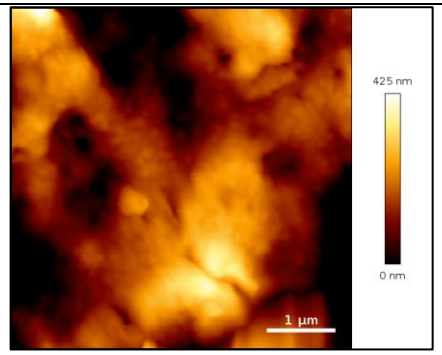	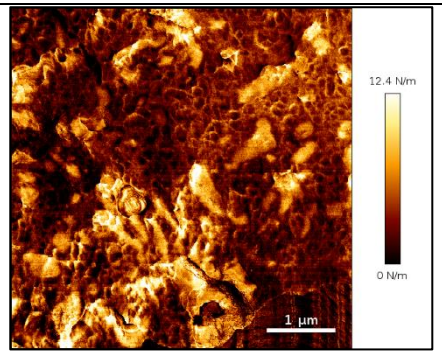	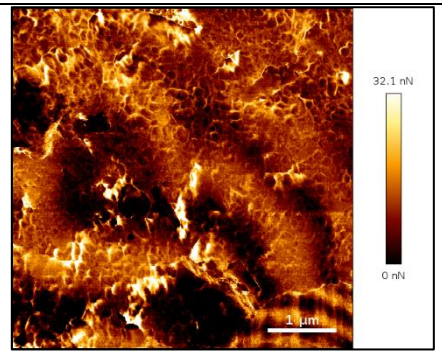
vP40	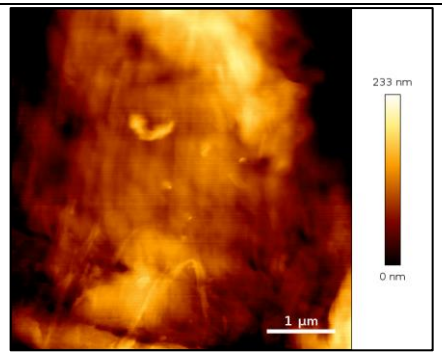	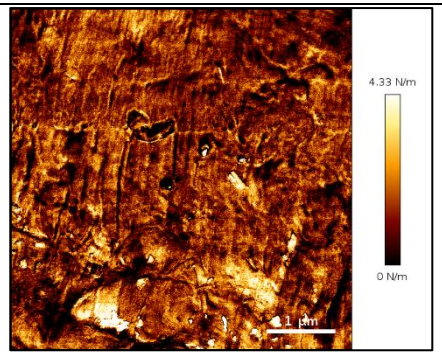	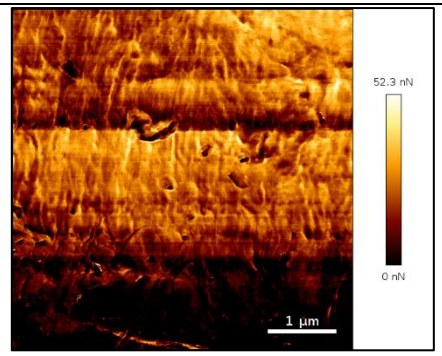

Appendix 7

vP50	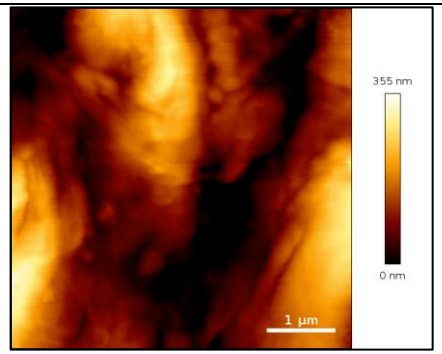	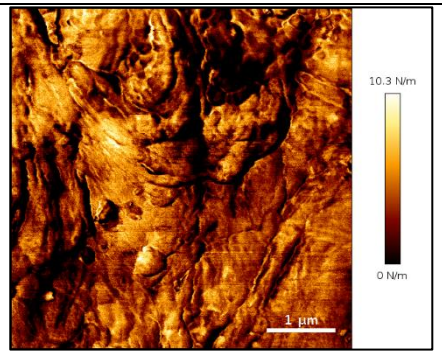	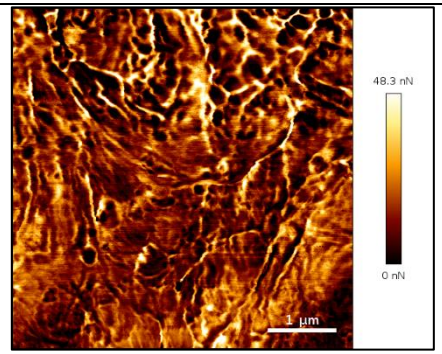
vP60	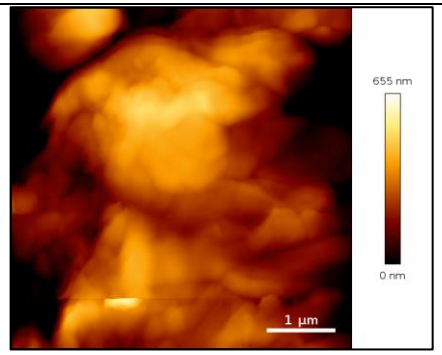	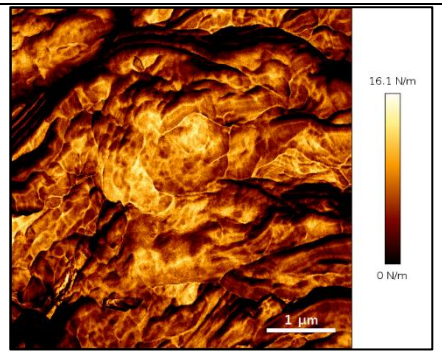	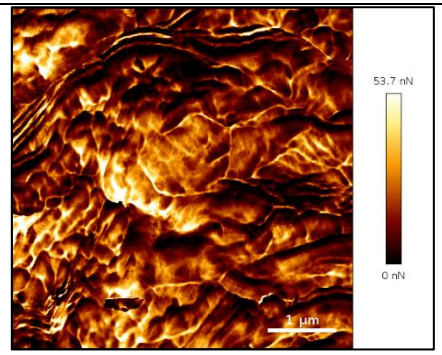
vP75	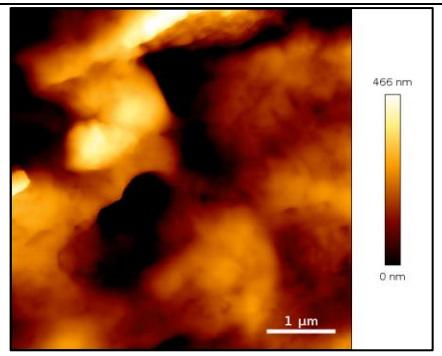	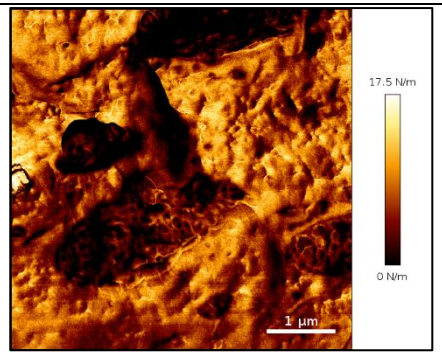	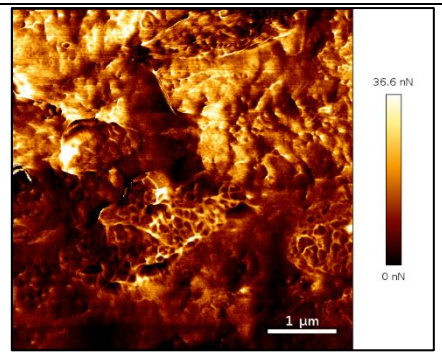

Appendix 7

vP80	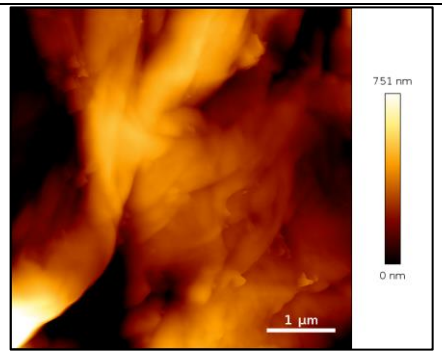	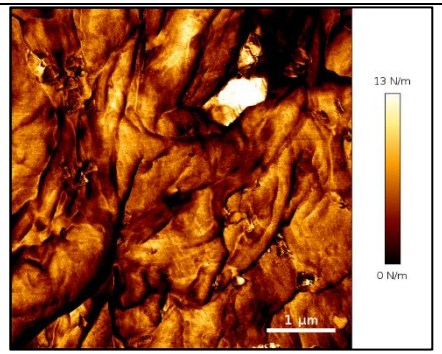	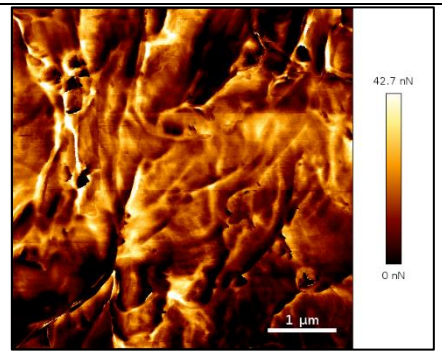
vP90	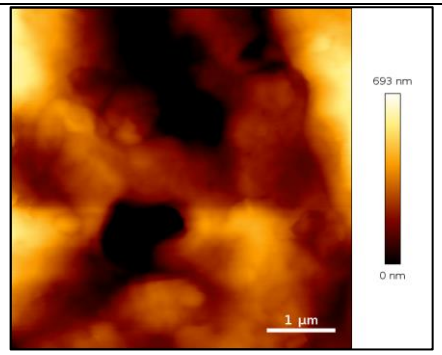	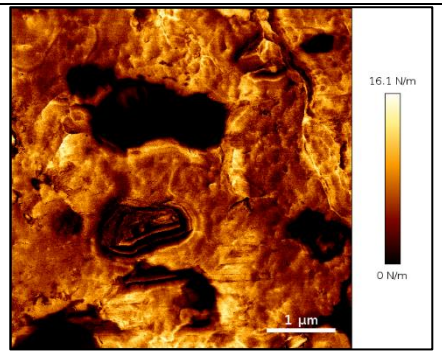	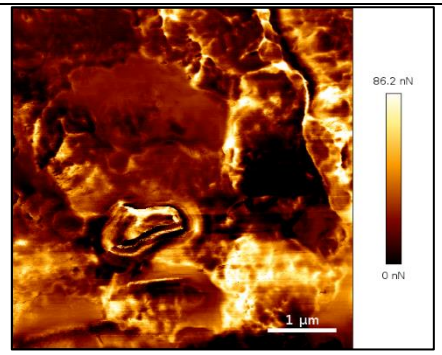
vPP	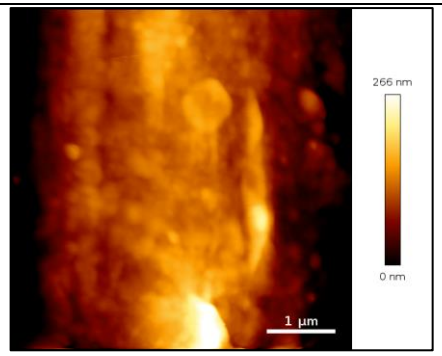	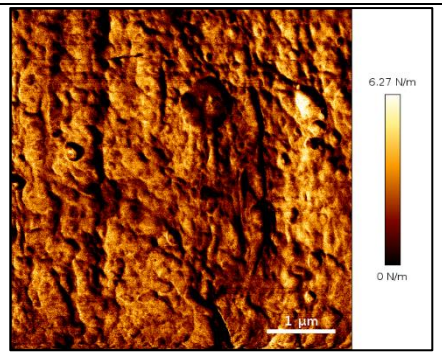	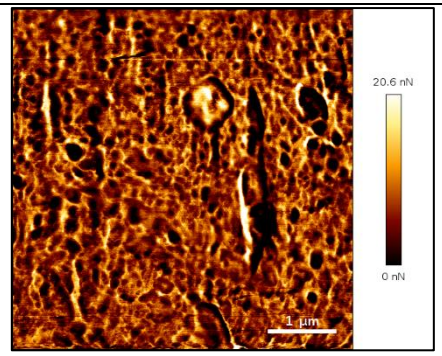

Appendix 8 AFM QI mode height, stiffness and adhesion images obtained at 512 x 512 pixels for rPP:rHDPE blends.

PP:HDPE Blend	Height, nm	Stiffness, N m^{-1}	Adhesion, nN
rHDPE	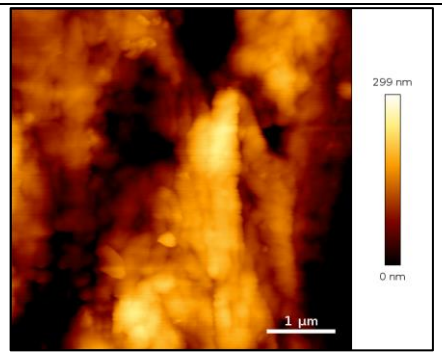	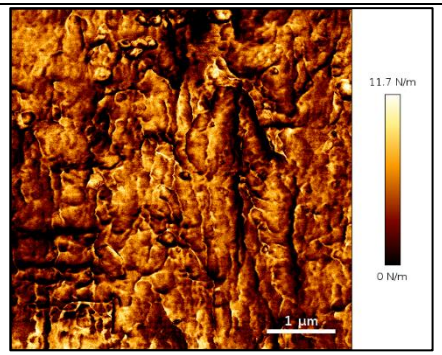	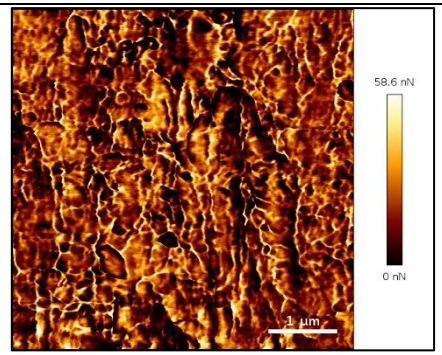
rP10	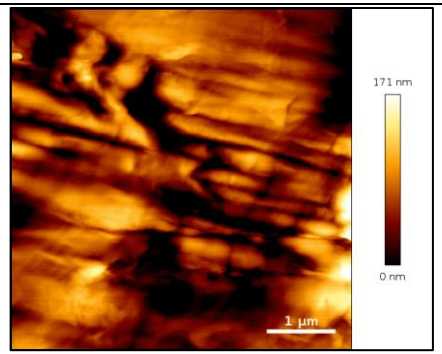	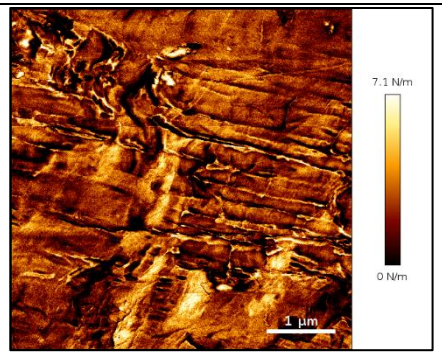	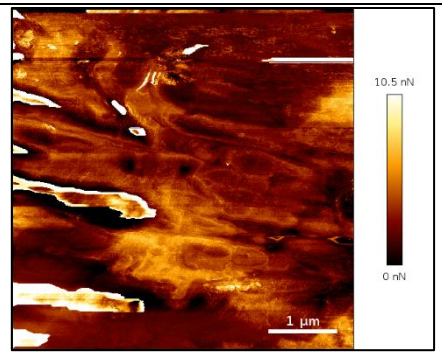

Appendix 8

rP20	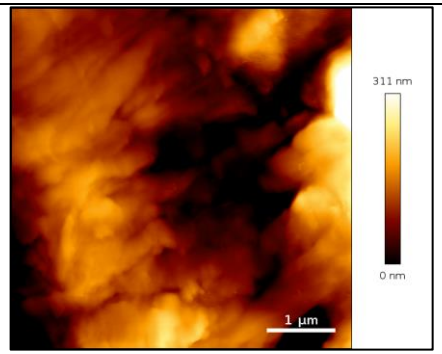	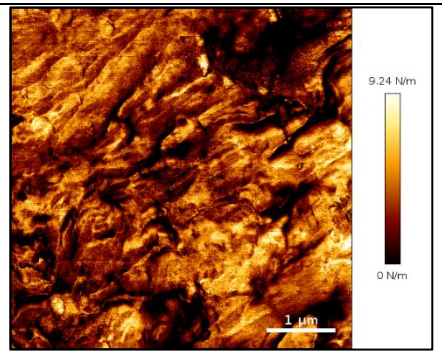	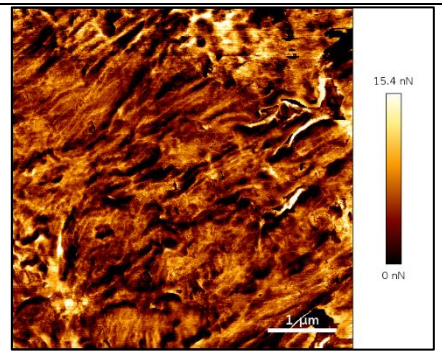
rP25	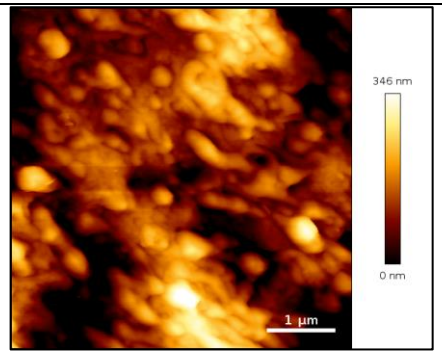	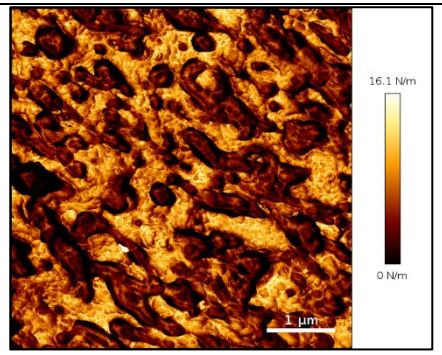	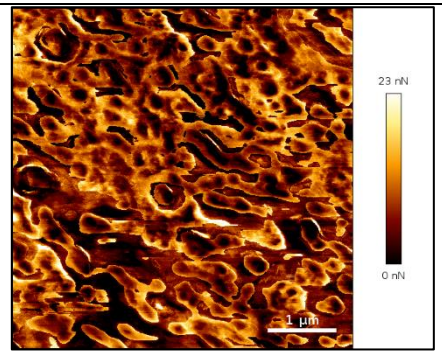
rP40	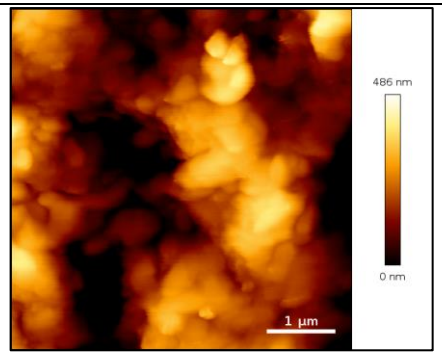	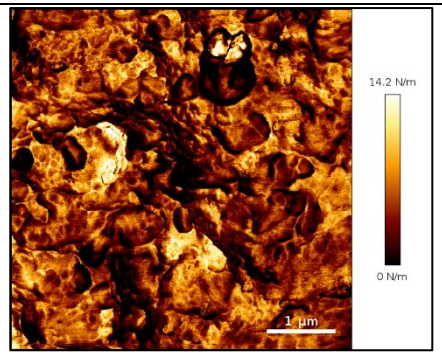	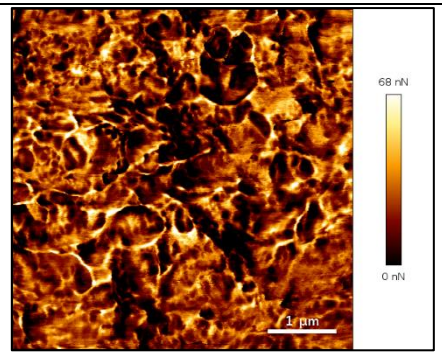

Appendix 8

rP50	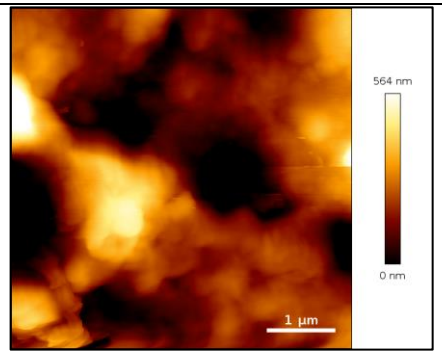	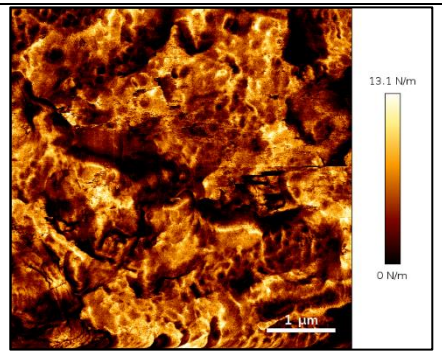	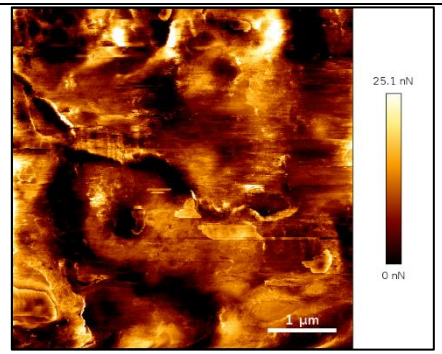
rP60	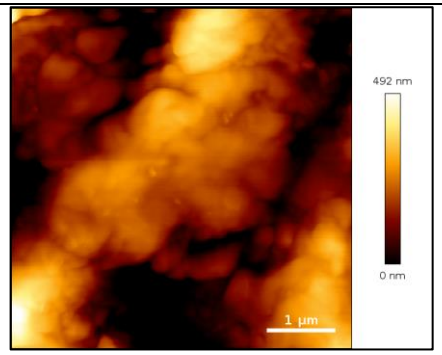	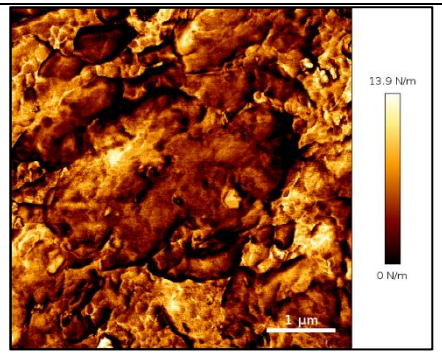	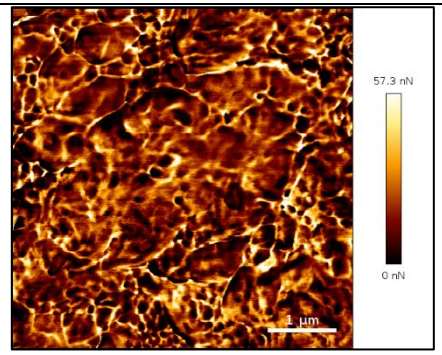
rP75	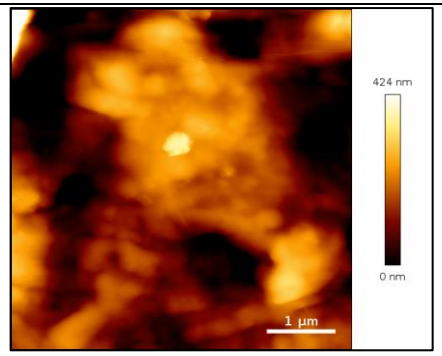	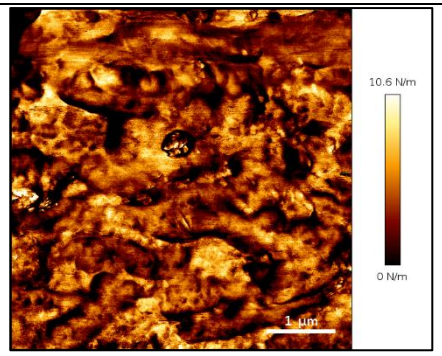	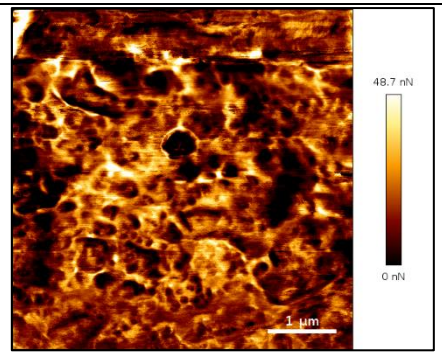

Appendix 8

rP80	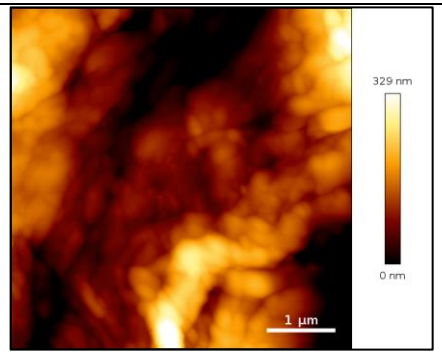	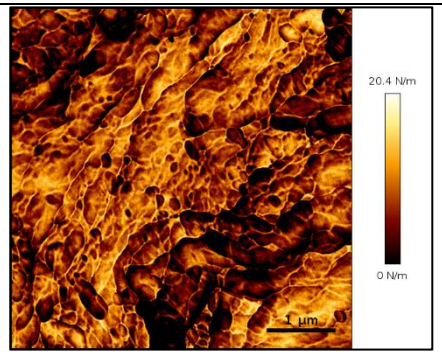	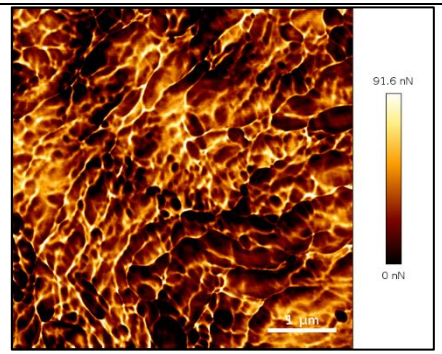
rP90	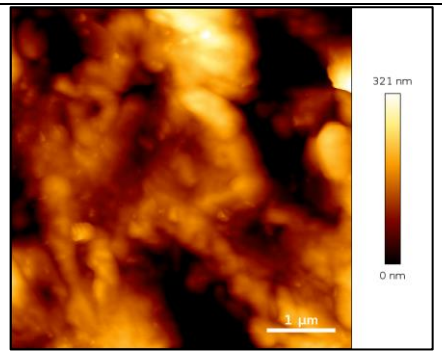	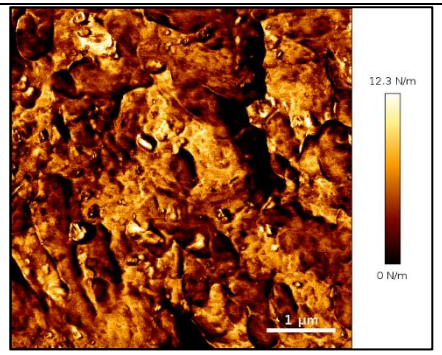	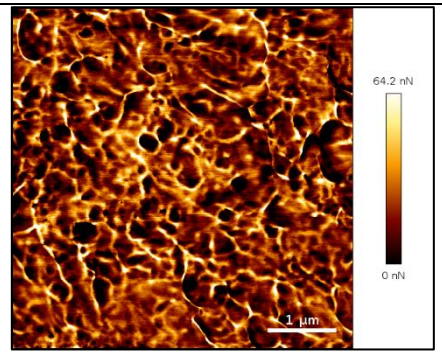
rPP